NATIONAL TECHNICAL UNIVERSITY
OF ATHENS
SCHOOL OF ELECTRICAL AND
COMPUTER ENGINEERING
SECTOR TRANSMISSION SYSTEMS
INFORMATION AND MATERIALS
TECHNOLOGY LABORATORY
MICROWAVE AND OPTICAL FIBER

Study and Design of waveguide Vircator

DOCTORAL THESIS

Panagiotis B. Betzios

NATIONAL TECHNICAL UNIVERSITY OF ATHENS
SCHOOL OF ELECTRICAL AND COMPUTER ENGINEERING
SECTOR TRANSMISSION SYSTEMS
INFORMATION AND MATERIALS TECHNOLOGY LABORATORY
MICROWAVE AND OPTICAL FIBER

Study and Design of waveguide Vircator

DOCTORAL THESIS

Advisory Committee: Ouzounoglou Nikolaos**,**Prof. NTUA Demeter Theodora-Kaklamanis, Professor. NTUA
Konstantina Nikita Professor. NTUA

Adopted by the seven-member committee of inquiry on 22 June 2009.

.....	.....	.....
N.Ouzounoglou Kath.E.M.P.	. Kaklamanis	K. Nikita
	Prof. NTUA	Prof. NTUA
.....	.....	.....
I.Stathopoulos Kath.E.M.P.	I. Vomvoridis	Ch. Kapsalis
	Prof. NTUA	Prof. NTUA

.....
I. Tigkelis
Assoc. Prof. UoA

.....

Panagiotis B. Betzios

Degree in Electrical and Computer Engineer NTUA

Summary

This report presents the study performed upon a particular type of microwave light, the Virtual Cathode Oscillator - Virtual Cathode Oscilla- tor or, as widely known, light Vircator. This paper summarizes the research that has been done on this type of lamps. Describe the high power microwave systems and summarizes the difficulties encountered. Developed physical principles, which are essential for the further understanding of many phenomena Managing governing the operation of the lamps. Described problems of classical physics, such as the motion of charged particles in the electromagnetic field, the fundamental Child-Langmuir Law for ideal vacuum diode, the emergence of virtual cathode in triode infinite plates in shorted diode and electronic packages. Re- rigrafontai phenomena of the lamps, including processes electronic Emission, plasma oscillations, electrical breakdown in vacuo and the behavior of the electrodes in cases cleavage in vacuo.

In working out an extensive study on the Vircator. Developed extensively the natural processes that lead to the production of microwave radiation from Vircator. It explains why it is extremely unstable their function but also because these tubes are an attractive and special class. Grows with analytical party way, the design method of a lamp Vircator and calculation sizes Direc- tion.

Subsequently developed a theoretical study and preparation of the experiment with the light waveguide Vircator. It describes the design of the lamp, the construction of the vacuum system, the high-voltage system and the preparation of experiments. Out extensive experimental results of the tests. Grow the difficul- ties which were addressed in the measurements because of the noisy environment of high voltage. The experimental results are recorded and compared with the theoretical predictions of the analytical lamp drive models. Out, yet, observations relating to the production of X-rays and the effect of the pressure of light in the microwave generation.

In this thesis still presented to extend the Vircator system which Commission persecuted by constructing a multistage impulse generator. The multistage Chart provision designed to drive the Vircator with higher voltages and currents to spread the power of microwave costs. We present the experimental results of the lamp test, the new high-voltage device.

In the last chapter developed recommendations for future research. Out ideas for optimizing the original system and proposals for use of the system as a tool in research areas such as electromagnetic compatibility, radar, the gas ionization study, plasma physics and high energy physics.

Keywords

Vircator, Microwave Tubes, electron beam, diode Vacuum, Virtual Descent, High Voltages, impulse generators, Vacuum Systems.

Abstract

This thesis presents the research that has been conducted on a special type of microwave tube, the Virtual Cathode Oscillator, or Vircator, as it is widely known. High power microwave systems are presented and the difficulties of these systems are examined. Physics principles, required for understanding the microwave tubes operation, are presented. Fundamental problems, such as the Child-Langmuir law for the vacuum diode, the formation of virtual cathode in the vacuum triode, in the short-circuited vacuum diode and in electron beams, are examined. Vacuum tube-specific terms, such as electron emission, plasma oscillations, vacuum breakdown and interelectrode plasma properties are demonstrated.

In the text, an extensive research regarding Vircators is included. The physical processes that lead to microwave generation are investigated. The inherent instability of Vircators as microwave generators is explained, together with all the facts that make them a special class of tubes. The method of designing a Vircator is analytically presented.

The theoretical research and development of the Vircator tube is demonstrated. The design of the tube, its construction, the vacuum system, the high voltage system, and the experimental work is fully explained. Extensive results are presented, together with all the difficulties that had to be solved. Experimental results are compared to theoretical predictions from analytical models of the Vircator operation. Observations of X-ray emission and the influence of vacuum conditions on the Vircator operation are also included.

Further development of a multistage high voltage generator is presented. This Marx generator was fully custom and was used for driving the Vircator tube with higher voltages and currents. More experimental results of this work are included.

In the final chapter, suggestions for further work are discussed. Ideas for enhancing the Vircator system are presented. The uses of a high-power, frequency stable, frequency tunable, light-weight Vircator system are discussed.

Keywords

Vircator, Microwave Tubes, Electron Beam, Vacuum Diode, Virtual Cathode, High Voltage, Impulse Generators, Vacuum Systems

Thanks

On this note I would like to first and foremost thank my family for the unconditional help and sympathy throughout the course of preparation of this thesis.

I thank Professor Mr. Nicholas Ouzounoglou for your interest breathed me to deal with the impressive world of tales and microwave high power vehicles, and for so far valuable discussions and advice.

For help, hospitality and patience, thanks to Professor. John Stathopoulos. Within the framework of fair play, gave me on top, triggers to implement the second largest multistage impulse device - at least in the area of the National Technical University of Athens.

For the extensive input and their help I thank John Written, Atha- Nasia Gida and John Gonos. I thank them for the valuable experience shared with me and for the significant contribution over the long duration of the investigational process.

"A hand science, nevertheless preserves tais meletais, a mathikas it were not so, recruit epistimais tais."

Isocrates

Athens, June 2009.

CONTENTS

1. INTRODUCTION

For decades, high-power microwaves are one area in which considerable research is conducted. Speaking of high-power microwaves, no one conjures devices with exotic names: magnetrons, klystrons, Gyrotrons. In many ways the fact that: it is possible to produce a strong electromagnetic a- ktinovolia other devices only by lamps. And the creators tend to baptize them with increasingly strange names, first gimmicky, secondly to perform that delicate distinctive feature, which it relies function of each invention. Saying light, we must forget the old glass lamps strengthened, admittedly with excellent quality, the weak signals from the needle of a record player. The microwave high power LEDs Direc- gountai of enormous powers and produce impressive light sizes. However, for this reason we call on the lights, they have some common characteristics with Asia Mi- sounding fragile brothers.

The high-power microwave tubes are metallic (and not glass), bulky structures, but require these shortcomings, namely the absence of air in order to operate. They necessarily two isolated electrodes, the cathode and the d- nodo, which should exhibit a potential difference. Making one parenthesis, we will remember that once the analytical chemistry called the cathode electrode that at whoever happens the process of reduction. If you do electrolysis, the cathode are attracted to the positive ions, cations, which employ electrons and become neutral indi- MA molecules. In the case of tubes, the cathode is the electrode that emits electrons in the device. This increase, in turn, is the electrode having ypsilote- po potential than the cathode, thus this attracted electrons, the cathode emits. A cathode and an anode, dry in an area without air, we have made the *vacuum diode*, A very important provision since this accelerate electrons, pro- ragoume ie what we call *electron beam*. Sometimes we have n- lektrodio collector or a control electrode, like the grid had the third CsCl lamps, but usually nothing further. The microwave high power LEDs is, from this perspective, simple rules, since all you need is the cathode and the anode, to create an electronic beam. The package, just bring re- ester its mission, which is to produce microwaves, falls onto the collector, which can be well designed to save heat energy and increase performance, or simply as metal walls lamp, if the fate of the electrons do not care. In fact, what we exploit are electrons traveling, which we are forced to follow perier-

any- tracks, in order to compel radiate in different regions of the elec- tromagnetic spectrum.

The operation of microwave tubes based on the existence of an electron beam, so what you basically need is to place a cathode RES-à-vis of an anode and applying an appropriate voltage so that the cathode to pull electrons, which want to go to rise. This property is very interesting, but the experiment was quite short and tedious if you do not care, in some way, the electrons run to the rise to "xe- Laugh" and to continue their journey, passing by *other* side. This re- tafernoume with sophisticated techniques, such as by making holes in the electrode of the upward jack or using metal grids (i.e. again with holes) or sometimes-financial simopoiontas very thin metal sheets (aluminum foil) to give a chance to e - tronic go climb easily. From that moment, the electrons re- rasoun the rise and continue their journey with as much speed gained by then, begins its exploitation: use magnetic fields to force the electrons circling; using periodic devices and put electrons running next to them so the induced fields in the walls to coordinated throughout with spatial harmonic components; microwave drive signals along with the package, so that the electromagnetic waves constantly absorbs energy from the electrons to their own advantage; disturb the beam with small signals and forcing the electronic rearranged into spatial structures that carry the brand image imposed on them, which then return in the form of enhanced radiation; sometimes, finally, stacked so many electrons in an area that these crowded and begin to perform various movements, trying to decommission thoun from this area in any direction. With this latest and homo- logoumenos odd technique we will deal a little more to this work.

We talked for microwave high power LEDs. The high power is easy to produce, sufficient to guide the passage of our lamp with voltages hundred thousand volt and be able to draw thousands of streams or tens of thousands am- pere. The electron beam then will have a *equivalent* power Gigawatt, from which we will manage somehow to get a portion of the power and do microwave radiation. The idea is simple, but its implementation has some evil points. Some Gi- gawatt is the strength of the Greek grid, so it can not be talking about the same thing. Indeed, in our case, we mean the instantaneous power of the device, ie a small stored energy, which is released in excessively short durations in order to increase the energy efficiency rate and boast that we achieved enormous power. The high-power lamps, they have de facto pulse therefore not a lot of money on the electric company pay nor the provision anticipates damaging effect of Joule, unless you really exaggerate. The power delivery is usually done using fire-knotes, which recharge late at a high voltage and discharged abruptly in light - load. Sometimes we use techniques to multiply the voltage and the shape so that he has *good properties*As fast rise time and fixed price requirements, however, are proving quite complex.

Driving lamp with high voltage remove electrons from the cathode and drive towards the anode. This is done by forced removal of electrons from the body of metal, and this happens when we vacuo.

If there was no gap, would occur ionization gas and there would be a bridging of the plasma anode-cathode gap. But this process, known as electrical ponent cleavage of the dielectric medium, does not accelerate electrons and can not produce fast-moving electronic beam. In high-power LEDs, the electric field that occurs between the anode and the cathode is so intense that the n- lektronia removed by a phenomenon characterized *FEDs*. If we design the appropriate rise, we managed to get the desired electronic high-power beam. The problem with the area of the passage is to create plasma from the electrodes. The intense emission of electrons and partial impingement on the rise, accompanied by a secondary phenomenon. The metal of the electrode melts and produces metal vapor, along with other trapped Toggle limits and organic elements, plasma creates starts the both side of the cathode and the anode side and gradually spreads to the passage. The plasma is the cause that shuts the lamp, since it bridges the gap, the voltage collapses and ceases the acceleration of electrons and hence the beam. Down who wondered how come some of microwave tubes to produce enough high power and not to speak of the above phenomenon. The truth is that these lamps not *considered* high power and generate the electron beam with *thermionic* manner. Heat ie cathode, which in turn emits only a cloud of electrons, which accelerated towards the anode. The currents but do not exceed a few tens of Ampere, because the way thermionic emission not bo- psi yield impressive rheumatic densities. That is why the Down Methods does not suffer from overheating and melting, to create plasma from the vapor of the metal and to bridge the gap of the vacuum diode.

Speaking of high-power microwaves, we can talk about a system. The lamp, which turns the power of the electron beam to electromagnetic solar irradiation is of course the protagonist. We care for the cathode materials, designing the anode and the space in which they will travel the electron beam and produce Asia Mi- krokymatiki radiation. We are concerned about the way you drive the necessary strong potential difference to the electrodes of the diode lamp, which raises problematic ming regarding the electrical insulation. We are interested in the microwave prop- quantities lamp, such as operating frequency, bandwidth, the maximum output power and efficiency. However, to implement and properly operate a system of high-power micro- wave, a set of subsystems must be designed qualifi- Xe. In principle, we can not omit the portion of electric power supply, which occupies multiple volume and hides several technical peculiarities. The form of the high voltage driver is often critical to the yields night lamp. Very often requires stable voltage and current, even for a short duration timing RH, in sizes that are far from insignificant. Other times required iota schyra magnetic fields to guide the electron beam, thus in- xanetai complexity and weight of the system. If the light is not Deci- absolutely tight, pumped and 'sealed' in very low vacuum (hard-sealed tubes), requires the accompaniment of the maintenance system of the vacuum device. Taking oven, usually done by waveguides or choanokeraies therefore requires the existence of suitable vacuum-air interface that keeps ste- ganotita and does not introduce damping to radiation. Finally, the supplied electrical in--effects, which comes either from the power grid, or accumulated

Tess or even by generating sets should be transformed into a ypsilote- po voltage level, more easily exploitable by the device will further multiply the voltage at the level of hundreds of thousands volt, to Direc- githei the microwave high power lamp.

In conclusion, then, we find that a high power microwave system is complicated. Starting from basic principles of dynamic electron, the design of such a system requires knowledge of materials technology, high voltage systems, vacuum technology, electromagnetic radiation transmission principles, electronics, circuit, metrology, deep detail. With this investigation, which is in constant progress, we are pleased enormous knowledge and in- Beira, constantly gained in all these areas. The light waveguide Vircator chosen as the center of this work, in which you will always open new fields of study, experimentation and evolution. This includ- report TAKES a very large portion of the acquired knowledge, experience and hitherto of experimental findings.

2. PRINCIPLES OF DYNAMIC ELECTRONIC

This chapter will present a set of figures features, which Euro- Ares meet, when we study the microwave vacuum tubes. They mainly concern the behavior of electrons in structures and interactions with electromagnetic fields. The electron beam is the carrier of energy, part of which is tapped to produce radiation. In the following paragraphs, will be presented with summary Kd the equations of motion of charged particles in the electromagnetic field in the classical and the relativistic region. They will present the basic concepts of plasma physics, plasma frequency and shielding Debye. We studied the provisions ment vacuum passage and how it led to the formulation of the classic Child- Langmuir law for the maximum current of the diode. Then, examining the phenomenon emergence of virtual cathode, both in classical flat shorted diode, and the electron beam. Finally, phenomena occur such as the emission of electromagnetic cations of metals and electrical breakdown between the electrodes under tension. Based on these fundamental concepts, we will consider in the next chapter the interactions those actions, which are responsible for producing radiation in that category of lamp, called a virtual cathode oscillators and are the subject of study of this work.

2.1. The Lorenz force and the equation of motion

In this paragraph we will soon present the classical equations of motion of charged particle in an electromagnetic field. Starting, mention the famous expression of power, exerted on a particle, which moves inside of electromagnetic field. The *power Lorenz* given by:

$$\mathbf{F}= q\left(\mathbf{E}+ \mathbf{v}\times\mathbf{B}\right). \qquad (2.1)$$

Vectors $\mathbf{E}$ and $\mathbf{B}$ obey the equations of Maxwell, which for the case of vacuum are:

$$\nabla \times \mathbf{E} = -\frac{\partial \mathbf{B}}{\partial t}\ , \qquad (2.2)$$

$$\nabla \cdot \mathbf{E} = -\frac{p}{e_0}\ ,$$

$$\nabla \times \mathbf{B} = m_0\mathbf{J} + \frac{12}{c}\ \partial\partial\ \mathbf{E}\ t\ ,$$

$$\nabla \cdot \mathbf{B} = 0.$$

The speed of light in vacuum is $c = 1\ \ e_0\ m_0 \big/ \sqrt{\text{While}}\ E0$ They are dielectric constant, and *M0* the magnetic permeability of vacuum. The current density **J** and the spatial charge density *p* associated with the continuity equation

$$\nabla \cdot \mathbf{J} + \frac{\partial p}{\partial t} = 0\ . \qquad (2.3)$$

As we know, the change in momentum of the particle because of Lorenz force is

$$\frac{d\mathbf{P}}{dt} = \mathbf{F} = q\ (\ \mathbf{E} + \mathbf{v} \times \mathbf{B}). \qquad (2.4)$$

In the non-relativistic momentum, the momentum of the particle is the product of mass, *m*With its speed, ***v***le **P** = *m***v** . The power connection and change of momentum applies to relativistic velocities, the momentum in this case is

$$\mathbf{P} = \frac{m\mathbf{v}}{\sqrt{1\ \ -v^{2}\big/\ c^{2}}}\ . \qquad (2.5)$$

The relativistic *factor Lorenz* defined as the amount

$$\text{f}c = \frac{1}{\sqrt{1-\ b\ 2}}\ , \qquad (2.6)$$

where *b* is the percentage of the particle velocity relative to the speed of light, namely:

$$\text{f}b = \frac{v}{c}\ . \qquad (2.7)$$

The relativistic momentum (2.5) is therefore based on the above,

$$\mathbf{P} = c\ m\mathbf{v}. \qquad (2.8)$$

From (2.4) by substituting (2.8), we obtain that

$$cm\frac{d}{dt}\mathbf{v} + m\mathbf{v}\frac{d}{dt}c = \mathbf{F} = q\left(\mathbf{E} + \mathbf{v}\times\mathbf{B}\right). \tag{2.9}$$

Solving for the acceleration, $\mathbf{a} = \mathbf{F}/m$, we can write that

$$\mathbf{a} = \frac{\mathbf{F} - \left(\mathbf{F}\cdot\mathbf{b}\right)\mathbf{b}}{\gamma m}. \tag{2.10}$$

In the non-relativistic region it holds that $c = 1$ and that $dg/dt = 0$, so the acceleration and the force is parallel. In relativistic region, however, the speed and power have different directions. For $\mathbf{F} \perp \mathbf{v}$ ($\mathbf{F}\cdot\mathbf{b} = 0$)

$$\mathbf{a}_{\perp} = \frac{\mathbf{F}_{\perp}}{cm}, \tag{2.11}$$

while $\mathbf{F} \,||\, \mathbf{v}$,

$$\mathbf{a}_{\parallel} = \frac{\mathbf{F}_{\parallel}\left(1 - b^2\right)}{cm} = \frac{\mathbf{F}_{\parallel}}{c^3 m}. \tag{2.12}$$

From the above expressions, it appears that the inertial relativistic mass appears different depending on the force and speed angle. In the case of force perpendicular to the speed, the inertial mass is

$$mt = c\,m, \tag{2.13}$$

while in the case of force parallel to the speed, the inertial mass is

$$ml = c^3 m. \tag{2.14}$$

Amounts in the literature are referred to as *transversely* (Transverse) and *longitudinal* (Longitudinal) mass respectively. The amount *gm* It is also known as *relativistic MA ga* particle, while *m* It is known as *rest mass*.

Equation (2.4) represents one vector relation of a system of conjugated secondary rovathmion differential equations. In the case of Cartesian coordinates that we

$$\begin{aligned}
\frac{d}{dt}\left(c\,mx\right) &= c\,mx + c\,mx = q\left(E_x + yBz - zBy\right),\\
\frac{d}{dt}\left(c\,my\right) &= c\,my + c\,my = q\left(E_y + zBx - xBz\right),\\
\frac{d}{dt}\left(c\,mz\right) &= c\,mz + c\,mz = q\left(E_z + xB_y - yBx\right).
\end{aligned} \tag{2.15}$$

The known mass correlation - energy from the special theory of relativity is that

$$E= mc^2 , \qquad (2.16)$$

where to m We symbolize the relativistic mass shows the particle. In the event of immobility is re- $E_0 = mc^2$ While in the case of motion is $E = c\ mc^2$. A cor- matidio moving, has a total energy as the sum of the rest energy plus kinetic energy, so that we can write

$$cmc^2 = E = E_0 + T , \qquad (2.17)$$

where to T we denote the kinetic energy of the particle. An electron which is initially at rest, when accelerated by a potential V Volts, alpha pokta kinetic energy $T = V\ [\ eV\ ]$ When expressed in eV. Therefore, from the production over relationship we can write that

$$fc = \frac{E_0 + T}{E_0} = 1 + \frac{eV}{mc^2} . \qquad (2.18)$$

For the case of the electron, the rest energy is ~ 511keV. Consequently, if, from zero initial speed, an electron accelerated by voltage VWill apoktisei1 tikistiko a relevant factor equal to

$$fc = \frac{511 + V[\ kV\ ]}{511} = 1 + \frac{V[\ kV\ ]}{511} . \qquad (2.19)$$

Using relation (2.6), we can visualize the change coefficient b of an electron accelerated by voltage V. The expression of coefficient b versus accelerate voltage is given by the expression

$$fb = \sqrt{1 - \frac{511}{511 + V[\ kV\ ]}}^{2} . \qquad (2.20)$$

The electron, being extremely light particle is accelerated at speeds approaching the speed of light with relatively small voltages. Instead, the proton, echo- ing almost 2000 times more mass is much smaller accelerations. Acceleration pourable from a voltage 1MV, a proton acquires speed only 4.6% of the speed of light, while a single ionized nitrogen reaches 1.2% of the speed of photo- Tos.

[1] Traditionally, for greater acceleration voltage of 500kV, the electron is now schetikisti- parties. In 500kV electron gained 86% of the speed of light, while at 660kV has 90% of the in-.

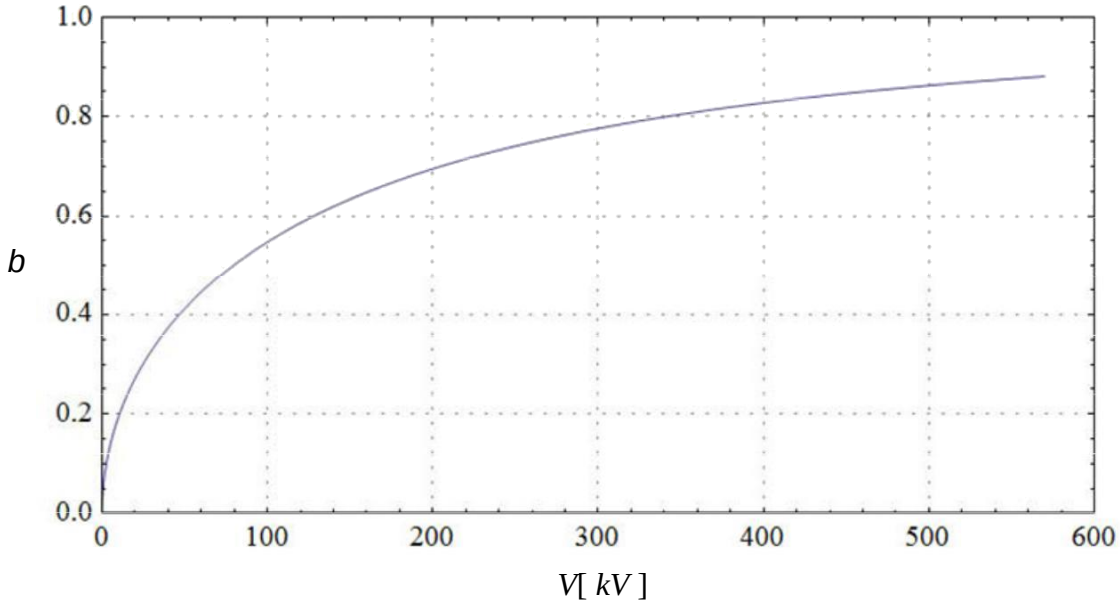

Fig. 2.1: The change of rate *b* the electron when it is accelerated by the potential difference *V*Expressed in kV.

Tab. 2.1: Relativistic coefficients b and c electron

Energy [keV]	Coefficient b	Factor c	Factor c3
0	0	1	1
10	0.19	1.02	1.06
20	0.27	1.04	1.12
30	0.33	1.06	1.19
50	0.41	1.10	1.32
100	0.55	1.20	1.71
200	0.70	1.39	2.69
300	0.78	1.59	4.00
500	0.86	1.98	7.74
1000	0.94	2.96	25.9
2000	0.98	4.91	119
3000	0.99	6.87	324
5000	0.99	10.8	1250

Then we present a list of weights and equivalent actions tranquility of elementary particles and a few atoms and molecules. Note that 1eV = -1.602 · 10-19 J and therefore the equivalent energy 1MeV mass is about 1.78 · 10-30 kg.

Tab. 2.2: Load and mass of elementary particles

	Electron	Proton	Neutron
Load *q*	-1.6 · 10-19 C	1.6 · 10-19 C	-
Mass *m*	9.11 · 10-31 kg	1.673 · 10-31 kg	1.674 · 10-31 kg
Idle Energy *E0*	0.511 MeV	938.259 MeV	938.566 MeV

Tab. 2.3: Energy tranquility of some atoms and molecules

	Atomic weight (amu)	Resting energy (MeV)
^{1}	1.00794	(1p, 1e) 938.77
^{2H}	2.01355	(1p, 1n, 1e) 1878.34
^{4}He	4.00260	(2p, 2n, 2e) 3756.67
^{12C}	12.0000	(6p, 6n, 6e) 11270.00
^{14N}	14.0067	(7p, 7n, 7e) 13148.40
^{16O}	15.9994	(8p, 8n, 8e) 15026.70
CH4	16.0425	(10p, 6n, 10e) 15025.10
NH3	17.0306	(10p, 7n, 10e) 15964.70
H2O	18.0153	(10p, 8n, 10e) 16904.20
N2	28.0134	(14p, 14n, 14e) 26296.70
O2	31.9988	(16p, 16n, 16e) 30053.40
CO2	44.0095	(22p, 22n, 22e) 41323.40
^{27Al}	26.9815	(13p, 14n, 13e) 25357.90
^{28Si}	28.0855	(14p, 14n, 14e) 26296.70
^{56}Fe	55.8450	(26p, 30n, 26e) 52595.00
^{64Cu}	63.5460	(29p, 35n, 29e) 60109.10

2.2. The Electron in Homogeneous Electric Field

Consider two infinite parallel plates, one (cathode) to position *x = 0* and potential zero and the other (anode) to position *x = d* and potential *F = V0*. This provision is known as *flat diode (Planar diode).* Assume for simplicity that an electron emitted from the cathode to the non-relativistic velocity $\mathbf{v}_0 = \{ x_0 , y_0 , 0\}$. The electric field between the reinforcement given by

$$\mathbf{E} = -\nabla F , \tag{2.21}$$

and potential *f (x)*, Between the two plates is calculated from the Laplace equation with *p = 0*:

$$\nabla^2 F = \frac{\partial^2 F}{\partial x^2} = 0 . \tag{2.22}$$

The potential is calculated from (2.22) as $F(x) = C_1 \cdot x + C_2$ and to the given boundary conditions leads to the expression

$$F(x) = \frac{V_0}{d} x, \tag{2.23}$$

while the electric field from (2.21), is

$$\mathbf{E} = -\frac{V_0}{d}\mathbf{x} = Ex\,\mathbf{x}\,. \tag{2.24}$$

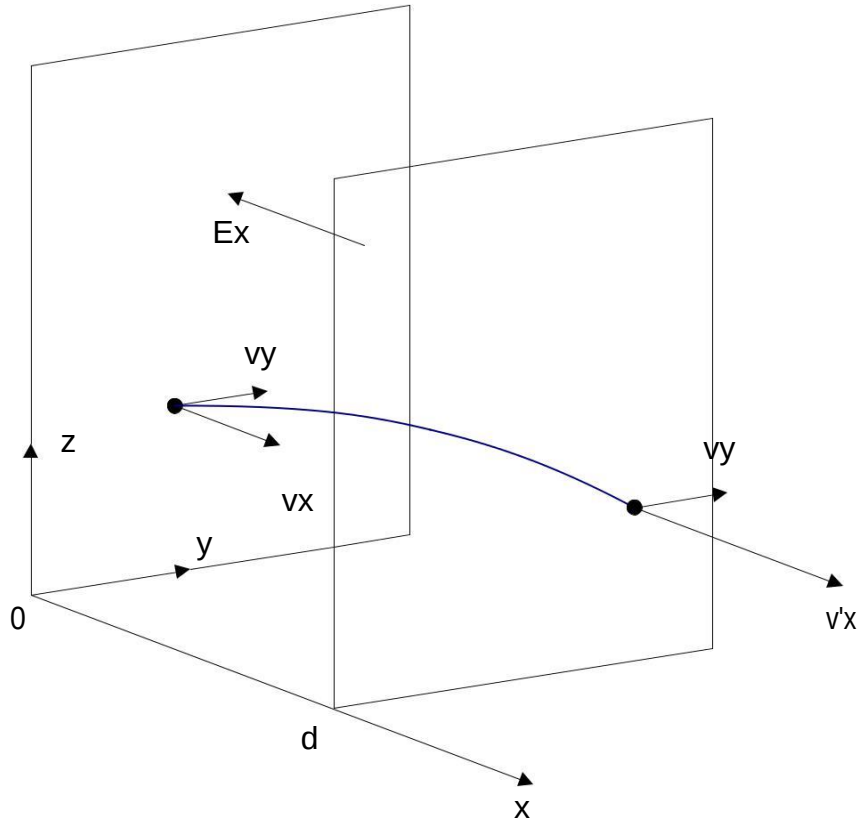

Fig. 2.2: The movement of an electron in the flat path without space charge.

From the equations (2.15) take on *c = 1*That

$$\begin{aligned} mx &= eEx\,, \\ my &= 0, \end{aligned} \tag{2.25}$$

which for the given initial conditions give

$$\begin{aligned} x &= \frac{e}{m_x} E_0\, t + x\,, \\ x &= \frac{1}{2}\frac{e}{m_x} E_0\, t^2 + x\, t, \end{aligned} \tag{2.26}$$

and

$$\begin{aligned} y &= y_0\,, \\ y &= y_0\, t. \end{aligned} \tag{2.27}$$

From the above expression for the displacement *y*, We can resolve with time *t* and replace the expression of displacement *x*. Then take the expression as a function of the track *x*,*y*, Which is

$$x = \frac{1}{2m}\frac{e}{y_0^2}E_x y + x_0 \frac{y}{y_0}, \qquad (2.28)$$

and it is, as we know, the equation of a parabolic trajectory. The change in kiniti- RH energy is from energy conservation:

$$T = T - T_0 = \frac{m}{2}(x^2 - x_0^2) = eV_0 \frac{x}{d}, \qquad (2.29)$$

hence that property originally particle accelerated by potential *V0*The final kinetic energy is *eV0*.

2.3. The Electron in Homogeneous Magnetic Field

Suppose that an electron has an initial velocity $\mathbf{v}_0 = \{x, y, 0\}$ and eiser- be EUR room where there is a magnetic field $\mathbf{B} = zB0$. From equation (2.4) taking WE DECLARE that

$$\begin{aligned} \frac{d}{dt}(me\,x) &= e(yB_0), \\ \frac{d}{dt}(me\,y) &= e(-xB_0), \\ \frac{d}{dt}(me\,z) &= 0, \end{aligned} \qquad (2.30)$$

in case of non-relativistic speed ($c \to 1$). The above system can a- gnoontas movement in z, to be written on the motion in one coordinate, say the x, by uncoupling the first two equations:

$$x = \frac{eB_0}{me}^2 x. \qquad (2.31)$$

Observe that the component $v_x = x$ as component $v_y = y$ show the character- ktiristiki frequency

$$oh = \frac{eB_0}{m_e}, \qquad (2.32)$$

characterized as *gyrosychnotita* (Gyrofrequency or cyclotron frequency) of electronic means in the magnetic field. For practical units for non relativistic in speed of the electron is the gyrosychnotita

$$f_c = \frac{c}{2\pi r_{oh}} = 28 \cdot B_0 \text{ [GHz]}, \tag{2.33}$$

wherein *B0* in Tesla. The radius of the circular motion of the electron occurs if in- xisosoume the magnetic force to the centripetal force by the relation

$$e \cdot v_{\perp} \cdot B_0 = \frac{me \cdot v_{\perp}^2}{rc} . \tag{2.34}$$

From the above relationship, whereas the magnetic field perpendicular to the velocity equals *vc*, relatively small *b*, take that

$$f_{rc} = 0.17 \frac{b}{B_0} \text{ [Cm]}, \tag{2.35}$$

wherein *B0* Tesla is in force

$$b = \sqrt{1 - \left(\frac{511}{511 + V_0}\right)^2} , \tag{2.36}$$

when the electron is accelerated by *V0* kV. To find the corresponding characteristics sizes (*fci, rci*) In single-charged ions, using the mass of the ion *mi* and for finding the *b* when the ion is accelerated by potential *V0*, We use the relation (2.36) the equivalent energy of the ion in keV.

2.4. Plasma Physics

A gas that is *ionization mode*So as to coexist free- pol positive (ions or protons) and negative current carriers (electrons) called *creature*. Many electrons in a plasma is coupled with individuals and sys- consequence of the positive and negative charges move about independently, allowing the plasma display large electrical conductivity. The physical and electrical properties of the plasma are quite different from those of solids and liquids of particulate, distinguishing it as one *fourth state of matter*. The term was originally used plasma by Langmuir and Tonks in a classical work of 1929 [1]. Borrowing an expression from blood plasma, through which blood cells are moving, characteristics as an ionized gas plasma, the agility that have electrons in the crowd of more cumbersome positive ions.

A creature can occur if you increase the temperature of a gas to such an extent so as to present high rate of ionization of atoms. In conditions

thermodynamic equilibrium, there is a correlation of body temperature and degree of ionization, which is described in the study of the Saha [2] and is given for monatomi- Kd gases, once ionized, by the relation [3]:

$$\frac{n_i}{n_n} = 2{,}405 \cdot 10^{21} \cdot T^{3/2} \frac{1}{n_i} \exp\left(-\frac{U}{kT}\right), \qquad (2.37)$$

where *T* the gas temperature, *U* The first ionization energy of the atom, *ni* the concentration of the ionised atoms in m-3 and *nn* the concentration of non-ionized atoms.

Plasma can also be produced by forced ionization methods of ventilation th, which have the effect of increasing the concentration of ionized atoms at higher prices than those under the thermodynamic equilibrium equation (2.37). The two most common methods for producing plasma in a laboratory environment is the photoionization (*photoionization*) And the *Electrical Discharge* gas. During fotoi- onismo, photons with energy greater than the first ionization energy impinging on the individual, thereby creating an electron-ion pair. Most people can be induced ionization radiation with a wavelength shorter than that of far ultraviolet light, as even by x-ray or gamma. The ionosphere of the earth, for example, is a natural fotoionismeno plasma. When electric representatives emptying gas, the electric field applied causes acceleration of electrons, which impinge on the atoms of the medium with a high energy and cause the ioni- tion. In this method, the plasma generated is "hot" electrons, since the kinetic energy acquired by the electric field is much more intense than that of positive ions.

Tab. 2.4: the first ionization energy of some persons

Element	Energy First I c Regulation (eV)	Wave Length (Nm)	Region
He	24.59	50.5	Extreme UV
Ar	15.76	78.7	
N	14.53	85.4	
O	13.62	91.1	
H	13.60	91.2	
Hg	10.44	118.8	Far UV
Fe	7.87	157.6	
Al	5.98	207.5	Middle UV
Na	5.14	241.4	
K	4.34	285.9	
Cs	3.89	319.0	Near UV

When the external driver, which provides the necessary energy to anti-plasma ionization actions removed, then the virus; electron and ion concentrations decrease gradually in thermodynamic equilibrium concentrations. In ergastiri- akes conditions recoupling process of free carriers is so fast that the creature was produced disappears in a split second. However, at low pressures, the volume recoupling lagging behind the recoupling the flank

the, which is the main plasma restore process in a state thermodynami- ment balance.

A plasma can be characterized by several properties such as, for example, if weakly or strongly ionized fully ionized, electrically neutral, warm or cold. Also a creature displays some very interesting properties, such as *oscillations plasma*, electrical screen or *Debye shielding*, and the displayed *mantle* (*sheath*), When the plasma is close to conductive surfaces. Significant these properties will be discussed below, which will examine how the elec- tronic caused vibrations, what is the meaning of the Debye shielding and the Debye length and how the creature ceases to be electrically neutral in the area around a metal body.

2.4.1. Plasma Oscillations

The Langmuir and Tonks first found that, in an ionized gas, electrons perform rapid oscillations with frequencies of the order gigakyklon while positive ions remain generally unaffected by running much slower oscillations [1]. The oscillator Dawson of electrons is a basic property showing a plasma, which is forced to a momentary electrical stimulation. In the plasma oscillations the- Tika ions are considered, in general, have the properties in comparison with electrons, and shall offer the necessary electrostatic restoring forces of the electronic cloud in their minimum potential energy state.

Assuming a plasma initially uniform and at rest, which is electric Kd neutral ion and electron concentrations equal to *ne* [M-3]. Suppose then that an external electrical field causes a small separation of fo- carriers, creating the edges of the area occupied by the two plasma regions, which appears, on the one positive and the other negative space charge. When the external electric field is imperative instantaneously interrupted, the electric field E has developed in the plasma due to the separation of bodies, tending to re naferei to its original state. However, the mobile electronic cloud, to round effects of the internal electric field is accelerated and, when the electronic transiting equilibrium removed again performing a simple pendulum motion. The frequency of this oscillation is called *frequency plasma electrons* (Electron frequency plasma).

In order to derive the expression frequency electronic oscillations of the plasma, we will assume that the ions are immobile and that the electric field Cou- lomb, which develops due to the separation of bodies, affects the movement of electronically according to the relation:

$$e \cdot \mathbf{E} = me \cdot \mathbf{r} . \qquad (2.38)$$

Having considered that the shift is in the axis x, we can aplopoiisou- the above equation the following relationship between measures of internal electric field *E* and acceleration of electrons x :

$$e \cdot E = me \cdot x . \qquad (2.39)$$

Moreover, the current density observed by the movement of electrons is

$$\mathbf{J} = p \cdot \mathbf{v} , \qquad (2.40)$$

We write the measures in the direction of motion obtain:

$$J = p \cdot x . \qquad (2.41)$$

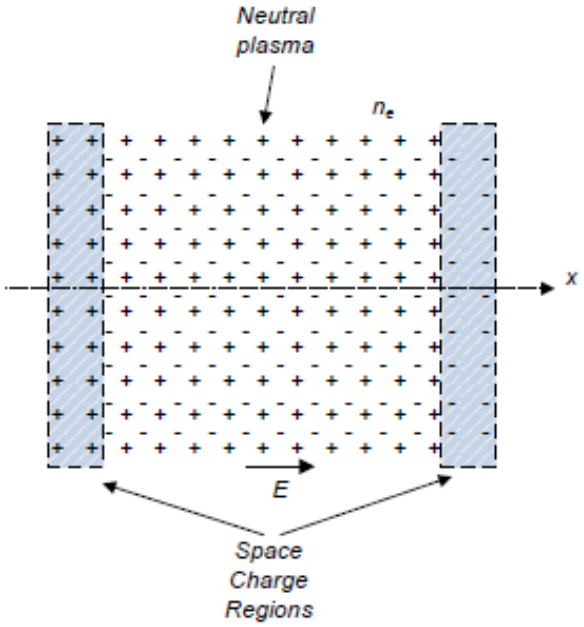

Fig. 2.3: In a neutral plasma instant an external electric field is applied, causing a shift of electrons in the direction x and consequently a separation of the bodies within the limits of the area occupied by the plasma.

The spatial charge density is $p = ne \cdot e$ and therefore paragogizontas once vs. time relation (2.41), we obtain that

$$J = ne \cdot e \cdot x . \qquad (2.42)$$

By law of Ampere, $\nabla \times \mathbf{H} = \mathbf{J} + e_0\mathbf{E}$, Paragogizontas once we receive the relationships night

$$\nabla \times \mathbf{H} = \mathbf{J} + e_0\mathbf{E} , \qquad (2.43)$$

while by law Faraday-Maxwell, $\nabla \times \mathbf{E} = -m_0\mathbf{The}$ We take that shifting the time derivative H is given by

$$\nabla \times \nabla \times \mathbf{E} = - m_0 \nabla \times \mathbf{The} \ . \qquad (2.44)$$

Therefore, equation (2.43) takes the form

$$- \frac{1}{m_0} \nabla \times \nabla \times \mathbf{E} = \mathbf{J} + e_0 \mathbf{E} \ . \qquad (2.45)$$

Observing that $\nabla \times \nabla \times \mathbf{E} = 0$, we take the approach that electrostatic

$$\mathbf{J} + e_0 \mathbf{E} = 0 \ , \qquad (2.46)$$

therefore, using the expression (2.42) for the time derivative of the current density, or (2.46) is, in the direction x:

$$ne \cdot e \cdot x + e_0 E = 0 \ . \qquad (2.47)$$

Substituting x from relation (2.39), we obtain that the electric field that shall follow the following expression:

$$E + \frac{ne \cdot e^2}{e_0 \cdot m_e} E = 0 \ . \qquad (2.48)$$

We notice that this secondary, with respect to time, dependence describes a simple harmonic motion with frequency is given by:

$$\sqrt{\frac{n \cdot e^2}{\varepsilon_0 \cdot me}} \ , \qquad (2.49)$$

η inviting and *frequency plasma electrons* (Electron frequency plasma). For practical sizes is $= {}^{e}oh$

$$f_{pe} = \frac{oh_p}{2Fr.} = 8.97 \sqrt{n_e} \text{ [Hz]}, \qquad (2.50)$$

with *ne* expressed in m-3.

For particles moving at relativistic speeds force $x = oh_p{}^2 \, x = Fs \, / cme$, and the repulsive force is reduced by the magnetic according to the expression (2.10) $Fs = eE \, s \left(1 - b^{\,2}\right) = eEs \, / c^2$, therefore

$$oh_{pe} = \sqrt{\frac{ne \cdot e^2}{e_0 \cdot c^3 \cdot m_e}} \ . \qquad (2.51)$$

Many times, the relativistic plasma frequency used only factor *gm* the denominator. However, The most logical extension of the frequency width of expression tions in relativistic area should incorporate longitudinal inertial mass *g3m*(2.14).

2.4.2. Debye Shielding

The Debye shielding is an important property that shows the creature. Let visas sumo a neutral plasma, into which a load in the form of foil. Without loss of generality we will assume that the shipment import is positive sign. Accordingly, this load will cause an electric field in both directions, which will pull the flex electrons of the plasma, so that the overall load on the disorder area be zero. The electric field in the plasma away from the disorder have prevented will continue to be non-not. Only natural plasma border will appear opposite sign separately party load quantity so much, osis load disturbance.

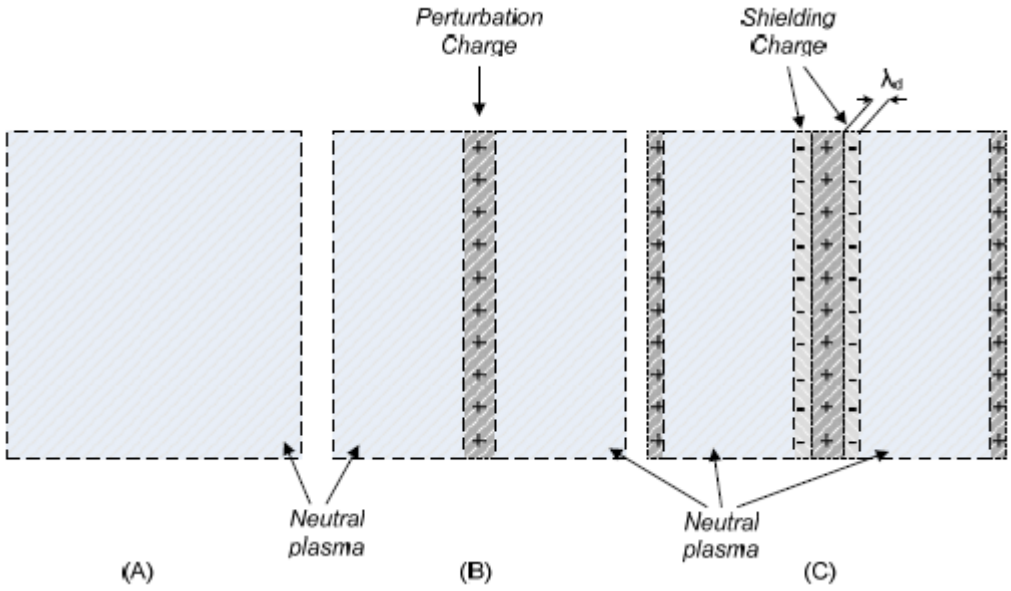

Fig. 2.4: In a neutral plasma, (A), a positive space charge is introduced, (B). This load causes an electric field pulls the boundary of the electrons from the plasma. In the surrounding plasma region remains electrically neutral, in other words the creature has *shield* the externally imposed electrical heterogeneity (C). Because of the electrical tronic, accumulated around the positive charge was introduced, it appears re- rissefma positive space charge in plasma boundaries.

Said property is known as *armor Debye*, Which results in an electrical disorder not perceived in the rest space occupied by the plasma. However, due to the thermal energy of electrons, the thickness of *mantle*

shield It is not infinitely thin, as it could theoretically be. The *mantle* (Sheath) extends a distance approximately equal to the quantity characterized *length Debye*. The length Debye defined by the ratio of the average speed of particles towards plasma frequency *op*. The average thermal velocity equals

$$u_x = \sqrt{\frac{kT}{m}}, \tag{2.52}$$

while the non-relativistic plasma frequency, with $oh_{pe} = (ne \cdot e\,2 / e_0 \cdot me)^{1\,2}$. Therefore,

$$\text{f}l_d = \sqrt{\frac{e_0 kT_e}{n\,e^2_e}}, \tag{2.53}$$

wherein the length *ld* called and length Debye. This quantity characterizes the depth of penetration of an electric field in a hot plasma.

2.5. The Law ChildLangmuir

In two classical works of the early 20th century, the Child [4] and Langmuir [5], edei- strated that in a passage of infinite plates, in which the anode can offer an unlimited number of positive ions or descent unlimited electron *without there is another body power* case by case, current, that can pass through the diode is given by the known *Law of "3/2"*. The Child and Langmuir, around the same period and thermionic emission by performing experiments in vacuum, showed that be- tween two parallel plates with a potential difference V, located at a distance x, the current density crossing the passage in the unit area, follow the relationship

$$J_{SCL} = \frac{\sqrt{2}}{9Fr}\sqrt{\frac{e}{esu}}\frac{V^{3\,2}}{m\;x^2}. \tag{2.54}$$

The above expression for *maximum current, limited by the space charge* (Space- charge limited current) on the flat path, formulated here *electrostatic mona- des1*. With eesu the electric charge is denoted in statcoulomb, while m It is the mass of particle. The following paragraphs will look at how we get the expression of the maximum current density for a given polarization and distance reinforcement (geometri- let) the diode when the cathode has arbitrarily large number of electrons on the record vacuum. We will also examine the expressions describing the current limitation on flat geometries with finite dimensions and a cylindrical passageway.

[1] The electrostatic unit equals 3.3356 · 10-10 Coulomb and 10 obtained by dividing the speed of light in vacuum, expressed in cm / s.

2.5.1. Planar Diode

To understand how the resulting relation (2.54), visas will Schumann cathode C with reference potential 0 and the rise in A charged potential *V*.

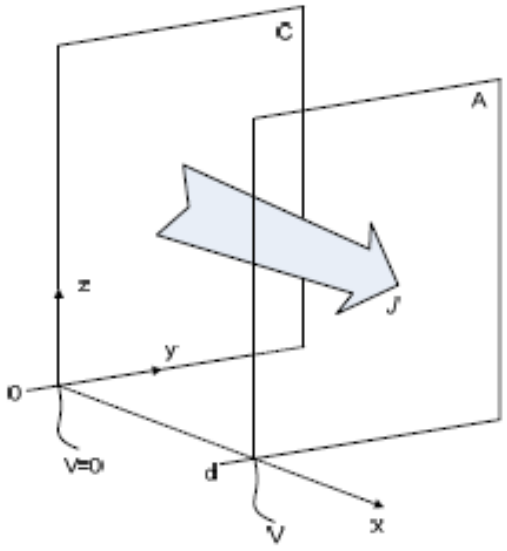

Fig. 2.5: The diode plates with infinite space charge.

Initially, and before any current flows in the passageway, the potential metavalle- Tai linearly between infinite slab, as the line PT of Fig. 2.6. If by some method, for example by heating or by irradiation, the cathode C initial CAM to emit electrons, they will be directed towards the anode, showing a current density *J* [A / m2]. The potential along the passage by increasing the flow rheumatism tion, will begin to change, as shown by the arrow in Fig. 6/2.

The speed of the electrons, even *u*It depends on the change in potential which have completed. Furthermore, the space charge *p* in a unit volume within the reinforcement equals *J / U*. If the potential at a distance from the cathode is *f (x)*Then the kiniti- RH energy of the electron is, with reference to the potential of the cathode,

$$\frac{1}{2}mU^2 = \frac{1}{2}mx^2 = eF(x), \qquad (2.55)$$

while the current density per unit area will be

$$J = \text{trailer} = p\,x\,. \qquad (2.56)$$

The Laplace equation for one-dimensional problem is

$$\nabla^2 F = \frac{\partial^2 F}{\partial x^2} = -\frac{p}{e_0}\,. \qquad (2.57)$$

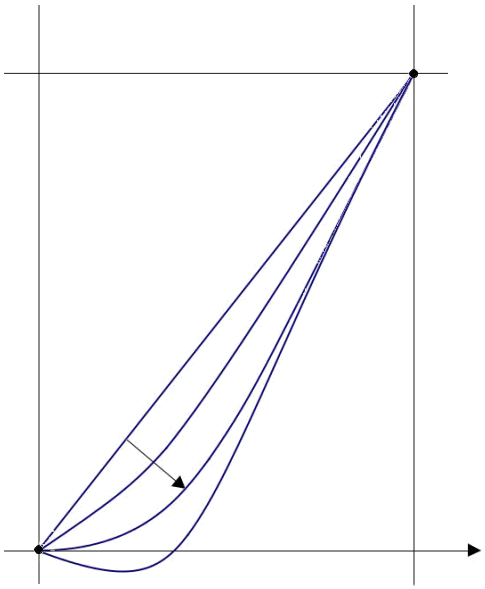

Fig. 2.6: Change in the potential path of infinite plates. The direction of arrow indicates the change in potential in the passage and increases the current (and thus the space charge) in that: (I) without power, (II) a small stream (III) current limited by space charge, (IV) potential barrier.

From equation (2.55), substituting $x = [2eF(x)/m]^{1/2}$ and by (2.56) we have the Laplace equation that:

$$\frac{\partial^2 F}{\partial x^2} = -\frac{J}{e_0 (2me)^{1/2}} \cdot \frac{1}{F^{1/2}} \qquad (2.58)$$

Multiplying the above relation $\partial F/\partial x$ we can complete by States and take

$$\frac{\partial F}{\partial x}^2 = \frac{4J}{e_0 (2me)^{1/2}} \cdot F^{1/2} + C. \qquad (2.59)$$

Considering the specific case of $\partial F/\partial x = 0$ at $x = 0$As well as that $F(0) = 0$, we get that C = 0. The visa did in $x = 0$ constitute essentially the assumption that the marginal situation because space charge in the diode field, the electrons leave the cathode with zero speed and enter the gap by accepting nil pediaki power. In this case, the diagram of potential in the passage has a horizontal tangent at point P. Any further increase in power and thus the space charge in the diode is impossible because it would create an allocation of resources, as shown by the dashed line IV in diagram of Fig. 2.6. This would mean that the electrons could no longer be decom- Thun from the cathode and move towards the anode, since the potential space forward

They will push the back surface of the metal. Continuing from the above production ratio, taking the square root of this, we get that

$$\frac{\partial F}{\partial x} = \frac{J^{1/2}}{e_0^{1/2}\left(2/m\,e\right)^{1/4}} \cdot F^{1/4} \quad , \tag{2.60}$$

while integrating and solving for the *J*We will take with $F(d) = V$ In that the potential in the flat passage varies as:

$$F(x) = V\frac{x^{3/4}}{d} \quad , \tag{2.61}$$

with *maximum current density* given by:

$$f_{JSCL} = \frac{4}{9} e_0 \frac{2e}{m}^{1/2} \frac{V^{3/2}}{d^2}. \tag{2.62}$$

The above relation is n*omos Child-Langmuir Flat diode*In SI units. For electrons, the above expression, we obtain that:

$$f_{JSCL} = 2.33 \cdot 10^{-6} \frac{V^{3/2}}{d^2} \quad [\text{A / m}], \tag{2.63}$$

with the *V* expressed in Volts and *d* in m. The relationship between the elementary electrostatic tion unit and the actual load of the electron is $eesu = 4IP_0 e\sqrt{}$ Towards $\sqrt{}$ comparison of relation (2.62) with (2.54).

The space charge of electrons existing in the space between the plates of the appointed period lowers the potential at any point in space, a limiting case in which the electric field at the cathode surface is zero. For example, a diode with thermionic cathode current does not increase beyond the limit prescribed by law Child-Langmuir, whether we raise the temperature of the cathode, wanting to force greater electron emission. To draw greater liquidity but the passage should either increase the potential of the anode or reduce the distance between the reinforcements. In terms of the commonly occurring sizes palmi- tions and relativistic microwave tubes, the Child-Langmuir Law on flat diode can be written as

$$JSCL = 2.33 \frac{V[MV]^{3/2}}{d[cm]^2} \quad [\text{KA / cm}], \tag{2.64}$$

and if, for simplicity, ignore the effects of the ends in a passage judicata finite area, we can write that

$$I_{SCL} \cong 2.33 \frac{A[cm^2] \cdot V[MV]^{3/2}}{d[cm]^2} \text{ [KA]}, \quad (2.65)$$

where to *A* denote the area of reinforcement of passage cm2. From these relationships can also be determined and *resistance* showing the passage, in conditions of maximum current, limited by the space charge [6]. This resistance is based on the above relationship for *ISCL*Is

$$Z_{SCL} \cong \frac{V}{I_{SCL}} = 429 \frac{d[cm]^2}{A[cm^2] \cdot V[MV]^{1/2}} \text{ [Z]}. \quad (2.66)$$

Note that, in a flat geometry diodes with finite size, relations (2.65) and (2.66) are approximate. Especially diodes *electronic field emission*Where, as we shall see, the electrons are released locally by microtip with great acidity, because of the intense electric field, it is difficult to precisely calculate the A surface in one, anyway, approximate estimate *ISCL*. For the case of relativistic electrons, namely V> 500kV, the relation (2.64) for the infinite passage can be written as follows: [7]

$$J_{SCL} = 2.71 \frac{1}{\frac{d[cm]^2}{1} + \frac{V[MV]^{1/2}}{0.511}} \cdot 10^{-8} \text{ [KA / cm}^2\text{]}. \quad (2.67)$$

We note that, while dependency on rising distance - descent *d*Is the same, the voltage dependence of the passage is somewhat different. In very large trends that in- pendence is J_{SCL} a V While at lower voltages approximates the classical law. The para-
Gontikas $J_{SCL} \cdot d^2$ the two cases varies as follows:

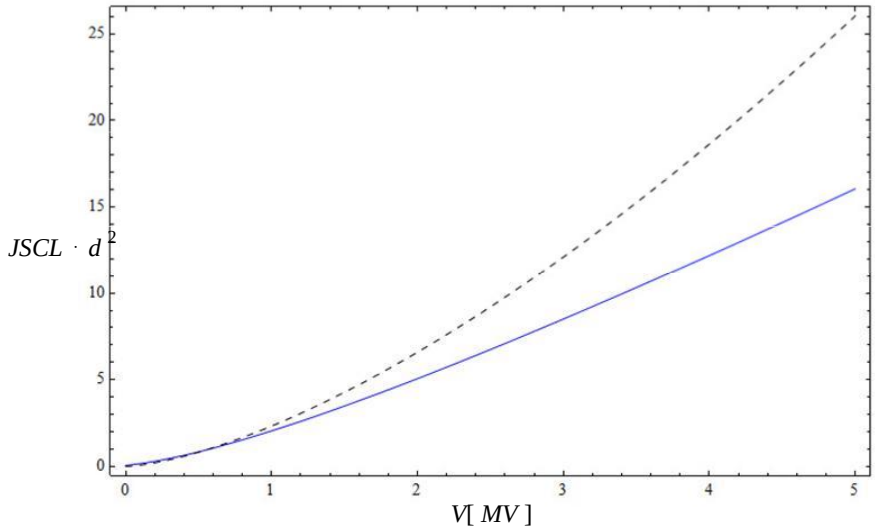

Fig. 2.7: Change agent $J_{SCL} \cdot d^2$ in diode infinite plates for classical and relativistic solution.

The above graph illustrates the fact that the non-relativistic Child- Langmuir law can be used with small error for voltages up to 1MV.

2.5.2. Flat Dimensional Finite Diode

Where the planar diode has infinite dimensions x and y, as is the case also in reality, the Child-Langmuir Law amended to incorporate the *increase* the maximum current density that production was maintained. Appearances limb enhance pediaki intensity and thus the maximum current density. Symbolizing *JSCL (1)* classical solution (2.62) and *JSCL (2)* the poly- importance for the passage to a finite one dimension of the cathode (cathode band-like cathode or circular form with finite radius) generally applies that *JSCL (2)* > *JSCL (1)*. Consider- ing diode with cathode form *Movie* width W and electrode spacing D, in the maximum current density observed is [8], [9]:

$$J\,SCL\,(\,2\,) \cong 1 + .3145\,\frac{D}{W}\,JSCL\,(1)\,, \tag{2.68}$$

whereas for *circular* cathode with a finite radius R and electrode spacing D, the maximum current density is observed [10]:

$$\text{f}J_{SCL}(2) \cong 1 \quad +.2647\frac{D}{R} \quad +0.0058\,\frac{D^2}{R}\,J_{SCL}(1). \tag{2.69}$$

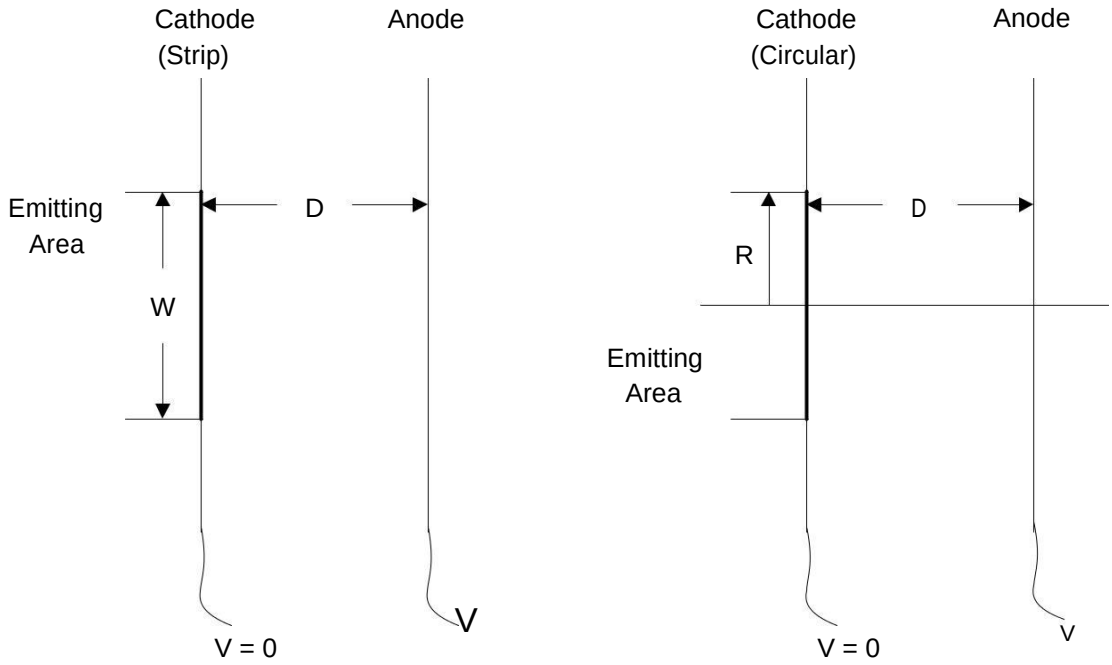

Fig. 2.8: Diode strip cathode finite width (left) and diode with a cyclical descent finite radius (right).

These equations can be adapted to expressions (2.64) and (2.67), for the simple and the relativistic solution respectively, and give a better estimate of the maximum current density, limited by the space charge flowing through the appointment of two or imiapeiri finite cathode.

2.5.3. Cylindrical Diode

The Child-Langmuir law may be extended accordingly and cylindrical geometry. If, for example, supposing that a conductor radius *rC* placed inside gov- lindrou radius *rA*Then the above investigation is made by solving the Laplace equation in cylindrical coordinates, namely

$$\frac{1}{r}\frac{\partial}{\partial r}\left(r\frac{\partial F}{\partial r}\right) = -\frac{p}{e_0} \quad . \tag{2.70}$$

Assume also that *unit long section* the thin cathode emitted power *I*Then the current density, the equivalent of (2.56) becomes,

$$I = 2\pi r\, r_{trailer} \quad . \tag{2.71}$$

Along with the energy conservation equation (2.55), which applies in this case, we can write that

$$r\frac{\partial^2 F}{\partial r^2} + \frac{\partial F}{\partial r} = \frac{I}{4\pi\varepsilon_0}\sqrt{\frac{2m}{eF}} \quad . \tag{2.72}$$

The above equation, boundary conditions $F(rC) = 0$, $F(rA) = V$ and $\partial F/\partial r = 0$ at $r = 0$May give the corresponding expression for cylindrical passage [5]. However, the above non-linear differential equation can not give a simple analytical solution for dynamic party. The Langmuir and Blodgett [11] approached the solution of (2.72) with the schesi1 (modified Meni here in units SI):

$$I = \frac{\text{Eight}}{9}\,\varepsilon_0\sqrt{\frac{2e}{m}}\,\frac{V^{3/2}}{b^2\,rA^2} \quad , \tag{2.73}$$

in which the rate *b* is basically the numerical solution of the relationship resulting from (2.72) if this replace the (2.73) and with the additional replacement $c = \text{Log}(rA/rC)$. The Langmuir and Blodgett exported the *b*as the solution of differential in- *xisosis*

---

[1] The work of Langmuir expression of the current for the cylindrical passage is given as $I = \frac{2\sqrt{2}}{9}\sqrt{\frac{e}{m}}\frac{V^{3/2}}{rb^2}$, expressed in electrostatic load units.

$$3b_2 \frac{\partial^2 b}{\partial c^2} + \left(\frac{\partial b}{\partial c}\right)^2 + 4b\frac{\partial b}{\partial c} + b^2 - 1 = 0 . \qquad (2.74)$$

The approach of the authors was through truncated numerical series, for which tables are given for finding the *b2*Depending on the price of *c* in [11]. Numerically solving the above differential equation shows the following dependence *b2* the ratio of radii *rA* and *rC*:

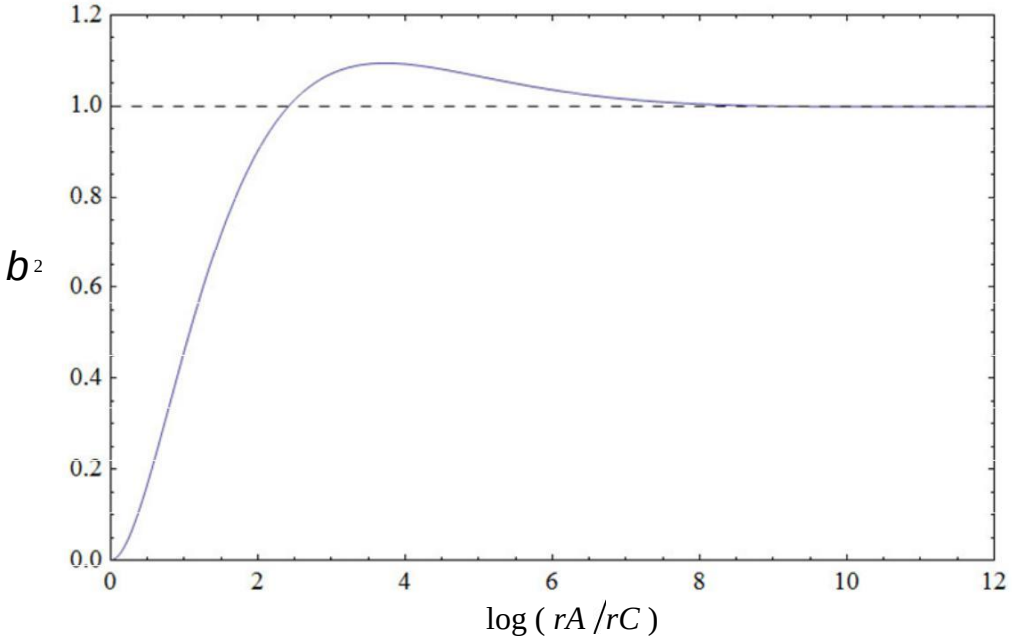

Fig. 2.9: The rate *b2* the relationship Langmuir-Blodgett for cylindrical passageway with *rC<rA*.

The solution, as is clear from (2.73) is exact for cylindrical passages in o what the descent is quite smaller radius from the anode (cathode - "wire"), while in case the size of the cathode approaching the rise The above is pos- making such an error. However, when the ratio of the radii up to about 1.7, the error is the limit of 5% [12].

In [12] there is an analysis of the law Langmuir-Blodgett for the cylindrical passageway and proposing expressions

$$J_{SCL} = \frac{4}{9}\varepsilon_0\sqrt{\frac{2e}{m}}\frac{V^{3/2}}{D^{1/2}r_C^{\beta/2}}\left(\frac{1}{\ln(rC/rA)}\right)^{3/2} \qquad \text{For rC> rA,} \qquad (2.75)$$

and

$$J_{SCL} = \frac{4}{9}\varepsilon_0\sqrt{\frac{2e}{m}}\frac{V^{3/2}}{D^{1/2}r_C^{\beta/2}}\left(\frac{1}{\ln(rA/rC)}\right)^{3/2} \qquad \text{For rC <rA,} \qquad (2.76)$$

current density when the difference $D = rA - rC$ They are relatively small. Relationships the cylindrical passage (2.75) and (2.76), as expressed here, below the coefficient 2p from the expression Langmuir-Blodgett, because the initial expressions refer to current from thin cathode unit length section.

In terms of the commonly occurring sizes and pulsed relativistic microwave ness lamps, rheumatic density *the cathode* is [6]

$$\text{f}JSCL = 2.33 \frac{V[MV]^{3/2}}{r_A[cm]\,r_C[cm]\,b^2}^2 \quad [\text{KA / cm}], \tag{2.77}$$

a good approximation for *b* to be

$$b = \frac{rC}{r_A}^{1/2} \sum_{n=1}^{\infty} Bn \left(\ln \frac{r_A}{r_C}\right)^{3/2}, \tag{2.78}$$

with B1 = 1, B2 = 0.1, B3 = 0.0167 B4 = 0.0024.

2.6. The View Virtual Cathode in tolls

Suppose that in a triode vacuum tube with infinite parallel electrodes, the Down Methods C produces electrons with thermionic emission. The electrons are accelerated toward the thin matrix G, which is maintained at a potential *VG,* and entering the space pleg- Matos - collector or "plate» (plate), P. P The collector also kept at zero pos- Namik. Moreover, we assume that all the electrons of the cathode are accelerated in the same manner and pass through the screen with the same speed and parallel paths. In the space CG, electronic transmission has capped rheumatic intensity stipulated by law
Child-Langmuir, (2.63),

$$JCG_{(sat)} = 2.33 \cdot 10^{-6} \frac{V_G^{3/2}}{z^2}^2 \quad [\text{A / m}]. \tag{2.79}$$

For low currents, the electrons approaching the armature P, or collected, or will be reflected, but in any case the space charge region in the GP generates a potential distribution such, *as if we had an equivalent emission from the armature P to the matrix G*. In other words, for any value of the injected current *JCG Asia Mi-*

located between curves I and III, as shown in Fig. 2.10. If, however, the current *J*, Entering the GP region exceeds the value *JGP (sat)*, Then it will create a situation where we do not have equivalent emission from the anode P to the grid G, under the present circumstances polarization and distance of reinforcement. The situation is not an equivalent emission from an electrode, located at a distance *F '= a0* called *virtual cathode*. It can be understood that, for the injection current in the region equal to GP *JGP (sat)*The virtual cathode of diode equivalent GF 'will be located at position *x = z*.

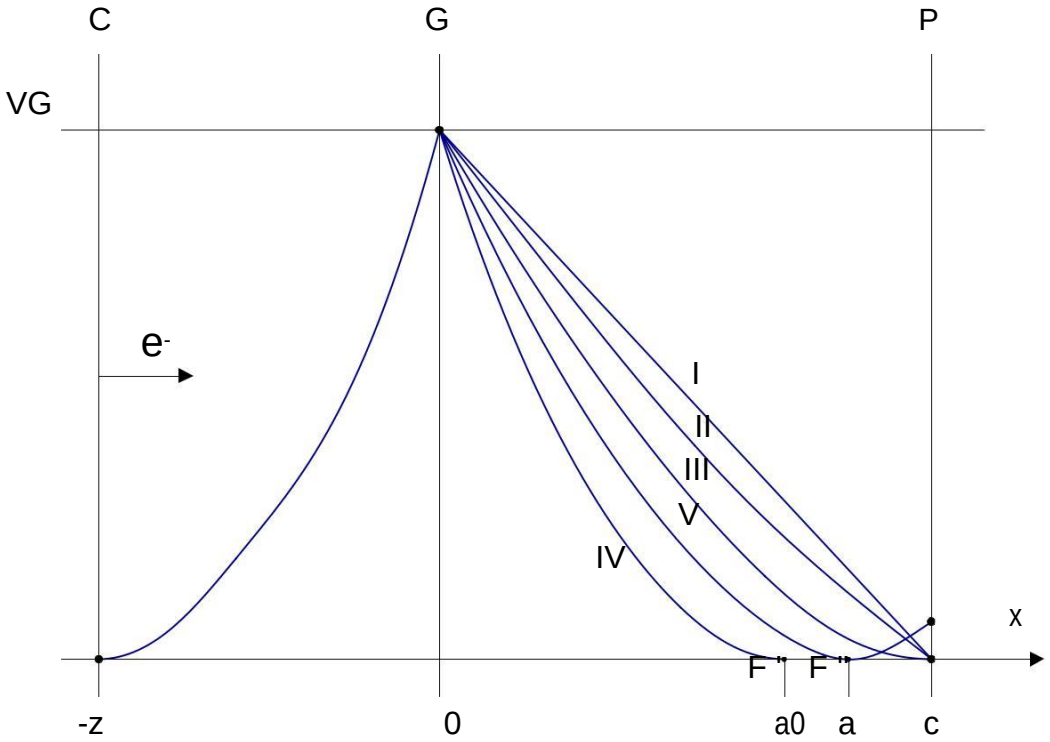

Fig. 2.10: Distribution of force in the region between grid G and reinforcement of alpha nodou P, for injected currents from area CG: (I) the absence of currents, (II) small liquidity automatically, (III) critical current region GP, (IV) formation of a virtual cathode, (V) virtual cathode reinforcement P slightly positive potential.

For the simple example of the three-way mentioned here, we find that in a threatened po problem with monoenergitika electrons, virtual cathode *F* ', Mathematics would constitute an absolute potential barrier from which the electrons could not cross and reach the reinforcement P. If, for continuation of this analysis, sub-put that P armature becomes slightly positive potential to tow portion of the electrons, the virtual cathode will move to P, the new location a. If shall be considered that the part of the incoming stream *J1*That the position of a virtual cathode is moved to P, is equal to *fJ1*Then the total effect spatial stream in the range 0-F '', is

$$J_{0F''} = (2 - f)J_1 = k\frac{V_G^{3/2}}{a^2}, \qquad (2.80)$$

while the region F '' - P spatial stream is

$$J_{F''P} = fJ_1 = k\frac{V_P^{3/2}}{(c-a)^2}, \qquad (2.81)$$

where to *k* We symbolize the constant 2.33 · 10-6 [AV-3/2]. The Tonks theory that inde-development in 1927 [13], makes the above approach to show that the three-way lamp, the import conical cathode causes negative resistance in the grid circuit G and collector P.

It follows from equations (2.80) and (2.81), by adding members, eliminated a and take it

$$cJ^{1/2} = \sqrt{k}\,\frac{VP^{3/4}}{f^{1/2}} + \sqrt{k}\,\frac{VG^{3/4}}{(2-f)^{1/2}} \quad . \tag{2.82}$$

In the above relationship, we can replace the quantity *J1* with an equivalent of from (2.80) if in this assumed that the rate of current negotiations pitches P is zero, ie *f = 0*. In this case the virtual cathode in accordance with the notation of Fig. 2.10, in place *a0*:

$$2J = k\,\frac{VG^{3/2}}{a_0^2} \Rightarrow J^{1/2} = \frac{\sqrt{k}}{\sqrt{2}}\,\frac{VG^{3/4}}{a_0} \quad . \tag{2.83}$$

Using the above expression for the current in the relation (2.82) and antikathisto-ing the normalized rates $v = VP / VG$ and $x = a_0 / c$, We receive following relationship:

$$v^{3/4} = \sqrt{p}\left(\frac{1}{\sqrt{2x}} - \frac{1}{\sqrt{2-f}}\right). \tag{2.84}$$

This expression can be represented parametrically for various values of regularity fied distance x wherein the dummy cathode may be formed. The conditioning were formed virtual cathode at zero initially tension the plate P will be a point that depends on the injected current *J1*. When a *VP = 0,* form the virtual cathode at a distance x Then the dependence of the current, which passes to the armature P (proportional *f*) Follows the tracks illustrated in Fig. 2.11.

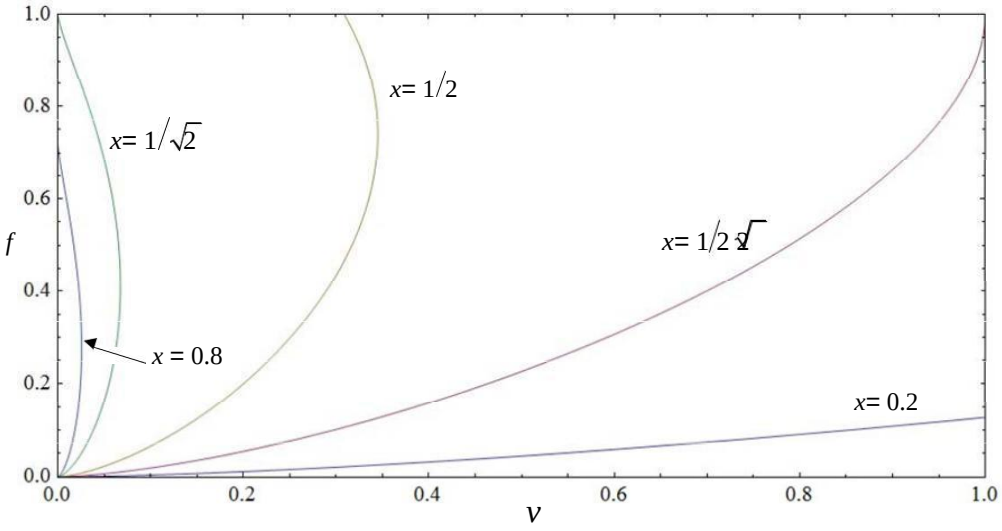

Fig. 2.11: Family curves relates the *v* with the *p*For various values of x .

We can distinguish the marginal case $x = 1/2\sqrt{2}$ Wherein a solution always have the *f*, With increasing v . The same is true for virtual cathode were formed conditioning distances less than $x = 1/2\sqrt{2}$. For values $1/2\sqrt{2} \leq x \leq 1/\sqrt{2}$, Are the curves v - f arriving to the Treaty $f = 1$ and continue onto the shaft for this in- xanomeno v , After passing through a section that presents data corresponding negative situation. Finally, values $1/\sqrt{2} \leq x \leq 1$, Curves v - f reaching the shaft f at a value, continue until they reach the point (v , f) = (0.1), then followed thoun axis $f = 1$ for growing v .

The analysis was made to show how, in a three-way, They may occur for some polarizations grid and plate, three current values, of which two are in positive resistance areas and one in the negative resistance region . It is also the simplest presentation of the Treaty that, *to be created been virtual cathode*, either diode flat plates, or in an inert space (Drift space - shorted diode flat plates), as we will examine later, should the injected current *exceed the marginal space charge current* characterizing this space. In the next section we will present *classical dimensional equations tions* to create a virtual cathode in an inert space injectable electronic de- term.

2.7. The Virtual Cathode in a short-circuit diode

The most commonly occurring cases virtual cathode display ness in microwave tubes, such as *virtual cathode oscillators*, Concerning those in which one electron beam enters an area without external electric re- project. Therefore, the shorted diode space charge is a simple al- Milled important system for the interpretation of the phenomenon lays virtual display output to inactive areas. The simplest analysis of this problem can be diexa- chthei, if we consider two infinite parallel thin grids, which are at a given distance apart and are maintained at the same potential. Grids these are essential for our analysis, two borders, which allow the free passage of electrons, but still maintaining the imposed Treaty of potential on their surface. This problem is, as we said, for the short passage and encircled referred to as the *classical* theory for displaying the virtual cathode in an inert space.

The problem, to which we refer, is illustrated in Fig. 2.12, where a space defined by borders two infinite conductive planes, which are kept in force *V0* and separated by a distance *d*. Rheumatic density distribution entering this place *J*[A / m2]. Conductive level (Fine mesh) not impede the passage of currents, Tosh. The classical theory is developed extensively by Birdsall and Bridges in [14]. The *oscillations* of *virtual cathode* Moreover, called many times and talanto- Birdsall-Bridges tions.

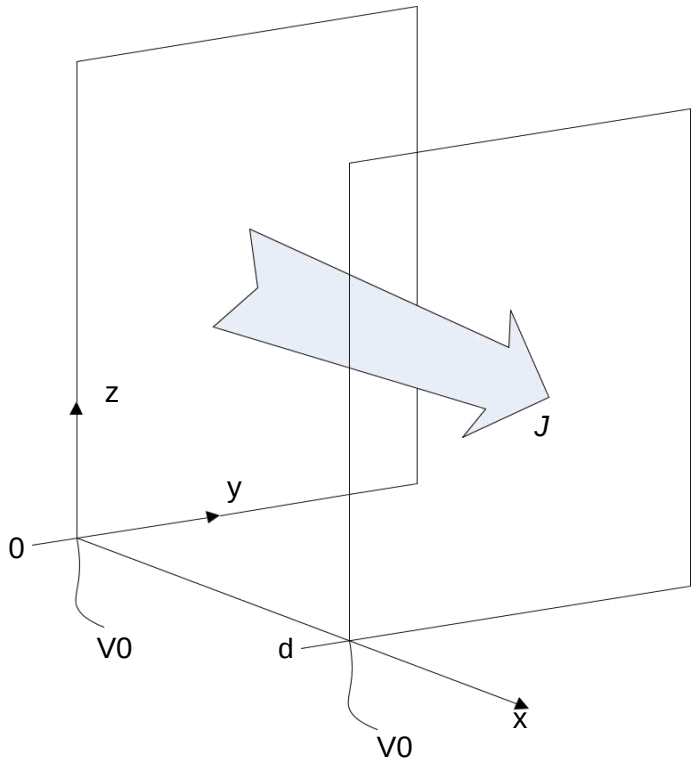

Fig. 2.12: The problem of shorted diode infinite plates.

For this visa we accept parallel, *nonintersecting* and *non anastrepsi- amid* orbits, while referring to non-relativistic speeds. This package is considered cold and absolutely monoenergitiki box, that all electrons enter with the same speed of *u*. Because of the small putative speed, the problem addressed electronic static, so we start writing the Laplace equation for the one-dimensional prob- lem:

$$\nabla^2 F = \frac{\partial^2 F}{\partial x^2} = \frac{d^2 V(x)}{dx^2} = -\frac{p(x)}{e_0} \quad . \tag{2.85}$$

With *p (x)* denote the spatial charge density, while *F* or *V (x)* We refer to the capacity of the passage. Conventionally, the injected current is

$$J = p(x)\, u(x) , \tag{2.86}$$

where *u (x)* It is the velocity of the particles. Speed (non-relativistic) is written as:

$$u^2(x) = 2\frac{e}{m} V(x) . \tag{2.87}$$

Solving for *V (x)*, We obtain

$$\frac{d^2V(x)}{dx^2} = \frac{J}{e_0\sqrt{2\frac{e}{m}V(x)}} . \qquad (2.88)$$

The above relation can be finished once transformed as

$$\frac{dV(x)}{dx}^2 = 4\frac{J}{e_0\sqrt{2\frac{e}{m}}}V^{1/2}(x) - V_m^{1/2} , \qquad (2.89)$$

the amount $Vm^{1/2}$ serving as role constant integration with the natural meaning of in- least potential in space. Where *Vm*> 0, the above is completed again and pre apparent parametric expression

$$\left(F^{1/2} - F_m^{1/2}\right)\left(F^{1/2} + 2F_m^{1/2}\right)^2 = a\sigma - \frac{1}{2}^2 , \qquad (2.90)$$

in which we replace *annealed* sizes $F = V/V_0$, $F_m = Vm/V_0$, $\sigma = x/d$. The fixed a clear

$$a = \frac{J}{4e_0\sqrt{\frac{2e}{3/2}V}} \frac{J}{} = 2.33\cdot10^{-6}\frac{}{V_{03/2}} , \qquad (2.91)$$

which is the injected rheumatoid density divided by rheumatoid density Child-Langmuir (2.62) of the passage by a distance equal to the reinforcements *d*Wherein the anode is at a potential *V0*. When the *a*= 1, effectively inject the shorted diode as current, as would support the biased diode Child-Langmuir with same Distillation importance electrodes and potential difference *V0*. The value of minimum force is from (2.90) as a function of the injected current a:

$$4F_m^{3/2} - 3F_m^{1/2} + \frac{a}{4} - 1 = 0 . \qquad (2.92)$$

H curve *fm* can be represented parametrically the above relationship, relative to a stream, displaying the behavior shown in Fig. 2.13.

H expression (2.92) has no solution *fm*> 0 *a*> 8, while the region «C-overlap», such designations was by Fay, Samuel and Shockley ([15]), will be shown to an unstable solution, concerning the appearance of the virtual cathode. Therefore, annealed currents with values of *a*= 0 so *a*= 8, the potential in the passage of little, which lies midway reinforcement and vary symmetrically about the center in- him. The change in potential in shorted diode for power from 0 to 8, is depicted in Fig. 2.14.

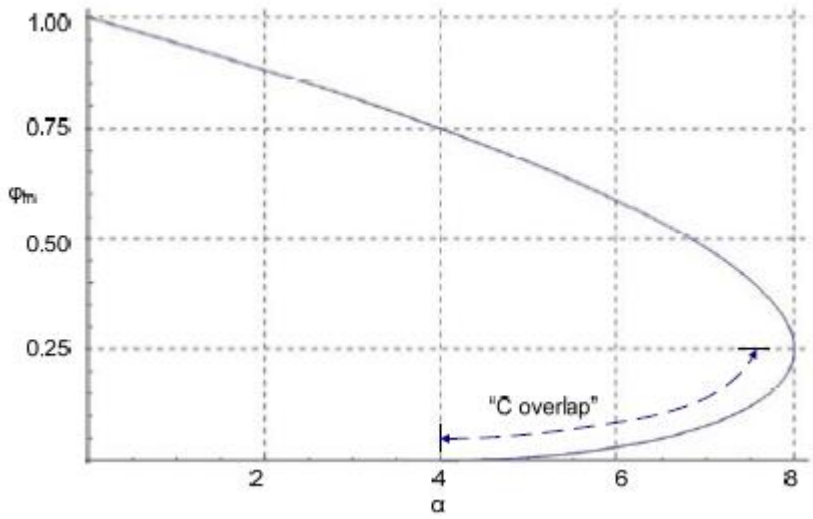

Fig. 2.13: The value of the reduced minimum potential function of reduced encheome- mind power to shorted diode.

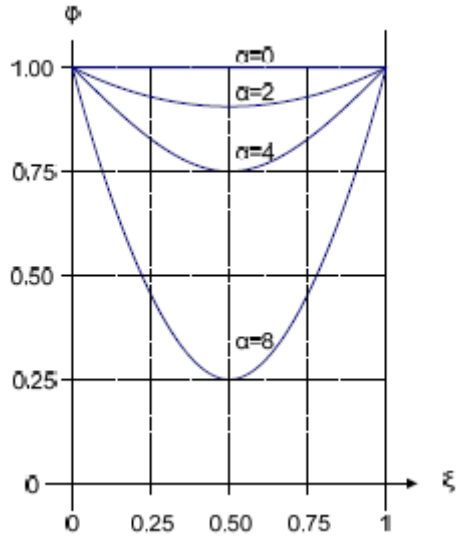

Fig. 2.14: Distribution of potential passageway for injected currents from 0-8 (anig- me sizes). Solutions fm> 0.

Since the value of the potential falls rapidly as a stream tends to 8, we can assume that *Vm* necessarily reset to a current value and causes load reflection and thus current, which was not considered in the analysis so far. This view essentially admits the appearance of the virtual cathode mathematical approach, since hitherto idealized natural approach does not allow a physical solution *Vm*= 0.

Considering that the potential in the shorted diode reset, there is a signifi- minus where the electrons stop moving. We will assume that a proportion of current, *f*, Propagates in the positive direction of *x* and a portion of the stream referred

klatai to the negative sense. Therefore, the right of point *xm*With *Vm*= 0, the fire-rheumatica is a density *f* · *a*And left this point, rheumatic density is the sum of the d-infused, *a*, And the reflected, *(1-f)* · *a*, Power. This situation leads to two regions I and II, with load densities

$$p_I(x) = \frac{J}{u(x)} + \frac{-(1-f)J}{-u(x)} = \frac{(2-f)J}{u(x)} \quad \text{For } 0 \le x \le xm \tag{2.93}$$

and

$$p_{II}(x) = \frac{f \cdot J}{u(x)} \quad \text{For } xm \le x \le d\,. \tag{2.94}$$

The velocity and therefore the energy of the particle is not dependent on the direction of movement, therefore by (2.85) (2.87), and the above expressions (2.93) and (2.94) that:

$$\frac{d^2 VI(x)}{dx^2} = \frac{(2-f)J}{e_0 \sqrt{\frac{2e}{m} VI(x)}}\,, \tag{2.95}$$

$$\frac{d^2 VII(x)}{dx^2} = \frac{f \cdot J}{e_0 \sqrt{\frac{2e\,VII(x)}{m}}}\,. \tag{2.96}$$

Completing the above expressions and posing *Vm*= 0, we obtain the same food- mo:

$$\frac{dV_I(x)_2}{dx} = \frac{4(2-f)J}{e_0 \sqrt{2\frac{e}{m}}} VI^{1/2}(x)\,, \tag{2.97}$$

$$\frac{dVII(x)^2}{dx} = \frac{4f \cdot J}{e_0 \sqrt{2\frac{e}{m}}} V_{II}^{1/2}(x). \tag{2.98}$$

Completing anew those relationships, with the Treaty *VI*=*VII*= 0 for *x*=*xm*, Lamvanou- me, converted variables:

$$F_I^{3/2} = (2-f)\,a\,(o - o_m)^2 \tag{2.99}$$

$$F_{II}^{3/2} = fa\,(o - o_m)^2\,. \tag{2,100}$$

The minimum position *xm=xm/d* calculated according to the percentage propagating power *f*from

$$o_m = \frac{f(2-f)^{1/2} - f}{(1-f)^2}, \quad (2.101)$$

while the relationship between the injected current *a* and fragment *f* They are

$$a = 2\frac{f(2-f)^{1/2} + 1}{f(2-f)}. \quad (2.102)$$

For very large values of *a*The percentage of current approaches propagated non not, while the total amount of the propagated current approaches the unit, that the power provided Child-Langmuir law on passage by distance *d* and difference possibility cial *V0*:

$$\lim_{a\to\infty} f_a = \lim_{f\to 0} 2\frac{f(2-f)^{1/2} + 1}{(2-f)} = 1, \quad (2,103)$$

$$\lim_{a\to\infty} o_m = \lim_{f\to 0} \frac{f(2-f)^{1/2} - f}{2(1-f)} = 0. \quad (2.104)$$

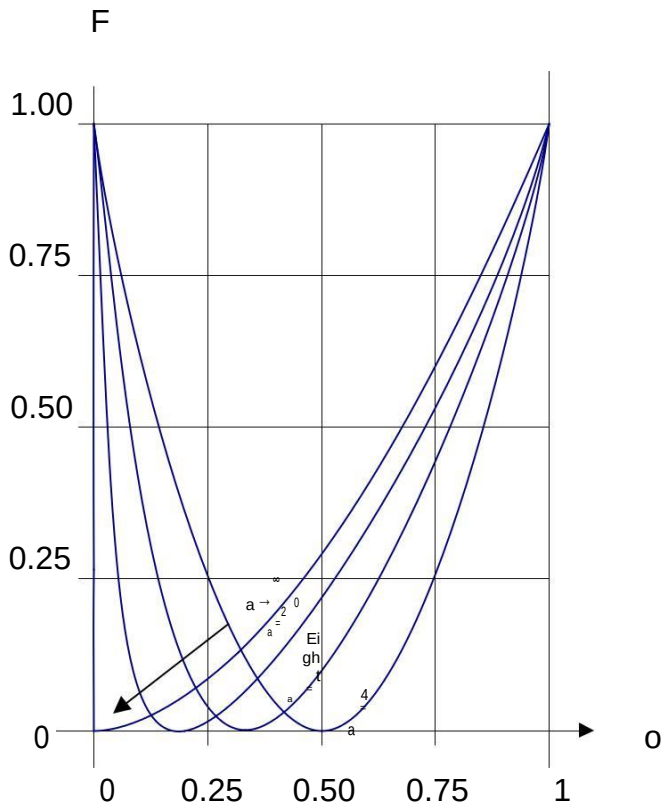

Fig. 2.15: Distribution of potential passageway for injected currents greater than 4 for solutions with virtual cathode (reduced size).

Therefore, where a very high density rheumatic introduced in shorted diode, virtual cathode formed in front of the input level, while the remaining space behave like diode Child-Langmuir, voltage diode V0. The solutions (2.99) and (2100) are depicted in the diagram of Fig. 2.15. The smallest current value allows solution with virtual cathode is about a= 4.

The previous analysis showed that, assuming virtual cathode, led to a set of solutions for 4≤a <∞, which overlaps the area "C-overlap" of poly- ing for dynamic *Vm* strictly greater than zero (non reflected power). These two solutions can be combined to cover all possible cases docu- cheomenon streams 0≤a <∞. The behavior can be described by a pseudo-time sequence of statements, as follows: As the current in the shorted diode increases from zero (item A, Fig. 2.16), passing through the point B, where a= 4, and can reach up to marginal price a= 8 (point C). The path A → B → C does not include, even, zero potential, but we are at the limit of the area where the *Vm* natural solution is greater than zero. Further growth a will lead to a potentially instantaneous transition of the system to the state D, which formed a virtual cathode in ¼ of the distance of the reinforcement, while the procedure vibrating current ($f \cdot a$) Is switched to a value slightly greater than 1. From point D with eiko- tronic cathode, further increase the current will push the system to the state E, with a smaller percentage propagated power and momentum of the virtual cathode even closer to the inlet electrode current . From the point D to reduce encheome- mind stream to the value $4 \cdot a$Will move to the point F, where the reflected power is marginally equal to 0, while the injected current is almost fully propagated to the output arms in position x=d. The points B and F are, however, different. Point B is a solution without virtual cathode, changing the dynamic as in Fig. 2.14, while the point F is solution with virtual cathode, by varying the potential such as in Fig. 2.15, always for prices a= 4.

Since this DC analysis, we find that the virtual cathode is re- lations, wherein the shorted diode switches by discontinuity. Furthermore, the two adjacent states B and F show another inherent instability of the system with virtual cathode. The states B and F have the same passing power but with different capacity allocation. These rules, already presented to the simple DC visa, showing the instability of the virtual cathode. Another useful sys- inference is that, to achieve conditions virtual cathode at shorted diode infinite slab, should the injected current is more than four times the equivalent, limited by the space charge current in that region. Using the Child-Langmuir law on the flat path or an earth paralla- this relationship for non-ideal geometries, we can arrive at some estimate of how much current is needed to display virtual cathode in a- SPAN space parallel plates absence external electrical field.

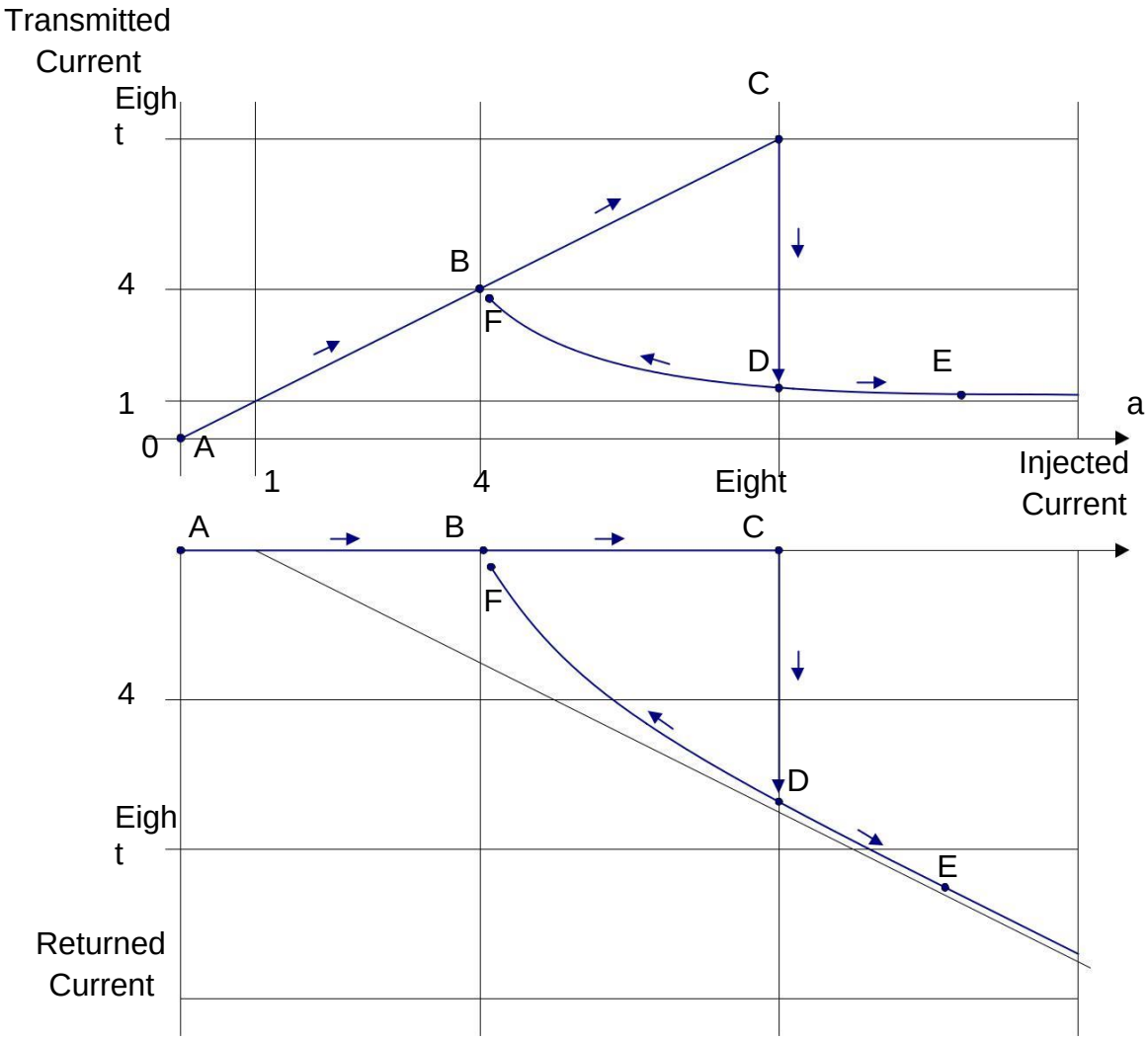

Fig. 2.16: Propagating and reflected power as a function of the injected stream a, including the transition from minimum potential in virtual cathode, when a = 8. For large values of a, the currents tend to the corresponding asymptotes.

2.8. Electron Beam with Spatial load

H most commonly occurring electron current distribution in the vacuum devices are η cylindrical electron beam. Produced using an Accelerating potential *V0* and enters idle space, which continues its course, absence of an external electric field with a kinetic energy that depends on the interactions of cor- matidion package. The electron beam is characterized in principle by its energy, which is practically equal to accelerate dynamic, expressed in eV. Key charac- teristics sizes of the beam also its diameter, rheumatic pyknoti- them and the total current.

H electron beam generated by a passage, which accelerates the electrons to a potential *V0*. Electrons can be produced by either a thermionic or a re- oxide emission and voltage correlation and the maximum current draw from the law Child- Langmuir, Eq. (2.63). For the passage that we can use any of the gen- nikefmenes expressions of the law, as the relativistic expression of the Law on. (2.67), the expression for finite dimensional diode on. (2.69), or the expression of the cylinder capacity

RH diode, (2.77), although the latter provision can not lead to production for the electronic "package". The Child-Langmuir law gives the maximum current density that can be derived from a cathode, which can provide arbitrarily large alpha algorithm electrons. Related, as we know, the voltage of the diode and the distance of the reinforcement, *d*In accordance with the expression

$$JSCL = 2.33 \cdot 10^{-6} \frac{V_{03/2}}{d^2} \left[A \cdot m^{-2}\right]. \qquad (2.105)$$

Based on this expression (although we could use the pre sengistiki Eq. (2.69)) we can say that an electron beam, generated by a circular area descending *prc2*Has *maximum* current

$$I_{SCL} \approx 2.33 \cdot 10^{-6} Fr. r_c^2 \frac{V_0^{3/2}}{d^2} [A]. \qquad (2,106)$$

From the above comparison, we can calculate the ratio of supply to the po- sotita *V3 / 2*, Resulting in the amount *P*:

$$fP = \frac{I_{SCL}}{V_0^{3/2}} \approx 2.33 \cdot 10^{-6} Fr. \frac{r_c^2}{d^2} \left[A \cdot V^{-3/2}\right]. \qquad (2.107)$$

The reason *P=I/V3 / 2* is the physical size characterized *perveance* package. D- The weight, which is standard in the field of vacuum tubes, probably derives from Pn but *pervade*, From the Latin *per-* (Cross-) and *vadere* (Spend). It is a natural analogue of the conductivity, which is evident from the line depending on the size of the passageway and the inverse dependence of the distance of the reinforcement. Without exact Greek translation, we propose using the term *dielefsimotita*, Meaning like in style with conductivity. The dielefsimotita one electron beam I / V3 / 2 can be quite different than the above threshold, which has been simplified left the Child-Langmuir Law for ideal flat passage. For a beam, which moves in an inert space, the dielefsimotita will equal the total current towards equivalent in- STEP in eV, at 3/2. Using the approximate Eq. (2.69), an electronically-derived circular beam cathode ray *rc*Which is the rise *d*Will have dielefsimotita

$$P = \frac{I_{SCL}}{V_{03}^{/2}} \approx 2.33 \cdot 10^{-6} \left[1 + .2647 \frac{d}{r_c} + 0.0058 \left(\frac{d}{r_c}\right)^2\right] \frac{r_{1.}^2}{r_{2c}^2} [A \cdot V\text{-}3/2]. \qquad (2,108)$$

The electron beam is repelling forces of the same of the space charge. The particles of a cylindrical beam will continue to move in parallel paths, unless rheumatic density is infinitely small. As the current carried by the electron beam is increased, the electrical forces cause progressive radial export of plosi. At very high speeds, the beam produces a magnetic field, which operates as a focusing power, reducing in this way the rate of expansion of

beam. Moreover, if the beam spread in space, which is a gas of low pressure background (density generally less than the spatial charge of the beam density), positive ions are produced, which contribute to a partial neutralization of the space of the cargo. The beam ionizes the atoms of the gas and pushes the walls of the releasable electrons, due to their low power. The positive ions, because of their large mass, are considered properties in the area. The production of positive ions decreased OF the effect of space charge by a factor of (1-*fe*). As we divided sitive to realize, with full neutralization of space charge, the electron beam is influenced by the magnetic field, resulting in the autofocus until point *Strangulation* (*pinching*), While no space charge neutralization, the beam will always *diverges* (*expanding*), A rate that depends on the energy and the spatial charge. When the beam is partially neutralize space charge of ions de- povathrou may occur either deviation or autofocus, depending on the prices received density *(1-fe) p0* and its energy, *c*. Analysis of electronic de- tions with space charge occurs extensively in [16]. Concepts such as peak beam current (limiting current), we will present below, grow as in the previous, and in [17].

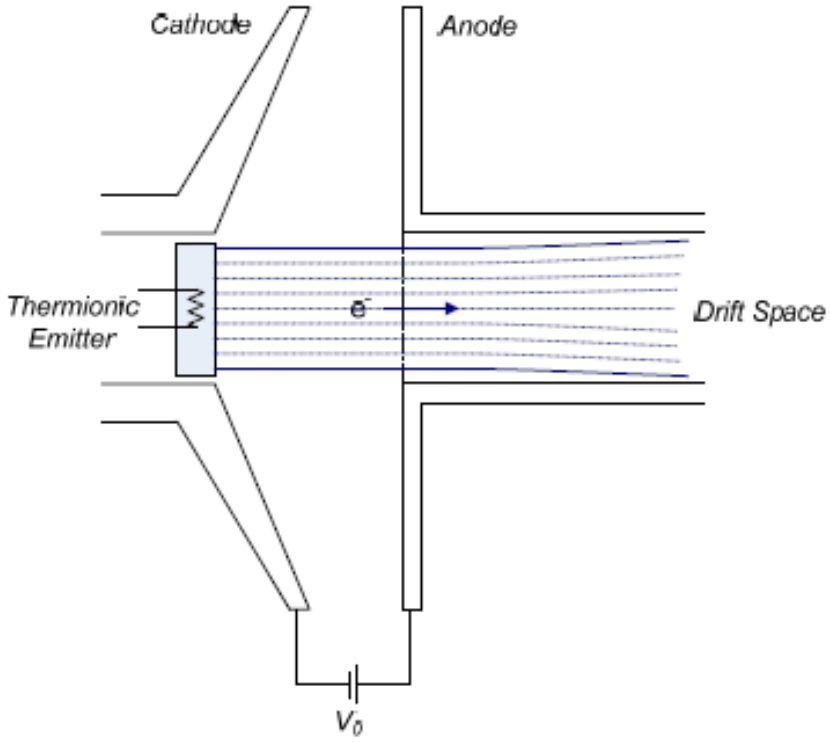

Fig. 2.17: Electronic beam produced by thermionic cathode type Pierce.

For the following analysis, we will make some assumptions. Firstly, the beam has a cylindrical beam section *a* and travels in a cylindrical beam tube *b*In non axis Mr. *z*. The change of the radius of the beam as a function of *z,* slow enough to ignore the longitudinal electric field *Ez* and the radial magnetic field *Br*. The a density of fire load beam and the spatial charge neutralization is fixed quantities within the limits of the beam and zero outside. The orbits of the particulate not intersect the beam is in stable condition, ie d / dt = 0 for all sizes.

2.8.1. Electronic Beam with space charge

To study the package we reason *fe*Resulting from real spatial deposits load distribution, with opposite sign and density *fer0*. The charge density of the beam is *ñ0*. If *fe*= 0, then we electron beam moving in absolute vacuum. The density current section is written, in a known ,:

$$J = \text{trailer} = \text{pelc}.$$

The relative power and current density of the package are:

$$J = \frac{Ia}{Fr.} .$$

The spatial beam load:

$$p_0 = \frac{I}{Fr.\ a\ u} = \frac{I}{Fr.\ a\ u_z} = \frac{I}{Fr.abc},$$

while the space charge beam neutralization:

$$p = p_0 (1 - fe) = Fr.\ aI^2 u (1 - fe) .$$

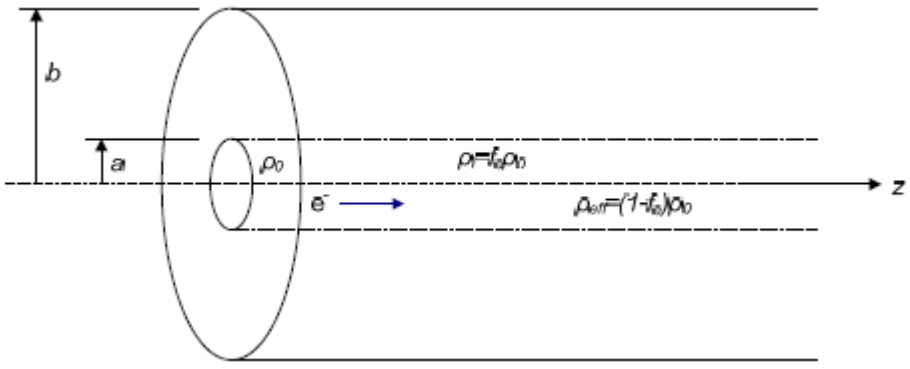

Fig. 2.18: Electronic beam a beam within the cylinder radius b, with a concentration of population fer0 background.

Applying the law of Gauss,

$$\int_0^e \mathbf{E} d\mathbf{S} = \int p dV , \qquad (2,113)$$

take to the axial electric field expression

$$E_r(r) = \begin{cases} \frac{p_0 (1 - f_e) r}{2\varepsilon_0} = \frac{I (1-f_e) r}{2\varepsilon_0 \pi a^2}, & r \le a \\ \frac{I(1 - f_e)}{2\varepsilon_0 \pi r}, & r > a \end{cases}. \quad (2,114)$$

Obviously, when f_e= 0, that is when we do not charge neutralization, holds:

$$E_r(r) = \begin{cases} \frac{p_0 r}{2\varepsilon_0} = \frac{Ir}{2\varepsilon_0 \pi a^2}, & r \le a \\ \frac{I}{2\varepsilon_0 \pi r}, & r > a \end{cases}. \quad (2,115)$$

From Ampere law,

$$\int_l \mathbf{B}\, dl = \mu_0 \int_S \mathbf{J} dS \quad (2,116)$$

calculate the azimuthal magnetic field, which shows:

$$B_i(r) = \begin{cases} \mu_0 \frac{Ir}{2\pi a^2}, & r \le a \\ \mu_0 \frac{I}{2\pi r}, & r > a \end{cases}. \quad (2,117)$$

The charge neutralizing considered *real estate* and therefore does not contribute to the magnetic re- slo. The potential in the case of this distribution is, completing the expressed importance of the electric field (2.114) ,:

$$F(r) = \begin{cases} V_s \left(1 + 2 \ln \frac{b}{a} - \frac{r^2}{a^2}\right), & r \le a \\ 2V_s \ln \frac{b}{r}, & a < r \le b \end{cases}. \quad (2.118)$$

In this regard, we have steadily

$$V_s = \frac{(1 - f_e) \rho_0 a^2}{4\varepsilon_0} = \frac{(1-f_e) I}{4\pi\beta_0 c} = \frac{30I}{\beta c} (1 - f_e), \quad (2.119)$$

which applies where the space charge neutralizing factor absent (f_e= 0). The maximum capacity in the axis of the beam is

$$V_{m,axis} = V_s \left(1 + 2 \ln \frac{b}{a}\right), \quad (2,120)$$

and the maximum electric field at the boundary of the beam is

$$E_a = \frac{V_s}{2} \quad \frac{60I}{a} \approx b_a \left(1 - f_e\right) . \tag{2,121}$$

Using the above expressions for the electric and magnetic field on. (2.114) and (2.117), the equation of motion (with B_z= 0)

$$\frac{d}{dt}\left(c\, m_r\right) = c\, m_r = e\left(E_r - z B_i\right) , \tag{2,122}$$

written as

$$c m_r = \frac{eI_r}{2\pi\varepsilon_0 a^2 b c}\left(1 - f_e - b^2\right). \tag{2.123}$$

For these expressions we consider that $z = u = bc$, $\varepsilon_0 \mu_0 = c^{-2}$ and that the magnetic field along the beam is negligible. Also

$$r = u_z \frac{d^2 r}{dz^2} = b^2 c^2 r'' , \tag{2,124}$$

therefore (2.123) becomes

$$r'' = \frac{eI_r\left(1 - f_e - b^2\right)}{2\pi\varepsilon_0 a^2 c\, mc^3 b^3} . \tag{2,125}$$

If we have no charge neutralization, using

$$1 - b^2 = c^{-2} , \tag{2,126}$$

the (2125) written

$$r'' = \frac{eI_r}{2\pi\varepsilon_0 a^2 c^3 mc^3 b^3} . \tag{2,127}$$

We define some characteristic quantities are widely used in sustain- vliografia for electronic packages. First we define the characteristic stream

$$I_0 = \frac{4\pi\varepsilon_0 mc^3}{e} \approx \frac{1}{30}\frac{mc^2}{e} , \tag{2.128}$$

with a value of about 17kA for electrons. Also define the parameter Budker, as

$$\text{f}vB = \frac{I}{I_0 b} \quad , \tag{2,129}$$

which for relativistic particles, equal to the ratio of the power of the beam to the feature stream *I0*. Finally, we define a generalized plasma frequency of De--term partly neutralized space charge,

$$\text{f}oh_p^{\,2} = \frac{e^2 n}{e_0 c^3 m}\left(1 - c^{\,2} fe\right), \tag{2,130}$$

with

$$1 - f_e - b^{\,2} = \left(1 - c^{\,2} fe\right)c^{-2}. \tag{2,131}$$

Beam current (2.111) is $I = p_0 Fr.\ a^{\,2}\, bc$ Hence the above relationship we can express as

$$oh_p^{\,2} = \frac{eI}{IP_0\, mcbc\, a^{3/2}}\left(1 - c^{\,2} fe\right). \tag{2.132}$$

Using the definition of the plasma frequency, the (2123) written

$$r = \frac{oh_n^{\,2}}{2}\ r. \tag{2,133}$$

The above relationship is important because it basically expresses the possible behaviors of the beam. If the generalized plasma frequency defined above is the- tion, ie when

$$f_e < \frac{1}{c^2} \quad , \tag{2.134}$$

the electron beam is *deviant* (Expanding). When the plasma frequency is negative, ie when

$$f_e > \frac{1}{c^2} \quad , \tag{2.135}$$

the electron beam is *convergent* and led ultimately to *strangulation* (*pinching*) From the same magnetic field. Finally, when applicable

$$\text{f}f_e = \frac{1}{c^2}, \tag{2,136}$$

the beam does not converge or diverge, and this expression is known as treaty in- toestiasis Budker (Budker self-focusing condition).

From the equations (2.130) and (2.132), we see that the plasma frequency depends directly proportional from the charge density and therefore inversely proportional to the cross section of the beam. Accordingly, the general equation *profile* beam, (2133), can not be completed unless we know the change of *op* the distance *z* and chro- only. Furthermore it is useful to eliminate the time and bring the distance *z*As an independent variable calculation of beam orbits. To solve the equation of the beam profile, we introduce a variable which will call general's qualifications dielefsimotita (generalized perveance), and is given by

$$\mathrm{f}K = \frac{I}{I_0} \frac{2}{b^3 c^3} \left(1 - c^2 fe\right). \qquad (2,137)$$

Generalized dielefsimotita not dependent on the radius of the beam as the plasma frequency. Using this definition, and the equation for the profile of the beam (2125), the trajectories described by the

$$r'' = \frac{K}{a^2} r. \qquad (2.138)$$

This equation can be applied to any particle within the de--term, with track radius $r \le a$. Given the assumption of non-intersecting trajectories, each particle performs motion, with scale factor r/a. In other words, the particles in the limits of the beam will always constitute the external borders, as it goes to the positive *z*. Considering the envelope of the package, we can put $r=a=rm$, Opo- then the previous equation is written as

$$rm\, rm'' = K. \qquad (2,139)$$

We note that *K* It is positive when we have divergent beam ($fe < 1/c^2$) and negative nity when we convergent beam ($fe > 1/c^2$). For divergent beam with zero in- *xoudeterosi, The envelope of the package described, replacing the (2139) the*
(2.137) with *fe*= 0, from equation ([18])

$$r\, r_{mm}'' = \frac{I}{I_0} \frac{2}{b^3 c^3}. \qquad (2,140)$$

To complete the expression (2.139) and describe the behavior of the envelope of the package, we believe that it enters the idle space with an initial radius *rm=r0* and *slope rm '=r0 '*In *z*= 0. To facilitate algebraic transformation tions, we define the variables adiastastes

$$R = \frac{r}{r_0^m}, \tag{2,141}$$

$$Z = \pm\sqrt{2K}\,\frac{z}{r_0} = \sqrt{2|K|}\,\frac{z}{r_0}, \tag{2,142}$$

$$R' = \frac{dR}{dZ} = \frac{1}{\sqrt{2|K|}}\,\frac{rm}{r_0'}, \tag{2,143}$$

wherein, where the positive sign is shown in *K* concerns divergent beam while the negative terms convergent beam. Writing (2139) as

$$\frac{d^2R}{dZ^2} = R'' = \pm\frac{1}{2R} \tag{2,144}$$

or

$$2R'\,dR' = \pm\frac{dR}{R}, \tag{2.145}$$

we can complete with $R=R0=1$ and $R'=R0'$ at $z=0$ and we have that

$$(R')^2 - (R_0')^2 = \pm\ln R \tag{2.146}$$

or, equivalently, that

$$R = \exp\pm\left(R'\right)^2 - (R_0')^2. \tag{2.147}$$

Integrating (2.146) will give

$$Z = \int_1^R \frac{1}{R'}\,dR = \int_1^R \frac{1}{\sqrt{(R_0')^2 \pm \ln R}}\,dR. \tag{2,148}$$

By changing the independent variable, now considering *R* 'From the (2147) have

$$dR = 2R'\exp\pm(R')^2 - (R_0')^2\,dR', \tag{2.149}$$

so the (2148) written as

$$Z = 2\exp\mp\left(R_0'\right)^2 \int_{R_0'}^{\sqrt{(R_0')^2 \pm \ln R}} \exp\pm\left(R'\right)^2 dR' \tag{2,150}$$

or, equivalently, as

$$\frac{z}{r_0} = \sqrt{\frac{2}{|K|}} \exp\left(\mp (R_0')^2\right) \int_{R_0'}^{\sqrt{(R_0')^2 \pm \ln R}} \exp\left(\pm (R')^2\right) dR' . \qquad (2.151)$$

The above expression gives the beam profile (radius *R*) Parameter as a function of the distance *z*. The parameters of this expression is the slope at the point of de--term (*R0* ') And generalized dielefsimotita *K*. The integral in expression (2.151) is of the form integral Dawson ([19], [20]). The above expression can be generalized imaging lished at distance axes *Z* and normalized radius *R*For different input slopes, beyond the parallel import (*R0* '= 0). Note that the analytical importance that admit little generalized dielefsimotita (|*K*| <1)

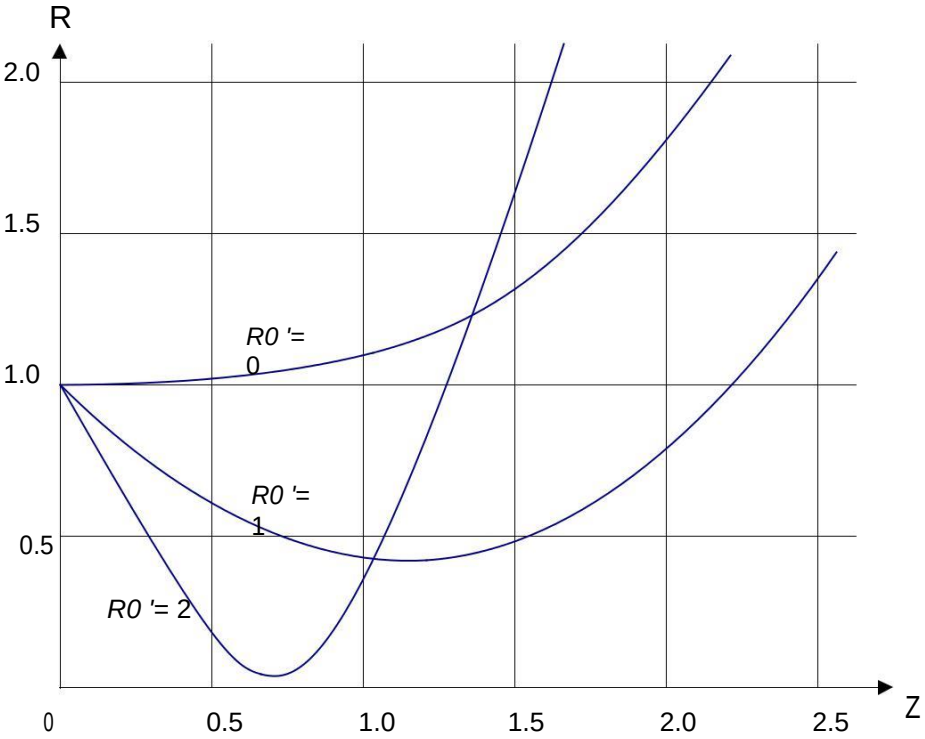

Fig. 2.19: Profile divergent electron beam, for three importing slopes.

When we load neutralization rate for which it is valid $fe > 1/c^2$, then we convergent beam (*K*<0), which *strangled* approximately

$$z \approx 0.8 \sqrt{\frac{2}{|K|}}\, r_0 . \qquad (2,152)$$

The mute point of the beam is many times spot with virtual cathode conditions, from which a portion of the electron beam can be scattered in the opposite direction to the negative *z*.

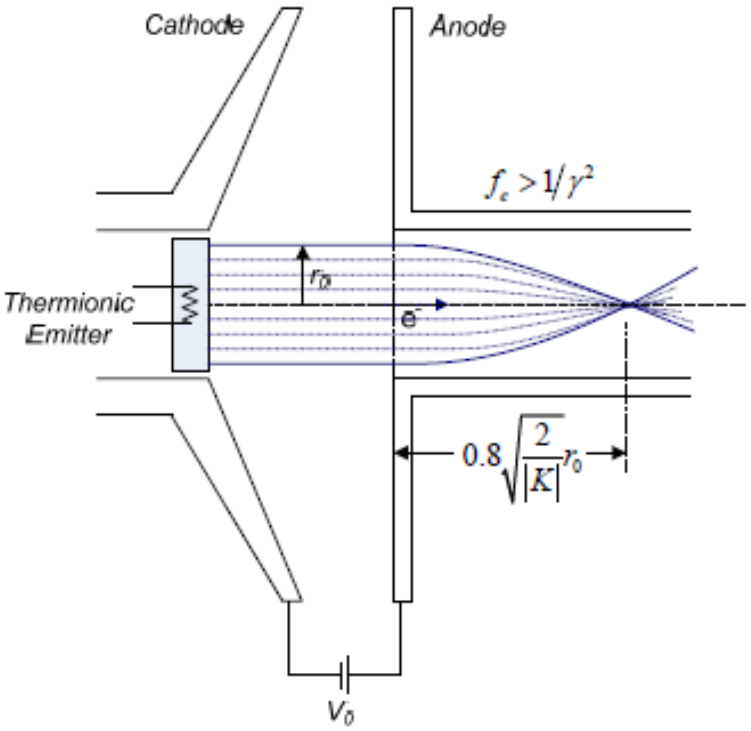

Fig. 2.20: Convergent beam collapses at a distance z and can be created CAM virtual cathode conditions.

2.8.2. Bundle with Complete Neutralization (Current Alfvén)

Suppose a beam propagates in space with full charge neutralization, re- Ladi force *fe* = 1. In this case it holds that

$$1- f_e - b^2 = \left(1- c^2 fe\right)c^{-2}, \qquad (2.153)$$

Therefore, by *fe* = 1, we obtain that

$$-b^2 c^2 = \left(1-c^2\right) . \qquad (2,154)$$

The dielefsimotita *K*From equation (2.137), is, using the above

$$K= - \frac{I}{I_0}\frac{2}{bc} . \qquad (2,155)$$

Therefore, the parameter Budker, (2.129), is related to the above expression of K in accordance with the

$$K= - \frac{2vB}{c} = - \frac{I}{I_0}\frac{2}{bc} . \qquad (2.156)$$

The Alfvén in [21] showed that the magnetic field of the beam is so strong that practically stops its propagation when we consider that

$$\frac{vB}{c} \rightarrow 1, \tag{2,157}$$

ie when the condition applies

$$\mathrm{f}I_A = I_0\, bc\ , \tag{2.158}$$

also called magnetic threshold current (magnetic current limit) or current Alfvén. In that regard, the particles become so strong radial component that stops practically any load propagation of the beam towards the positive *z*. The Treaty (2158) translates into practical units as $IA \approx 17bc$ [KA] for electrons.

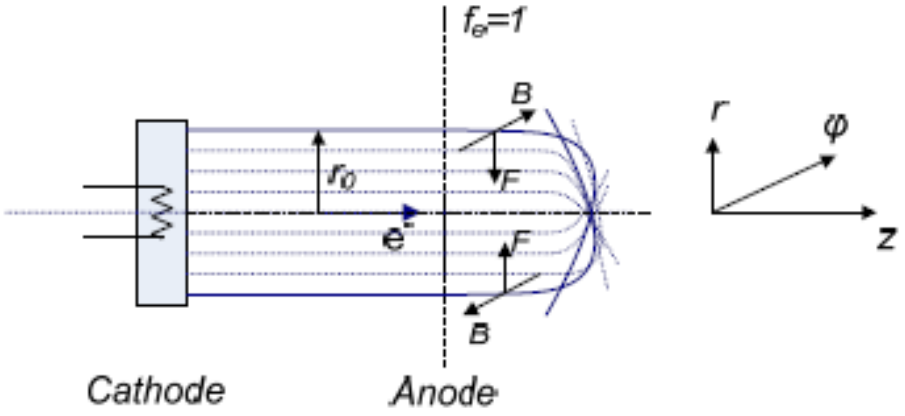

Fig. 2.21: Convergent beam to limit Alfvén.

2.8.3. Beam Infinite Magnetic Field

To solve the problem of virtual cathode display, a package which is not permitted to change its shape due to internal traction repulsive forces, we consider the following provision: we assume that the body is cylindrical, with a radius *a,* and moves within a very strong parallel magnetic field in radius cylinder *b* (See. Fig. 2.22). The electronic beam, space charge is intense, not described entirely by energy *eV0*But its potential, and therefore the kinetic energy, is a function of radial position. In other words, the energy of the beam having a dependency QUESTION by potential *f (r)* and is described by a relativistic factor of the form

$$c(r) = 1 + \frac{eF(r)}{mc^2}\ . \tag{2,159}$$

The beam has a load concentration, which is a function of the radial compo- nent, *n (r)*And we can write for this Poisson equation in cylindrical sys- tem, ie

$$\nabla^2 F = \frac{1}{r}\frac{d}{dr}\left(r\frac{dF}{dr}\right) = \frac{en(r)}{e_0} \quad . \tag{2,160}$$

In the above relationship, the charge density has been replaced by the product of the concentration operators, *n*, On the elementary charge, *e*. With a completion we receive akti-sulfonic electric field,

$$Er = -\frac{dF}{dr} = \frac{e}{e_0 r}\int_r^r n(r)\, rdr \quad . \tag{2,161}$$

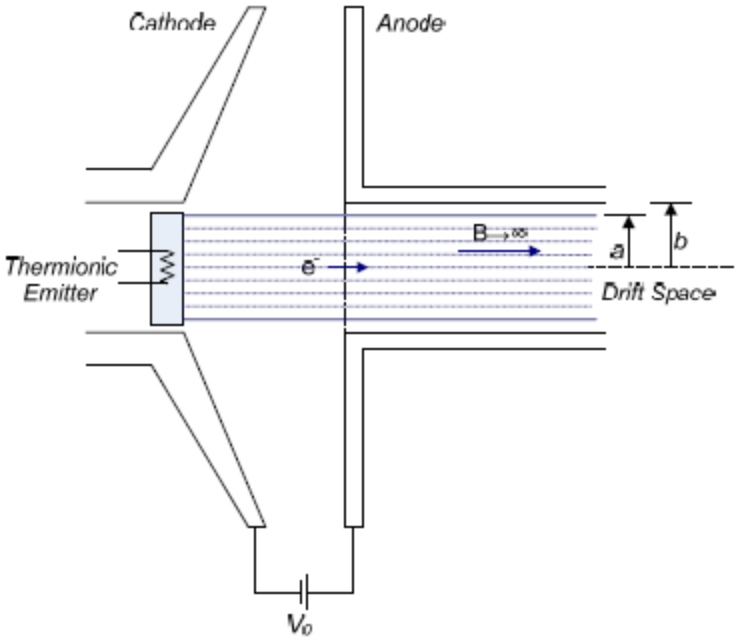

Fig. 2.22: Electronic beam forced in straight trajectories by imposing very strong magnetic field.

Rheumatoid density

$$J(r) = p(r)\,u(r) = en(r)\,b(r)\,c \quad . \tag{2,162}$$

In accordance with the principle of conservation of energy, the second is related to the potential of the package as

$$b(r) = \sqrt{1-\frac{1}{c(r)}^2} = \frac{\sqrt{2mc^2\,eF(r) + eF(r)^2}}{mc^2 + eF(r)} \quad . \tag{2,163}$$

The total beam current is

$$I = 2Fr.\int_0^a J(r)\,rdr = 2Fr.\,ec\int_0^a n(r)\,b(r)\,rdr\,. \qquad (2.164)$$

The equation Poisson (2.160), the equation of rheumatic density (2.162) and the relative differences maintenance of energy (2163) are three relationships between the four variables *f (r)*, *n (r)*, *J (r)* and *b (r)*. By selecting one of them as stable, for example liquidity but, we can write that *I=pa2J*, So from (2,162):

$$n(r) = \frac{I}{ecFr.\,a^2 b(r)}\,. \qquad (2,165)$$

From (2.160) to (2.163) and (2.165) gives the differential equation

$$\frac{1}{r}\frac{d}{dr}\left(r\frac{dF}{dr}\right) = \frac{I}{e_0 cFr.\,a^2}\frac{mc^2 + eF(r)}{\sqrt{2mc^2\,eF(r) + eF(r)}}\,, \qquad (2,166)$$

which identifies the potential, assuming uniform density rheumatic Community. If, instead of the potential use the relativistic factor *c (r)*The above- ther equation can be transformed as

$$\frac{1}{r}\frac{d}{dr}\left(r\frac{dc}{dr}\right) = \frac{eI}{e_0 mc^3 Fr.\,a^2}\left(1 - \frac{1}{2}\right)^{-1/2}\,. \qquad (2,167)$$

These representations are integrated numerically. In non-relativistic region, wherein *bc*= (*2ef*/*m*) 1/2, equation (2,166) written

$$\frac{1}{r}\frac{d}{dr}\left(r\frac{dF}{dr}\right) = \frac{I}{e_0 cFr.\,a^2\left(2e\,mc^2\right)^{1/2}}F^{-1/2}\,. \qquad (2,168)$$

For simplicity we assume that the electron beam satisfies the inert space, so that the beam is *r=a=b*. With this assumption we omit the term 1 + 2ln (*b*/*a*), Which appears when *a<b* (See. Eq. (2.118)). Assuming that f = 0 in the center of the package, we conclude that the above equation has the solution

$$F(r) = \frac{9I}{16IP_0 c\sqrt{2e/mc}}\,\frac{r^{4/3}}{a^2}\,. \qquad (2,169)$$

Assuming that the outer sheath of the beam energy is *f (a)=F*, Calculate the dielefsimotita package as

when we talk about electrons. This visa gives the value of that power, for which we have marginal virtual cathode formation in the center of the electron beam. The Olson and Poukey ([22]) came to the general relativistic type

$$\text{f}I_L \approx I_0 \frac{b(c-1)}{1+2\ln(b/a)}, \qquad (2{,}171)$$

which expresses the maximum current beam infinite magnetic field, with the energy of electrons in the beam center marginally zeroed. However, the general analytical RH solution (2.168) indicates that the maximum current passage occurs when the possibility cial to the axis of the beam is not zero, but slightly greater, approximately 0.174*F*. The dielefsimotita beam (when *r*=*a*=*b* and *f (0)*= 0.174*F*.) Are relatively larger and has the honor

$$km \approx 32.4 \cdot 10^{-6} \text{ [A} \cdot \text{V-3/2]}. \qquad (2{,}172)$$

According to Bogdankevich and Rukhadze ([23]), the maximum value of the current computerized package calculated from (2.167) as

$$\text{f}I_L \approx I_0 \frac{(c^{2/3}-1)^{3/2}}{1+2\ln(b/a)}, \qquad (2{,}173)$$

while the Nation and Read ([24]) suggest the expression

$$\text{f}IL \approx 8.5 \frac{(c^{2/3}-1)^{3/2}}{\ln(b/a)} \text{ [KA]}, \qquad (2.174)$$

for aggregations that do not occupy the entire transit area. In case *a*=*b*, in strongly relativistic region, expression of Bogdankevich and Rukhadze approximation gizei magnetic threshold current Alfvén, $I_A = I_0 bc/$. Recall that the characteristic quantity *I0* set to $4IP_0\ mc\ 3\ /e$, with price about 17kA for electrons. The three representatives marginal beam current phrases shown in Fig. 2.23 on ratio b / a = 1.5.

For the general case of "hollow" electron beam with an inner radius *rmin* and outer radius *rmax*Within a cylinder of radius *b*The denominator of the equation for the maximum current can be replaced by the quantity ([17])

$$1-f(e)+2\ln(b/r_{\max}), \qquad (2{,}175)$$

where

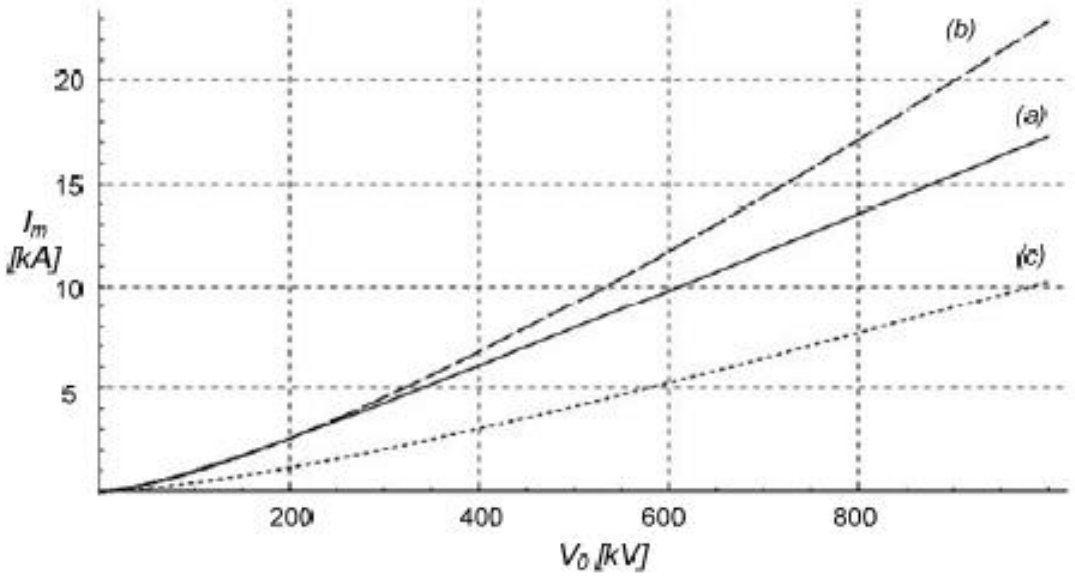

Fig. 2.23: Maximum current electron beam within infinite magnetic field without charge neutralization. (A) Olson and Poukey, 1974. (b) Bogdankevich and Rukhadze, 1971. (C) Nation and Read, 1973. Ratio b / a = 1.5.

$$f(e) = \frac{(1-e)}{1-e^2}\left|\frac{\ln(1-e)}{e}\right| , \qquad (2,176)$$

with *e*=*rmax*- (*rmin*/*rmax*).

How powerful should be the "infinity" magnetic field in the above visa re- riorismenis electron beam? In order to maintain a relatively constant cross-section of the beam, the required magnetic field should be at least [6]

$$B_{"Inf"} \sim \frac{0.34}{r_b}\sqrt{\frac{Ib}{8.5bc}} \quad [T] \qquad (2,177)$$

with beam current, *Ib*Be expressed in kA, while the radius of the beam, *rb*In cm. A set 1kA, radius 1cm, energy 500keV, would require a magnetic field around 100mT to remain concentrated. The required magnetic field afxa- focus Neta important as reducing the kinetic energy of the beam.

2.9. Electronic Transmission Mechanisms

By electronic transmission referring to those electrons acquire sufficient energy to be released from a metal surface and escape, theoretically, to infinity. A metal body can be modeled as a well pos- Namik, with electrons having an energy distribution given by the distribution
Fermi-Dirac:

$$f(W)\,dW = \frac{\text{Eight}\,\underline{Fr.}_3\,m_2^{\frac{3}{2}}\,W^{\frac{1}{2}}\,dW}{2\,h^2\left(\exp\frac{W-E_f}{kT}+1\right)}\,. \qquad (2,178)$$

At a temperature of absolute zero, electrons in the body of metal katalamva- mind energy levels up to the level of Fermi, energy

$$E_f = \frac{h^2}{\text{Eigh}\;2me\;\text{t}Fr.}\left(3n\right)^{\frac{2}{3}} \qquad (2,179)$$

The energy difference from the Fermi level to the top of the well potential, re- composed and *work* or *output energy* (Work function), *Ew*.

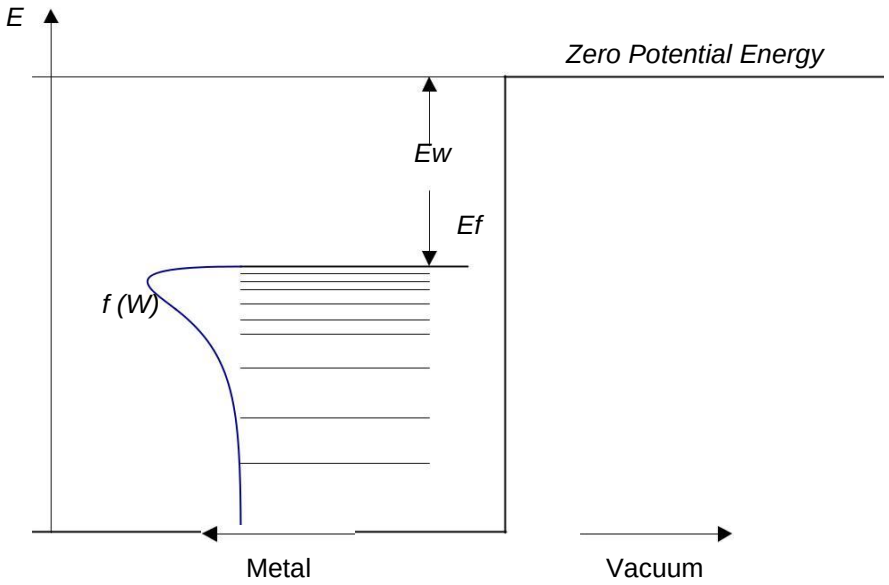

Fig. 2.24: The energy levels of the metal and the vacuum at a temperature of absolute non-isopropylidene. To remove an electron from the metal and to escape to space, should be offered energy at least equal to *Ew*.

Depending on how is the release of electrons from the me- metals body, we can categorize the electronic transmission in *thermionic*
(Thermionic), *FEDs* or *cold* (*field* or *cold emission*) *thermionic assisted by field* or *Schottky* (Field assisted thermionic or T-F) and *photoelectric* (Photo-electric). Elec- tronic transmission can also be caused by bombarding the metal with electronic, atoms or ions, so we are dealing with cases *secondary* electronically transmit and electronic Auger type show. The most important forms of elec- tronic emission is thermionic emission, field emission and emission of T-F, which we will examine below. In the case of photoelectric emission, the pre spipton photon must have an energy higher than the energy *Ew*. Under these circumstances there is a finite probability that the photon to transfer energy into

an electron Fermi level or lower, resulting in the push out of the area of the metal. Accordingly, incident particles can cause secondary electronic emission, but the kinetic energy must be arke- large, of the order of keV. The incidence of ionized atoms or atoms in excited states with excitation energy greater of *Ew,* can lead to apodie- their erection, while release of a photon having energy sufficient to push another electron out of the area of the metal. This phenomenon is the electronic type RH Auger emission.

2.9.1. Thermionic emission

Raising the temperature of the metal, the electrons in the metal occupy levels higher than the Fermi level and increases the number of electrons that can acquire kinetic energy greater than the energy output. The phenomenon studied by Richardson and Dushman early last century. The Richardson 1901 [25] observed that the current from a heated filament increases in a nonlinear manner as a function of temperature and 1911 resulted in the relationship, the o- what later reviewed by Dushman [26] and is the law *Richardson-Dushman* for thermionic emission:

$$fJ_T = AT^2 \exp - \frac{E_w \cdot}{kT} \qquad (2,180)$$

In the above expression, A is the constant of thermionic emission and equals

$$A = \frac{4Fr.\, eme_2}{\frac{k}{h^3}} \cong 1.2 \cdot 106\, A \cdot m^{-2} \cdot K^{-2} \quad , \qquad (2.181)$$

while *T* denotes the absolute temperature and *k* the constant Boltzmann, which in appropriate units is 8.617 · 10-5 eV · K-1. With *h* symbolized the constant of Planck, *e* It is the elementary charge and *me* the mass of the electron. The thermionic emission plays an important role at very high temperatures, on the order of hundreds or thou- sands degrees Kelvin, and depends significantly on the work function of the electron from the body of metal, *Ew*. Note that the most commonly used metal in Thermionic cathodes are tungsten, W, with a melting point of 3695K and the first ionization potential equal to 7.86 eV and rhenium, Re, with a melting point of 3459K and raw ionization potential equal to 7.83 eV [27].

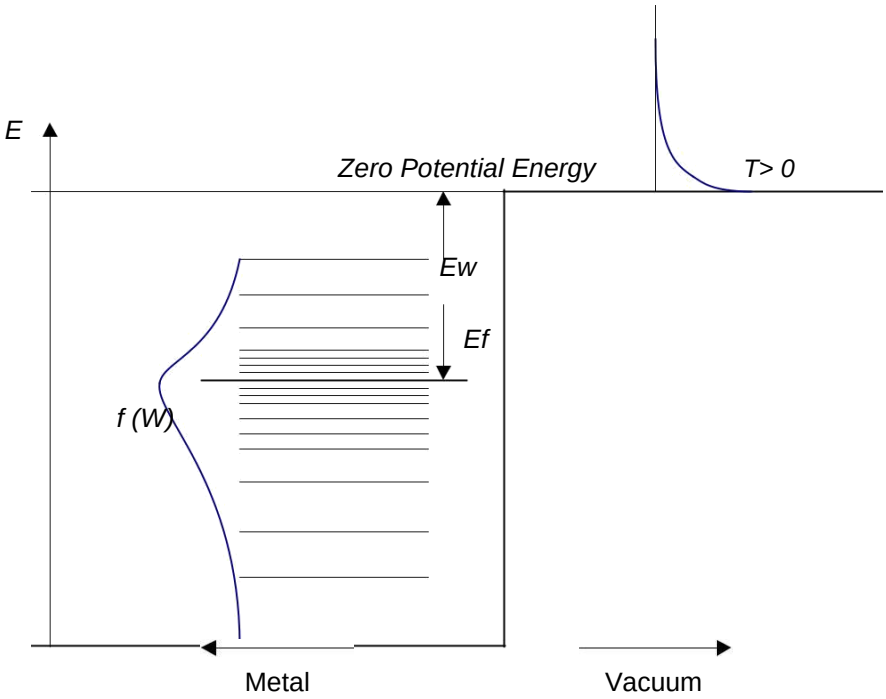

Fig. 2.25: The thermionic emission of: increasing the temperature of the metal a number of electrons may acquire energy greater than *Ew* and escape from me- tallow.

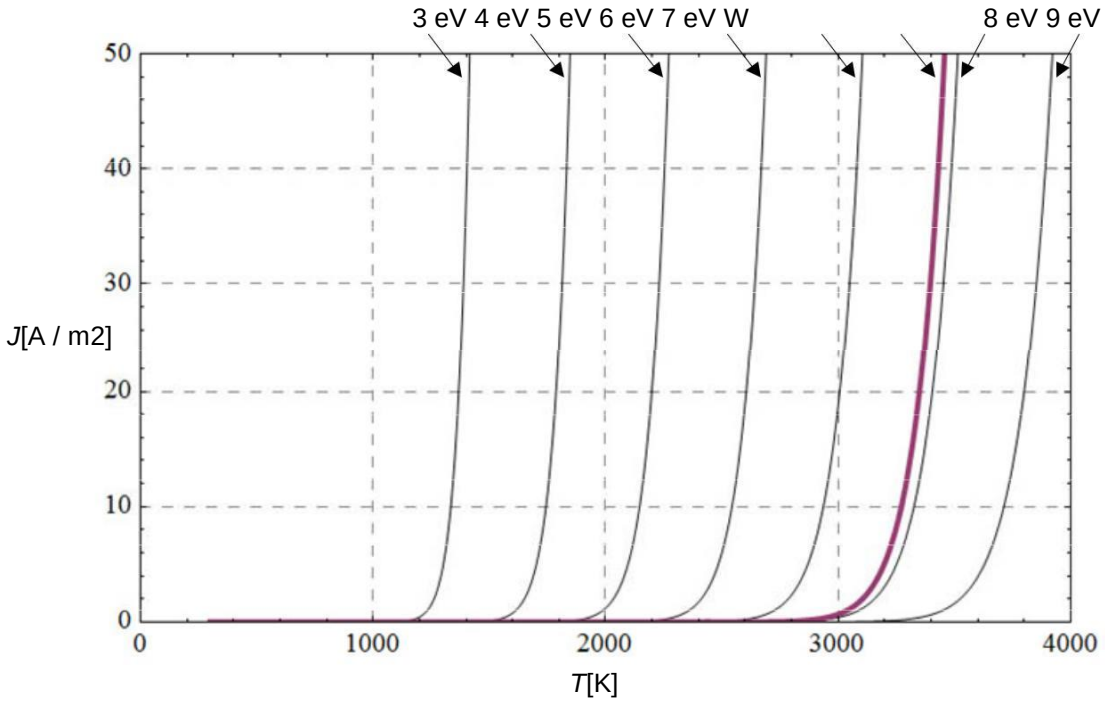

Fig. 2.26: The thermionic emission becomes remarkable for very high temperatures, proportionate accordingly always output energy of an electron from the metal. Tungsten should be heated to temperatures near the melting point, in order to obtain very me- milk thermionic currents.

2.9.2. Field Emission

When an electric field is imposed *E*The energy in the area outside of the metal decreases with slope *eE*. The potential barrier is reduced by the amount [28] [29]:

$$W = \sqrt{\frac{e^3 E}{4\pi P_0}} \quad , \tag{2,182}$$

as shown in Fig. 2.27. This rate is also called *rate aid Schottky aid*. The presence of strong external electric field also decreases the rea- weight the potential barrier that electrons have a non-zero probability to pass, in *tunneling effect* (Tunneling effect), as illustrated in Fig. 2.27. If the temperature is T = 0, then the probability of having electrons pass through the potential barrier is expressed by the relation *Fowler-Nordheim* for *emission Milli field* (*field emission*) or *cold emission* (*cold emission*) [30] and is given by

$$J_F = CE^2 \exp\left(-\frac{D}{E}\right). \tag{2,183}$$

In this expression, *E* It is the electric field in the vicinity of the surface of the metal, and the coefficients *C* and *D* They are given by [28]

$$C = \frac{e^3 E_f^{1/2}}{2\pi h \left(E_f + E_w\right) E_w^{1/2}} \tag{2,184}$$

and

$$D = \frac{8\pi \left(2me\right)^{1/2} E_w^{3/2}}{3he} \quad . \tag{2,185}$$

In the above expressions, *h* is the constant of Planck, *Ew* is the work function of the metallow, *Ef* is the energy Fermi, *e* the elementary charge and *me* the mass of the electron.

The Fowler-Nordheim equation is written as [31]

$$J_F = 6.2 \cdot 10^{6} \frac{E_f^{1/2}}{\left(E_f + E_w\right) E_w^{1/2}} E^2 \exp\left(-6.8 \cdot 10^{6} \frac{E_w^{3/2}}{E}\right) \quad [\mathrm{A/cm}^2], \tag{2.186}$$

where the actions *Ew* and *Ef* It is in eV and *E* the electric field strength in V / cm. The relationship Fowler-Nordheim for FEDs shows that class pediakes in- required intensity of 108V / cm, in order to receive electronic densities in the range of 102-103A / cm2.

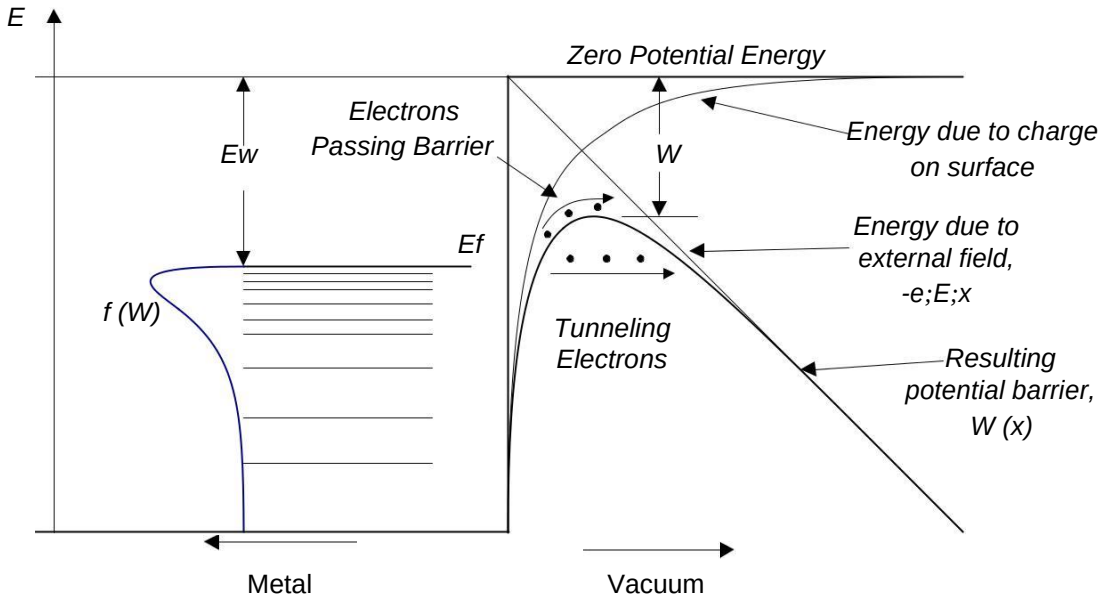

Fig. 2.27: The FED: The externally imposed field decreases the potential-barrier and allows electrons to pass through and leave the metal. Also in- taxanes the probability of tunneling.

Considering that the dividing metal surface - vacuum is in place *x*= 0, the expression of the potential barrier for electrons in the presence of an external electric field, becomes ([29], [31]):

$$W(x) = -\frac{1e}{4IP_0}\frac{^2}{4x} - eEx \,. \qquad (2,187)$$

In the above expression, the second term is derived from the applied electric re- slo, and the first term is the potential energy of the particle, because In contrast to the sign of charge collected on the surface of the metal, which is equivalent to an idol at position -x within the metal. Including the effect of the virtual load, the Law of field emission should be corrected by a pro- ragonta ([31])

$$a = (1 - y)^{1/2} \,, \qquad (2.188)$$

where

$$y = 3.8 \cdot 10^{-4} \frac{\frac{1}{E}^{1/2}}{Ew} (1 - y)^{1/2} \,. \qquad (2,189)$$

2.9.3. Combined Broadcast

The combination of thermionic emission and field emission is elec- tronic *emission T-F* or broadcast *Schottky*. The synergistic effect of electric field and

thermionic emission has led to rapid increase in rheumatic density observed. An approximate relationship for the transmission T-F is given by Hantzsche in [32], wherein the rheumatic density calculated by

$$J_{TF} \cong (AT^2 + BE^{9/8})\exp\left(-\frac{1}{C + E^2}\right)^{-1/2}, \qquad (2,190)$$

in which the coefficients *A*,*B*,*C* and *D* They can be found in tables in [28] and [32]. Indicatively, in copper, with output power *Ew*= 4.5eV, at a temperature of 2000K (zero imposed electric field), the thermionic current density of the (2180) appr *JT*= 22 A / m2. If the electric field is 2 · 109 V / m (in core temperature of absolute zero), electronic field emission from the (2183) is *JF*= 3.9 A / m2. However, if the factors temperature and electric field act simultaneously the combined emission of T-F is *JTF*= 1.2 · 106 A / m2. This observation becomes apparent that the combination of thermionic emission and electric field leads to a significant strengthening of rheumatic density.

There is however a critical point and any necessary pediakes tensions to be applied to a diode, to receive significant current values for the electronic transmission. As we saw from the previous example, even for tech- Rust pediakes tensions of the order of 109 V / m, the field emission current is very small, only a few A / m2. The above pediaki intensity practically equivalent to 10MVolt voltage application on a flat path, whose reinforcements are just 1cm. A- ntilamvanomaste that this is impossible in every respect (voltage magnitude, diile- ponent strength). However, the FED is normal practice emission elec- cations from the cathodes, even at room temperatures, ie far from the catalytic growth area of the electronic emission because of thermionic phenomena mind. The reason the FEDs finds practical application, even in small BRAKE diodes tions, is *local strengthening pediakis intensity* acute geometries and other non-ideality on the surface of the metal. The feature size, as will be seen, is *field amplification factor* (Field enhancement factor).

2.10. The amplification factor of Pediakis Intensity

Relation (2.183), on the field emission at low temperature, and the relation (2.190) for the combined emission of T-F receive satisfactory prices when pediaki volume is too great. For example, in simple field emission at low temperature, a completely simplified expression by the approximate coefficients (magnitude) is as follows [30]:

$$J_F \cong 10^{-6} E\exp\left(-\frac{10^9}{E}\right). \qquad (2.191)$$

The above expression gives satisfactory rheumatic densities (> 10A / cm2) for pediakes intensities of around 1010V / m or more. Even if electronic emitting T-F, that accretion rates, due to the combined action thermio- victory emission and electric field is of the order of 104 required pediakes tensions have price too high. So the question becomes how to have De-effective field emission cathodes, once so great pediakes tensions can not be brought into passages. Specifically, we apply the cathode voltage of tens or hundreds kV, while the distance to the rise of the order of a few centimeters, which would pediakes tensions in the region of 107V / m. The answer lies in the fact of *aid* electric field acute geometries as spikes or fine needles on the surface of the conduit and from areas of epifanei- let in which insulating materials are deposited particles.

Assuming that a passage infinite plates spaced distance *d* Schumann applied potential difference *V*Then the electric field at the surface of the electrodes, as everywhere in the space, you will be *E = V / d*. But in areas of the surface with anomoio- form, the electric field is altered and presents more value, which can be written as follows:

$$fE = b\frac{V}{d}. \qquad (2,192)$$

The coefficient b in the above expression is called *field amplification factor* (Field en-hancement factor). Any geometry escapes passage infinite parallel plates, wherein the electric field is equal to the ratio *V / d*Exhibits maximum electric field party larger than this, in a region of space. These areas are usually located in places abnormal geometry of the electrodes.

2.10.1. Pediaki Strengthening of Spikes

The sharp protrusions on a surface is a strong geometry, which is presented very strong field amplification effect. If the geometry of the cutting edge approaches lives cylinder with spherical head, as illustrated in Fig. 2.28, then from [28], the intensity of pediakis factor results approximately equal to

$$fb \approx \frac{2\frac{H}{r}+1}{\ln 4\frac{H}{r}+5}-2. \qquad (2,193)$$

A ratio of height / radius equal to 10 implies pediaki aid about 5 times, while a ratio equal to 100 causes strengthening field 33 times. The reinforced field appears on the edge of the peak.

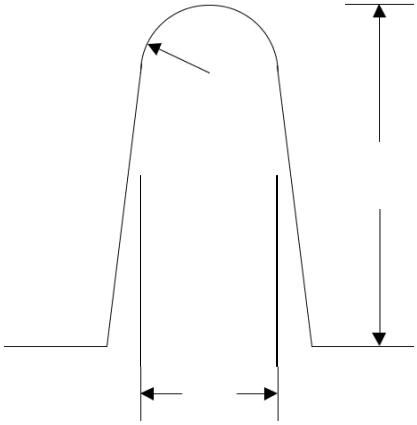

Fig. 2.28: Typical approximate peak geometry.

The spikes in the capacity of the strong support of the electric field, already been used by a Spindt cold cathode electron emission. The cathodes of cold-emission type Spindt ([33]) are implemented by making micrometric peaks in a trilayer structure of metal - insulator - metal, as illustrated in Fig. 2.29. With modern microelectronics technologies can be made one of such arrays cess micrometer or nanometric peaks, with the nose radius of hundreds or de- bins Å. Therefore, small-imposed field between the electrodes, strong pediakes tensions may be presented, allowing large field emission current from the device.

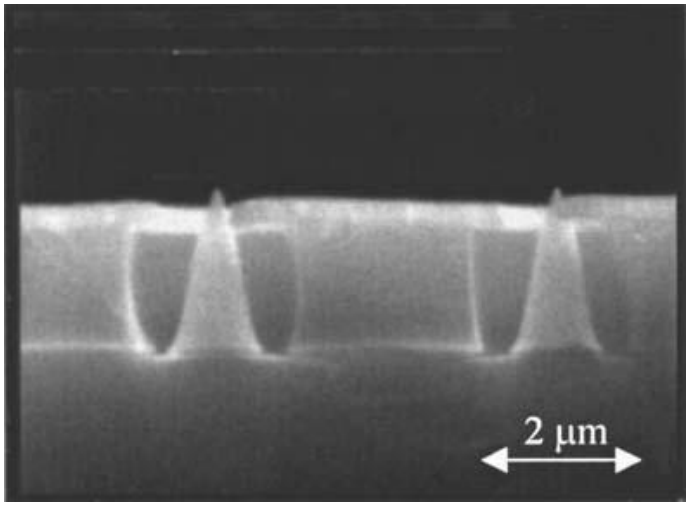

Fig. 2.29: Element cathode type Spindt (cross-section). From ([34]).

The electronic field emission is a very small area at the tip of aich- bution, so the device is sensitive to effect Joule. By requiring greater voltage and thus forcing larger amount of current to ekly- been from the top of each cone, the tip explodes due to overheating and destructive slice completely. Example damaged item Spindt shown in the following picture. Left shows a cone array, while the right shows a con- testrammeno item. Indeed, the explosion has caused a crater cone, a material has melted and has spread radially the original point.

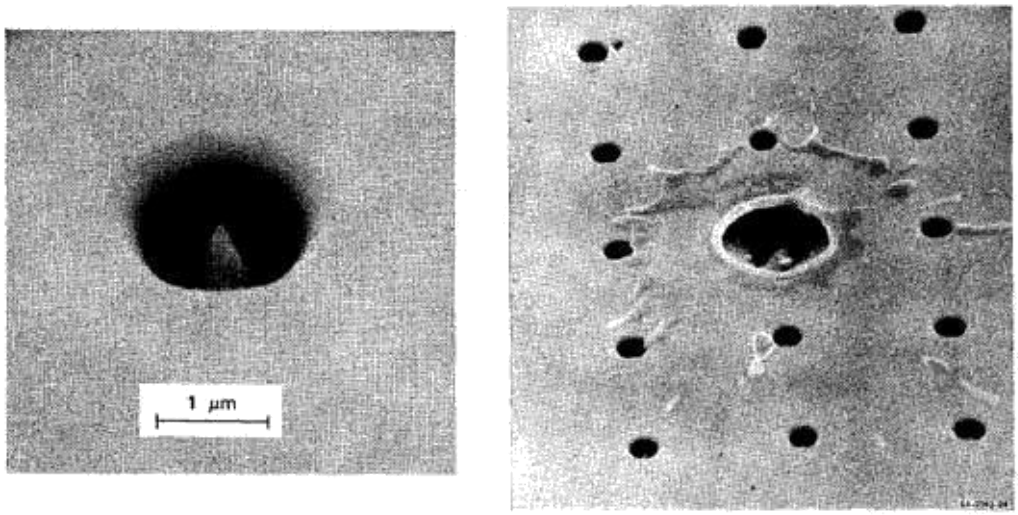

Fig. 2.30: Element type glide Spindt (left) and data is destroyed (de- Xia). From ([35]).

Each individual element has a maximum power capacity of the order of a few tens or hundreds mA. Always depending on the size of the peak, typically specific maximum current from each cone can reach 150mA ([35]) and with improved re- Methods can be taken over 200 each cone ([34]), without cause irreversible damage to the elements. The maximum electric field at the cutting edge provided by the Nottingham effect melting point of intense field emission ([35]),

$$\mathrm{f}E = 1.88 \cdot 106\, F^{1\,2} Tc\ . \qquad (2{,}194)$$

In this respect, the *F* is the work function of the metal in eV and *Tc* the tempera- ture of the metal melt.

A Spindt type array, with a transmission element per 3um can give liquidity but of the order of 100 / (3 micrometres) 2 · 104 = 1100A / cm2. Improving the performance of each cone and thickening the array can take even greater fire-rheumatic densities. The specificity of cold emission cathodes is their sensitivity to i-schyro field, resulting cathodes these can operate only small voltages of the order of a few hundred Volt. To the electronic currents emitted can be used in high power microwave tubes must acquire energy hundreds keV. Therefore, to use an array of Spindt to microwave lamp should be shielded from the high voltage, so that the field emission current is able to accelerate the alpha paitoumenes effects.

In microwave tubes medium and high power, the tendency is to use Thermionic cathodes or explosive emission cathodes (explosive emission cathodes). The Thermionic cathodes typically use small metallic yarn, which thermai- nontai from DC to lefkopyroseos temperatures, so emit electrons through the phenomenon Richardson-Dushman.

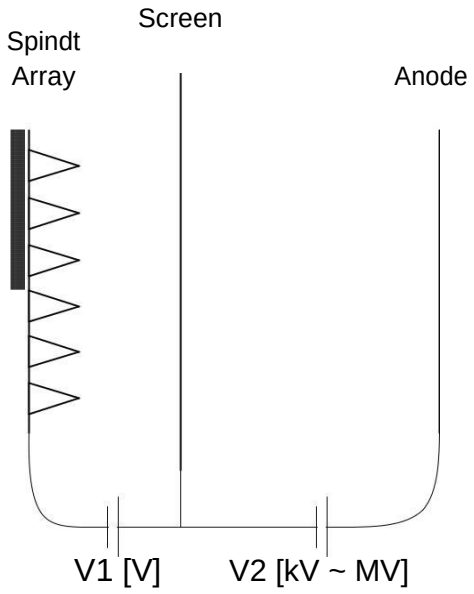

Fig. 2.31: Array Spindt for high-power LED.

The disadvantage of thermionic cathodes is that they have small emitting surface, and can not perform very dense currents of hundreds of A / cm2, as required for the production of highly concentrated electronic links. Typical continuous wave klystron using electronic bundles several tens A, which accelerates Commission action tens or hundreds of keV. In such klystron, as in Al-say average power tubes, the electron beam is usually produced from Thermionic lays periods. In high power LEDs necessitate electronic beams with currents of many thou- sands A, which can not be obtained from Thermionic cathodes. In general, cathodes are used explosive emission, which undergo cleavage by very iota schyro electric field and generate their surface multiple molten points (as in the case of Fig. 2.30) which are converted to metal vapor plasma. The explosion of the cathode caused by the large pediaki intensity, which pre- calls strong field emission current from tiny areas. These regions are then melted and produce a very hot plasma, which is continuously fed from the material of the electrodes. During this process, the plasma cathode operates as a source of infinite power theory, which accelerated towards the anode of poly- XVIA. The disadvantage of the explosive emission is *Bridging* the gap of the passage of the increasingly expanding plasma, thereby shorting the electrode and an end of the phenomenon of acceleration of electrons. Bridging the gap depends on the electric field in the gap, the temperature and the plasma material is made at speeds of the order of 1 ~ 10cm / microseconds. The explosive electronic emission from cold cathodes is a very simple method of making electronic De--term. The package, however, has big noise and varying characteristics due to the dynamic variation of the characteristics of the diode. The field emission cathodes like array Spindt, better alternatives because they are destroyed, can operate for longer periods and provide electronic beams Tific best features. The disadvantage is the increased complexity in their construction and their susceptibility to overheating phenomena Joule.

2.10.2. The Triple Point (Triple Junction)

The triple point is a three compound materials with different refraction indices. The most commonly occurring geometry is the compound of a metal, a diile- tronic equipment and air or vacuum. Considering that the metal has infinite diile- ponent fixed, the pediakes lines are always perpendicular to the surface. The vacuum or air having a relative dielectric constant equal to 1, while the insulating material has a dielectric constant greater than unity. The association of the three materials, considering that the metallic Member of flat, we can distinguish two geometries. The first eikonize- geometry Tai in Fig. 2.32 (a), wherein the dielectric medium forms an angle less than 90 degrees with the conduit. The phenomenon of refraction, under the law of Snell, leads to a "deviation" of pediakon lines near the point of union. Intuitively we understand that the physical geometry that leads to a decrease in field strength at the point of union.

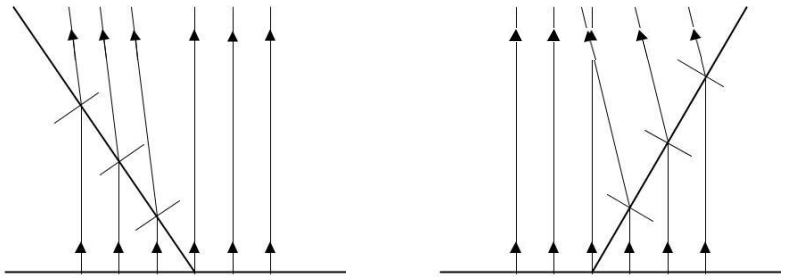

Fig. 2.32: The refraction of pediakon lines in the triple point.

The other case the triple point compound is shown in Fig. 2.32 (b). In this geometry, the dielectric forms an angle greater than 90 degrees with the conduit. Following the refraction of pediakon lines, we see that a convergence region created by intersecting lines, which, as we know, has no physical sense. What actually occurs is very large amplification of the electric field around the region of the triple point. The consequence of this distortion of the field, is to enhance the electron emission at the point of union. Since the apparent pediaki aid is large enough, it may cause electric ponent split, which comes from the triple point. For this reason, when designing support insulators or transit, care is taken to avoid im-
meia metal compound, air and dielectric, the angle of air-metal below
90th.

2.11. The Power Break the Void

The division of a gap, which is empty, or *vacuum decay (Vacuum break- down)* is a completely different phenomenon from the break gaps, which mo- They are communicated by dielectrics, such as, for example, ambient air. In the case of the void, the "material", which will form the conductive path for the installation of the electric arc decomposition, offered by the same electrodes.

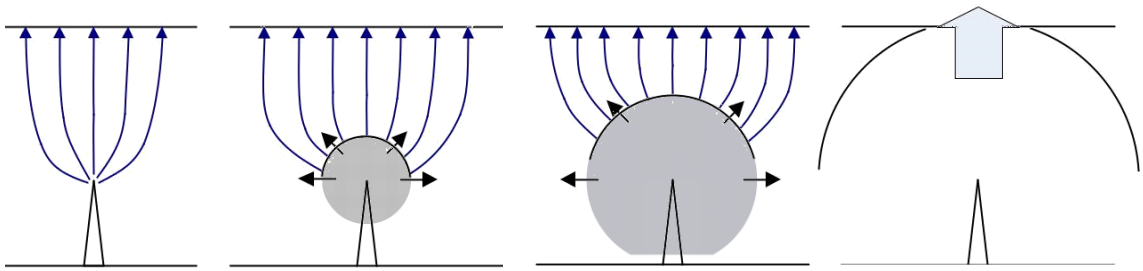

Fig. 2.33: Due to field emission, caused global consistency with emission melting point of the metal and the plasma production.

By imposing the voltage in the gap, some parts of the descent begin to emit electrons, according to the laws of electronic field emission, such ekfraze- Tai from the relationship *Fowler-Nordheim*. Imposing tension in the gap creates pediaki E- intensity, which strengthened locally by microtip (Fig. 2.33) or triple points pre- sented, said residue being at the electrode surface (Fig. 2.34).

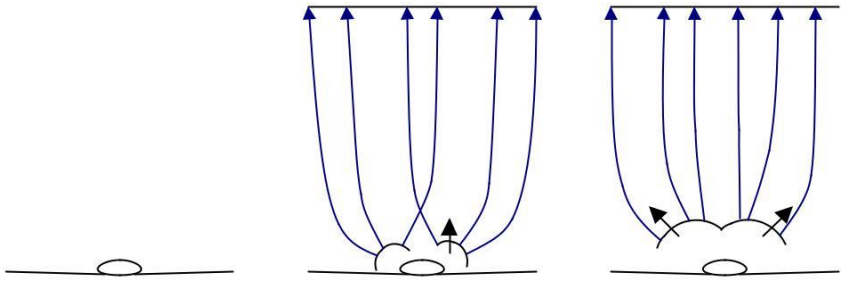

Fig. 2.34: Decomposition Start a triple point surface impurity.

In Fig. 2.33 (a) and Fig. 2.34 (a) the field enhancement occurs, for example, the edge of a peak or the triple point of an impurity, adhered to the surface. In this region the electron emission begins, which is typically much of limited extent. Result of field emission is the warming of the region that emits electronic flow at such high temperatures, which may be of fusing both of organic impurities, and the cathode metal itself. As a result (see. Fig. 2.33 (b) and Fig. 2.34 (b)), a microplasma of ionized gas appears around the area originally provided by the field emission current. The width this term because of electrostatic field but also because of thermal diffusion, expand at all directions and represents an ideal electron source. Let im- cut at this point that the expansion of the plasma in the gap is quite contrary co- and chaotic process, however, for the sake of simplicity, we consider that there is o- moiomorfa with relatively constant speed. From the point that the descent "covered" to a sufficient degree by the plasma, the diode switches from the transmit mode *Fowler-Nordheim*, to space-charge limited electronic transmission. The front of plasma- Tosh longer functions as ideally descent and as it expands towards the anode, under the law *Child-Langmuir*, Increasingly impinging on current increase (see. Fig. 2.33

(C) and Fig. 2.34 (c)). Very often, because of the growing power of the passage, there is fusion of the anode and contribute to progressively bridge the gap with their upward plasma. This phenomenon, however, not shown in the simplified formation Kd charts of previous images.

The continuous increase of power in the fairway, always depending on the Child-Langmuir law and the ability to drive the external circuit, contribute to more pronounced heating of the electrodes and ultimately bridge the gap from plasma. At this point (see. Fig. 2.33 (d)), the diilektrodio plasma is a conductor very Asia Mi- Cretan resistance to the passage of current. Since the driving source (external circuits nd), which caused the breakdown of the gap has at its disposal sufficient load will continue to flow current in diode, which is the *vacuum arc (Vacuum arc).* In very simple terms, therefore, we can approach the electrical breakdown in the Capital Law in three stages: First, a large positive voltage on the diode causes emission Milli scope of certain points with a strong geometrical disorder, presenting me- turkey coefficient pediakis aid. Then, if the field emission current EI so strong enough, the cathode is melted in points prevailing intense electronic representatives procession. The generated plasma spreading is an electron reservoir, being pushed towards the anode, and the diode is now governed by the Child-Langmuir theory. Finally, the contribution of the descent, but sometimes the rise in diilektrodio plasma, the gap is bridged and *vacuum decay* switches to electric *vacuum arc*A the- arc molten metal, which is constantly fed by melt material of electrode charge.

2.12. The Diilektrodio Plasma

Saw where cleavage of the vacuum passage, that the full bridge the gap precedes the plasma output from the electrodes, due to local melting of materials. He next electrode materials, for example stainless steel, aluminum or copper, to be an important parameter in the behavior of the decay of the vacuum diode. The metal used in the electrodes, may still have a significant amount of adsorbed gas, such as hydrogen (H, H2), water (H2O) and other gases (CH4, NH3). Also, the electrodes may be coated by metal oxides, at a height of several atomic layers, as well as to have deposits of organic and non compounds on their surface. The material of the electrodes, the prosrofi- me gases and other factors play a crucial role in spreading speed of the plasma in the passage and in the behavior of the collapse of the gap.

By imposing the voltage, the cathode of a vacuum diode begins to be covered by term width typically in the first few tens nsec, while the rise begins to emit plasma few tens nsec later ([36], [37]). The metal vapor plasma spreading rate is small, of the order of 1cm / microseconds. For example, in [36] are recorded speeds for stainless steel at 0.4 ~ 0.5cm / microseconds for copper electrodes at 0.55 ~ 0.65cm / microseconds and aluminum electrodes at 0.8 ~ 0.95cm / microseconds. The speed in- Lie plasma depends on the temperature, according to the relation

$$u = k\sqrt{k_B M/T}\,. \qquad (2.195)$$

The temperature of the plasma are a direct function of the passing current. Therefore, by passage in a Child-Langmuir, the electric field and hence the applied voltage and the geometry of the electrode greatly affect the heat dissipation of the plasma- Tos. In microwave source of high power, such as Vircators, the imposed voltages on the order of hundreds of kV, resulting in the displayed electric fields are hundreds kV / cm. Cathodes covered with fabric or cathodes from anthrakonima- the show spread speeds in the range of 2 ~ 3cm / microseconds. The coating technique of the cathodes with cesium iodide, CsI, dramatically reduces the spreading speed, because the mass of Cs atoms and I is significantly higher [38].

The Miller, [39], has presented a paper on the behavior cathodes re- coated with fabric (velvet). The process starts with vacuum split on the in- surface should be a thread because of the intense electric field exists in limited Xe. The electric field absorbing the permissible spatial stream, according to the law of *"3/2"*. This current causes overheating of the plasma column which ektei- Neta to thermal velocity. Where clusters (tufts) carbon fiber, which are distance *d* *The spreading speed of the plasma cathode can be estimated from

$$u = 100 \frac{d}{d} V^{1/2} \text{ [M / sec]}, \qquad (2,196)$$

where *d* the anode-cathode distance and *V* It is the positive trend in Volt. In conclusion, the main issue affecting the explosive emission cathodes

bis is to generate plasma from the electrodes, resulting in short-cycling of the vacuum passage. Important is the purity of electrodes. The importance of materials uses very high vacuum, ie metal parts which have undergone cleaning tion and heat treatment improves the collapse times the gap. However, the metal parts and particularly the metal cathodes do not offer the advantages of cathode carbon fiber or fabric, which is the very biggest in number of electronic broadcast areas and therefore larger rheumatism tions densities. Instead, textiles and carbon fiber, however good preparation cleaning and have undergone, hold very large amounts of adsorbed light gases, mainly hydrogen, methane and water vapor. Accordingly, the cathodes of this type are useful only in small repetition rates and low total party number of pulses. The coating of the cathodes with cesium iodide, CsI, offers a tho- rakisi of carbon high atomic weight, which maintain low speeds of spreading, even in very strong electric fields. As a result, production can meet more extensive in duration microwave pulses [40] .The cathodes these form extensive field research in high power microwaves.

3. High Power Microwaves

Provided *High Power Microwaves*

The development of high power microwave sources made possible by the introduction of en- Welfare of *pulse or percussion* in the electricity sector. The rapid return of electricity saved with instantaneous power levels, reaching the 100TW, enabled designing vacuum tubes, which operate these short while but huge voltage and currents for generating microwave pulses with powers of several GW. For this reason, each lamp high iota schyos is inextricably linked to the electrical system, it provides the necessary pulsed electrical power. The design of the electrical system, storage of electricity and the method rapid performance of the lamp - load parameters critical to the quality of the electron beam and therefore to export Asia Mi- krokymatikis power.

The high-power sources can be categorized according to the bandwidth of the output. The latest classification is given in [41] and can be summarized as in- referred to as:

Tab. 3.1: Categorization HM Radiation Sources

Characterization	Percent Range PBW	Speech Zone BR
Narrowband	PBW <1%	BR <1.01
Mesoband	1% <PBW <100%	1.01 <BR <3
Sub-hyperband	100% <PBW <163.4%	3 <BR <10
Hyperband	163.4% <PBW <200%	10 <BR

The definitions given on the BR and PBW are:

$$BR = \frac{fH}{fL} \quad . \tag{3.1}$$

$$PBW = 200 \frac{BR - 1}{BR + 1} \quad . \tag{3.2}$$

Depending on the type of lamp, ie whether the generated radiation is narrowband or broadband, the requirements of drivers with impact force change signifi- cantly. For example, a microwave narrowband component, even if operated in a pulsed manner, generates a pulse sequence of a few tens or hundreds nsec with well defined microwave frequency. This condition requires an electronic RH package "good", which is characterized primarily by steady *accelerates Nusa trend* stable *Current Price*, in addition to other characteristics, such as *temperature* (Electron temperature), *brilliance* (Beam brightness), *sharing actions* (Beam emittance), etc. The monochromatic electron beam is essential to the sys- coupled to the electromagnetic wave in the architecture designed to ekasto- either narrowband light. Instead one broadband or wideband light based on driving a "d" electrical pulse in a radiative device. The shock current radiates at frequencies covering a wide range of the electromagnetic spectrum Tosh and if this requirement is to produce an electric pulse with as quickly as rise time and a shorter duration. Based on this con- fication, the microwave narrowband sources are fairly high complexity, both on the lamp, and the storage section, and driving electric iota schyos while microwave wideband sources have less complexity, the main concern mainly in part on the production of electrical pulses of very short duration, on the order of a few nsec, with sub-nanosecond rise times.

3.1. Structure High Power Microwave System

A high power microwave system may occupy the entire space em- abdomen or be a truly portable system transportable on a small truck. The entirety of which is typically composed of the following (see. Fig. 3.1): Firstly required primary power source (prime power). This can be simple alternating voltage 220V, energy from a generator or DC voltage from an electric accumulators. Thereafter follows a transformation of the capital of low voltage in a readily usable level high voltage as a me- alternating low power transformer ratio of 500: 1 or a generator Cockroft-Walton (trans- formed power). In this manner, the voltage is transformed to a level suitable for use in an amplification system voltage but not very cumbersome in terms of insulation requirements and capacitive elements. Here is a step multiplying the voltage, which in most cases is a Marx generator (pulsed power). This step raises the voltage typically used voltage level in high power lamps, which may vary in 300-400kV even up 1-2MV. The energy stored longer driven in microwave poly-

XVIA, which is the converter «DC» energy RF. Perhaps intervention challenged a circuit configuration of the electric pulse (pulse forming network), which imparts the electrical pulse driven lamp in a desired shape, e.g. rectangle or trapezoid, with short rise times and low ripple peak. Ithin E lamp (tube) the electron beam is generated, which is usually schetikisti- KH or almost relativistic. By appropriate interactions extracted microwave radiation from the energy beam. The generated microwave power may be driven in a compression subsystem of the microwave pulse (microwave pulse compression), an increase of the instantaneous power, and a mesh transformation rate of the microwave, for example for coupling of a circular waveguide kyma- todigo rectangular. Are eventually transmitting means, which may be a choanokeraia or a mirror.

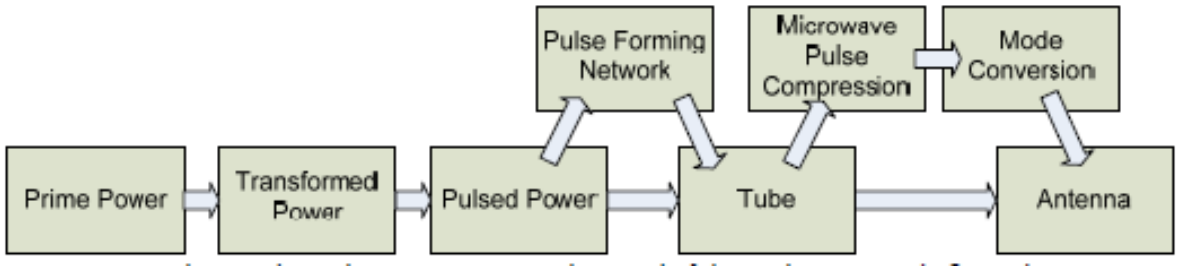

Fig. 3.1: The parties to a high power microwave system. Additional (optional accessories Train) sectors shown in the diagram.

3.2. Pulsed Power

There are generally two ways of producing electrical pulse to a load, the gov- limits storage of electric power be either capacitive or inductive. In the case of capacitive storage, as shown in Fig. 3.2 (a), a capacitor is loaded dynam- in a wide voltage V0. With the *closing* switch S, the voltage of the capacitor odigei- Tai instantaneous load Rload. If no resistance and the switch is ideal, then the rise time of the voltage across the load is zero. If epagogi- tion electricity storage, as shown in Fig. 3.2 (b) the switch S EI- yes initially closed and the coil flows through a very large current, which is limited only by the capacity of the current source I0. With the *opening* switch S, the coil current is then forcibly load Rload. The two techniques described a- wear the fundamentals *closing switch* (Closing switch technique) and *opening switch* (Opening switch technique) for driving the installed energei- let a storage element to the load.

The basic idea behind the impulse force is: store energy slowly, either a capacitive or an inductive element and discharged with a strong transient load, which may be for example a microwave generator high power. The primary power supply should have no great demands on DC power.

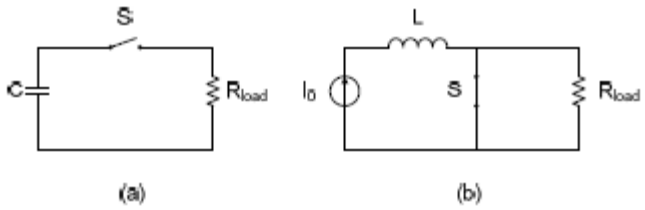

Fig. 3.2: Capacitive (a) and inductive (b) a method of generating pulses.

The charging of the capacitor in the case (a) may be performed while a very high voltage, but with currents of a few mA. Charging coil if (b) bo- psi to about several kA current source but a voltage driving few Volt. Therefore the required "primary" power is on the order of hundreds of Watt or few kW.

3.3. Single-stage generators

By single-stage generator that characterize the device, which storage kefei electric power to a single element, capacitor or inductor. The stored energy through technical closing (electrostatic storage) or opening switch (magnetic tostatiki storage) driven by pulsed mode at light-load, where take place the desired processes. The most common types of single-stage generator are VDE-a type generators and VDE-b, which are used for production of standard voltages impulse form [42].

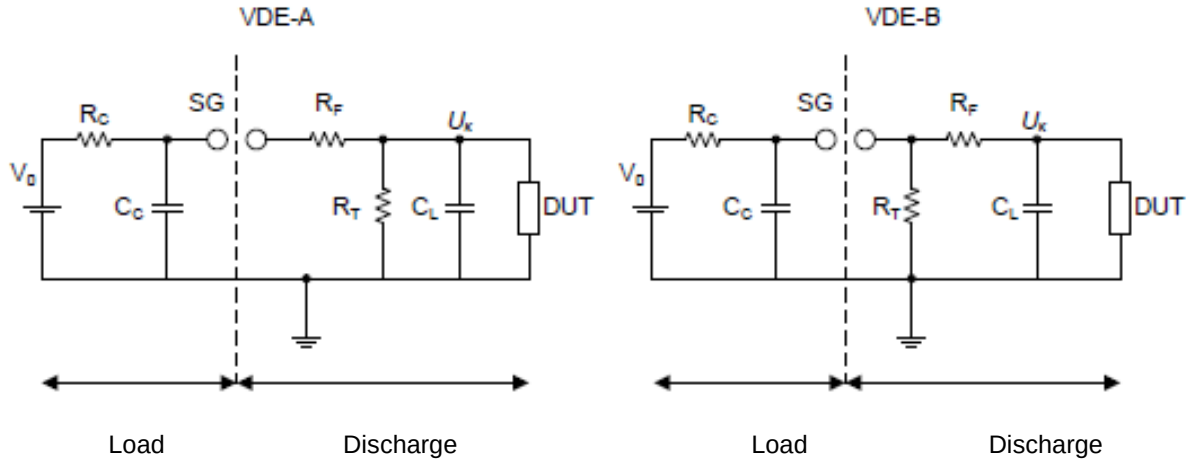

Fig. 3.3: Single-stage shock generators trends in VDE-a and VDE-b.

In the above circuits, the details that determine the behavior of the E contain a provision symbolized as follows: V0: charging voltage, RC: Load resistance, CC: cargo tisis Capacitor (Charge Capacitor), SG: Spark Gap (Spark Gap), RF : Resistance Front
(Front Resistor), RT: Resistance Tail (Tail Resistor), CL: Capacitor Load (Load Capacitor), DUT: Essay (Device under Test). The load capacitor CC, is charged by a high voltage through a current limiting resistor. Once the voltage reaches the desired level, the appropriate set scintillator SG cleaved and the voltage

charging capacitor is transferred to the remaining circuit. If there is no sample for examination, the trend *UK* across the capacitor CL has diploekthetiki form by expression:

$$U_{\kappa}(t) = aV_0\left(e^{-\frac{t}{\tau_1}} - e^{-\frac{t}{\tau_2}}\right).$$

Depending on the circuit, VDE-a or VDE-b and data values can be calculated stoun the characteristic times t1 and t2, the maximum value of the voltage is transferred to the load, *UK, max*As well as the rise time and tail. Conversely, given the Commission desirable waveform (anode and tail time) can be calculated apaitoume- images data values of the impulse generator. The most widely used outbreak STICK waveform, the waveform *1.2 / 50*With a time 1.2msec forehead and half time range 50msec. For impulse voltage 1.2 / 50, elements selected from the approaches STICK types RT = 1410 · n · (TF /CC) , the tail resistance, and RF = 333/n· (TR /CL) ,
the front resistance. With *TR* and *TF* denote the front and tail times respectively, expressed in microseconds and *n*The ratio of the width of the impulse voltage to the charging voltage (approximately 0.8). The capacitors are expressed in nF. Typical values for the production of impulse voltage 1.2 / 50 with VDE-b circuit CC = 6000pF, CL = 1200pF, RT = RF = 9500 and 416O. For more detailed calculations single-stage shock generating installations the reader is referred to [42].

3.4. Multiple generators

In a previous section we described how, in a simple way, can lead to a load Sumy impulse voltage or current. However, when the pulse power requirements are MV or several kA, these techniques are insufficient. Especially in case of outbreak ment trend is widespread technique of multiplication. Clearly capacitors withstand MV trends are unprofitable to manufacture because it will import so bulky and unwieldy. Also, the required DC voltage for charging a capacity of this standard MV, are difficult to produce with any technique, such as a transformer and rectifying ming ultra high voltage. Given these difficulties, to para- goume voltage of several hundreds of kV or MV, using the principle of hyperproliferative voltage, based on the loading of many parallel capacitances by a moderately high voltage, for example 100 or 200kV, and then the series charging their representatives. The most commonly used multiplication circuit voltage is the Marx generator (Marx generator), a circuit invented by German
Erwin Otto Marx in 1923.

In a generator Marx, capacitors C are charged in parallel from the source V0, through resistor R1 and the resistor R. If all the switches S are closed simultaneously, the capacitors are momentarily connected in series. If the Marx generator is densely knotes N (N *steps*), Then across the load Rload appears voltage theoretically equal NV0. If there are no reactors in the circuit and the resistance of the load is re- Terah ohmic, the voltage will reach its peak, NV0, almost instantaneously.

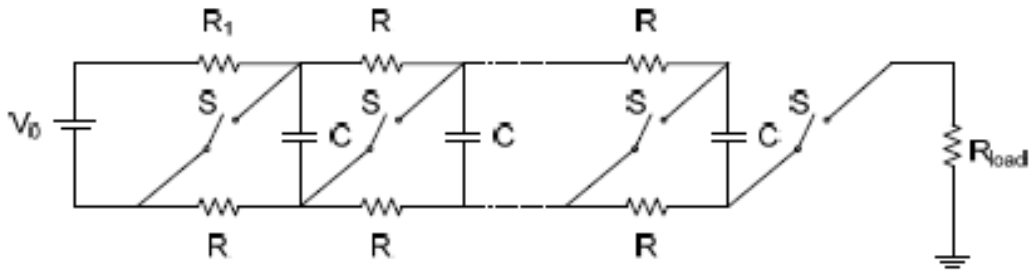

Fig. 3.4: Marx generator circuit for multiplying the voltage.

The total capacitance of the Marx generator is C / N, because the series mains capacitors and hence the voltage on the charge decays exponentially with time constant t = RloadC / N. An important condition for the Marx generator is the resistance of the load is sufficiently lower than the load resistors R, that the voltage is apportioned almost entirely on the Rload. The switches S is usually simple gap spark (spark gaps) and sometimes triggered gaps or type trigatron thyri- blinds.

3.5. Interaction Microwave Production

Electrons can produce electromagnetic radiation through certain mechanisms, which are used to classify according microwave tubes. The operation of the microwave sources based on -*phase* (*coherent*, From the Latin *cohaerere* = I'm connected) electromagnetic radiation emission from electron groups. The grouping of electrons (bunching) in a lamp is crucial, because it leads to overlapping of accidental irradiation of individual electron in a random phases, resulting in-phase and therefore of enhanced radiation, which can be extracted from the microwave lamp. In other words, the characteristics of the device cause spatial and temporal changes in the originally uniform electron beam, resulting in a grouping of electrons and energy extraction therefrom, to produce or aid of microwave radiation.

The main production mechanisms of radiation from charged particles (electronic) is the radiation *Cherenkov* or radiation *Smith-Purcell*, Radiation -*pass ing* (*transition* radiation) and radiation *Bremsstrahlung* (From the German bremsen = slow down and Strahlung = radiation) [43], [44].

The Cherenkov radiation occurs when electrons move in a medium speed of ue, greater than the phase velocity uph of electromagnetic waves in this me- both. The phase velocity is uph = c / n, where c is the speed of light in vacuum and n is the refractive index of medium. Irradiation Smith-Purcell, which occurs when the electrons pass near a periodic structure, can be regarded as a form of radiation Cherenkov. The periodic structure of the device results in the night it is shown wavenumber kz, and hence a phase velocity uph = w / kz, which is lower than the speed of light, close to the periodic structure region. LEDs based on radiation from passing electrons by periodic structures are too pulp say, with key representatives of the TWT lamps, VWO and Orotron. The lights with periodic structure called and LEDs Cherenkov (Cherenkov devices). If online kinei- Tai straight beam with a guiding magnetic field parallel to the beam, the indicator

called O-type Cherenkov. If the electron beam is moved perpendicularly to a magnetic field, performing a circular path, the light is called M-type Cherenkov. Leading representative lamp M-type Cherenkov is the magnetron.

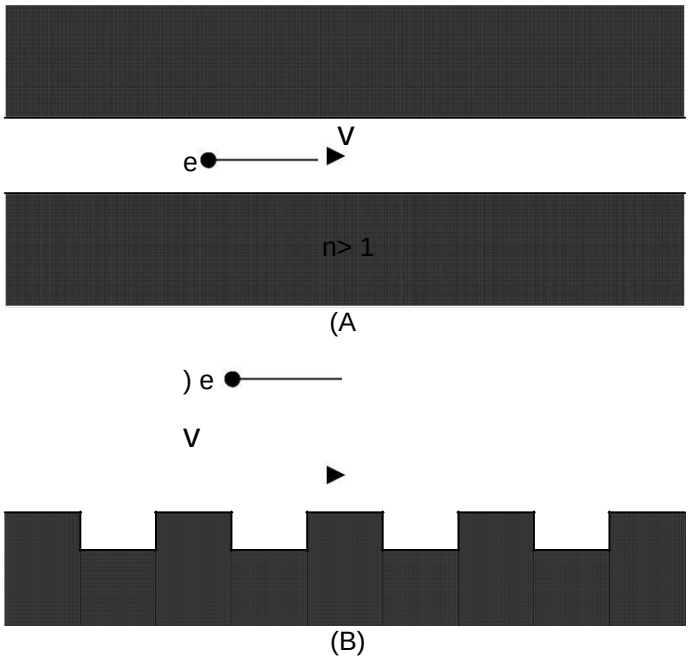

Fig. 3.5: radiation Cases (a) Cherenkov and (b) Smith-Purcell. In the first case the electrons travel channel in a dielectric medium with a refractive index n> 1. In the latter case the electrons move close to a periodic structure.

Transit radiation occurs when electrons pass through the boundary between two regions with different refractive index or transiting through discontinuities conductivity Sciences bodies, such as grids, irises, and voids (see. Fig. 3.6). Example tubes based on the phenomenon that the Klystron, the Reflex Klystron and Mono- tron.

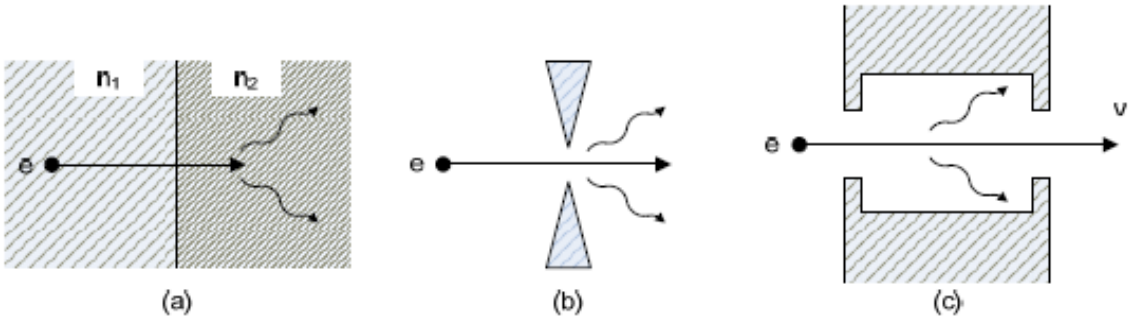

Fig. 3.6: Active Radiation cases: (a) the electron moves from one material to another with different refractive indices. (B) the electron passes through a conductive diaphragm. (C) the electron passes through a cavity.

The Bremsstrahlung, or else braking radiation, allegedly first discovered by Nikola Tesla in his experiments between 1888 and 1897 and confirmed AP- gotera by Wilhelm Roentgen and the discovery of the rays X. The Vremsstrahlung

It occurs when the electrons change their speed due to electrical or magnetic fields. The lights, which are based on this phenomenon is mainly the family lights, using magnetic fields to force the electron beam into a spiral. Invited Cyclotron Resonance Masers (CRMs), as a basic parameter of the radiation is *gyrosychnotita* (Gyrofrequency or cyclo- tron frequency), (2.32), and the change due to the relativistic factor affecting the mass of the electron. The entire class of round-tubes (Gyrotrons) such as gyro-monotron, the gyro-klystron, the gyro-TWT and gyro-BWO are bremsstrahlung equivalently of Cherenkov linear electron beam tubes. Category Vremsstrahlung tubes are the Free Electron Lasers (FELs), in which the electron beam passes through a periodically alternating magnetic field, also called un-dulator or «wiggler» (see. Fig. 3.7 (b)). The Vircators and Reflex Triodes can be regarded as lamps as Bremsstrahlung, since the radiation due to deceleration BRAKE lantoseis electrons. However, the classification is not common because the lamps are based on the creation of the virtual cathode, which acts as agent slowdown electrons, while lacking the magnetic field causes the spiral tracks, exploiting Gyrotrons for generating microwave radiation.

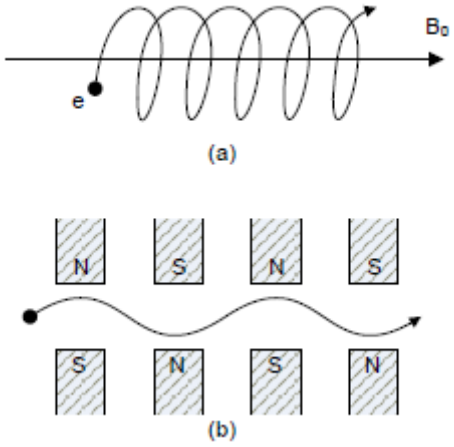

Fig. 3.7: Cases radiation Bremsstrahlung: (a) in a constant magnetic field and (b) a periodic magnetic field.

To produce or enhance the microwave radiation in a lamp, the electronic RH beam must carry some of the energy of the electromagnetic wave. In other words, a negative work should be brought by the microwave field in the electron beam. This work is proportional to the intensity of the high frequency electric field and the interaction length of the beam with it. Therefore, as the voltage of the beam increases, and thus the relativistic factor, they should also increase the dimensions of the lamp. Also, the electric field intensity of the wave generated can result in electrical breakdown in the tube, thus increasing the force; th output necessarily lead to large physical dimensions of the lamp. However, in large-field beam interaction lengths are very critical synchronization of the motion of electrons and the high frequency electromagnetic field.

4. Virtual Cathode Oscillators

The *Oscillators Virtual Cathode* (**Vir**tual **Cat**hode **O**scillato**rs** - ***Vircators***) Form a class of microwave sources based on the injection of an electronic de--term in a cavity, a current value greater than the local *maximum current, included defined by the space charge* (Space-charge limited current) this range. The gen- Scion has resulted in the formation of *virtual cathode*, Which is responsible for a number of processes involved and lead to the production of microwave radiation. With broad categorization of the previous chapter is the Vircators Bremsstrahlung lamps, but are completely the philosophy of key repre- sentatives of this group, the Gyrotrons and Free Electron Lasers. Invited poly- chnies *space charge* (Space charge devices), because the microwave production beginning in Vircators and variations are radically different from all other micro wave tubes.

The Vircators generally consist of two parts, the area of *diode* (Diode re- gion) or anode-cathode region (A-K), wherein the electron beam is accelerated, and the area in which the virtual cathode is formed. This region is called, and coun- weight shift (drift space), or idle space, where electrically isolated from the region of the passage. We can say that a Vircator like a triode with virtual cathode playing the role of the third electrode. Besides, the Vircator arose from the three-way lamps, after observations of the formation of virtual re- Methods and phenomena that accompany it. According to the notation which is presented in Fig. 4.1, the injected current in the aggregate space, to form the cathode eikoni- RH should be

$$f_0 J = J_{SCL[1]} > J_{SCL[2]} . \qquad (4.1)$$

In the above expression, *J0* is the current of diode (range [1]), which we consider passing the inert space (area [2]) through the infinitely fine mesh of alpha nodou. As mentioned in Chapter 2, the current of the diode is determined by the present law alte Child-Langmuir, relation (2.63), or the law *"3/2"*. With appropriate modifications, the liquidity but *J0* It can be expressed in relativistic area ratio (2.67), and finite geometries, relation (2.69). This is the maximum current of the diode, limited by space charge, where the cathode emits electrons at zero work function. With *JSCL [2]*, Denotes the maximum spatial stream of inert space (area [2]), as pro- rousiastei in paragraphs 2.6, 2.7 and 2.8. Meeting the above Treaty will

result in delayed portion of the electron beam by the strong space charge and forming a region *virtual cathode*. The theoretical development, described in paragraphs 2.6, 2.7 and 2.8, provides for maximum spatial streams where the ideal of infinite three-way reinforcement, the ideal shorted diode infinite reinforcements and symmetric electron beam into infinity Direc- fur magnetic field. In Vircators, the idle space is not included in any of those three conditions therefore the maximum spatial stream *JSCL [2]* It can not be determined accurately only be assessed using the above analytical models.

As previously mentioned, the virtual cathode is a region in which the electronic have lost kinetic energy, causing such portion be returned Fei to the anode or to accelerate in other directions. The appearance of the virtual cathode is the prerequisite and the phenomenon exploited by Virca- tors to produce microwave radiation.

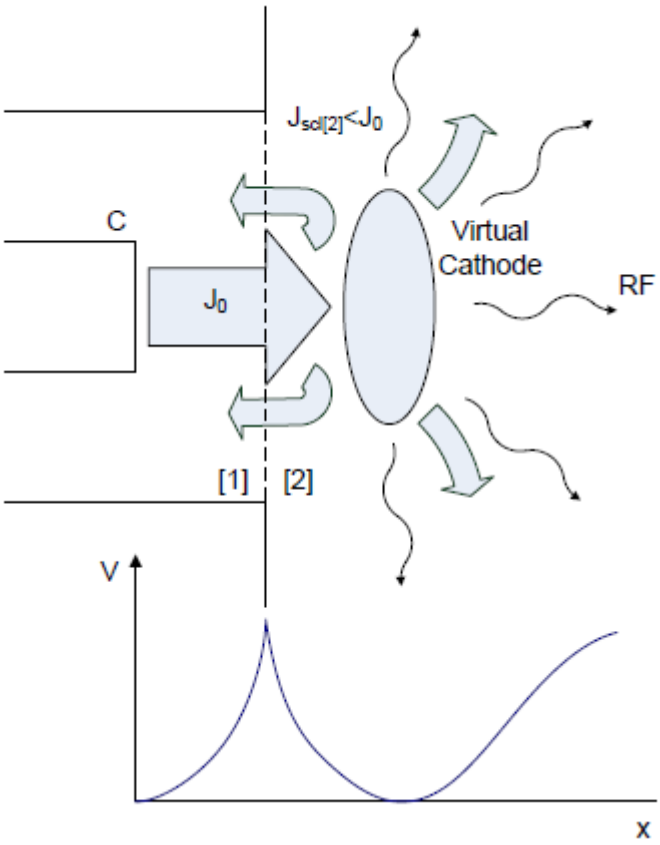

Fig. 4.1: The virtual cathode oscillator and the change in potential at the site. In [1] we denote the area of the diode, while [2] the inert space in which schimatize- Tai virtual cathode.

The basic processes that produce microwave radiation under conditions of emergence of virtual cathode oscillations is both the virtual cathode itself (virtual cathode oscillations), the other oscillations of electrons between the carried

sional and virtual cathode (electron reflex oscillations). Specifically, the "fysali- da" of electrons having decelerated to very low energies, which constitute the region of the virtual cathode, may be subject to local *oscillations plasma- Tosh* and spatial *load oscillations*. Equivalently, the *place* and *voltage* the import Connick cathode is unstable quantities, subject to temporal changes. The BRAKE lantoseis virtual cathode is directly linked to the density of the electronic package in the virtual cathode area and also depend on the existence of ions, either from individuals remaining air within the device or by metal atoms, which sublimed due to the strong current of the actual cathode and mesh anode. Therefore, vibration of eikoni- ment cathode directly connected to the local plasma frequency electronic de--term (beam frequency plasma). The phenomenon of oscillations trapped electronic s between the real and the virtual cathode and called *reflection* electrons (electron reflexing). These two mechanisms lead, in general, observation ness microwave signals at frequencies remote from each other, results confirmed experimentally ([45], [46], [47]).

The Vircators, to produce the required electron beam, usually driven by an impulse high voltage source and low internal resistance. Primarily used generators Marx, which are adjusted to provide maximum power at a relatively stable trend in low load conditions because the diode con- Methods - climb Vircator presents, at the time the mikrokyma- tive radiation observed ohmic resistance of a few tens Ohm. In fact, what happens is the beginning of a breakdown of the gap passage AK because of the high voltage applied between the cathode and the anode. However, before you bring oli- RH bridge the gap from the plasma between the electrodes, Fields was evoked tensions, arriving and $1010 V / m$, Forcing a large number of electrons move towards the anode with high accelerations. Despite what syntelou- phenomena are the anode-cathode region, the current always follows the law of the Child- Langmuir. Seemingly stream may *exceed* the value J0 for the passage calculated, for example, by the relationship (2.69). However, this is because the positive ions *counteract* to a degree *electronic space charge*And in addition the *plasma between electrodes* (Interelectrode plasma) contribute greatly of change of geometric characteristics of the diode, mainly *Diminishing* the apparent distance *d*Between anode and cathode and enlarging the area phenomenon *S* electrodes. These phenomena, however, encountered in the operation of the Vircator lamp and affect output, we will consider in detail below.

Regarding the rise of lamps, is commonly used grid of stainless steel in high permeability (> 50%) and aluminum foil (<20 microns), which allows a large part of the electron beam to pass unimpeded. In educa- tion way, a large part of the current of the diode can reach the area, which is characterized by a generally smaller, as mentioned above, critical spatial stream. The cathodes used in Vircators are usually formed with strong micrometric roughness, to facilitate the emission of electrons due be- pediakis the displayed intensity. In cases in Vircators chrisimopoiei- Tai magnetic field to maintain the electron beam about parallel to di- efkolynsi forming the virtual cathode and better trapping electrons between the real and virtual cathode.

4.1. Display Radiation Mechanisms in Vircators

On lamps Vircator, electrons are accelerated to the anode-cathode gap, per- ensure the rise, mesh-like or very thin metal foil in a space in which, because of the fierce space charge, some electrons of the beam stop grubbing completely, forming virtual cathode. The production of microwave radiation in a Vircator is attributable to vibrations of electrons between the real and virtual cathode (reflexing), secondly to vibrations and post falls situations of virtual cathode itself. Both these processes lead, in general, on observation of microwave signals at discrete frequencies together. The reflexing frequency calculated from the time it takes an electron, in order to travel from the cathode through the anode, the virtual cathode and be returned psei. The oscillations of virtual cathode in position and intensity directly related to the plasma frequency of the electron beam, which is injected into the inert space.

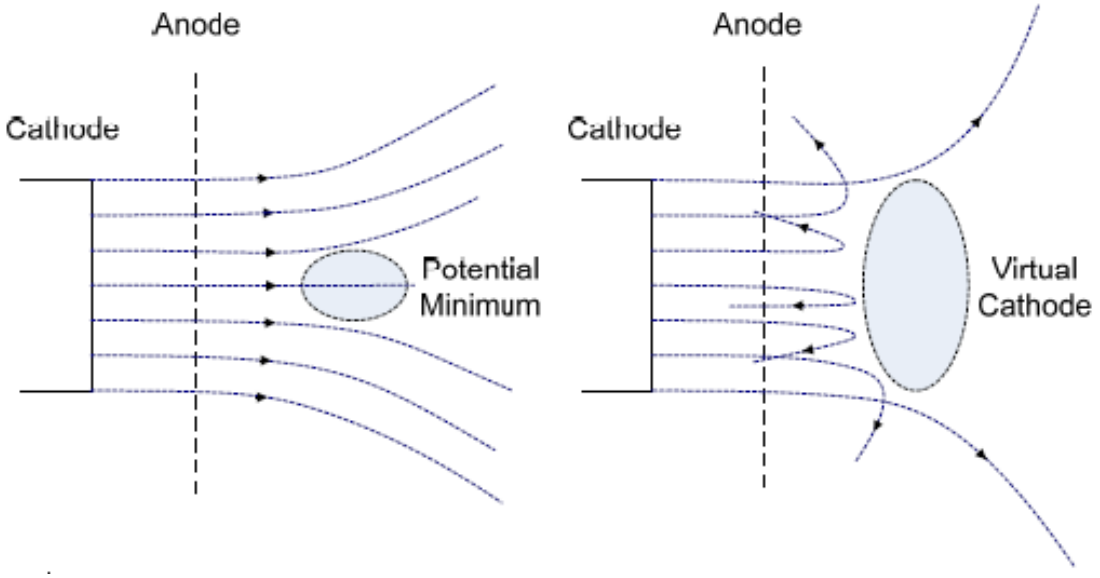

Fig. 4.2: The formation of a virtual cathode and the "explosion" of the electron beam. Left one shows the image of the beam, as the draft appears in potential due to the space charge. Without a magnetic field and charge neutralization, the beam gradually grew to deviate. Right we have the image of the package, only the virtual lays Give formed.

4.1.1. Reflexing Phenomenon

Assume that the stream released from the cathode and the anode has passed sufficiently large value so that part of the electrons following and passing the anode be retarded because of the developed space charge. D- that mentioned in paragraph 2.6 for the case of infinite three-way parallel reinforcement, virtual cathode will be created, ideally perfect symmetry

electronic and non-intersecting trajectories, just as much as the distance AK. And the pos- Namik will be around as long as the potential of the actual cathode. It can be seen that the non-infinite symmetry and chaotic behavior of the virtual cathode resulting in large variations in the location, extent and potential of virtual re- methods. However, in order to examine the phenomenon of reflection of electronic s, we will assume that the virtual cathode formed from the anode at a distance equal to the distance of the gap AK and that this capacity to its limits are equal to the pos- Namik cathode.

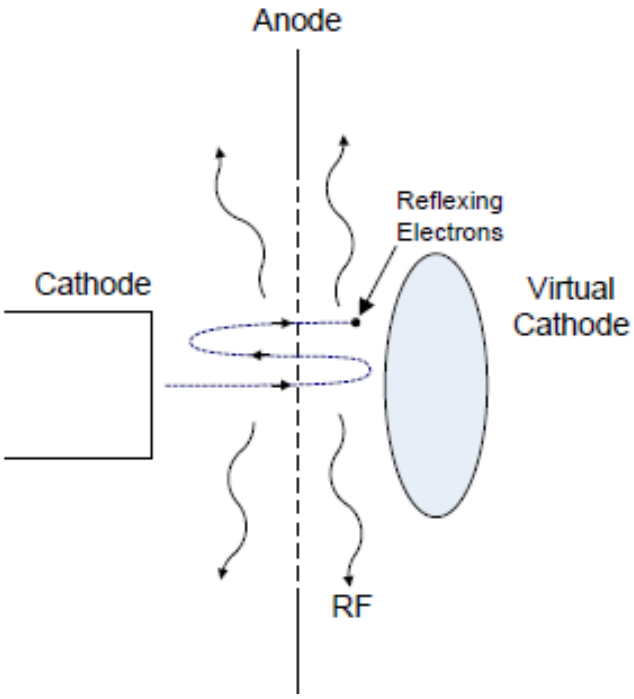

Fig. 4.3: Production of RF oscillations of electrons between real and virtual cathode.

An electron passing through the anode-cathode gap AK, since the virtual cathode formed accepts slowdown from the virtual cathode, stops and epitachyne- Tai again towards the anode. The total time required in order for the electrolysis ene perform a cycle in the order C-A-VC-A-C, theoretically equal to

$$T = 4t_{AK}, \qquad (4.2)$$

where *TAK* is the time taken for an electron to travel from the cathode to the anode, accelerated by the applied electric field in the gap. The electric field party, both in the gap A-R, and the space between anode and virtual lays Two clearly uneven.

Non Relativistic Approach uniform electric Field

We can estimate the time it will give us the time of motion (4.2), if we consider that the electric field is homogeneous. Since the relationship for non-relativistic ki-

ment of an electron in a homogeneous electric field (2.26), without initial velocity, we obtain that

$$ft_{AK} = \sqrt{\frac{2m}{e}}\frac{d}{\sqrt{V_{AK}}}\ , \tag{4.3}$$

where *d* is the rise distance - descent and *VAK* It is the voltage across the diode. In the above expression directly included the assumption that *Ex = VAK / d*. The frequency resulting from this simple homogeneous electric field is approximately

$$f_{fREFL} = \frac{1}{4t_{AK}} = \frac{\sqrt{V_{AK}}}{4d}\sqrt{\frac{e}{2m}}\ . \tag{4.4}$$

Therefore, for a Vircator a typical anode-cathode spacing value equal to 15mm and diode voltage equal to 200kV, the assessment of the above frequency oscillator reflex Dawson is 2.2GHz. The above expression is a first demonstration of the dependence of the frequency of reflex oscillation of the square root of the voltage of the diode Vircator [48] and the inverse of the frequency dependence from the gap A-R, *d* [49] i.e.

$$f_{fREFL} \alpha \frac{\sqrt{V_{AK}}}{d}\ . \tag{4.5}$$

Relativistic Approach uniform electric Field

We can return to the equations of motion (2.15) and consider the event that the relativistic factor is equal to one. In this case we have that

$$\frac{d}{dt}(c\ mu) = eE\ , \tag{4.6}$$

therefore replacing the value of y, we obtain

$$\frac{d}{dt}\frac{mu}{\sqrt{1-u^2/c^2}} = eE\ . \tag{4.7}$$

Conventionally, with *m* denote the mass of the electron, with *e* elementary cargo TLC and *E* the electric field accelerates. Completing the above relationship, for non deniki initial velocity, we obtain that

$$\frac{mu}{\sqrt{1-u^2/c^2}} = eEt\ . \tag{4.8}$$

Solving this expression in terms of speed shows

$$u(t) = \pm \frac{eEt}{m\sqrt{1+\left(\frac{eEt}{mc}\right)^2}}\ . \tag{4.9}$$

From this relationship for speed, we can calculate the temporal variation of the position, based on the general expression $u = x$. If we define the quantity $m = eE/m$, to *simplification of performances, The integral of the speed in time gives*

$$x(t) = \pm \int_0^t \frac{m}{\sqrt{1+\left(\frac{m}{c}\right)^2 o^2}}\, odo, \tag{4.10}$$

where we believe that the initial position of the particle is x (0) = 0. Setting new integration variable $q = mx/c$, we have that

$$x(t) = \pm \int_0^t \frac{m}{\sqrt{1+\frac{mx}{c}}}\, od\, o = \pm \int_0^t c\, \frac{\frac{mx}{c}}{\sqrt{1+\frac{mx}{c}^2}}\, do \Leftrightarrow \tag{4.11}$$

$$x(t) = \pm \frac{c^2}{m} \int_0^{q=\frac{mx}{c}} \frac{q}{\sqrt{1+q^2}}\, dq.$$

For the indefinite integral of the above expression holds that $\int \frac{q}{\sqrt{1+q^2}}\, dq = \sqrt{1+q^2}$, super-

fore we come to the result

$$x(t) = \pm \frac{c^2}{m}\left(\sqrt{1+\left(\frac{mt}{c}\right)^2}-1\right). \tag{4.12}$$

From the expression for the shift, we can solve for the year *t* and calculate the required duration of transition from the cathode to the anode, an electron moving in a uniform electric field with relativistic velocity of. If we replace the quantity $m = eE/m$and assume that $E = V\,AK/d$, the *positive solution for the period of transition from the anode to the cathode is*

$$t_{AK} = \frac{d}{\sqrt{V_{AK}}} \sqrt{\frac{2m}{e} + \frac{V_{AK}}{c^2}}, \tag{4.13}$$

and corresponding frequency equal to $f_{REFL} = \frac{1}{4t_{AK}}$:

$$f_{REFL} = \frac{1}{4t_{AK}} = \frac{\sqrt{V_{AK}}}{4d} \sqrt{\frac{ec^2}{2mc^2 + eV_{AK}}} . \tag{4.14}$$

Other Approaches to Frequency Reflexing

In practical units, the reflexing frequency can be accessed from [6]

$$f_{fREFL} \cong k \frac{b}{d} \text{ [GHz]}, \tag{4.15}$$

the distance A-C, d, expressed in cm, and *k*= 2.5 ~ 7.5. For small voltages (non schetiki- STICK area), the multiplier *k* takes the value of 2.5, while for major trends, where the speed of the electron quickly approaching the speed of light in the gap, the rate shall be taken 7.5. This type is more useful in relativistic BRAKE ye, because the multiplier quickly converges to the value 7.5. For large diode voltages, the Woo [50] suggested that the reflexing frequency can be estimated better than the expression

$$f_{fREFL} = \frac{4.77}{02d} \ln\left(c0 + c\sqrt{-1}\right) \text{[GHz]}, \tag{4.16}$$

wherein the distance A-C, d, expressed in cm. For lower voltages, the above law me- tavalletai like $fREFL$ a $V_{AK} / \sqrt{d}$. Generally, Non-homogeneous potential in the region *diode, Transition time from the cathode to the anode can be calculated from the gen- eral expression*

$$t_{AK} = \int_{x_C}^{x_A} \frac{1}{u_e(x)} dx . \tag{4.17}$$

These proposed models for reflex oscillations are summarized in Fig. 4.4, for two cases- anode-cathode spacing, 15mm and 25mm. The relativistic approach (4.14) converges very quickly to a constant value, which is determined sub- stances urban by the time it takes a particle to the speed of light to pass through the gap passage. The model Woo, (4.16), although small Accelerating potentials gives higher frequencies, following the non-relativistic approximation (4.4) until the 2.5MeV, and from then on starts and it tends to a limit value.

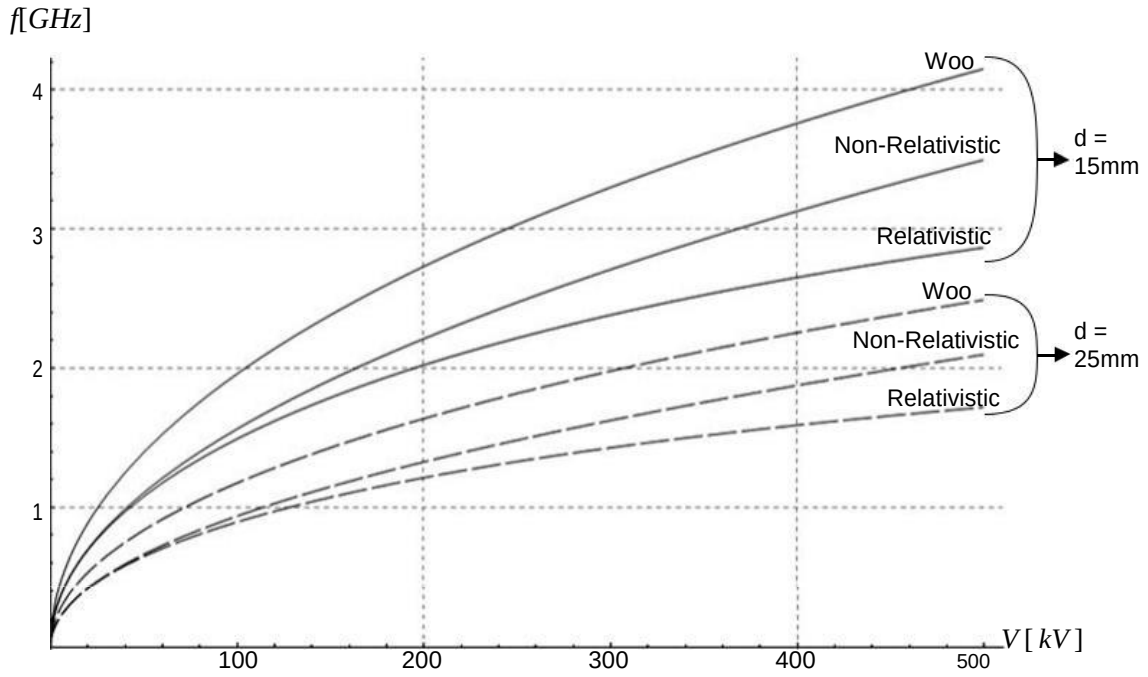

Fig. 4.4: The frequency of reflex oscillations under three theoretical models, two anode-cathode distances.

These models for reflex oscillations applied when the electric field EI- so homogeneous and when the distance of the virtual cathode from the anode is equal to the distance of the actual cathode from the anode. In fact, the area of the virtual cathode far are clearly defined, which contributes signifi- nificant uncertainty in these idealized approaches.

4.1.2. Oscillations of a Virtual Cathode

On lamps Vircator, besides the electrons oscillate between real and virtual cathode, there another key mechanism production mikrokyma- tion radiation. The dummy cathode may be a radiator, because the oscillations both in place, and in the spatial charge or, equivalently, the possibility cial [6], [47]. The virtual cathode oscillator behaves as a damper, which offers energy through electron beam that feeds load. The space charge of virtual cathode oscillations empirically placed between the frequency ([47], [50], [51])

$$f f_p \le f_{OSC} \le 2\sqrt{Fr.}\, f_p , \qquad (4.18)$$

where in here *fp* express frequency plasma electron beam. In literature the relativistic plasma frequency of the electrons of the beam as it will normally attributed [52]

$$f o h_p^2 = \frac{ne\,e^2}{cme} \quad \text{or} o h_p^2 = \frac{ne\,e^2}{e_0 cme} , \qquad (4.19)$$
$$4Fr.$$

for amounts expressed in Gauss system or SI respectively. However, since the night talanto-plasma electrons relates direction generally parallel to the axis of the ki- ent, it is preferable to use the longitudinal relativistic mass (longitudi- nal relativistic mass), which is equal to $m_{\|}$ = *c* 3*m* [16]. Accordingly, the plasma frequency
for relativistic region should preferably be taken as oh_p^2 = 4*Fr.* (*ne e* 2 / $c^3 me$) or
oh_p^2 = (*ne* $e^{2/}$ $e_0 c^3 me$), for amounts denominated in a system Gauss or SI respectively. In above expressions with *ne* denote the density of the electron beam and *c* the relativistic factor of the electrons when they pass through the anode. From the above density neutralize any charge from the presence of positive ions tion may be removed, so that the charge density of the electron beam is:

$$n_{e,eff} = n_{e,beam} - n_{ion} . \quad (4.20)$$

The expression for the beam plasma frequency can be written into practical units as [6]

$$ff_p = 4.08\sqrt{\frac{J\ kA\ /\ cm^2}{bc}}\ [\text{GHz}] \quad (4.21)$$

In [52] it would appear oscillations of virtual cathode made in characteristics frequencies

$$ff_{OSC} = \sqrt{+ 2Fr.\ f_p\ \ k - \frac{1}{2}}\ , \text{K} = 0,1,2, \ldots \quad (4.22)$$

they receive, for k = 0, the center frequency of oscillation of virtual lays period is $fOSC \cong 2.2\ f_p$, K = 0,1,2, ... In [53], the frequency of the virtual oscillation
cathode was estimated to be $fOSC \cong 2.14\ f_p$.

4.2. Factors Affecting the Microwave Output

Easily see that the basic processes that lead to production for Asia Mi- krokymatikis radiation in a Vircator, depend on a number of parameters which, during the phenomenon, far constants are. For examples but the oscillation of electrons between the real and the virtual cathode is strongly dependent on the position of the virtual cathode, the actual distance of the anode and cathode, which decreases from the plasma generated between the electronic Dio, and by voltage applied to the passage of the Vircator. The position and the oscillations of the virtual cathode depending on energy, which enters the inert space the electron beam and the electron density and hence rheumatoid density beam, *J*. The power reflected from the virtual Down

Methods for the region of the passage of the Vircator affects the spatial density of the diode currents, Tos, and thus the electron beam as a whole. Moreover, the voltage and current supplied to the passage from the external circuit, such as a generator Marx, show significant temporal variation, so we can not talk about sta- kets external parameters in an array with light Vircator. Still, the virtual cathode itself presents chaotic behavior, since the load reflecting to the anode, the plasma oscillations performs the spatial distribution of load, anything but clearly some are. Finally, several parameters even as the materials of the anode and the cathode, the vacuum in the tube and the microwave characteristics koilo- Community within which the virtual cathode is formed, are important in the charac- teristics of a microwave pulse Vircator.

4.2.1. Properties Gap Anodou Kathodou

Assume without loss of generality, that we refer to Vircator negative driving, in which the rise and the body kept at a reference potential and the cathode driven the strong pulse of very high voltage of negative polarity. As a result, the cathode emits strong field emission current from microtip and abnormalities in geometry, which, in the next step, resulting in a risk of explosion of material from the cathode and progressively cover the surface lays output plasma. The plasma generated by the explosive emission (explosive emission) is responsible for the strong currents for very large microwave iota scheis but for the short duration of the phenomenon radiating.

The plasma cathode serves as an ideal descent, which provides arbitrarily me- turkey many electrons in the passage at zero output task. The currents in an explosive emitting diode is larger than any configuration lays thermionic cathode output or field emission. The explosive emitting diodes are the only ones They can contribute tens kA power per cm2 of surface. However, the equivalent import so the spread of the plasma at the interface due to thermal processes diffuse ing and the strong electric field, leading to bridge the appointed period of a conductive plasma. Since bridging or *collapse* the gap, the diode ceases to accelerate electrons and therefore the electron beam that feeds the virtual cathode disappears. The explosive electron emission from cold con- Methods is very simple method of producing package. The package, however, has a large noise from eo (not monoenergitiki) due to the dynamic variation of the characteristics of the diode.

The materials of the electrodes can be varied: stainless steel, aluminum, copper, graphite. These are an important parameter in the behavior of splitting of the vacuum diode. The metal used in the electrodes, may still have a significant amount of adsorbed gas, such as hydrogen (H, H2), water (H2O) and other gases (CH4, NH3). Also, the electrodes may be coated by metal oxides, at a height of several atomic layers, as well as to have deposits of organic and non compounds on their surface. The material of the electrodes, the prosrofi- me gases, the geometry and other factors play a critical role in the rate of spreading of the plasma in the diode and the behavior of the collapse of the gap.

The creature in the path can come from both the rise and the laid structure. The materials of the electrodes and the purity of playing an important role in spreading speed diilektrodiou plasma. Depending affects the original Deci- anode-cathode distance and the associated electric field that occurs in the fairway. The propagation velocity of the plasma cathode and the anode can kymaine- Tai area of 1cm / microseconds up to 10cm / microseconds [54], resulting in the passage gap of several mm a useful life up 50nsec only. This speed is mainly dependent on the local plasma temperature, which can anerche- Tai to several thousand degrees.

In one Vircator, the cathode is usually circular in shape, with a radius *a*. If agnoisou- the phenomena of limbs, the current in the diode is initially

$$ISCL = J\,SCLFr.\,a^2 \quad , \tag{4.23}$$

or, in practical units,

$$ISCL \cong 2.33 \frac{\frac{Fr.a}{2}}{d[\,cm]} \frac{[cm\,2]\cdot V[\,MV\,]\,3/2}{2} \text{ [KA]}, \tag{4.24}$$

as required by law Child-Langmuir. In the above expression, d is the distance alpha nodou- cathode. The expansion of the plasma electrodes results in enlargement of the front of the cathode and the reduction in the distance between the reinforcements. E- pomenos, the area of the cathode can be approximated by the expression

$$S(t) \cong Fr.\,r^2(t) \cong Fr.\,(a + u\,K\cdot t)^2 , \tag{4.25}$$

where *uK* the spreading speed of the plasma cathode, a phenomenon the- oroume that occurs in every direction.

Similarly, the anode-cathode distance, initially equal to *d*Decreases with time at a rate of - $u \cdot t$Hence the apparent distance of reinforcement is

$$d(t) \cong (d - u\cdot t)^2 . \tag{4.26}$$

In this relationship, *u* It is the cumulative spread speed of cathode plasma alpha nodou in the fairway.

As will be appreciated, the amount of current passing through the passage increases with a rate virtually fourth grade, since the radius of the cathode increases linearly, so the area in square rate with the amount *d2* likewise decreases with square rate with respect to time. Therefore, the current of the diode, responsible primarily for the plasma frequency Vircator, vary with time, and the change is done rapidly, while the spreading speed of the plasma becomes greater. Moreover, the apparent decrease in the distance between reinforcement directly affects the frequency of reflex oscillations,

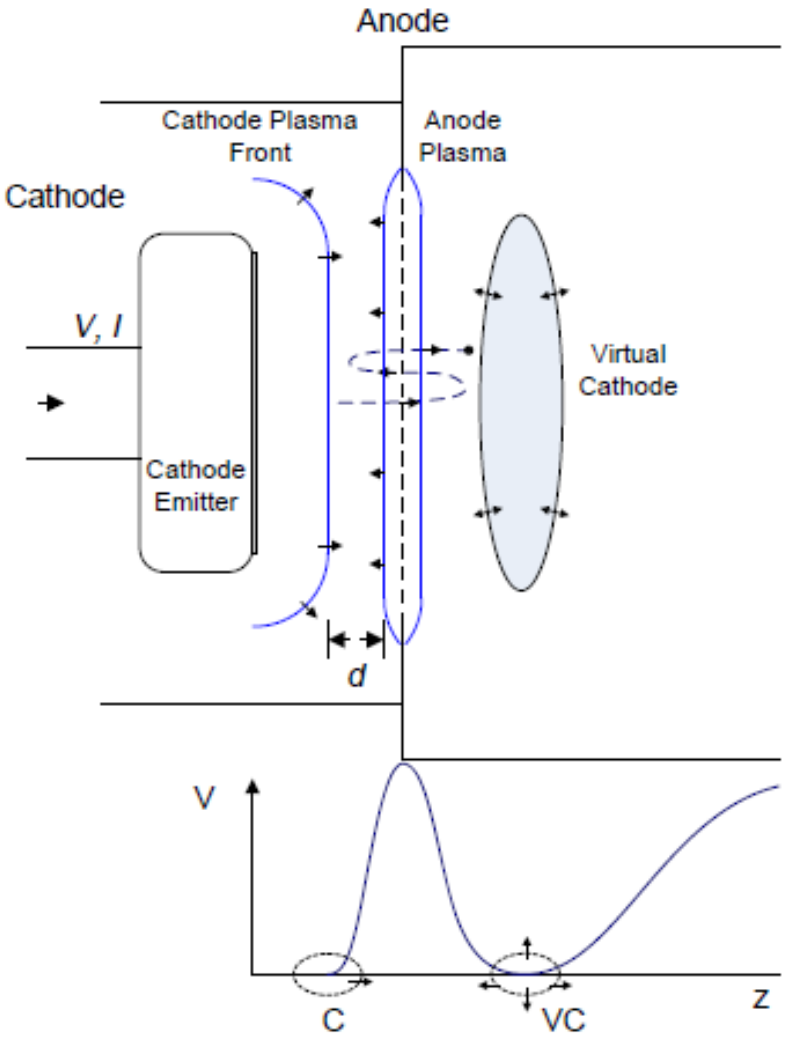

Fig. 4.5: Schematic depiction of the change of the characteristics of the diode.

pushing, inversely, to higher prices. Already, intuitively, it is a- ntilipto that pumping ever higher current from the source that feeds the passage of light results in a change of trend, *V*, Thereby further re- shifting the frequency of oscillation reflex, the energy of the elec- tion beam and turns the plasma frequency of the Vircator.

4.2.2. Voltage and Current Driver

Driving a Vircator about trends, starting at 100kV and reach up and 5MV. Currents capable of producing strong microwave radiation, are in the range of tens or hundreds of kA. As is understood, no source driver is not able to provide such amounts of power with a stable and no fluctuations. The most common method of driving Vircators performed multistage krousti- tions generators Marx. This method consists in charging a capacitor bank in a medium-high voltage and then discharging them in series to the lamp. As a result, the driving voltage of a diode Vircator is the product of the cargo tisis voltage capacitors on their total number. However, we find it easy

voltage and the driving current depends on the total energy stored in the densely knoton and the resistance macroscopically showing the passage of light. Both the finite stored energy, capacity and nonlinear sys- nartisi current-voltage vacuum diode constitute a source-load system with exo- ha nonlinear behavior. Therefore it is impossible to stably maintain the voltage and current of a Vircator.

A direct consequence of non-stability voltage and drive current is the slippery importance of output frequency. We have seen that the frequency reflexing of electrons depends on the square root of the tension, Fig. (4.5), which we repeat here:

$$\text{T}_{fREFL}\text{a} \qquad \frac{\sqrt{}_{V_{AK}}}{d} \; . \tag{4.27}$$

Moreover, the frequency oscillation of the virtual cathode depends both on the energy of the beam (voltage) and the current of the diode. For example, an estimate of the oscillation of the virtual cathode is determined by the empirical expression (4.21), which we mention again here:

$$\text{f}f_p \qquad = 4.08\sqrt{\frac{J\ kA\ cm^{-2}}{bc}} \quad [\text{GHz}] \tag{4.28}$$

It is obvious that the current and the driving voltage directly affect two key microwave radiation producing devices. Variation of voltage and liquidity Matos during phenomenon, result in slippage of frequency output of a Taq Vircator, by any mechanism if it is derived. In the complexity of driving problem can be added the change of geometric characteristics of the diode, because of production and plasma expansion, according to what we mentioned in the previous paragraph. The transient behavior of a Vircator, which is driven by capacitive source, is treated in more detail in the following paragraph, 4.3.6.

4.2.3. Effect of Magnetic Field

The Vircators form a class-tales in which the magnetic field is not required, except in the case of Reditron ([55], [56]), as will be presented in paragraph 4.5.5. The Reditron uses rise to ring opening by passing similar tubular beam (annular beam), thus the magnetic field necessary for the alignment. But apart from this case, the theoretical SO and experimental results regarding the use of magnetic field in reflex tri- ode Vircators and axial Vircators are vacillating as to whether the use magniti- tion field improves the strength or not. For example, the output of the reflex triode dramatically reduced by applying a magnetic field, ([57]), which is developed and theoretically [58] for the case of coaxial Vircator.

The presence of magnetic field appears to potentiate the presence of only frequencies: at the cost of the total energy of the microwave pulse ([59]). In

weak magnetic fields, virtual cathode has greater freedom spatial kinise- s, thereby producing radiation at a plurality of harmonics in a chaotic manner. The energy of the generated microwave is bigger, but the range is clearly smaller relevance.

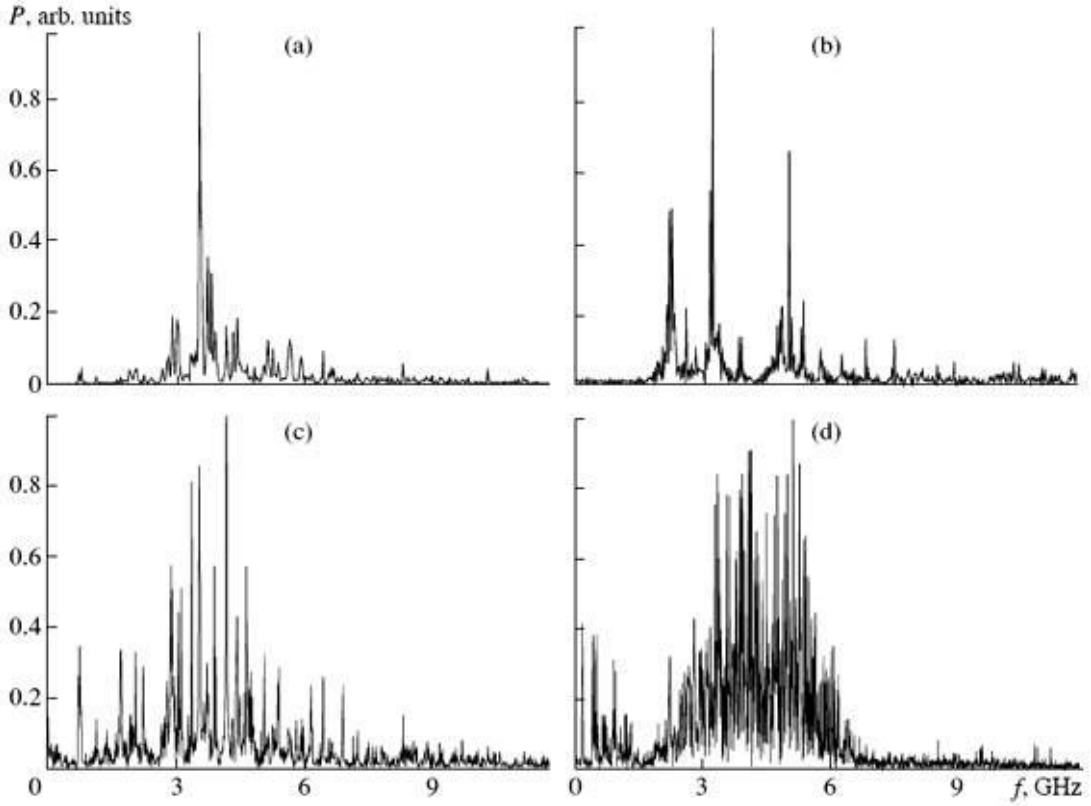

Fig. 4.6: Spectrum microwave output, imposed for various magnetic fields. (A) 40kG, (b) 20kG, (c) 6kG, (d) 0kG. From [59].

In experiments it has also been observed in other cases increasing frequency by applying a magnetic field [60], and that the magnetic field has no effect on output frequency, while having little negative effect on the strength of the bulb ([61], [62]) . From theoretical studies also seem to be no cases in which the inhomogeneous field increases performance because Gyrotron effect ([63]). In the case of Reditron, the microwave radiation is absent when there is no magnetic field, but here are de- an optimum field value, in which the yield is highest ([64]).

4.2.4. Void in Lights Vircator

The level of vacuum in Vircator tubes and Reflex Triode is a parameter with relative tolerance. Intuitively, better vacuum will result in a longer lifetime of the virtual cathode, however, the generated plasma from the cathode and upward structure seems to be much more significant effect on persons and ion concentration in the interaction region. Furthermore, a gap of about 10-4Torr implies a density of atoms of the order of 3 · 1018m-3. An electron beam 1kA, 100keV and section 5cm2, (numbers are very conservative for a Vircator), has electron density

2 · 1019m-3, almost an order of magnitude above. Considering the likelihood ioni- tion of a person from the electron beam, the effect of residual gas in the behavior of a Vircator seems to be little space for the bulb to 10-4 Torr. In [65], as in the present study (see. Par. 6.5), it seems that mikrokyma- tive output of a Vircator remains equally strong vacuum even *worst* 10-3 Torr.

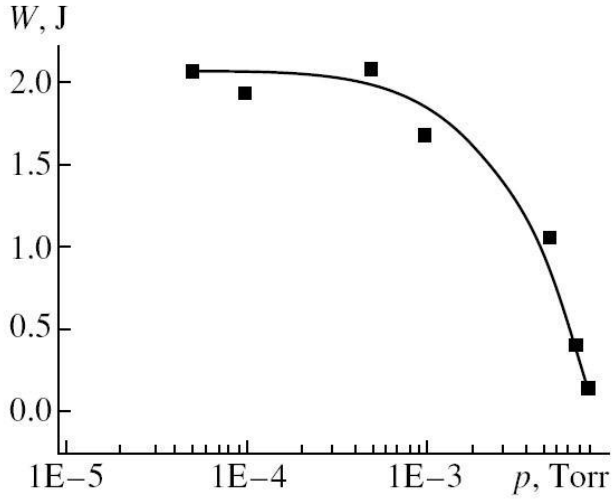

Fig. 4.7: The energy of the microwave pulse a Vircator, according to the in- vacuo ithin lamp (Selemir et al., [65])

However, there appears to be a threshold around 10mTorr, above which is of Conduct the Vircator changes drastically: the diode breaks down more quickly, more in gas decomposition mechanism (Townsend and drain) and filled with plasma, while Asia Mi-krokymatiki output practically disappears. In Reflex Triode of Kapetanakos et al. the vacuum tube is 10-4 Torr ([48]), while in the Reflex Triode [66], the gap stands at about the same level, 7.5 · 10-5-10-4Torr. In other cases, such as the C-Band axes sulfonic the Vircator [67] and Vircator - Reflex Triode of [68], the vacuum is maintained at 10- 5Torr. In Reditron oscillator of Davis et al., The gap is at 3 · 10-5 Torr ([55]). In other reports the vacuum is maintained at even lower levels, but it seems that something tech- TolC not important.

The number of the lamp can be estimated from the ideal gas law,

$$PV = NkT\,, \tag{4.29}$$

where *P* is the pressure, *V* volume, *T* the temperature, *k* the Boltzmann constant, and *N.* the number of gas atoms in the volume V. For convenience we use the relationship Avogadro, that at 273K and a pressure 1atm, 6.023 1023 atoms ideal gas occupying a volume of 22.4 lt.

The density of electrons in the electron beam can be calculated from the relationship $J =$ *trailer* Substituting $J = I_{beam}/Sbeam$, $u = bc$, $b = 1 - 5112/(511 + Ebeam[\ keV\ ])^2$ and $p = ne/e$.

Tab. 4.1: Pressure and Number of People Gas at Normal Temperature

Pressure [Torr]	Concentration of People [m-3]
10^{-2}	3.2 1020
10-3	3.2 1019
10-4	3.2 1018
10-5	3.2 1017
10-6	3.2 1016
10-7	3.2 1015

Tab. 4.2: Density Differential Ties, Cross Section 10cm2

Electronic Beam	Electron concentration [m-3]
1kA, 100keV	~ 1019
1kA, 300keV	~ 7 · 1018
5kA, 100keV	~ 5 · 1019
5kA, 300keV	~ 3.5 · 1019
10kA, 300keV	~ 7 · 1019
10kA, 600keV	~ 6 · 1019

It seems that the dense electronic packages with load densities of 1019-1020 [m-3] antagonize one equivalent dense gas when the pressure is ~ 10-3Torr. With this observation we can conclude that Vircators work as expected, when the gas pressure of the lamp is at most equal to the electron density of the injected electron beam.

The iterative operation of Vircator results in release and accumulation of gas, which comes from collisions of electrons with cor- but lamp. The pressure prevailing within the tube affects the course of micro wave pulse, as it enhances the phenomena of collapse of the gap of the passage and elimination of the virtual cathode from background ions. Therefore, the party system pump station lamp must be constantly connected and in operation, in order to ensure the iterative mode. For light having undergone adequate re-tharismo, there is an empirical formula, linking the length of micro-wave pulses, the pumping speed of the vacuum and the frequency of repetition. This relationship is the [69]

$$t[\,ns] < 20\,\frac{S[lt/sec]}{R[\,Hz]}\quad , \tag{4.30}$$

For example, we can achieve microwave pulses of duration 100nsec, with a repetition rate of 1kHz, if the pumping speed is 5000lt / sec. Of course, such a pumping rate is unrealistic. If instead we use a realistic pumping rhythm, which are the 50lt / sec, we can theoretically achieve pal- mousse duration 100nsec repetition rate 10Hz.

4.3. Classical Method Design Vircator

In one design Vircator, taken in principle in mind both widely acceptable microwave radiation producing devices. The first of these is the importance of electrons trapped between the real and the virtual cathode mechanism laid invites reflexing frequency. The second mechanism is associated with the "density" of import conical cathode. This process is related to the frequency of plasma n Electronics beam (beam frequency plasma).

4.3.1. Design Frequencies

The traditional approach is to consider the formation of a virtual cathode at a distance approximately equal to the actual distance of the cathode-anode, *dAK*. As mentioned above (see. Παρ. 4.1.1), reflexing frequency can be approximated as a non-relativistic

$$f_{REFL} = \frac{1}{4t_{AK}} = \frac{\sqrt{V_{AK}}}{4d}\sqrt{\frac{e}{2m}}\ , \qquad (4.31)$$

or relativistic as

$$f_{REFL} = \frac{1}{4t_{AK}} = \frac{\sqrt{V_{AK}}}{4d}\sqrt{\frac{ec^2}{2mc^2 + eV_{AK}}}\ . \qquad (4.32)$$

According to the above, the frequency reflexing, at moderate voltages can pre sengisthei from expressions

$$f_{REFL} \cong k\frac{b}{d}\ [\text{GHz}], \qquad (4.33)$$

wherein *k*= 2.5 ~ 7.5, as we go from small voltages to relativistic region. This type is more useful in relativistic tendencies because the multiplier quickly converges to the value 7.5. At higher voltages, the most widely used and diadedome- screen relationship Woo,

$$f_{REFL} = \frac{4.77}{02d}\ln\left(c0 + c\sqrt{-1}\right)[\text{GHz}], \qquad (4.34)$$

with the *d* used in cm.Charaktiristiko all above expression is inversely dependent on the distance *d=dAK* and looser straight accessories importance than the voltage of the diode, *VAK*.

We mentioned in par. 4.1.2 that the second production process radiation on Vir- cators related to the 'density' of the virtual cathode. This process is co dedemeni the plasma frequency of the electron beam (beam frequency plasma).

In the non-relativistic region, the plasma frequency of the electron cloud schetize- Tai with density according to

$$0 \quad h_p = \sqrt{\frac{ne^2}{e_0 m}} \quad . \tag{4.35}$$

In relativistic regions, the plasma frequency is usually obtained as a

$$oh_p = \sqrt{\frac{ne^2}{e_0 cm}} \quad , \tag{4.36}$$

where the denominator put the relativistic mass of the electron. This item uses live some attention because if we talk about longitudinal oscillations, should take into account the longitudinal inertial mass, which equals *g3m*, Ie

$$oh_p = \sqrt{\frac{ne^2}{e_0 c^3 m}} \quad . \tag{4.37}$$

Therefore, for operations over 500keV, wherein the coefficient c is equal to 2 and alpha nevainei rapidly estimated beam plasma frequency can vary significantly. The oscillations of virtual cathode empirically placed in the area

$$f p \le f OSC \le \sqrt{2} Fr. f p \; . \tag{4.38}$$

The plasma frequency of the beam, as we can see, depends on the density of the electron beam and its energy via the agent *c*. To calculation Excellence density electron beam, the known types of current density used

$$J = trailer = ne\, bc. \tag{4.39}$$

For a beam radius applies

$$J = \frac{I}{Fr.a^2} \quad , \tag{4.40}$$

therefore

$$n = \frac{\frac{I}{Fr.a^2 e}}{bc} \quad , \tag{4.41}$$

hence

$$oh_p = \sqrt{\frac{Ie}{e_0 mFr.a^2 bc}} \quad , \tag{4.42}$$

where we use the relativistic mass *gm*. In the above relation *pa2* It is the cross-sectional area of the beam, and *b* It is the ratio of the velocity of the particles relative to the speed of light. With *c* denotes the relativistic factor Lorenz. Ypenthymizou- with that where neutralization of background ions, the rate of thrust of the narrowing space charge is introduced

$$p = p_0 (1 - f_e) = \frac{I}{Fr.a^2 bc} (1 - f_e). \tag{4.43}$$

The rates *b* and *c* related to the energy of the electron, according to

$$b = \sqrt{1 - \frac{511}{511 + V[kV]}^2} \tag{4.44}$$

and

$$c = \frac{511 + V[kV]}{511} = 1 + \frac{V[kV]}{511}. \tag{4.45}$$

According to the above, the expression for the beam plasma frequency can be written into practical units as

$$f_p = 4.08 \sqrt{\frac{J\,kA\,cm^{-2}}{bc}} \quad [\text{GHz}] \tag{4.46}$$

4.3.2. Diode Area

In Vircators output of the electron beam becomes explosive electronic emission from the cathode, under the influence of a very strong electric field. The emission of electrons starts locally with type field emission devices Fowler-Nordheim or combined broadcast Thermal-Field (broadcast Schottky). Very quickly, the cathode undergoes melting, is covered by the plasma and the electron emission switches to release Child-Langmuir. The front of the plasma acts as ideal descent, providing arbitrarily large number of electrons in the fairway. Ideally passage threatens resources plates has a maximum current density, limited by the space charge, equal to

$$JSCL = 2.33 \cdot 10^{-6} \frac{V^{3/2}}{d^2} \quad [\text{A / m}]. \tag{4.47}$$

The above relationship is known n*omos Child-Langmuir Flat diode*In SI units. In terms of the commonly occurring sizes and pulsed relativistic mikrokymati- tions lights, the Child-Langmuir Law on the flat path can be written as

$$JSCL = 2.33 \frac{V[MV]^{3/2}}{d[cm]^2} \text{ [KA / cm]}, \quad (4.48)$$

while, according to what has been mentioned in par. 2.5, for the case of relativistic n-lektronion, the relationship to the infinite diode can be written as:

$$JSCL = 2.71 \frac{1}{d[cm]^2} \frac{V[MV]^{1/2}}{0.511 + 1}^2 -.8471 \text{ [KA / cm]}^2. \quad (4.49)$$

The cathode is generally circular in shape, with a radius *a*. If we ignore the effects of the limbs, the current in the diode is initially

$$ISCL = J\,SCL Fr.\, a^2, \quad (4.50)$$

or, in practical units,

$$ISCL \cong 2.33 \frac{Fr.a^2 [cm^2] \cdot V[MV]^{3/2}}{d[cm]^2} \text{ [KA]}. \quad (4.51)$$

For *circular* descent with finite radius *a* and electrode spacing *d*The maximum power of fire a density is observed:

$$J_{SCL\,2\text{-}D} \cong 1 + .2647 \frac{d}{a} + 0.0058 \frac{d^2}{a} J_{SCL,\,1\text{-}D}, \quad (4.52)$$

in other words, the spatial density of the current slightly increases, these phenomena limb.

From the expression of spatial stream, we can calculate the apparent alpha ntistasi gap

$$Z = \frac{V}{I_{SCL}} = \frac{V}{S \cdot JSCL}. \quad (4.53)$$

Note that the gap due to plasma expansion phenomena, presents dynamics. The anode-cathode distance decreases with re- rose of time, at a speed which can range from 0.1 cm / microseconds up to 10cm / microseconds. The collapse speed of the gap depends on the material and the condition of the electrodes, the applied voltage and the partial pressure of the background gas present in the passage area. Furthermore, the phenomenon emva-nearly the reinforcement can be varied and in particular to increase, as the plasma

surrounding the cathode, the embracing like luster and extends radially in all directions. Therefore the diilektrodio plasma affects both the rising distance - re- Methods *dAK*, And the size, particularly the cathode, S.

4.3.3. Electronic Beam

To create a virtual cathode in an electron beam, should the value of the current to exceed a threshold value. The electron beam, as long as there is no charge neutralization of positive ions background is always deviant. In an electron beam without charge neutralization, which is kept focused on an infinite magnetic field, the maximum value of current that can pass calculated as

$$IL \approx 17 \frac{\left(C^{2/3}-1\right)^{3/2}}{1+2\ln\left(b/a\right)} \text{ [KA]}, \qquad (4.54)$$

and even suggested the expression

$$IL \approx 8.5 \frac{\left(C^{2/3}-1\right)^{3/2}}{\ln\left(b/a\right)} \text{ [KA]}. \qquad (4.55)$$

Higher current injection attempt by the values in the above production models, leading to virtual cathode forming the axis of the beam. Thontas still trying to channel more current to the beam, the virtual cathode deposits continuously receives greater extent in the stack and moving closer to im- minus insertion.

To establish descent in a shorted diode infinite plates, should the price of the spatial power to overcome the momentary value of 8*JSCL* and transfers dropped less to a value 4*JSCL*. Speaking infinite shorted diode with distance reinforcement *d* and beam energy *V*The *JSCL* in this case is nothing more than the equivalent of the Child-Langmuir Law

$$JSCL = 2.33 \cdot 10^{-6} \frac{V^{3/2}}{d^2} \text{ [A / m]}. \qquad (4.56)$$

For cases where the electron beam is not limited by a strong magnetic field, the principle to display virtual cathode is channeled stream "significantly larger" than the sizes laid down in the one-dimensional theory. In any arrangement suitable customize theory electron beam and diode infinite plates to estimate a current threshold required for creating virtual cathode conditions.

4.3.4. Magnetic Field

In order to maintain a relatively constant cross-section of the beam, the required long gnitiko field should be at least

$$B_{\text{"Inf"}} \sim \frac{0.34}{r_b}\sqrt{\frac{I_b}{8.5bc}} \quad [\text{T}] \tag{4.57}$$

as we have stated in par. 2.8.3. In this magnetic field, the electrolysis JIA are gyrosychnotita, which is, in practical terms,

$$fc = \frac{c}{2F_{r.}} = 28 \cdot B_{0h} \text{ [GHz]}. \tag{4.58}$$

Generally, gyrosychnotita to Vircators not observed in microwave output, omega However it is advisable to take into account.

4.3.5. Calculation Sizes

Consider the cylindrical symmetry Vircator, with output waveguide radius *b*= 5cm. We have available voltage generator ~ 200kV, low internal resistance, and epithymou- to emit radiation around 2GHz. The relatively more precise frequency estimate to Vircators the frequency reflex. So we start, having assumed the tendency to define the gap diode to place the frequency reflex ko- dumping the desired frequency. According to the frequency of calculation models reflex, for *VAK*= 200kV, reckon with tests that *dAK*= 1.6cm are:

Tab. 4.3: Estimated Frequency Reflexing, 200kV, *dAK*= 1.6cm

Non-relativistic Model (4.31)	Relativistic Monte-Member of (4.32)	Model (4.33) *k*= 4.5	Model (4.34)
fREFL= 2.07GHz	*fREFL*= 1.89GHz	*fREFL*= 1.95GHz	*fREFL*= 2.55GHz

The average of these estimates is the 2.1GHz, so we set the initial distance of the anode-cathode gap to 1.6cm. Placing frequency reflexing, have largely determine the maximum current density that can be a- ntlithei the passageway. This is because, given the frequency and voltage of the diode, E- humus define the anode-cathode distance required and thus the maximum current density, *JSCL*. Under the Child-Langmuir Law for the infinite diode is approximately 80A / cm2. In the calculation we *VAK*= 200kV and *dAK*= 1.6cm.

From circular radius descent *a*= 2cm, the initial power estimate, *I=pa2JSCL*Is ~ 1000A. Using the precise relationship circular passage finite akti- image on. (2.69), we obtain that the value of the diode current is ~ 1240. The maximum current of the electron beam radius 2cm, which move within 5cm tube in threatened po magnetic field is ~ 730A (56A / cm2), according to Eq. (2,173) of Bogdankevich and Rukhadze. The classical approach of Birdsall and Bridges, for flat short-

klomeni diode with a theoretical distance of 5cm reinforcement would require rheumatic density 33A / cm2, for virtual cathode formation in the center of the distance of reinforcement. This amount is calculated four times rheumatic density for short-circuit diode Meni spaced 5cm reinforcement and energy package 200keV (see. Par. 2.7). For the estimated size of the package, the total current shows about ~ 500A. According to these estimates, an amount of power over the beam 700A (56A / cm2) must enter the idle space in order to form a virtual cathode. From the calculated maximum gismeno diode current, 1240, a grid with 60% permeability leaves ~ 740A stream passing the inert space and form virtual cathode.

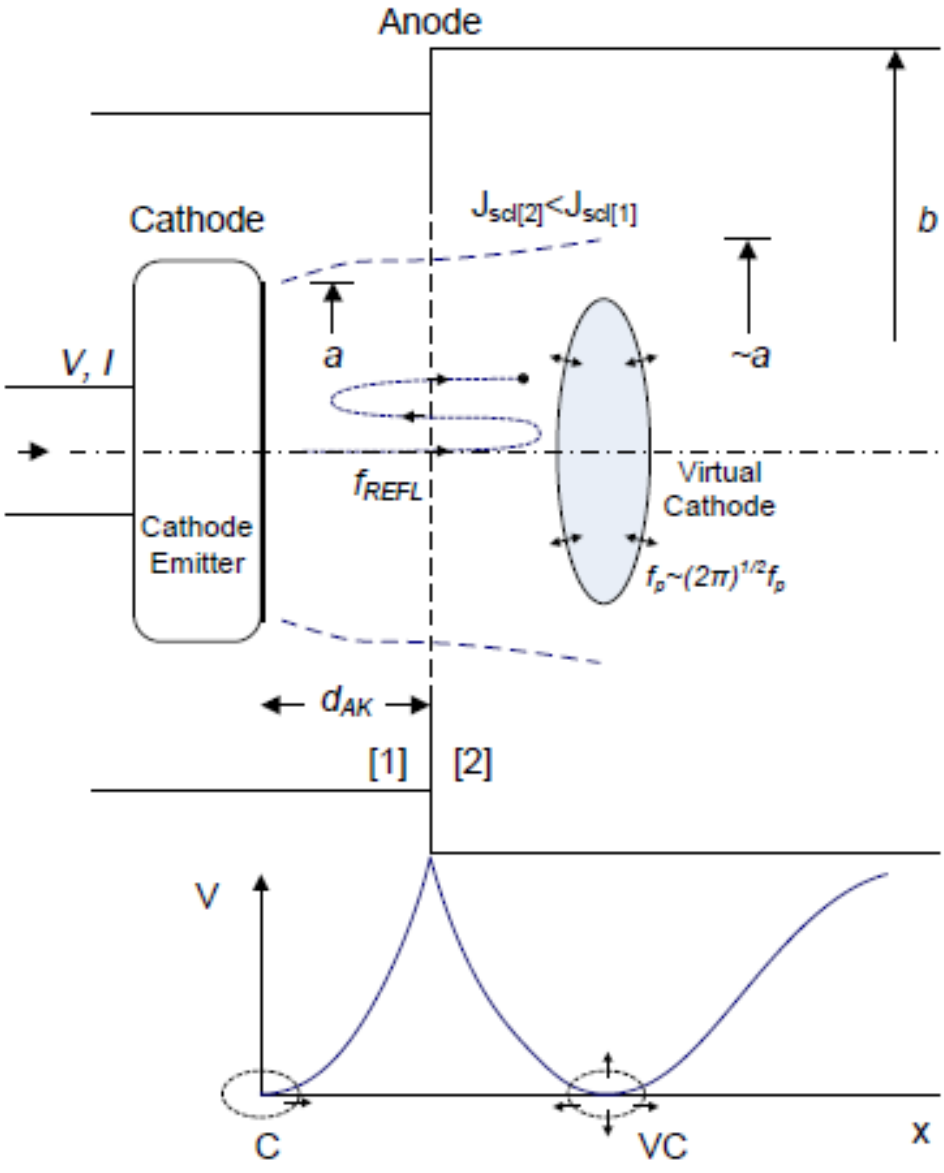

Fig. 4.8: Design Vircator. Initial conditions.

Then the foregoing calculations, the matrix allows further adjustment of the current density of the beam and consequently the frequency of this plasma. Given beam current ~ 740A, the radius thereof, ~ 2cm, and her energy, ~ 200keV, we can calculate the plasma frequency of De--term. The non-relativistic approach gives plasma frequency 1.19GHz, while schetikisti- RH approach, using the coefficient Lorenz *c*Gives plasma frequency 1.01GHz. Non-usual approach, using the coefficient *c3*Gives even smaller beam plasma frequency, 0.72GHz. Using the empirical observation that the frequency

oscillation of the virtual cathode positioned between prices *fp* and (2n) 1/2*fp*, Difference judging cases 1.19≤*fVC0*[GHz] ≤2.99, 1.01≤*fVC1*[GHz] ≤2.53 and 0.73≤*fVC3*[GHz] ≤1.82
for estimation using the relations (4.35), (4.36) and (4.37) respectively. Despite regar- ding gross errors of estimation, the estimated range of virtual cathode oscillations containing the desired frequency of 2GHz (except *c3*-based approach of frequency plasma Community).

Tab. 4.4: Calculated Sizes Vircator 2GHz, 200kV (t = 0 nsec).

Beam waveguide output *b*	5cm
Cathode ray, *a*	2cm
Anode-cathode distance, *dAK*	*1.6cm*
Diode voltage, *VAK*	*200kV*
c	*1.39*
b	*0.69*
Matrix permeability, *i*	*60%*
Diode current, *I*	*1240A*
Passage resistance, *Z*	*160O*
Passing beam current, *Ibeam*	*760A*
(Peak beam current*inf. B*)	*730A*
Shorted diode *dSCD=b*	*500A (4 · pa2JSCL)*
fREFL (*c*= 1)	*2.1GHz*
fREFL (*c*)	*1.9GHz*
fREFL (Benford)	*2.0GHz*
fREFL (Woo)	*2.5GHz*
<FREFL>	*2.1GHz*
fVC (*c*= 1)	*1.2≤fVC [GHz] ≤3.0*
fVC (*c*)	*1.0≤fVC [GHz] ≤2.5*
fVC (*c3*)	*0.7≤fVC [GHz] ≤1.8*

Since the frequency of oscillation of the virtual cathode can ex ante be determined within a relatively small range, the imposition of an iota diosychnotitas can push the oscillations of the virtual cathode in the desired region.

The problem, however, is what happens in the time evolution of the phenomenon, the Vircator. We know that the field emission cathode is covered in were first liberalized rate of plasma, so the apparent size of the diode progressively changing. The plasma cathode extends in all directions and especially towards the anode, a plasma velocity which may range from 0.1cm / microseconds up to several cm / microseconds. Furthermore, the anode is overheating and local melting, thereby contributing anodic plasma in the passage area. In the following schematic representation it seems likely to change the dimensions of the passage, after a few hundred nsec. We ignore the anode plasma and believe that the cathode plasma spreads evenly to the anode.

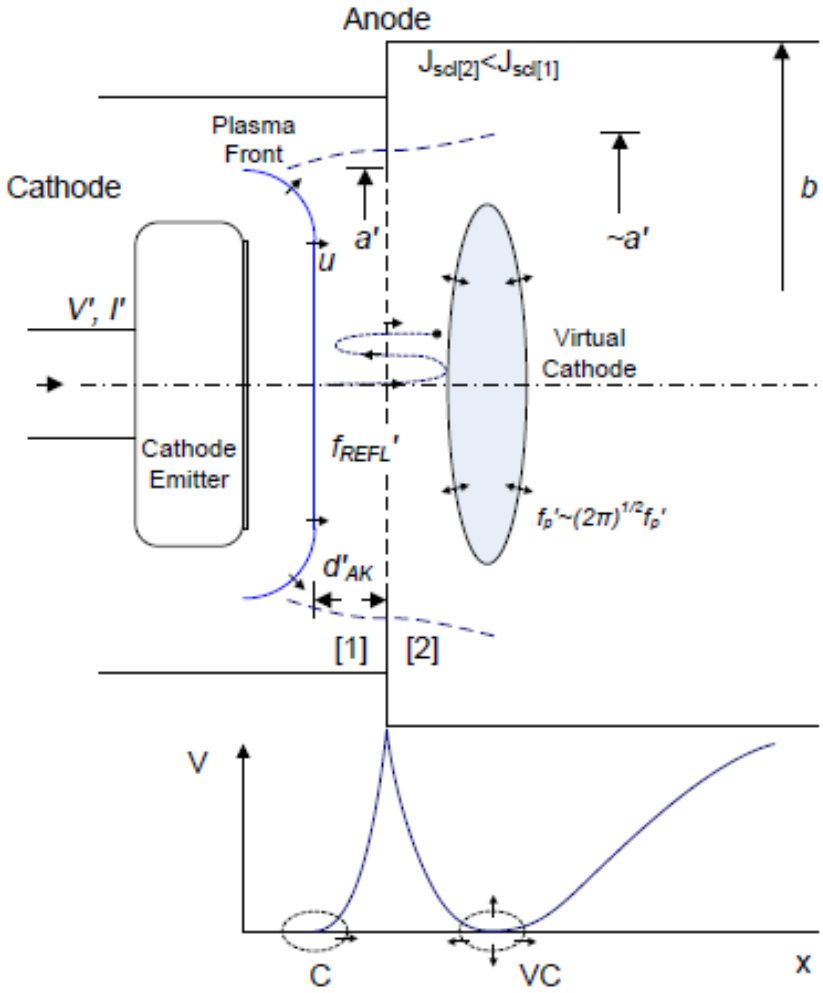

Fig. 4.9: Design Vircator. Evolution phenomenon.

The gap now has a new distance, *d'AK*. Suppose that the new gap is half of the previous one, namely 0.8cm. The front of the plasma is expanded radially by a distance *dAK* - *d'AK*= 0.8cm. Thus the "new" within the cathode is 2.8cm. The Direc- tion passage is practically impossible to have been maintained at 200kV, given the sensor until now loss of impulse load device and the additional reduction of alpha ntistasis gap. Suppose that the trend in the passage this time has fallen to 120kV. Following the same methodology as before, we calculate the new figures Vircator, at time t1.

We note that with shorter distance reinforcements, larger cathode surface and relatively smaller bias voltage, the current of the diode increases dramatically, reaching 4kA. Corresponding increases the amount of current flowing to the anode, in the area of the virtual cathode. Since the conditions for forming virtual re- Methods in inert space not change dramatically, the effect in this phase kathi- replaced very intense. The frequency reflex and the plasma frequency have been othi- upwardly and apparently removed far from the design frequency.

Tab. 4.5: Calculated Sizes Vircator 2GHz, 120kV (t = t1 nsec).

Beam waveguide output *b*	5cm
Cathode ray, *a '*	2.8cm
Anode-cathode distance, *d'AK*	*0.8cm*
Diode voltage, *V'AK*	*120kV*
c	*1.23*
b	*0.59*
Matrix permeability, *i*	*60%*
Diode current, *I*	*4000A*
Passage resistance, *Z*	*30O*
Passing beam current, *Ibeam*	*2400*
(Peak beam current*inf. B*)	*460A*
Shorted diode *dSCD=b*	*400A (4 · pa'2JSCL)*
fREFL (*c*= 1)	*3.2GHz*
fREFL (*c*)	*3.0GHz*
fREFL (Benford)	*3.3GHz*
fREFL (Woo)	*4.0GHz*
<FREFL>	*3.4GHz*
fVC (*c*= 1)	*1.7≤fVC [GHz] ≤4.2*
fVC (*c*)	*1.5≤fVC [GHz] ≤3.8*
fVC (*c3*)	*1.2≤fVC [GHz] ≤3.1*

But in order to gain a picture of the transition behavior of Vir- cator, we will consider a very simple case of driving, which, however, describes the reality enough. Considering that Vircator driven by a charged coun- ritikotita, which is discharged through the diode lamp, we will calculate the characteristics of the design sizes, as well as the phenomenon develops.

4.3.6. Transition Behavior Vircator

The temporal variation of Vircator size must be taken into account in schedi- silver lamp. An important factor is the impulse generator, which drives the poly- XVIA. A typical case is that of a simple capacitive discharge sys- correlation capacitors (generator Marx), with capacity egermeni *C*, Charged in an equivalent voltage *V0*. According to the theory of Marx generators, (Fri 3.4), if available *N* capacity capacitors *Ci*(*N levels*), Which is charged at a voltage *Vi*Then when representatives charge will appear to the load voltage theoretically equal to *V0=NVi*. The overall-capacity of the Marx generator is *C=Ci/N.* because the series, longer connecting capacitor of. The capacitor discharge circuit via a diode Vircator illustrated in Fig. 4.10.

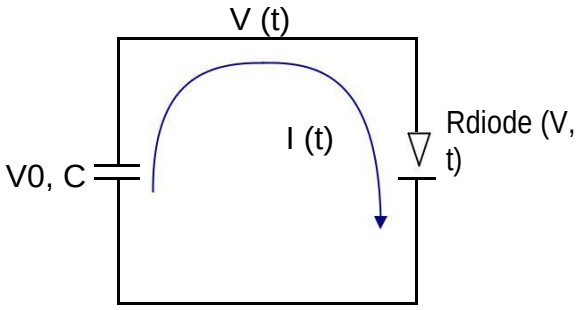

Fig. 4.10: Discharge capacitor using vacuum diode.

At time t = 0, the capacitor C, charged voltage *V0*, Connected across the diode. We believe that because of the strong field the diode switches instantly to conduct Child-Langmuir. In other words we consider that the entire surface of the flat circular passage (see. Fig. 4.8) is covered by an instantaneous plasma infinitesimal thickness which is able to offer arbitrarily large number of electrons in di- progress. Note that before the complete coverage of the cathode plasma occur, emfanizo- are scattered small "jets" plasma (plasma jets) points to the strongest geometric anomalies ([70]). For this simple circuit, the dependency of current from the voltage given by the load of the capacitor,

$$I = \frac{dQ}{dt} = C\frac{dV}{dt}. \tag{4.59}$$

The current of the diode is described approximately by the expression

$$I \cong kS(t)\frac{V^{3/2}(t)}{d^2(t)}, \tag{4.60}$$

where $k = 2.33 \cdot 10\text{-}6$ constant of the planar diode in units SI [AV-3/2], *S (t)* It is the phenomenon of the cathode area and *d (t)* It is the apparent distance of reinforcement. The radius of the descent, first price *a*Increases over time at a rate $u \cdot t$Wherein *u* plasma propagation velocity (see. Fig. 4.9). Therefore, the area of the diode can be approximated by the expression

$$S(t) \cong Fr.\, r^2(t) \cong Fr.\,(a + u \cdot t)^2 \tag{4.61}$$

Similarly, the anode-cathode distance, initially equal to *d*Decreases with time with regulated MD $-u \cdot t$Hence the apparent distance of reinforcement is

$$d(t) \cong (d - u \cdot t)^2. \tag{4.62}$$

Equating the capacitor current with the current of the diode, we get the following differential equation:

$$C\frac{dV}{dt} = k\,Fr.\,(a + u\cdot t)^2\frac{V^{3/2}}{(d - u\cdot t)^2} \qquad (4.63)$$

This equation we see that it has two analytical solutions,

$$V = \frac{2Cdu\,(d - tu)\sqrt{V_0}}{\pm 2Cdu\,(d - tu) + kFr.\,u\sqrt{\quad}\,(\quad)\,kFr\,\sqrt{0}\,(\quad)\,(\quad)\,(\quad)}\,, \qquad (4.64)$$

resulting in the requirement *V (0)=V0*. From these solutions, one *not* having terminals for positive time and therefore represents the voltage in the circuit. The yield, as vlepou- with, depends on all the parameters of the circuit and the diode. Starting at *V0* and reset the time *t=d/u*. For this example, to in- VERVIEW behavior sizes of interest, we set the following sizes: *k*= 2.33 · 10-6A / V3 / 2, cathode beam *a*= 0.020m, reinforcement distance *d*= 0.016m, geometric anode mesh permeability *n*= 50%, plasma propagation velocity *u*= 2cm / microseconds = 2 · 104m / sec, initial voltage capacitor *V (0)=V0*= 200kV, capacitor capacitance *C*= 10nF. The voltage of the diode, the radius of the cathode and the anode-cathode distance mate- layout employed earlier in the static approach, in order to place the micro- wave output as close as possible to 2GHz. In this dynamic approach, the two solutions of the differential equation of the trend shown below.

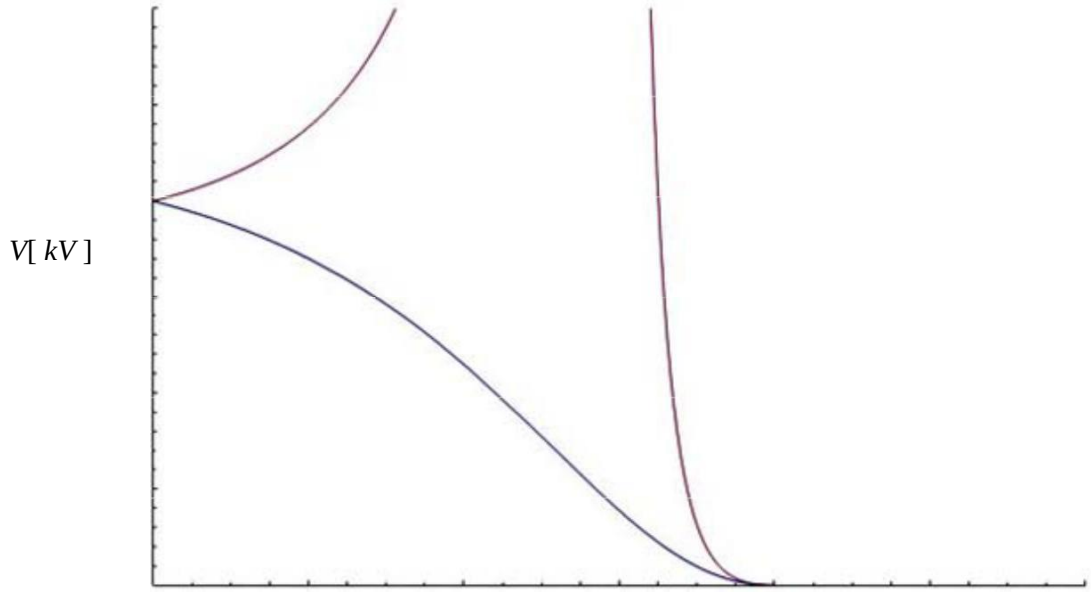

Fig. 4.11: Voltage in diode.

One of the two solutions shows the expected behavior of the discharge of fire knoti to the point shorting the diode, which occurs at time 0.8msec

(0.016 / 2 · 104 sec). Using the equation of voltage in the circuit, calculate the frequency reflexing of the expressions of par. 4.1.1, properly replacing chro- winning distance dependence of reinforcement, non-relativistic as

$$f_{REFL} = \frac{\sqrt{V}}{4\left(d - u \cdot t\right)}\sqrt{\frac{e}{2m}}, \tag{4.65}$$

or relativistic as

$$f_{REFL} = \frac{\sqrt{V}}{4\left(d - u \cdot t\right)}\sqrt{\frac{ec^2}{2mc^2 + eV}}. \tag{4.66}$$

The spacing of the two estimates is small, and further decreases with time and reducing the capacitor voltage. Interestingly the analysis is rapid removal of the frequency from the original design frequency (2GHz), from the very beginning of the phenomenon. Then appears a region slowest of change towards the end of the phenomenon of the collapse of the diode. In this region, between 600 and 800nsec, the voltage is too low, below 50kV, but the rate of discharge of the capacitor and the apparent dimensions of the passage creates condi- tions suitable for stabilizing the frequency reflexing. An important factor for the occurrence of such stabilizing regions is the capacitor size of the charging voltage and the speed of the plasma, a factor that depends yli- party and the purity of the electrode. By appropriate selection of these parameters can be achieved a plateau fixed frequency, long time a duration of, in the desired zone.

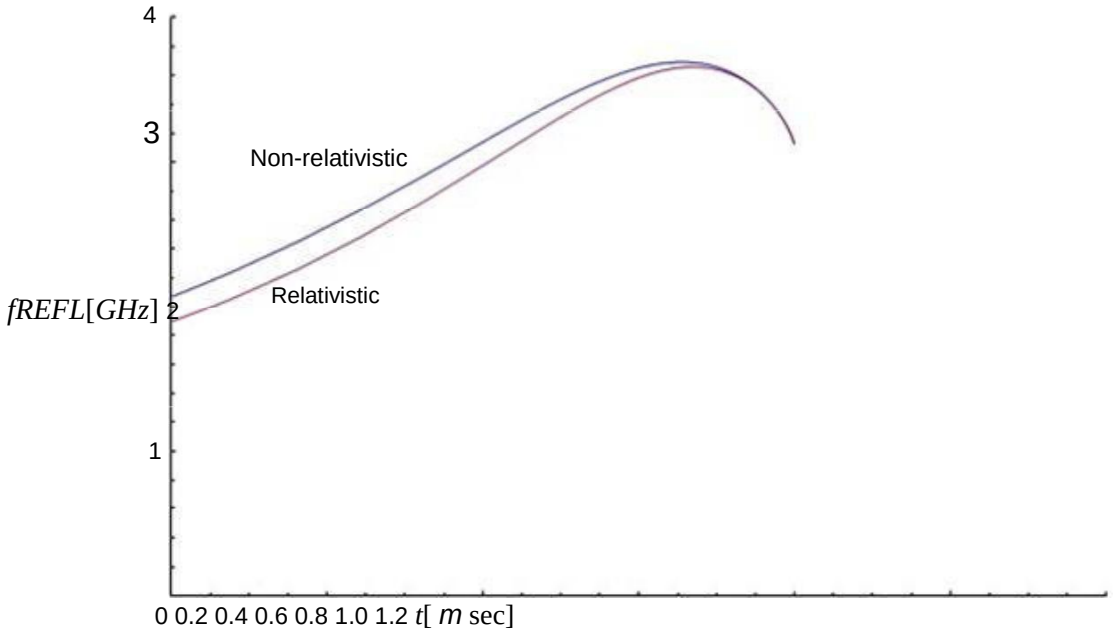

Fig. 4.12: Theoretical frequency Reflex.

Using expression found for the voltage of the diode, we can export goume stream Child-Langmuir passageway. We use the expression for circular passage finite dimensions (2.69)

$$J_{SCL}(2) \cong 1 + 0.26 \frac{d}{r} J_{SCL}(1), \tag{4.67}$$

to write

$$I_{SCL} \cong kS(t) \frac{V^{3/2}(t)}{d^2(t)} 1 + 0.26 \frac{d(t)}{r(t)}. \tag{4.68}$$

Substituting the equivalent area of the cathode and the distance of the reinforcement with the appropriate time dependencies, we take the relationship

$$I_{SCL} \cong 2.33 \cdot 10^{-6} Fr.(a + u \cdot t)^2 \frac{V^{3/2}}{(d - u \cdot t)^{1/2}} + 0.26 \frac{d - u \cdot t}{a + u \cdot t}, \tag{4.69}$$

which varies as follows:

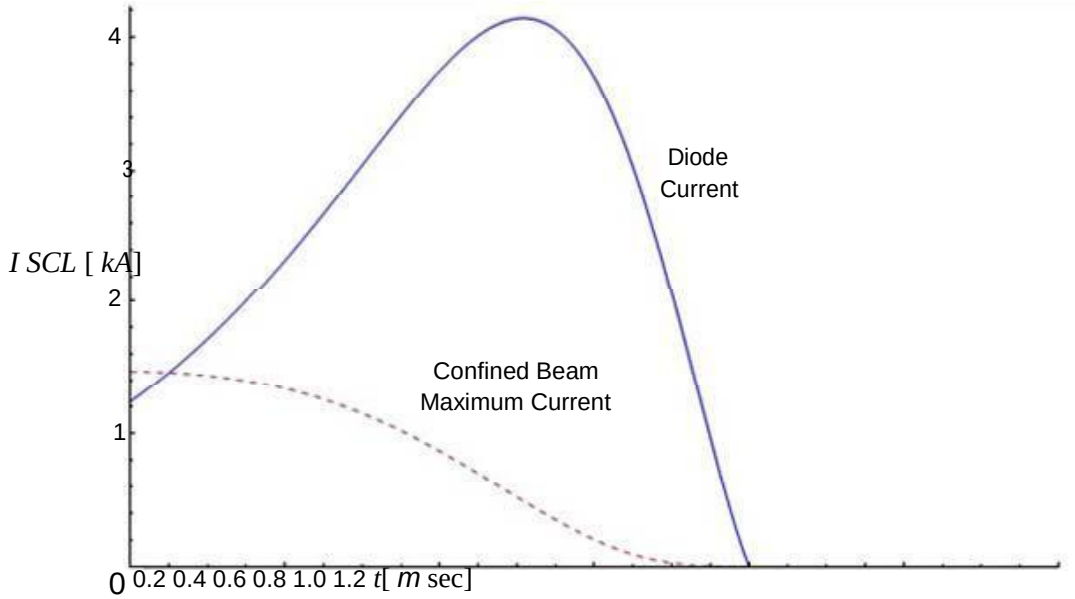

Fig. 4.13: The current in the diode.

In the above image, the stream is shown in the fairway. Recall the point in- how Eq. (4.54) provides a maximum power electron beam in the presence of infinite magnetic field. Considering the geometrical permeability of the matrix, the dotted line illustrates the same amount of current. Replacing the timing dependencies where necessary, the current in the diode should ideally be EI- yes more than:

$$I_{diode} > 17 \cdot 10^{3} \frac{1}{n\%} \frac{\left(1 + \frac{V}{511 \cdot 10^{3}}\right)^{2/3} - 1}{1 + 2 \ln \frac{b}{a + u \cdot t}} \quad [A]. \tag{4.70}$$

Given the absence of magnetic field, a much larger current value De--term, as in the case of the 0.4msec until 0.8msec may be deemed sufficient to install virtual cathode in inert space. The maximum beam current deteriorates with time, it is an amount that depends on the energy of the beam and thus the voltage of the diode.

The impedance of the diode can be represented by dividing the voltage V by the calculated space charge current, equation (4.69):

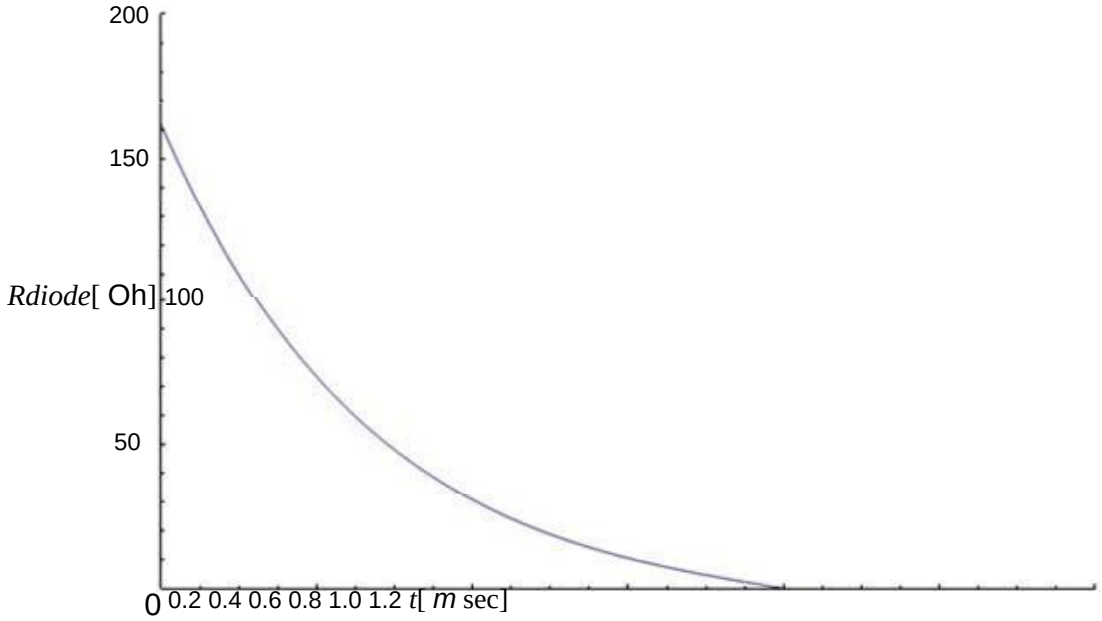

Fig. 4.14: The resistance of the diode.

H resistance of the diode is much greater before the phenomenon, essentially described in this analysis. Before the time *t*= 0, the cathode emits electronic field emission current Fowler-Nordheim, Fig. (2183). The resistance of the diode in this region starts a theoretical infinite value and varies according to the combination of the electronic field emission from all the small projections and the development microplasma the cathode surface. By the time the cathode surface theoretically covered the entire plasma (*t*= 0), there is a transient, which lasts a few tens nsec [66].

H plasma frequency of the electron beam, which enters the inactive area can be calculated from the relativistic equation (4.42). In this expression in place of the current package *I*, Substituting the amount (4.69) multiplied by the geometrical permeability of the matrix, *n*. In the denominator of the equation (4.42) we make the appropriate anti-time dependence of the radius of the cathode, which we assume and radius of the beam. The change of plasma frequency is described by

$$f_p = \frac{1}{2Fr.}\sqrt{\frac{e\cdot(n\%)\cdot 2.33\cdot 10^{-6}\cdot \frac{V_f^{3/2}}{(d-u\cdot t)^2}1 + 0.26\,\frac{d-u\cdot t}{a+u\cdot t}}{e_0\, m\, b c\, c}}\,, \qquad (4.71)$$

where the coefficients b and c depend on the tension in the passage and described by equations (4.44) and (4.45). The power and energy of the electron beam are the main factors that affect the value of the plasma frequency. However, the electron beam is derived from a passage of which the current is expression law Child- Langmuir. The simplifications in the above equation translate relationship to plasma frequency, from current to voltage relation context with behavior similar to reflexing frequency. This is shown in the graph, illustrating the chro- tronic change of plasma frequency of the electron beam.

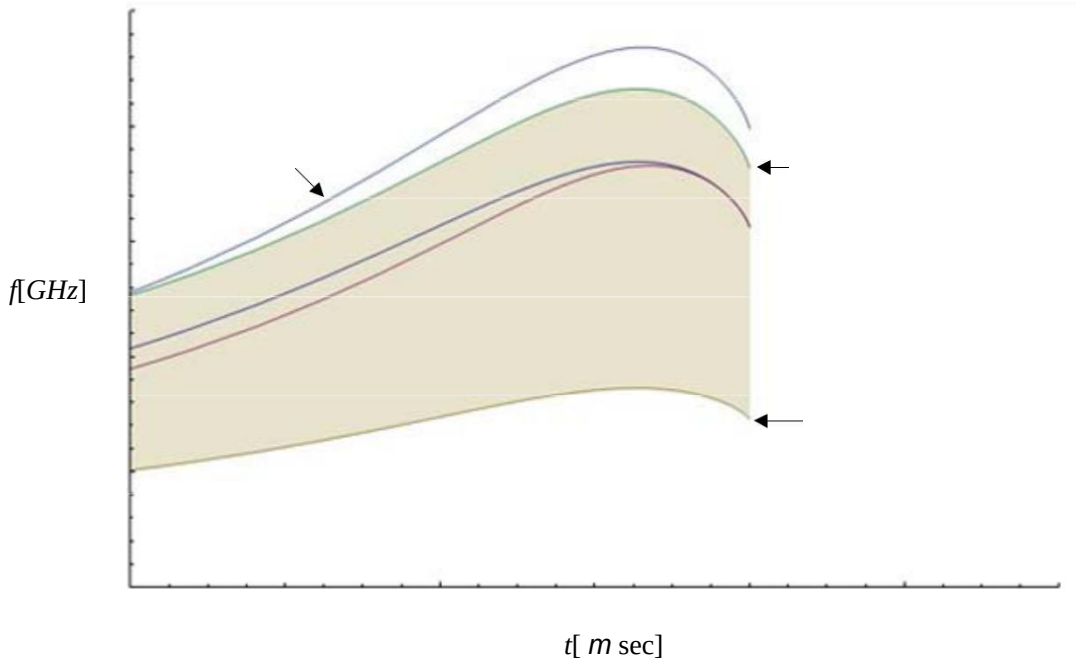

Fig. 4.15: The calculated frequencies reflex and plasma.

The frequency of oscillation of the virtual cathode, according to what has been referred behave in par. 4.1.2, is between the values *fp* and (2n) 1/2*fp*. In the above graph marks the area defined by this empirical observation. Still marked the two estimates of frequency reflexing, non-relativistic and relativistic, O that described in par. 4.1.1. Finally made and the assessment of Woo, on. (4.16), according to which "the frequency of Vircator determined by the relationship with a margin of 20%" ([50]). It is evident that a fairly large range of possible mikrokymati- KON frequency defined by the theoretical models. Therefore, the fixing sys- gkekrimenis output frequency of "free» (free-running) Vircator is difficult. Forcing the output at fixed frequencies is achieved using methods lock the output, such as coordination procedures and appropriate parametropoi- against voltage and dynamic dimensions of the passage.

The procedure described in this paragraph, uses the classical equations current-voltage vacuum diode, to assess the dynamic change of macroscopic sizes of the passage of Vircator. The circuit model is used by the discharge of a capacitor, charged to an initial voltage, via diode lamp. By appropriate selection of the size (*C*,*V0*,*d*,*a*,*u*,*n%*), We have the possi- ity to identify desired frequency ranges, always with limitations or uncertainties involve theoretical models of radiation Virca- tors. Point intense uncertainty is the diilektrodio plasma. Catching re- Methods of plasma may not be complete, resulting in only a region thereof to provide current to the diode. As a result we glide behavior equivalent area smaller course. The propagation velocity of the plasma in the space between n- lektrodion is another parameter great randomness. The existence of pre-plasma coming from the rise should count when the current volumes in the fairway is large and the electric field is intense. If the electrodes are from i- chloride material and have undergone the same purifying treatment, it can be considered that the gap collapses with the same speed, both in the cathode side, and the side of the anode. Small plasma expansion velocities (<1cm / microseconds) They can generally be achieved by high purity electrodes where hydrogen and water vapor are missing the greatest possible extent by adsorption. To achieved purity of the electrodes, should the cathode and the anode to klivanisthoun many hours at a high temperature and quickly placed in the gap of the lamp. Furthermore 'education »(conditioning) of the gap, using high voltage in a high vacuum, can rid the electrodes of adsorbed gases. The diapera- matrix lity affects current density passing in an inert space, wherein the virtual cathode is formed. This parameter shifts the grammoskia- certain area of Fig. 4.15 accordingly. Increasing the permeability of the matrix leads to increased density of electron beam and hence to increased frequency plasma Taq.

Experimenting with the parameters of the circuit can lead to finding Timoleon Sciences with better predicted behavior. For example, by selecting a radius lays Output *a*= 0.030m, distance reinforcement *d*= 0.017m, geometric anode grid permeability *n*= 60%, plasma spread speed *u*= 3cm / microseconds = 3 · 104m / sec, initial tension of fire knoti *V (0)*=*V0*= 200kV and capacitor capacitance *C*= 6nF, take the diagrams of Fig. 4.16. The projected area output frequency, these parameters are more focused around 2GHz around the time of the diode operating range. H diode collapses about 560nsec, while the current of the diode, from 100nsec to end the phenomenon is considerably larger than the maximum beam current within the magnetic field reaches threatened. The resistance, which is not shown here, starting at 80O Once the theoretical start collapse of the gap, and decays until the bridging of plasma passage. The maximum power at the diode (product *VI*) Exceeds 500MW during the first 200nsec phenomenon.

$V[\ kV\ ]\ f\ [GHz\ ]$ And $I\ [\ kA]$

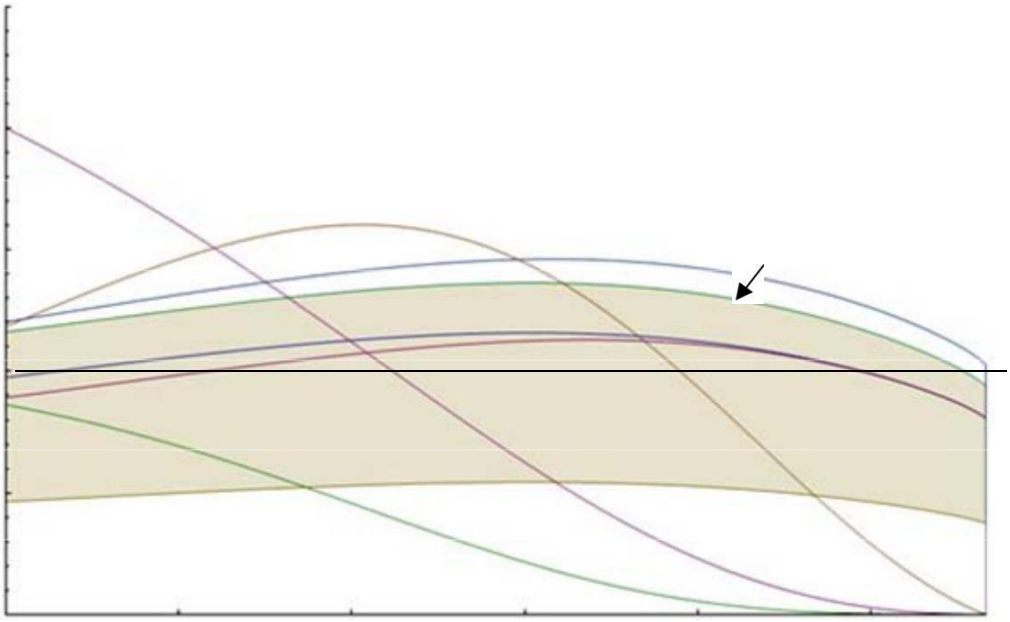

$t[\ m$ sec]

Fig. 4.16: (a) diode voltage, (b) diode current, (c) Required power, (d) Frequency reflex, (E) Relativistic frequency reflex, (f) frequency plasma beam, (g) Frequency plasma- Tosh beam on (2n) 1/2, (h) Estimated Woo.

4.4. Evolution of lights Vircator

The first reference to light Vircator done in 1979, the patent of Kapetanakos et al. [48], which describes the first lamp Reflex Triode Vircator, ie a poly- XVIA Reflex Triode without control electrode of backscatter electrons (see. Fig. 4.17). In this patent is found for the first time the possibility offered to produce microwave radiation, using the phenomenon of formation *virtual cathode*. In published work, which was preceded by the same group ([57]), it is the first observation that, driving a strong positive pulse in d- nodo a Reflex Triode, can be produced microwave radiation because of schi- ming virtual cathode , and that the output frequency is, the in- farmozomeni voltage passageway linear dependence factor V1 / 2 and inversely proportional dependence on the distance of the anode-cathode gap. The experiments referred to voltage levels ranging from 250kV to 400kV. The microwave power from this first light Vircator was approximately 100MW at X-band.

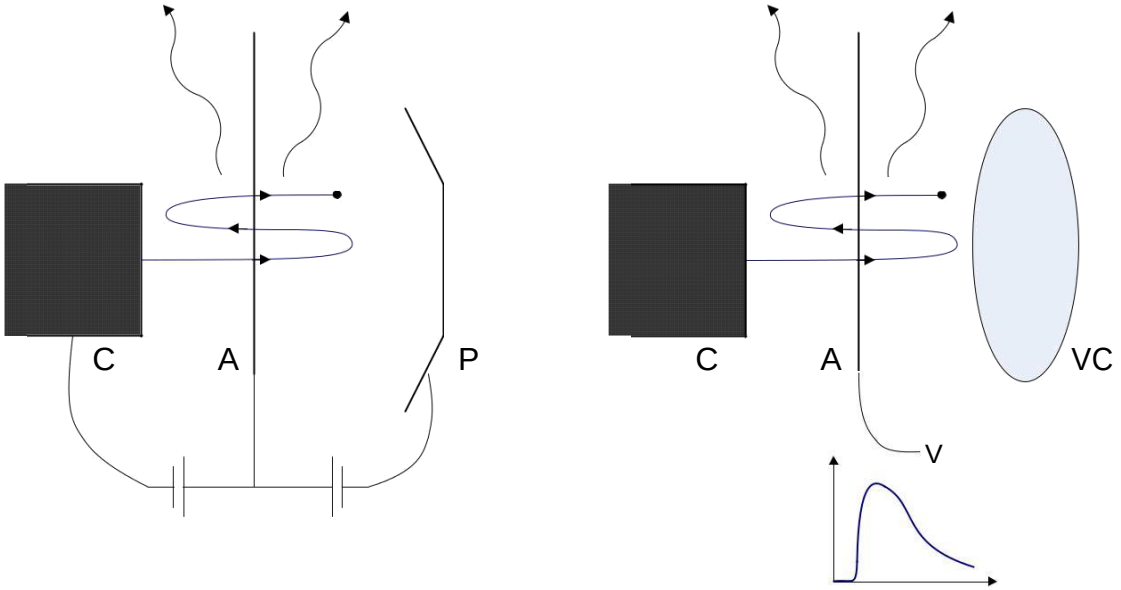

(A) (B)

Fig. 4.17: Reflex Triode (a) and Reflex Triode Vircator (b). In the first case the oscillator Dawson electrons are controlled anode voltages (A), cathode (C) and n- lektrodiou control (P). In the second case the reflections of epityncha- electron nontai the virtual cathode formed.

In 1982, Sullivan ([71]) establishes the first patent for axial Vircator. In in- fefresi, the Sullivan claims that can achieve outputs of microwave BRAKE ment of 1GW, with the rather unreal performance of 30%. Note that no gen- ometria Vircator not record both high yields with standard performance to gov- raging 6% ([55], [72], [73]) and in some cases up to about 10% ([74] , [75]). Interest in the study of Virtual Cathode Oscillators continues katochy- ronontai some more patents, such as Brandt 1985 [76], the Kwan and Snell from Los Alamos in 1988 [77], which is the first description of *Reditron* Vircator with anode slotted, and other (Ohkawa, 1988, [78], Schumacher et al., 1990, [79], Convert and Brasile, 1992, [80], Durand, 2004, [81]).

The power achieved during the initial period of studies Vircator lights (1980- 1990) exceeded Gigawatt. Some experimental results listed are: 500MW at 17GHz, with Axial Vircator [47] · 200-500MW at 0.4-5.5GHz, with Reflex Tri- ode Vircator [49] · 1.6GW at 2.46GHz, with Reditron oscillator [55] · 1.4GW at 8.2GHz with Re- flex Triode Vircator [68] · 1.4GW at 3.9GHz, with Reditron oscillator [56] · 4GW at 6.5GHz with Axial Vircator [82] · 7.5GW at 1.17 GHz with Axial Vircator [83]. In the overview of RF Hoeberling and MV Fazio [84] reported that 8GW power observed by light Vircator, while the summary of Alyokhin et al. [53] states that recorded the astonishing amount of power of 22GW by experiment with virtual cathode. This experiment Aurora, in which a beam of 10MeV, 250kA, driven in classical geometry reflex triode, gave power of more than 20GW at frequencies up to 1GHz [85]. These experimental results were obtained with Kd simple geometries lights (Reflex Triodes, Reditrons and Axial Vircators), which we present below. The driving them in all cases about trends of several hundred kV and currents of several tens of kA, ie the simple and direct way to apply very strong impulse voltage from

pulse generators. This observation, however, that the microwave spectrum lights are not concentrated and their performance is relatively low, on the order of a small percentage point rate, has now turned its field of study in technical growth phase of alpha FOOT and blocking microwave oscillations of virtual re- methods.

H development of computer codes made it possible to study the dynamics of Conduct of Vircators. The oscillations of virtual cathode, a very complex and charac- primary school phenomenon, and the consequent production of microwave radiation would be practically impossible to predict with some accuracy without the use of computational methods of don. So-called Particle-In-Cell codes (PIC Codes), used for these simulations, solving Maxwell's equations and the equations of motion of the particles in space. They usually use the two-step technique «leap-frog», in which the already calculated fields and particle positions define the pos- nameis exerted on all particles in the interaction space, while stays and these forces are used to assess new places and new fields distributions. The most commonly used codes PIC simulations Vir- cators is MAGIC ([67], [86], [87], [88], [89]), the KARAT ([90], [91], [92]) and o XOOPIC ([93], [94], [95]) but others, such as ISIS ([55]), the SPIFFE ([96]) and CCUBE ([97], [98]).

H study on Vircator lights has focused on methods to increase the performance and optimization of the individual parts, especially the cathode and the anode. Researched techniques, such as using two anode grids ([90], [99], [100]), which define a small region of electromagnetic interaction of the beam and that of the lamp, optimal for pre-configuration and grouping of electrons package. Also, use is made of discontinuities, such as leaves, irises and cavities for achieving coordination of pro- ragomenis microwave radiation in a microwave quirks ([101], [102] [103] [104]), so that the microwave radiation acquire limited spectral content at a desired frequency. Even investigated the replacement of traditionally used cathode covered with cloth, usually velvet (velvet cathode), cathodes from carbon fiber (carbon fiber cathodes) [72], or

from metal cathodes with micrometric roughness ([105], [106], [107]), which charac- Rassia by either mechanical means (micromachining) or chemical means (etching), in order to have longer life relative traditional.

Finally, another area of research in Vircator lamps is the effect of magniti- tion field, the coupling with a light of another type, the construction of hybrid structures with virtual cathode or even parallelism Vircator, to achieve microwave resonance and increase the received microwave power. A typical experiment of the first year was driving Vircator by magnetron ([108], [109]), which could be observed under some conditions, forcing the output of the Vircator the driving frequency. Also, although not common, is examined Steia several times to impose magnetic field at Vircators, ([64], [60], [110], [61], [62]), while geometries Reditron, the using magnetic field is mandatory ([55], [111]). The magnetic field can bring about improvement but also deteriorating yields ing to Vircators and the usual practice is not used. A variation

Vircator by periodic slow wave structure (slow wave structure) is Virtode [112], a hybrid form Axial Vircator TWT structure and the waveguide output which epityncha- TAKES 16% yield. Several more hybrid forms with virtual cathode ray tubes described

fontai in [91] and consider a scenario microwave coupling Vircators ([113], [114], [115]).

4.5. Geometries Vircator

The philosophy in Vircator tubes is relatively simple: a strong current, which shall be fixed by the Child-Langmuir restrictions in space AK, enters an area, the feature stream bounded by the space charge is small enough - than. As a result, the electron beam "explodes" and simultaneously creates the virtual cathode, starting all those mechanisms generate mikrokyma- tion radiation. The geometries used in Vircator lamps is varied. Usually used geometry type reflex triode, the axial geometry (axial Vir- cator), the coaxial geometry (coaxial Vircator) and vertical outlet geometry (verti- cal extraction Vircator), which will examine separately below. In any case, the cathode leads an electronic current very high price through the anode, which has a grid format or a very thin sheet, in the space on the other side of the anode. The anode should have sufficient permeability to the Y- high energy electrons, since it is the input window of the beam at coun- po, to which the virtual cathode is formed. The anode is most provisions grounded and connected to the body of the Vircator, while the cathode is driven to a negative voltage impulse. This is the standard provision *negative bias* lamp Vircator. E- nallaktika can descent to maintain a zero potential and rising to Direc- githei a pulse of positive voltage impulse. This drive is usually used in the geometry of the reflex triode [48] as the provision *positive bias* Lamp Vircator.

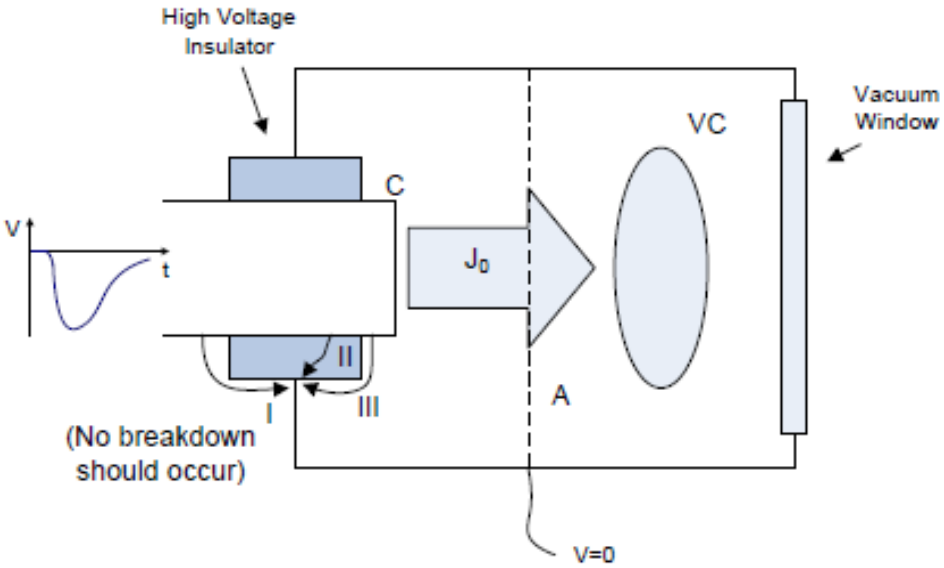

Fig. 4.18: Example Vircator negative driving.

In the negative bias, the cathode is the electrode of the high voltage and must be electrically insulated from the body with an insulator Vircator transit (see. Fig. 4.18). In contrast, the positive polarization, the rise is the high voltage electrode and

therefore it must be electrically isolated from the body of the Vircator a suitable insulator (see. Fig. 4.19). In any case, the design of the insulator must be tech- toia to withstand pediaki tension between the high voltage electrode and the body of the lamp. Also there should be no case of in- formation electrical arc to the grounded body, both from the inside of the bulb, and from outside it. In other words, the impulse voltage leading the Vircator should form electronic drain only between the cathode and the mesh anode.

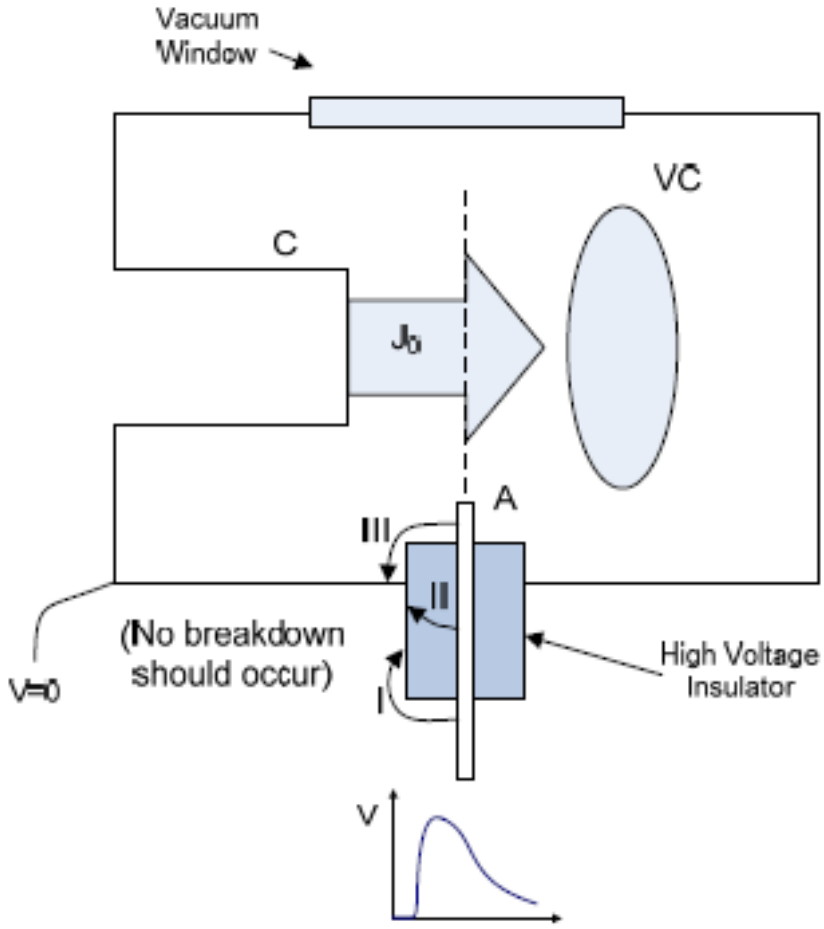

Fig. 4.19: Example Vircator positive driving.

The cases are illustrated undesirable electrical breakdown can occur out in the above figures, Fig. 4.18 and Fig. 4.19. These cases are: (I) Generator arc or creeping discharge from the outer side of the lamp, between electrode charge high voltage and the lamp body, (II) piercing the insulating material at some point with great intensity and local pediaki (III) arcing or creeping discharge on the surface of the insulator from the inside of lychni- let. Also the dimensions of the passage area must be such that the electron beam is guided directly to the mesh of the anode, without dispersion in the re- rivlima or support means of the mesh, which may be a solid ring me- tallikos .

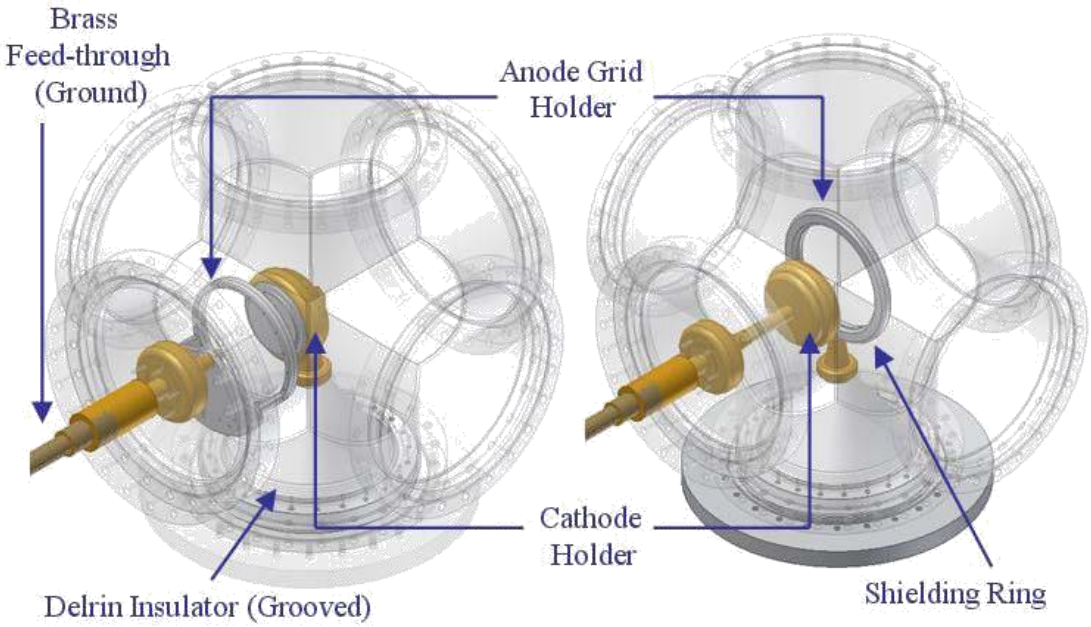

Fig. 4.20: Negative (a) and Positive Polarity (b) Reflex Triode Vircator ([106]). Construction EI-yes based on a standard vacuum accessory, link six routes (6-way cross). At the bottom is the insulator passage, which may lead to the cathode (a) or the anode (b) with a pulsed voltage. From left distinguished a piston, which supports the matrix of the anode or cathode respectively, at a variable distance from the electrode high voltage.

4.5.1. Geometry Press Reflex Triode

H reflex triode with a virtual cathode is practically the first form lamp Vircator implemented, and the most common. Indeed, this patent has ob- chyrosei team researcher Ch. Kapetanakos 1979 [48]. The construction of the first re- flex triode included a rise circular form grid, which was supported by an electrode leading pulse of positive voltage to the lamp. In Reflex Triode Vircator, electrons from the cathode are accelerated by the electric field passing through the mesh of the anode to form a bubble of virtual cathode on the other side of the web. The operating principle of reflex triode with a positive bias eikoni-Zeta in Fig. 4.21.

Electrons following periods, as they pass the rise encounter ahead the virtual cathode and pushed back to the area of the actual cathode. Per- Nontas again rise encounter the electrical field of the passage A-K, in which slows again, forcing the thus an oscillation between actual and eikoni- ment cathode. The reflex triode with a virtual cathode can still be driven with a negative voltage pulse to the cathode [49], the case illustrated in Fig. 4.22.

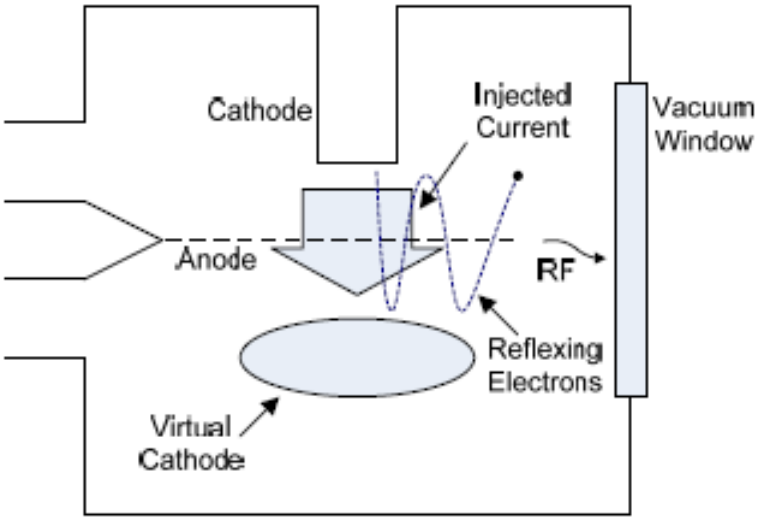

Fig. 4.21: Vircator type Reflex Triode with driving pulse to rise. The reflex triode Vircator not in the strict sense, because the extraction is due to the microwave trapping electrons between real and virtual cathode.

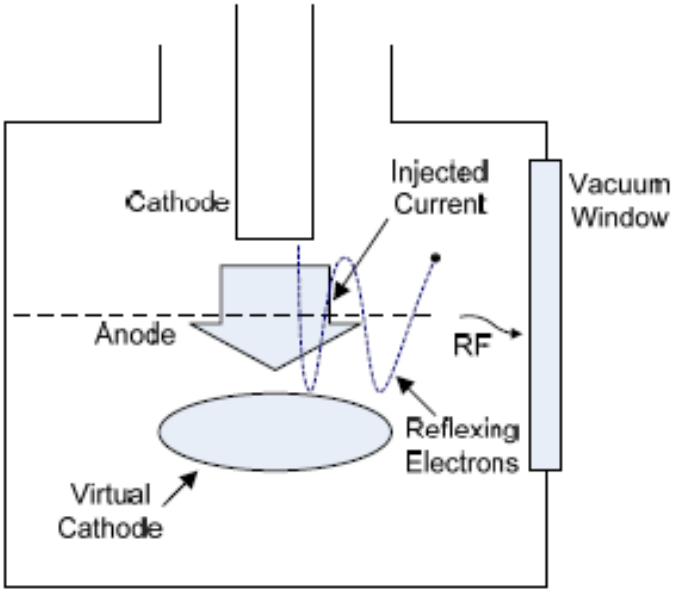

Fig. 4.22: Vircator type Reflex Triode with driving pulse to the cathode.

The body of a reflex triode may be a cylindrical waveguide, to which is fitted an outlet window of microwave radiation. Its location is such that it favors the microwave extraction, produced by troubled Dawson electrons between real and virtual cathode. The most common practice in reflex triodes is to use standardized vacuum components, such as crosses ConFlat various calibers. For example, in Fig. 4.23, shows a typical practical embodiment reflex triode Vircator [116]. In this figure we see that in a cross ConFlat, dimension 8 ", 4-way, is attached to the left of the system d- Pumping, the right cathode with a mechanism for moving the electrode, while the back side is attached to the insulator bearing the the anode electrode. On the front is mounted a standard large diameter glass window for export of microwave radiation.

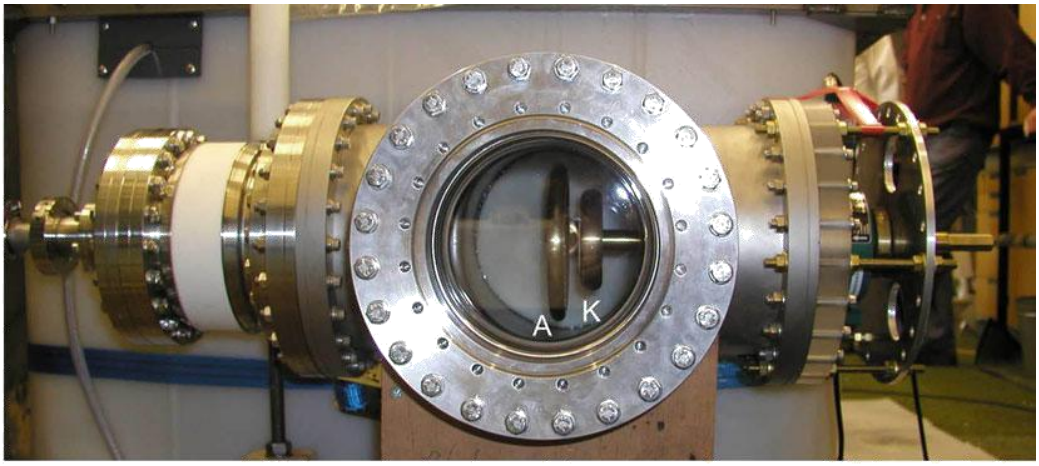

Fig. 4.23: Vircator type Reflex Triode. The pulse is driven to rise. Left is customized vacuum pump (not visible) through a dielectric ceramic liaison bodies, for electrical isolation of the pump from the impulse land [116].

Experiments with Reflex Triode Vircators:

Mahaffey et al .:

The first substantially light published by microwave radiation extraction experiment Vircator placed in 1977 by Mahaffey et al. [57] and in the patent that later patented [48]. Logged microwave power 90MW in the X band (around 11.6GHz), with positive trends driving 250-350kV, from generator resistor importance 7O & Currents 25kA peak. The yield of the experiment was estimated to be about
1.5%.

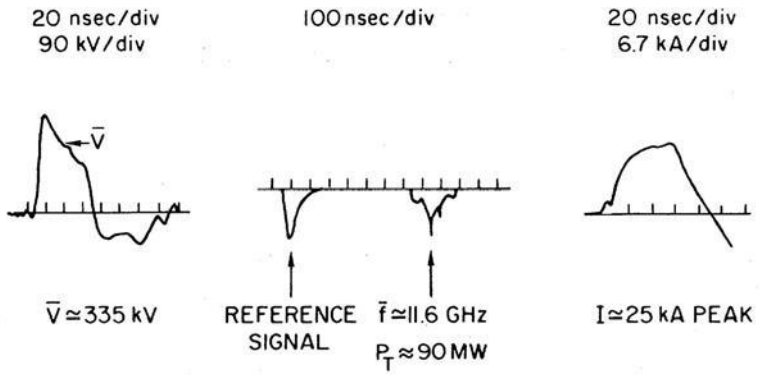

Fig. 4.24: Voltage, current and power of microwave radiation [57].

In the same paper we present the dependence that displays the output frequency of the applied voltage, for some types of cathode and for various anodou- descent distances. What we observed is that the output frequency is proportional to V1 / 2, and is inversely proportional to the distance A-K. It is confirmed that the general expression of the output frequency, which is, as we have seen above ,:

$$f f \text{ a } \frac{\sqrt{V_{AK}}}{d_{AK}} . \qquad (4.72)$$

The experimental results on [57] shown in the diagrams of Fig. 4.25 and Fig. 4.26.

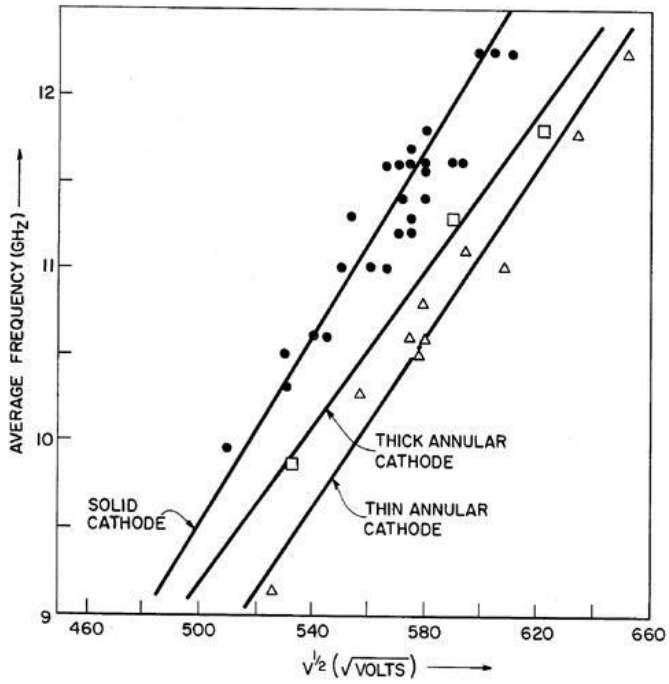

Fig. 4.25: The output frequency of reflex triode, a function of the driving voltage, for as various cathodes [57].

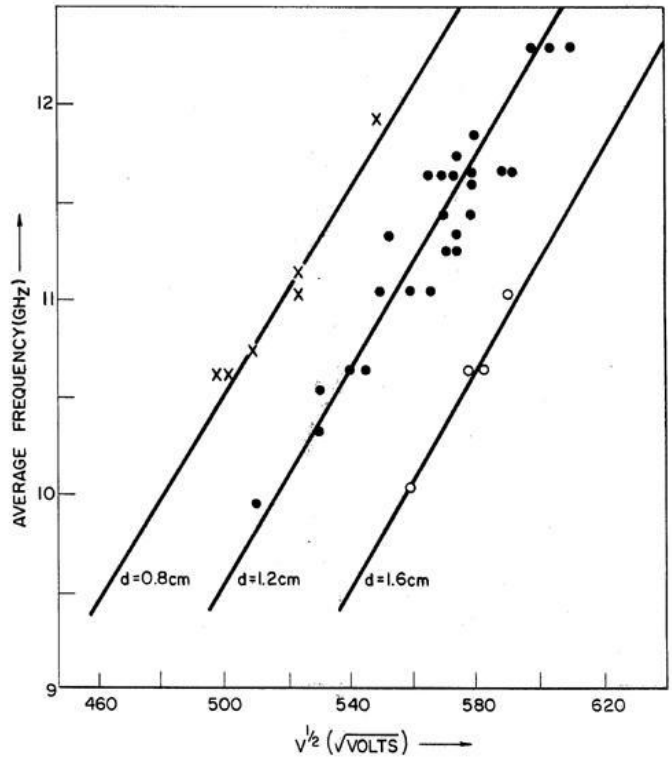

Fig. 4.26: The output frequency of reflex triode, a function of the driving voltage, for as various distances anode - cathode [57].

Price et al .:

The experiment of Price et al., The Vircator II [49], produced up to 500MW mikrokymation power in various low frequencies, the L, S and C bands. The specific Vircator was very large. Used cathodes 20 cm diameter and 60 cm distance and AK to 18cm. His body had Vircator inner diameter 80cm. DRAINAGE microwaves done with waveguide WR-510, with excitation at 1.15 GHz and WR-1500, with excitation at 393MHz, to study lower spectral content. The diode driving voltages amounted to 600-800kV and driving currents 50- 120kA. The very large lamp favor the existence of multiple rates, omega However the experiments in this indicator showed the existence of a dominant regulated me, who during the pulse passed at a frequency of about 200 με 400 MHz. This behavior is logical, because of the change in voltage in the passage as the phenomenon progresses, as well as the gradual reduction of the gap anodou- cathode, due to the spread of the plasma between the electrodes. Measurements edei- strated the typical inverse dependence of the center frequency of the anode-cathode distance of the lamp.

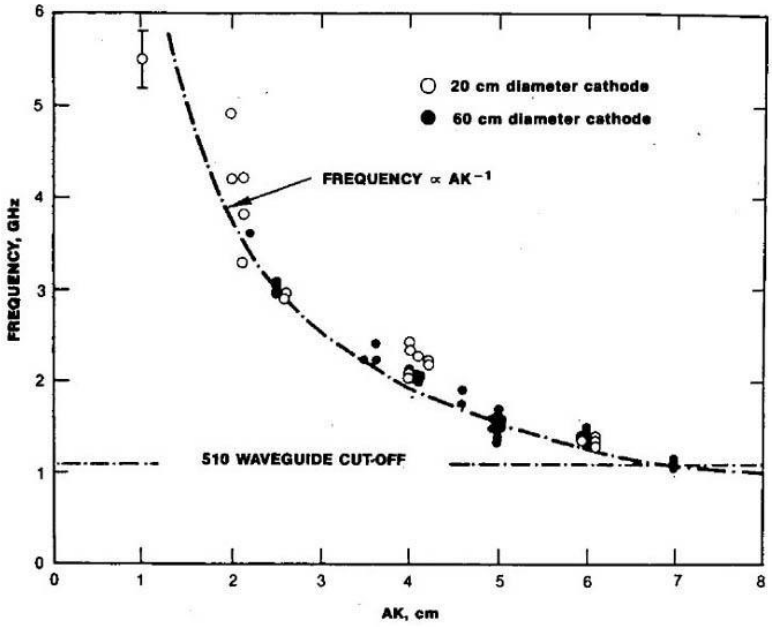

Fig. 4.27: The output frequency of reflex triode versus distance A-K, [49].

Hwang and Wu:

A new experiment with Reflex Triode Vircator yielded microwave power of more than 1GW. In the work of Hwang and Wu, [68], a Vircator, with two symmetric waveform digous WR-650 for export radiation yielded a total maximum power 1.4GW in various frequencies between 8 and 12 GHz, with the dominant frequency of 8.2GHz . Voltage odigi- ing 1.2MV and current 54kA, the above Vircator 450MW power observed in
8.2GHz, 30MW at 9.3GHz, 81MW to 59.3MW at 10.4GHz and 11.85GHz, on each output port. Total yield was estimated at about 6%. The vacuum in the tube was BRAKE ment of 10-5 Torr, while the anode-cathode distance of 1cm. It was also observed that

the diameter of the cathode plays an important role in the output power, maximum output can be reduced signifi- a 3.3cm diameter cathode coated fabric (velvet).

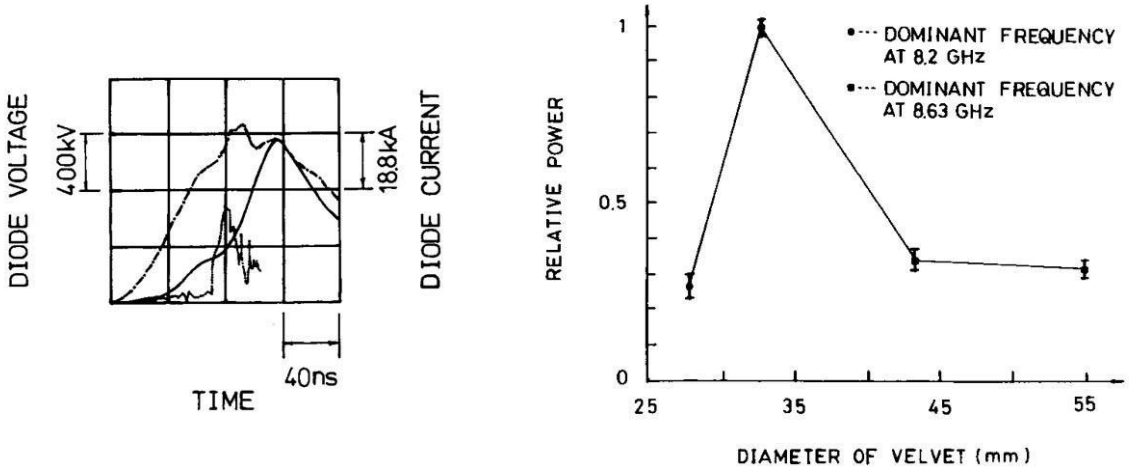

Fig. 4.28: Left: voltage waveforms, current and displaying microwave signal; Tosh. Right: Relative microwave power depending on the diameter of the cathode. Hwang and Wu, 1993 ([68]).

Didenko et al .:

An experiment with reflex triode Vircator showed that the cavity, which is formed by the virtual cathode and the microwave radiation is acquired, plays an important role in the power output of the lamp. The Didenko et al., [75], produce 1.2GW microwave power S-Band leading the Vircator with 540kV and current 18kA, achieving a return of 12%. They observed that the internal metal body of the lamp functions as syntonizo- next cavity, which greatly favors the production of microwave radiation

From this study it was also clear that the stability of the microwave output and efficiency of the lamp depend heavily on drive voltage diode of Vircator. Critical parameter is the driving pulse stable plateau ("flat-top"), with a duration of around 50-100nsec.

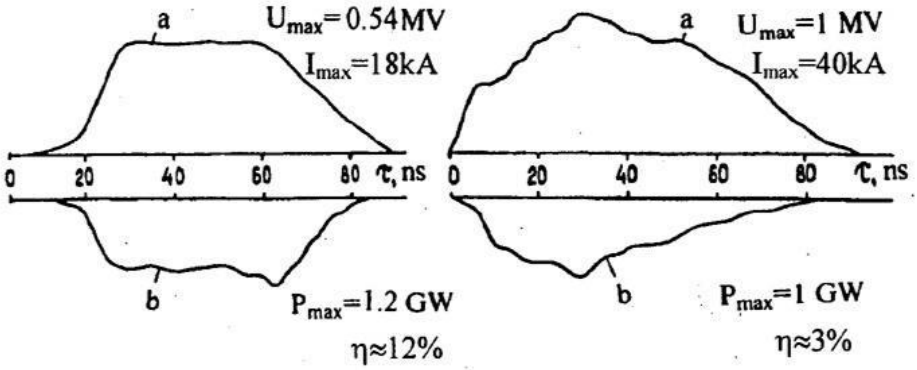

Fig. 4.29: The characteristics of the driving voltage pulse affecting quite a microwave tional output [75].

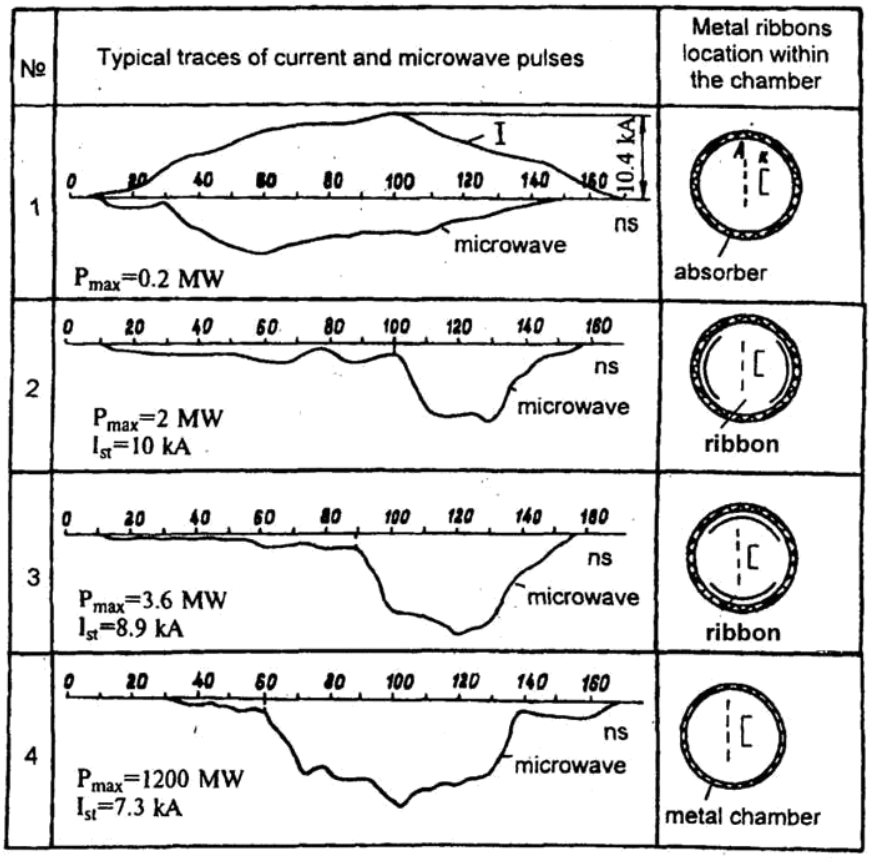

Fig. 4.30: The Didenko et al., [75], they found that, by placing an absorbent material or different sheets within the lamp output is significantly affected.

Huttlin et al .:

The Aurora is probably the largest pulse generator strong relativistic electron beam with energy of about 10MeV and current 250kA load 35O. It was examined the possibility of generating microwave radiation by application of the virtual cathode phenomena mind creation. Using an array reflex triode, with transit rise Food 1.22m the Huttlin et al. produced more than 20GW iota microwave power constraints to frequencies below 1GHz [85]. The anode used aluminum sheet thickness 16mm, while the anode distance - descent was 23cm. In the body of reflex diode attached six waveguides WR-975, cut-off frequency 605 MHz, for export of microwave radiation, which placed 27 cm below the anode. Driving passage recorded about 6.5MV and 300kA, which means a passage resistance of about 22O.

Holt et al .:

In the [117] describes a reflex triode, which is driven by the compression generator inductive energy. Generators using such a coil, which flows through current. Eventually, using explosives, is compression of the stored in--effects due to the rapid reduction of the active length of the tube. The defendant re-stream from this process is driven by the load switch (more

for pulse generators of this type are discussed in [118]). In this imple- mentation was achieved output 4MW to 3.8GHz by a pulse duration of about 100ns. The anode used was a stainless steel mesh with a permeability of 70%, while the voltage on the diode was 100kV, relatively small Vircator data. The vacuum diatirou- when the 7.5 · 10-6Torr. The yield is estimated at about 1%, but in this work is a report that the compression of the current reaches 40kA, so this would mean return of 0.1%. Possibly the total power output is measured at the initial charging of the coil, before the eruption of the solenoid.

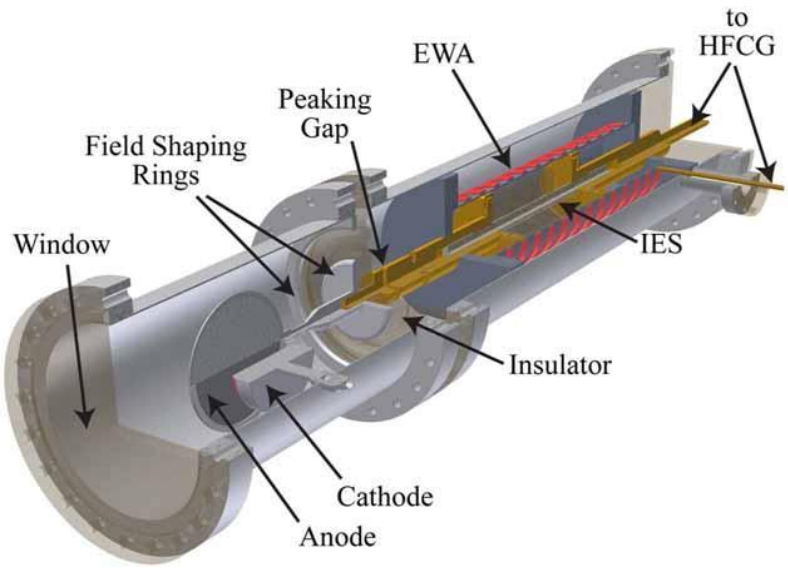

Fig. 4.31: Reflex Triode Vircator, driven by inductive energy storage. , Or the same term of validity is done using explosive ([117]). IES: Inductive energy storage, EWA: exploding wire array, HFCG helical flux compression generator.

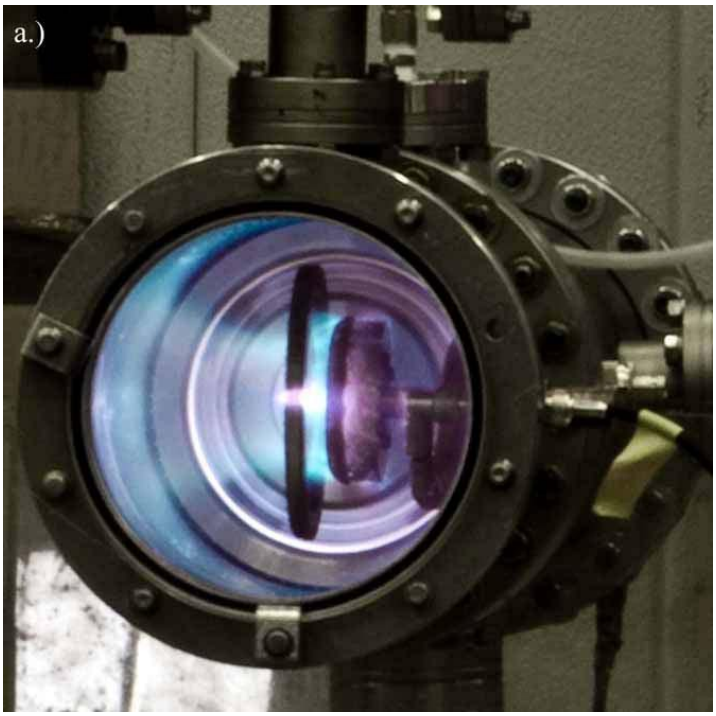

Fig. 4.32: Picture of the plasma generated during the operation of the Reflex Triode Vircator [117]. The polarization is positive and this trend led to the rise.

Particularly interesting is the image of the plasma generated in the light (see. Fig. 4.32). The plasma is generated mainly due to the ejection of material from the cathode and the anode in the space. Light emission is from ionized fo- carriers that undergo energy transitions within the band of visible light, i.e. few eV. The plasma channel deviates to the walls of the device, which is grounded, and occupies a large part of the periphery of the cavity.

4.5.2. Axial Geometry

The axial Vircator (axial Vircator) has cylindrical symmetry and the space in which the virtual cathode occurs, is electrically isolated from the region of the anode-cathode appointed period. The direction of travel of the electron beam and the direction of extraction of the microwave radiation are generally parallel, opposed to the reflex triode Vircator. Therefore, the specific type Vircator characterized as "axial" export (axial extraction) unlike reflex triodes, which presented live "radial" or "vertical" export (radial or vertical extraction). The axial geometry as in triode geometry, two phenomena compete production tional microwave radiation. The first is the trapping of electrons between the actual ment and virtual cathode, while the second is the oscillations in space and the intensity E of the bubble of the virtual cathode. Axial Vircators usually designed so that electronic oscillations are coupled with a TM pace digou waveform output. This practice is used because the virtual cathode and the electronic, which are trapped in the potential well between the real and virtual cathode perform oscillations in the axial direction z of the Vircator. Therefore renders easier coupling with Ez and Hf components of the electromagnetic field of a TM rate.

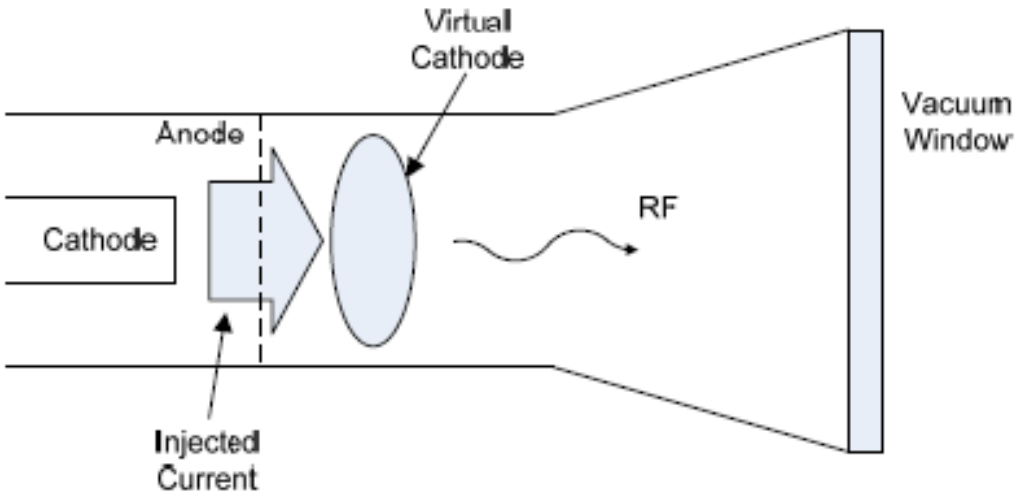

Fig. 4.33: Vircator axial geometry. The cathode, the anode and the body of the E Vircator contain a cylindrical structure and export of microwave radiation is generally a cylindrical waveguide in a direction parallel to the injected current.

Experiments Axial Vircators:

H. A. Davis et al .:

In 1985, the Davis et al. at Los Alamos produced with axial force Vircator 500 ± 130MW to 17GHz and 100 ± 30MW area from 30 to 40GHz [47]. For anode was used a foil thickness of 6 microns, a 0.4 to 0.9 cm from the cathode. The drive voltage of Vircator stood at 1.2 with 3MV and current from 75 to 90kA. The FWHM pulse duration was about 60nsec with a rise time 40nsec. The gap in the lamp was approximately 3 · 10-5 Torr.

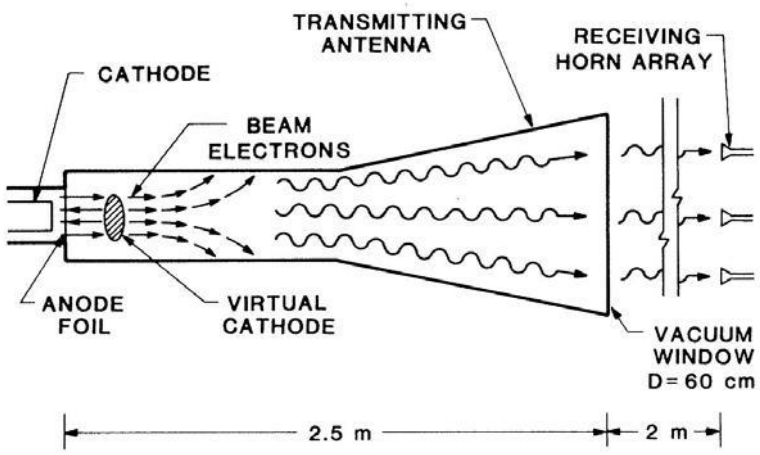

Fig. 4.34: Axial Vircator [47].

According to the authors, the microwave power, presented the lowest frequency of 17GHz, due to the frequency reflexing of electrons between the real and the virtual cathode. The potency observed in the zone of 30-40GHz may be due either to the longitudinal vibrations of the virtual cathode, when the address of the centerline of the Vircator, or to create second harmonic by electrons backscattered from the virtual cathode, raising microwave radiation by half the period of their movement.

S. Burkhart:

In 1987, S. Burkhart, using axial Vircator, recorded more than 4GW force to 6.5GHz [82]. In this experiment, an electron beam schetikisti- RH 2MV used, 6O, while the anode-cathode distance to this me- measurement was 2cm. Smaller gaps showed that bias the output frequency to the sta- tion, and the change in diameter of the cathode had no significant effect on the frequency of the generated microwave radiation. The rise was foil re- objectives 0.3 to 1 mil (1mil = 0.001 "= 25mm). The gap in provision was maintained at levels Asia Mi- krotera of 6 · 10-5 Torr. The cathodes used had diameters from 59 to 87mm, with 0.7mm deep etched grooves, spaced 0.8mm and coated porous carbon, to achieve greater electronic emission.

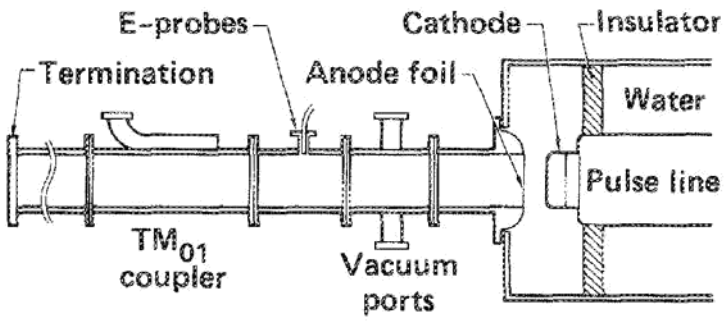

Fig. 4.35: Order experiment with axial Vircator of [82].

The performance of this experiment was around 3% for the measurement at 4GHz. Also observed in the frequency shift upwards during the pulse of 60nsec used to drive the diode.

R. Platt et al .:

In 1989, Platt et al. They produced the impressive power of 7.5GW to 1.17 GHz mate-mopoiontas axial Vircator [83]. They used an electronic beam 4MV and tensions ing 80kA, which was channeled through an aluminum mesh 0.25mm thickness in gov- lindriko waveguide diameter 19cm. The vacuum tube was maintained at 5 · 10-6 Torr, while the radiation emitted by a choanokeraia diameter 1.22m, through a door production from acrylic glass (lucite) thickness 7.62cm.

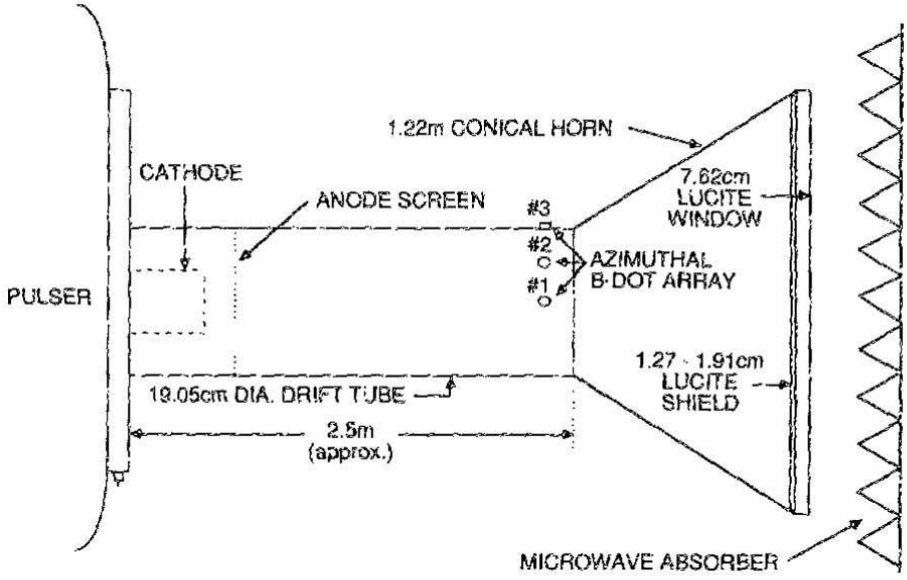

Fig. 4.36: The axial Vircator of [83].

A series of eight shock force produced 7.5 ± 0.5GW to 1.17 ± 0.02GHz, pulsed Asia Mi-Cretan duration of the order of 10nsec. The yield strength of this experiment was estimated at 5.3%.

K. G. Kostov et al .:

The KG Kostov and NA Nikolov, a series of experiments with a fixed axial Vircator digoun magnetic field produced potencies of about 15MW in the range of 11 to 22GHz ([61], [62]). The voltages were 200 to 480kV, while the currents from 2 to 7kA. From the experiments in this Vircator found that the magnetic field has no effect on output reflexing frequency while having little negative effect on the strength of the lamp. Note that the views on the effect of magnetic field on Virca- tors divided, with the prevailing habit is *non* use. Exception constitute LEDs Vircator type Reditron, in which use magnetic field is necessary. The gap in this indicator was maintained at about 10-4Torr, while the rise was mesh stainless steel (stainless steel mesh), 0.5mm thickness. The cathodes used by Kostov et al. They have diameters of 10, 20 and 30mm, while the distance A- K was from 3 to 7mm. Lamp pumped at a point near the diode region (see. Fig. 4.37), since the simultaneous evacuation of inert space on the other side of the anode, enabling the matrix permeability of 70%.

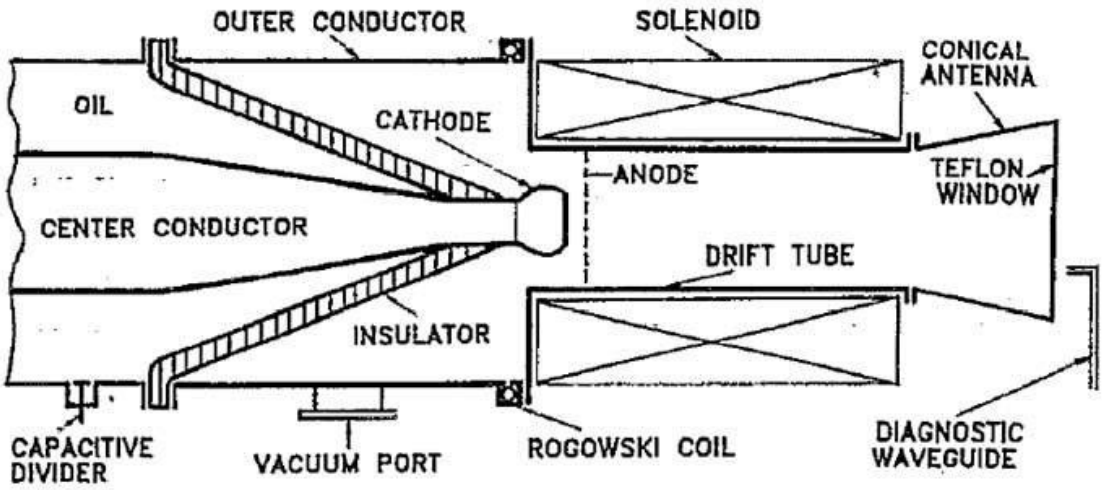

Fig. 4.37: The axial Vircator with guiding magnetic field (from [62]).

In the first study of two ([61]), the researchers claim that the strongest source of electromagnetic radiation is reflexing of electrons between the actual ment and virtual cathode, leading to the appearance in the spectral content of about 12GHz. Weaker microwave radiation in the area over the 15GHz attributed to oscillations of the virtual cathode. In the second study, however, ([62]), it is probable that the main radiation source is the oscillation of the virtual cathode. There is talk of only one center frequency, which for specific shaping (cathode diameter 30mm, dA-K = 4mm) does not change significantly under the influence of the magnetic field (see. Fig. 4.38). However, other configurations of the experiment with Asia Mi- kroteres cathode diameters, leading to apparent dependence of microwave frequencies: the relationship

$$f = k \cdot \sqrt{\frac{J}{b \cdot c}} \quad , \tag{4.73}$$

concerning the dependence of the oscillation frequency of the virtual cathode (affiliated with the frequency plasma beam) of the injected current density *J*And the parameters b and c of the electron beam. These researchers conclude that the output due to oscillation of the virtual cathode, because assess- importance for the reflex frequency as given by

$$f_{refl} = \frac{1}{2Fr} \cdot \frac{u}{2d}, \qquad (4.74)$$

(See. The reference [62]) leads to much lower frequencies than those observed. It made even a simple attempt to justify the patient ing round effects of the magnetic field in the frequency, on the grounds that this maintains the radius of the beam constant, thus not changing the spatial current density and thus in- pektasi plasma frequency for the same parameters experiment.

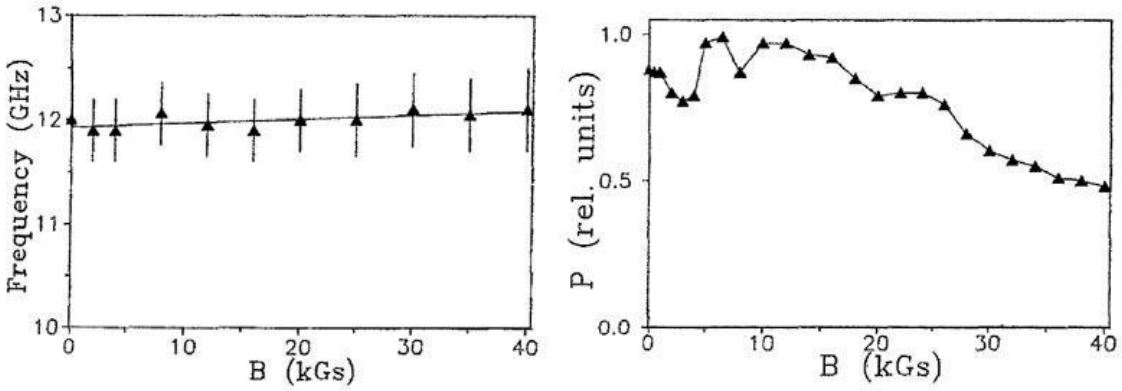

Fig. 4.38: Influence of the magnetic field in the frequency and strength of the axial Vircator [62]. Ray Cathode 30mm gap and A-K 4mm.

E.-H. Choi et al .:

The team of EH Choi received from around the axial force Vircator amounts of 200MW in 6.7-7.2GHz [67] and 5.5GHz [119]. In the first case, driving the lamp was with 290kV and 21kA, with a gap of A-K equal to 5mm, while in the second case 240kV, 23kA, and a gap of 4mm. The gap in provision was about 10-5 Torr.

In the [119] is the estimate that the anode gap - cathode closed by a rate of about 3cm / microseconds, due to the plasma generated. Also, for different gap distances, the largest power of 200MW observed for 4mm gap, and even displayed at the lower frequency of the experiments, the 5.5GHz. In this case, the microwave irradiation appeared under high anti situation diode and large gap voltage, which means a large relativistic sys- coefficient and therefore less beam plasma frequency. Recall that frequency section of the plasma beam invite quantity *oh* $_{p} = \sqrt{ne^2 / e_0 cm_e}$.

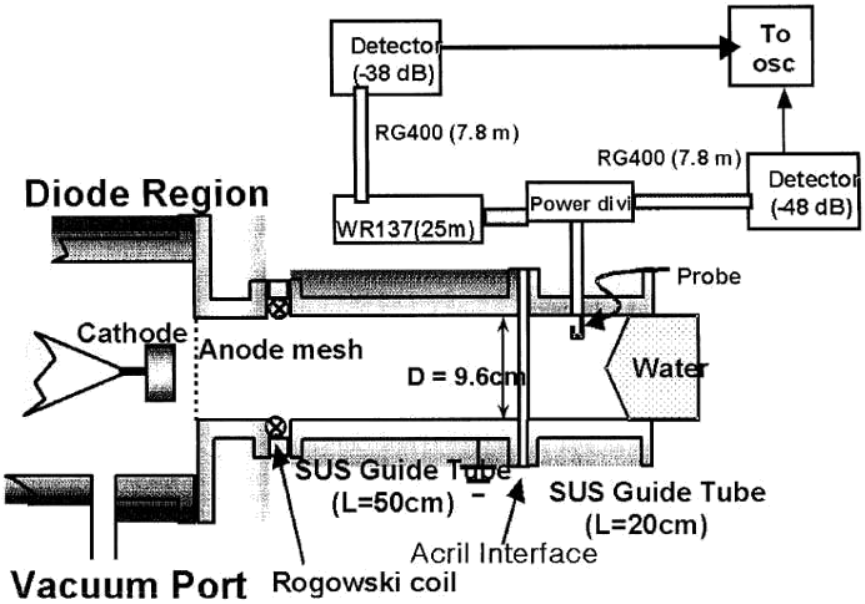

Fig. 4.39: The experimental setup of [119].

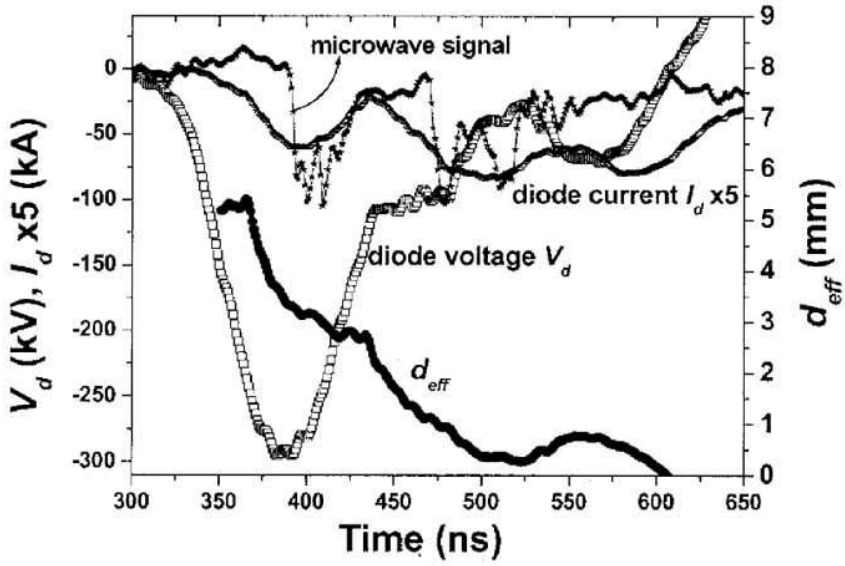

Fig. 4.40: Voltage Waveforms, and microwave power output Vircator. Com- ing is shown and the time evolution of the gap A-K, because of the creation and of spreading plasma passageway ([119]).

4.5.3. Coaxial Geometry

The coaxial Vircator (coaxial Vircator) having cylindrical symmetry, but the current of the diode is radial as opposed to axial Vircator, in which the current is injected along the centerline. The cathode has a greater radius than the anode and encloses. The current of the diode forming the virtual cathode in the anode interior Kd near the centerline of the device (see. Fig. 4.41)

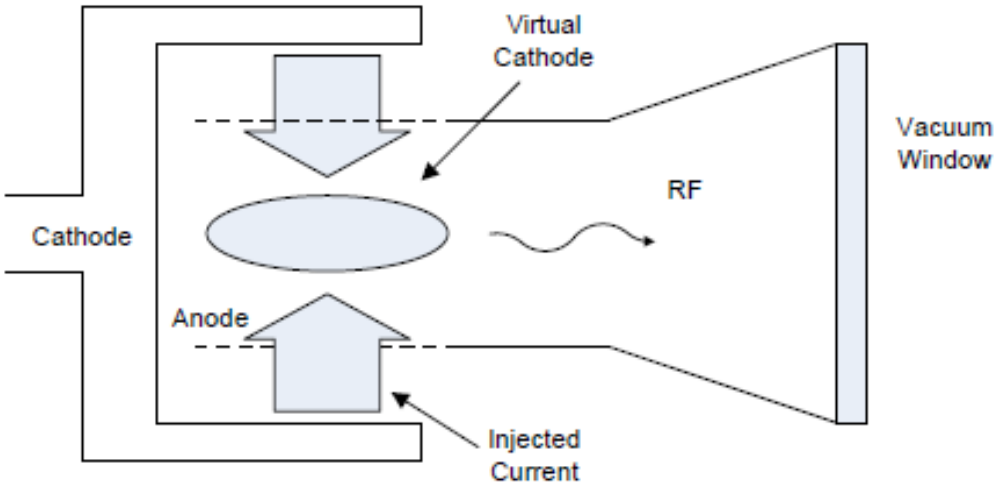

Fig. 4.41: Vircator coaxial geometry. The cathode, the anode and body Vircator have cylindrical symmetry, however, the stream is passed radially through the mesh, forming a virtual cathode. The export of microwave radiation is a cylindrical waveguide in a direction perpendicular to the injected current.

The arrangement allows the diode electron oscillations in the radial component, stimulating mainly cylindrical TE rate in Vircator.

Experiments with Coaxial Vircators:

W. Jiang et al .:

The team of W. Jiang experimented with coaxial Vircator driving the lamp with pal-mousse 500kV, 40kA and duration 30nsec. The radius of the cathode was 13.1cm, 9.9cm the anode and the cathode was covered with fabric (velvet) with width 3cm. The rise was a cylindrically shaped stainless steel mesh. The experiments gave Asia Mi- krokymatiki radiation 400MW to 2GHz, with a corresponding power electronic beam equal to 18GW, thus defining a yield of 2% [120].

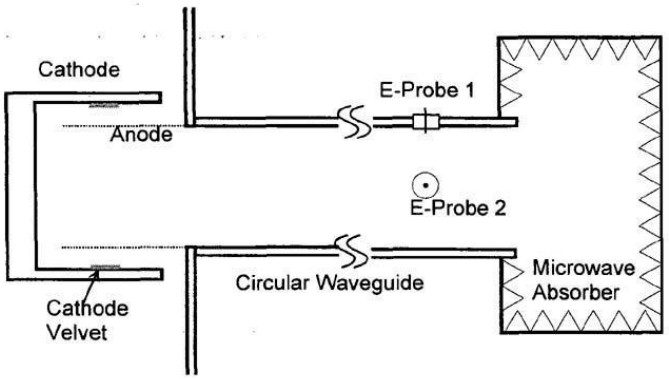

Fig. 4.42: The coaxial Vircator of W. Jiang et al. (From [101]).

By using a metal foil as microwave reflectors within the cylindrical anode and spaced 3.6cm from the imaginary radius through the cathode fabric strip achieved power increase of about 2.2 times,

reaching 900MW power ([73], [101]). According to the authors, the frequency re- flexing of electrons between the real and virtual cathode should be

$$f_{refl} = \frac{1}{4T} = \frac{1}{4} \int_{r_{VC}}^{r_A} \frac{1}{e} dr^{-1} \cong 1.3GHz , \quad (4.75)$$

the frequency of oscillation of the virtual cathode, as described under [52], resultant oversight equal

$$f_{osc} = \frac{Fr.}{\sqrt{2}} f_p \cong 3.5GHz . \quad (4.76)$$

The frequency, which is determined experimentally and, as mentioned 2GHz, βρίσκε- Tai somewhere in between. The difference may be due both to the deviation from the reasoning be- frequency reflexing, for which unilaterally taken the path be- tween the anode and the virtual cathode, and in fact the interaction region of the virtual cathode, with the area of diode, since these two are not electrically isolated in this experiment coaxial Vircator.

K. Y. Sung et al .:

In an experiment with coaxial Vircator, the KY Sung et al. 244MW produced microwave radiation, to 5.47GHz, with a yield of 2.75% [87]. Driving the passage about 245kV and 36kA a 12-point Marx generator charging voltage 50kV per grade. The cathode EI- yes aluminum, while the rise of a cylindrical stainless steel mesh. The gap varies between 4 and 8mm. The gap in Vircator experiment maintained at 10- 5Torr, while the cylindrical output waveguide diameter 9cm, and the corresponding cutoff frequency of approximately 2.4GHz. An acrylic window (Plexiglas) thickness 2cm is topo- thetimeno in choanokeraia output.

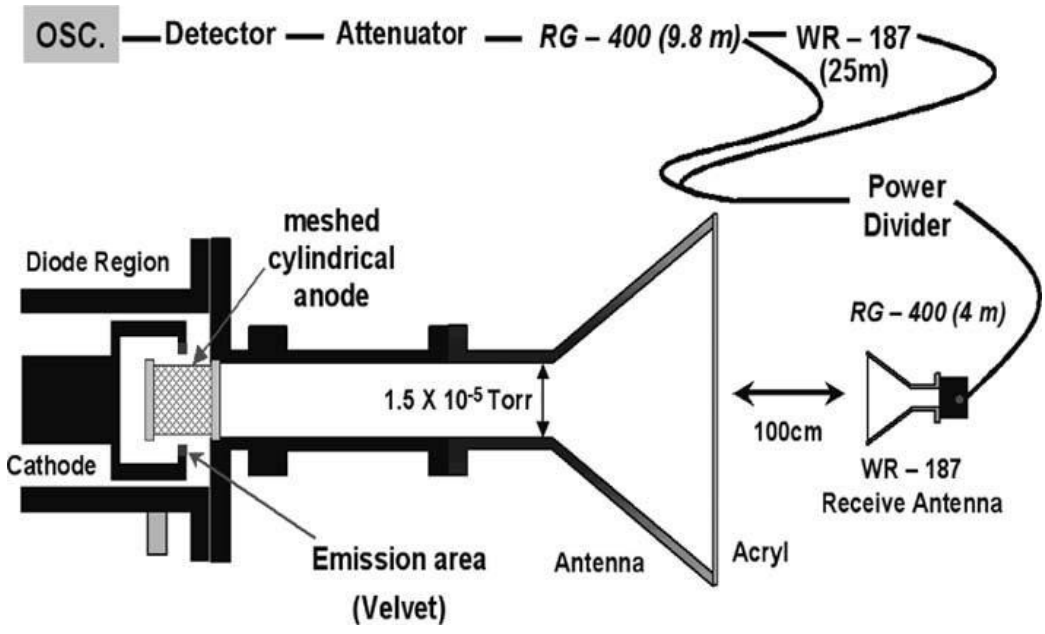

Fig. 4.43: The coaxial Vircator of KY Sung et al. (From [87]).

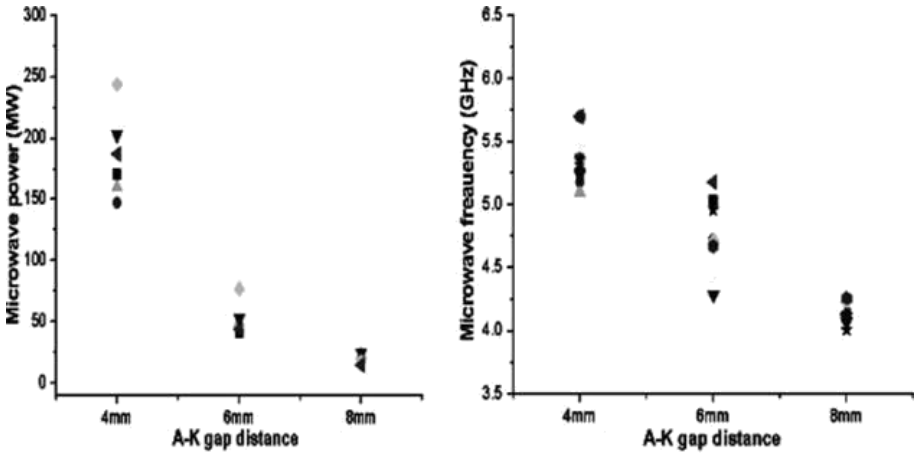

Fig. 4.44: The effect of the gap A-K in the power and output frequency of the omoaxonition Vircator [87].

From the experiments appear inverse frequency dependence of the length of the cross gap in the passageway, and the results are quite close to estimates made using the PIC MAGIC code.

W. Jeon et al.

We refer substantially to the same Vircator in the foregoing, by which the W. Jeon et al. They managed to take more than 1GW microwave power allazo- ing certain parameters of the device [121]. Placing the gap anodou- cathode to 10mm 1GW received power at 3.38GHz, 28% yield, whereas with proper positioning of a metal sheet thickness of 20mm, at a distance of 80mm from the position of the cathode the microwave power is increased to 1.5GW, with corresponding performance unreal 45%. Driving the passage was to 246kV voltage and current of 14kA. Despite the gen- fry that such performance has never been reported again and is quite yperektimime- screen, this test provides image sizes that can be achieved by careful selection of the parameters of a Vircator.

4.5.4. Geometry Vertical Exhaust

The Vircator vertical or lateral outlet (transverse or side-extracted Vircator) poieitai usually used for export of microwave radiation on TE10 rate a gov- matodigou rectangular. The electric field of the anode-cathode path is parallel to the short dimension of the waveguide, and usually there is complete electrical isolation of the diode region from the output waveguide. The vertical exhaust geometry can be used as a variant of reflex triode, where the anode is based on a point within the usable space of the waveguide and not in Eudivine walls. In this way, the movement of electrons between the real and virtual cathode can be coupled with the best electric field TE10 regulated me. If the rise is in line with the walls of kyma- todigou, more emphasis on coupling the oscillations of virtual lays period with microwave field.

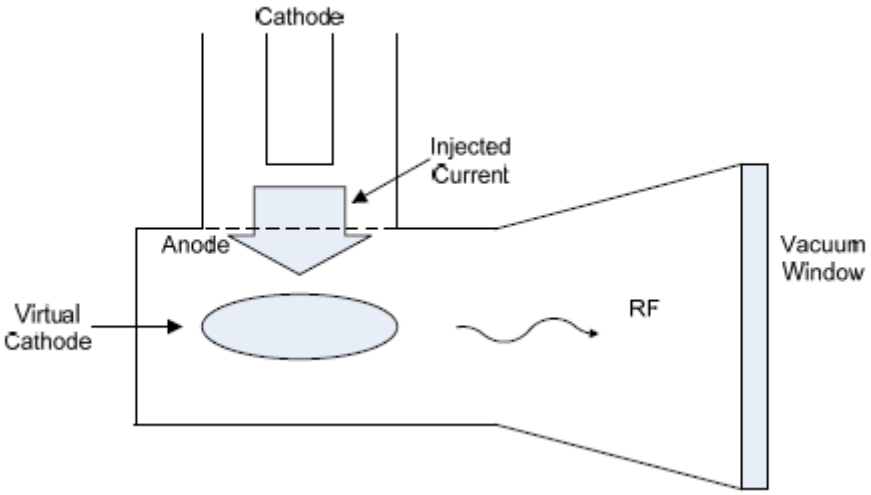

Fig. 4.45: Vircator vertical geometry. The Vircator body is formed of gov- matodigo rectangular section, while the current is led from the mesh of the anode is generally positioned on the long side of the waveguide. The export of micro- wave radiation is in the direction perpendicular to the injected current.

O Vircator vertical exhaust has the advantage that it can be directly coupled to standard choanokeraies rectangular for export and irradiation of microwave power. It also has the special feature of the export mikrokyma- tion radiation mainly in the rhythm TE10, the contribution of the other rates to be much lower [6].

Experiments with Side-Extracted Vircators:

Benford et al .:

The group of Benford, Sze, Woo and Harteneck did some experiments with Vircator Down foster export, achieving 350MW microwave power ([122], [123]) to drive the diode voltage and current 1MV 100kA. The performance of experiments calculated to approx 0.6%. Used waveguide dimensions 12.7x6.4cm, rising from certi- Member of aluminum 25mm thick and 5cm diameter cylindrical flat cathode. The clearance passage was 1cm. The vacuum was approximately 5 · 10-5Torr, with some pistons borou- as to modify the distance of the virtual cathode from short-circuiting of m- particle surface of the waveguide and the distance from the opposite side (see. Fig. 4.46). The occurrence of radiation bands observed were 8.9, 9.10, 10-11 and 11- 12GHz, with the majority appear in 9-10GHz. It was found that the creation of the microwave radiation is due more to the behavior of the virtual cathode, despite the phenomenon of trapping of electrons in the well potential-between real and virtual cathode.

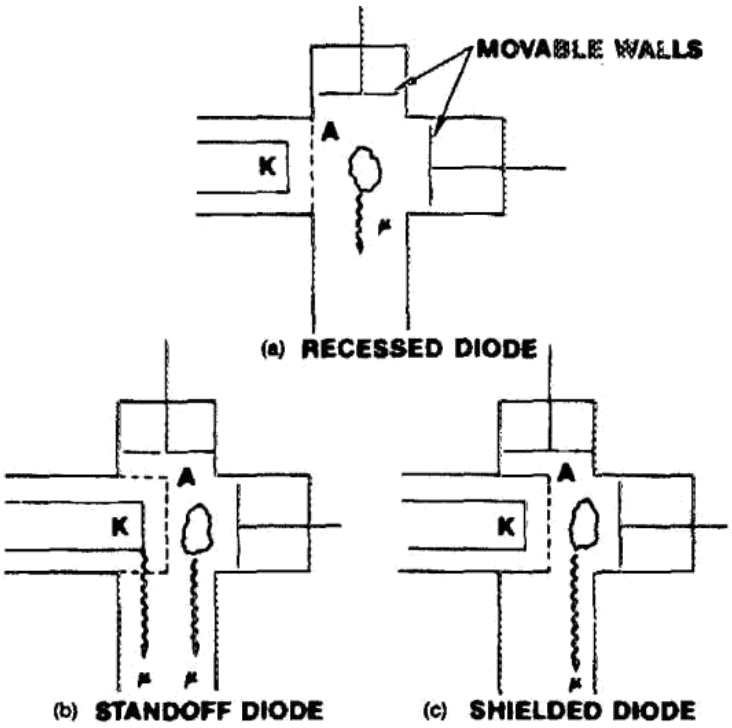

Fig. 4.46: Ways of formation of the geometry of the diode within the waveguide of export of radiation [123].

In the experiments described, the case of (c) (see. Fig. 4.46) gives ptocho- particular results, followed by the configuration (a). The symmetrical shaping of the cathode-anode-cathode virtual system within the waveguide (b) di- beyond what best results microwave output. This is probably due to the exploitation of both reflex oscillations of electrons, and the oscillations of the virtual cathode.

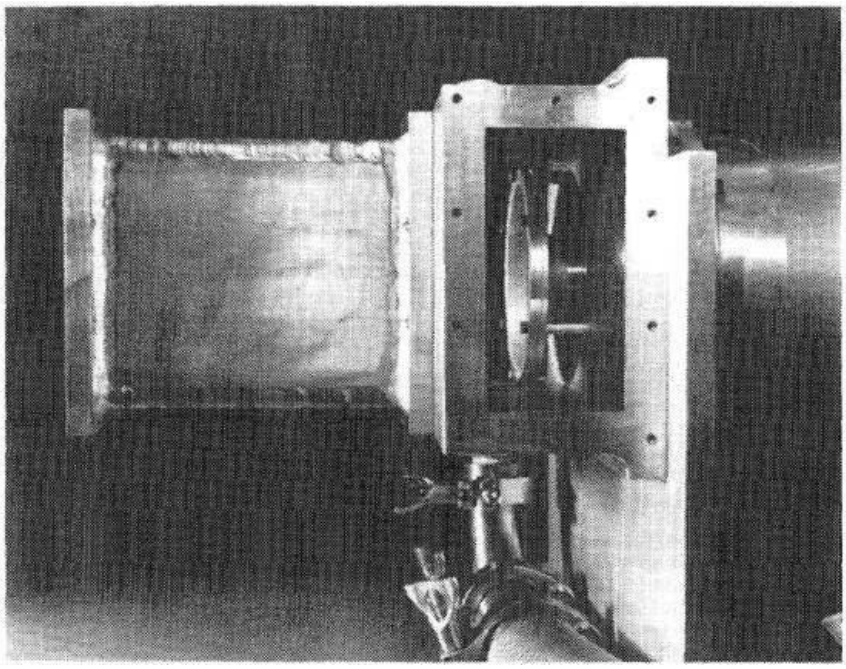

Fig. 4.47: Vircator vertical geometry [123]. The cathode and the anode grid vrisko- are within the useful area of the waveguide.

Hwang et al .:

The Hwang et al., Using a similar device to Benford et al., Produced 120MW microwave radiation at 8.63GHz, together with smaller amounts of power at higher frequencies (75MW at 9.75 GHz and 60MW in 10.53GHz) [124]. Driving the diode was voltages from 660kV up 1.2MV and currents from 37 to 88kA. Used anode foil 15mm thickness and waveguide in-Exit type WR650. The vacuum was maintained at 10-5 Torr.

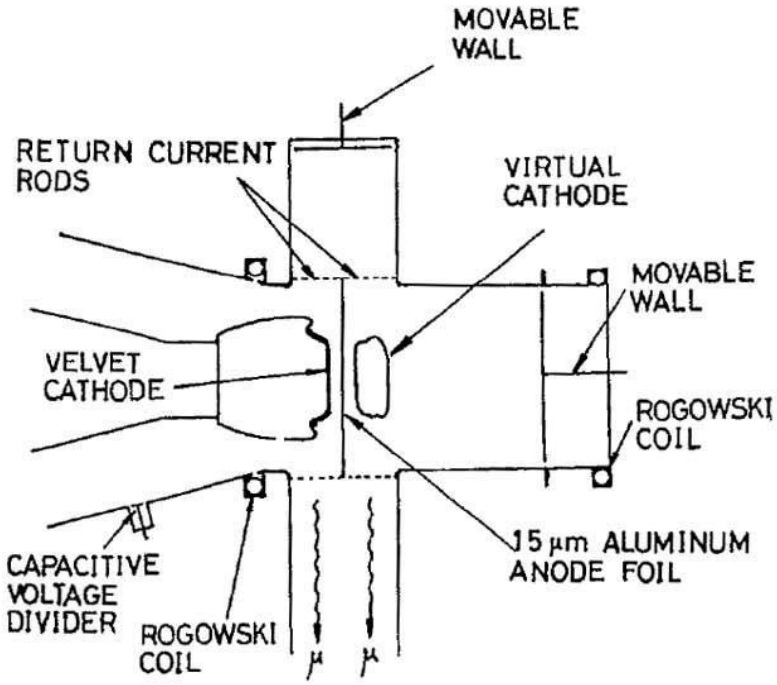

Fig. 4.48: Vircator vertical geometry with emphasis on coupling reflex oscillation (from [124]). The anode is parallel to the middle of the small dimension of the waveguide.

It was observed that the output is not influenced by the movable members (see. Fig. 4.48), which showed that, in this experiment was not created conditions favorable to tune the microwave radiation. The output frequency influenced by the intensity of the injected current to the lamp and the anode-cathode distance.

In a modification of the above experiment ([68]), the Hwang and Wu placed two identical outputs antisymmetry in the layout, using waveguides WR650. Comments exit 1.4GW to 8.2 GHz, noting a yield of around 6%. The Direc- tion for this output was 1.2MV and 56kA. Used cathode cover to close Meni fabric (velvet) within 1cm from the anode and diameters 2.8cm, 3.3cm, 4.3cm and 5 cm, with a diameter of 3.3cm to achieve said results. The anode was again sheet aluminum, 15mm thick, which was placed in the middle of the short dimension of the waveguide output, for reasons of symmetry. The vacuum was maintained at 10-5Torr. In each of the two outputs of the lamp were measured
450MW at 8.2GHz, 30MW at 9.3GHz, 81MW to 59.3MW at 10.4GHz and 11.85GHz. Note that in the above experiments, the microwave output appeared in were first liberalized percentage TE10 rate.

4.5.5. Geometry Press Reditron

The lamp Reditron (**R**eflected **E**lectron **Di**scrimination Oscillator) is a variant of the axial Vircator, we have seen previously. It was suggested some time after the simple alpha xoniko Vircator, the same team of scientists in Los Alamos (see. [47] and [56], and US Patent 4730170, [77]). To reset the effect of electrons engage reverse sthoskedazontai the virtual cathode in the region of the passage, is used *annular* electron beam (*annular beam*) thicker anode, bearing schi- term. The cathode is designed to emit electrons in the form of ring; type beam, which is accelerated towards the anode and passes therefrom through suitably shaped circular slot.

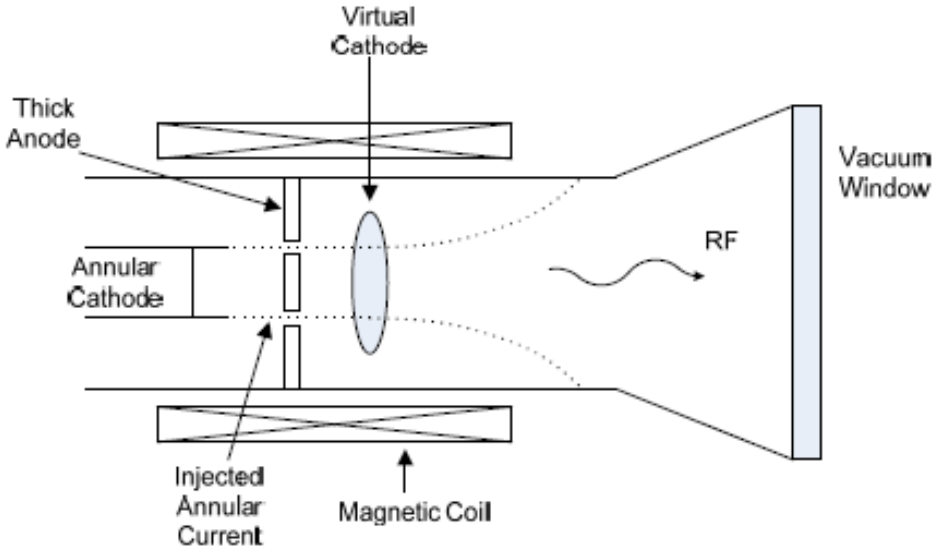

Fig. 4.49: Vircator formula Reditron. The peculiarity of Reditron lamp is the rise slit, which does not allow the return of electrons in A-K, apokleio- ing microwave output from the phenomenon reflexing.

The geometry used is cylindrical magnetic field. The backscatter electrons from the virtual cathode leads heavily on the rise. EI- so practically negligible percentage of electrons that manage to return to the diode region, therefore, the microwave generating mechanism in Reditron light is only the oscillations of the virtual cathode. In this sense, the Reditron is a real virtual cathode oscillator.

Experiments Reditron Vircator:

H. A. Davis et al .:

The team HA Davis in Los Alamos, after axial Vircator, made its first and im- mantikotera experiments Reditron type lamp. The first version of the lamp, as pre- sented in [56], produced 1.4 ± 0.3GW microwave radiation in the 3.9 ± 0.4GHz.

The lamp, namely the area of the passage and the first 16cm of the waveguide outlet, located in a magnetic field with an intensity ranging from 0 to 30kG. The descent was 6cm diameter and the emitting surface had a thickness of 0.05cm. The distance from the rise ranged from 1cm to 3.7cm, while the rise was forming the required slot, supported by three points, covering about 6% of the electron beam. The output waveguide was cylindrical, diameter 18cm, length of 1.25m, while the edge was appended a choanokeraia length 1.25m. The device was vacuum 3 · 10- 5Torr. By varying the gap from 1.7 to 3.7cm, the voltage of diode varied by 1.4MV to 1.9MV, the flow passage 48 to 35kA, and the propagated current from 14 to 20kA. The best results were achieved for magnetic field 5kG, and anode-cathode distance equal to 2.6cm.

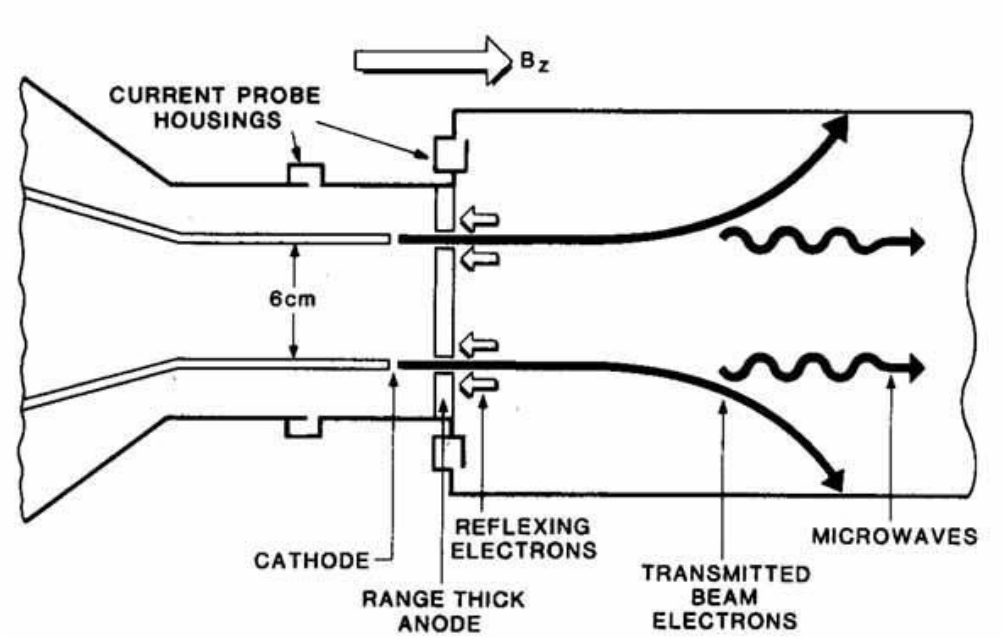

Fig. 4.50: Reditron Vircator (from [111]).

The output frequency of Reditron falls with increasing gap A-K, while remaining relatively unaffected by changing the driving magnetic field [111]. The dominant output rate was the TM02.

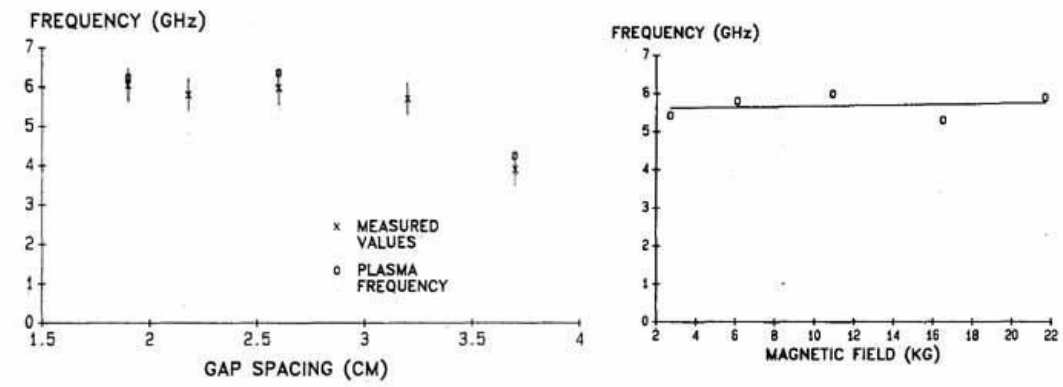

Fig. 4.51: The output of Reditron Vircator versus gap A-R (left) and magnetic field (right) for clearance 2.6cm. (From [111]).

In [55] the performance Reditron Vircator estimated at approximately 5.5%. Received 1.6GW to 2.46 GHz, with driving the diode voltage 1.3MV and current 22kA. The blank of the lamp was in 3 · 10-5Torr, while the magnetic field was 7.3kG.

4.5.6. Geometries with Resonant Cavity

To improve the performance of a Vircator and concentrate the spectral content of the microwave output closer zone technical in- gkleismou virtual cathode inside a cavity used. Phenomena observed PRIMA lock when the frequency of "free» (free-running) Vircator is near the resonance frequency of the cavity within which the virtual cathode is formed.

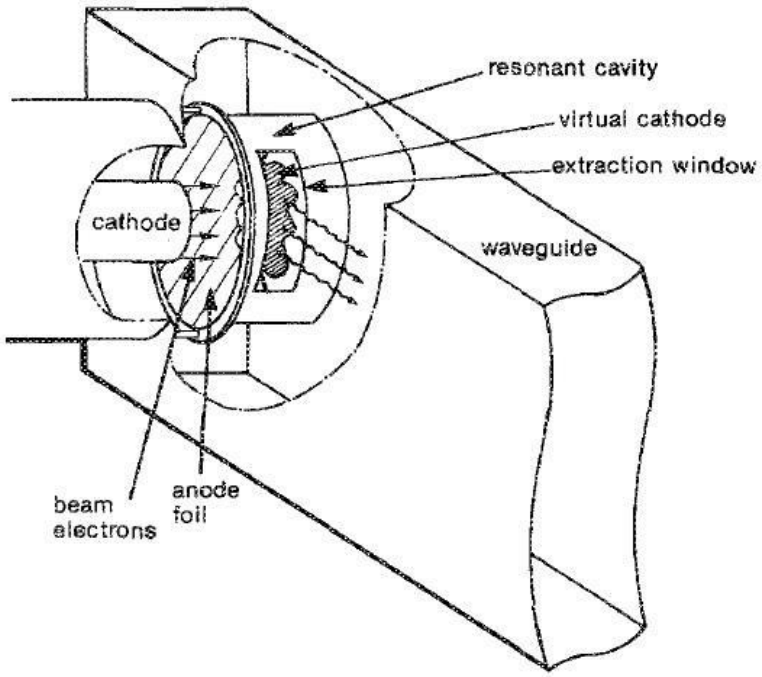

Fig. 4.52: Vircator vertical exhaust resonant cavity [125].

For example, [125], the Benford et al. They received up to 320MW in various quantities resonance frequency in the band 3.5-4.5GHz, changing the dimensions of the enclosing Com- versity of virtual cathode (see. Fig. 4.52). Improved output for the resonant cavity was about 1.5 times than that without cavity, while the "incompatible" koiloti- them showed reduction of the microwave output. Moreover, slippage of frequency (chirping) in Vircator without cavity was to 1000MHz, while periorizo- cavity when at 200MHz. Driving the above experiment was done by electron beam 1MV, 100kA, 65nsec. The output waveguide was rectangular 12.7cm * 6.4cm. The clearance passage was 2.1cm and the diameter of the cathode 5cm.

In the case of the coaxial Vircator, which has been presented previously (see. Par. 4.5.3) has been using the reflector, which is mounted to the outlet of poly- XVIa, at some point of the circular waveguide. The reflectors are shaped such tape or annular screen ([102], [103], [121]).

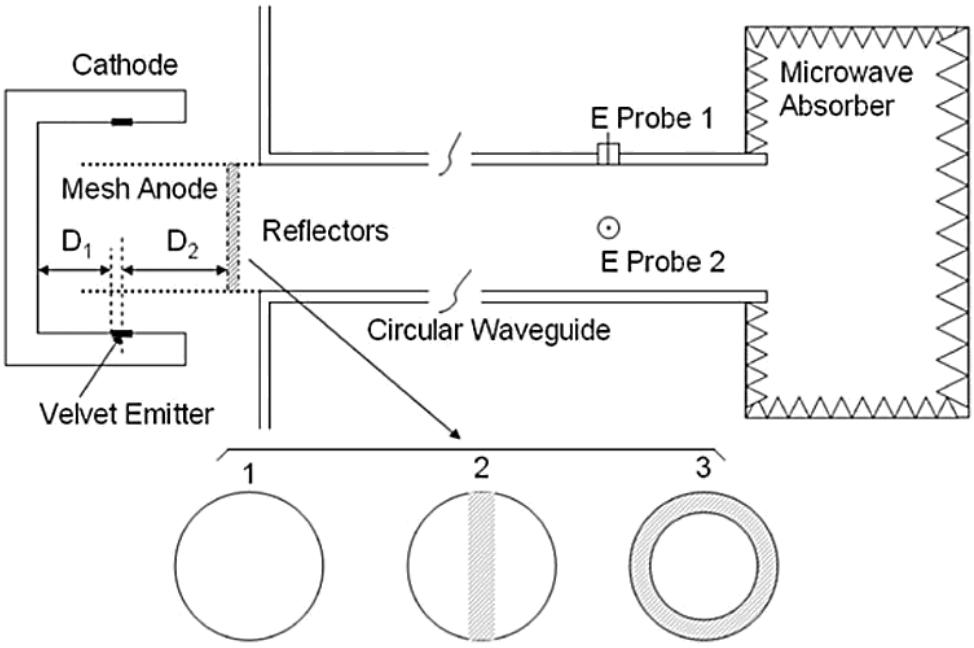

Fig. 4.53: Vircator coaxial geometry with a cavity formed by anaklasti- hours [103]. A similar provision is studied in [121].

In such cases, the use of reflector showed an increase of the microwave radiation, where the formed cavity has natural frequencies near the frequencies of free Vircator. But when the parameters of Vircator (diode voltage and current density) determine other center frequencies, use reflectors leads to re- tapiesi of microwave radiation.

4.5.7. Geometry Dual Rise

To improve the efficiency of a microwave Vircator, there is the possibility to precede formation of the electron beam before it enters the coun- po which form the virtual cathode. This idea seems to be used initially in Split Cavity Oscillator (SCO) [126], wherein a small shielded cavity used (pillbox cavity), by which the electron beam passes. Within the Com- koiloti- is an additional grid, the vertical velocity of the electrons, which Generator two interrelated imikoilotites that modulate the electron beam through the issues raised quirks. In the case of vertical Vircator of export dual rise [92], between two sheets or grids form a region where electric field develops and shapes the beam. With suitable dimensions of selected, can reduce the chaotic effect of scattered elec- ments to current diode as well as to achieve better coupling for the electronic beam with the quirks of cavities.

The S. D. Polevin, S. A. Kitsanov et al. two papers ([100], [92]) show results for Vircator double rise. The study of the Vircator is primarily simulations and dimensions of the cavities are: small cavity height, ~ l / 8 long cavity height, ~ l / 2 small cavity shorting distance Centre of the electron beam, ~ 3min / 4 large cavity fault distance from the center of the beam, ~ 3min / 4 coupling slot (see. Fig. 4.54), l / 30. In the first work ([100]) was observed microwave power 300MW at 2.65GHz, with a 5% yield.

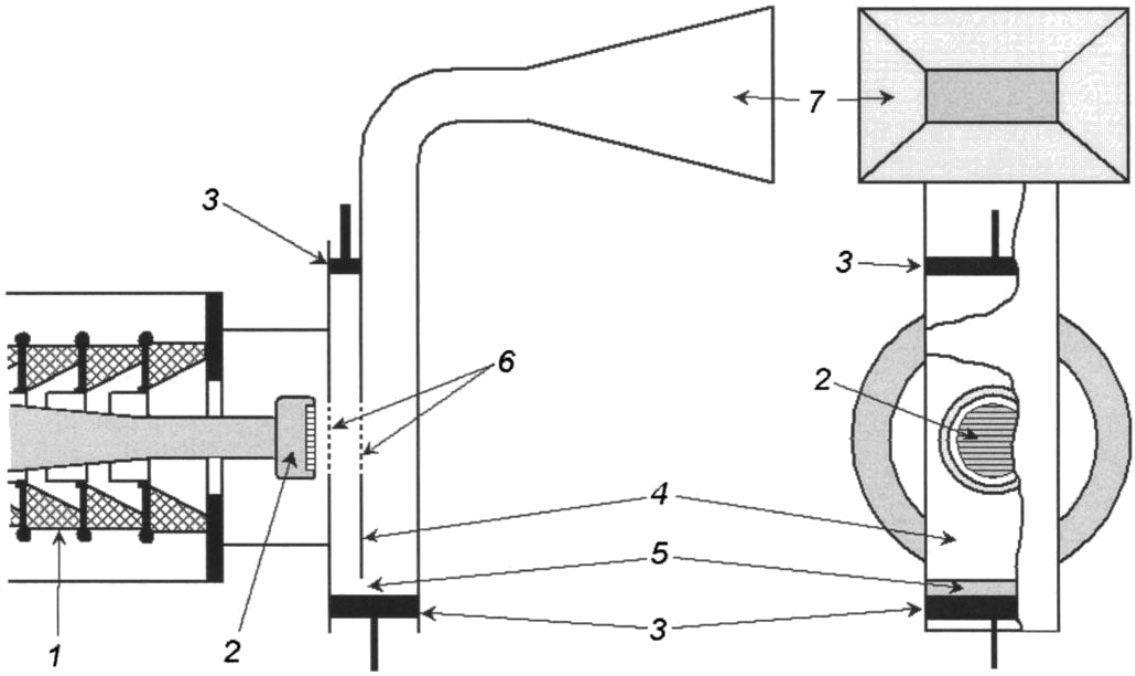

Fig. 4.54: Vircator vertical exhaust with dual anode [92]. 1-insulator, 2-cathode short circuit resonance 3-, 4-wall waveguide, 5-coupling slit 6-leaf or mesh anodes, 7-choanokeraia emission (in vacuo).

The duration of the microwave pulse was 50nsec. During the pulse, the voltage was varied from 520kV to 300kV, while the flow passage of the 9kA to 14kA. Despite the change, the rate remained relatively stable, which is attributable to the provision resonance properties. In the second work ([92]), the same provision, was recorded 1GW power in 2.1GHz. Driving the diode was 1MV voltage and current of 20kA. With the new drive data, the distances modified short circuits to match the desired new frequency, while the anode-cathode distance was set to 2cm. In any case, the export of microwave radiation egi- ve to rate TE10.

4.5.8. Other Geometries with Virtual Descent

To find rules that will optimize their properties glide eiko- victory as microwave radiator examined various hybrid geometry triennial devices with virtual cathode. Two characteristic is Orotron iconic Down Methods (described along with other hybrid devices in [91]) and Virtode, a combination Vircator structure and slow wave, a corresponding traveling wave tube [112]. The case of Virtode, has experimentally studied, shows an improvement of 1.6 BRAKE ment of the microwave power corresponding single TWT, where the intrinsic frequency of oscillation of the virtual cathode is the same as the frequency of operation of the TWT.

5. Development System Vircator

As part of this research effort was made to develop a System Operator production microwave high power, a central element Vircator vertical exhaust, in what has been reported for this type of lamps. The Vir- cators are simple in conception but promising microwave sources, States with large power capability and output frequency setting. They work almost exclusively as oscillators, however there is evidence that they can behave as a amplifier microwave radiation. For the development of the experiment with the light Vircator studied various parameters and, to the extent permitted, made forecasts for the future development of the system. We chose to design a Vircator vertical exhaust (see. Par. 4.5.4), because this can produce microwave radiation at a rate TE10, and easily connect to standard choanokeraies. The compart- flow sections examined was the way of channeling the high voltage in the Capital mind chamber lamp through a crossing high voltage insulator sealed in the Capital Law, the design of Vircator vertical exhaust radiation using rectangular kymatodigou with coordinated cavity, the possibility of amending the cathodes are used, the ability to easily change the anode grid and the regu- half of the resonator in order to achieve some behavior closed roof frequency Vircator. This chapter will present all aspects of the design on the lamp itself, as well as the systems that they allow the operation, ie the vacuum system, the high-voltage system and the measurement system, the microwave radiation, and voltage and current to the Vircator, during operation. The next chapter will present the hitherto results and findings on the whole persuasive suture

5.1. Lamp Design

The lamp itself is one Vircator vertical exhaust radiation in- built on a waveguide WR-430, large dimension 4.3 "and small dimension equal to half. The output waveguide, wherein the virtual cathode is formed, placements were two panels to form a resonant cavity, the length of which is controlled by the distance of the panel from the short rear side of the waveguide. Top on the long side of the waveguide was a

metallic neck in which is placed the insulator passage of high voltage and fixed grids of the rise of Vircator. The metal neck is in the upper flange, similar in dimensions to ConFlat DN100CF, and groove in o- what place the ring strikes the seal with the insulator. At the bottom of the throat is slit in which is placed the fixture securing the mesh anode. The high voltage insulator designed overhead function therefore has a height several corrugations, to increase the length erpy- tion. Also constructed several cathodes, which can easily be changed in the device. Finally, there was a concern about the way in which it can be changed coordinated Vircator, changing the length of the resonant cavity, wherein the virtual cathode is formed. The general view of the lamp appears to model in Fig. 5.1. The individual parts of the lamp design will present in detail in the following paragraphs.

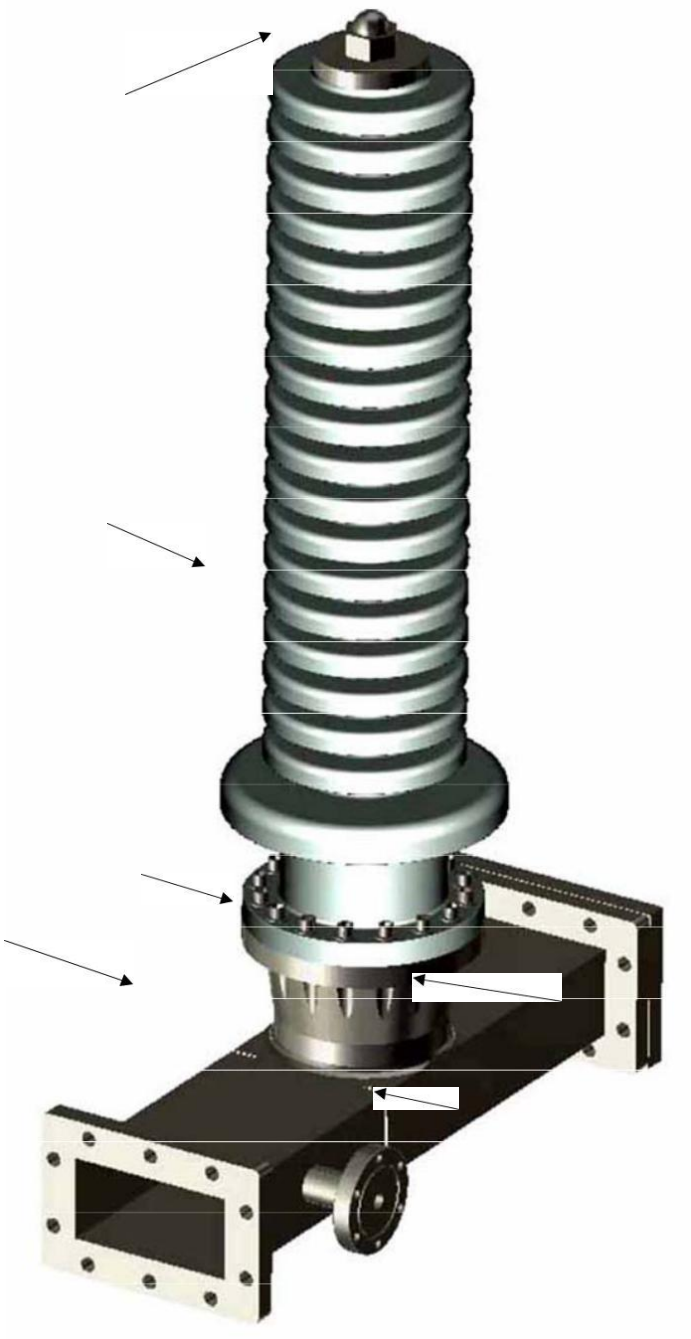

Fig. 5.1: Model of Vircator built.

Fig. 5.2: The Vircator, as received from the machine shop.

5.1.1. Lamp House

The body of the lamp is built upon a waveguide WR-430. The kymatodi- gos has been long dimension 4.3 "(10.92cm) and a dimension equal to half the me- feline. The rate TE10 cutoff frequency is equal to

$$f_c = \frac{c}{2Fr.}\sqrt{\left(\frac{nFr.}{a}\right)^2 + \left(\frac{mFr.}{b}\right)^2} \quad \begin{matrix} n=1 \\ m=0 \end{matrix} \rightarrow f_{a=0.109m} \quad c10 \quad =1.37GHz\,, \quad b=a/2 \tag{5.1}$$

while the subsequent rates TE20 and TE01 have cutoff frequency of 2.75GHz. Since Vircators vertical radiation extraction dominated by the rate TE10 with re-

opportune parameters of driving and coordination can theoretically pety- humus monorrythmiki and coordinated exit microwave radiation in the range of 1.4 to 2.75GHz, while going up even more in the frequency, the output can still be taken in the first waveguiding rate. On the long side of the waveguide opened circular diameter hole 104mm, ie almost the entire length of the long side, and at this point has been tagged a cylindrical socket for the high voltage insulator transit. The metal neck is 85mm high and the top flange has a groove in which the O-ring seal is positioned. The flange is an outer diameter of 6 inches, with 16 holes threaded 6mm and D- are similar in dimensions to ConFlat DN100CF (see. Fig. 5.3). Basically, the metal lai- ber has a small protrusion, wherein the fitting is secured to the grids which are screwed anode. In this way, the grid of the anode is almost in line with the long side of the waveguide, in order to avoid large the internal discontinuities.

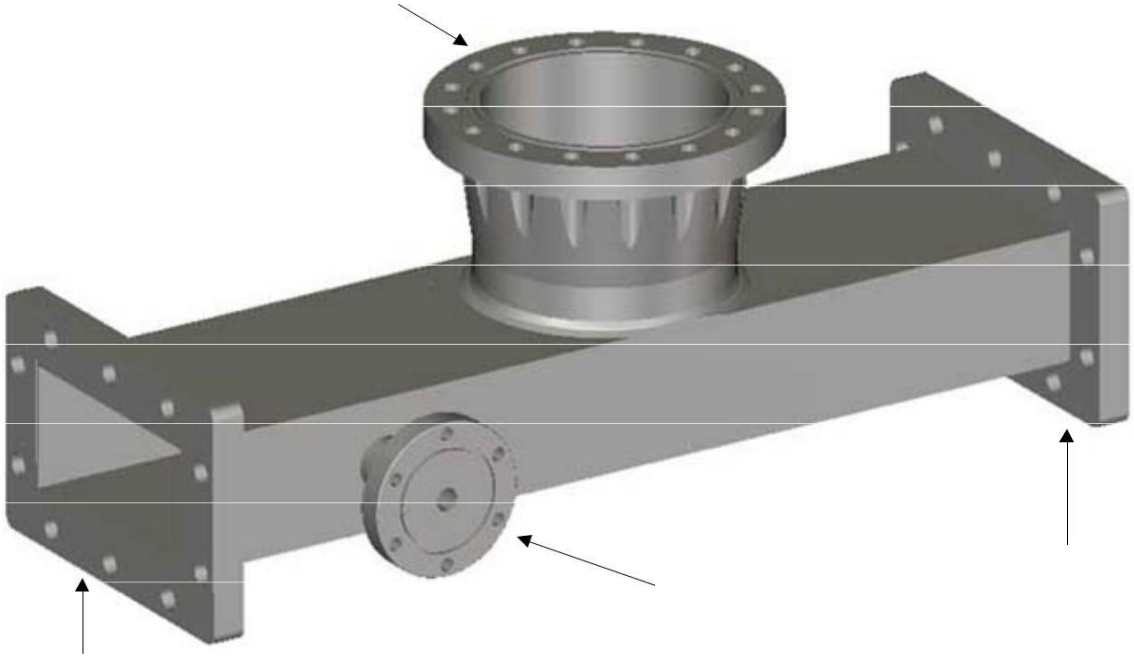

Fig. 5.3: The body of the lamp, a waveguide WR-430.

For the pumping section a hole 15mm opened to the outlet of the waveguide and was glued a small slot flange outer diameter of 2.75 inch. The pumping of air through this opening is not effective because the conductivity d- Pumping of this section (diameter 15mm x length of 50mm) is small. However, the hole purposely selected to have small dimensions, not to disturb the microwave field within the waveguide. As we will see below (Fri 6.1), the vacuum in the waveguide is estimated to be about two to three orders of magnitude above the void that exists in ionic pump used, taking into account the conductivities of all piping, used to connect the pump with the lamp.

The waveguide placed two metal plates - irises in close proximity to the metal neck (see. Fig. 5.4), which is perpendicular to the long side and perpendicular

them to the length of the waveguide and having width of about 15mm. So leave a pro- rathyro dissemination opening approximately 80mm. The area formed by the iris and variable rear short, may identify a cavity with a certain natural frequency, which may force the output of the corresponding Vircator epithymi- coordination.

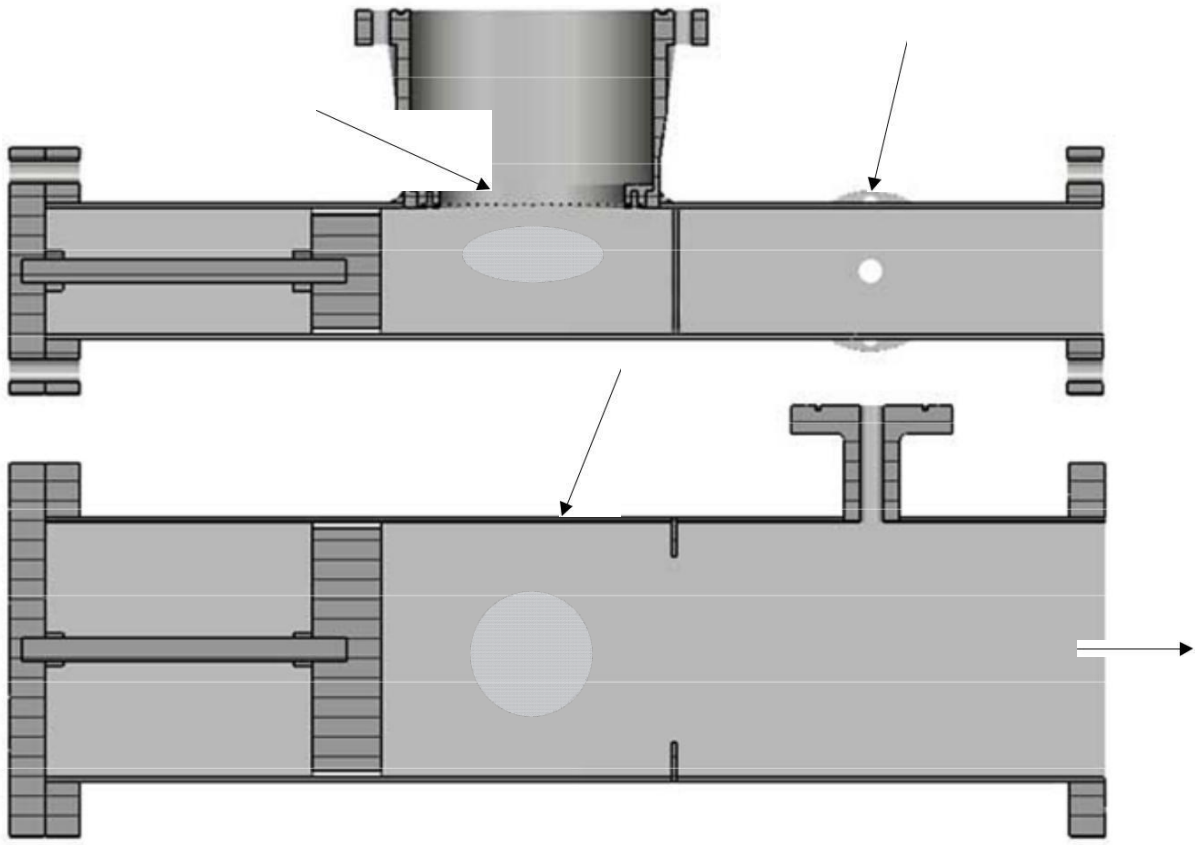

Fig. 5.4: Upper: side section and bottom: horizontal section of the Vircator body. There shall irises placed, the point to place the grid of anode and me- tavlito back short.

The equivalent conductivity *jB* of irises placed can be calculated according to what developed in [127].

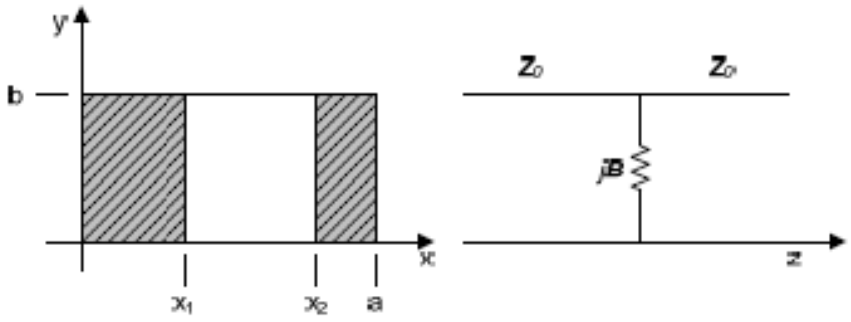

Fig. 5.5: Aperture in waveguide section axb, equivalent item.

The simplified expression for the conductivity *symmetric* aperture is given by

$$B=\frac{2F}{b_1 a}\csc\frac{\underline{Fr.}\,\underline{d}}{2a}\cos\frac{{}_2\underline{Fr.d}}{2a}+\mathrm{S.}_{n=3,5,\ldots}\frac{(\underline{a}\,\underline{Fr.})\,\mathrm{C.}_n}{{}_2}-\underline{n}_{r_{n1}^2}, \tag{5.2}$$

where

$$\csc i=\frac{1}{\sin i}\ , \tag{5.3}$$

$$d=x_2-x_1=a-2x_1\ , \tag{5.4}$$

$$C_n^2=\frac{nFr.^2}{a}-\kappa_0^2\ , \tag{5.5}$$

$$k_0=oh\sqrt{,}^{e_0 m_0} \tag{5.6}$$

and

$$b_1=\left|{}_1^{C}\right|\ . \tag{5.7}$$

In the above sum, the rates used *Pn1,* up to class 5, and applies

$$P_{31}=3a_2\left(a_{22}-1\right), \tag{5.8}$$

and

$$P_{51}=5a_2\left(2\,a_{24}-3a_{22}-1\right), \tag{5.9}$$

where

$$a_2=\frac{1}{2}\cos\frac{\underline{Fr.x}}{a}{}_1-\cos\frac{\underline{Fr.x}}{a}{}_2=\sin\frac{\underline{Fr.d}}{2a}\sin r.\frac{F\,2x+d}{2a}{}_1. \tag{5.10}$$

The amount *B* is a positive number, therefore the irises of this type are characterized by induction baffles. It relaxed depending on the frequency and increasing function of the iris range, x1. The B impedance infinite when the rea- weight of each iris is equal to half of the large dimension of the waveguide, ie D- when opening the iris, *d*Becomes equal to zero.

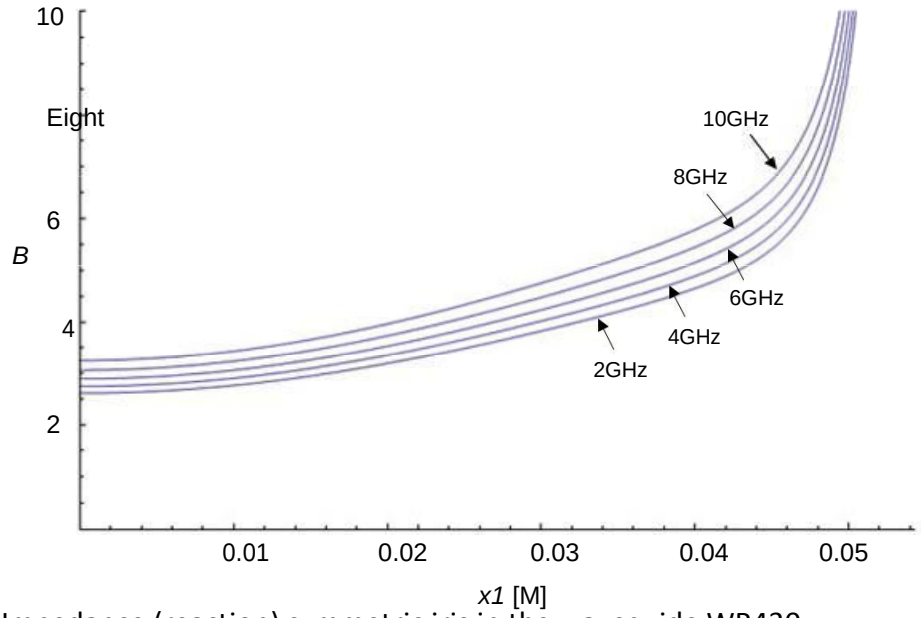

Fig. 5.6: Impedance (reaction) symmetric iris in the waveguide WR430.

For the rear short used an aluminum block, a thickness of 2mm Asia Mi- krotero than the inner cross section of the waveguide, which is dressed with a sheet of Teflon thickness 2mm. The metal block was constructed to have a length equal to about lg / 4 at 2GHz, divided by the square root of the dielectric constant of Tef- lon. This will achieve a better theoretical behavior stele- objectives as shorting.

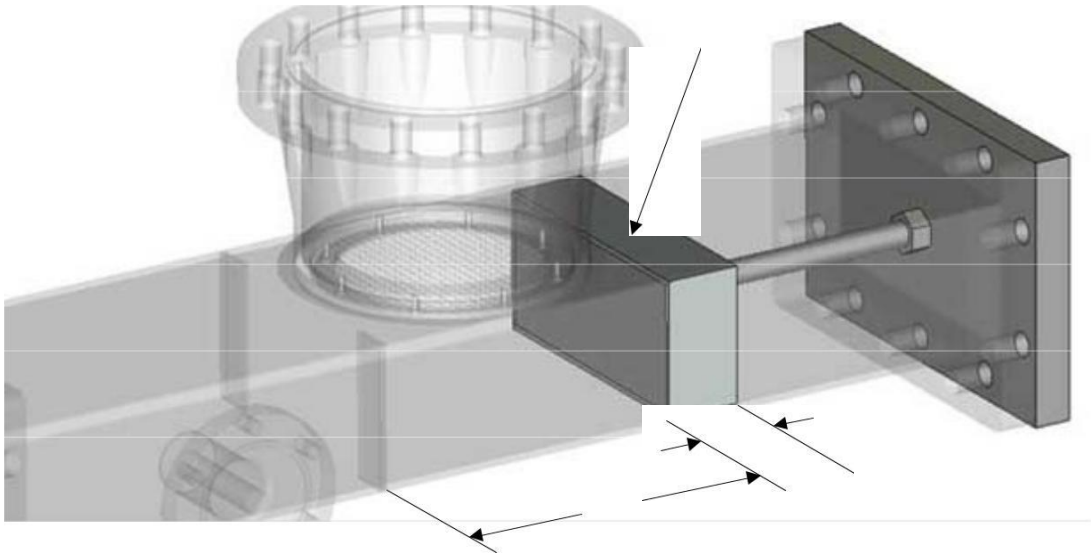
Fig. 5.7: The short rear.

Good contact of the plastic waveguide arcs coaxial straight-line transmission bution, which transforms a virtual anoiktokykloma the back in a virtual short circuit at the front. Since the wavelength in the waveguide is

$$l_g = \frac{c}{f} \frac{1}{\sqrt{1 - \frac{c}{2a}^2}}, \quad (5.11)$$

the length of the stem, $l_g / 4e_r$ appr 3.5cm for calculating frequency
the 2GHz. The strain was initially positioned so as to form the cavity length 125mm with the two irises. This cavity, 109.2x54.6x125mm, has idiosychnoti- the 1.82GHz, as calculated using Microwave Studio of CST. For various cavity lengths we can extract the change of the first natural frequency as apeiko- shown on the Fig. 5.8. The back side of the waveguide sealed successfully using wire lead, diameter 0.5mm, which is clamped between the two flantzes and was very good seal.

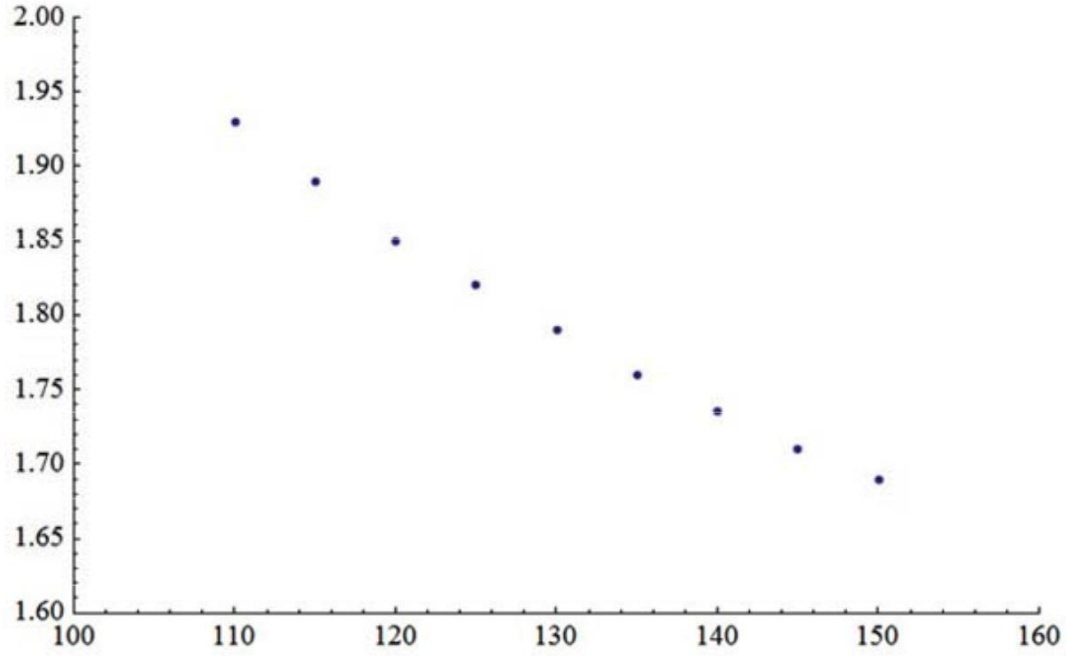

Fig. 5.8: cavity resonance frequency in waveguide WR430.

5.1.2. Crossing High Voltage Insulator

For the insulator crossing a plastic polymer insulating material used, quite hard, readily processable workshop and high strength. This is the Ertacetal or Acetal as generally known. The family of plastics Acetal (polyoxymethylene plastics) has properties that differ according to their chemical the Recommendation. The precise characterization of the polymer used for the construction is not known, but then given a table summarizing iota competence of plastic polyoxymethylene [128] and compare them with the known Teflon.

Tab. 5.1: Properties Acetal Copolymers and DuPont Teflon

Name	Polyoxymethylene (POM)	DuPont Teflon®
Density	1.29 ~ 1.47 g / cm3	2.14 g / cm3
Hardness (Shore D)	75 ~ 88	56
Melting Point	160 ~ 175 ° C	260 oC
Specific resistance	~ 1016 Oh-cm	> 1018 Oh-cm
Dielectric Constant	3.70 ~ 4.30	2.1
Dielectric Strength	165 ~ 850 kV / cm	530 kV / cm

The Acetal has some better properties compared to Teflon, so it was chosen. First is fairly harder than Teflon and therefore better processable. Secondly it is significantly lighter than Teflon, about 40%. Also it has arke- large dielectric strength. In the worst case, the dielectric strength is 160kV / cm, which can reach up to more than 800kV / cm, however, this parameter does not have any information. The Acetal is much larger dielectric constant, around 4. This raises some points of attention and concern the high voltage and especially the dielectric-metal contacts and the presence of triple points where there may be heavy concentration pediakon Lines . Main drawback of this polymer is low heat resistance since the melting point is only 160oC. This does not permit its heating, in order to be vacuum conditioning of the insulator.

Insulator passageway Vircator designed to operate in an open environment, with the side of the inlet of the high voltage to be in the air. Therefore predicted long creepage distance and total tall insulator, a little more than 50cm. From the center of the insulator passing shaft stainless steel SS-304 with cross Ø16mm. The last part of the insulator serves the needs sealing the lamp.

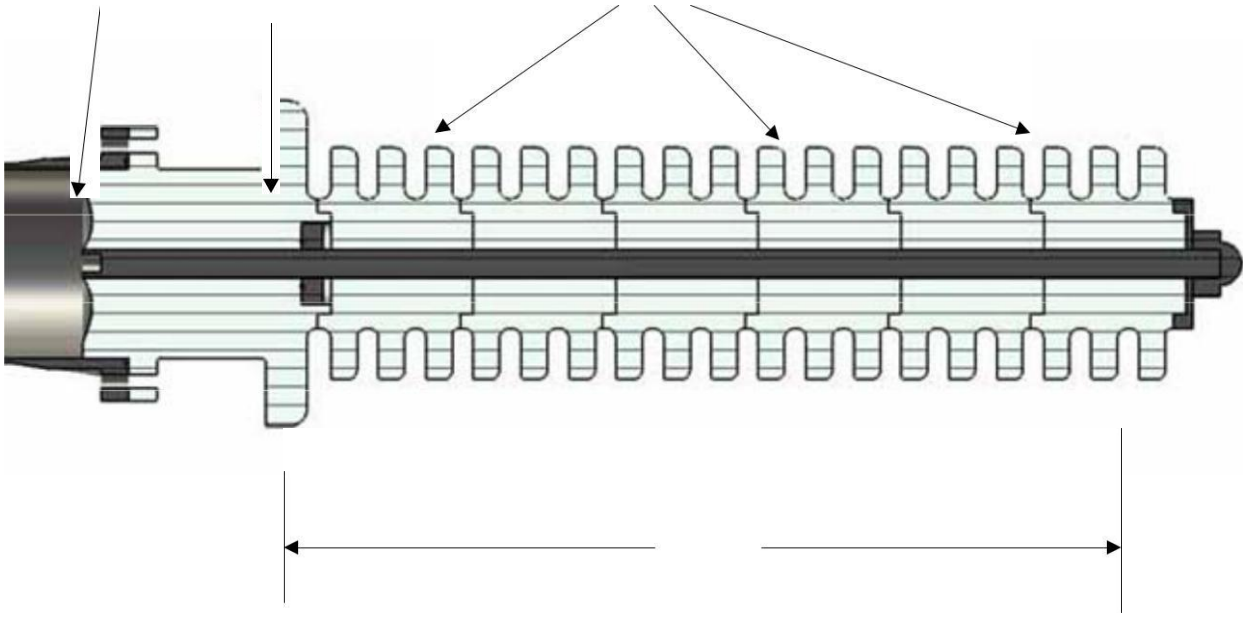

Fig. 5.9: Intersection of designed insulator.

In the compound of the metal neck region of passage Vircator is circular groove in which is placed the ring of hard polymer (Viton® O-ring), to achieve sealing contact of the gasket with metallic diphenylmethyl neck waveguide. Also, a small stainless steel cylinder is stuck on the shaft of the transfer high voltage and bears less importance for grooved ring Viton. At this point, the shaft is screwed together with the polymer and in- xasfalizei tightness in the high-voltage electrode contact and the insulating material (see.
Fig. 5.10).

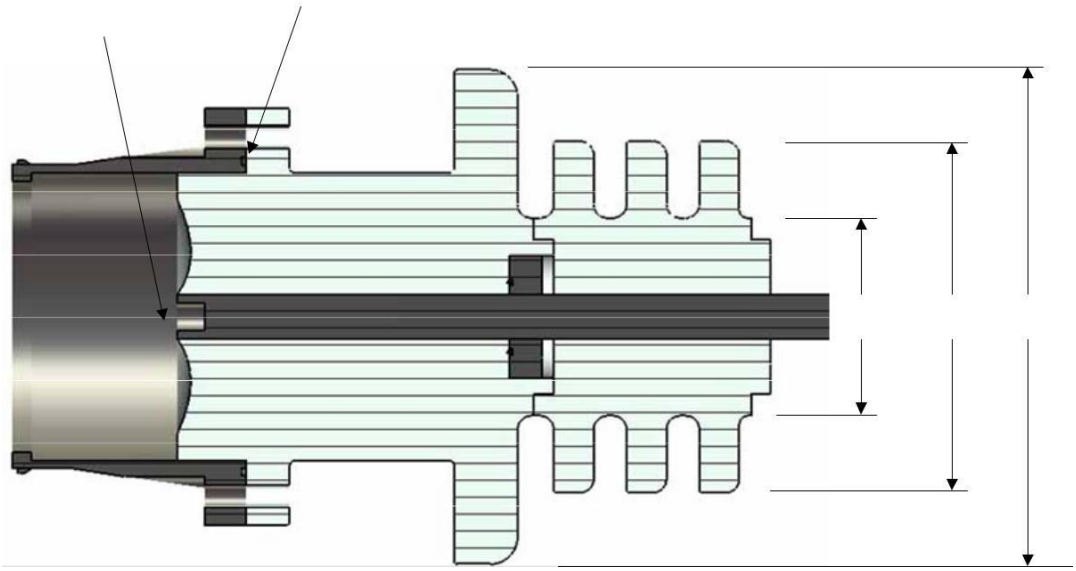

Fig. 5.10: Intersection of insulator designed, detail.

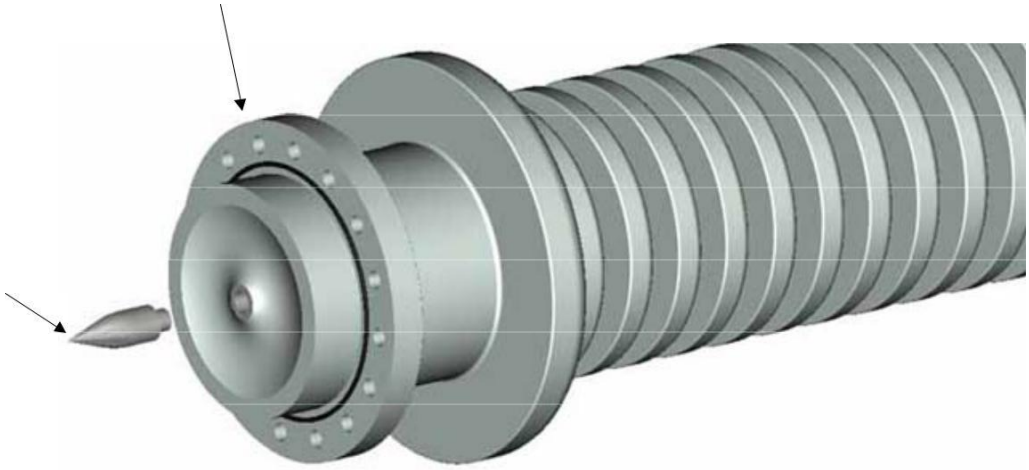

Fig. 5.11: Perspective view of the intended insulator. The cathode is removable.

The top portion has a greater thickness, for better electrical shielding of electrode charge high voltage from the metal walls. This, like the rest of the Subpart, make very good mechanical contact with the center conductor in order to reduce as far as possible stresses from high voltage at the interface of the conductor and the polymer. The compound of the insulator to the metal neck of the waveguide is made by

gasket similar in dimensions to ConFlat DN100CF, outer diameter of 6 inches, with 16 holes M6 (see. Fig. 5.11).

O Transit insulator has a triple point in the high-voltage electrode compound, dielectric and vacuum. This point is designed so that the angle of the dielectric to the metal to be slightly smaller than 90o, in order to avoid condensation of pediakon lines and start creeping discharge therefrom. The walls of me- metals neck shielded by a cylindrical insulating ring of the same material, 1cm thick (see. Fig. 5.12). This provision ensures that the evacuation would begin the descent, in this case the displayed spike, is headed towards, on the grid of the anode. Also, the bushing ensures good fixation of the anode to the lower portion of the metal neck.

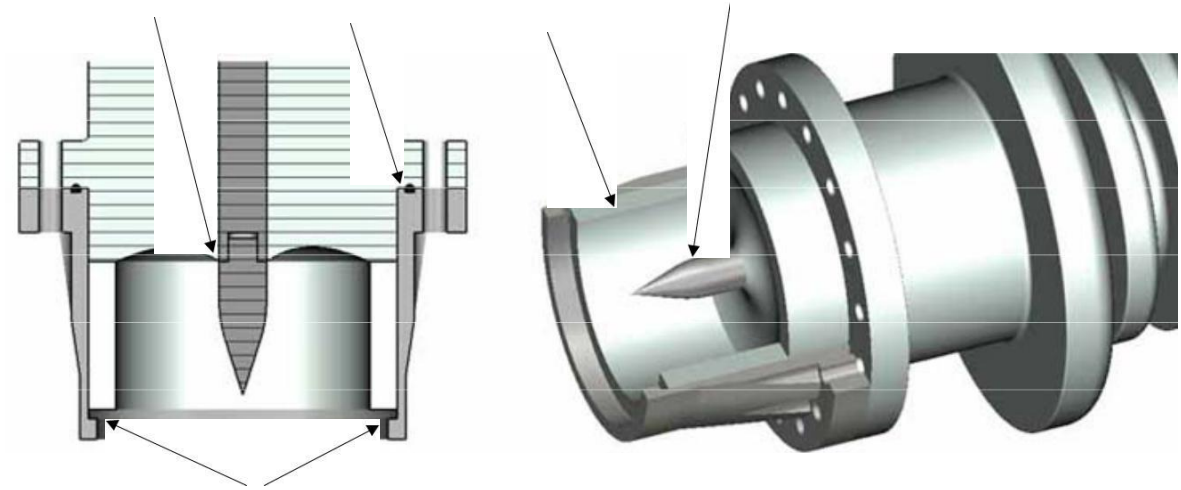

Fig. 12.5: The area of the diode, a pin-type cathode.

In Fig. 5.12 shows the triple point in cathode compound, dielectric and the Capital mind surroundings. Also distinguished point in which is placed the Viton® O-ring seal, the ring locks in the region of passage of the toicho- automatically and stuck waveguide metallic neck in which is placed the mo- notiras. At the lowest point of the neck there is a slot on the rise, which used steel mesh.

5.1.3. Diode Area

The area of the passage is on the same blank with the body of the lamp, which is notified by the conservative pumping device connected to the waveguide of the slot (see. Fig. 5.1). The area of the passageway constituted by the mesh of the anode and the cathode. The anode is fixed to a circular member, at the bottom of the metal neck sup- port insulator, and terminals used in the cathode changed efko- la, the slot at the edge of the insulator (see. Fig. 5.11). The bottom insulator transit and metallic neck, along with the anode, forming a re- Rioja of approximately 60mm (59mm from where the pin is screwed to the upper surface of the grid) and a diameter of 86mm. The rise is beneficial opening di-

measureless 80mm, while a dielectric ring height 50mm and 10mm thick tenderers additional electrical shielding the internal portion of the metal neck of the cathode (see. Fig. 5.14). When installing a terminal at the cathode, it must be taken into account the dimensions and distribution of the electric field, in order, the electron beam is guided directly to the grid of the anode rather than the side walls.

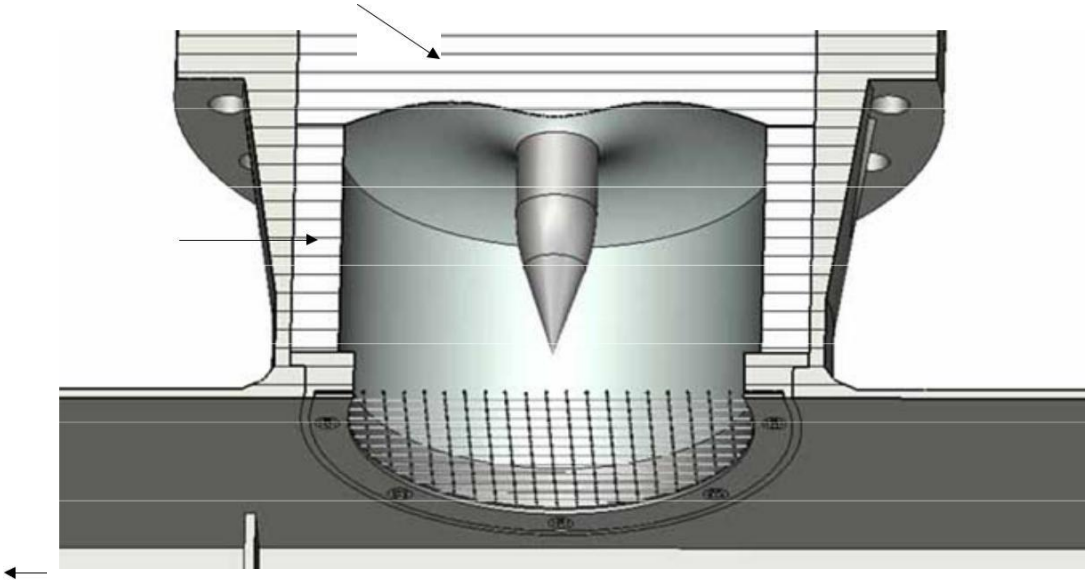

Fig. 5.13: The area of the passage, in perspective section, the anode and a cathode pin type mounted.

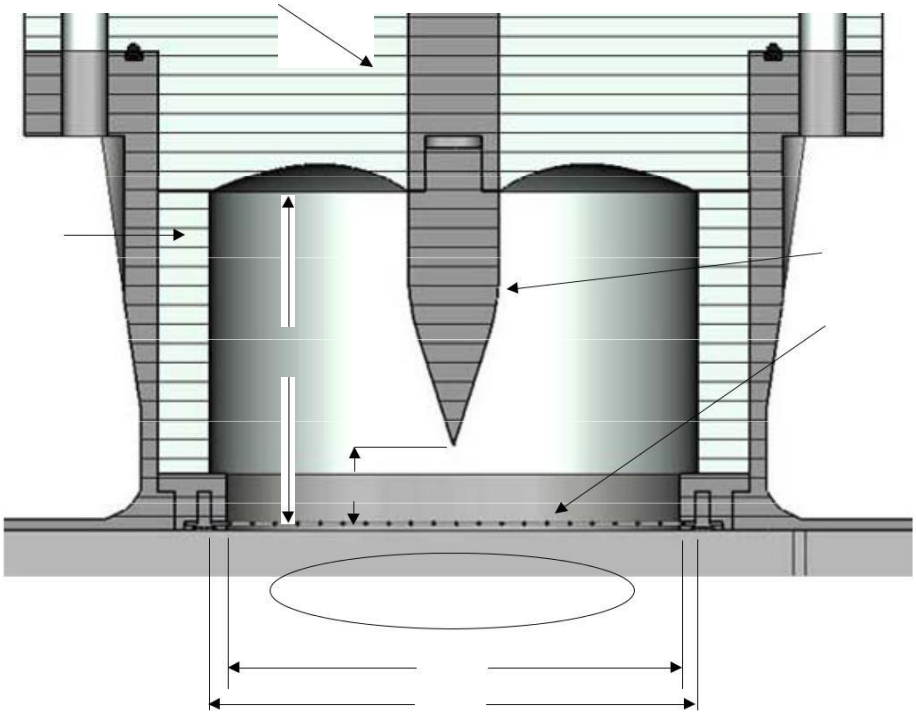

Fig. 5.14: The area of the passage in side sectional view. Some time dimensions of the project.

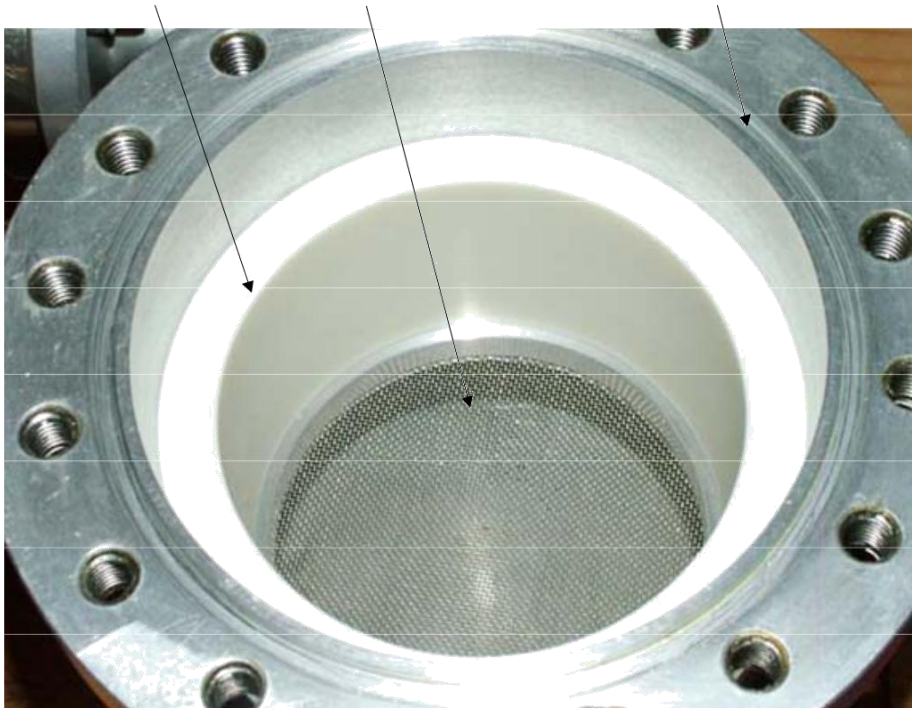

Fig. 5.15: View of the anode and the mounting point of the insulator passage.

5.1.4. Anode

To support the anodes, built a metal part supporting upward xeidoton meshes used, previously cut circle. The accessory has a small diameter guide 90mm, which placed the grids and fixed from one minutes 1mm thick ring. This ring has eight im- meia screwing and ensures that the anode is flat and grounded to the body of the lamp. At the anode tested various types of commercially available stainless steel mesh, with thicknesses of 0.52mm to 0.12mm and densities of 30 holes / inch, 150 holes / inch. The grids, which commonly used, we call "1", "3" and "6". The mesh number "1" comprised 30 holes per inch, with a hole opening 0.587mm, 0.26mm diameter wire and free surface ~ 48%. The mesh number "3" carries 60 holes per inch, with a hole opening 0.263mm, 0.16mm diameter wire and surface should be free in- ~ 39%. The mesh number "6" bring 150 holes per inch, with a hole opening 0.109mm, 0.06mm diameter wire and free surface ~ 41%. It is the thinnest of all available meshes and has an intermediate rate of free surface.

H perspective view of the component of the anode shown in Fig. 5.16.

H placing the anode becomes the base of the metal neck of the waveguide, the web being situated practically in line with the long side of the waveguide. The available "window" of the beam diameter is 80mm. Note that, the cathode used should be dimensioned so that the electric arc Direc- geitai on the grid and not in the support hoop.

Fig. 5.16: The fixture of metal mesh anode.

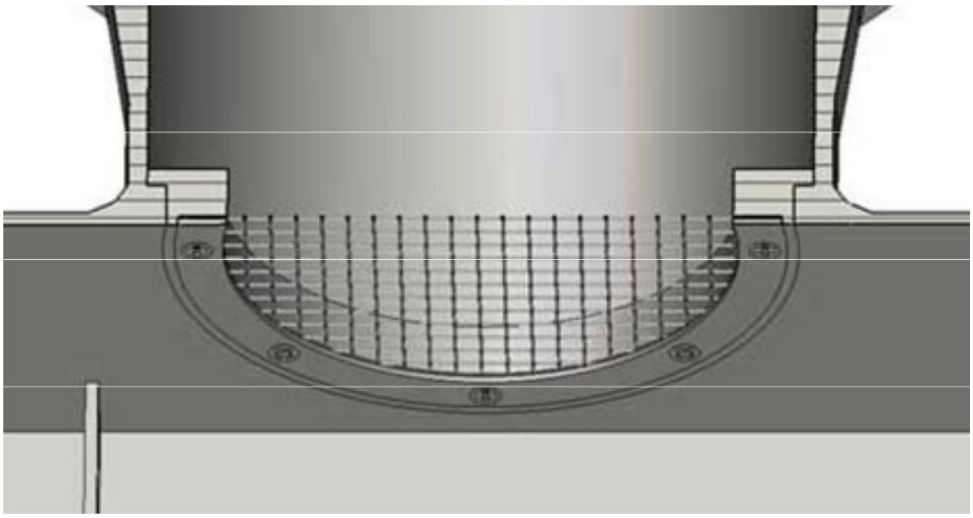

Fig. 5.17: Placing the anode grid to the lamp.

Before designing the particular component, was used a plastic ring-lios, the underside of which sticking matrices using resin and conductive silver paste (asimopasta). However, this method was abandoned and was constructed in the above fixture, allowing easier changing anodes and better thermal, electrical and mechanical contact of the anode mesh to the body of the lamp. The manufactured part, with a grid mounted, shown in the following import Kona.

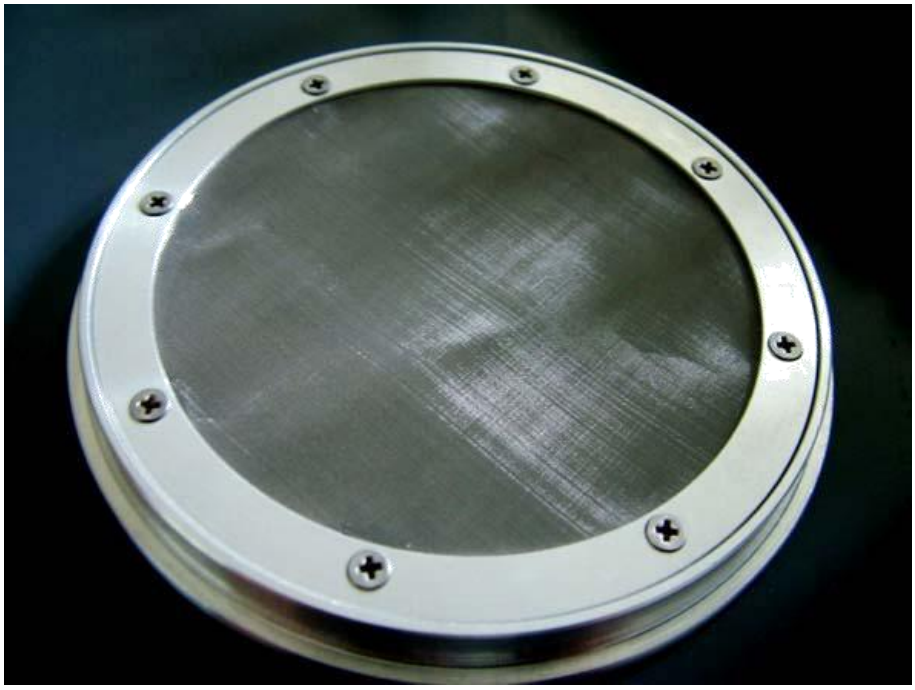

Fig. 5.18: Support ring with mounted grid.

5.1.5. Descent

Insulator high voltage crossing is designed cathodes changing as terminals, using thread 10mm (see. Fig. 5.10 and Fig. 5.11). With dimensions namely, the cathodes must be designed so that the electron beam is guided directly to the grid of the anode. For cathodes cylindrical section, can we simple way to extract the maximum radius of the cathode, in co nartisi the anode-cathode distance in order not driven evacuation around the edge of the mesh support member. The dimensions of the phenom- nontai design in the following illustration, Fig. 5.19.

Since the collar has a height of about 10mm, if the anode-cathode distance is less than 10mm, the allowable radius of the cathode should have the E- pendence d <40 - r To theoretically preferred routing to the grid rather than to the rim. If the anode-cathode distance is greater than 10mm, then it says to pre- principle applies

$$d< \sqrt{(d - 10)^2 + (40 - r)^2} \ , \qquad (5.12)$$

namely

$$d< (40 - r)^2 \quad +100/20 \ . \qquad (5.13)$$

Based on these expressions, we can design the nomogram of Fig. 5.20.

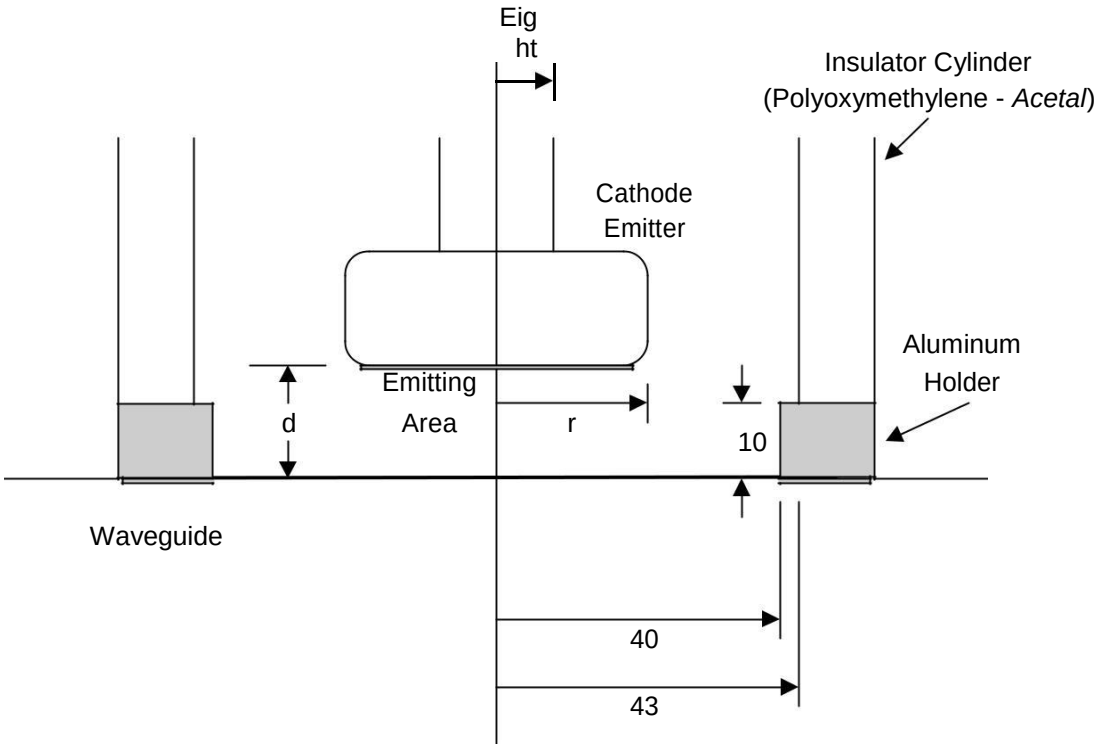

Fig. 5.19: The dimensions of the structure in the passageway area.

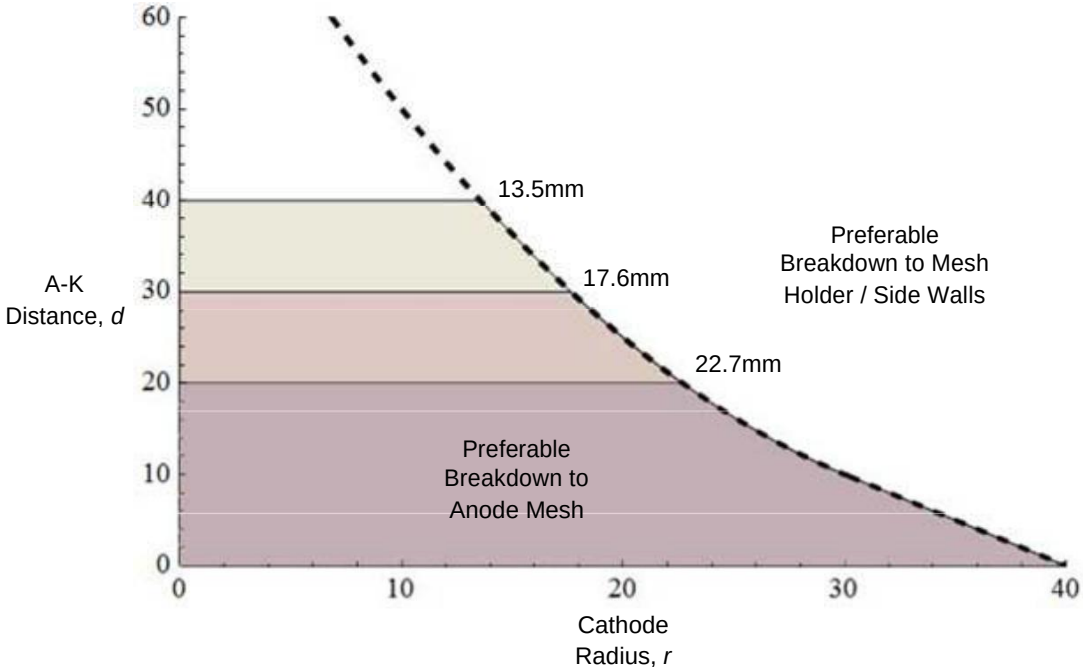

Fig. 5.20: Simplified nomogram for maximum allowable radius cylindrical cathode.

For example, if the distance dAK selected 10mm, the theoretical maximum radius of the cathode may be 30mm, but taking account of local irregularities of the field at the edge of the cathode and the anode of the flange, the radius must be made even smaller. If the distance dAK selected 20mm, the maximum radius of the cathode is 22.7mm, while dAK equal to 30mm, the radius becomes theoretically 17.6mm. For distances

we have chosen for the experiment, d = 15mm and d = 25mm, the corresponding maximum estimated cathode rays are 25mm and 20mm.

5.2. Vacuum Window

In order to extract the microwave radiation from the lamp, the use of a suitable window, which is sealed in the gap and allows governed tation of microwaves, without significant losses. The windows can be constructed of several insulating materials such as acrylic glass (Plexiglas, Lucite), from Teflon, from simple glass or ceramic materials. For this application was used a microwave window of ceramic material, attached to the waveguide dimension links WR430. This box, manufactured by Var- ian, is made for use with S-band Klystrons very high microwave powers, of the order of 200kW CW. Can accept water cooling and has insignificant loss RF (see. Fig. 5.21). The window is made of a white ceramic material, which has a diameter of disc form about 130mm. In Fig. 5.21 exploded distinguished side situated at atmospheric pressure. In this figure, the window is fitted and sealed onto the lamp, while slots are divided the de- dropsyxis available. Certainly, for the intended mode of impulse tube, the cooling installation is not necessary, since the total energy at impact is very small.

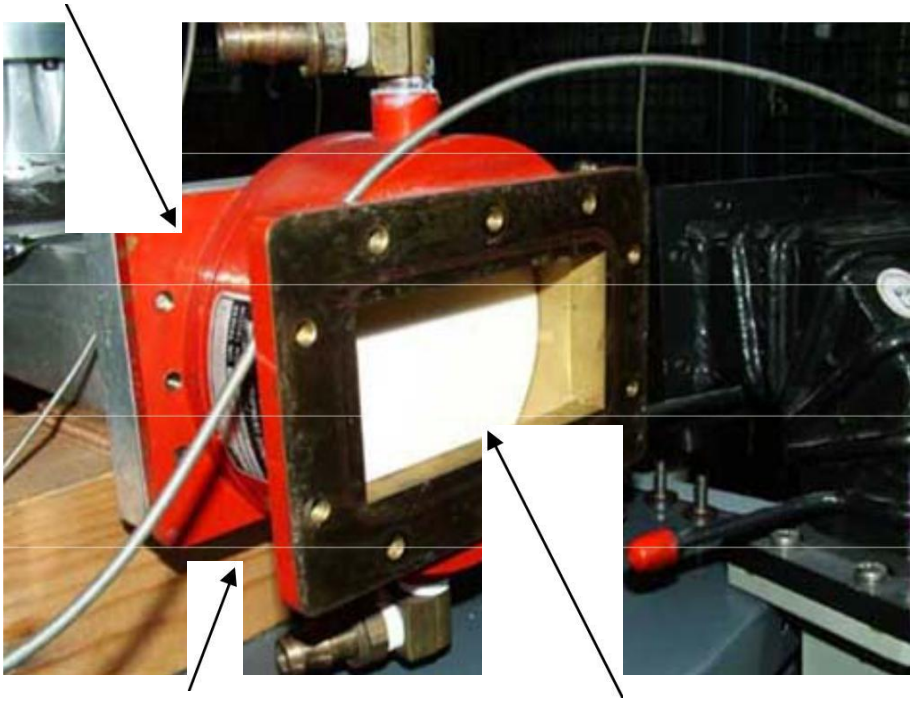

Fig. 5.21: The ceramic window dimension WR430.

The window is made to function in TE10 pace WR430, there- fore theoretically operate in the range of 1.4 to 2.75GHz. To the finding been the microwave behavior of the window, two adapters from Type-N used in the waveguide corresponding profile. These adapters are also designed for operation in the first pace, so clear conclusion for the propagation and reflection coefficients of the window can be exported in the range of 1.4 to 2.75GHz. The device, tested in Network Analyzer concludes with schematically in Fig. 5.22.

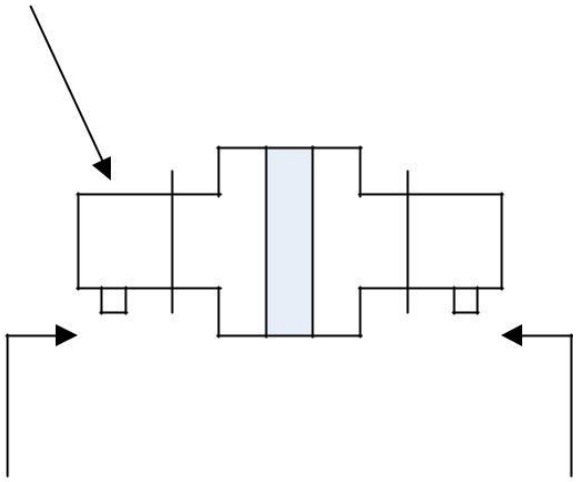

Fig. 5.22: Measurement of loss of the ceramic window.

From this measurement it was found that the window is actually excellent behavior at frequencies of 1.54GHz, with minimal losses of around 0.1- 0.2dB. Especially for the requirements of specific window, his performance is very good. If you must pass 200kW continuous power from the window, the losses are of the order of 5KW. The ratio is small, however, a significant amount of heat to be dissipated from the water. For frequencies above the 2.65GHz begins po- lyrrythmiki proliferation therefore can not be exported clear conclusion on the coefficient diffusion and reflection of the window, at least with certain adjustments from coax to waveguide system. The reflectance and the diffusion coefficient sys- netting adapters and apeikonize- window Tai in Fig. 5.23. The corresponding behavior with minimal differences, presented with reference to port 2, since the layout is symmetrical.

After testing, the window placed on the body of the lamp, on the side of the exit. For sealing of the two surfaces of used wire, lead-Mo- thickness 0.5mm, which was placed around the opening kymatodi- Woo, between the flanges of the bulb and the ceramic window. With leaks following measurements (leak detection with helium detector), it was found that the sys- gkekrimeni technique is very good and does not allow air flow, rather than really considerable extent on medium-high vacuum areas of interest.

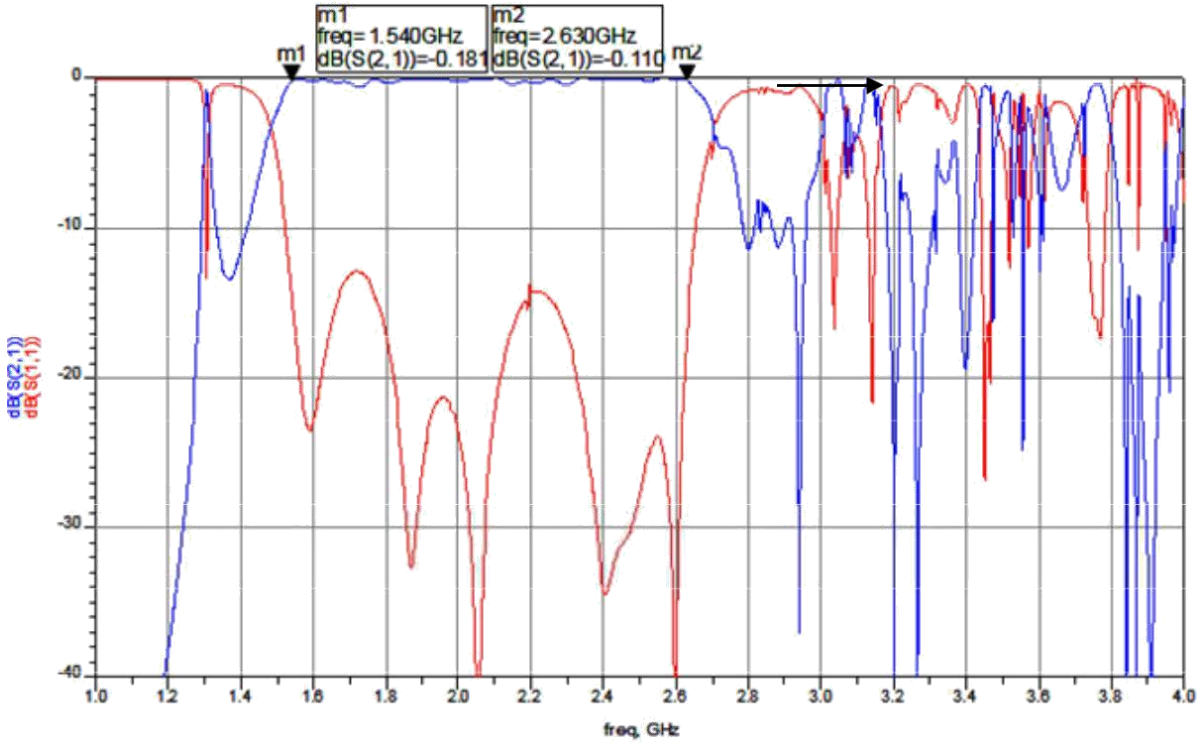

Fig. 5.23: The reflection and diffusion coefficients of netting adapters and the Capital ramikou window.

5.3. Vacuum System

On lamps Vircator, vacuum, without an important parameter is kept at medium levels - high vacuum in areas 10-3 to 10-7Torr (see. Par. 4.2.4). To reach this level of pressure, using a mechanical pump, which lowers the pressure from atmospheric to vacuum levels medium (~ 10-3Torr), and an eductor, which further lowers the pressure. In this experiment use was made of a type of oil pump and a rotary vane pump ionization (ion pump), speed antli- ing S = 100lt / sec. The tube was connected to the drainage system in the manner are illustrated down in pattern of Fig. 5.24. Both the mechanical pump (rotary vane pump), and the ionization pump (ion pump) are excised from the body of the lamp by means of Central mind valves (valve A and valve B). Moreover, it fitted and an indicator thermocouple (thermocouple gauge), which measures the pressure in the device in the range of ~ 1000Torr (~ 1Atm) up ~ 1Torr. The ionization pump is able to lower the pressure in Chart provision up beneath 10-8Torr, however, can operate is required to connect to a volume with a pressure of 5 · 10-3Torr. The ionization pump operating at a voltage 5kV, which is provided by an appropriate power supply. The power supply has a current and voltage indications (*Iion, Vion*) From which we can infer the level-pressure, which is the body of ionization pump.

In order to draw air from the lamp starts the pump unit and opens the valve body B. If the lamp is free from adsorbed gases, the pressure is lowered relatively quickly by the 2-3 · 10-3Torr. At this point kleinou- with the valve B and gradually open the valve A. During the first phase of antli- ing, we can have an indication of the pressure in the order of the thermocouple and me- tritiko institution connected (pressure readout).

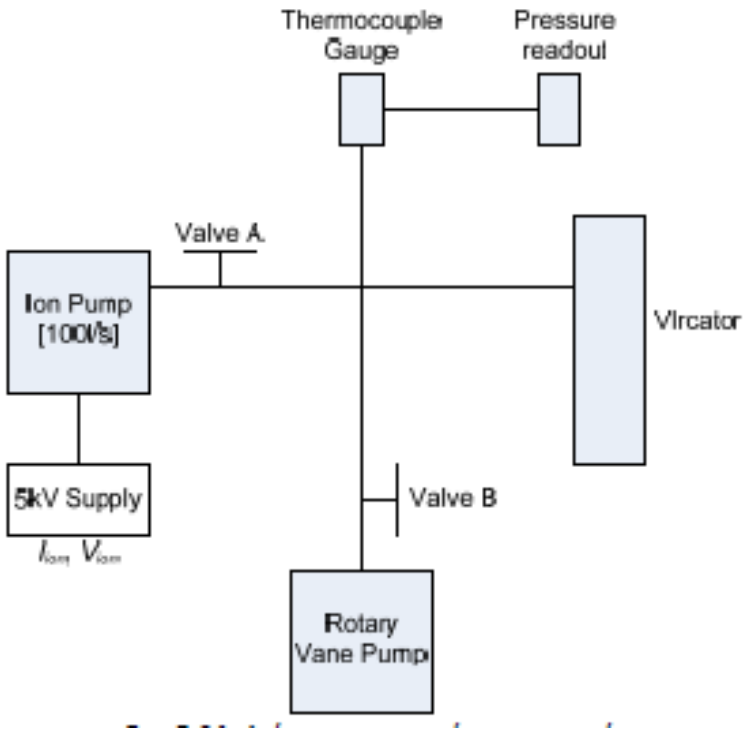

Fig. 5.24: Diagram of the vacuum system.

The ion pump, which is already operating and draws its volume, connected to the rest of the system, which is much greater pressure. At this point there is a strong increase of the pump operating current (ionization current) and the power supply voltage drop. After reducing the initial high pressure, the pump operating current decreases slowly and tends to a minimum price, which is the state of balance of pressure in the system. At this point, all system leak six- saving it to the pumping capacity of the ion pump.

In Fig. 5.25 distinguishes the system used in testing of the system vacuum, which was finalized in subsequent experiments. The Vircator is connected with the mechanical pump and the ionization pump via piping and netting valvi- don and the thermocouple gauge gives an indication of the pressure in the range of atmospheric pressure to 10-3Torr. From this point onwards, the gap in provision calculated indirect sauce, the ionization current of the ion pump, taking into account the overall conductivity of the pipe until his body Vircator (see. Par. 6.1). During testing of the system it was also possible to use leak detector (leak detector), which chrisimopoi- et helium (He) as a tracer gas. The system, which is not shown here, in this syndee- Tai pumping device and detects the presence of helium, giving the corresponding leak rate. Spraying sun at various points of the device (associations, welds, flanges), can be seen if there is a local point, which shows stronger leaks. Thus, some solder into the body of the lamp Com- covered with aluminum adhesive resins in order to reduce still re- rissotero leaks lamp (see. Fig. 5.26), with some success.

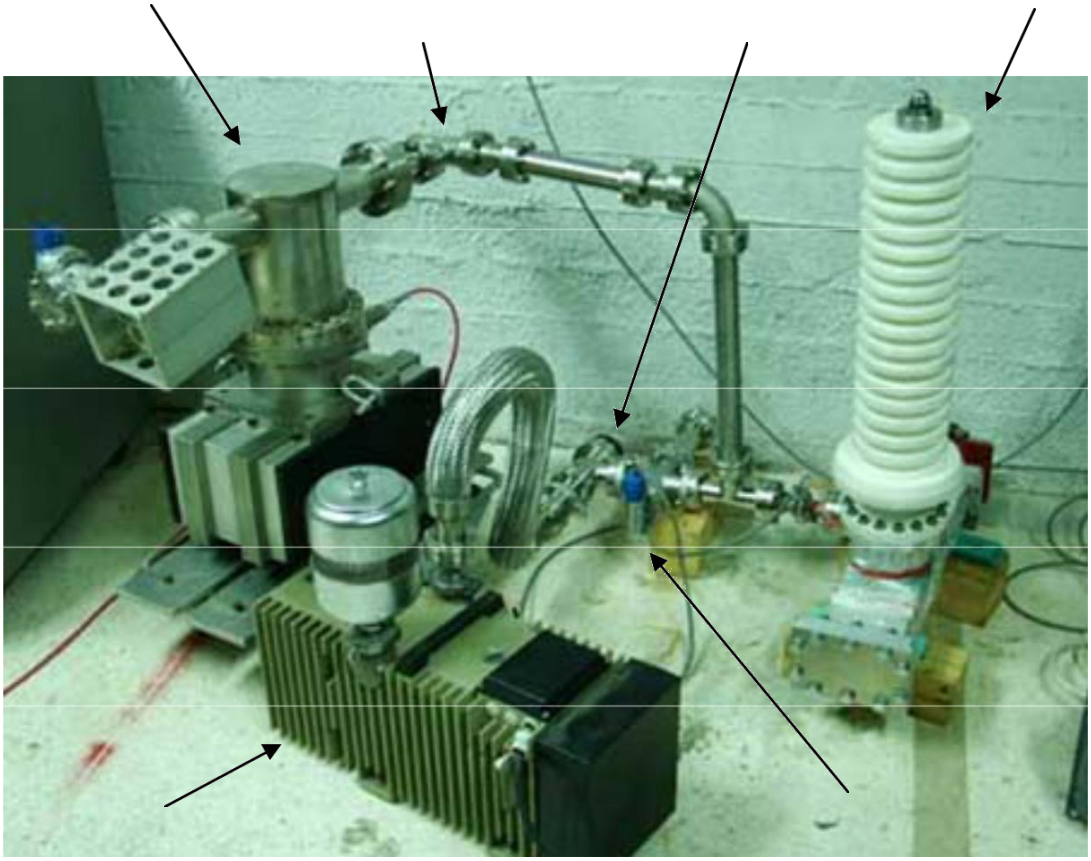

Fig. 5.25: Initial vacuum system tests.

Fig. 5.26: Coating resins in order to reduce leakage in the compounds of the lamp.

5.4. Microwave Attenuator

To record the microwave radiation from the Vircator, a simple kymatodigikos attenuator constructed, which is placed at the output of the lamp. For this purpose was used a piece of waveguide WR430, a length of about 50cm, which placed an absorbent material similar to that used in 'concerns choikous chambers. The sponge material cut into 11.0x5.5cm profile with sloping shape as shown in Fig. 5.27. The length of the inclined portion is 20cm. Added another long section 10cm, to achieve the desired total attenuation. Adjusting well to input port is critical, while adjusting the output port is not en- differ much. With the large slope of the material can be achieved a smooth transition from the air, and therefore a good fit with the load reflection coefficient remains small. The desired value for the reflectance to be located as far as possible under 10dB.

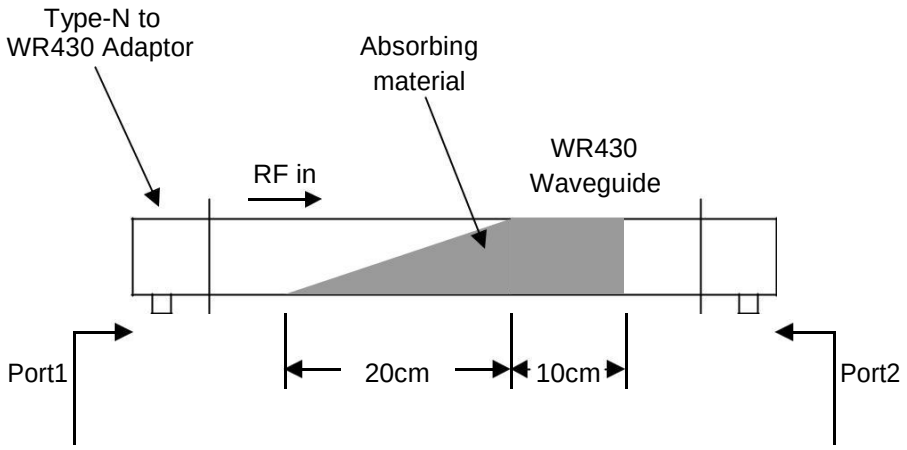

Fig. 5.27: Measurement of microwave attenuator.

The quantity of the absorbent material was chosen attenuation sygkekrime- portion mind is about 40dB. Roughly triangular piece displays weakened importance of the order of 20dB, 20dB, while others show the parallelepiped piece length 10cm. The attenuator measured by network analyzer and displays the behavior shown in Fig. 5.28. By measuring the microwave attenuator observed sible one dependent attenuation with frequency, as it is provided the depth of penetration $d = (Fr. f BDSM) -1 2$. Adjustment to port 1 (S11) is very good and specifically, the range of the first rate is always below -10dB. For the region over the 2.6-2.7GHz we can not draw firm conclusions, because the N-type in WR430 adapters are no longer operating in monorrythmiki area. Estimated however, the weakening of the load is 37dB at 1.5GHz, 40dB at 2GHz and decline reaches 45dB at 2.5GHz. From then on can only be predicting weakening or linear or model $(f) -1 2$ extending the behavior that has the material in the range 1.5-2.5GHz. The charge was placed in a microwave tube together with the microwave window, as illustrated in Fig. 5.29.

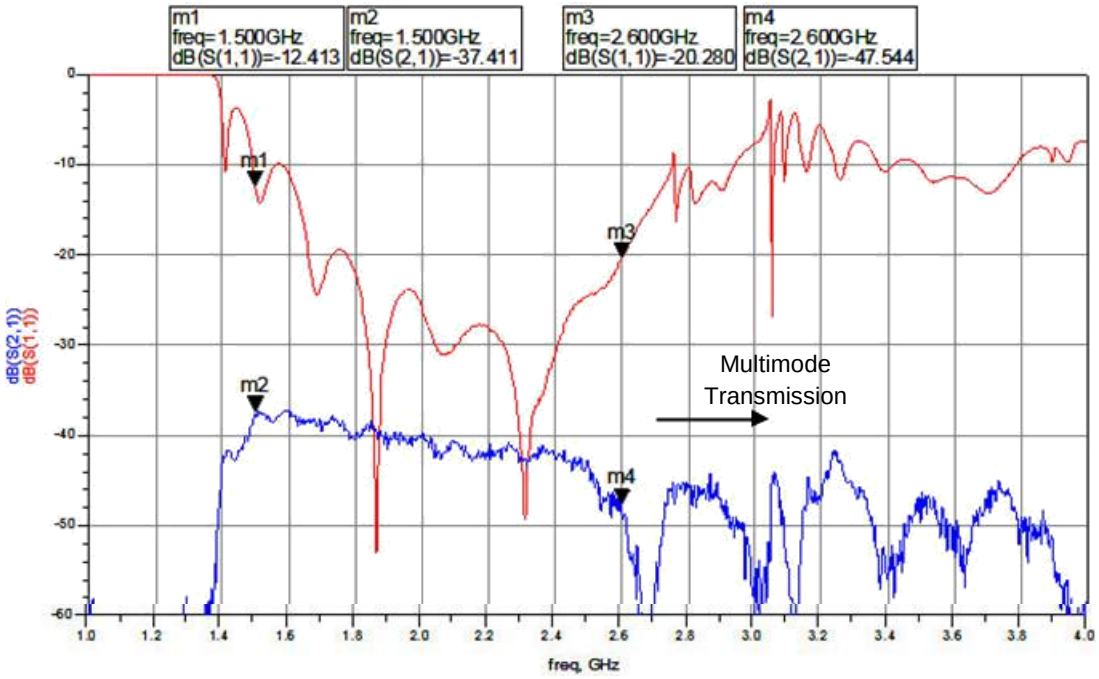

Fig. 5.28: reflection coefficient and distribution of microwave attenuator.

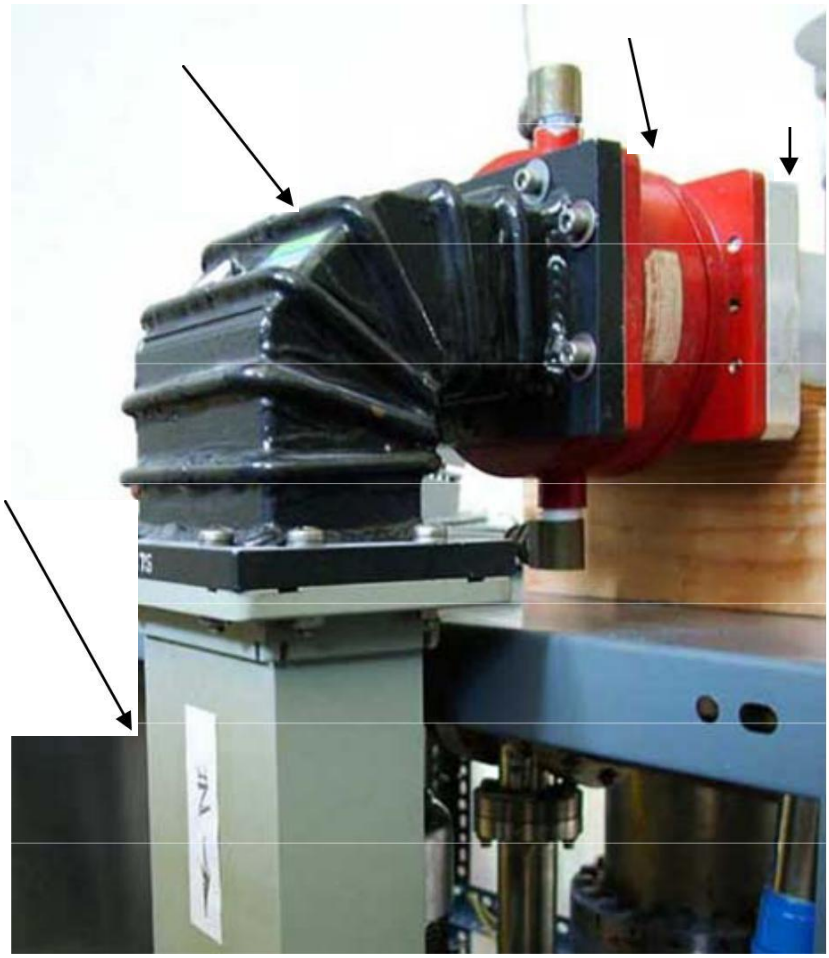

Fig. 5.29: The microwave window and the microwave load-attenuator established within the output of the lamp.

5.5. Single-stage Hammer Device

To make the first series of experiments with light constructed, assembled was one-step device impulse voltage with detachable generator of High Voltage Laboratory of NTUA. Per VDE-b [42] circuit implemented was one its amended form of the circuit 1.2 / 50 with less RF front resistance, to achieve faster waveforms and larger currents. The values of the data were used for the generator are: charging capacitor (charge capacitor) CC = 6000pF, alpha- ntistasi front (front resistor) RF = 208O, comprising two resistors connected in parallel 416O, tail resistance (tail resistor) RT = 9500, and capacitor load (load capacitor), configured as a voltage divider with CH = 1200pF and CL = 504nF. With these elements, but with front resistance equal to 416O, receive, with good accuracy, the standard waveform 1.2 / 50. Using resistance 208O forehead produces a waveform shape of about 0.6 / 50. The load capacitor, molded capacitive voltage divider, giving a reason relegation 1: 420. This ratio is further ypovivaze- using probe ratio relegation 1: 100.

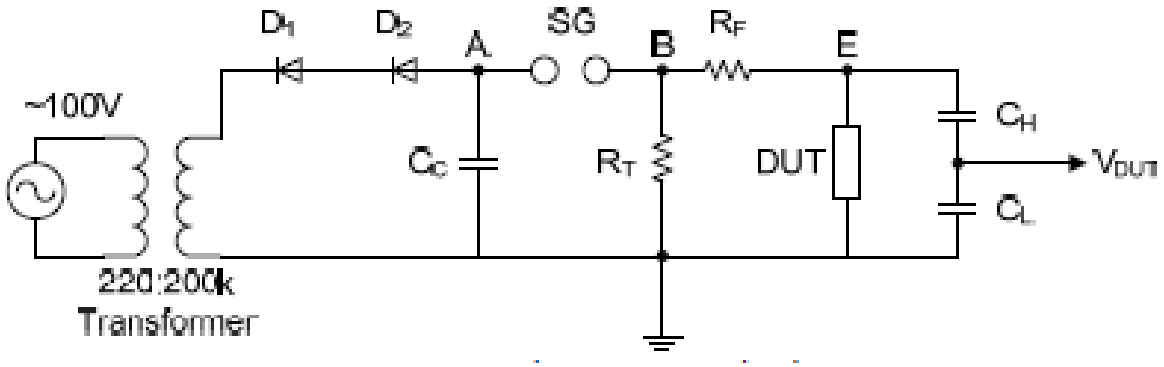

Fig. 5.30: Single-stage impulse device

The charging of the capacitor CC is a imianorthosi output transformer 220V / 200kV. Since all components used have a maximum operating voltage of 140kV dc, the adapter works with primary voltage up to 100V ac. With the given transformation ratio (~ 1000: 1), the rms output of the transformer is 100kV, which gives upstanding 140kV dc for a maximum charging voltage of the capacitor CC. To lift using two diodes, D1 and D2, so as not to exceed the maximum voltage function, the 140kV. This could happen on the negative periods of the alternating voltage, a positive charging voltage of the capacitor or vice versa. The primary is powered by an autotransformer, which is controlled by a bank manipulations enabling rectified dc voltage to any value. The bank handling also enables variation of the spark gap SG. The voltage divider formed by the capacitors CH and CL is connected in parallel with the light-specimen (DUT).

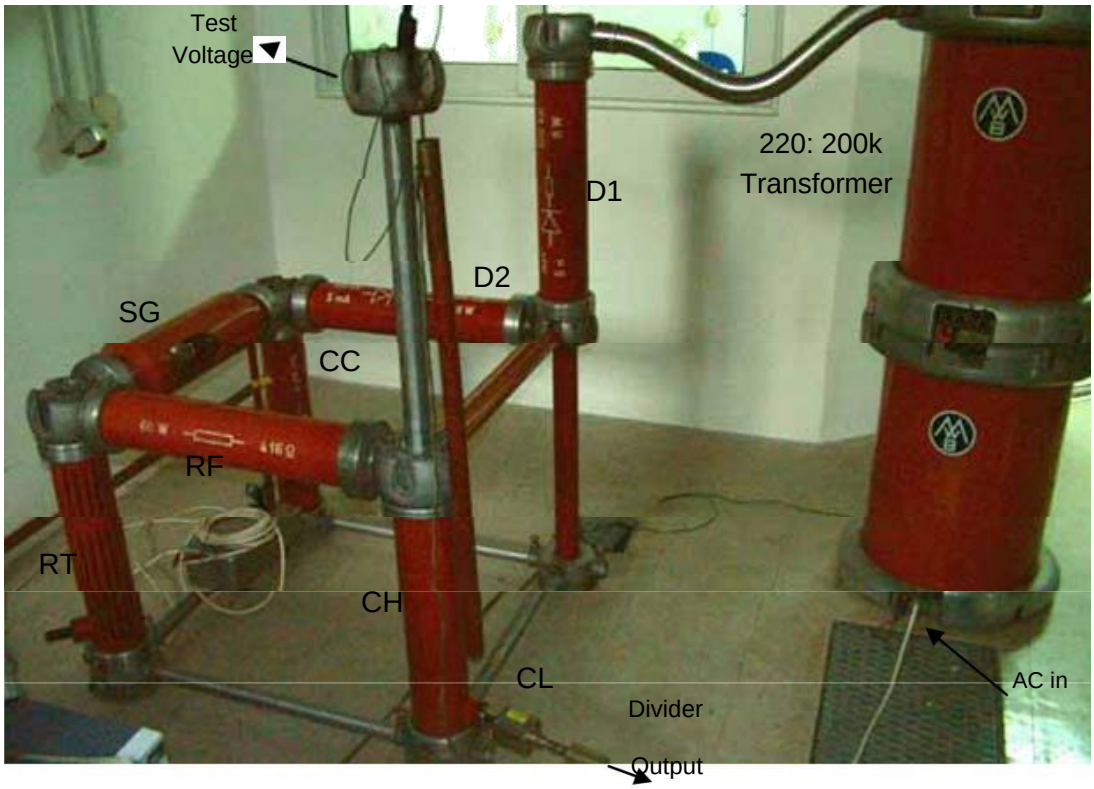

Fig. 5.31: Experimental single-stage impulse device at High Voltage Laboratory of NTUA.

In Fig. 5.31 shows the releasable form of the impulse generator of utilization was for the first experiments with Vircator. Right distinguish lassomenis alternator voltage transformer, which rectifies through diode D1 and D2, voltage negative policy ness charging the capacitor CC. Through, bridged by the electric arc, spin- thiristi balls when the voltage reaches a certain value, the capacitive load is driven to the discharge circuit. Distinguish the tail resistors (vertical), forehead (horizon), the capacitive divider and the node from which we receive the impulse test voltage.

The peculiarity of this impulse device is that it uses resistance to frontal and capacitive divider for measuring the voltage. This results in the deceleration of the front and limit current, because, at the time of Chart secondment gap of the spark plug, the charge of the capacitor CC is driven by the corresponding situation in the RF specimen and the capacitive divider. As a result, front rising to a time constant of about t = RFCH = 208O · 1200pF = 250nsec, if we consider the circuit of Fig. 5.30. In other words, the front rises relatively slowly and takes over from 0.5msec to a maximum value. While down split appointed output of the lamp, the voltage across the lamp, the capacitive divider is the same. Also, the coun- exception of preservatives divider offers the greatest amount of power to the lamp after are located in parallel. However, this trend often has not had time to rise significantly since the collapse of the gap of the lamp starts at much lower voltage. Faster waveform would result in the exploitation of idle gap and consequently the start of the collapse at higher voltages.

This impulse device can be simulated in no-load condition, when we get the following chart of the output voltage and BRAKE ing the charging capacitor CL:

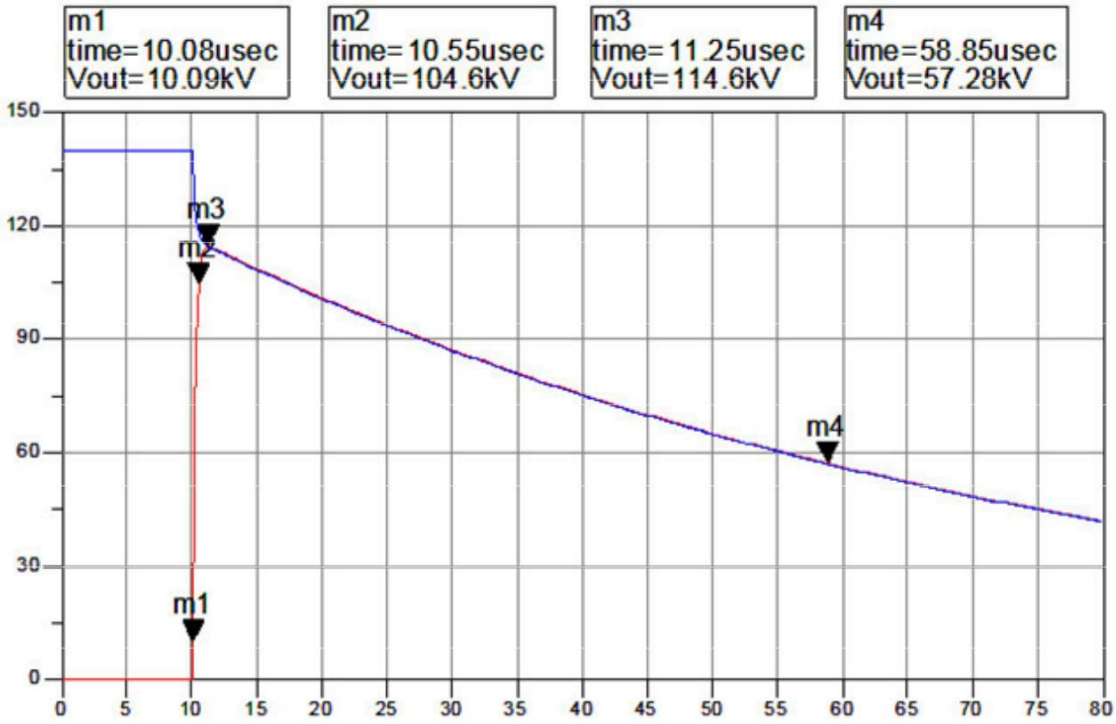

Fig. 5.32: Simulation of the output voltage and the voltage of the charging capacitor.

We believe that the capacitor CC has an initial voltage equal to the maximum permitted, ie 140kV DC, which have resulted from recovery 100kV AC voltage from the transformer. At the time t = 10msec, the spark plug gap (ideal switch) cross spatai and capacitor load is transferred to the output, ie the sample (if de- pirche) and the capacitive divider, which is connected in parallel. The voltage E has a rise time 10% -90% of the order 0.5msec, as expected, since we modified the standard circuit 1.2 / 50, putting half face resistance. The potential maximum impulse device are 114kV, which means a rate of return presented rectified voltage to a maximum impulse equal to 81%. The time required for the rise from zero to the maximum is 1.2msec, while the half-width time is on the order of 58msec. The impulse waveform depreciates through the tail resistor of 9500. Due to limited available data, it is possible to achieve faster times front to fully exploit the available width voltage. Also, replacement of the alpha- ntistasis brow short despite the fact that it would be one solution, there was Tested through because the charging capacitor is fated discharges in short-circuits, so this is not diakindynefthike.

6. Experimental Results System Vircator

The first stage of testing Vircator lamp became the High Voltage Laboratory of NTUA, using a single-stage impulse device by VDE-b, capable of Direc- tion to 140kV DC. In the laboratory the pumping device was installed, which was found to be working satisfactorily and creates a vacuum in the light of the order of 10-5 Torr. The lamp was attached to the microwave radiation extraction window and microwave attenuator, which, as described in the preceding paragraph (par. 5.4), was implemented by placing the absorbent material within the waveguide, with trapezoidal shape suitable for achieving the required adjustment and epi - setpoint attenuation. To draw conclusions about the behavior of poly- XVIA, measure the microwave output directly to a digital oscilloscope, as well as the test voltage and the current of the lamp through the ground, with currents, converter Tosh. Several problems concerning the recordings of signals and due to the percussive device and intense transients encountered, resulting to capture clear waveforms, from which we can study the lamp of Conduct in relation to such driving levels. All issues such regarding this stage of testing, will be discussed in subsequent paragraphs.

6.1. Vacuum System

Having determined and controlled vacuum system is necessary for the light (see. Par. 5.3), the two pumps, primary mechanical ionization, placed in a roller box and grounded appropriately connected to the lamp, which is placed thereon (see. Fig. 6.1). To document the function of the vacuum system ml topothetithi- the microwave window and the insulator passage to the lamp, while the back side of the waveguide sealed with blind flange waveguide WR430, using syrma- Tos lead thickness 0.5mm. The microwave window sealed well with the gov- matodigo with lead wire, while the insulator passage, as we have seen, is sealed using polymer ring (Viton O-ring). The mechanical oil pump uses voltage 110V, and for this purpose a step-down transformer is used 220 / 110V. The oil pump is stopped to be used when the pressure reaches the level of 2 ~ 3mTorr, so it is possible to link the ionization pump with the volume of the bulb. Currently sealed and comes off the oil pump, while

ionization pump undertakes to continue pumping interconnected volumes at lower pressure levels. The ionization pump requires voltage 5kV, which is provided by power supply capacity 5kV / 200mA.

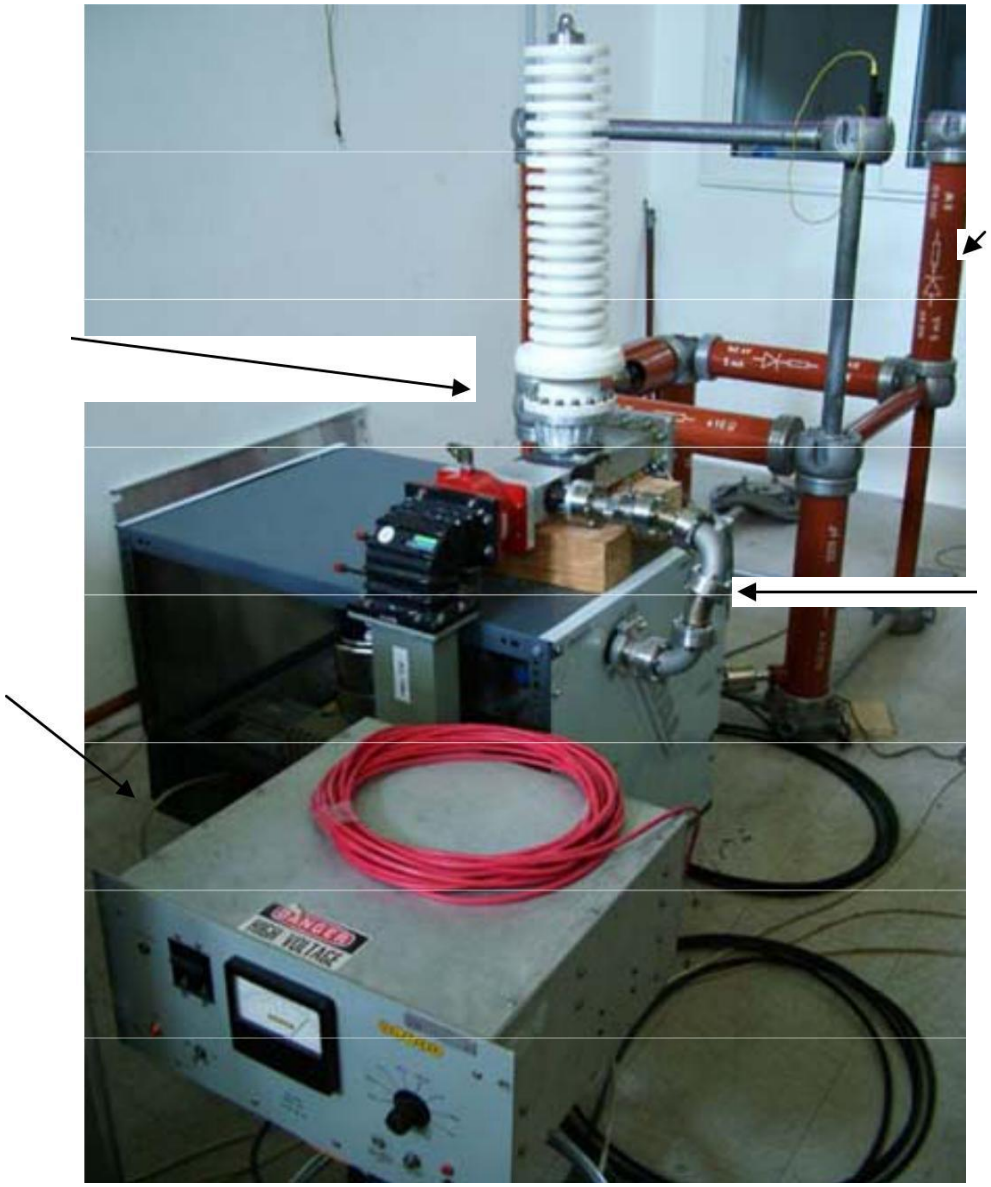

Fig. 6.1: Installed experimental setup

At the beginning of the pumping process, since the light is disconnected very com- chthei for any necessary alterations or maintenance, the pressure must be lowered by one a- tmosfaira (760Torr) in high vacuum levels (~ 10-5Torr), about eight classes chamilote- pg. A feature of the vacuum systems is the rapid adsorption of gas atoms in the metal walls, when in contact with air. The adsorbed Toggle limits as O2, N2, H2, vapor H2O, aggregates and organic gases, occupy many stoi- vades metal mesh and contribute to a very large volume of trapped gas, which should be gradually drawn. The best procedure to bleed

krynsi adsorbed gas is steaming (bake-out) of each component, to be used in the vacuum system. By autoclaving at temperatures of 300-400oC for some time, the gas atoms that are prosrofi- me to the surface, are removed to a large extent, whereby the component syndee- out in a vacuum system has sharper internal surfaces and pumping becomes BRAKE chytera. When a component which is left at atmospheric pressure for a long time (several minutes or hours), connected to a vacuum system, there is a long delay, to achieve the maximum possible vacuum. For example, a volume of some liters, free of adsorption and leaks can be pumped vacuum 1mTorr a diaphragm pump in 5 minutes. The corresponding time for the same volume, one with no klivanisthei and remains at atmospheric pressure has importance for some time, can amount to several hours.

In this experiment it is necessary to disconnect and opening the lamp for changes in the anode and cathode of the lamp. As a result, the volume to be pumped regularly comes into contact with air. When this occurs, it is abrupt gas adsorption to the walls and the mechanical pump is far lower the pressure on the mini- mum possible achievable, which is about 1mTorr. To avoid long operation of the pump many intermediate pumping cycles are few minutes. In govern- these Cluj, the valve A closed (see. Fig. 6.2), the mechanical pump is connected with the poly- XVIA through valve B and the pump. After some minutes of operation, valve B is sealed and the mechanical pump is isolated, while the light is now left without antli- night. Through indicator thermocouple, clearly the pressure increase in the system, the top in bold and then more slowly. With this procedure, we take advantage of the release of adsorbed gas at a partial vacuum of space, in order not to fatigue the mechanical pump long operation. By repeating this process several times, the vacuum system gradually exempted from a large part of adsorbed gases and the mechanical pump may eventually lower the pressure on 2mTorr about. From these pressure levels (point crossover), may start to operate the ionisation pump, drawing instant very large currents around 1 ~ 2A. To switch to the ionization pump, mechanical pump should be isolated by closing the valve B and the volume be connected been the ionization pump through valve A. From this step (2 ~ 3mTorr) and emer- of the ionization pump lowers the pressure slowly until the minimum achievable vacuum. The vacuum is achieved practically equalization pumping capacity provi- ment to the total leakage of the system, such as leakage through cracks kolli- tions flanges, joints and diffusion of light gases in the atmosphere through the metals. The approach of this condition is slowly bleed after krynthoun all adsorbed gases from the interior surfaces of the device, and may require several days of pumping.

For the provision was implemented, pumping non autoclaved system pipes and tube from mechanical pump may require up to 10 cycles of pumping of 10 minutes with breaks of 30 minutes, so the pressure is lowered to 2mTorr easily. With such a procedure, when the pressure reaches 2mTorr and the system is isolated, the pressure rises relatively slowly, about 1mTorr every 5 minutes.

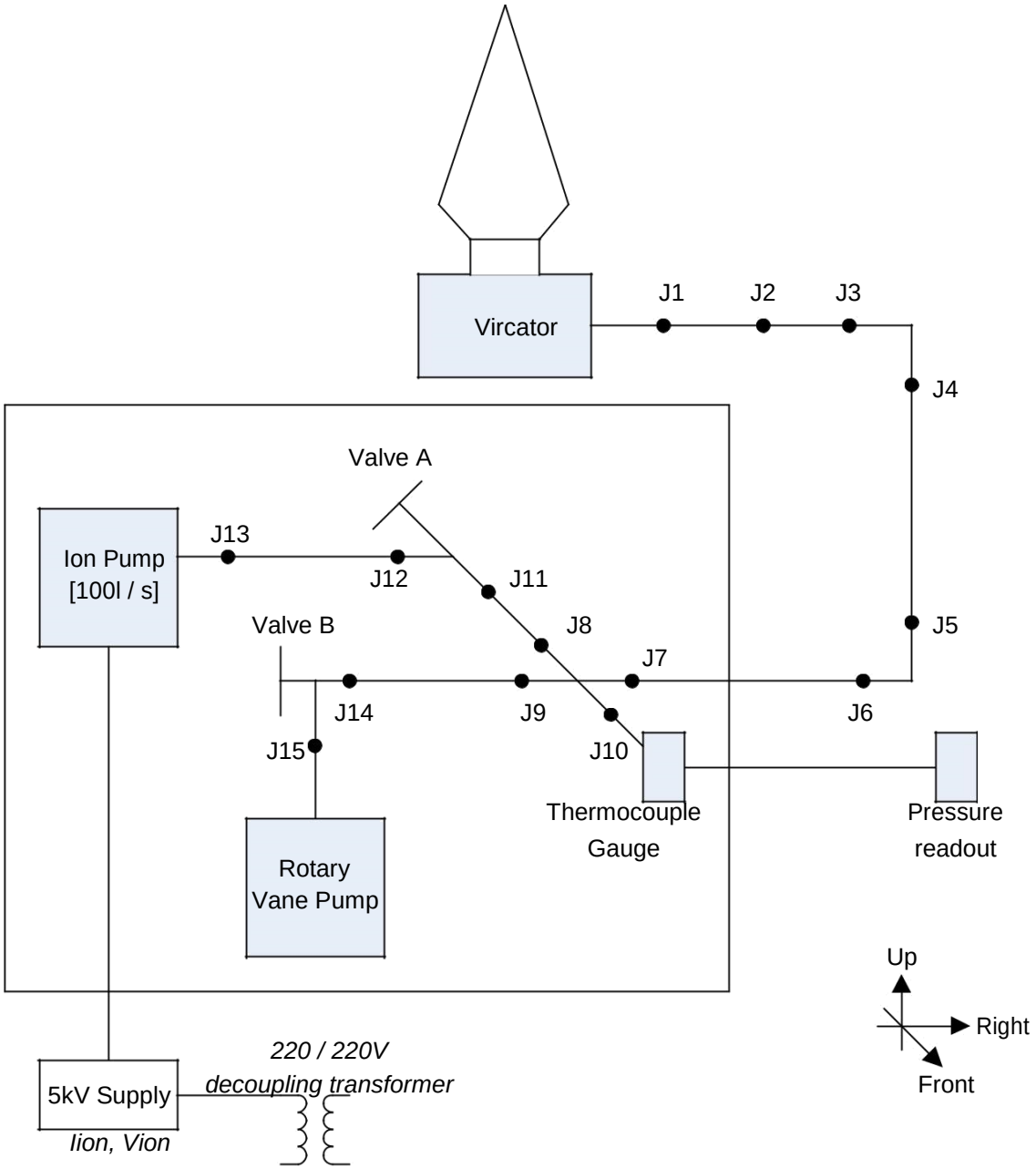

Fig. 6.2: Diagram of the vacuum system.

The purity level of the system is no longer satisfactory to connect the ionization pump. Binding of Ion Pump the remaining volume is made by gradually opening the valve D, whereby the ionisation current rises up to 50mA, and then decreases exponentially. Typical times during the first pumping with Ion Pump is the first 1-2lepta 10mA, 5mA in the next 20 minutes, 3mA in the next hour, 2mA in the next two hours. The ionization pump operates continuously, thus the next day there is ionization current of about 0.5mA, while the other two or three days of pumping, the pump ionization current reaches 0.2mA. The total minimum in- EVEL ionisation current, observed the arrangement is approximately 0.16mA (160) after one week pumping. When the sample has reached the mini- mum achievable pressure lamp can be disconnected from the drainage system and increase internal pressure very slowly.

Tab. 6.1: Pipe Network System Vacuum and Associations

Department / Association	Length [mm]	Cross-section [mm]	Description
Vircator-J1	~ 60	Ø15	Straight Tube
J1			3 Joint 2.75 "ConFlat (CF) Flanges
J1-J2	~ 110	Ø22	2 Ø22 Kwik-Flange (KF) Adapters
J2			2 Joint 2.75 "CF Flanges
J2-J3	~ 80	Ø30	Flexible Tubing (Spiral)
J3			2 Joint 2.75 "CF Flanges
J3-J4	~ 90	Ø34	Solid 90o Bend
J4			2 Joint 2.75 "CF Flanges
J4-J5	~ 80	Ø30	Flexible Tubing (Spiral)
J5			2 Joint 2.75 "CF Flanges
J5-J6	~ 90	Ø34	Solid 90o Bend
J6			2 Joint 2.75 "CF Flanges
J6-J7	~ 80	Ø34	2 Ø34 KF Adapters (Straight Tube)
J7			2 Joint 2.75 "CF Flanges
J7, J8, J9, J10		Ø34	4-Way Cross with 2.75 "CF Flanges
J7-J8	~ 80	Ø34	90o Bend through 4-Way Cross
J8			2 Joint 2.75 "CF Flanges
J8-J11	~ 80	Ø30	Flexible Tubing (Spiral)
J11			2 Joint 2.75 "CF Flanges
J11-J12	~ 120	Ø34	90o Bend through Valve A
J12			2 Joint 2.75 "CF Flanges
J12-J13	~ 110	Ø34	Straight Tube
J13			2 Joint 4 "CF Flanges
J13-Ion Pump	~ 130	Ø60	Straight Tube
J7-J9	~ 120	Ø34	Straight Path through 4-Way Cross
J9			2 Joint 2.75 "CF Flanges
J9-J14	~ 200	Ø34	Straight Tube
J14			2 Joint 2.75 "CF Flanges
J14-J15	~ 120	Ø34	90o Bend through Valve B
J15			2 Joint 2.75 "CF Flanges
J15-Mech. Pump	~ 80	Ø34	Straight Tube

Since the indicator thermocouple (Thermocouple gauge) has functional area let by 1mTorr to 760Torr, we have direct indication of pressure in the device, the region below 1mTorr, i.e. when it is connected to the ionization pump. The m- direct the light can be measured indirectly by the pump ionization current. The liquidity but ionization translates into pressure on the pump by which dependence Zeta presented in Fig. 6.3.

To calculate the pressure of the lamp must estimate the conductivity of pipeline from the pump to the lamp, through the route J13 -> J1, as illustrated in Fig. 6.2.

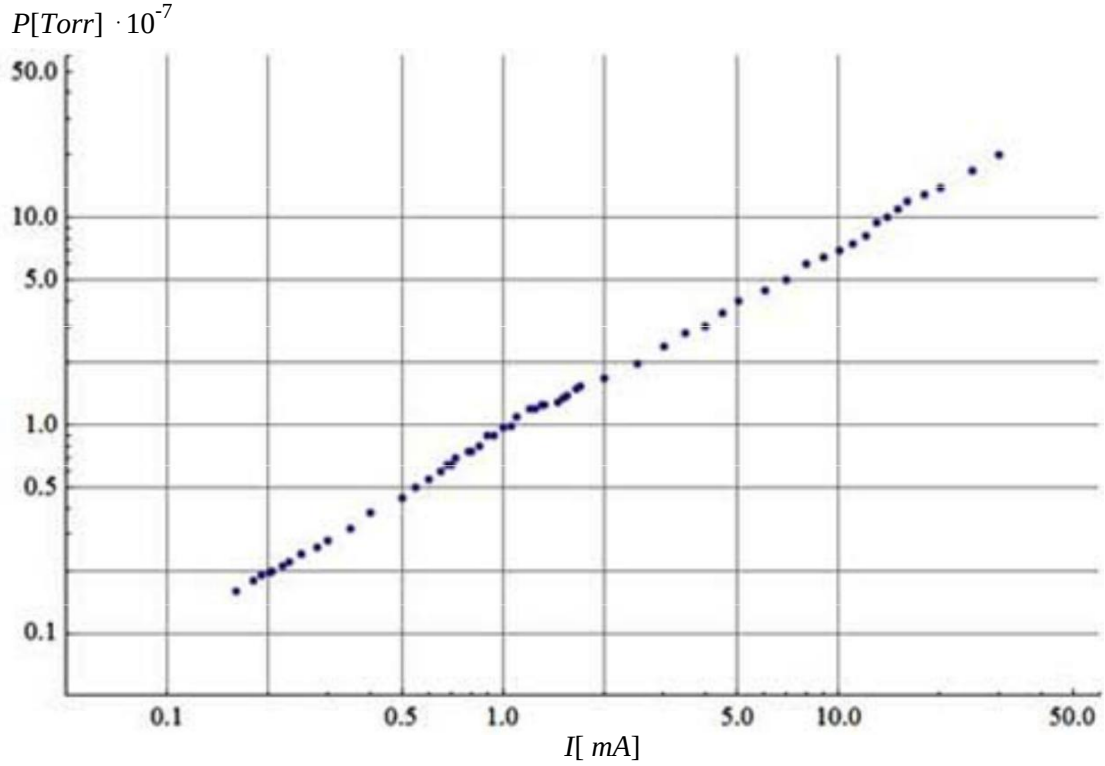

Fig. 6.3: Empty the pump function of the ionisation current

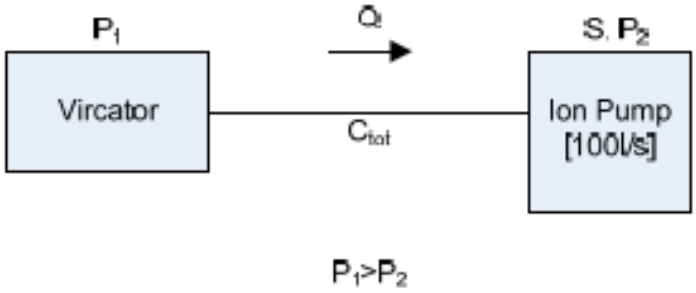

Fig. 6.4 Simplified circuit for calculating the pressure in the specimen.

Conductivity *C* a cylindrical tube defined as the ratio

$$C = \frac{Q}{P_1 - P_2}, \tag{6.1}$$

where to *Q* denotes the gas flow and *Pi* pressures of tumors, the tube connects. However, the conductivity is a variable which depends on the geometrical characteristics of the tubing and tubular sections applicable [129]:

$$C = 1.16aA \text{ [Lt / s]}, \tag{6.2}$$

where *A* is the cross section of the conductor in cm2, and a is a dimensionless number which depends on the ratio *l / d* (Length / cross section) of the tube and is spread probability of a person or the molecule through the tube.

Tab. 6.2: Piping Route Network Vircator-Ion Pump

Department / Association	Length [mm]	Cross-section [mm]	Coord. "A"	Conductivity [lt / s]
Vircator-J1	~ 60	Ø15	0.22	~ 0.45
J1-J2	~ 110	Ø22	0.19	~ 0.83
J2-J3	~ 80	Ø30	0.30	~ 2.46
J3-J4	~ 90	Ø34	0.30	~ 3.15
J4-J5	~ 80	Ø30	0.30	~ 2.46
J5-J6	~ 90	Ø34	0.30	~ 3.15
J6-J7	~ 80	Ø34	0.32	~ 3.45
J7-J8	~ 80	Ø34	0.32	~ 3.45
J8-J11	~ 80	Ø30	0.30	~ 2.46
J11-J12	~ 120	Ø34	0.25	~ 2.52
J12-J13	~ 110	Ø34	0.26	~ 2.63
J13-Ion Pump	~ 130	Ø60	0.35	~ 11.5

The total conductivity *truly independent* tumor connected in series is equal to the relation

$$\frac{1}{C_{tot}} = \frac{1}{C_1} + \frac{1}{C_2} + \frac{1}{C_3} + \ldots \tag{6.3}$$

However, this type can be used in the case between the cor- linoseis inserted large volumes, of which we have apparently devel- heading of gas. In case the pipes are connected together without leaving large volumes, the potential for the spread should be amended to compounds according to the theorems described in [129]. In order to submit accountants pressure prevailing in the lamp, will build the diagram of Fig. 6.4 and we will calculate the total conductivity between Ion pump and kyma- todigo, based on the relationship (6.3) and assuming that the part from the connector J2 to the connector J13 is a long section with section 810mm 30mm. We conclude the alpha Sequence table conductivities:

Tab. 6.3: Simplified Network Piping Route Vircator-Ion Pump

Department / Association	Length [mm]	Cross-section [mm]	Coord. "A"	Conductivity [lt / s]
Vircator-J1	~ 60	Ø15	0.22	0.45
J1-J2	~ 110	Ø22	0.19	0.83
J2-J13	~ 810	Ø30	0.05	0.40
J13-Ion Pump	~ 130	Ø60	0.35	11.5

The total conductivity is therefore:

$$C_{tot} \cong \left(\frac{1}{0.45} + \frac{1}{0.83} + \frac{1}{0.40} \right)^{-1} \cong 0.17 \text{ [Lt / s]}. \tag{6.4}$$

About the same result would end using (6.3) for all pipeline gimotites of Tab. 6.2. Therefore, at best, the conductivity of the connection

Vircator-Ion pump is 0.17lt / s. We know that the pumping speed S of a pump is a structural size and for many pumps is a constant quantity for the designed operating range. For Ion Pump we use, we believe that, throughout the operating range, the pumping speed is equal to 100lt / s, according to its standards. The pumping speed is expressed by the relation

$$S = \frac{Q}{P}, \tag{6.5}$$

where *Q* the gas flow to the pump and *P* the pressure prevailing therein. There- fore, on the basis of (6.1) we have

$$C_{tot} = \frac{Q}{P_1 - P_2} = \frac{S \cdot P_2}{P_1 - P_2}. \tag{6.6}$$

Solving for the desired, i.e. the pressure *P2*, We will have

$$P_1 = P_2 \frac{S + Ctot}{C_{tot}}. \tag{6.7}$$

After S = 100lt / s, and Ctot = 0.17 lt / s, clear $P_1 \cong 600 P_2$. Since overestimate conductivity pipeline, we believe that the pressure in the tube is about three orders of magnitude greater than the pressure present in the ionization pump. From the vacuum test series the lamp was found that the lowest point of operation of ionization pump with currents of about 0.16mA (160m), which correspond to a pressure of 1.6 · 10-8Torr. Consequently the gap in the waveguide is in the range of 10-5 ~ 2 · 10-5Torr, which is deemed sufficient for the operation of the lamp. Worth Notes been that after each pulse, elimination of gases from the cathode and the anode is arke- large, so it takes about 5min to restore pressure to the previous levels. Yes, register the pressure after each impact, using the thermo- couple gauge, showed release gases that cause increased pressure from 0.2mTorr up 2mTorr where appropriate, which is affected, as can be a- ntilifthoume, the purity of surfaces The material of the electrodes, the size of the cathode and other factors.

6.2. Measuring Device

To draw conclusions about the behavior of the lamp, we measure the voltage, current and the microwave signal directly to an oscilloscope 2GHz bandwidth and sampling 20GSamples / s, the DSO80204V of Agilent ([130]). The voltage of the impulse generator is led to the lamp probe and simultaneously to a party a capacity divider, to which the high voltage is lowered at a 1: 420. The capacitor ypsi- glycol capacitive voltage divider is 1200pF / 140kV and low capacitor is 504nF. The capacitive voltage divider is divided further comprises a differential probe with a 1: 100 and is led to the oscilloscope in port 50R. The probe lowered

voltage used is MD200 of Schaffner ([131]), with unknown bandwidth 70MHz and output impedance, which is designed to drive the signal to a high- impedance oscilloscopes. The registration of the mark by 50 ohm oscilloscope probe E has resulted in further division of the voltage by about half. Parallel testing high-impedance and 50 ohm oscilloscope revealed that the sinking of BRAKE ing because of driving small load resistance is a factor of about 0.6, there- fore, the lamp voltage is recorded by the oscilloscope degraded **70000 times** (Ratio 42000 / 0.6).

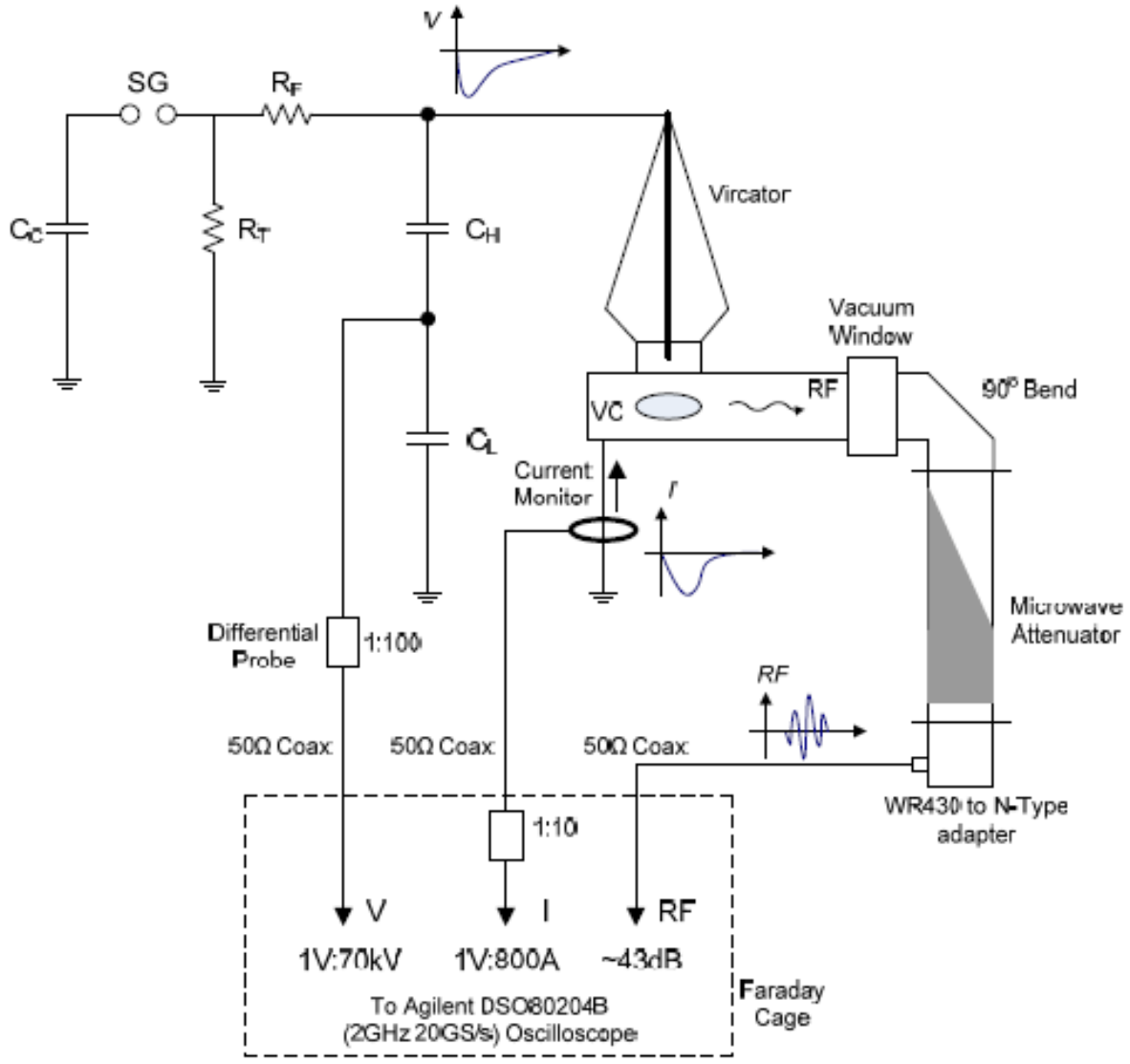

Fig. 6.5: The diagram of the measuring device of the first stage of Virca- tor experiments

The current measured is the lamp ground current, and recorded via a current transformer (current monitor). This is the transformer currents, Tosh 1025 of Pearson Electronics ([132]), with Bandwidth 4MHz, maximum current 20kA and transformation rate 25Volt / 1kA an open load. At 50W this relationship, according to the manufacturer, is half, ie 12.5V / 1kA. Therefore used one extra attenuator 10: 1 (20dB), so as to degrade the signal in the order of 1.25V for each 1kA passing current. In other words, the transformation

They are **1V / 800A** current. This signal is fed to the second channel of the same digital oscilloscope. Finally, the microwave signal, after undergoing attenuation of micro- wave load at the output of the lamp, is driven via coaxial cable to the third channel of the oscilloscope, where he recorded for the range of 1.4GHz (sum of WR430 waveguide) up to ~ 2GHz, which It is the analog bandwidth of palmo- graph. The attenuation is variable in frequency and varied, as are illustrated down in the diagram of Fig. 5.28, with an average value of about **43dB**, If we calculate the total losses of the coaxial cable used by the light sensor until the log.

The three channels, RF, current and voltage, respectively driven in the channels CH1, CH3 and CH4 oscilloscope DSO80204V of Agilent, which is located within a shielded cage and powered by an isolation transformer 220 / 220V. Inside the cage there is also an arrangement of two WR430-to-N-Type adapter connected together (back-to-back), so that the microwave signal is still a high-pass filtering term with lower cut-off frequency of 1.4GHz. The arrangement within the container shown in Fig ents were formed. 6.6.

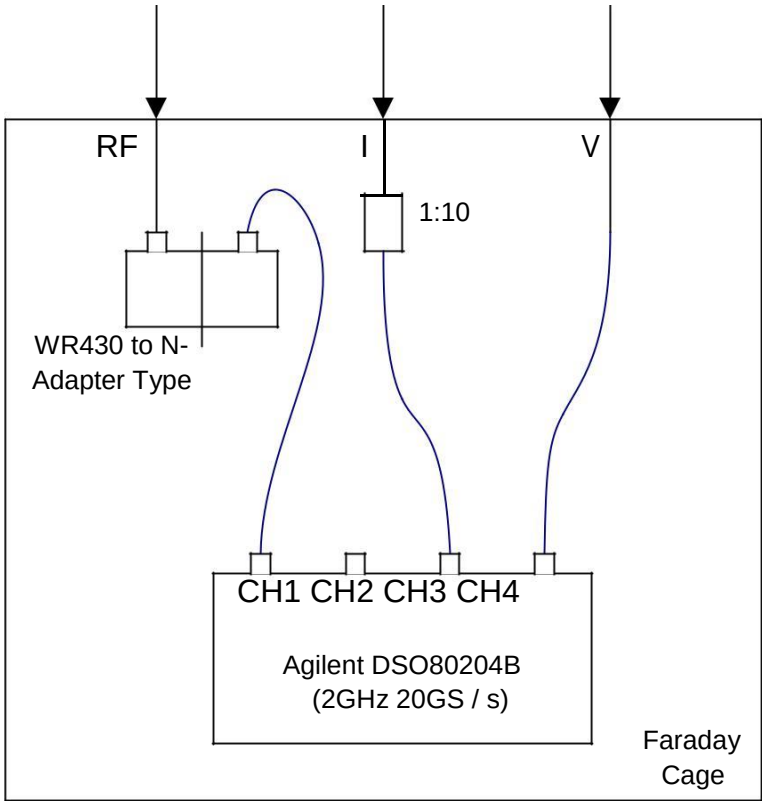

Fig. 6.6: The metering device into the cage Faraday, in the Lab. High Voltage NTUA.

The tests found that the grounding and shielding is of paramount simasi- let for measurements close to high voltage. Crowd cables, connectors and adapters were tested and changed, before the signals received, be as possi- clean and free from parasitic and transients, due to the percussive device itself and the bank handling. Coaxial cables other and within (!) The cage significantly affected, unless they have very good armor and if not too tight connections, the points paremval- be submitted attenuators, probes, transducers and other links. In order to solve

all proofing problems consumed several days in tests of recorded tor- signals and comparison of each channel separately, and combinations me- the tween, until you confirm that the channels count correctly without being affected only to a small extent on the device of high voltage.

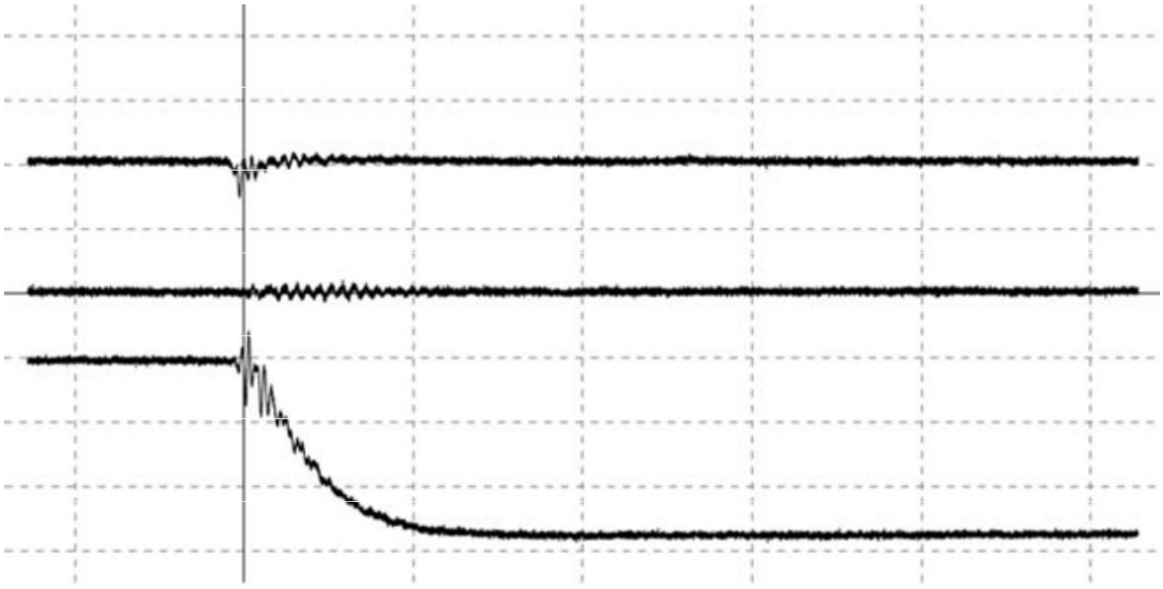

Fig. 6.7: Taken Voltage signals Power and Light Output for impulse test voltage ~ 100kV.

In the picture above shows the recording of a typical maximum impact with the lamp disconnected from the high voltage. The arrangement and the measuring system is completely installed, but the Vircator is the "air". The trend recorded in specific maximum price 1.463Volt, signal corresponding to impulse voltage amplitude 102kV. The current channel recording on a small label on the principle of impulse voltage, whoever it may be due to displacement currents at the time of discharge. This signal has a value of 250mV, corresponding to currents of the order of 200A. To this is added where appropriate interference of high voltage device on the recording channel. Finally, we see the channel of the microwave signal, which is the channel for which became the biggest concern about external interference. In a typical maximum amplitude shock, noise occurring in the RF channel is very Asia Mi- Cross, about 1mV. Ideally, after the lamp is disconnected, there would be no signal observed in this channel, which is practically achievable. Since noise and offsets of the channels of voltage and current, the power *sub- accounted* as offered to the passage of the lamp has an estimated final uncertainty the rate of 1MW, if the striking voltage width ~ 75kV, and 2MW, where the impulse voltage width ~ 100kV DC.

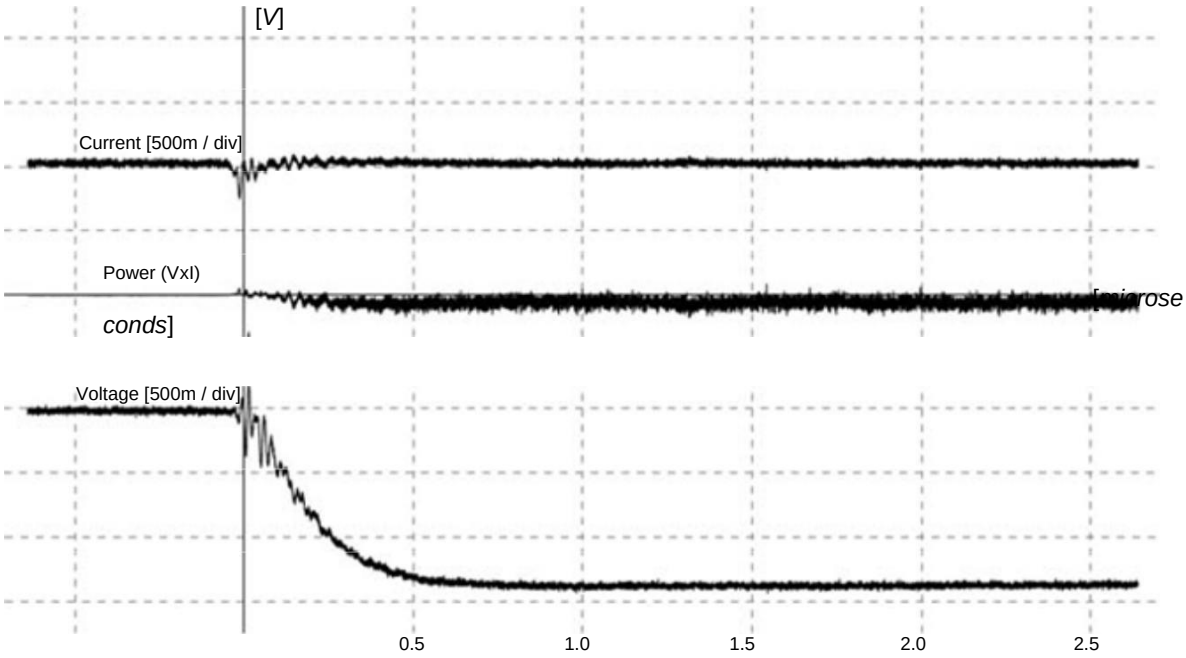

Fig. 6.8: Taken Voltage signals Current and multiplying them on impulse test voltage ~ 100kV. The noise of the product corresponds to uncertainty about power 2MW.

6.3. Lamp Testing

We saw in the preceding paragraphs (Par. 5.3, 6.1), the lamp control in terms of tightness and maximum practically achievable vacuum. The lamp was checked for leaks with a He leak detection system and confirmed that after satisfactory discharge of adsorbed gases, the vacuum reaches the levels of the waveform 10-5Torr digo. This pressure is the assessment made by the pumping capacity of Ion Pump used, the pressure therein and the overall conductivity of cor- linoseon, used in the lamp-pump connection. This gap is sufficient to operate the Vircator, since we have seen that in the literature referred to vacuum levels of 10-4 to 10-7 Torr, and even until 10-3Torr appears that the microwave power is not affected. We saw further that the lamp is designed with two re- Tasman, to form a cavity of variable length in z-axis of the waveguide. Placed a short circuit at the rear, so that the cavity length is 125mm, in order to impose an eigenfrequency coordinating the virtual cathode in the range of 1.8GHz (see. Fig. 6.9).

Then we will describe the tests relating to light with regard to Asia Mi- krokymatikes of parameters and different potencies finally recorded, leading the light to the VDE-b-step impulse generator of 140kV.

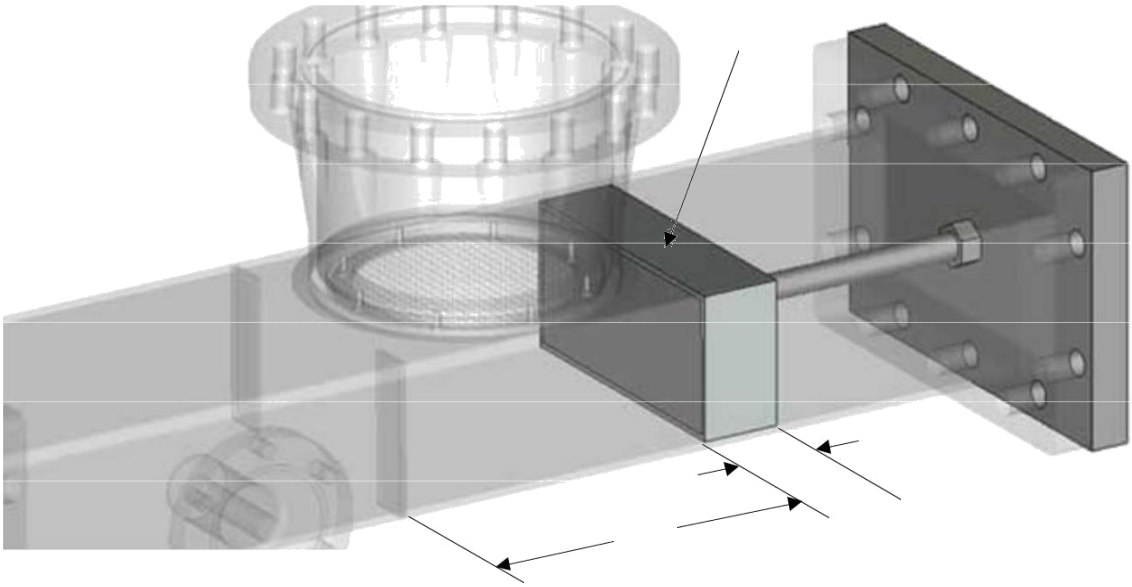

Fig. 6.9: The inside of the waveguide Vircator, the cavity formed.

6.3.1. SParametroi of Vircator

The lamp was tested for the reflection coefficient S11, when viewed from the micro wave window to the waveguide. Using a network analyzer (network analyzer), we measured the reflectance of the light in vacuo, no space without the insulator and without the anode (see. Fig. 6.10). The results show small differentiations vacuum and without vacuum, but more marked differences when there is no mo- notiras. Not surprisingly, when we remove the grid anode, the reflectance changing behavior completely.

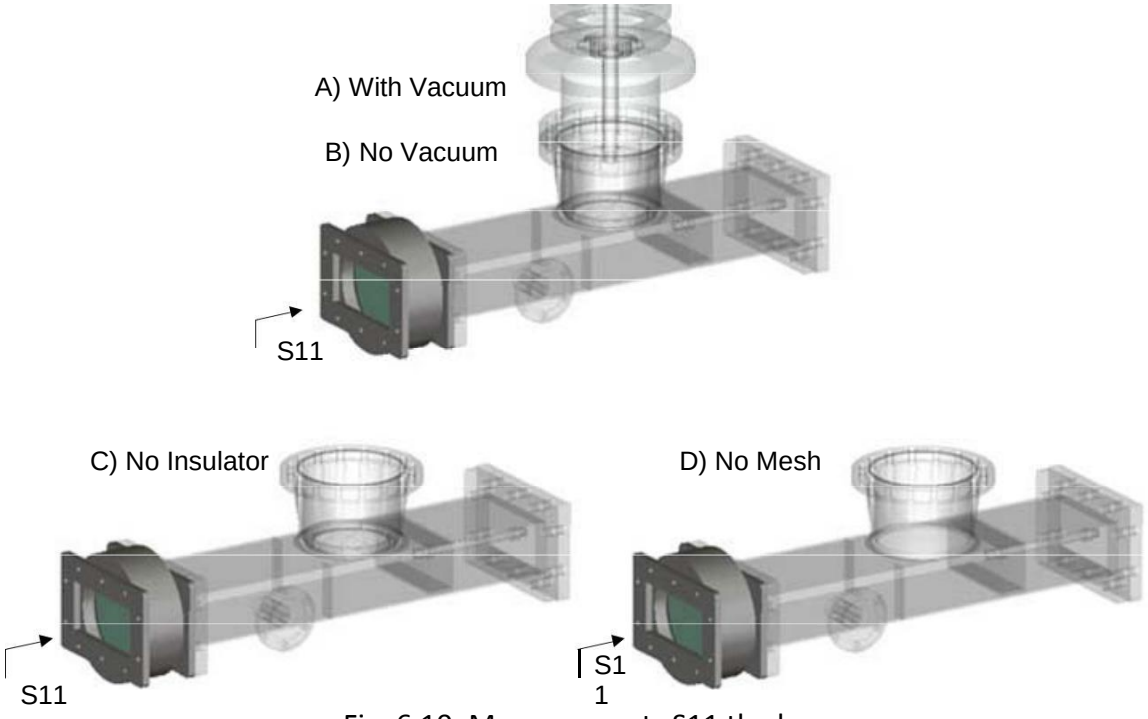

Fig. 6.10: Measurements S11 the lamp.

In the cases A) and B), the effect of the vacuum is limited to slightly displace some characteristic resonance frequencies, since virtually slightly alters the dimensions of the waveguide due to the external atmospheric pressure. For example, when the lamp is in vacuum, appear pale both known transition frequencies: one part of the window (see. Fig. 5.23), the other part of the waveguide, at 1.480GHz and 1.308 respectively, while the cavity resonance frequency observed reitai to 1.870GHz. Two more characteristic frequencies of unknown origin re- ratirountai to 2.245GHz and 2.297GHz (see. Diagram Fig. 6.11 above). When the light EP sulfate at atmospheric pressure, the switching frequency of the window still it would appear at 1.308GHz, the waveguide transition frequency occurs at 1.488GHz and the cavity resonance frequency occurs at 1.877GHz. Slightly displaced wells at 2.275GHz and 2.342GHz (see. Diagram Fig. 6.11 below).

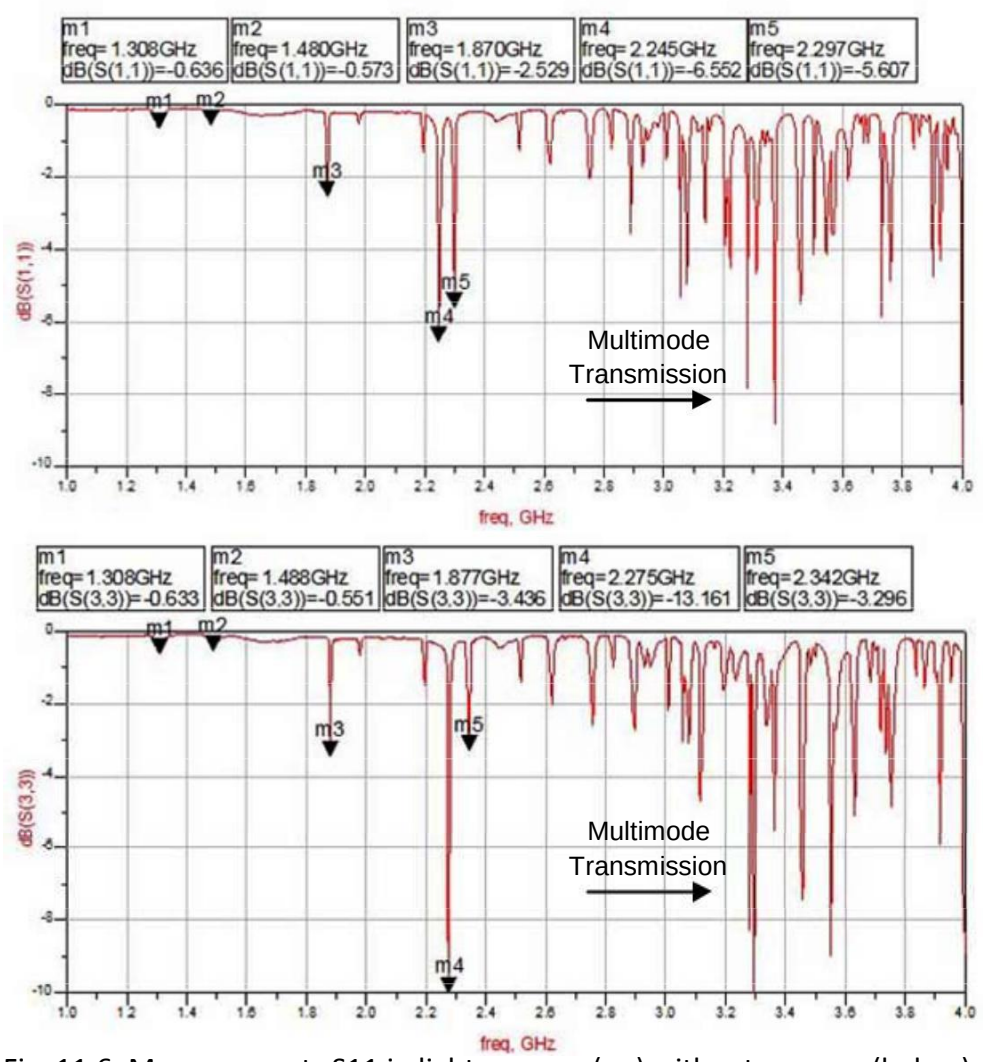

Fig. 11.6: Measurements S11 in light vacuum (up) without vacuum (below).

Removing the insulator passage, an additional draft presented in 1.488GHz, with several large bandwidth, which may be due to cyclical de- cceptance anode, which now makes full contact with the waveguide (see. Diagram Fig. 6.12 above). Wells at 2.275GHz and 2.342GHz still

They appear at the same frequencies. Removing finally the grid anode, a significant diffusion occurs for frequencies above 2GHz, which is justified by the leakage of the microwave signal into the circular hole of the upper side of the waveguide (see. Diagram Fig. 6.12 below). For this measurement of utilization was the matrix "No.1", with 30 holes per square inch, 0.26mm wire thickness and a free surface of 48%.

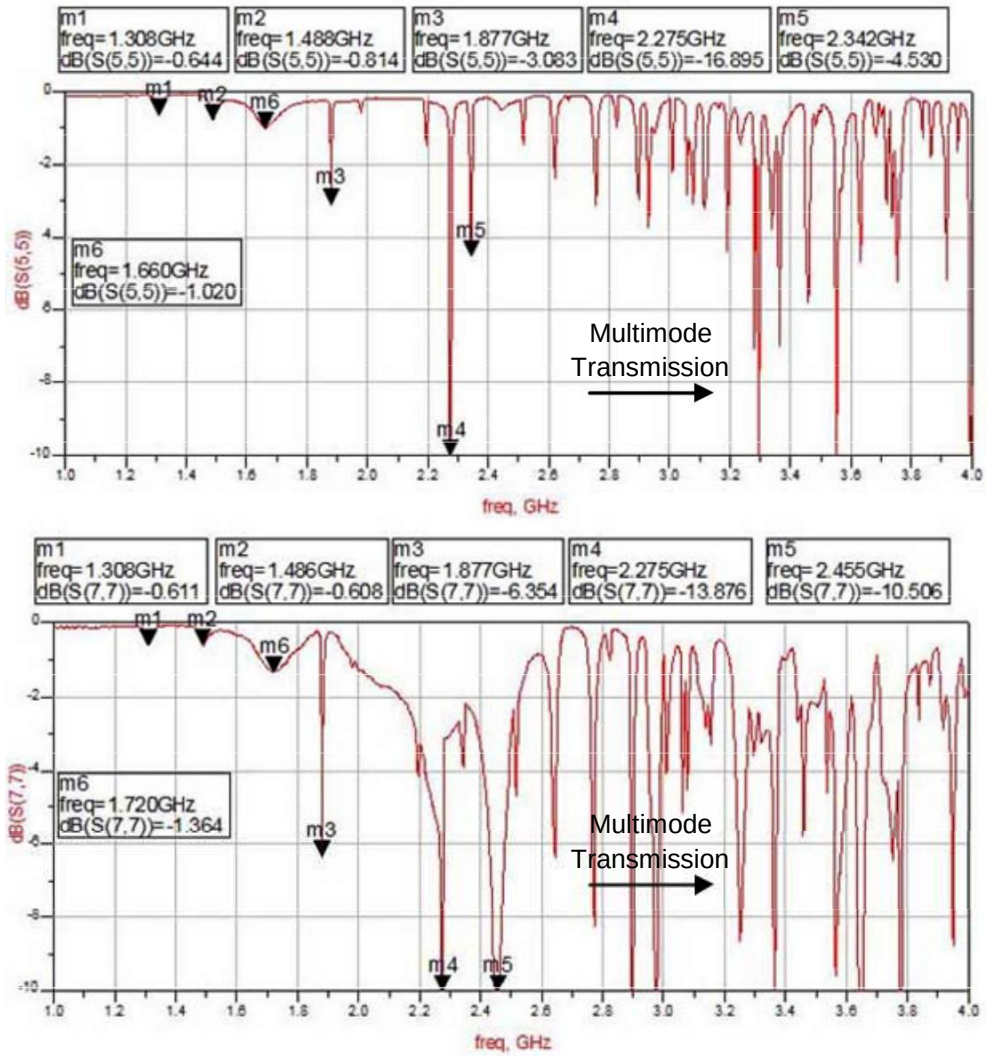

Fig. 12.6: Measurements S11 to the lamp without the insulator (top) and without the insulator and the anode mesh (under).

The most important conclusion from these measurements is the observation that the frequency of ~ 1.87GHz always appears almost identical to the frequency cavity lation coordination 125mm * 109mm * 54.6mm (125mm waveguide WR430). Under Microwave Studio of CST, this frequency is 1.82GHz (see., And Fig. 5.8). This suggests the presence of a small Q in resonator and any load from the walls, and the short rear, which, as we have seen, is a parallelepiped block of aluminum with a length of 35mm, coated with Teflon thickness 2mm, whereby there is a path microwave sional signal backward.

6.3.2. Testing in Single-stage Impulse Generator

The first tests were done with the Vircator layout VDE-b, we have described previously (see. Ex. 5.5), with front resistance RF = 208O, charging capacitor CC = 6000pF and load capacitor CL = 1200pF, formed simultaneously as a capacitive divider with low voltage capacity 504nF (division ratio 1: 420). The provi- ment may cause the lamp to a maximum impulse voltage of 115kV, with a rise time of 10% -90% approximately equals 500nsec and shock current, which largely provided by the capacitive divider and generally depends on the transition instead - situation showing the anode-cathode gap of the lamp.

Fig. 6.13: Experimental Device with Impulse Generator VDE-b.

Tests were made to light with various combinations of cathodes and anodes, the opoi- s will be described. The practice was recorded characteristic variables lamp for alternating drive voltage from the bank equal to maneuver **~ 50**, **~ 75** and **~ 100V** AC. The driving equivalent to that DC charging voltage of the capacitor CC equal to **~ 64kV**,**~ 96kV** and **~ 128kV** respectively. Given the rate of impulse voltage device performance, 0.81 (see. Par. 5.5), the LED being driven by impulse voltage **~ 52kV**,**~ 78kV** and **~ 104kV**, shape 0.6 / 50. The diode lamp, depending on the configuration of gap, happened often withstand voltage of the first or the second-level load. Only for certain configurations, such as spheroidal cathode at a distance d = 25mm from the anode or cathode cylindrical with concentric grooves, tychai-

ve observed strength of the gap even in impulse voltage of ~ 104kV. The following screenshot shows the three typically used percussive trends, o- what obtained by charging primary voltage of 50, 75 and 100V AC. The percussive shown here width 52kV, 79kV and 102kV respectively. Some transients, which occur at the origin, due generally to ypsilote- pn charge level and is a typical phenomenon for aerial percussive devices.

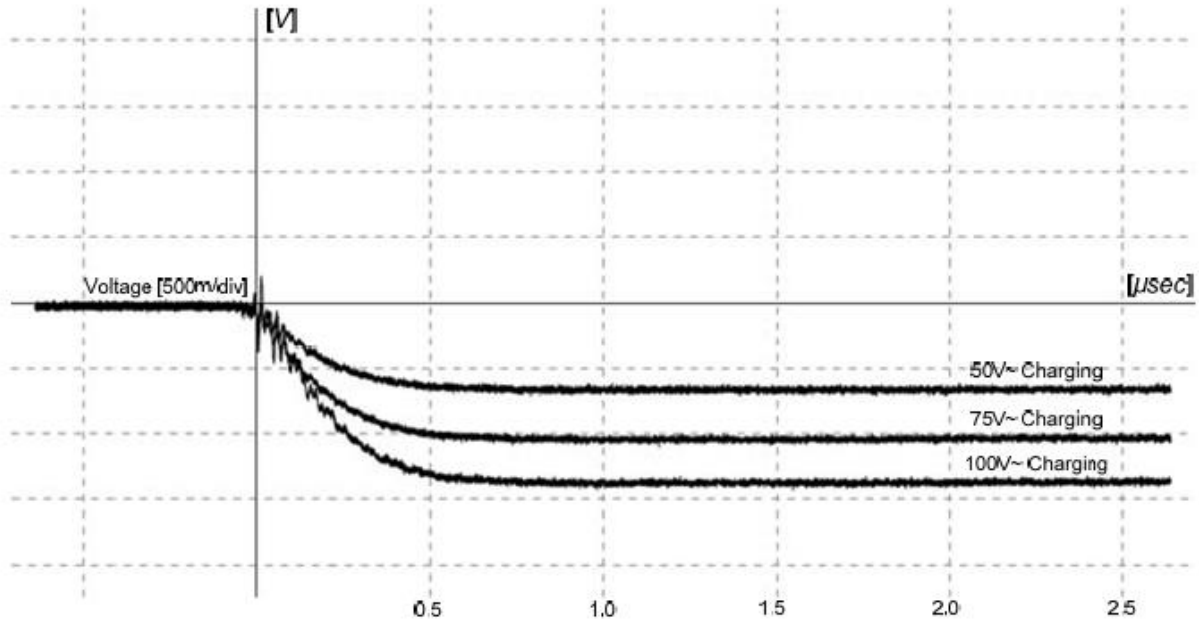

Fig. 6.14: The three used impulse test.

Driving from the impulse of ~ 104kV has given average values observed specific maximum from 50kV up to full price peak, where the cleavage occurs in the tail of the impulse voltage. Also, the currents occurring are rates of up to 700A over 2kA, depending on the configuration of the passageway. In Tab. 6.4 are included some typical voltage and current sizes of the lamp, driving capacitor charged to ~ 128kV and hence impulse voltage amplitude ~ 104kV (primary voltage ~ 100V AC).

Tab. 6.4: Observed Maximum Voltage-Power Lamp (VC = 128kV, VK = 104kV)

Formation	<Vmax> [kV]	<Imax> [A]
Pin Cathode, dAK = 15mm	~ 56	~ 900
Pin Cathode, dAK = 25mm	~ 75	~ 1000
Velvet Cathode, dAK = 15mm	~ 64	~ 900
Velvet Cathode, dAK = 25mm	~ 70	~ 1000
Multipin Cathode, dAK = 15mm	~ 85	~ 1600
Ridged Cathode, dAK = 15mm	~ 100	~ 2000

The maximum trend before collapsing the passage of Vircator. The maximum current is displayed in much later, when there has been a complete bridging the diake- mind from plasma. At this time, the voltage of the diode is sufficiently lower than the maximum and thus the maximum value of voltage and current are separately sizes coun- Piq important. As we will see, the voltage and current waveforms show

lots of useful information on the behavior of the gap when examined jointly. The information that can be extracted is the maximum power supplied to the device by multiplying the voltage by the current, and the resistance that displays the appointment Give, as the collapse of the gap evolves. For example, we present two records for the voltage and current of the lamp as well as another product, to form a pin diode type cathode, with a distance AK equal to 25mm. The waveforms shown below are factors ~ 70000V / V for voltage, 800A / V for the power, 56MW / V for the power diode.

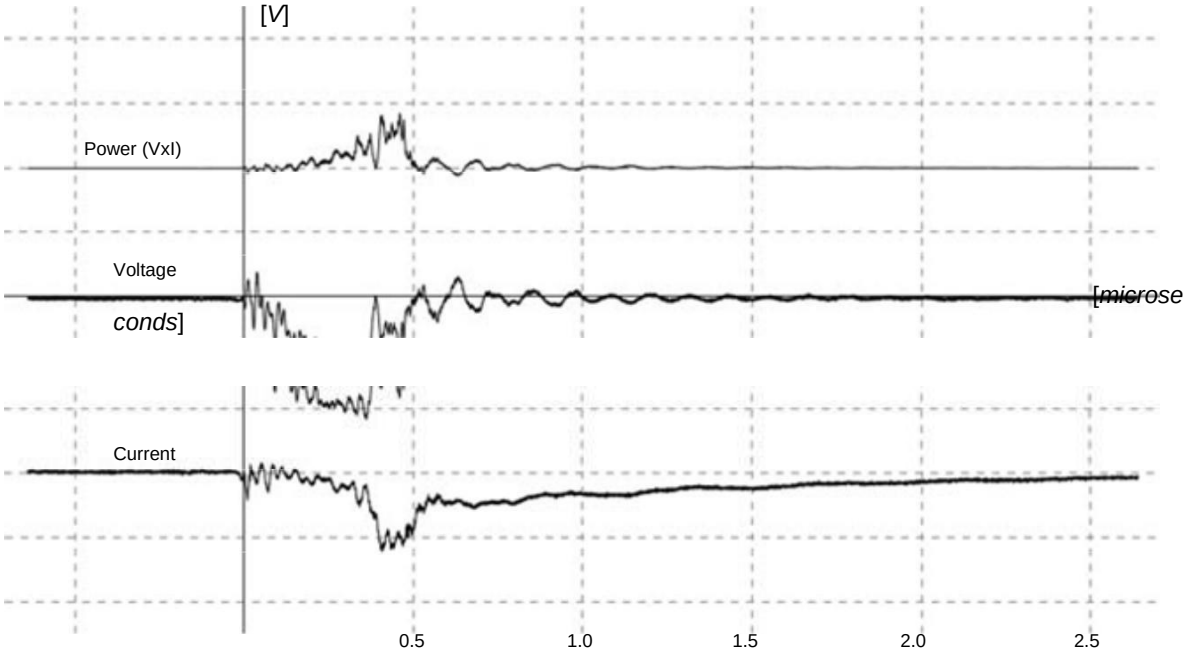

Fig. 6.15: Voltage, Current and Power Diode, Case 1. (Imax = 980A, Vmax = 81kV, Pmax = 47MW). Descent Pin, dAK = 25mm.

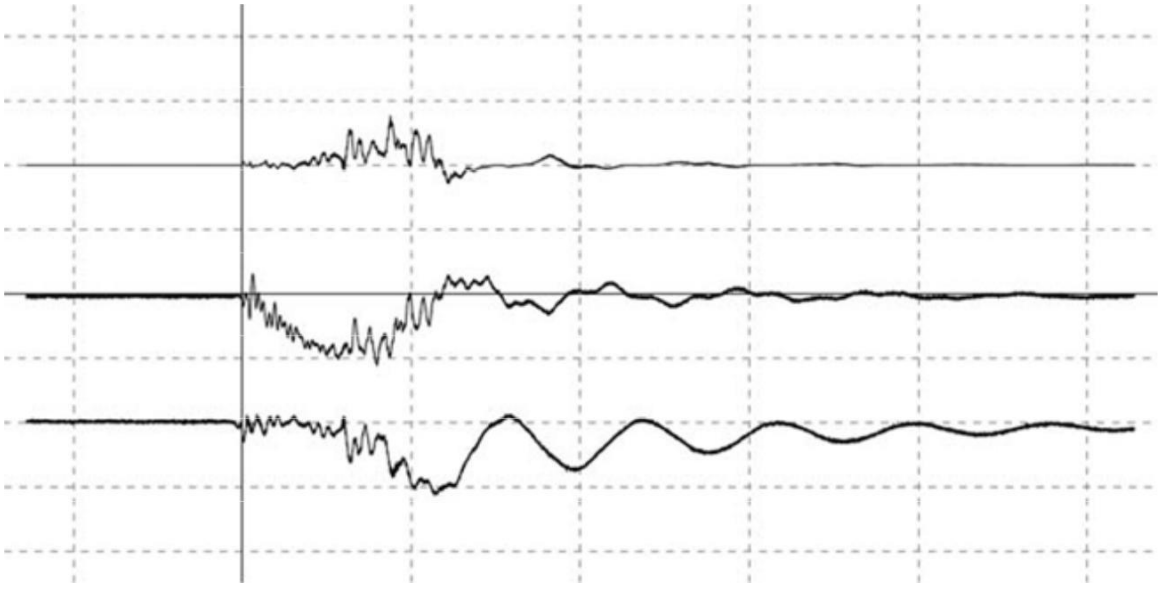

Fig. 6.16: Voltage, Current and Power Diode, Case 2. (Imax = 910A, Vmax = 78kV, Pmax = 43MW). Descent Pin, dAK = 25mm.

Of the two functional recordings, we can observe two behaviors, a gently decaying drive diode and a rocking. In the first case (Fig. 6.15), the voltage (main signal) rises until the xekina- where the collapse of the gap, so the approximately 0.4msec, the current rises rapidly, and the voltage decreases. For 100nsec about the stream remains approximately 900A, while the BRAKE importance is significantly suppressed after the 500nsec remains oscillating around zero. This stream, after 500nsec, following gradual extinction and it is the current of the capacitor CC, which is discharged gradually through the front RF resistance of 208O and, bridged plasma-diode lamp. The maximum power of the diode is approximately 47MW and is observed when current tends to take their maximum rate even before the voltage collapse completely.

In the second case, and while the diode is still directly polarized, the maximum BRAKE importance reaches 78kV, the current 910A and the maximum power in the diode is 43MW. However, this impact (Fig. 6.16), the situation is somewhat different. The voltage gradually goes inde- passageway and at a point, about 300nsec, starts collapse diake- mind. The voltage decreases, while the current continues to increase, until about 600nsec, whereby the voltage to the lamp is reversed, due to the bridge diode and the inductance of the circuit showing the impulse device and the lamp. At that point, the tide now seems to follow a new behavior, a very smooth oscillation. The of Conduct is being observed quite often, when the voltage across the diode quickly collapsed due to the sudden imposition of a closed loop oscillations between coun- exception of preservatives divider and diode lamp. This phenomenon is also observed in other experiments with Vircators, the voltage and current waveforms ([46], [119]), due to the strong inductance of lamp-loop capacitive element. In our experimenting arrangement with impulse generator VDE-b, these oscillations are observed when, always have the same period, slightly less than 400nsec, that is one reason li- frequency greater than 2.5MHz.

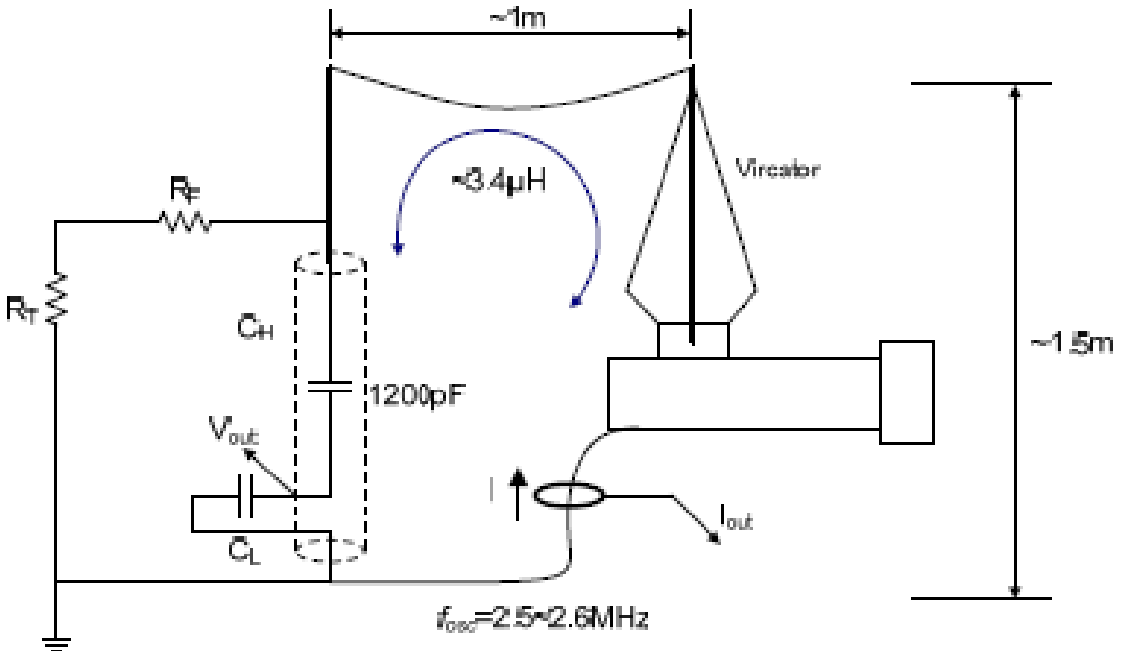

Εικ. 6.17: Εμφάνιση ταλαντώσεων ανοικτού βρόχου.

The oscillations of power completely justified, since the inductance of vro- Hu the capacitive divider and lamp, a total length of more than 4m, resulting in non. Specifically, square measuring 1m, considering that apotelei- Tai of circular cross section conductor 1cm, the inductance resulting 3.6mI. If the cross section of the duct is 10cm, the inductance resulting ~ 1.7M ([133], [134]). The period of 400nsec translates to a frequency 2.5MHz, which results from LC circuit with elements C = 1200pF and L = 3.4m. This value, L = 3.4m, is justified by the size of the loop of the capacitive divider and Vircator. Based on these observations, when the observed current is switched to the smooth harmonic behavior, we believe that it is installed in the passage of the arc tube and the cathode to the anode of Vircator is completely short-circuited by plasma.

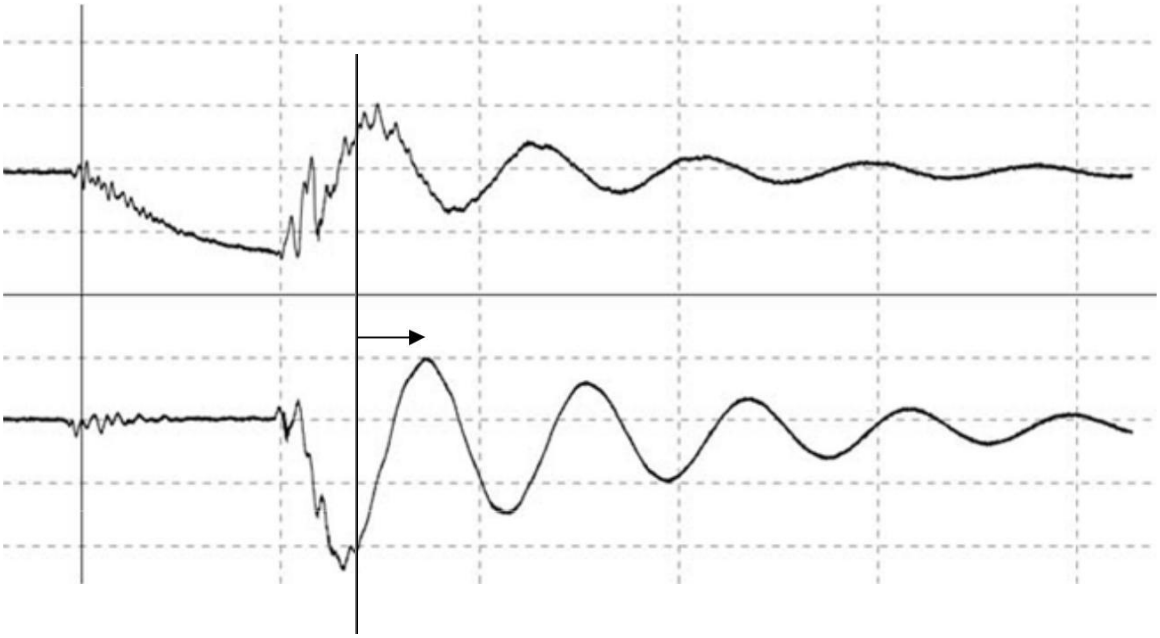

Fig. 6.18: Example showed strong oscillations in the fairway. Sandblasted sfai- steroid descent, impulse voltage 104kV, Vmax = 100kV, Imax = 1900A.

From the records it is clear that power in the gap during those periods the voltage has not completely collapsed when that gap is not fully bridged. The time during which significant potency observed in the passage of the lamp is of the order of 300nsec to the specific impulse device, always depending on the configuration of the passageway. In the graphs below, a dotted line is noted as the time where the voltage changes polarity, while the waveform of the current switches to smooth variation. This point marks the closing of the plasma channel.

6.3.3. Descent Pin (d = 15mm)

For experiments with waveguide Vircator and testing with the armrest assembly VDE-b, the cathodes widely used were the cathodes type pin, because, as we shall see below, provided the larger sizes microwave aktinovoli-

let. The tip cathodes exhibit rapid decomposition of the gap of the passage, due to their geometry, and therefore relatively low driving voltage of the lamp. The slow rise time of the forehead means the limited drive voltage levels, since the gap begins to crumble even before the trend reaches the largest possible Timoleon Mes. The currents observed are of the order of 1kA the case of the maximum driving voltage of impulse type 0.6 / 50, the width 100 + kV.

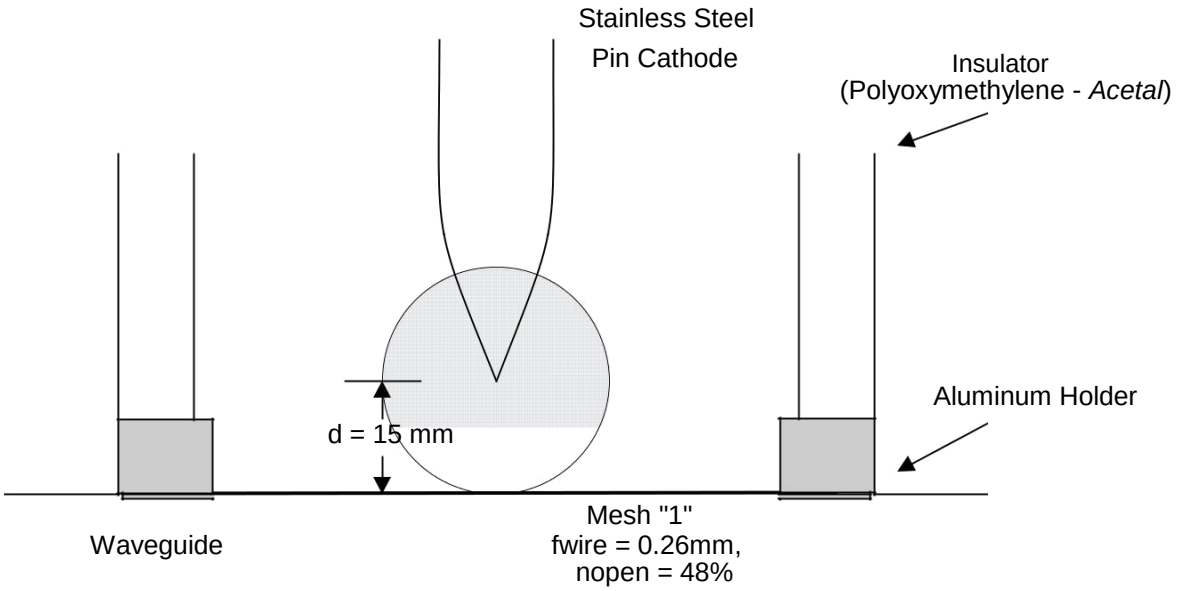

Fig. 6.19: Configuring a pin diode cathode and dAK = 15mm.

This configuration had split the gap on all three voltage levels tested, while microwave output, always present, showed rapid in- crease with increasing diode driving levels. The mesh number "1" comprised 30 holes per inch, with a hole opening 0.587mm, 0.26mm diameter wire and free Commis- surface ~ 48%. It is the grid used widely by all current available because it has the highest percentage of free surface.

6.3.3.1. Macroscopic Experimental Sizes

The following tables lists the recorded peak voltages, current and power in the passage for at least ten (10) iterations, a charging pri- tefontos of 50, 75 and 100V AC. According to what has been stated in paragraphs 5.5 and 6.3.2, the loads they give impulse *0.6 / 50*With maximum widths 52, 78 and 104kV. The voltage, current and power of the diode are given as mean and the calculated dispersion *p*the recorded maximum, in any state of charge, with semiotics $\langle X \rangle \pm 1 \cdot sx$.

Tab. 6.5: Descent Pin dAK = 15mm, Mesh "1" (Measurements 27-02-2008)

Load	50V AC	75V AC	100V AC
Max Surge	~ 52kV	~ 78kV	~ 104kV
Current Ion Pump	0.3 ~ 0.4m	0.3 ~ 0.4m	0.3 ~ 0.4m
Lifting	3 ~ 4mA	5 ~ 6mA	7 ~ 8mA
Voltage typical	32.9 ± 1.5kV	47.4 ± 2.6kV	56 ± 1.7kV
Typical Power	323 ± 58A	604 ± 67A	841 ± 72A
Power typical	6.2 ± 0.9MW	17.1 ± 1.7MW	27.9 ± 2.4MW
RF typical	**0.5 ~ 3W**	**2 ~ 15W**	**10 ~ 70W**
Efficiency typical	4 · 10-8 ~ 5 · 10-7	10-7 ~ 5 · 10-7	10-7 ~ 2 · 10-6
RF max recorded	**9W**	**50W**	**270W**

Tab. 6.6: Descent Pin dAK = 15mm, Mesh "1" (Measurements 02/29/2008)

Load	50V AC	75V AC	100V AC
Max Surge	~ 52kV	~ 78kV	~ 104kV
Current Ion Pump	0.3 ~ 0.4m	0.3 ~ 0.4m	0.3 ~ 0.4m
Lifting	3 ~ 4mA	4 ~ 6mA	6 ~ 8mA
Voltage typical	33.3 ± 1.2kV	45.0 ± 1.0kV	56.7 ± 3.0kV
Typical Power	351 ± 48A	565 ± 37A	820 ± 41A
Power typical	6.8 ± 0.8MW	16.5 ± 1.6MW	29.1 ± 3.8MW
RF typical	**1 ~ 5W**	**1 ~ 15W**	**10 ~ 60W**
Efficiency typical	10-7 ~ 6 · 10-7	10-7 ~ 10-6	3 · 10-7 ~**3 · 10-6**
RF max recorded	**6W**	**19W**	**70W**

Tab. 6.7 Descent Pin dAK = 15mm, Mesh "1" (Measurements 14-04-2008)

Load	50V AC	75V AC	100V AC
Max Surge	~ 52kV	~ 78kV	~ 104kV
Current Ion Pump	0.2 ~ 0.25m	0.2 ~ 0.25m	0.2 ~ 0.25m
Lifting	1.9 ~ 2.3m	2.8 ~ 3.8mA	3.5 ~ 4.2m
Voltage typical	38.4 ± 2.0kV	52.0 ± 2.4kV	66.2 ± 3.3kV
Typical Power	440 ± 70A	744 ± 74A	1073 ± 107A
Power typical	8.8 ± 1.3MW	21.6 ± 4.9MW	39.0 ± 7.1MW
RF typical	**1 ~ 3W**	**3 ~ 15W**	**10 ~ 50W**
Efficiency typical	10-7 ~ 3 · 10-7	2 · 10-7 ~ 10-6	2 · 10-7 ~**2 · 10-6**
RF max recorded	**10W**	**24W**	**150W**

Tab. 6.8: Descent Pin dAK = 15mm, Mesh "1" (Measurements 11-07-2008)

Load	50V AC	75V AC	100V AC
Max Surge	(Not out)	(Not out)	~ 104kV
Current Ion Pump	-	-	0.2 ~ 0.25m
Lifting	-	-	3.5 ~ 4.5m
Voltage typical	-	-	54.3 ± 1.7kV
Typical Power	-	-	788 ± 112A
Power typical	-	-	26.5 ± 1.2MW
RF typical	-	-	**10 ~ 100W**
Efficiency typical	-	-	8 · 10-7 ~ 1.2 · 10-5
RF max recorded	-	-	**320W**

H estimated pressure in the passage area is as current of Ion Pump in mA at the moment before impact, multiplied by 10-4 Torr (see. par. 6.1). Therefore the 0.2mA corresponding to 2 · 10-5Torr. The current of the ionization pump the moment of impact rises rapidly (within approximately 0.5sec) about one order of magnitude above. Longer impulse voltage causes greater surge current of ionization pump.

H pin cathode distance 15mm presented the second strongest mikrokyma- Tikas signals after distance spike 25mm in this series of experiments. Based on the calculated losses, o Vircator with this descent showed maximum katage- written power in the band of 1.4 to 2GHz, equal to about 320W. The microwave output, with relatively large power fluctuation is typically between 10 to 100W for the majority of shock. The increase in drive voltage of the lamp reflected in a marked increase in microwave output power.

The diagrams in the solid line show measurements made consecutive days (results Tab. 6.5 and Tab. 6.6), while the dotted plot shows recorded sizes cycle experiments performed much later (results Tab. 6.7). The measurements of the last table (Tab. 6.8) were trying to determine the x-ray radiation of the device at the maximum operating voltage of specific experiment therefore received both lower charge levels. However, the results of this case are consistent with the results for the impulse of 104kV, the Tab. 6.5 and Tab. 6.6. Account has also been quite strong ness microwave signals with a maximum recorded value of the order of 320W, the biggest we got for the cathode pin 15mm format and distance from the anode.

The graphs of raw measurements converge much and also have small dispersion in their values. The experiments were repeated later (dotted line on these representations), show a relatively higher voltage diode respective ha more current and therefore more power in the diode lamp.

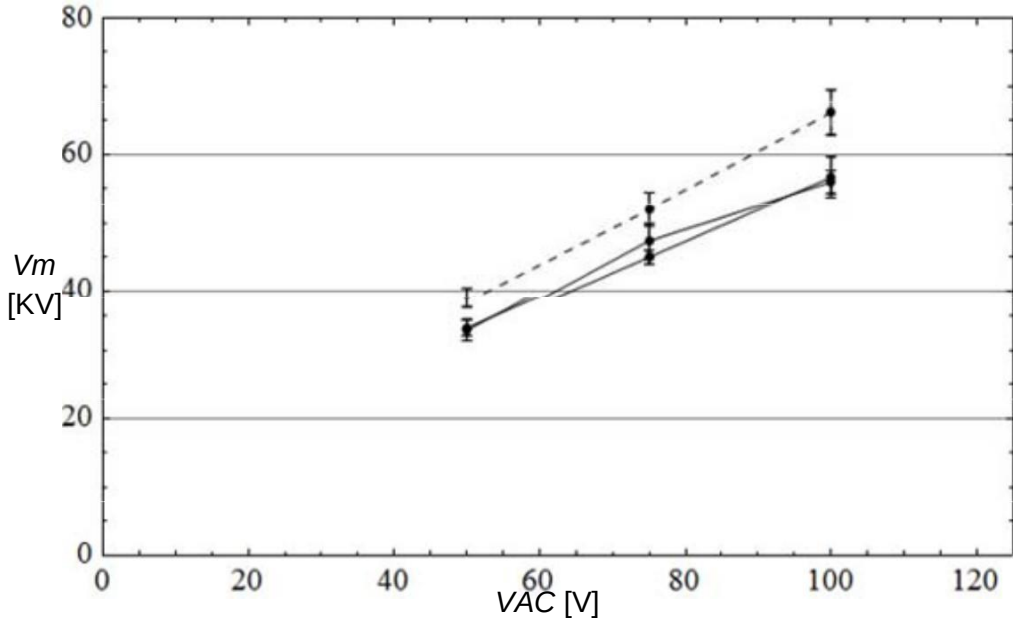

Fig. 6.20: Maximum voltage diode. Descent pin, dAK = 15mm, mesh no. '1'. Dotted diagram: later repeat experiments.

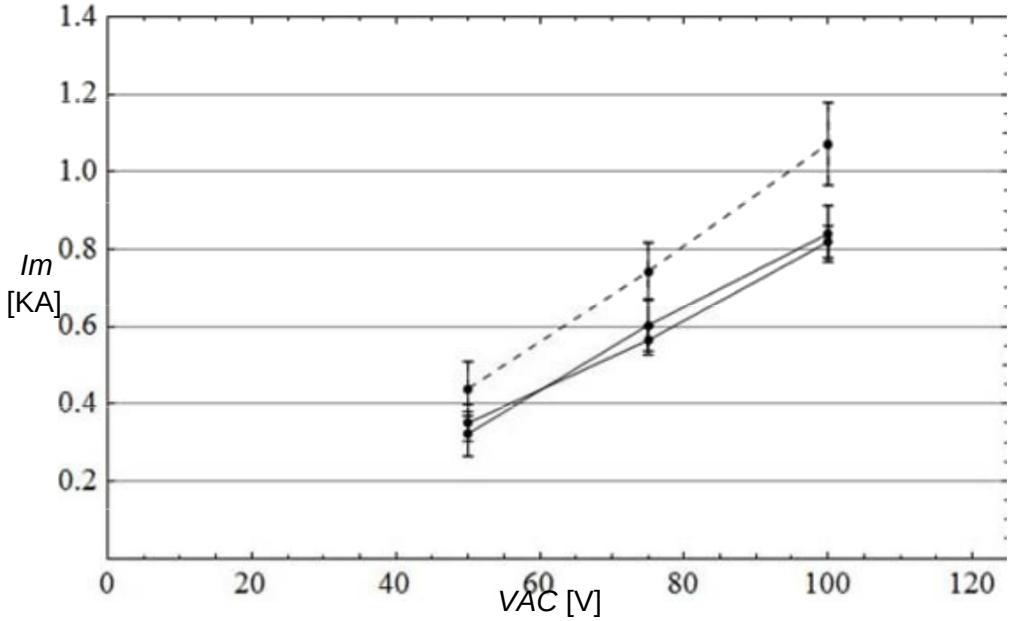

Fig. 6.21: Maximum diode current. Descent pin, dAK = 15mm, mesh no. '1'. Dotted diagram: later repeat experiments.

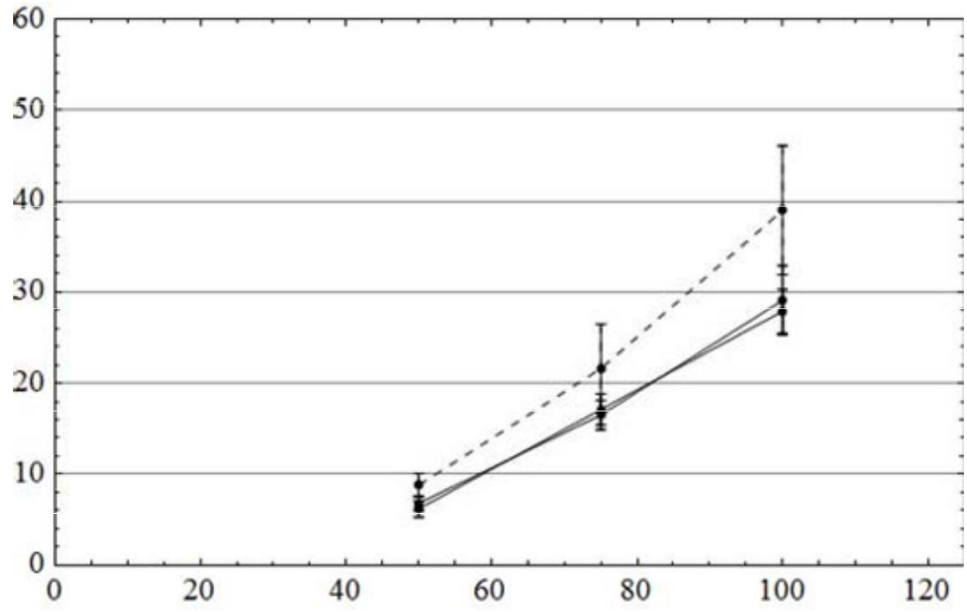

Fig. 6.22: Maximum power diode. Descent pin, dAK = 15mm, mesh no. '1'. Dotted diagram: later repeat experiments.

6.3.3.2. Model Discharge Capacity by Diode

At maximum test voltage, the impulse of 100kV, the trend "anticipates" to anel- sulfate up to 60kV in most cases, as depicted in the diagram means maximum voltages of Fig. 6.20. Once, the voltage does not rise CHANGE Member of he would this possibility, we consider that the virtual collapse of the diode gap has begun. At the time this call t = 0, and we consider that the capacitors

of the high voltage capacitive divider, capacity *C*= 1200pF, charged voltage *V0*, Connected across the diode. We believe that the diode switches instantaneously explosive electron emission and behavior Child-Langmuir. In other words we con- sider that the entire bottom surface of the "flat" and "circular" passageway covered by a stiff Plate plasma infinitesimal thickness which is able to offer o- sodipote large number of electrons in the passage.

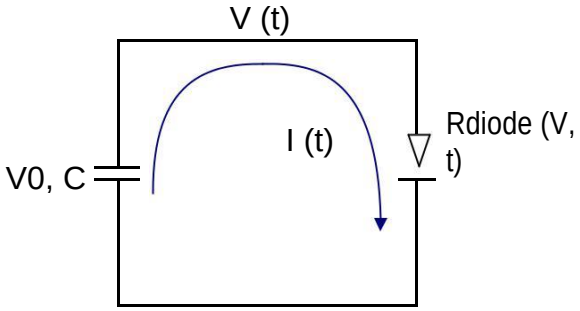

Fig. 6.23: Discharge capacitor using vacuum diode.

As mentioned in paragraph 4.3.6, the dependence of the current from the voltage di- in by the relation for the load capacitor,

$$I = \frac{dQ}{dt} = C\frac{dV}{dt}, \tag{6.8}$$

while the current of the diode is described approximately by the expression

$$I \cong kS(t)\frac{V^{3/2}(t)}{d^2(t)}, \tag{6.9}$$

where *k*= 2.33 · 10-6 constant of the planar diode in units SI [AV-3/2], *S (t)* It is the phenomenon of the cathode area and *d (t)* It is the apparent distance of reinforcement. The radius of the descent, first price *a*Increases over time at a rate *u* · *t*Wherein *u* plasma spreading speed, while the anode-cathode distance, initially equal to *d*, Is reduced with time at a rate of -*u* · *t*. The area of the passage gap and the phenomenon can be approximated by the expressions

$$S(t) \cong Fr.\, r^2(t) \cong Fr.\,(a + u \cdot t)^2, \tag{6.10}$$

$$d(t) \cong (d - u \cdot t)^2. \tag{6.11}$$

Equating the capacitor current by current passage, a differential take the following equation, to which solve for the voltage:

$$C\frac{dV}{dt})^2 = kFr.(a + u \cdot t \quad \frac{V^{3/2}}{(d - u \cdot t)^2}. \tag{6.12}$$

For this configuration, we set the following sizes: cathode ray *a*= 0.001m, reinforcement distance *d*= 0.015m, geometric matrix permeability upward Output *n*= 48%, plasma spread speed *u*= 5cm / microseconds = 5 · 104m / sec, initial voltage capacitors fh *V (0)=V0*= 60kV, capacitor capacity *C*= 1.2nF. The radius of the cathode is set to 1mm, since it is a pin, while the plasma spreading rate is set equal to 5cm / microseconds because the measurements it was found that the collapse of the gap takes about 300nsec.

Using expression found for the voltage of the diode, we can export goume stream Child-Langmuir passageway. We use the expression for circular passage finite dimensions (2.69)

$$J_{SCL}(2) \cong 1 + 0.26\frac{d}{r} J_{SCL}(1), \tag{6.13}$$

to write

$$I \cong kS(t)\frac{V^{3/2}(t)}{d^2(t)}\left(1 + 0.26\frac{d(t)}{r(t)}\right). \tag{6.14}$$

Substituting the equivalent area of the cathode and the distance of the reinforcement with the appropriate time dependencies, we take the relationship

$$I_{SCL} \cong 2.33 \cdot 10^{-6} Fr.\left(a + u \cdot t\right)^2 \frac{V^{3/2}}{(d - u \cdot t)^2}\left(1 + 0.26\frac{d - u \cdot t}{a + u \cdot t}\right). \tag{6.15}$$

Recall that, for one electron beam without charge neutralization, which is kept focused on an infinite magnetic field, the maximum value of current that can bring, is calculated as

$$I_L \approx 17\frac{\left(c^{2/3} - 1\right)^{3/2}}{1 + 2\ln\left(b/a\right)} \text{ [KA]}, \tag{6.16}$$

This amount is an indicator to display virtual cathode area is therefore used as a benchmark for the current flowing through the waveguide cabin mo of Vircator. With *a* symbolized the radius of the beam, while *b* denoted the radius of the metal cylinder, from which the beam passes. Note that in kyma- todigiko Vircator experiment there cylindrical symmetry in the area of eikoni- ment cathode, therefore use as *radius* it *half* the large dimension of waveguide WR430, ie approximately 5cm. Considering the geometrical permeability of the matrix, we can depict the maximum current in the beam waveform digiko chamber. Substituting temporal dependencies where necessary, the current in *diode* They should ideally be *most* from:

$$I_{diode} > 17 \cdot 10^{3} \frac{1}{n\%} \frac{\left(1 + \frac{V_{23/32}}{511 \cdot 10^{3}}\right)^{-1}}{1 + 2 \ln \frac{b}{a + u \cdot t}} \quad [A]. \tag{6.17}$$

Given the absence of magnetic field, probably one much larger beam current value can be judged sufficient to install virtual cathode in inert space. Solving the linear model and reflecting the change of aggregates, we receive the following graph:

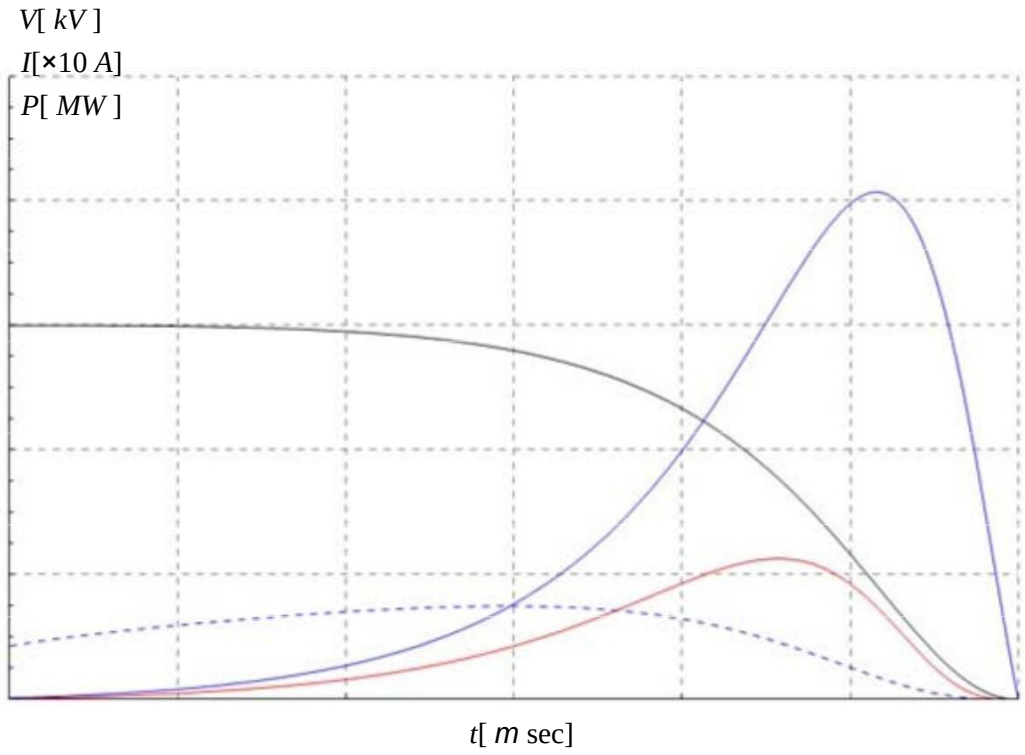

Fig. 6.24: Theoretical variation of voltage, current and power pin cathode dAK = 15mm, for drive voltage 60kV, capacity capacitor 1.2nF, speed katarref- ing gap 5cm / microseconds.

We see that the stream starts by a very small price, while the voltage varies quite slowly. As the phenomenon progresses and the cathode increases to effect almost emva- while reducing the distance between electrodes, the current provided by the capacitor in the diode rises rapidly. The phenomenon lasts 300nsec. The theoretical power the diode reaches 22MW. The maximum current in the diode is slightly larger than 800A.

Based on the calculated voltage and current figures, we can calculate the predicted output frequencies Vircator, based on theoretical models for reflex oscillations and the oscillations of the virtual cathode. Using in- xisosi voltage in the circuit, calculate the frequency reflexing of the expressions of par. 4.1.1, properly replacing the temporal distance dependence of reinforcement, not relativistic, as

$$f_{REFL} = \frac{\sqrt{V}}{4(d - u \cdot t)} \sqrt{\frac{e}{2m}} \quad , \tag{6.18}$$

or relativistic as

$$f_{REFL} = \frac{\sqrt{V}}{4(d - u \cdot t)} \sqrt{\frac{ec^2}{2mc^2 + eV}} \quad . \tag{6.19}$$

The spacing of the two estimates is small, and further decreases with time and reducing the capacitor voltage.

The plasma frequency of the electron beam, which enters the inactive area can be calculated from the relativistic equation (4.42). In this expression in place of the current package *I*, Substituting the amount (4.69) multiplied by the geometrical permeability of the matrix, *n*. In the denominator of the equation (4.42) we make the appropriate anti-time dependence of the radius of the cathode, which we assume and radius of the beam. The change of plasma frequency is described by

$$f_p = \frac{1}{2Fr.} \sqrt{\frac{e \cdot (n\%) \cdot 2.33 \cdot 10^{-6} \cdot V^{3/2} \cdot \frac{d - u \cdot t}{(d - u \cdot t)^2} + 0.26 \cdot \frac{d - u \cdot t}{a + u \cdot t}}{\varepsilon_0 m_{bc} c}} \quad , \tag{6.20}$$

where the coefficients b and c depend on the tension in the passage and described by equations (4.44) and (4.45). The frequency of oscillation of the virtual cathode, agree- to what has been reported in par. 4.1.2, is between the values *fp* and (2n) 1/2*fp*. In Fig. 6.25 noted: the area defined by frequencies prices *fp* and (2n) 1/2*fp*The two estimates of frequency reflexing, non-relativistic and relativistic, as described in par. 4.1.1. Finally made and the assessment of Woo, on. (4.16), according to which "the frequency of Vircator is determined by the in- it with a margin of 20%" ([50]).

Note that, from Fig. 6.24, we note that after the first 150nsec, the current is strong enough to allow the display of virtual cathode. However, by the time she and then the geometrical and electrical characteristics of the circuit seems to remove the output frequencies in the area over the 2GHz. However, it is important to note that there is the area in which the current in the diode is sufficiently strong to have virtual cathode formation. Com- ing, possible output frequencies (mainly lower plasma frequency) passing through the region of 1.8 to 2GHz. For this configuration, the maximum current that provides the linear model is 800A, to collapse the gap in 300nsec. The power in this case amounts to 22MW. Faster collapse gap because larger BRAKE plasma spread smelter will mean larger diode currents. Namely the model can predict the contribution of the charging capacitor of 6nF, which is connected to the capacitive divider through the ohmic resistance of 208O. Also, there is provided the effect of the inductance of the circuit, however, of change in current is not dramatic, so the inductance playing leading RG Member of limiting current value.

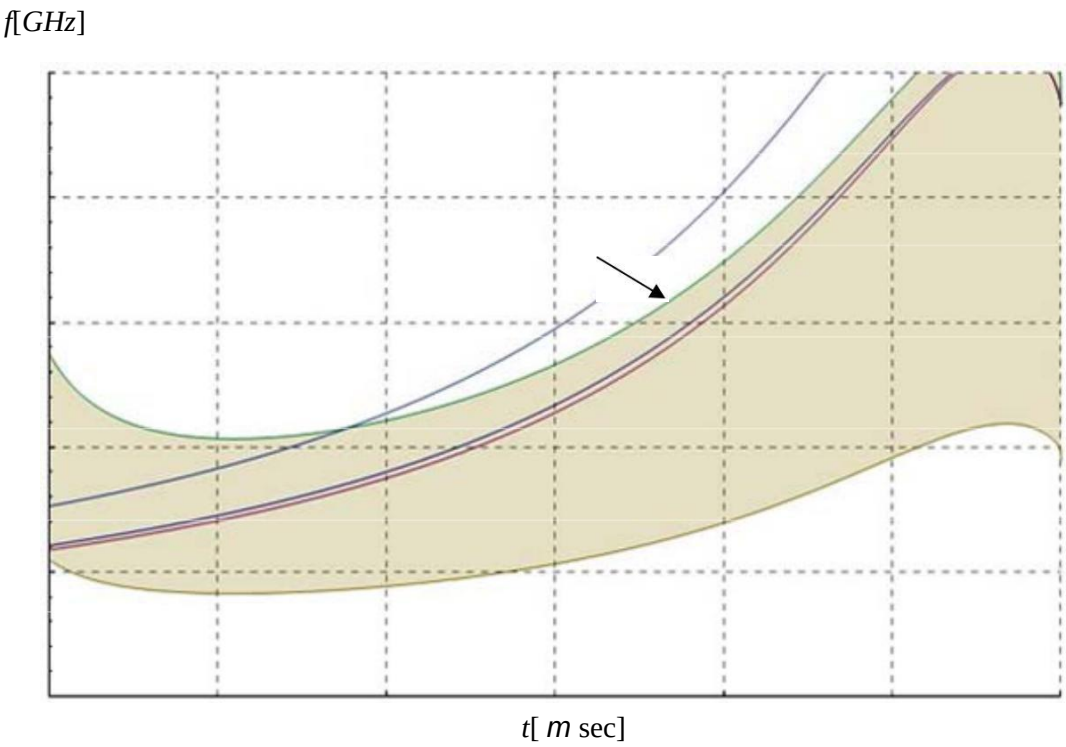

Fig. 6.25: Output frequency Assessments Vircator with pin cathode dAK = 15mm, for discharge voltage 60kV, capacitor 1.2nF, with spacing collapse speed 5cm / microseconds.

6.3.3.3. Typical measurements

Case A (55kV, 780A, 31MW, 5cm / microseconds)

In the following measurement we have a typical microwave exit configuration of the pin diode cathode spaced 15mm from the mesh anode. The voltage applied to the diode and from a point and then begins to appear some liquidity but in the fairway. Sometime around 200nsec the imposition of impulse voltage, the current increases rapidly, because the collapse of the gap has greatly decrease the resistance of the diode and allows significant spatial stream to cross the passage. In im- minus this indeed observed intense microwave radiation. By 450nsec about current is maintained high, about 700A, and then the voltage to the lamp is reduced to zero indicating the closing of the passageway. The voltage reaches the maximum value of 55kV, with maximum current of 780A. The offered power to the passage of Vircator is 31MW. The microwave pulse exhibits a duration 200nsec, as strength in the gap is reasonable. The passageway collapses within 300nsec about. From the point of 450nsec and the emer- there is a slight trend reversal, which indicates the closing of the passage of plasma, 450nsec about. The collapse of the pin-diode matrix in this case takes about 300nsec.

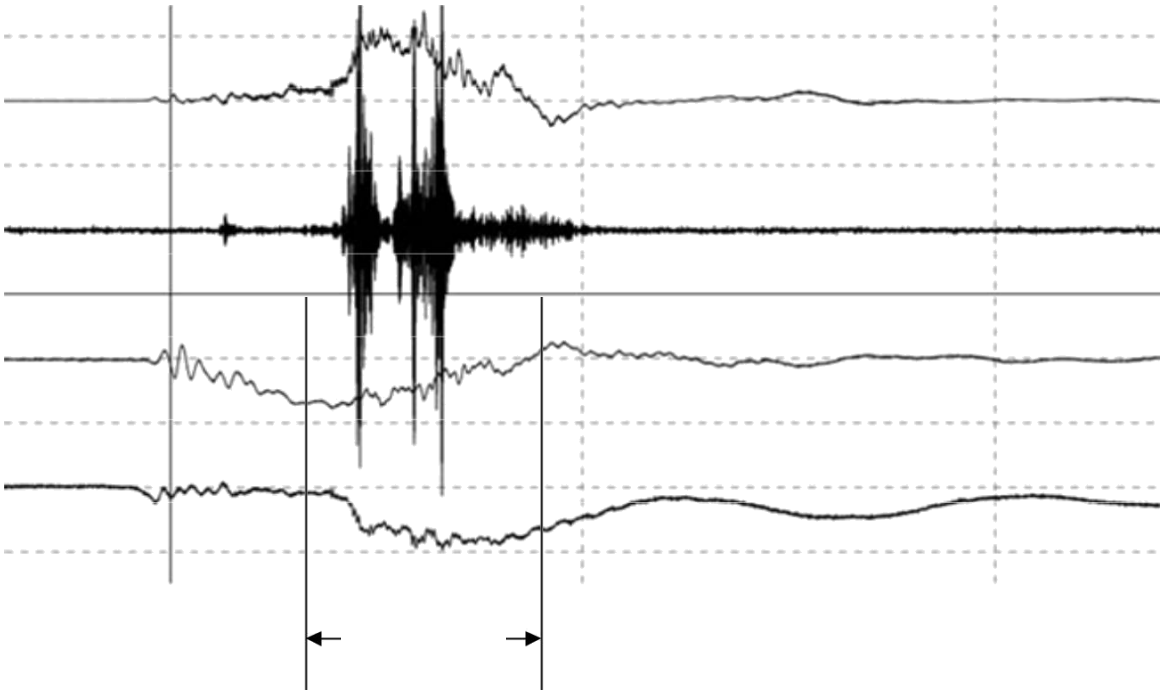

Fig. 6.26: The Descent pin, dAK = 15mm (measurement 20080227m47): Vmax = 55kV, Imax = 780A, RFmax = 30W, Pmax = 31MW.

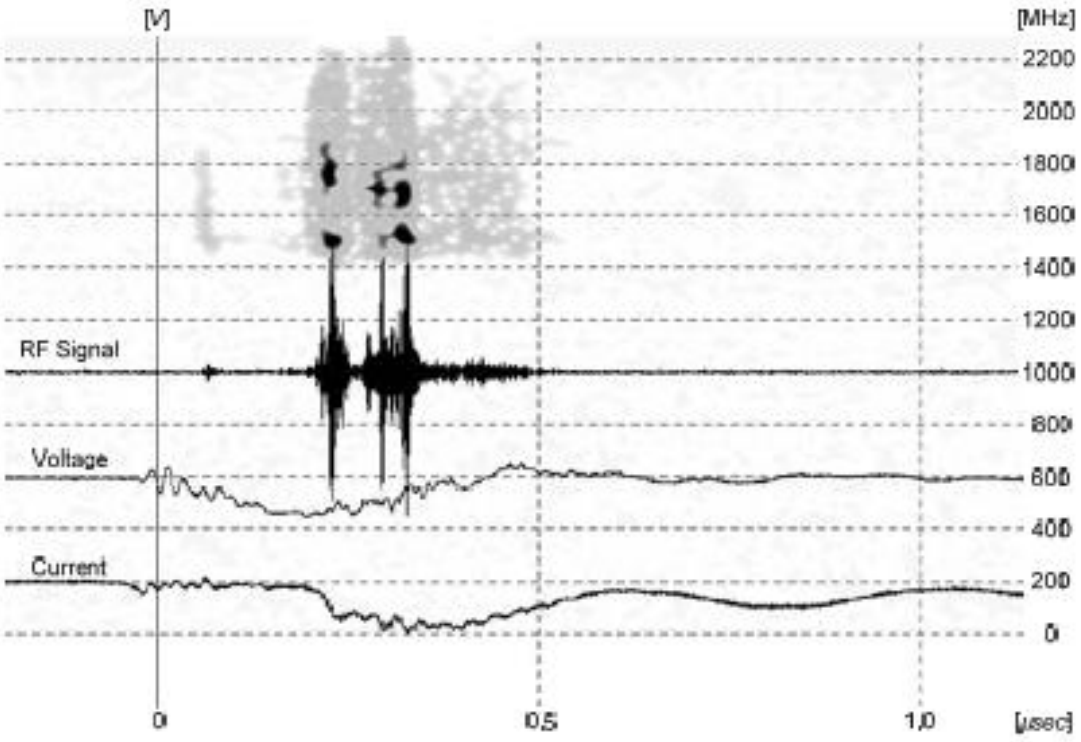

Fig. 6.27: The Descent pin, dAK = 15mm (20080227m47 measurement) Show time-range.

In the time-range display (time-frequency representation) of Fig. 6.27 has en- somatothei spectrogram in grayscale, with the right frequency range (0 to 2200MHz), and the same horizontal time axis with the three oscillograms. The dark color shows the regions with the strongest spectral content. For re- Example, the first powerful microwave pulse shows strong spectral contents are at 1450-1500MHz and around 1800MHz. Strong signals below are content again around the 1450-1500MHz and a second portion in the range of 1600-1800MHz. The spectral content at 1450MHz rates are probably lower fix- ing the threshold, while reducing the frequency observed in the most "high-pitched" the tracks, probably due to the voltage reduction, which meanwhile has been made.

It is interesting to see the representation of speech

$$R_{diode} \cong \frac{|V_{real}|}{|I_{real}| + d} , \qquad (6.21)$$

in well-defined sizes of driving, ie shortly after the applied voltage and by the time the voltage across the diode is reset. At this time, the signals of voltage and current are free of transients of impulse voltage and *resistance* the passage is well defined. Reversing the BRAKE ing and stopping the arc leads to recording waveforms, not representing any real resistance. The amount S is a small number, which is set equal to 1A, and added to the value of the actual current normalization denominator close to zero. The above accounting expression, which a- ntikatoptrizei the resistance of the diode in the period of imposition trend will apeikonizou- by then alongside the corresponding graph of recorded signals for thought.

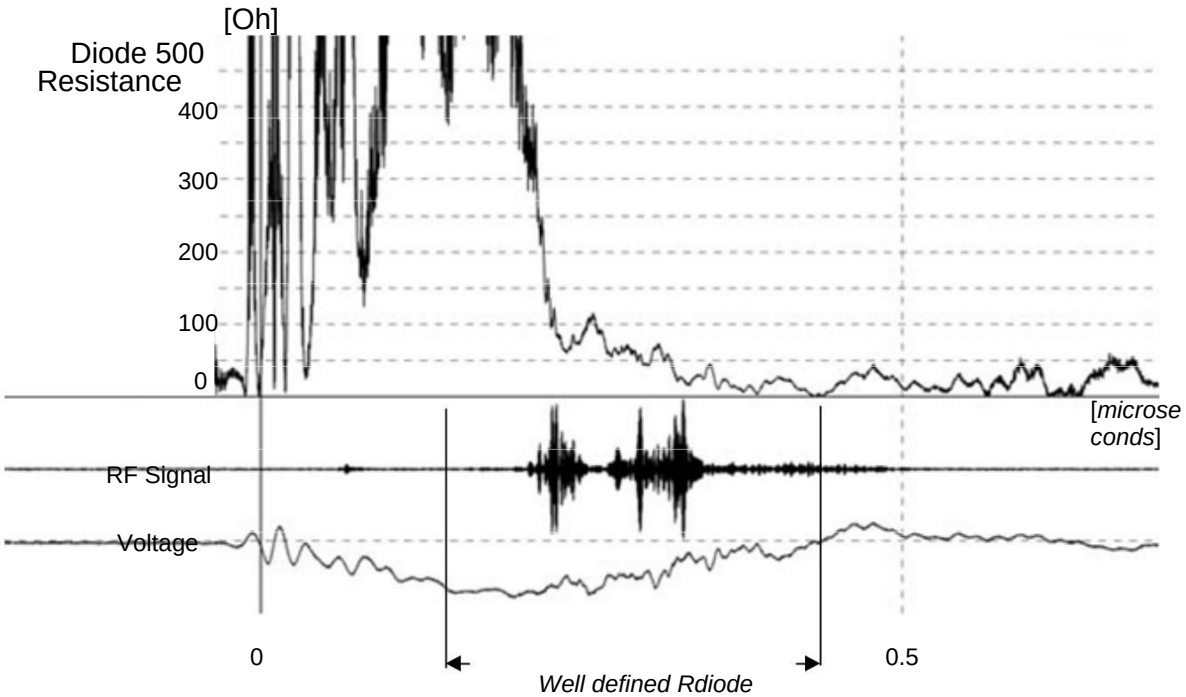

Fig. 6.28: The Descent pin, dAK = 15mm (measurement 20080227m47): diode impedance.

A useful observation in the diagram of Fig. 6.28 is the change in resistance of the diode, the time is well defined. Well defined gap resistance have since dampen transients principle until the signifi- minus undergoing polarity reversal trend in the gap. Starting from a theoretically very large value, the resistance decreases rapidly as the decay progresses, until it is reset. Interestingly, the fact that the microwave radiation occurs when the resistance of the diode is below 150O and up to about 20-30.

Case B (56kV, 840A, 27MW, 5cm / microseconds)

In the following measurement have a typical microwave output from forming passageway, the tip cathode spaced 15mm from the mesh anode. The voltage reaches the maximum value of 56kV, while the maximum current is 840A. The offered power to the passage of Vircator is 27MW.

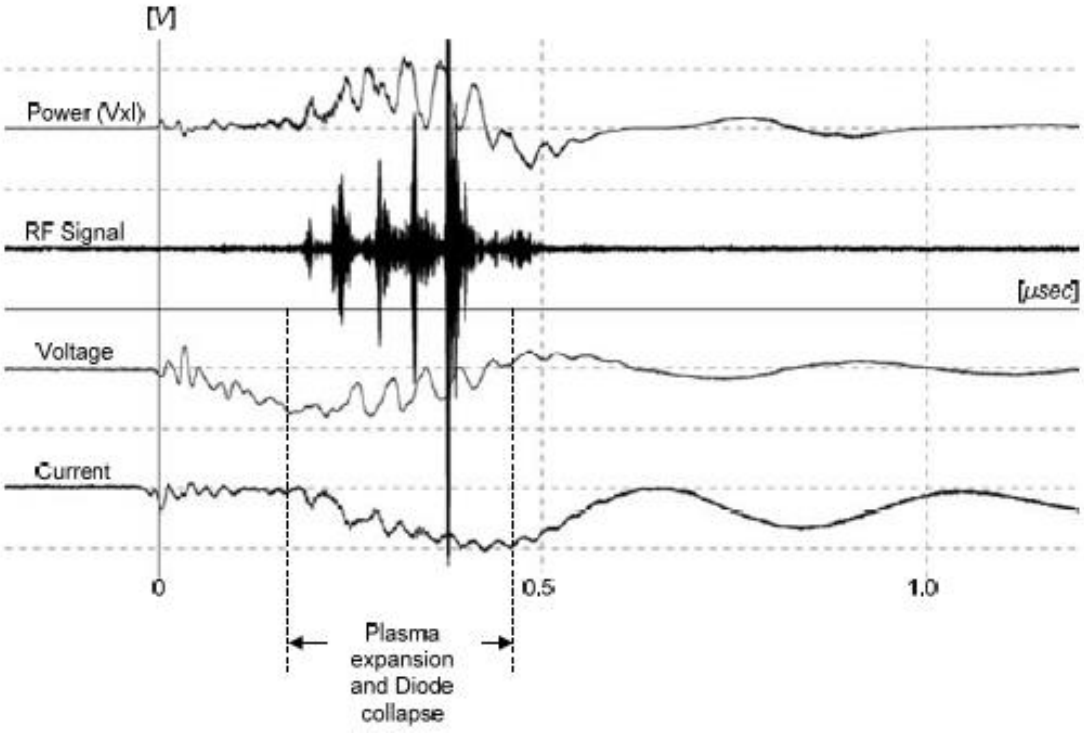

Fig. 6.29: The Descent pin, dAK = 15mm (measurement 20080229m25): Vmax = 56kV, Imax = 840A, RFmax = 50W, Pmax = 27MW.

The interest in the measurement of Fig. 6.29 macroscopic undulation is shown exhibiting the voltage and power of the diode, in combination with the observed microwave ness signal. The four consecutive microwave pulses progressively next by increasing power, which occurs at local maxima negative voltage bias and locally specific maximum force in the passage, presence of a large current. This behavior indicates that the current value of the diode presence accelerate voltage is crisis sima importance for the microwave output. Indeed it seems as if the current playing important role in the tendency, after the successive maxima are progressively less-

oumeni trend but an increasing current. The collapse of the pin-diode matrix in this case takes about 300nsec.

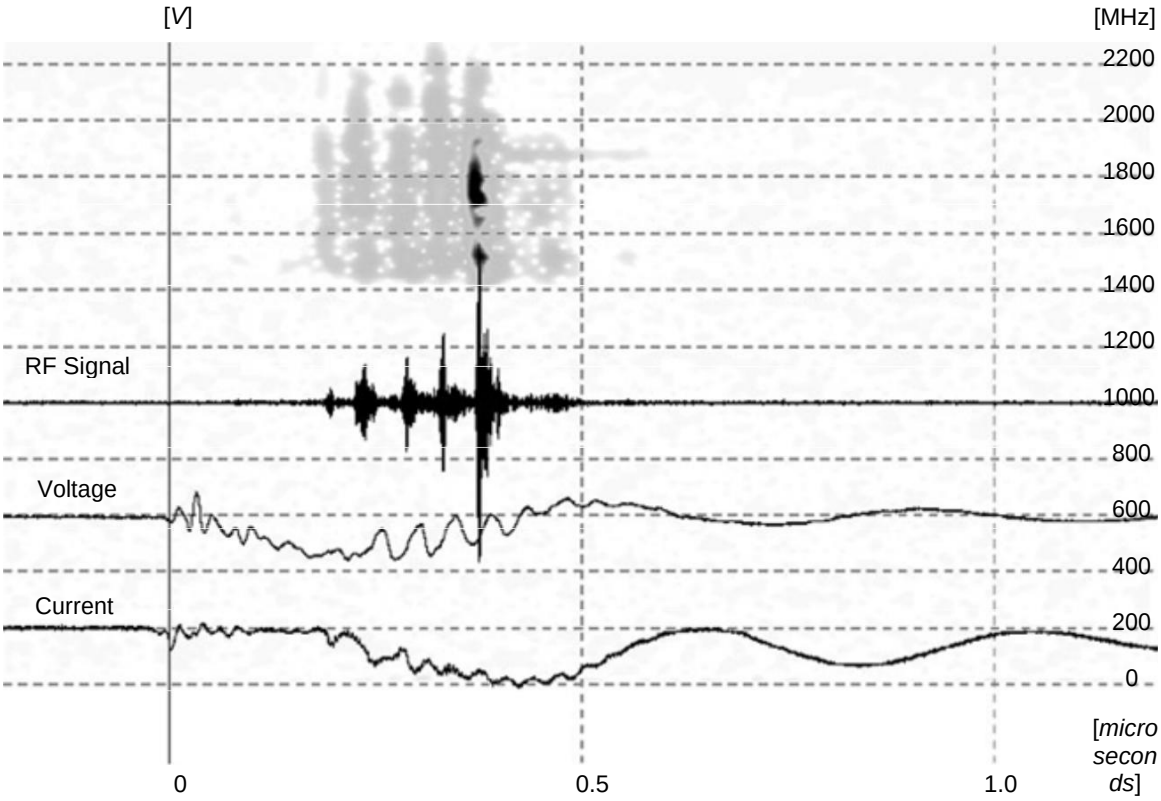

Fig. 6.30: The Descent pin, dAK = 15mm (measurement 20080229m25): time-imaging spectrum.

In the time-range display (time-frequency representation) of Fig. 6.30 has en- somatothei spectrogram in grayscale, with the right frequency range (0 to 2200MHz), and the same horizontal time axis with the three oscillograms. The tech- leftaios and powerful pulse captures spectral content at 1500MHz and in the range of 1700 to 1850MHz. Especially, from 0.5msec onwards shows a trace of spectrogram, frequency of ~ 1850MHz. These signals are probably indi- cate for coordination around 1800MHz, where trying to sys- coordinators lamp by means of the cavity. There remains indication spectral content below 1400MHz, which can occur because cleavage of the first rate.

The change of the passage resistance in this experiment is shown in Fig. 6.31. In time we may consider proper expression of resistance, production keep the microwave irradiation occurs in intervals, in which the corresponding distance is small, about, price. Characteristically, the last and strongest pulse ap- appears when the resistance of the diode is about 30O. Correspondingly, the two previous vol small pulses occur when the resistance of the diode is lower than 50 ohm.

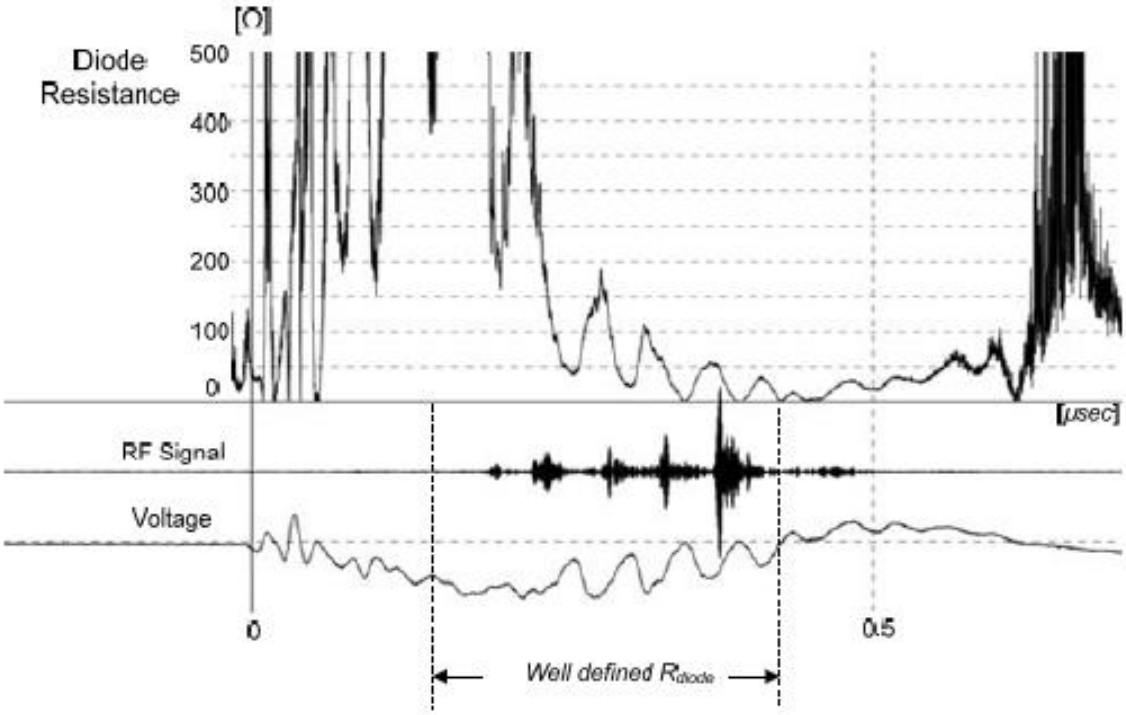

Fig. 6.31: The Descent pin, dAK = 15mm (measurement 20080229m25): diode impedance.

Case C (62kV, 860A, 29MW, 5cm / microseconds)

In this measurement, we have a different microwave exit from the configuration of the passage to the cathode tip. The voltage reaches the maximum value of 62kV, while the maximum current is 860A. The offered power to the passage of Vircator is 29MW. Without displaying a momentary maximum signal, as in previous re- characteristic we record the microwave signal in this case shows a steady behavior, macroscopically, validity, for a period of about 200nsec.

In the time-range display (time-frequency representation) of the case has incorporated the spectrogram in grayscale, scaled frequencies to the right (0 to 2200MHz), and the same horizontal time axis with the three palmo- graphs, such and previous composite images. The dark color shows the regions with the strongest spectral content. Exit without much coherence pre- sented in the zone from 1450MHz up to 1850MHz. There seems to be a central trend in output frequency around 1700MHz.

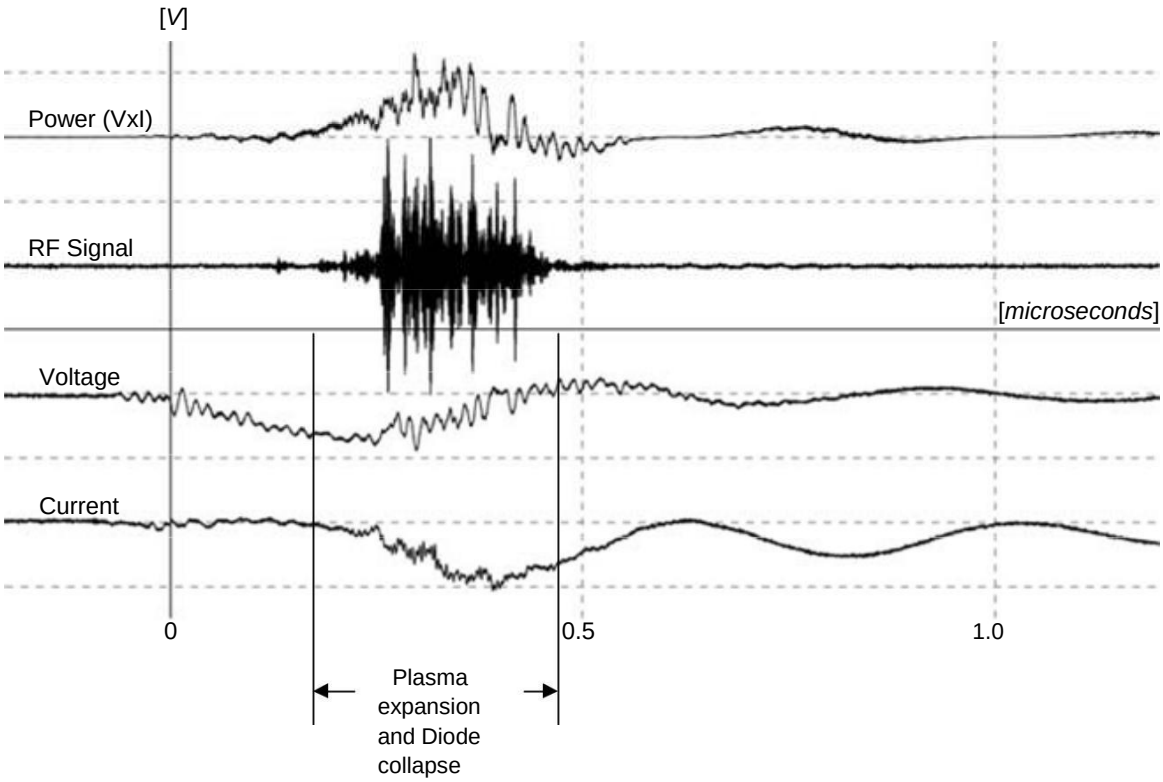

Fig. 6.32: The Descent pin, dAK = 15mm (measurement 20080414m32): Vmax = 62kV, Imax = 860A, RFmax = 5W, Pmax = 29MW.

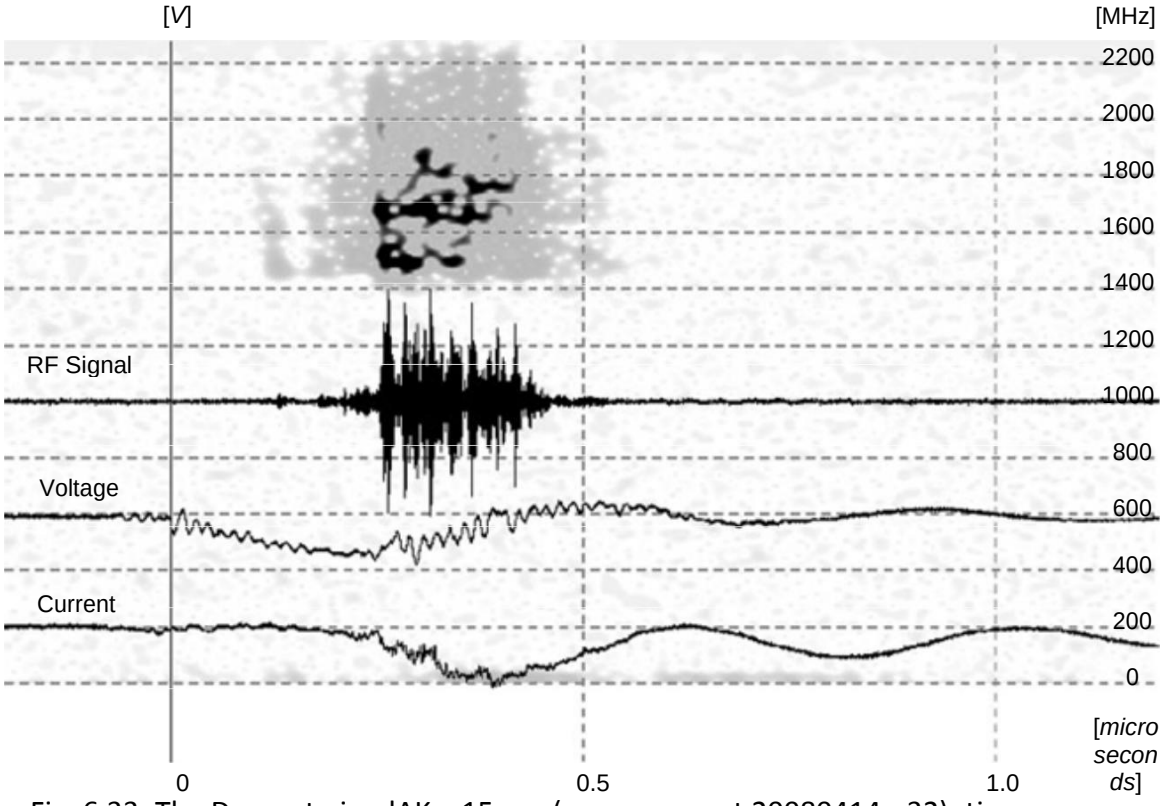

Fig. 6.33: The Descent pin, dAK = 15mm (measurement 20080414m32): time-imaging spectrum.

In this example, the path travels a relatively long period of near zero voltage and displays a small inverse voltage on the 500nsec, after the imposition of impulse voltage. Therefore, the resistance has no physical sense after 500nsec, as a ratio of the signal voltage to the current. A small area, prior to this time, and maintains a very low resistance below 50 ohm, which is the limit of the error due to the fluctuation around zero.

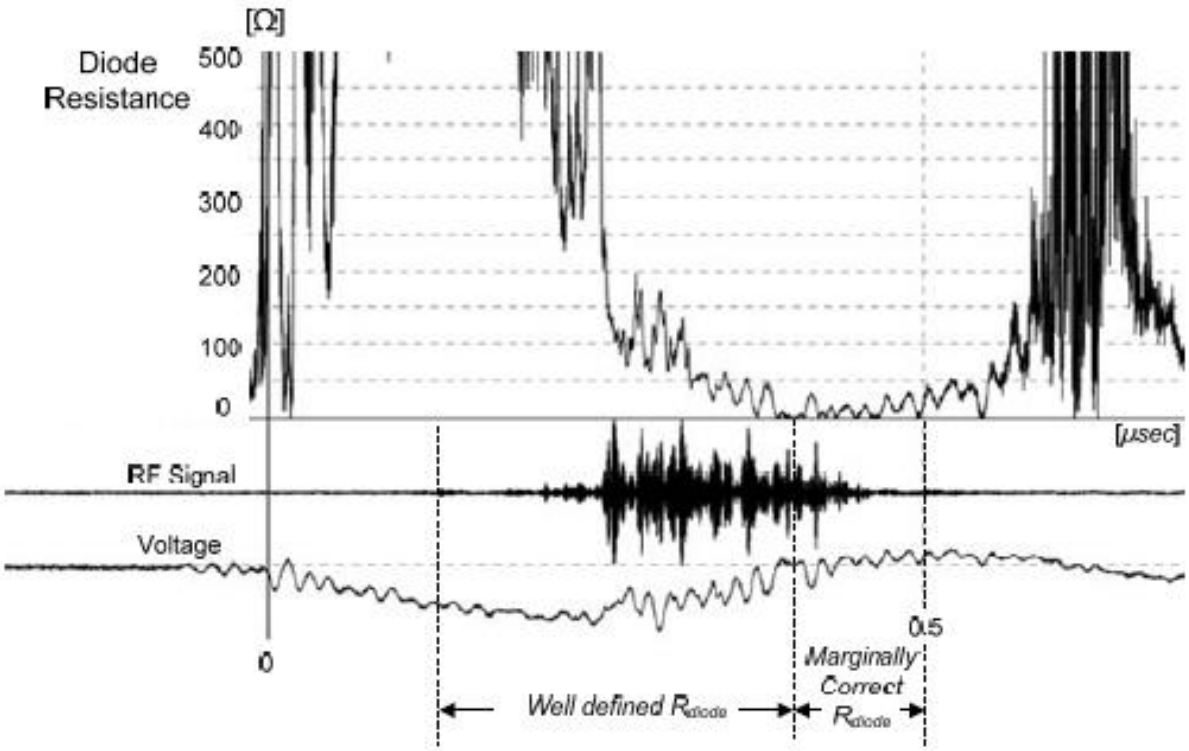

Fig. 6.34: The Descent pin, dAK = 15mm (measurement 20080414m32): diode impedance.

As apparent from the above diagram, the microwave radiation starts to occur, when the resistance of the gap is below 100 ~ 150O. Microwave radiation persists slightly towards the end of this phenomenon, although the gap is almost bridged plasma. The large current flowing in the passage, together with the possible existence of area not covered by plasma contributes to electron beam enters the area of the waveguide with a speed and feeds the virtual cathode load.

Case (53kV, 730A, 25MW, 4cm / microseconds)

H following is a case in which no loop oscillations occur.
H diode collapses approximately 350nsec, and there is a fairly strong mikrokyma- trade mark for measurements with this type of configuration. The voltage reaches the maximum value of 53kV, while the maximum current is 730A. The offered power to the passage of Vir- cator is 25MW.

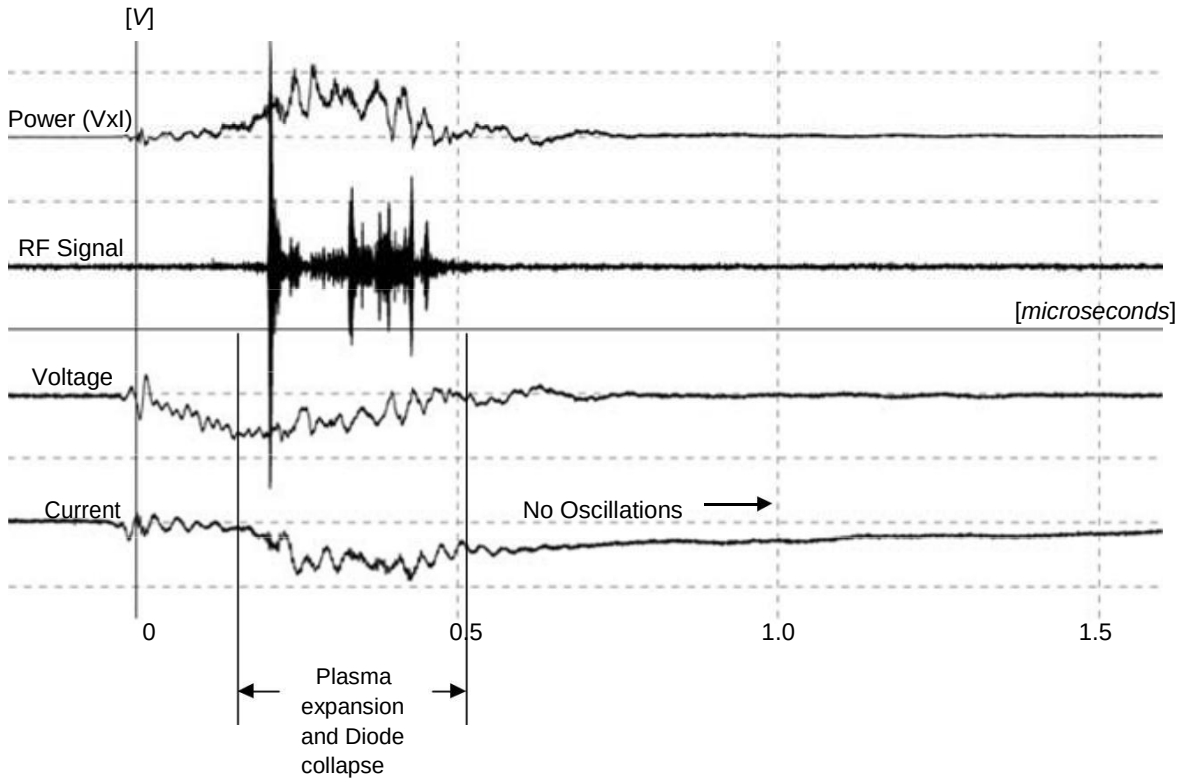

Fig. 6.35: The Descent pin, dAK = 15mm (measurement 20080711m00): Vmax = 53kV, Imax = 730A, RFmax = 140W, Pmax = 25MW.

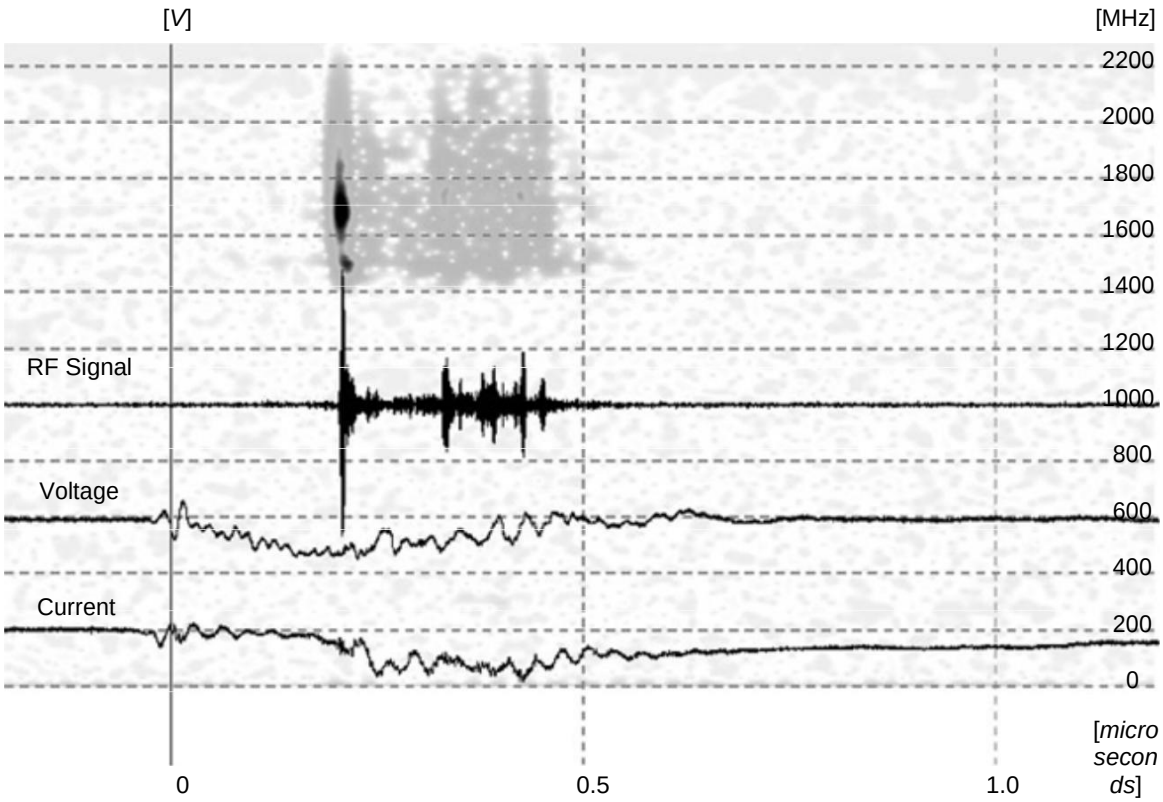

Fig. 6.36: The Descent pin, dAK = 15mm (measurement 20080711m00): time-imaging spectrum.

The time-range imaging, Fig. 6.36, it appears that the initial strong mikrokyma- tion pulse has spectral content around 1700MHz. It appears when the voltage is about 50kV, while the current is still small. If a model representatives charging capacity through passage Vircator, according to what has been developed in paragraph 4.3.6, if the collapse last 350nsec, current passage will fta- the CAM 800A, the power in the passage will reach 20MW but the Treaty of power for virtual cathode formation will begin to be satisfied after the first 150nsec. How- ever, in this stage, and then the Vircator output frequencies provided above the 2GHz, there is therefore the possibility that the original strong microwave signal unrelated to virtual cathode oscillations, but by passing a strong current that excites the first rate. Also, what happens to time t = 300nsec with t = 500nsec be remnants of output Vircator, which, moreover, probably the- places them well above 2GHz.

The resistance of the gap, in the period observed radiation range a few tens of ohms. The first and most powerful pulse occurs when the voltage is still high enough, approximately 50kV, while the impedance of the gap is 120O. Over 0.5msec gap is filled by plasma, while stabilizing the voltage over the 0.7msec enables us to estimate the plasma channel resistance diode, which is below 20O.

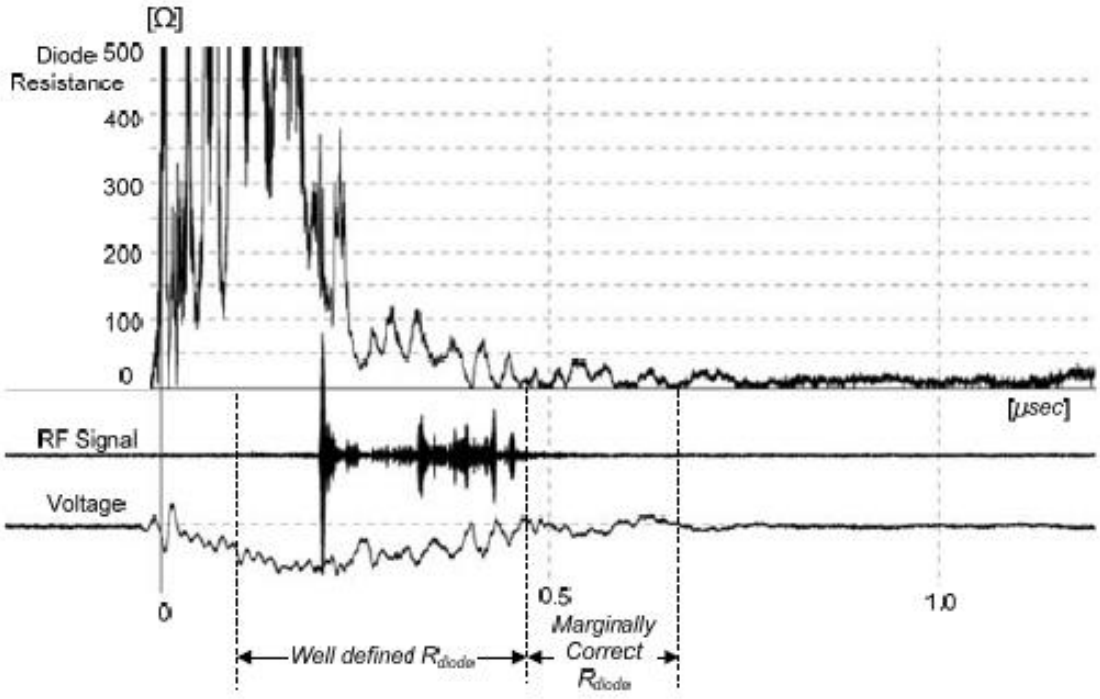

Fig. 6.37: The Descent pin, dAK = 15mm (measurement 20080711m00): diode impedance.

In the above cases, a gap should be from the time when the voltage stops rising in the prescribed rate and a current starts flowing in the passage, until a zero voltage and normalization of power. The phenomenon lasts about 300nsec. Thus, for this geometry, namely stainless steel pin at 15mm distance from the anode stainless mesh, the BRAKE cast spread plasma passageway estimated at ~ 5cm / microseconds.

The diilektrodio plasma estimated to be due to hydrogen released by potential for adsorption to the surface of the electrodes. Hydrogen is the most common pros- adsorbed gas in metals, which may occupy too many internal layers of metal wire. Also, an ordinary molecule adsorbates metals is water, which can be attached to the surface of the metallic Lu but encapsulated and inside. No. of other atoms and molecules vriske- Tai trapped at the electrodes, thus released at the time of applying voltage. The plasma is initially diilektrodio source cathode which is heated dramatically as starts flowing electronic field emission current. However, the plasma begins to evolve from the anode, where a significant amount of current starts to strike the grid and to the heat at high temperatures. The plasma formation starts sooner, but this phenomenon is relatively slow in the early stages of evacuation ing. The plasma is generally limited to a small sphere around the tip of the pin. Until this sphere to spread significantly, the *maximum current limited by space charge* (Space-charge limited current), between plasma around the pin and the rise, it is still small and does not appear in waveforms. Accordingly, the corresponding dimension of the passage is large enough not observed pronounced collapse BRAKE ing. Therefore, bridging the passageway *appear* occurs at time 300nsec, while the duration of effect may be somewhat larger. Recall that the Langmuir Child Act flat passage is:

$$\text{f}JSCL = 2.33 \cdot 10^{-6} \frac{V^{3/2}}{d^2} \quad [\text{A / m}], \tag{6.22}$$

the geometry of the passage to affect primarily the fixed factor. There- fore, the development time and spread plasma, the observed liquidity but, proportional to the amount

$$\text{f}I_{SCL}(t) \text{ a } S(t) \frac{V(t)^{3/2}}{d(t)^2} \text{ a } k Fr. R(t)^2 \frac{V(t)^{3/2}}{d(t)^2}, \tag{6.23}$$

growing at *fourth* order, due to plasma-anode distance and equivalence "area" of the diode, if the voltage held relatively constant. Indeed, in case diode pin-plate in a vacuum, the Mesyats and Litvinov [135] suggest that the current can be calculated by an expression of the form

$$I_{SCL}(t) = 2.33 \cdot 10^{-6} \frac{V(t)^{3/2}}{(d - ut)^2} \cdot S_{eff}(t) \cdot k(t), \tag{6.24}$$

$$S_{eff}(t) = Fr. \cdot (ut)^2$$

wherein the area and the steadily *k* It has a dependence of the form $k(t) \approx 5(d - ut)/ut$. The amount *u* the spreading speed of the plasma in the passage and d is the initial anode-cathode distance. In this regard, the constant originates directly from the law Child-Langmuir.

The rapid growth of spatial power is reflected in the rapid collapse of the impedance of the diode just before the point begins to emfanize- Tai microwave radiation (see. Fig. 6.28, Fig. 6.31, Fig. 6.34 and Fig. 6.37) In the above relationship, we denote the time dependencies of the distance of the "passage" with anode plasma- *d*With *V* inclined to the passage and *R* the radius of the plasma sphere.

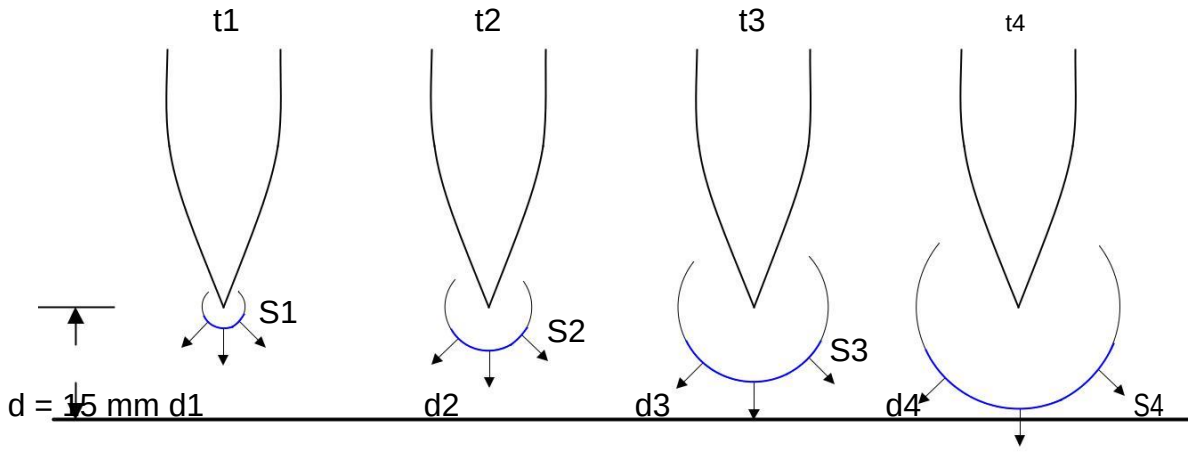

Fig. 6.38: Simplified plasma display development stems from the cathode.

The point at which allegedly happens bridge the gap, that is, where the trend has been reversed and the current ripple goes to smooth sine behavior (see. Fig. 6.26, Fig. 6.29 and Fig. 6.32). This is due to applic- stays oscillations LC, between the capacitive divider and the inductance of the capacitor vro- Hu-Vircator, as already mentioned.

There are cases in which vibrations do not occur. Characteristic is the example of Fig. 6.35. In this case, the voltage across the diode is not reversed po- TE for some time, resulting in feeding of the arc of the impact load capacitor *CC*. The discharge circuit is no longer capacitor *CC*The front resistance *RF* and Shorted Vircator. The capacitive divider has paid most of the load during the first stage of decomposition, to zero voltage (short-spinning diode). It is apparent that the plasma in the passage is a very good reason pipeline, since the voltage across the diode of the Vircator is practically zero, while the current is kept sufficiently large value. The resistance of the plasma column in this case appears to be some Z, calculated by the ratio of voltage to current passage. The expression of power after the collapse of the diode is determined by the discharge of the capacitor impact *CC*Through the front drag *RF*. In our case, *CC*= 6000pF and *RF*= 208O. This is an exponential discharge of the residual charge of capacitor *CC*With a time constant of ~*RFCC*.

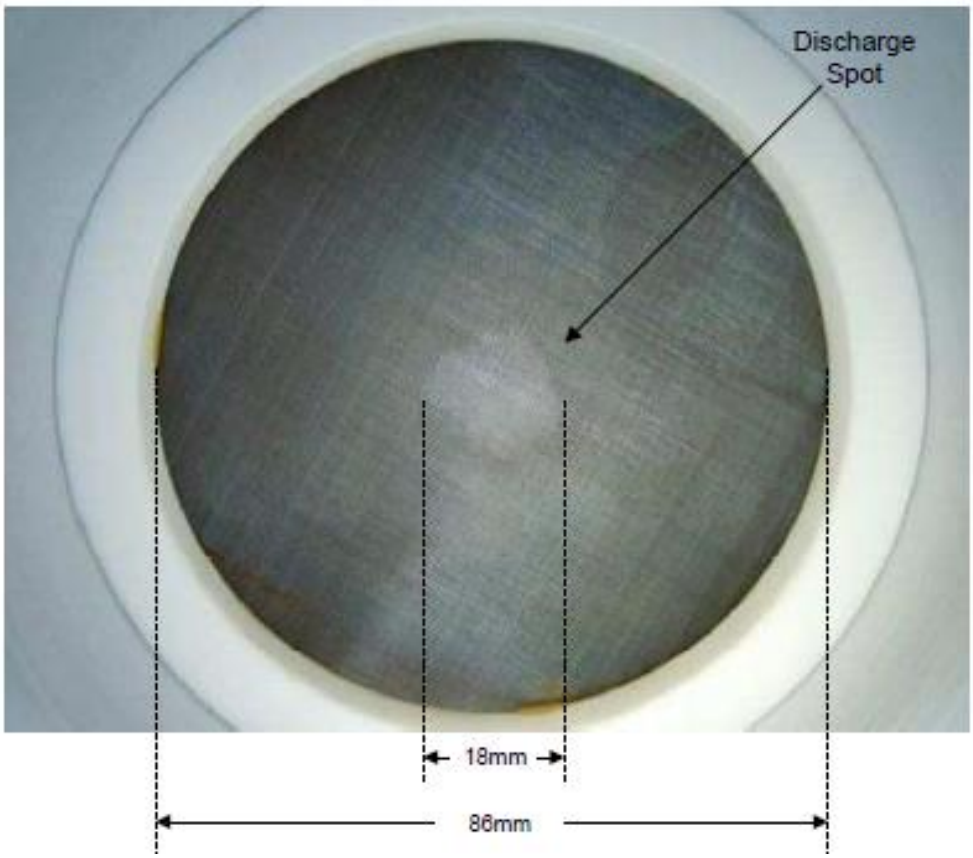

Fig. 6.39: Trace the rise, after ~ 200 impacts. Descent pin, dAK = 15mm.

6.3.4. Descent Pin (d = 25mm)

The pin cathode with the anode-cathode distance of 25mm, presented the most importantly results in microwave output of Vircator. Therefore in- n pin cathode distance 25mm from the anode, used to substantiate confirmed effect of the rise in the characteristics of the device grid. The voltage, which appeared collapse of the gap, is greater than in the case of the pin spaced dAK = 15mm. The pin-cathode distance 25mm It was used also for documenting the effect of the vacuum at the outlet of the Vircator. These experiments were performed with the matrix. No. "6" and a negligible effect on the microwave output was observed for pressures up to ~ 10-3Torr, as will be mentioned below (see. Par. 6.5). The mesh number "1" comprised 30 holes per inch, with a hole opening 0.587mm, 0.26mm diameter wire and free surface ~ 48%. The mesh number "3" carries 60 holes per inch, with a hole opening 0.263mm, 0.16mm diameter wire and surface should be free in- ~ 39%. It has lower free surface of the matrix "1", therefore expected lower microwave output from the anodes to the previous screen. The mesh number "6" bring 150 holes per inch, with a hole opening 0.109mm, 0.06mm wire cross measure free surface and ~ 41%. It is the thinnest of all available matrices and has an intermediate coefficient of free surface, thus anamenou- by microwave output between the matrix "1" and "3". Also in the grid with the greatest chance to present premature.

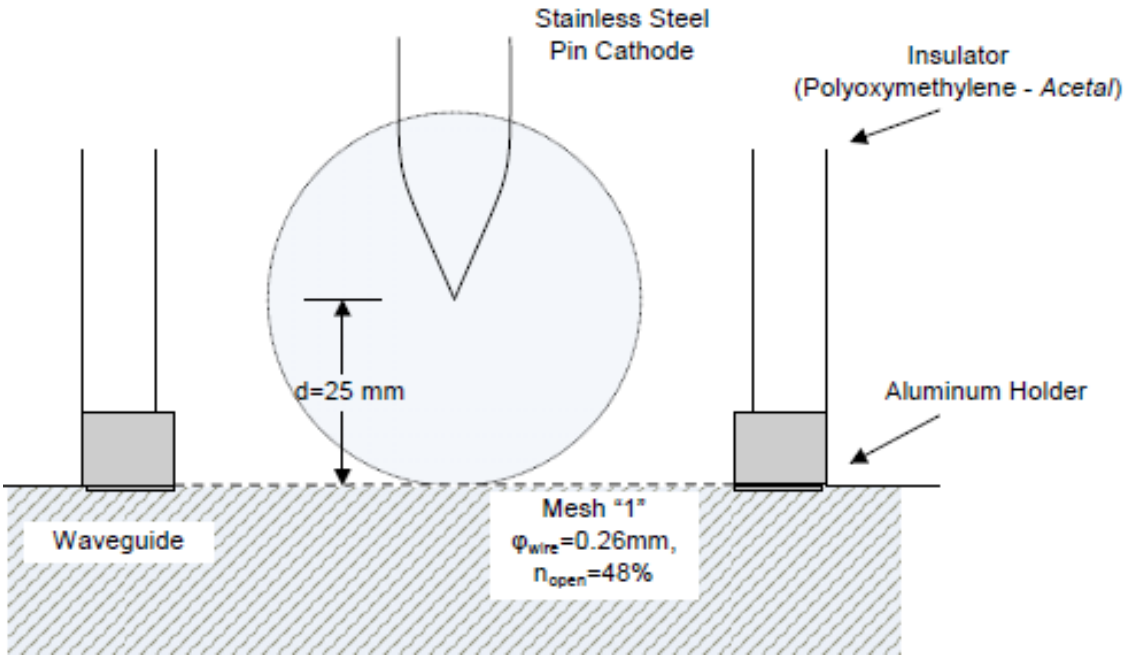

Fig. 6.40: Configuring a pin diode cathode and dAK = 25mm.

6.3.4.1. Macroscopic Experimental Sizes

The following tables lists the recorded peak voltages, current and power in the passage for at least ten (10) iterations, a charging pri- tefontos of 50, 75 and 100V AC. According to what has been stated in paragraphs 5.5 and 6.3.2, the loads they give impulse *0.6 / 50*With maximum widths 52, 78 and 104kV. The voltage, current and power of the diode are given as mean and the calculated dispersion *p*the recorded maximum, in any state of charge, with semiotics *<X> ± 1 · sx*.

Tab. 6.9: Descent Pin dAK = 25mm, Mesh "1" (Measurements 08-05-2008)

Load	50V AC	75V AC	100V AC
Max Surge	~ 52kV	~ 78kV	~ 104kV
Current Ion Pump	0.16 ~ 0.20mA	0.18 ~ 0.21mA	0.25 ~ 0.27mA
Lifting	1.9 ~ 3.5m	2.5 ~ 4.5m	3.5 ~ 6.5m
Voltage typical	39.7 ± 1.9kV	64.8 ± 4.4kV	76.0 ± 3.1kV
Typical Power	304 ± 51A	548 ± 106A	989 ± 175A
Power typical	6.3 ± 1.6MW	21.2 ± 3.6MW	39.3 ± 4.7MW
RF typical	**0.1 ~ 0.6W**	**1 ~ 10W**	**10 ~ 100W**
Efficiency typical	2 · 10-8 ~ 10-7	10-7 ~ 8 · 10-7	10-7 ~**10-5**
RF max recorded	**0.8W**	**16W**	**430W**

Tab. 6.10: Descent Pin dAK = 25mm, Mesh "1" (Measurements 05/09/2008)

Load	50V AC	75V AC	100V AC
Max Surge	~ 52kV	~ 78kV	~ 104kV
Current Ion Pump	0.20 ~ 0.22mA	0.24 ~ 0.26mA	0.21 ~ 0.26mA
Lifting	1.9 ~ 3.1mA	2.5 ~ 5mA	4 ~ 7mA
Voltage typical	42.8 ± 1.8kV	61.7 ± 1.6kV	75.2 ± 2.6kV
Typical Power	391 ± 64A	781 ± 145A	1104 ± 170A
Power typical	8.0 ± 0.9MW	19.3 ± 1.7MW	40.8 ± 5.5MW
RF typical	**0.5 ~ 3W**	**1 ~ 10W**	**5 ~ 40W**
Efficiency typical	4 · 10-8 ~ 5 · 10-7	8 · 10-8 ~ 7 · 10-7	10-7 ~**10-6**
RF max recorded	**9W**	**25W**	**50W**

Tab. 6.11: Descent Pin dAK = 25mm, Mesh "3" (Measurements 14-05-2008)

Load	50V AC	75V AC	100V AC
Max Surge	(Not out)	~ 78kV	~ 104kV
Current Ion Pump	-	0.21 ~ 0.23mA	0.25 ~ 0.26mA
Lifting	-	2.8 ~ 3.5m	3.5 ~ 5mA
Voltage typical	-	54.5 ± 0.9kV	66.9 ± 3.8kV
Typical Power	-	529 ± 87A	743 ± 133A
Power typical	-	19.5 ± 3.2MW	28.8 ± 6.0MW
RF typical	-	**0.5 ~ 3W**	**1 ~ 10W**
Efficiency typical	-	4 · 10-8 ~ 5 · 10-7	5 · 10-8 ~**10-6**
RF max recorded	-	**12W**	**30W**

Tab. 6.12: Descent Pin dAK = 25mm, Mesh "3" (Measurements 19-05-2008)

Load	50V AC	75V AC	100V AC
Max Surge	~ 52kV	~ 78kV	~ 104kV
Current Ion Pump	0.18 ~ 0.19mA	0.17 ~ 0.22mA	0.20 ~ 0.35mA
Lifting	1.6 ~ 2.5m	2.5 ~ 4.1mA	3 ~ 5mA
Voltage typical	37.0 ± 0.5kV	55.7 ± 1.9kV	68.0 ± 3.1kV
Typical Power	314 ± 42A	523 ± 89A	712 ± 200A
Power typical	6.9 ± 1.5MW	17.3 ± 4.3MW	25.1 ± 4.8MW
RF typical	**0.1 ~ 0.6W**	**1 ~ 3W**	**1 ~ 15W**
Efficiency typical	10-8 ~ 10-7	5 · 10-8 ~ 5 · 10-7	5 · 10-8 ~**10-6**
RF max recorded	**0.7W**	**10W**	**25W**

Tab. 6.13: Descent Pin dAK = 25mm, Mesh "6" (Measurements 10-06-2008)

Load	50V AC	75V AC	100V AC
Max Surge	~ 52kV	~ 78kV	~ 104kV
Current Ion Pump	0.24 ~ 0.32mA	0.21 ~ 0.26mA	0.26 ~ 0.30mA
Lifting	1.8 ~ 4mA	3 ~ 5.3mA	4 ~ 7mA
Voltage typical	36.1 ± 0.6kV	57.0 ± 2.5kV	71.9 ± 2.6kV
Typical Power	342 ± 58A	552 ± 142A	929 ± 290A
Power typical	5.5 ± 0.8MW	14.8 ± 2.6MW	29.2 ± 7.8MW
RF typical	**0.2 ~ 0.6W**	**1 ~ 10W**	**1 ~ 30W**
Efficiency typical	2 · 10-8 ~ 3 · 10-7	10-7 ~ 10-6	3 · 10-8 ~**4 · 10-6**
RF max recorded	**1.7W**	**20W**	**100W**

Tab. 6.14: Descent Pin dAK = 25mm, Mesh "6" (Measurements 11-06-2008)

Load	50V AC	75V AC	100V AC
Max Surge	~ 52kV	~ 78kV	~ 104kV
Current Ion Pump	0.20 ~ 0.25m	0.20 ~ 0.25m	0.20 ~ 0.30mA
Lifting	1.8 ~ 3mA	3 ~ 5mA	4 ~ 7mA
Voltage typical	42.4 ± 2.6kV	61.7 ± 1.8kV	74.4 ± 3.0kV
Typical Power	380 ± 55A	662 ± 187A	860 ± 197A
Power typical	7.0 ± 1.3MW	19.5 ± 2.0MW	32.9 ± 4.5MW
RF typical	**0.2 ~ 1.5W**	**1 ~ 10W**	**3 ~ 20W**
Efficiency typical	4 · 10-8 ~ 10-6	10-7 ~ 9 · 10-7	10-7 ~**10-6**
RF max recorded	**5W**	**17W**	**45W**

Tab. 6.15: Descent Pin dAK = 25mm, Mesh "6" (Measurements 17-06-2008)

Load	50V AC	75V AC	100V AC
Max Surge	~ 52kV	~ 78kV	~ 104kV
Current Ion Pump	0.18 ~ 0.22mA	0.22 ~ 0.28mA	0.25 ~ 0.32mA
Lifting	1.8 ~ 3.1mA	2.5 ~ 5.2mA	4 ~ 8mA
Voltage typical	49.3 ± 1.7kV	61.7 ± 4.3kV	76.9 ± 1.7kV
Typical Power	311 ± 51A	703 ± 239A	1100 ± 306A
Power typical	6.3 ± 1.6MW	16.3 ± 3.7MW	33.2 ± 8.0MW
RF typical	**0.1 ~ 0.2W**	**0.2 ~ 5W**	**0.5 ~ 20W**
Efficiency typical	10-8 ~ 5 · 10-8	10-8 ~ 7 · 10-7	5 · 10-8 ~**2 · 10-6**
RF max recorded	**0.5W**	**12W**	**45W**

H estimated pressure in the passage area is as current of Ion Pump in mA at the moment before impact, multiplied by 10-4 Torr (see. par. 6.1). Therefore the 0.2mA corresponding to 2 · 10-5Torr. The current of the ionization pump the moment of impact rises rapidly (within approximately 0.5sec) about one order of magnitude above. Longer impulse voltage causes greater surge current of ionization pump.

H pin cathode with 25mm distance from the anode showed the strongest out of all configurations tested with the single-stage impulse device. The captured were first liberalized power 500W approached in the observation zone, ie ~ 1.4 ~ 2.1GHz. The grid is "1", the highest permeability, 48% had larger amounts of power. Since the configurations grids "3" and "6", with permeability 38% and 41% respectively, the latter showed slightly larger amounts of power. However, Asia Mi- krokymatiki output is greatly reduced, relative to the configuration with the matrix "1". The conclusion drawn from the above is that the passing the kyma- todigo stream is so critical that even in this subthreshhold guide area of our experiments, a slight decrease in permeability plexus Tos translates to a substantial reduction force.

Diode behavior. Pin dAK = 25mm, matrices '1' and '3'.

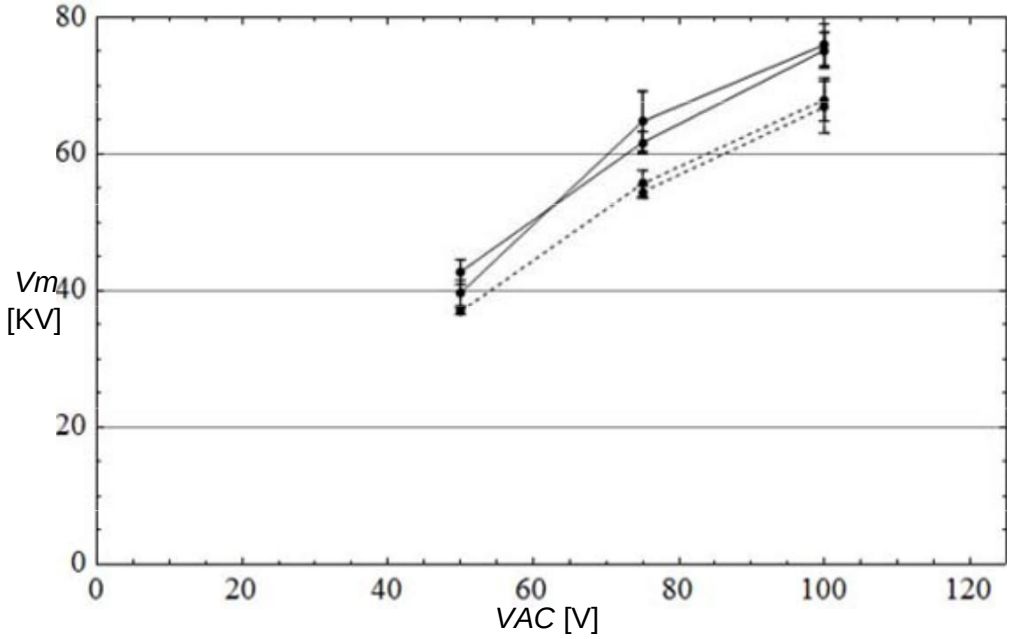

Fig. 6.41: Maximum voltage diode. Cathode tip, dAK = 25mm, mesh Nos. "1" (solid lines) and matrix. No. "3" (dotted lines).

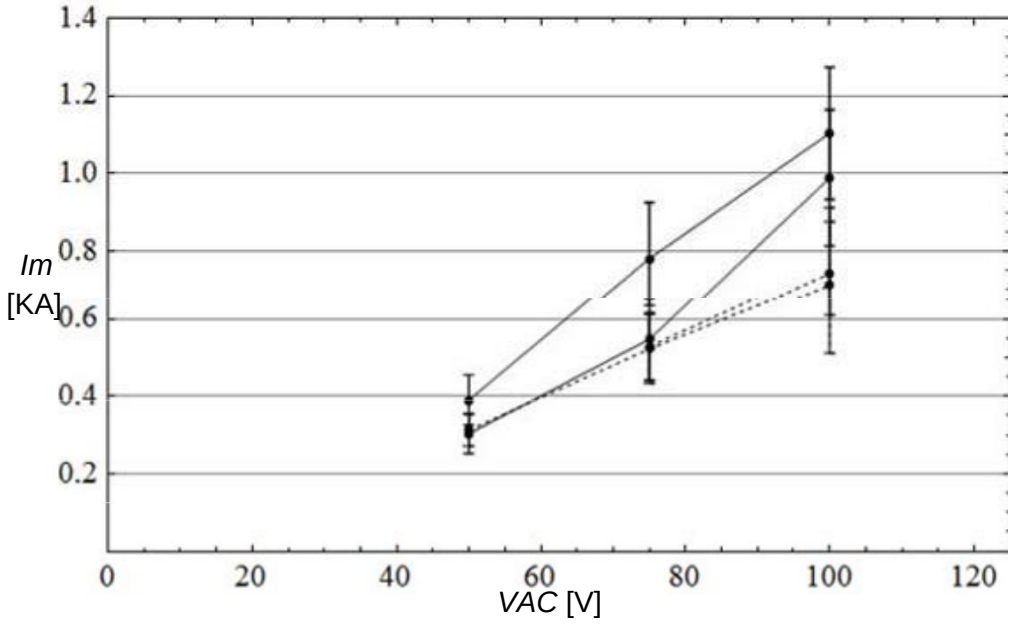

Fig. 6.42: Maximum diode current. Cathode tip, dAK = 25mm, mesh Nos. "1" (solid lines) and matrix. No. "3" (dotted lines).

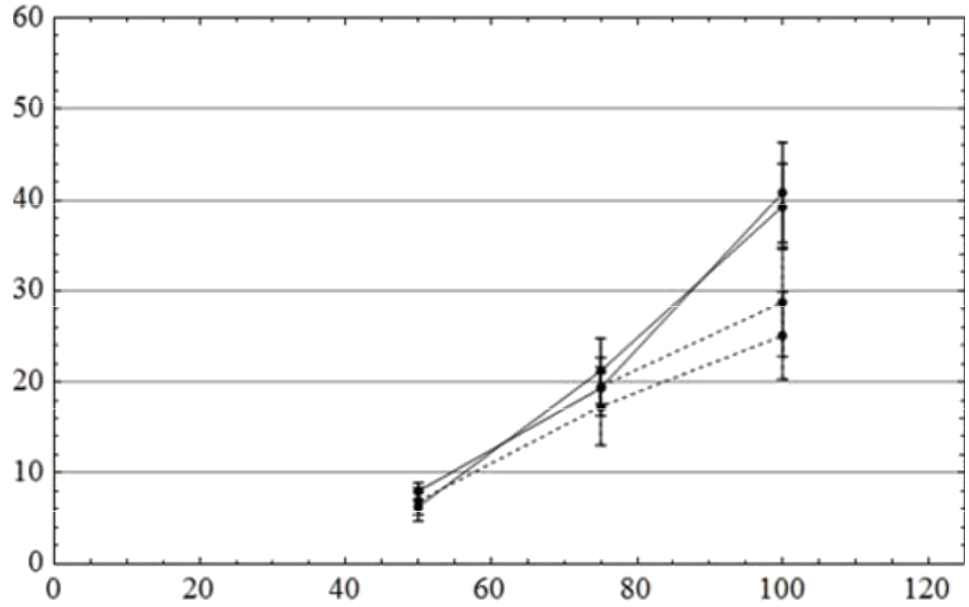

Fig. 6.43: Maximum power diode. Cathode tip, dAK = 25mm, mesh Nos. "1" (solid lines) and matrix. No. "3" (dotted lines).

Diode behavior. Pin dAK = 25mm, Grids "1" and "6".

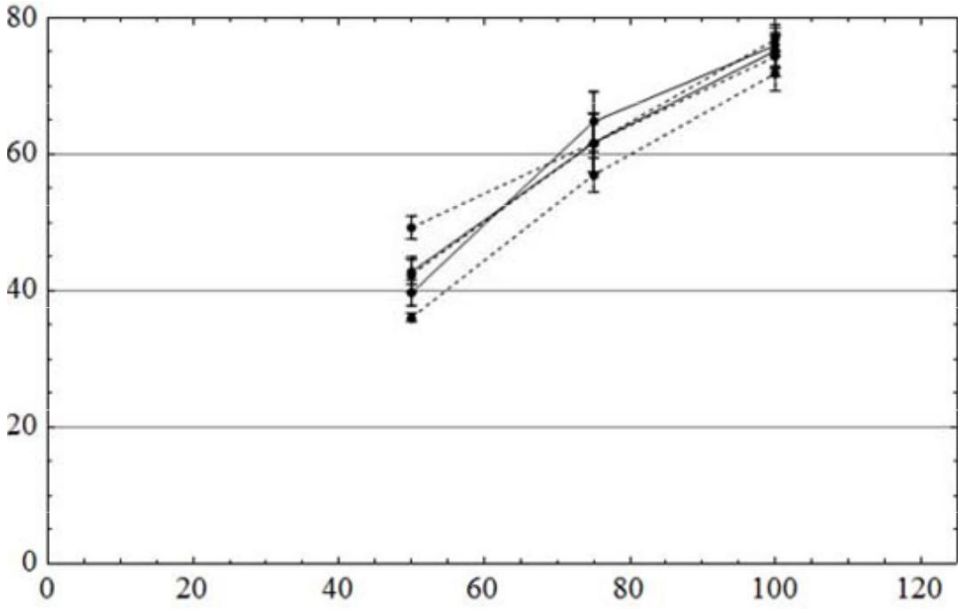

Fig. 6.44: Maximum voltage diode. Descent pin, dAK = 25mm, mesh no. '1' (continuous lines) and grid no. "6" (dotted lines).

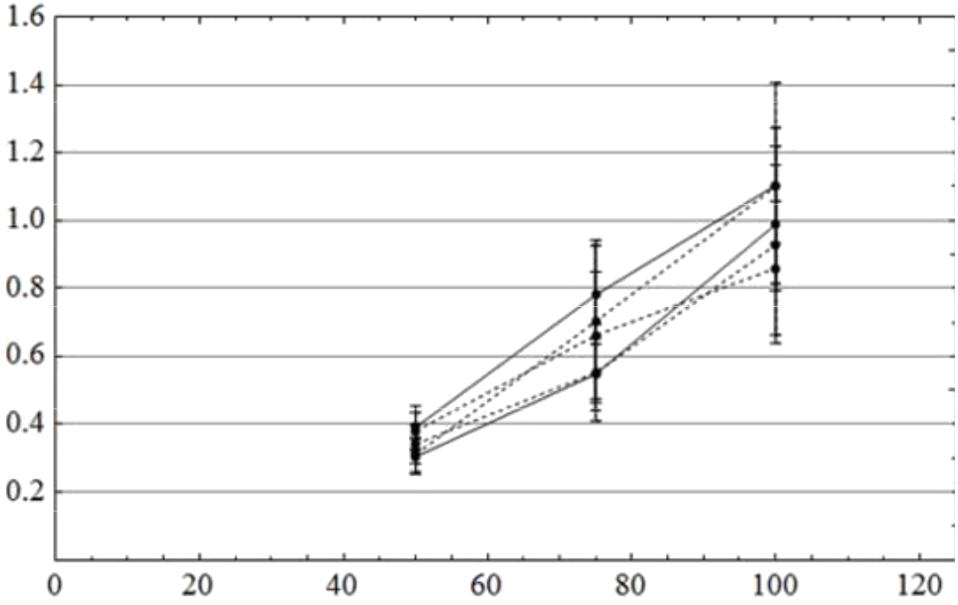

Fig. 6.45: Maximum diode current. Descent pin, dAK = 25mm, mesh no. '1' (continuous lines) and grid no. "6" (dotted lines).

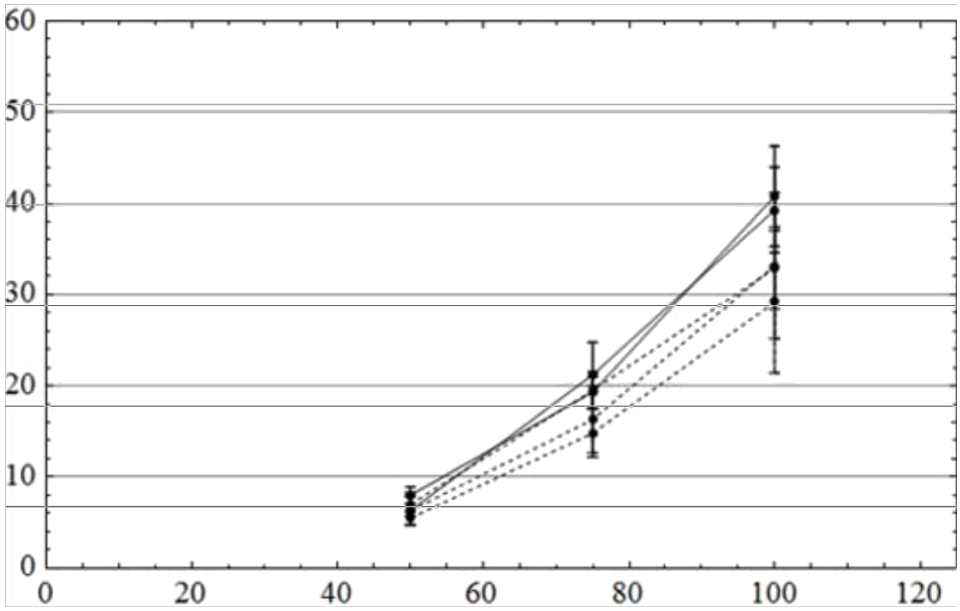

Fig. 6.46: Maximum power diode. Descent pin, dAK = 25mm, mesh no. '1' (continuous lines) and grid no. "6" (dotted lines).

Compare Conduct passages. Pin dAK = 25mm and dAK = 15mm, mesh "1".

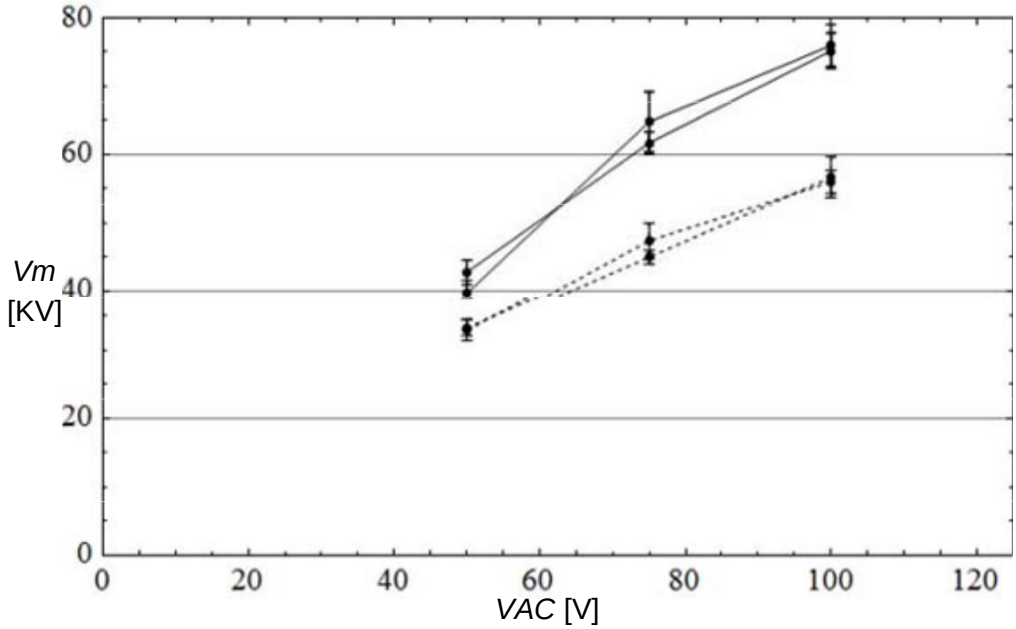

Fig. 6.47: Maximum voltage diode. Descent pin, dAK = 25mm (solid lines) and dAK = 15mm (dotted lines), mesh no. '1'.

As expected, the longest distance of the electrodes in aki- Group cathode dAK = 25mm enables greater endurance of the gap, with respect to the cathode tip dAK = 15mm.

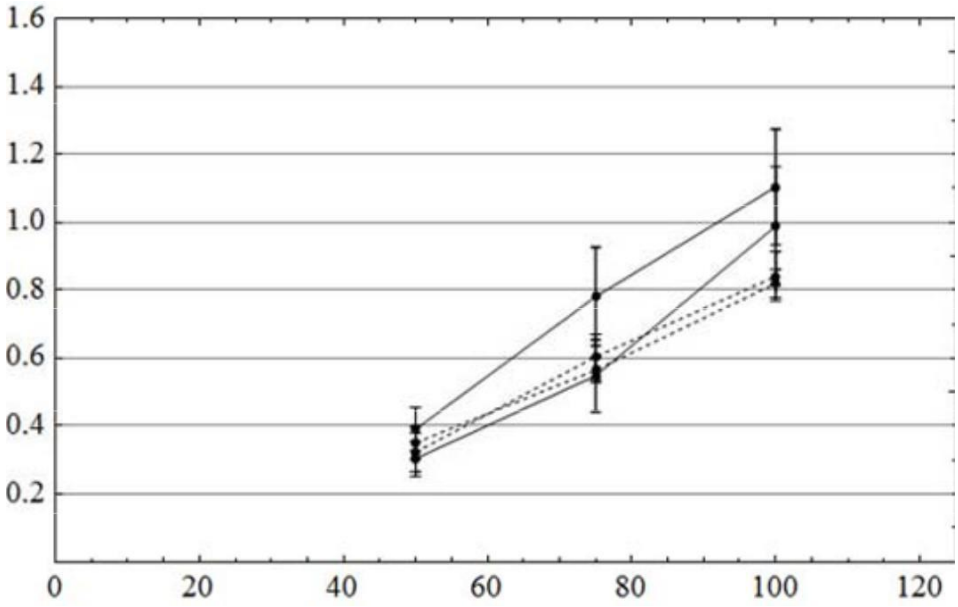

Fig. 6.48: Maximum diode current. Descent pin, dAK = 25mm (solid lines) and dAK = 15mm (dotted lines), mesh no. '1'.

The pin cathode dAK = 25mm shows generally higher peak currents from the spike in dAK = 15mm, because, in the last stages before bridging the gap, the plasma sphere has expanded to a radius greater value allowing therefore higher prices Child Langmuir stream passage. To apparent area of the cathode-anode plasma channel is greater.

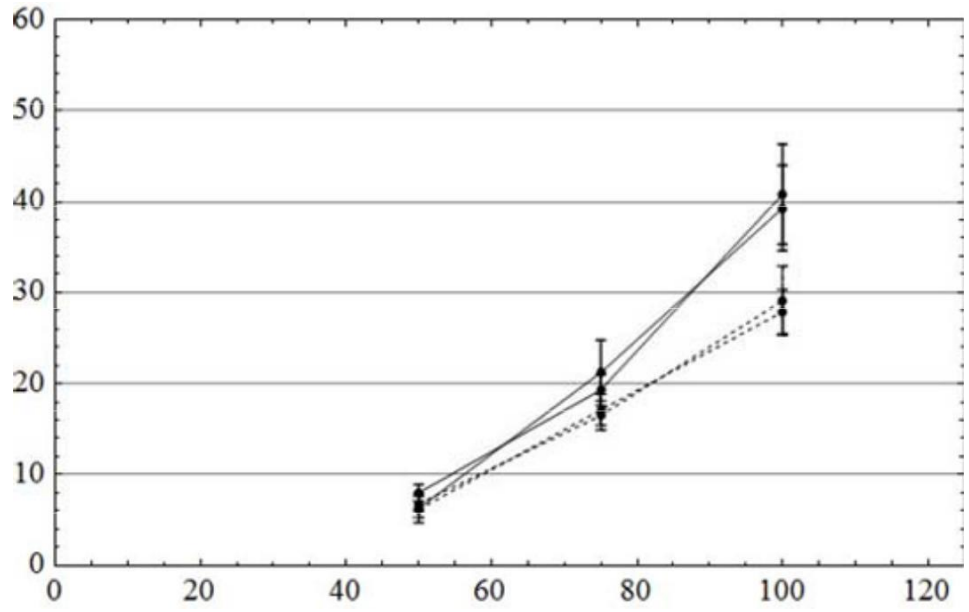

Fig. 6.49: Maximum power diode. Descent pin, dAK = 25mm (solid lines) and dAK = 15mm (dotted lines), mesh no. '1'.

As expected, the pin diode with larger electrode spacing, for the same lattice, is more power consumed. It seems, in fact, the trend super linear increase in power in the passage by increasing the driving voltage. The two configu- foseis show little power dissipation values in all series of experiments.

The behavior of the passage in time is quite chaotic and displays at the timing RH during the break, crowd behavior. This is due to a single point detonation microplasma the top of the pin, which extends in a chaotic manner plasma sphere until the mesh anode. The way the collapse of the gap, observing the time change in the trend, sometimes show a smooth reduction and sometimes abnormal behavior changing, reflecting the random behavior of the plasma column generated between ilektrodi- s. Also, the bridging of the gap times show great dispersion, with times from 300nsec up 800nsec.

6.3.4.2. Model Discharge Capacity by Diode

For this configuration, we set the following sizes: cathode ray *a*= 0.001m, reinforcement distance *d*= 0.025m, geometric matrix permeability upward Output *n*= 48%, plasma spread speed *u*= 6cm / microseconds = 6 · 104m / sec, initial voltage capacitors fh *V (0)*=*V0*= 80kV, capacitor capacity *C*= 1.2nF. The radius of the cathode is set equal to

1mm, because it is a spike, while the plasma spread speed is set equal to 6cm / microseconds because among other measurements, some of them had collapsed gap within 400nsec. Following the procedure described, and in par. 6.3.3.2, we form the following representations: In Fig. 6.50 show the analytical solution of the diode voltage and the current of contributing passage Vircator. A- Fu we find the dependence of the voltage in the gap, we can extract the energy of the electron beam and the area of which is set equal to the phenomenon emva- almost cathode. Of those sizes and the permeability of the grid upward period, we can calculate the diode current required to feed the kymatodigiki cavity with critical peak beam current. This stream, par- symbolized by the dotted line, it should leak passage to enter in conditions of virtual cathode display in kymatodigiki cavity, according to the in- xisosi (4.70). The passageway leads to more current than is necessary after the first 220nsec. From that moment onwards we can predict what will be referred menomenes frequencies output Vircator, based on the theoretical models of literature. In Fig. 6.51, since we know the voltage and current flowing through the diode, can illustrate approaches for frequency reflex and to sys- frequencies of the oscillations of the cloud of virtual cathode.

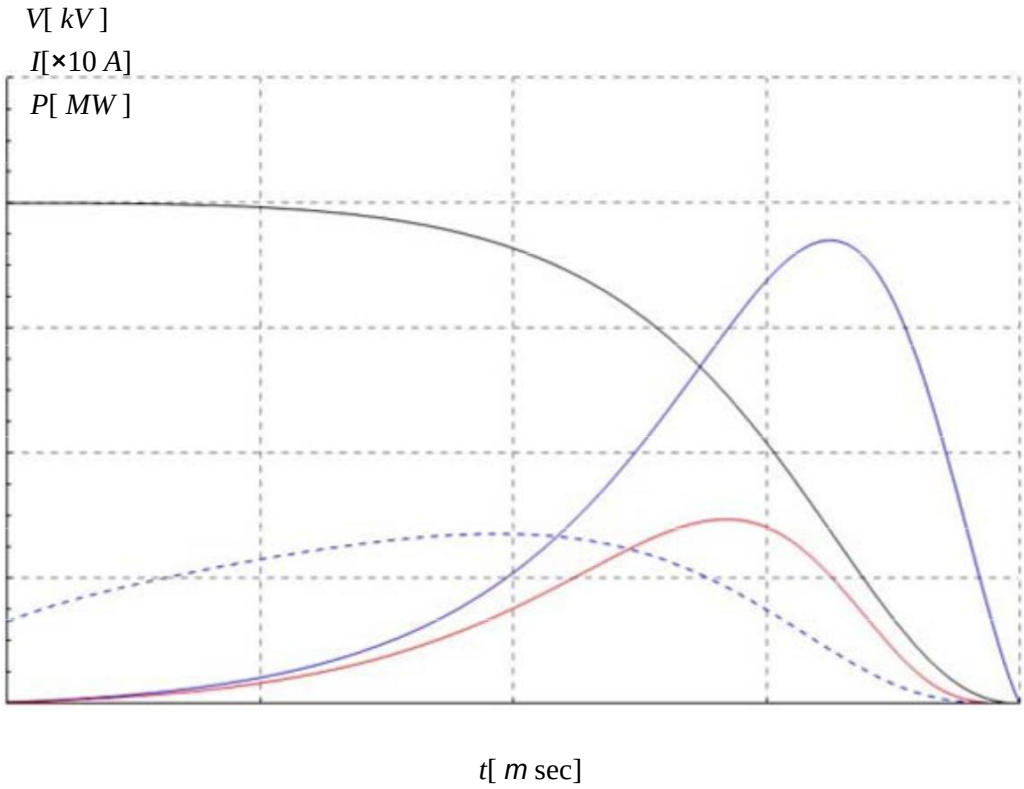

Fig. 6.50: Theoretical variation of voltage, current and power pin cathode dAK = 25mm, for drive voltage 80kV, capacity capacitor 1.2nF, speed katarref- ing gap 6cm / microseconds.

The plasma frequency of the electron beam, which enters the inactive area can be calculated from the relativistic equation (4.42). In this expression in place of the current package *I*, Substituting the amount (4.69) multiplied by the geometrical permeability of the matrix, *n*. In the denominator of equation (4.42) anti

properly we make the time dependence of the radius of the cathode, which we assume and radius of the beam. The change of plasma frequency is described by (4.71), where the coefficients b and c depend on the tension in the passage and described by equations (4.44) and (4.45). The frequency of oscillation of the virtual cathode, according to what has been reported in par. 4.1.2, is between the values *fp* and (2n) 1/2*fp*. In Fig. 6.51 noted: the area defined by frequencies prices *fp* and (2n) 1/2*fp*, Both estimates of frequency reflexing, non-relativistic and schetiki- spotty, as described in par. 4.1.1. Finally made and the assessment of Woo, on. (4.16).

We note that after the first 220nsec, the current is strong enough to shall become possible to display virtual cathode but the geometrical and electrical characteristics of the circuit seems to remove the output frequencies in periodic Xe over the 2GHz, however not far away. The possible output frequencies (the frequency reflex oscillations and lower plasma frequency) transiting include vehicles of 1.8 to 2GHz. For this configuration, the maximum current that provides the Secre- nomic model is ~ 750A, to collapse the gap in 400nsec. The power in cases importance this amounts to 30MW. Faster collapse gap because larger velocity plasma spreading ties implies larger diode currents.

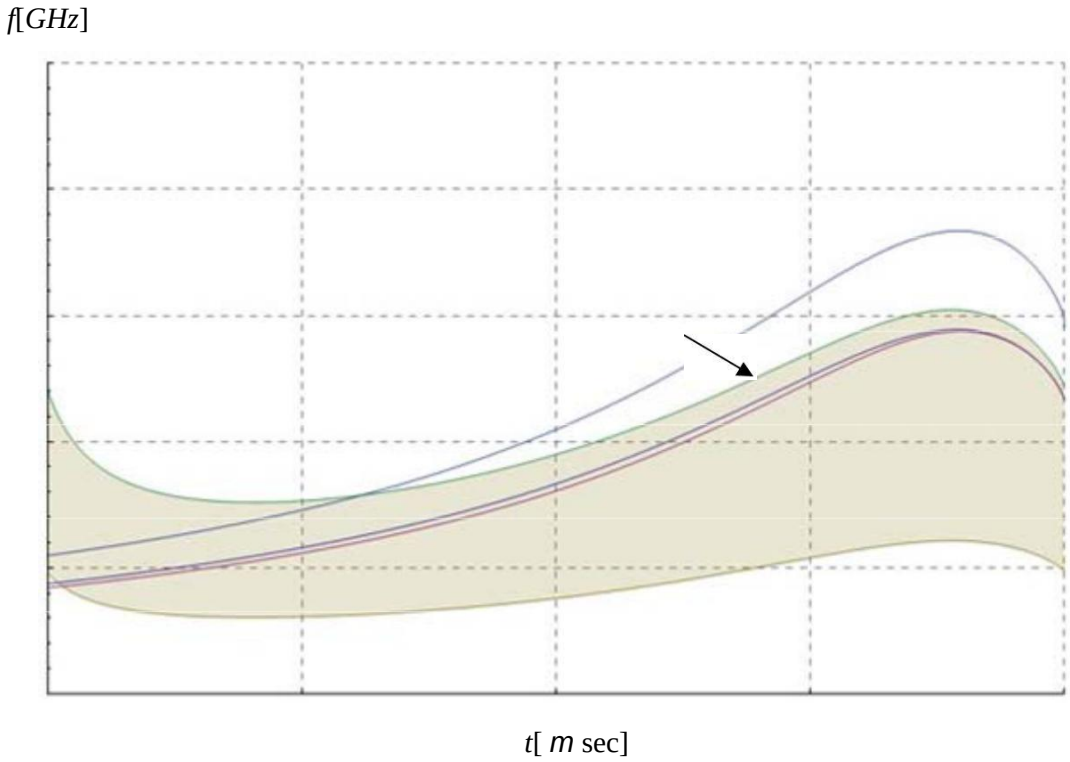

Fig. 6.51: Output frequency Assessments Vircator with pin cathode dAK = 25mm, for discharge voltage 80kV, capacitor 1.2nF, with spacing collapse speed 6cm / microseconds.

It is important to note that there is a region in which the current in the di- progress is strong enough to have virtual cathode formation. Also, projections for output frequencies passing through the region of 1.8 to 2GHz.

6.3.4.3. Typical measurements

Case A (82kV, 890A, 42MW, 5cm / microseconds)

In this iteration, the voltage across the diode is no great reversal and under the current waveforms depreciates smoothly. As the voltage rises, re- ratireitai a small increase in power up to the point where a sudden re- tarrefsi trend, accompanied by a sharp increase in supply and a strong pulse RF. As shown in Fig. 6.54, resistance at this point is about 70O with previous sharp decline from much higher prices. The gap pre- sented a general instability in characteristics throughout the course of the phenomenon, the bridge, while a second signal strength appears just before 500nsec, at a time of strong current and apparent gap resistance of about 30O. The period in which the diode collapses approximately 500nsec, thereby yielding a plasma spread speed in the passage of approximately 5cm / microseconds. Abrupt serial decreases in voltage at the beginning of the phenomenon may be due to electrical breakdown phenomena that are not localized in the tip region and the matrix but also the wider chamber accommodates the passage.

The time-range display of Fig. 6.53 shows that the first powerful microwave output is broad spectral content covering the band from 1600MHz up to 1850MHz. Here patient output while just before 0.5msec, the second powerful micro- wave pulse has a spectral content in 1800MHz, at 2GHz and suspicion for larger frequencies than 2.2GHz.

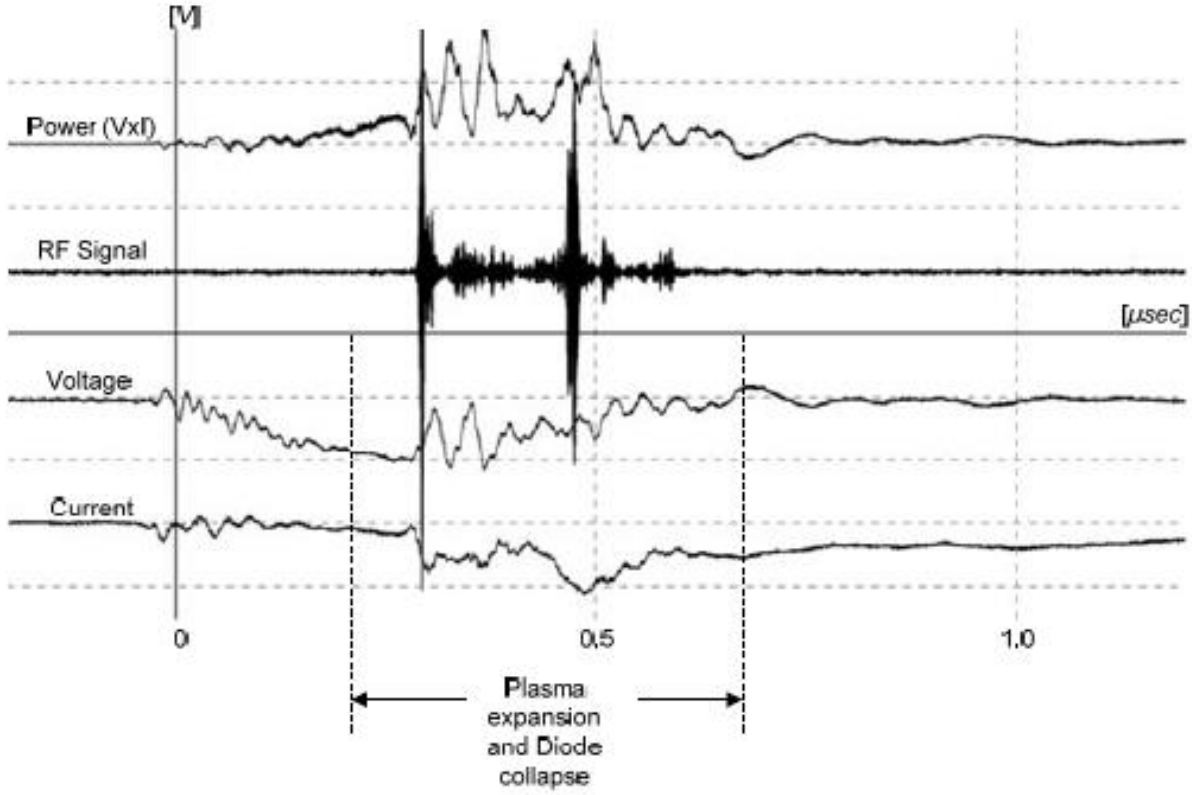

Fig. 6.52: The Descent pin, dAK = 25mm, mesh no. '1' (measured 20080508m48): Vmax = 82kV, Imax = 890A, RFmax = 130W, Pmax = 42MW.

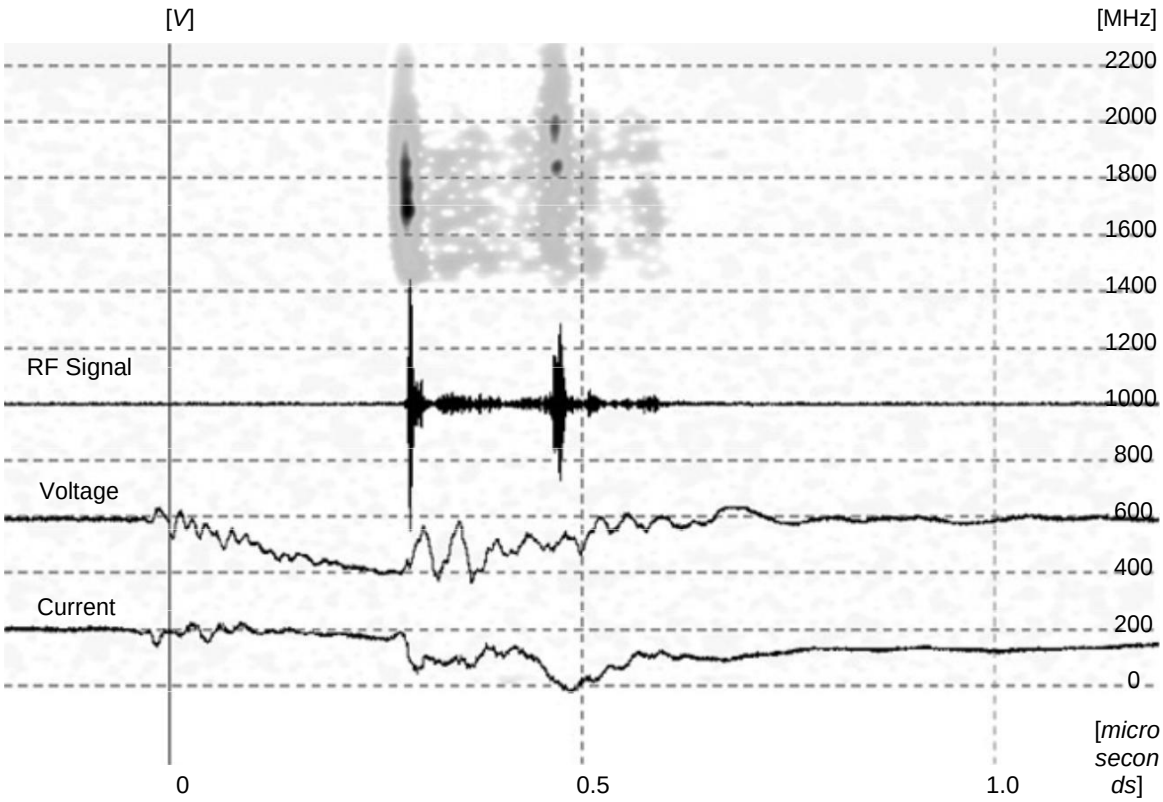

Fig. 6.53: The Descent pin, dAK = 25mm (measurement 20080508m48): time-imaging spectrum.

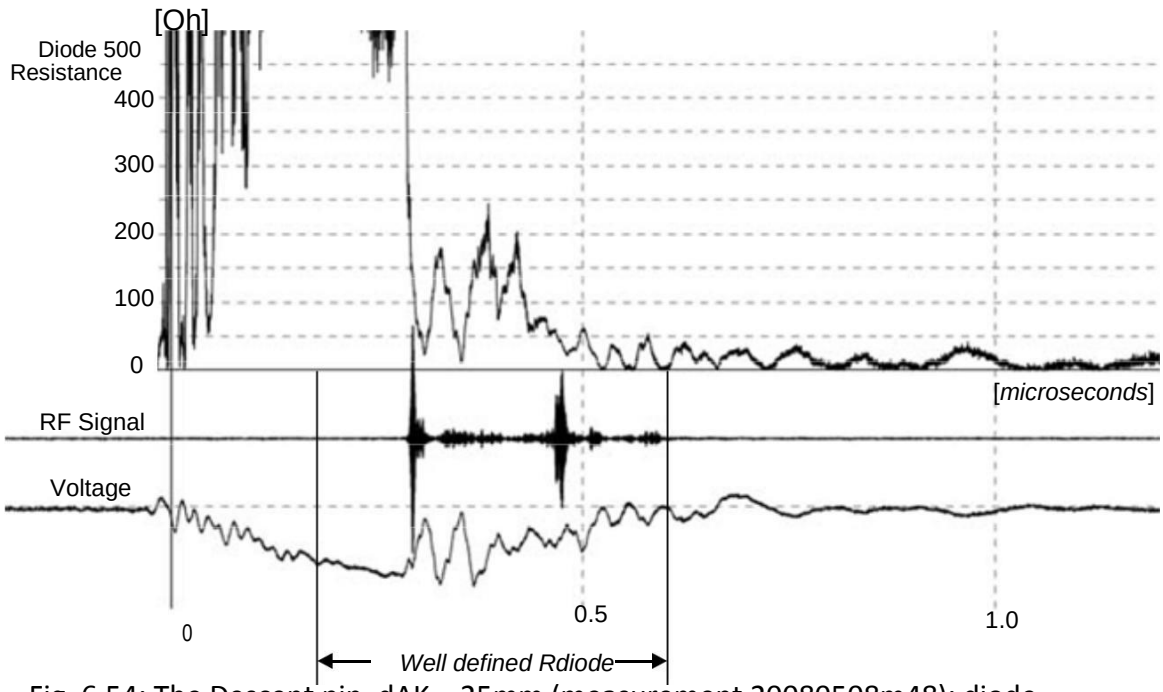

Fig. 6.54: The Descent pin, dAK = 25mm (measurement 20080508m48): diode impedance.

Case B (82kV, 980A, 47MW, 5cm / microseconds)

This event is the strongest recorded pulse in far observations by-step impulse device VDE-b. The validity of the order of 0.5kW, while giving greater power efficiency in RF we hold about 10-5. The diode is several variations in the characteristics of sizes and collapses in about 500nsec. During phenomenon existing Tai two zero voltage by the normalization of the current, which indicates the total bridging the gap. The propagation speed of the plasma is of the order of 5cm / microseconds, corresponding to the time of collapse of the gap. However, early in the zero voltage diode may mean even higher-speed plasma them. The microwave output is observed the time period the current import so large, the resistance of the gap is of the order of 20 to 50 ohm.

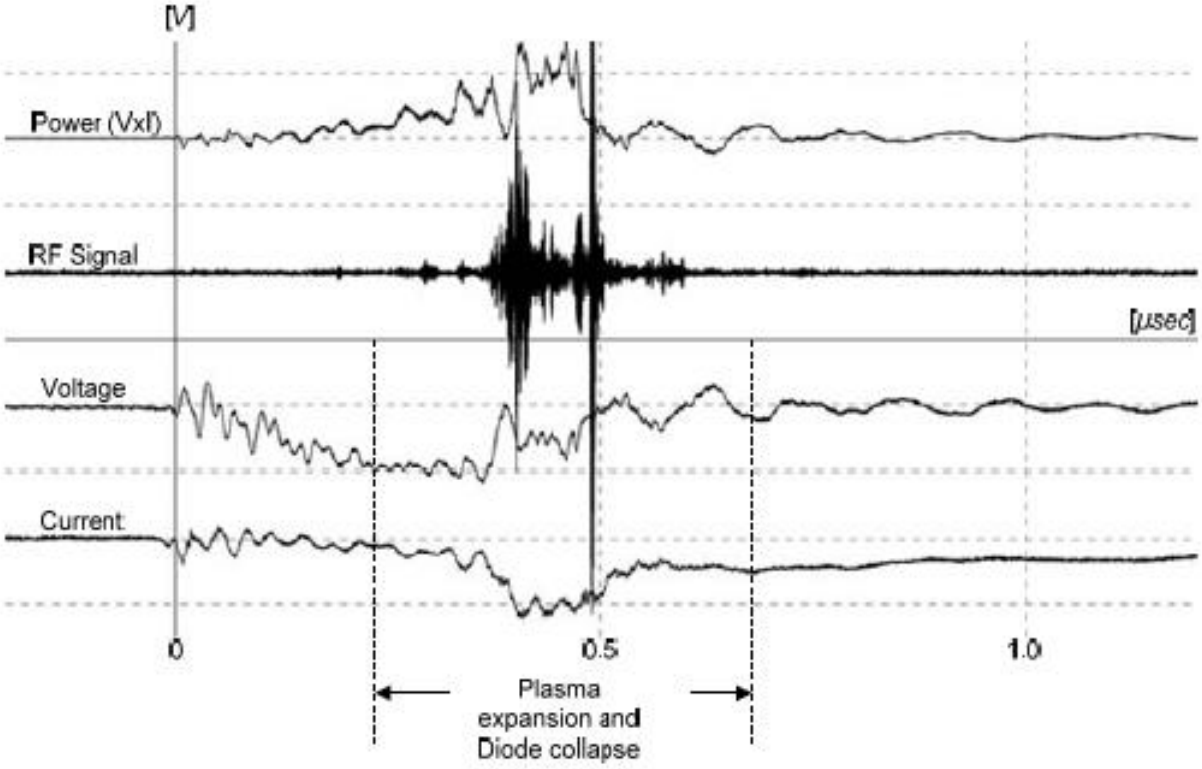

Fig. 6.55: The Descent pin, dAK = 25mm, grid Nov. «1» (20080508m57 measurement): Vmax = 82kV, Imax = 980A, RFmax = 430W, Pmax = 47MW.

In the time display the spectrum of such registration, we observe that the fa- tive content of the stronger, analog, signal located between the
1600GHz and 1800GHz.

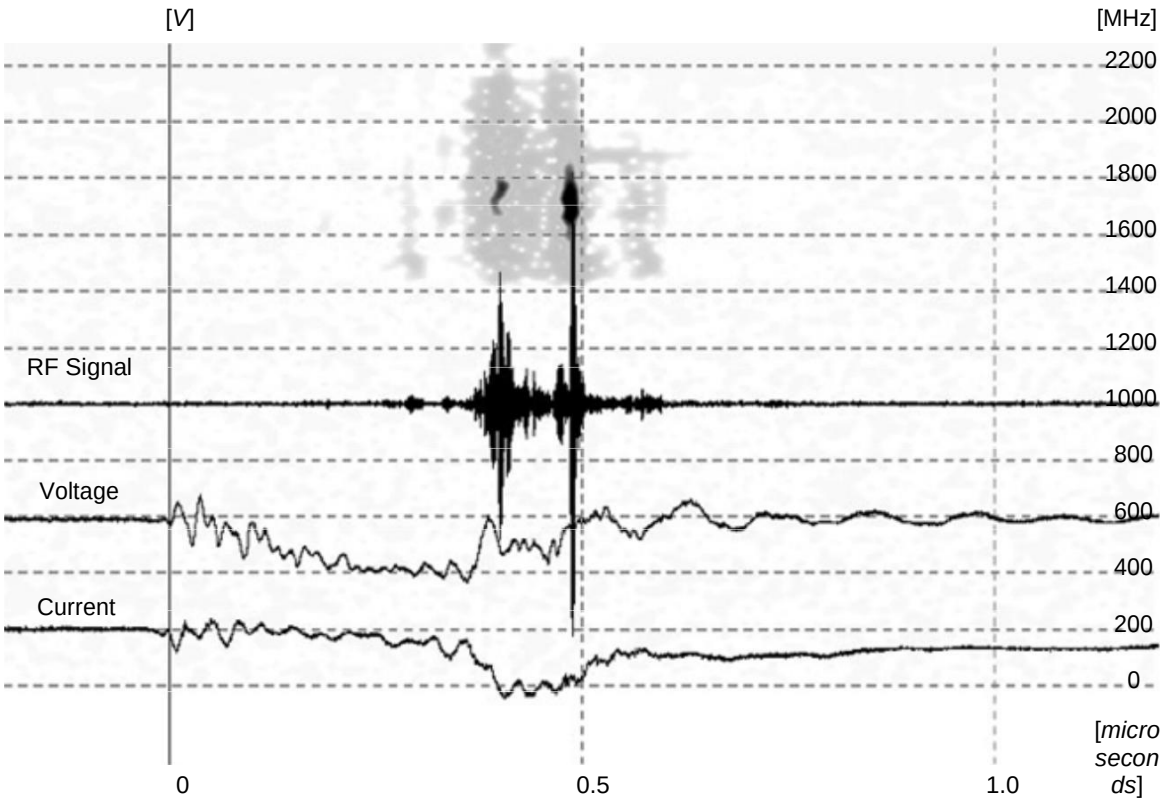

Fig. 6.56: The Descent pin, dAK = 25mm (20080508m57 measurement) Show time-range.

From the depiction of the change of the resistance of the gap, it is apparent that force; Ph microwave output is observed when the resistance of the diode is lower than 50 ohm.

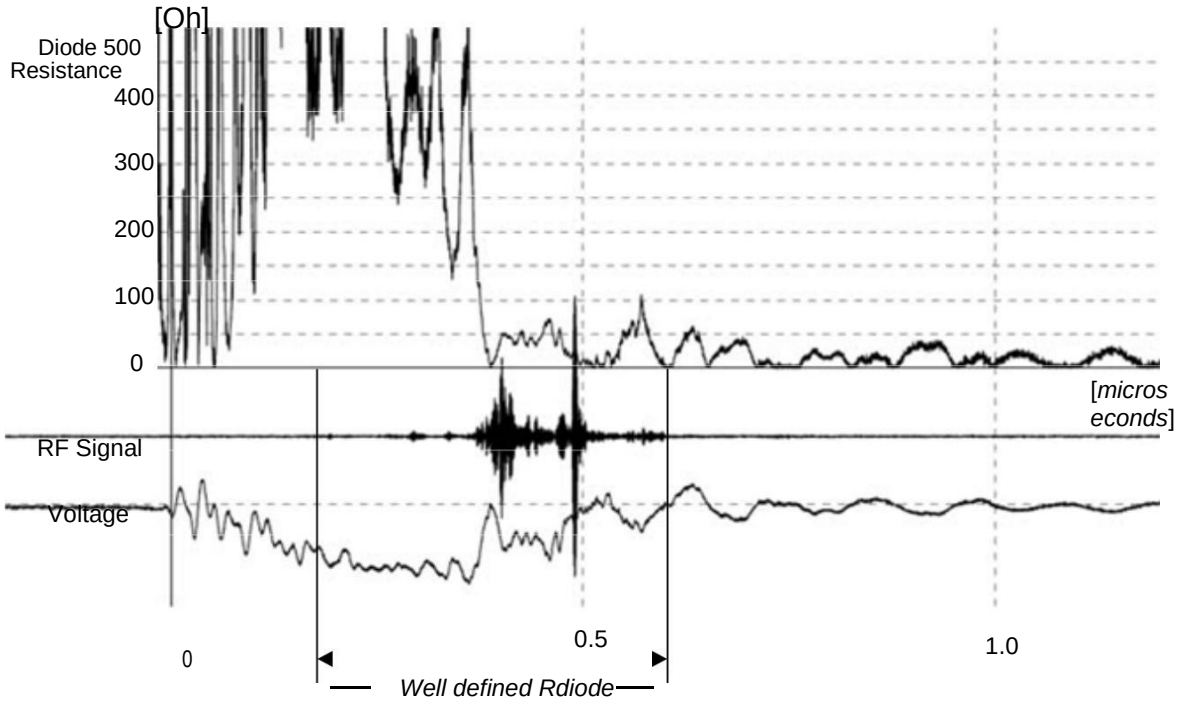

Fig. 6.57: The Descent pin, dAK = 25mm (20080508m57 measurement): diode impedance.

Case C (76kV, 1200A, 40MW, 6cm / microseconds)

The following case shows the classical sudden collapse plate pin spacing behavior with distance dAK = 25mm. Spike looks at first De-gives a small electronic current, which, since its appearance and 150nsec about growing slowly, while in 0.4msec about this growth is rapid. The appointment Give collapses into 400nsec, giving a speed jumper ~ 6cm / microseconds. The bridge in this case probably contributes strongly both the cathode and the anode. The a sharp change in sizes during the time period between 0.4 and 0.5msec explained, if we consider that the grid is intense local heating and produces anode width term. In this test, the microwave radiation occurs when the corresponding distance of the gap has been less than 100O until the diode bridge of complete Rus.

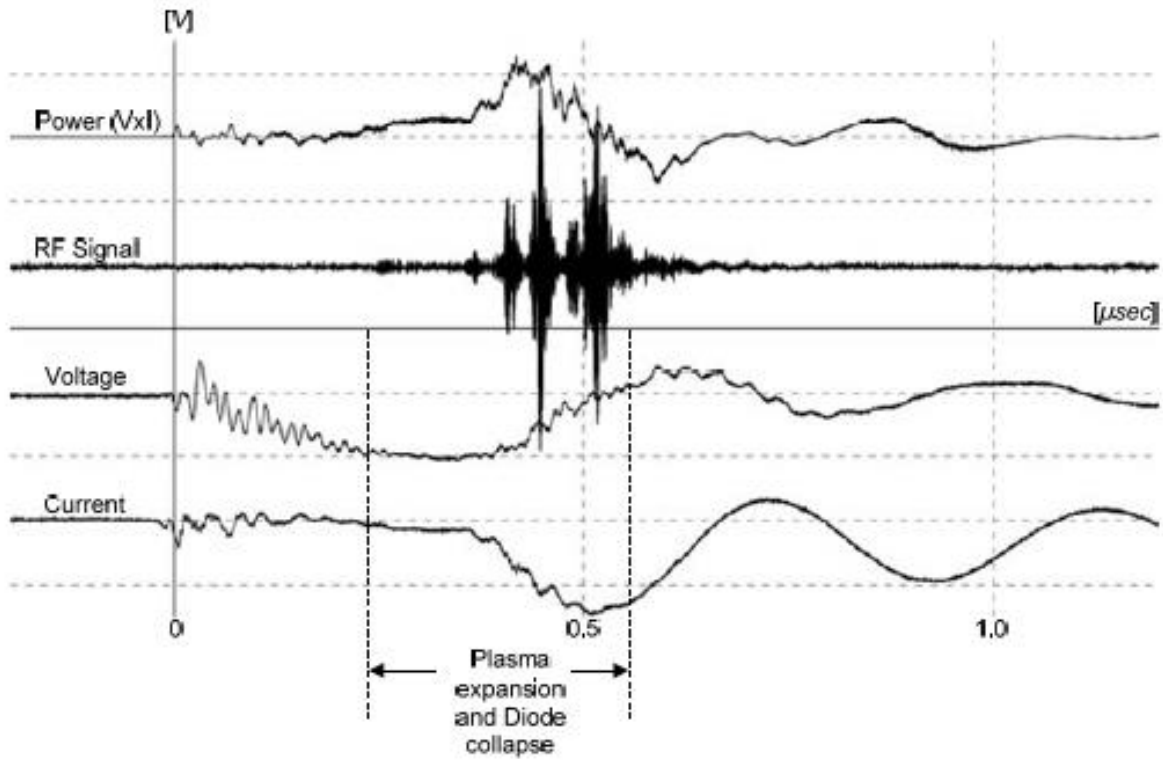

Fig. 6.58: The Descent pin, dAK = 25mm, mesh no. '1' (measured 20080509m47): Vmax = 76kV, Imax = 1200A, RFmax = 15W, Pmax = 40MW.

The display time range of a specific test, Fig. 6.59, is interesting because microwave signals occur in two frequency ranges. The first and strongest signal is cleaner spectral content, localized from 1500MHz up to 1700MHz. The signal, which follows, has spectral content of the sensor until the 1700MHz 2000MHz.

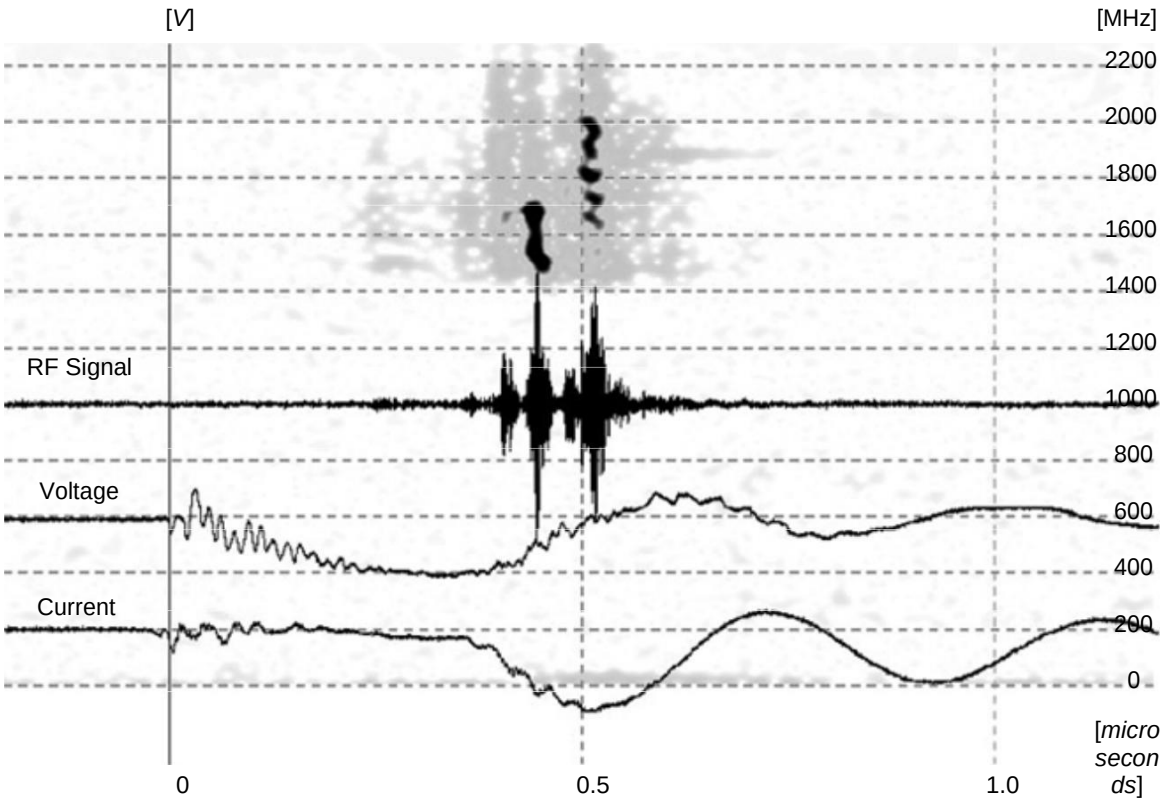

Fig. 6.59: The Descent pin, dAK = 25mm (20080509m47 measurement) Show time-range.

The change in resistance of the diode, Fig. 6.60, shows that the microwave solar irradiation displayed strong resistance values below 50 ohm.

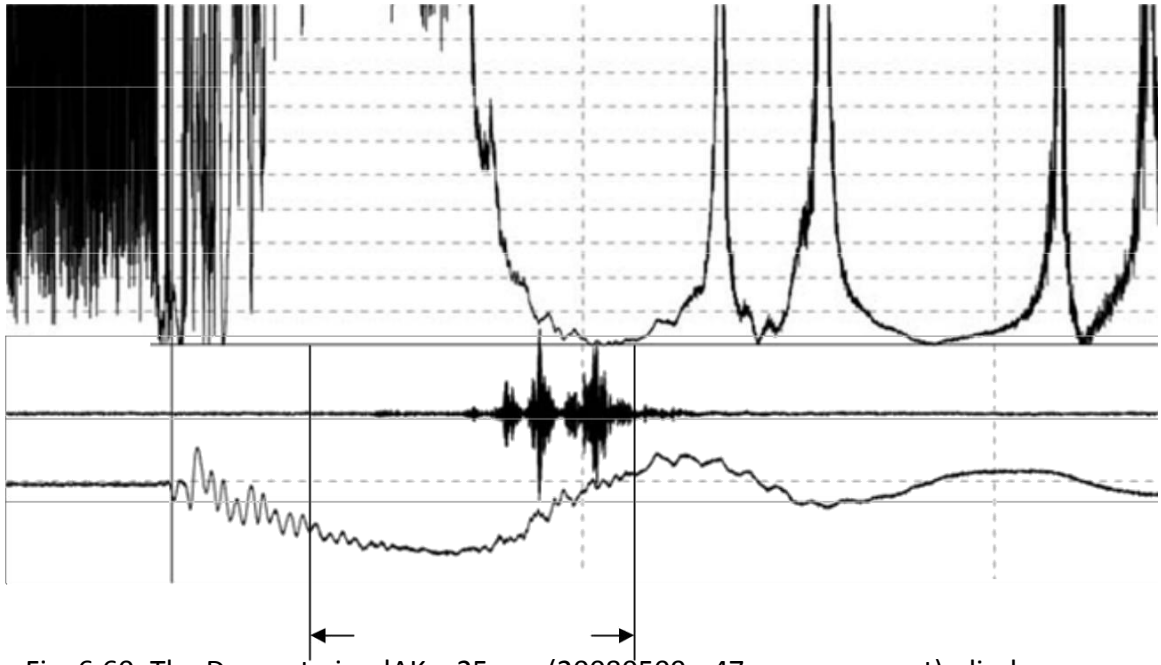

Fig. 6.60: The Descent pin, dAK = 25mm (20080509m47 measurement): diode impedance.

Case (64kV, 660A, 21MW, 3cm / microseconds)

The following test, which was obtained by the spike and matrix "3" is a char- raktiristiki case of very slow collapse of the gap. The passage in this case lasts "life" on the 800nsec, from which we calculate a speed in- Lie plasma close to 3cm / microseconds. This configuration showed very regularly such lifetimes, which probably attributed to the smaller proportion freedom to the surface, relative to the matrix "1". The dense weave is perhaps best heat removal from the incident area of elec- tronic culvert. It of course, quite simply, this grid has been different but a Member or greater purity than previous. Since hydrogen and Y- dratmoi are critical for the behavior of the gap at the time of cleaving, the purity of the metal from such blends important. In this recording we notice a very smooth decrease in impedance of the gap and patient radiation, throughout this time. RF however gi- Neta important, when the resistance of the gap is between 50 and 20O with ko- currents dumping at 600A.

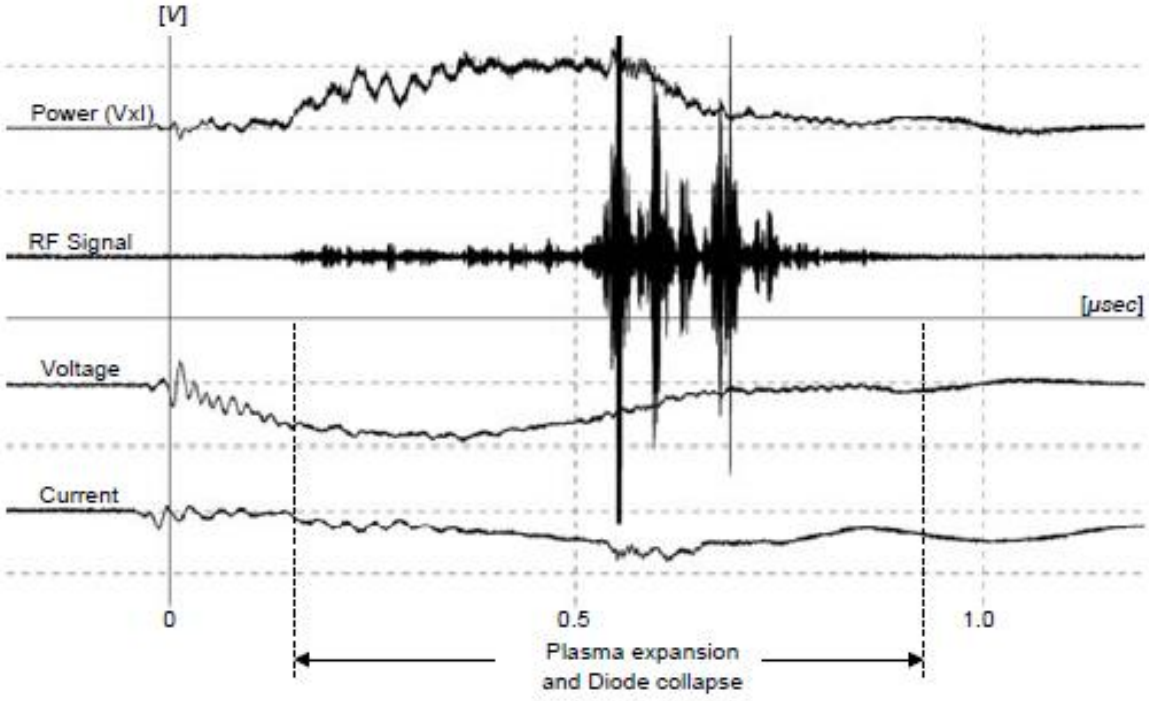

Fig. 6.61: The Descent pin, dAK = 25mm, grid Nov. «3» (20080514m19 measurement): Vmax = 64kV, Imax = 660A, RFmax = 12W, Pmax = 21MW.

While there is a high voltage in the gap and the current is about Asia Mi- Cro recorded weak high-frequency signals in the output. However, once the current CAM pera- some critical value and reaches 400A, shortly after the first 500nsec, the first strong signal appears. The time-range chart shows that the content of the raw signal is from 1600MHz up to 1800MHz, and followed by a second signal with frequencies around 1800MHz. As the phenomenon is completed, the storage costs less crocheted spectrum cohesion. Depicting the ratio measured voltage to current in the diode, we take very interesting diagram of Fig. 6.63. Resistance They are shown

live very smooth transition as the phenomenon progresses while proportionally stronger microwave irradiation occurs when the resistance of the diode is lower than 50 ohm.

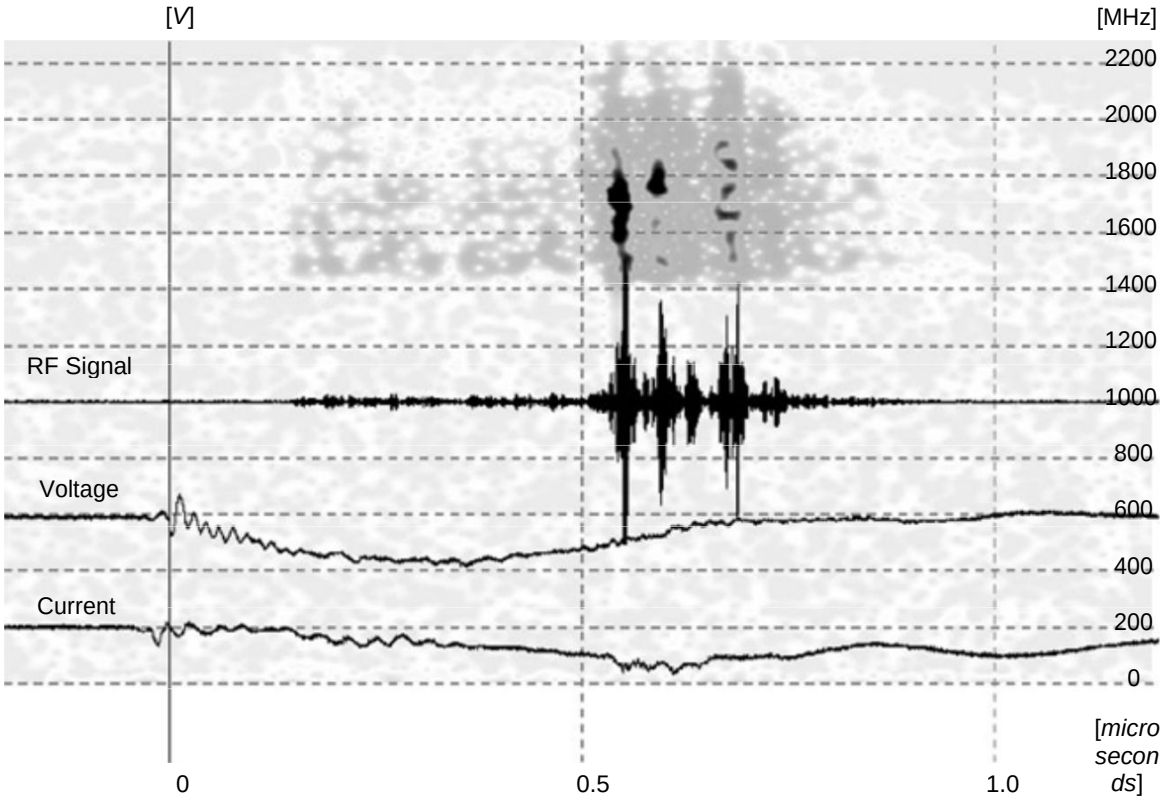

Fig. 6.62: The Descent pin, dAK = 25mm (20080514m19 measurement) Show time-range.

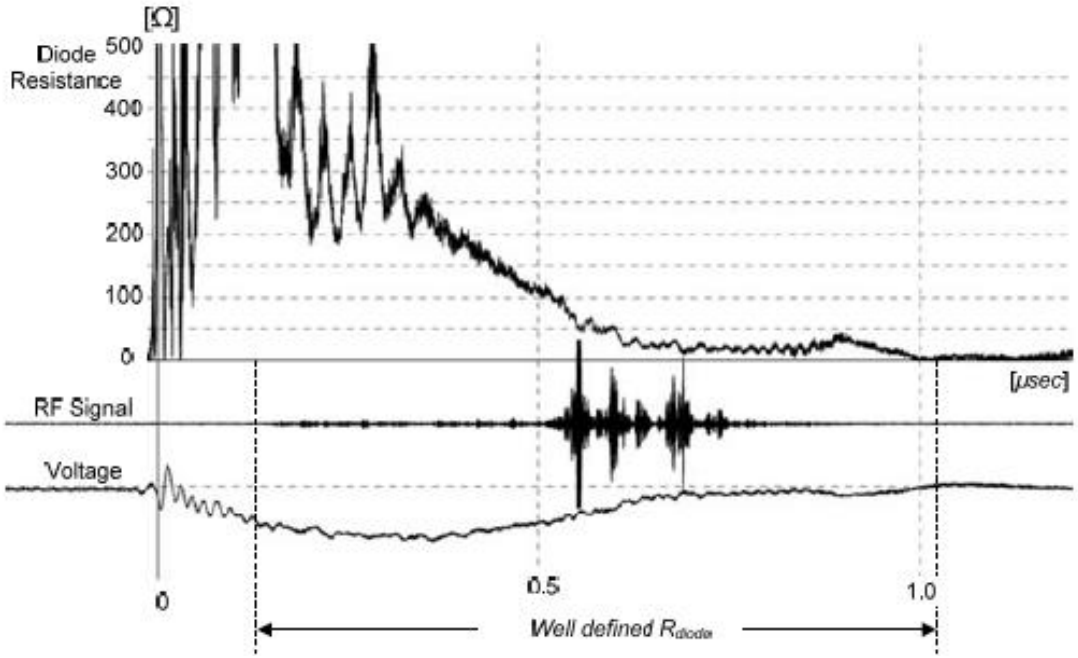

Fig. 6.63: The Descent pin, dAK = 25mm (20080514m19 measurement): diode impedance.

Case E (68kV, 700A, 28MW, 5cm / microseconds)

This record indicates one of the strongest microwave pulses for forming a pin diode cathode and grid number "6". The strength of the signal me- turkey is over 100W, and many weaker signals are on course 400nsec. The diode exhibits unstable behavior with the stream afxomeione- Tai during that pulse. The gap collapses in about 500nsec, giving a plasma spread speed of 5cm / microseconds. The powerful microwave signal D- appears when the resistance of the gap is 60O. From time spectrum diagram of Fig. 6.65, shows that the frequency content of the signal strength is between
1600MHz to 1800MHz.

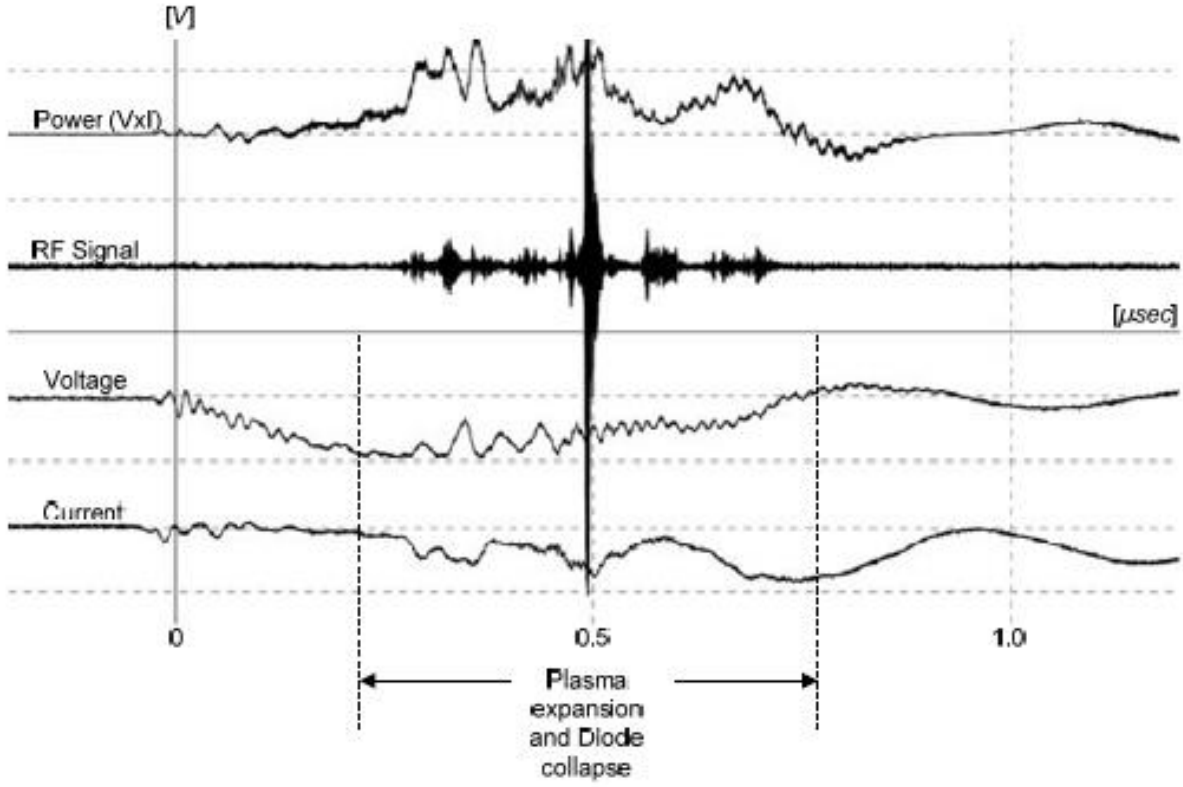

Fig. 6.64: The Descent pin, dAK = 25mm, grid Nov. «6» (20080610m51 measurement): Vmax = 68kV, Imax = 700A, RFmax = 105W, Pmax = 28MW.

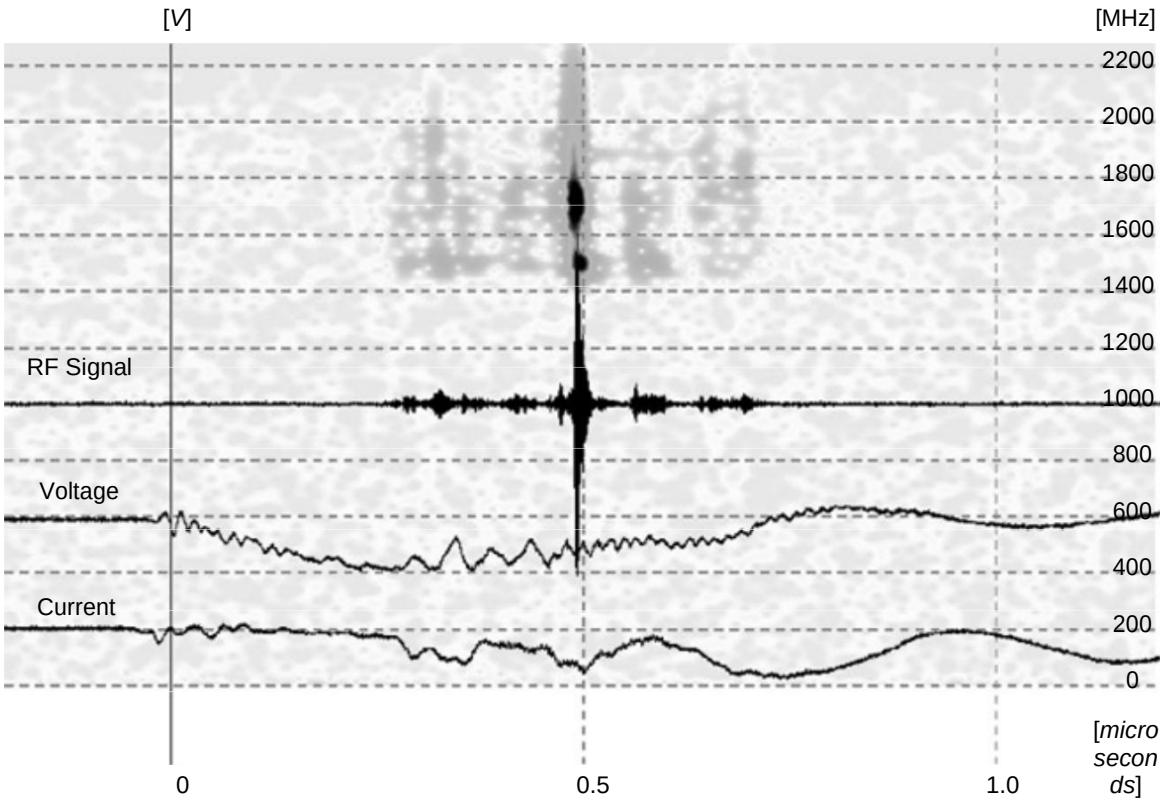

Fig. 6.65: The Descent pin, dAK = 25mm (20080610m51 measurement) Show time-range.

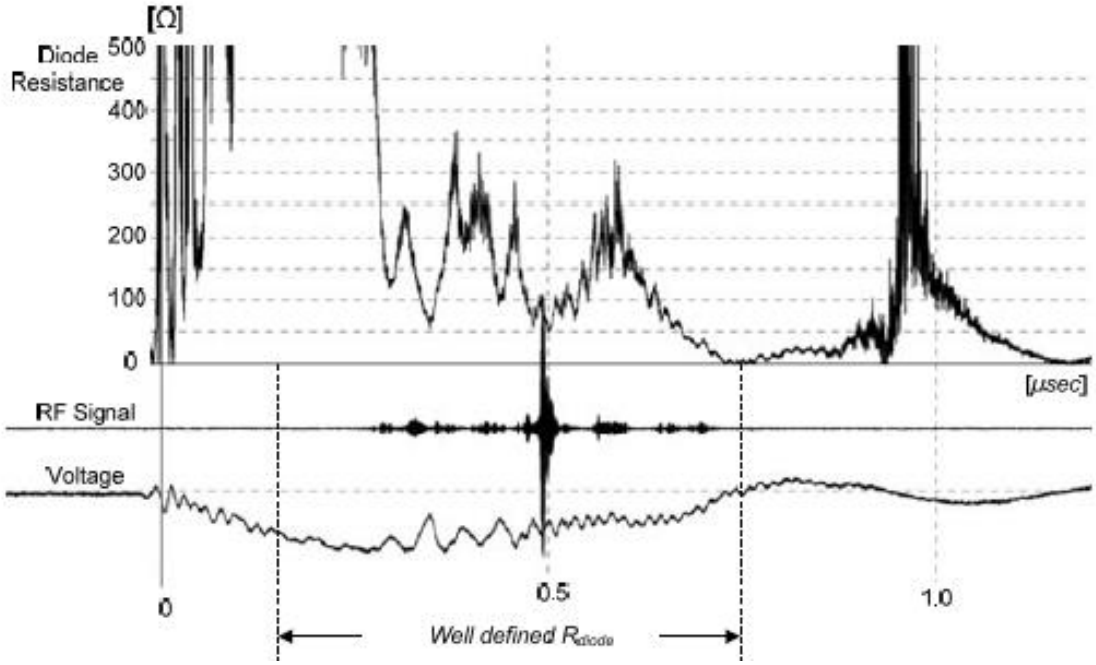

Fig. 6.66: The Descent pin, dAK = 25mm (20080610m51 measurement): diode impedance.

Case F (70kV, 1250A, 34MW, 8cm / microseconds)

In this recording we have one case of fast bridging the diode. The Asia Mi- krokymatiko signal is approximately 35W and diode collapses into 300nsec, which implies speed bridging over 8cm / microseconds. The stronger the microwave signal occurs when the apparent resistance of the gap is 70O.

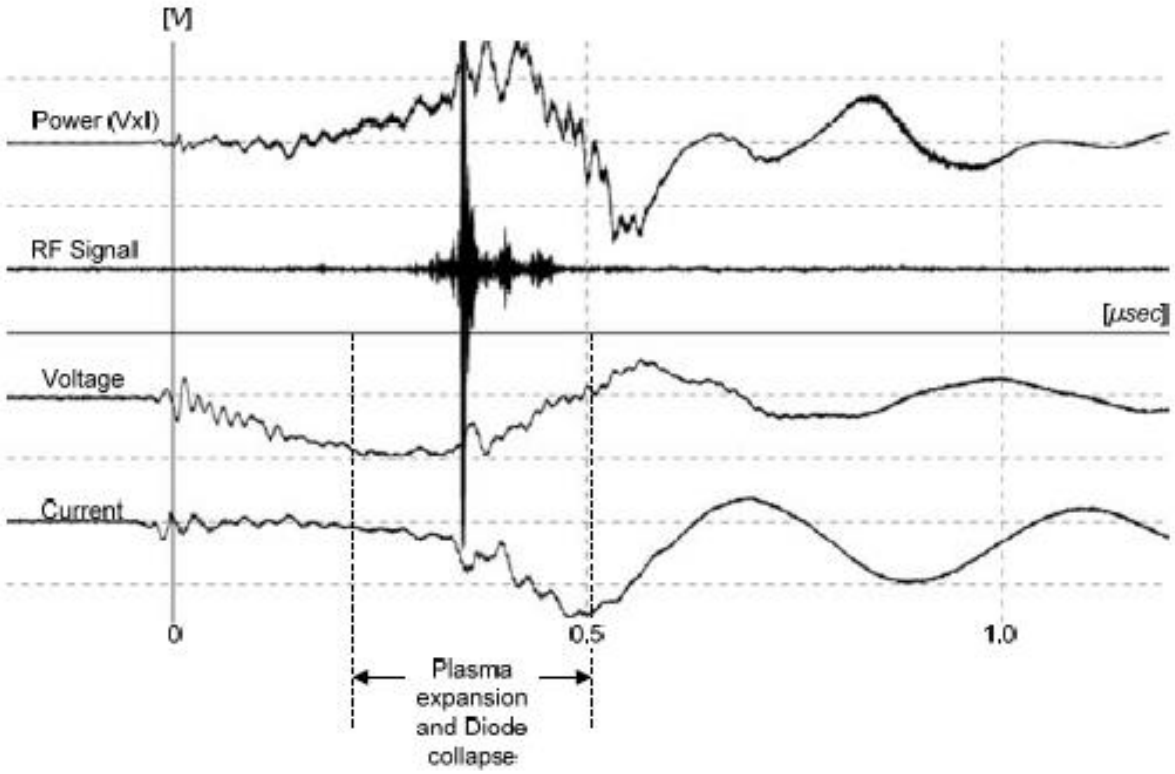

Fig. 6.67: The Descent pin, dAK = 25mm, grid Nov. «6» (20080611m49 measurement): Vmax = 70kV, Imax = 1250A, RFmax = 35W, Pmax = 34MW.

From time spectrum diagram of Fig. 6.68, it appears that the frequency periechome- only the strong signal is between 1500MHz to 1800MHz.

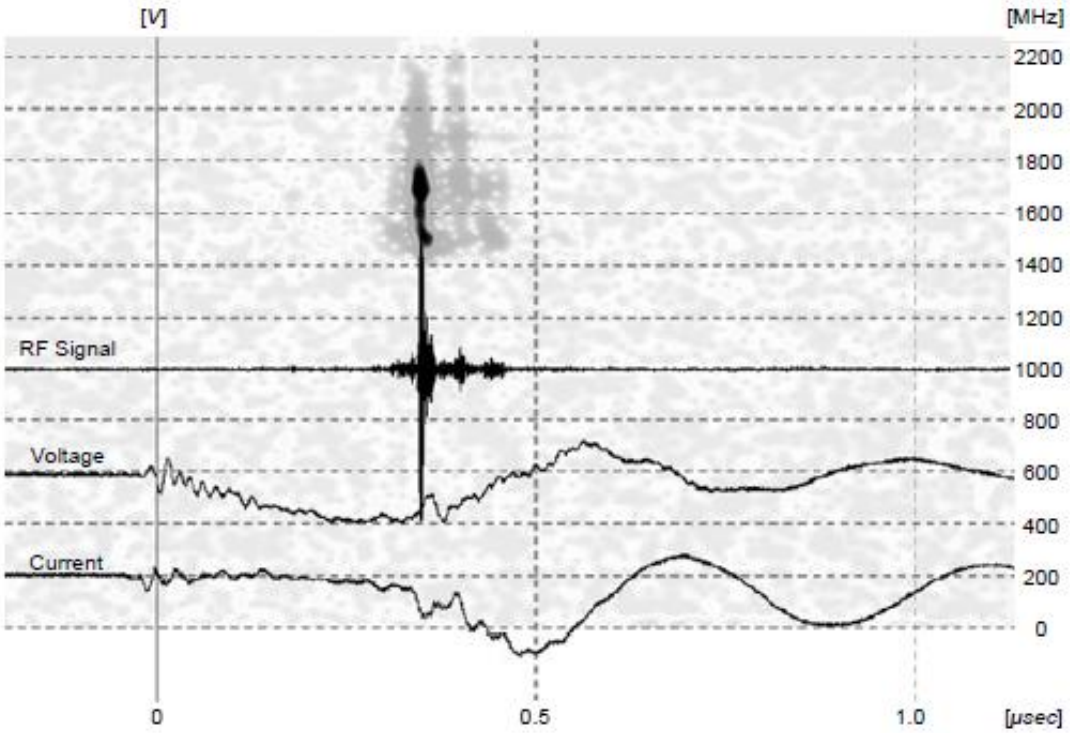

Fig. 6.68: The Descent pin, dAK = 25mm (20080611m49 measurement) Show time-range.

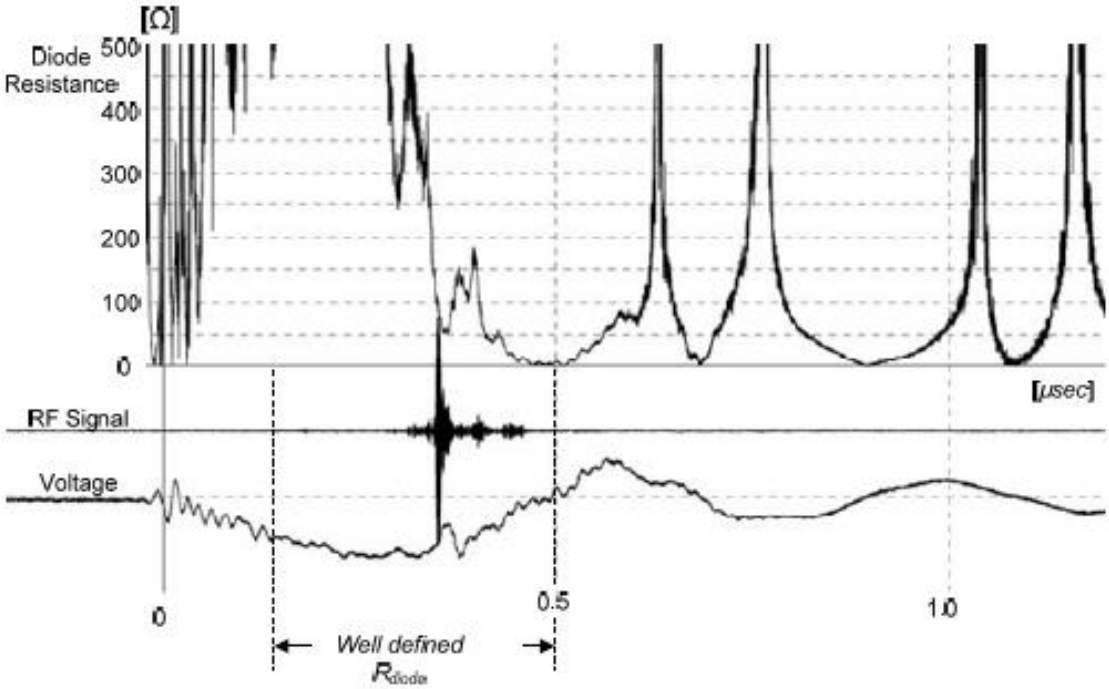

Fig. 6.69: The Descent pin, dAK = 25mm (20080611m49 measurement): diode impedance.

In the above cases, a gap should be from the time when the voltage stops rising in the prescribed rate and a current starts flowing in the passage, until a zero voltage and normalization of power. The sys-

conduct the pin-diode matrix in this case is the largest tychaioti-. The collapse phenomenon can last from 300nsec up 800nsec, with conse- quently, the spread velocity of plasma in the diode can be calculated between ~ 3 and ~ 8cm / microseconds. The case where the gap collapses speed 8cm / microseconds (see. Fig. 6.67) may be justified only by rapid plasma creation side upward period, resulting in a cumulative collapse of the passageway on both sides. The re- event of slow collapse of the gap (see. Especially Fig. 6.61 and Fig. 6.64) dikaiologei- Tai, assuming plasma derived mainly from the cathode to the anode not sys- ucts to bridge the gap.

If the pin with dAK = 25mm have more cases smooth representatives charge diode, the current is not switched to oscillatory behavior. The slow collapse of the gap seems to provide scope in the capacitive divider discharged smoothly through the passage of the Vircator. After the closing of the passage of plasma, the arc is fed by the residual charge of capacitor cargo tisis through front resistance *RF*.

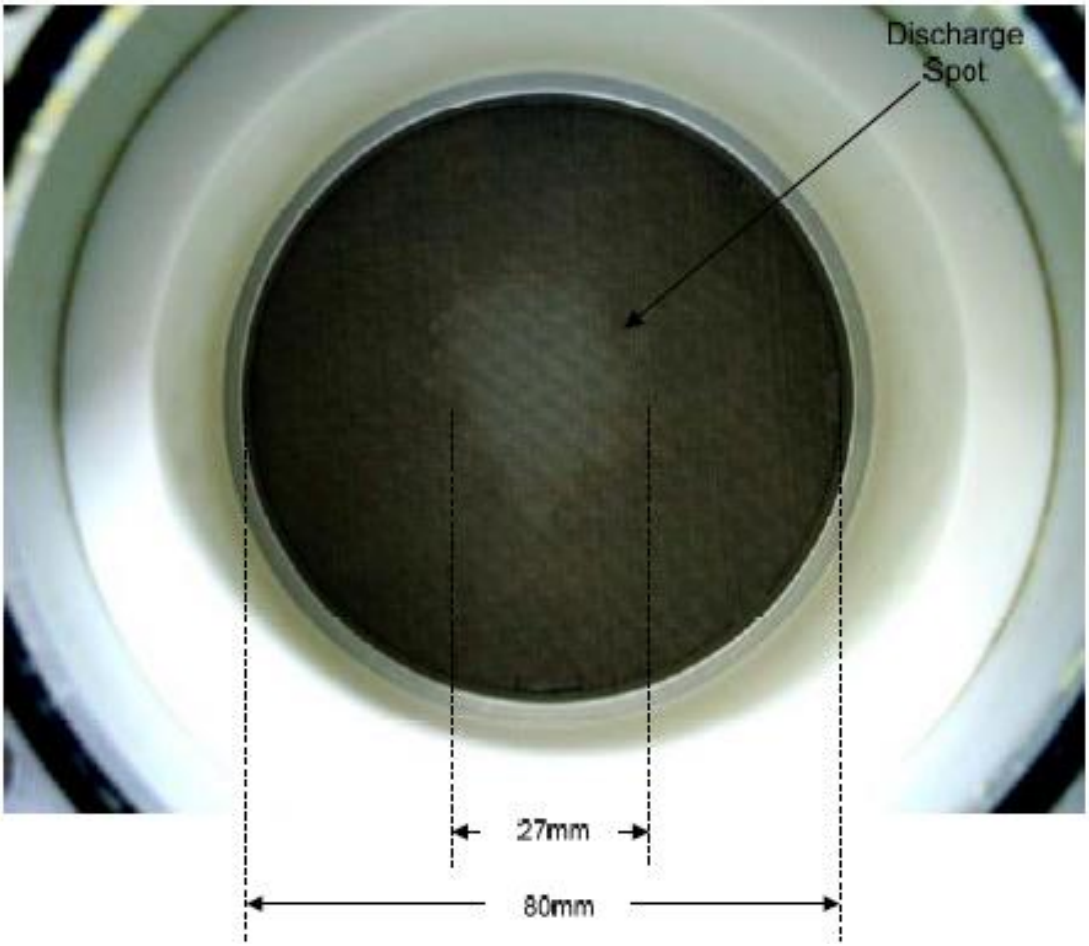

Fig. 6.70: Trace the rise, after ~ 200 impacts. Descent pin, dAK = 25mm.

6.3.5. Ductile Descent with Fabric (d = 15mm)

In order to achieve an increase of the surface of the cathode and total liquidity Matos, tested geometry of the spheroid terminal, fabric-covered, here velor (velvet). The use of cloth is a traditional technique for

increase rheumatoid density emitting a cathode. The fibers of the fabric are points on which the pediakis intensity factor is strongest Tattoo. The large surface area decreases the resistance of the gap as the re- tarrefsi progresses, resulting in higher drive currents. With respect to the cathode aki- same distance Group, cathode fabric showed a higher breakdown voltage, al- Milled similar current and power. The mesh used is the number "1". Comprised 30 holes per inch, with an opening hole 0.587mm, 0.26mm diameter wire and free surface ~ 48% and proven to provide the best governed tation in electronic culvert and virtual cathode formation, as shown by ded from the pin cathode (see. par. 6.3.4). The configuration of the passageway shown in Fig. 6.71. Pin stainless steel dressed fabric (velvet), which was stretched in good surface and glued to the neck of the terminal insulating film.

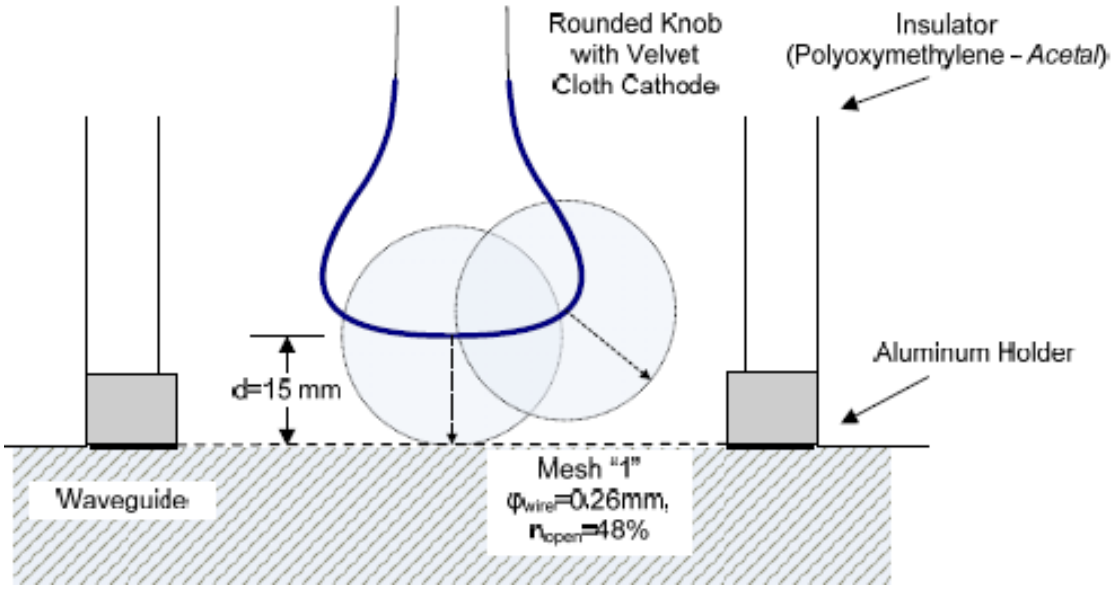

Fig. 6.71: cathode diode configuration covered with fabric and dAK = 15mm.

Based on the nomogram of Fig. 5.20, the maximum diameter of the cathode for a distance 15mm from the anode is about 50mm. Since the diameter of the probe so EI- 42mm, we can safely say that the drain of electrons injected into the grid anode rather than the mesh support hoop.

6.3.5.1. Macroscopic Experimental Sizes

The following tables lists the recorded peak voltages, current and power in the passage for at least ten (10) iterations, a charging pri- tefontos of 50, 75 and 100V AC. According to what has been stated in paragraphs 5.5 and 6.3.2, the loads they give impulse *0.6 / 50*With maximum widths 52, 78 and 104kV. The voltage, current and power of the diode are given as mean and the calculated dispersion *p*the recorded maximum, in any state of charge, with semiotics $\langle X \rangle \pm 1 \cdot sx$.

In early tests, the passage presented to withstand the impulse voltage of 52kV (BRAKE night charging primary 50V AC), but this changed in the coming days. Passageway E- PAPSE withstand voltage of 52kV, probably due to local destruction yfasma- Tos, causing change in the properties of the gap.

Tab. 6.16: Descent with Fabric dAK = 15mm, Mesh "1" (Measurements 09/04/2008)

Load	50V AC	75V AC	100V AC
Max Surge	(No decay)	~ 78kV	~ 104kV
Current Ion Pump	0.21mA	0.21 ~ 0.36mA	0.22 ~ 0.35mA
Lifting	×	6 ~ 8mA	8.5 ~ 9.5mA
Voltage typical	×	59.7 ± 1.2kV	62.3 ± 2.4kV
Typical Power	×	650 ± 32A	891 ± 47A
Power typical	×	20.6 ± 0.9MW	28.9 ± 2.4MW
RF typical	×	**0.3 ~ 1W**	**2 ~ 6W**
Efficiency typical	×	10-8 ~ 10-7	9 · 10-8 ~**3 · 10-7**
RF max recorded	×	**3W**	**8W**

Tab. 6.17: Descent with Fabric dAK = 15mm, Mesh "1" (Measurements 10-04-2008)

Load	50V AC	75V AC	100V AC
Max Surge	~ 52kV	~ 78kV	~ 104kV
Current Ion Pump	0.21 ~ 0.29mA	0.25 ~ 0.30mA	0.31 ~ 0.37mA
Lifting	3 ~ 4mA	5.2 ~ 7.2mA	8 ~ 9.1mA
Voltage typical	48.5 ± 2.5kV	56.2 ± 1.9kV	64.8 ± 1.7kV
Typical Power	307 ± 29A	653 ± 87A	944 ± 59A
Power typical	5.6 ± 1.4MW	17.8 ± 2.5MW	30.0 ± 1.4MW
RF typical	**0.1 ~ 0.4W**	**0.5 ~ 5W**	**0.5 ~ 6W**
Efficiency typical	10-8 ~ 3 · 10-7	10-8 ~ 3 · 10-7	2 · 10-8 ~**4 · 10-7**
RF max recorded	**4W**	**7W**	**12W**

H estimated pressure in the passage area is as current of Ion Pump in mA at the moment before impact, multiplied by 10-4 Torr (see. par. 6.1). Therefore the 0.2mA corresponding to 2 · 10-5Torr. The current of the ionization pump the moment of impact rises rapidly (within approximately 0.5sec) over an order of magnitude. Longer impulse voltage causes greater surge current of ionization pump. The gassing seems to be lower during the second day of tests. On the first day of me- measurement, the gap presented to the impulse withstand voltage of 52kV, which is why we have two points on the first day measurements.

H Descent with fabric and dAK = 15mm showed weak microwave output, which in no way approached the figures showed the spike in the same distance from the anode. The trend in the passage is greater than the measurements to pin. This is very reasonable because the visual smoothness of the cathode creates narrower passageway. Furthermore the fabric may function as electrical shielding to a certain extent. Only locally, the fibers of the fabric, developed release centers plasma- Tos (cathode spots), but which spread with maximum speeds as hydrogen, about 3cm / microseconds. Also, it is very likely driving the diode with relatively "small" impulse voltages of 100kV not be sufficient to launch an impres-

sive effect collapse of the passageway to create a plurality of small pockets of intense electronic emission surface of the fabric. Also, the fact that, in the coming days, splitting the diode was the low impulse voltage of 50kV indicates that some local fabric disaster resulted in lower electrical resistance of the device.

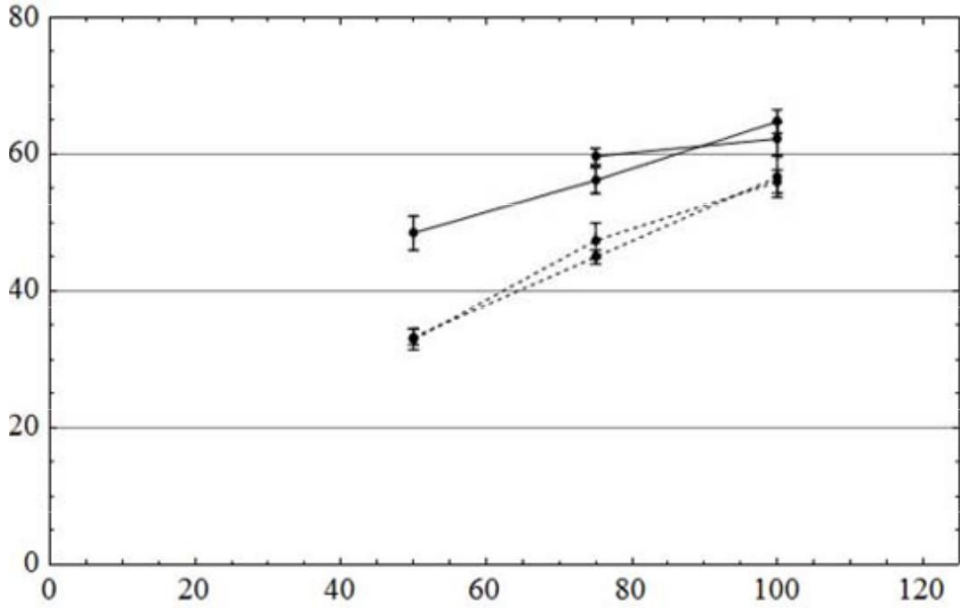

Fig. 6.72: Maximum voltage diode. Descent with fabric, (solid lines), the pin cathode (dotted lines). Grid no. "1" dAK = 15mm.

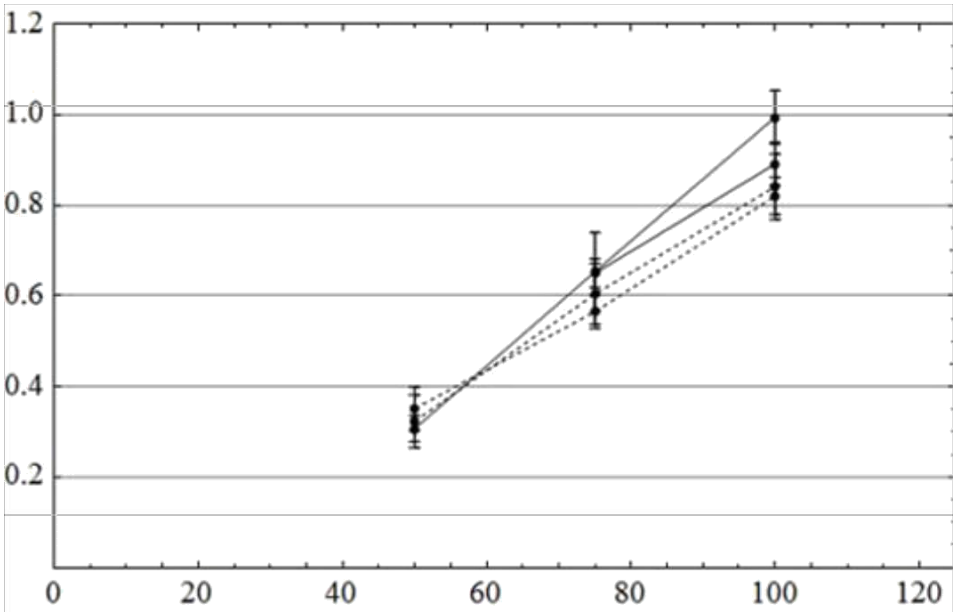

Fig. 6.73: Maximum diode current. Descent with fabric, (solid lines), the pin cathode (dotted lines). Grid no. "1" dAK = 15mm.

The currents in the passageway with the fabric correspond to the currents that are observed in the passage of the cathode tip to the same distance. This forces us to sys-

conclusion that only a point (spot) of the surface of the spheroid terminal emits electrons from the cathode. Therefore, the macroscopic behavior of the stream of con- Methods are almost like the pin cathode. We come to the same conclusion and the average price of power displayed on passage Vircator, with this configuration, as shown by the following chart.

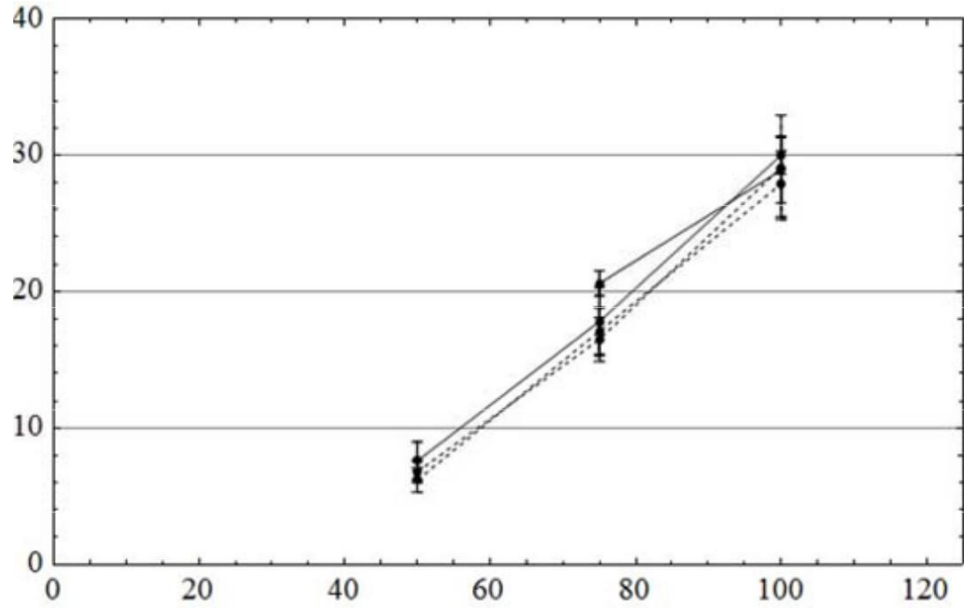

Fig. 6.74: Maximum power diode. Descent with fabric, (solid lines), the pin cathode (dotted lines). Grid no. "1" dAK = 15mm.

6.3.5.2. Model Discharge Capacity by Diode

The cathode material, although the electrode surface is signifi- cantly larger displays currents depending on the cathode tip. This probably goes Contracting because the plasma release region is the entire surface of the Tl of the cathode facing the anode, but a small spot, from which starts the electronic culvert. The collapse voltage, current and power of the gap filler is para where the cathode tip and the cathode spheroids. If the cathode is produced by explosive emission of electrons across the surface, we would find a faster collapse of the voltage in the gap. Therefore, we are illustrated sumo two solutions, one with "radius" electron emission equal to 2mm, and a cathode having a radius equal to 10mm, since the diameter of the probe is 42mm. In the first case, the evacuation theory comes from a single spot on the surface, while in the second case, the electronic transmission becomes greater area. In the first case, a cleavage surface involves small gas production and therefore short plasma spread speed (even u= 5cm / microseconds), while in the second case, large amounts of power mean higher plasma speeds (even u= 8cm / microseconds). With these assumptions fill the remaining figures monte- Lou: k= 2.33 · 10-6A / V3 / 2, distance reinforcement d= 0.015m, geometric permeability plexus Tosh anode n= 48% initial voltage capacitor $V(0)=V0$= 65kV, capacitor capacity

C= 1.2nF. The discharge capacitor visa through the diode lamp is developed in Fri 4.3.6 and in para. 6.3.3.2.

The first discharge event illustrated in Fig. 6.75. The diode is bridged in 300nsec (typical observed half) with a maximum current of 800A and a maximum power ~ 25MW. Once we find the dependence of the voltage in the gap, we can extract the energy of the electron beam and the area of which is set equal to the phenomenon ap- vadon descent. Of these quantities by the permeability of the matrix of alpha nodou, we can calculate the diode current required to trofodotei- Tai kymatodigiki the cavity with critical peak beam current. This current notarial lizetai the dotted line. The passageway leads to more current than is necessary after the first 150nsec. From that moment onwards we can predict what will import so the expected output frequencies Vircator, based on the theoretical models of the literature.

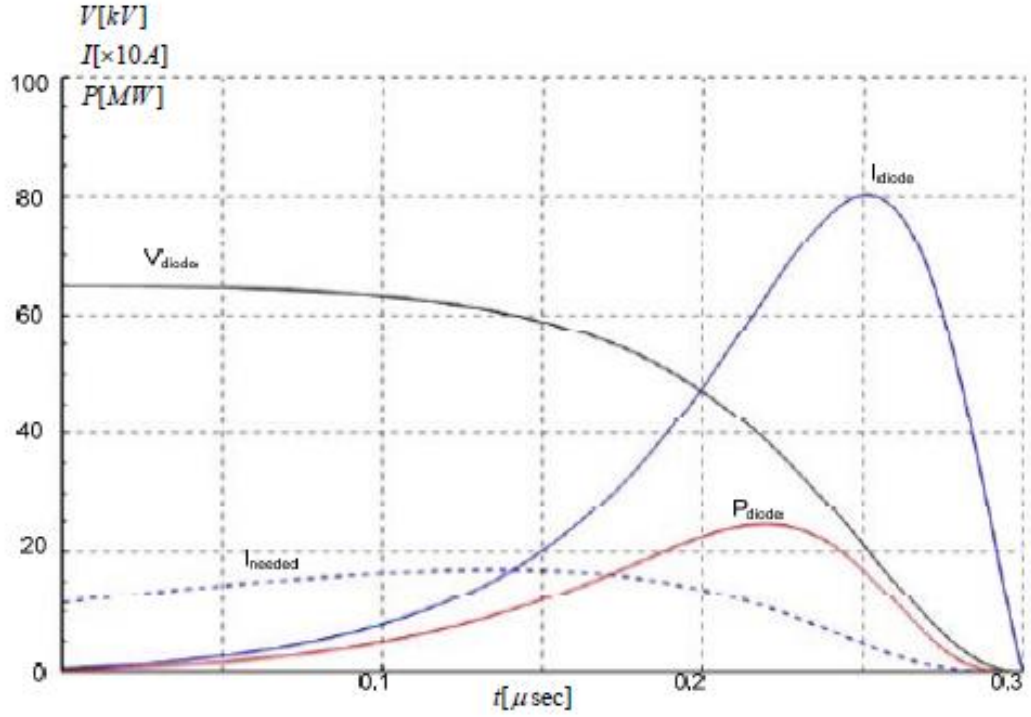

Fig. 6.75: Theoretical variation of voltage, current and power at the cathode with fabric and dAK = 15mm, for drive voltage 65kV, capacity capacitor 1.2nF, speed katarref- ing gap 5cm / microseconds (the case of short-emitting surface).

The frequency of oscillation of the virtual cathode, according to what are referred brought in par. 4.1.2, is between the values *fp* and (2n) 1/2*fp*. In Fig. 6.76 Read off: the area defined by frequencies *fp* and (2n) 1/2*fp*The two estimates sys-
frequencies reflexing, non-relativistic and relativistic, as described in par. 4.1.1. Finally made and the assessment of Woo, on. (4.16) for the output frequency of a Vircator. After the first 150nsec, when the diode leads necessary currents ap- emergence of virtual cathode, the output frequencies seem to have spent the 2GHz, which is the observation area.

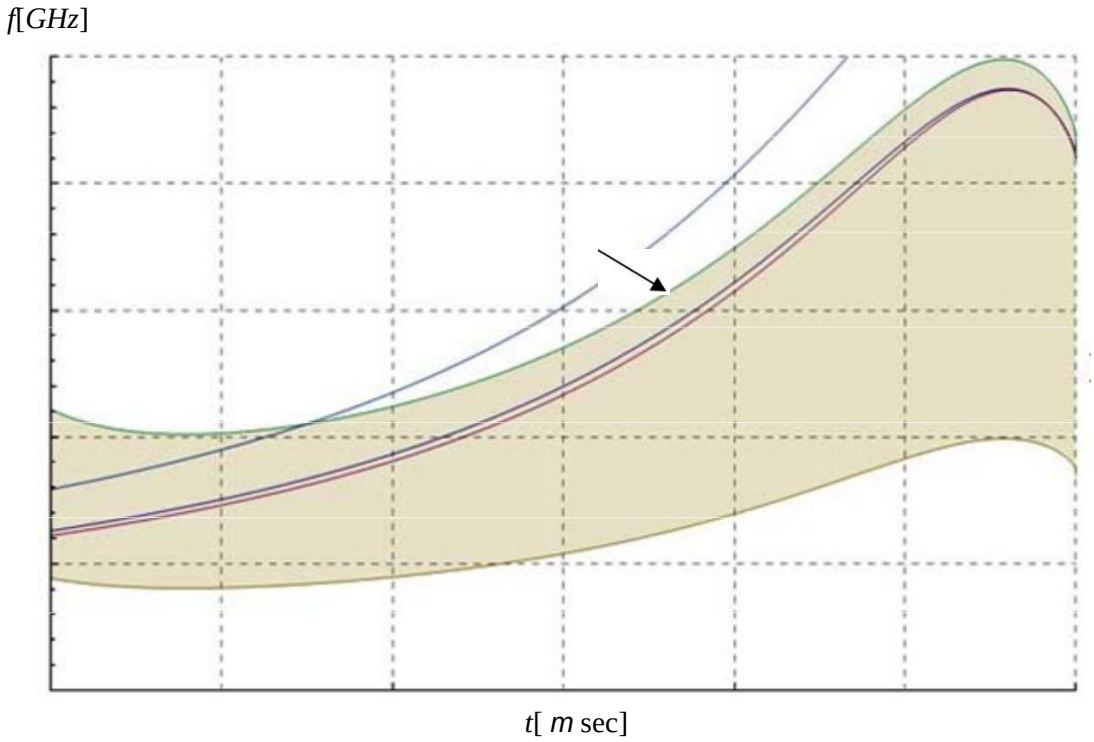

Fig. 6.76: Output frequency Assessments Vircator with descent with fabric and dAK = 15mm, for discharge voltage 65kV, capacitor 1.2nF, with spacing collapse speed 5cm / microseconds (the case of short-emitting surface).

The second case discharge shown in Fig. 6.77. The diode is bridged at ~ 200nsec (theoretical time), with a maximum current of 850A and a maximum power ~ 30MW. Having found the dependence of the voltage in the gap, we can draw the energy for the electronic beam and the area of which is set equal to the apparent area of the cathode. Of those sizes and the permeability of the anode grid, can we calculate the diode current required to feed the kyma- todigiki cavity with critical peak beam current. This stream is denoted by the dotted line. The passageway leads to more current than necessary already after the first 50nsec. From this moment on, we can see what will be referred menomenes frequencies output Vircator, based on theoretical prediction models.

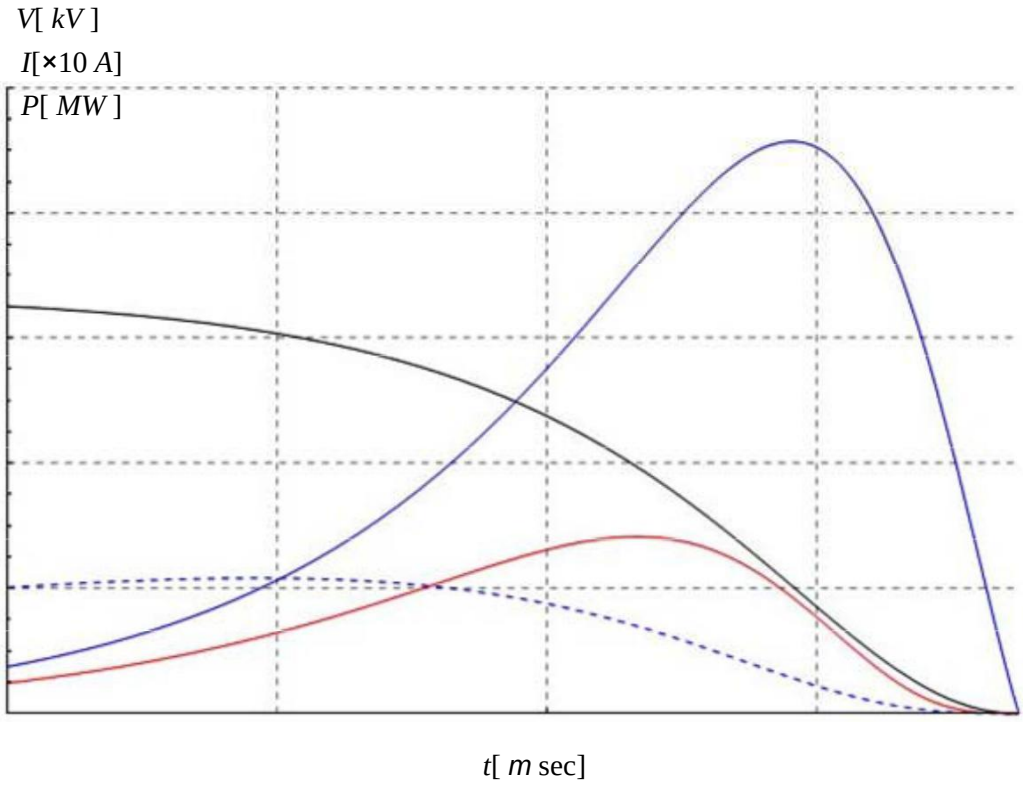

Fig. 6.77: Theoretical variation of voltage, current and power at the cathode with fabric and dAK = 15mm, for drive voltage 65kV, capacity capacitor 1.2nF, speed katarref- ing gap 8cm / microseconds (case of a large emission surface).

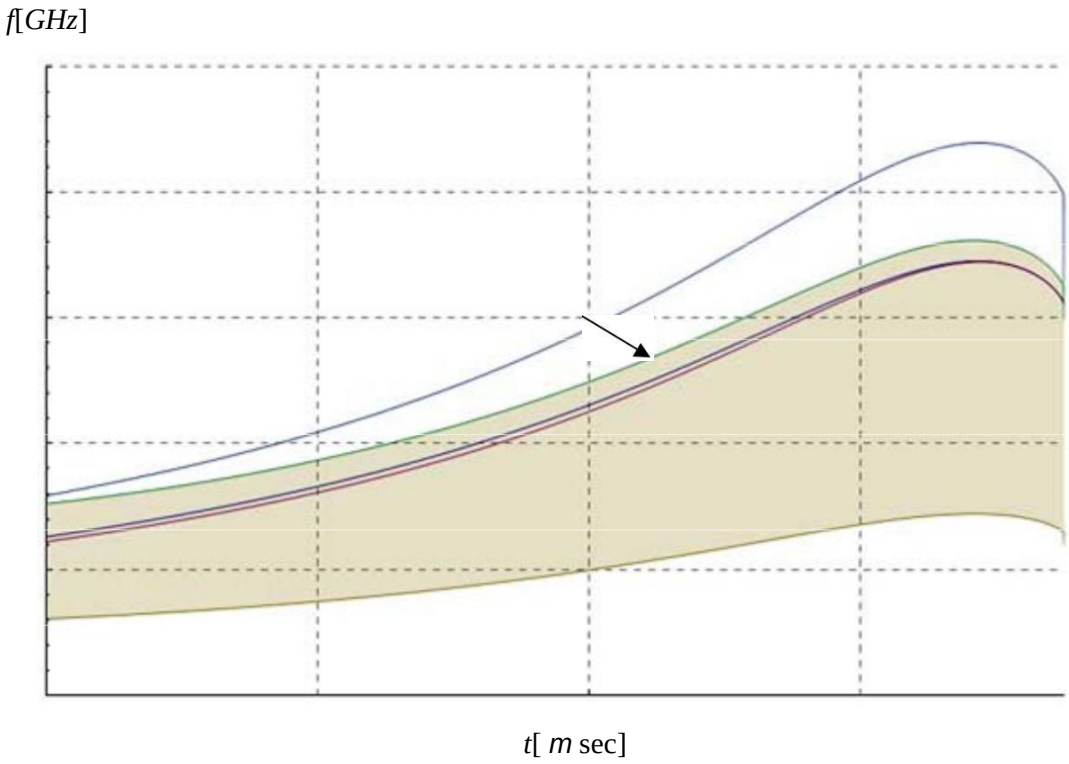

Fig. 6.78: Output frequency Assessments Vircator with descent with fabric and dAK = 15mm, for discharge voltage 65kV, capacitor 1.2nF, with spacing collapse speed 8cm / microseconds (case of a large emission surface).

The high electron emission from the cathode surface with cloth has as a result the passage manages too early to provide high currents in the gap and therefore the inert space kymatodigikis cavity. Taking 50nsec as threshold display the virtual cathode, the output frequencies from this point onwards can be estimated from the diagram in Fig. 6.78. We note that there has time window, during which the reflex frequencies and plasma to pass through the region 1.8GHz to 2GHz, which in theory helps to have optimum exit waveguide Vircator.

6.3.5.3. Typical measurements

Case A (58kV, 890A, 23MW, 5cm / msec)

H subsequent recording is a typical impact with a particular configuration. The repeatability of experiments is very good, for each day conducted the experiment. The microwave power is small, the diode current is around 900A, while the collapse of the gap takes approximately 300nsec. The graph offering of power in the gap is very smooth, while the surrounding microwave vriske- Tai very well localized in space, where there is strength in the gap. The next resistance phenomena diode follows omalotati decline by law-like quadratic time dependence. From this observation we assume that the plasma generated, shows no significant radial expansion and is heading to climb steadily. The microwave power occurs when the resistance of the gap is below 100O and maximized when done 30 ~ 40O. These figures are production fillers with observations made in the configurations of diode with pos- cathode pin.

H time spectrum display, Fig. 6.80, showing range extending the range of 1600MHz to 2GHz. The predictions from the models for that night stood as shown in the diagram of Fig. 6.76 and Fig. 6.78, showing that the specific loop-through output may be due to vibrations of the virtual cathode, with frequencies close to the plasma frequency.

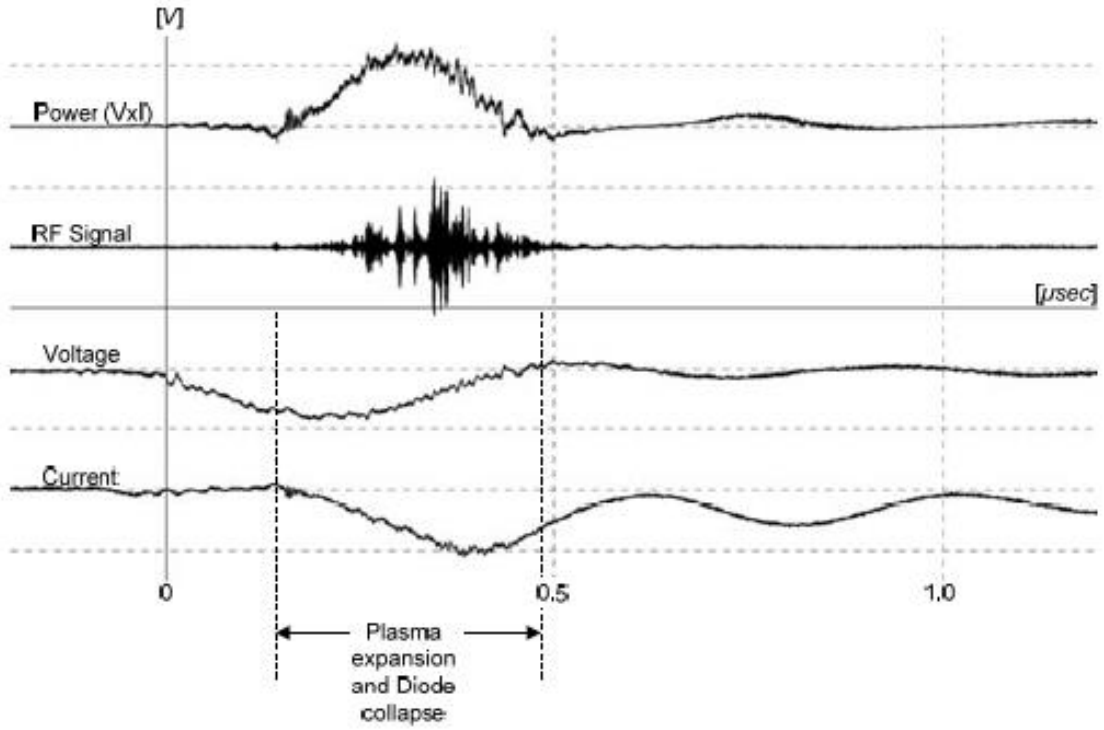

Fig. 6.79: The Descent fabric, dAK = 15mm, mesh no. '1' (measured 20080409m43): Vmax = 58kV, Imax = 890A, RFmax = 3W, Pmax = 23MW.

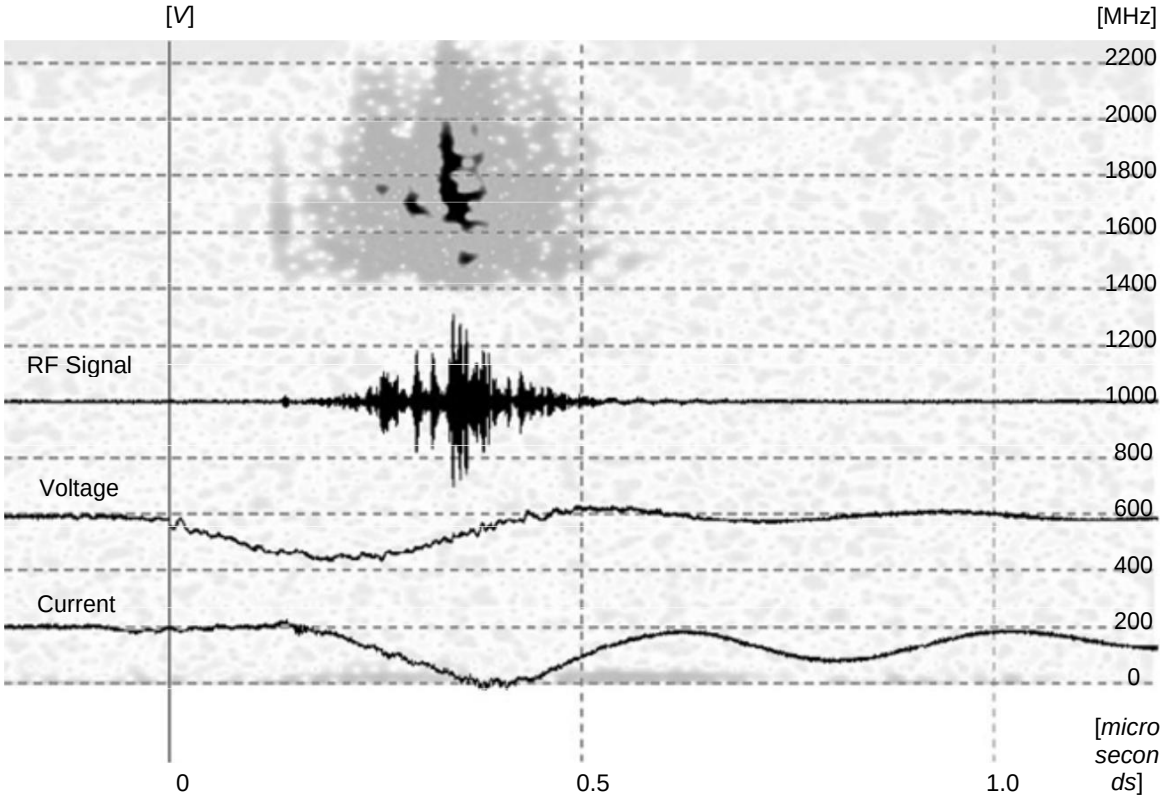

Fig. 6.80: The Descent fabric, dAK = 15mm (measurement 20080409m43): time-imaging spectrum.

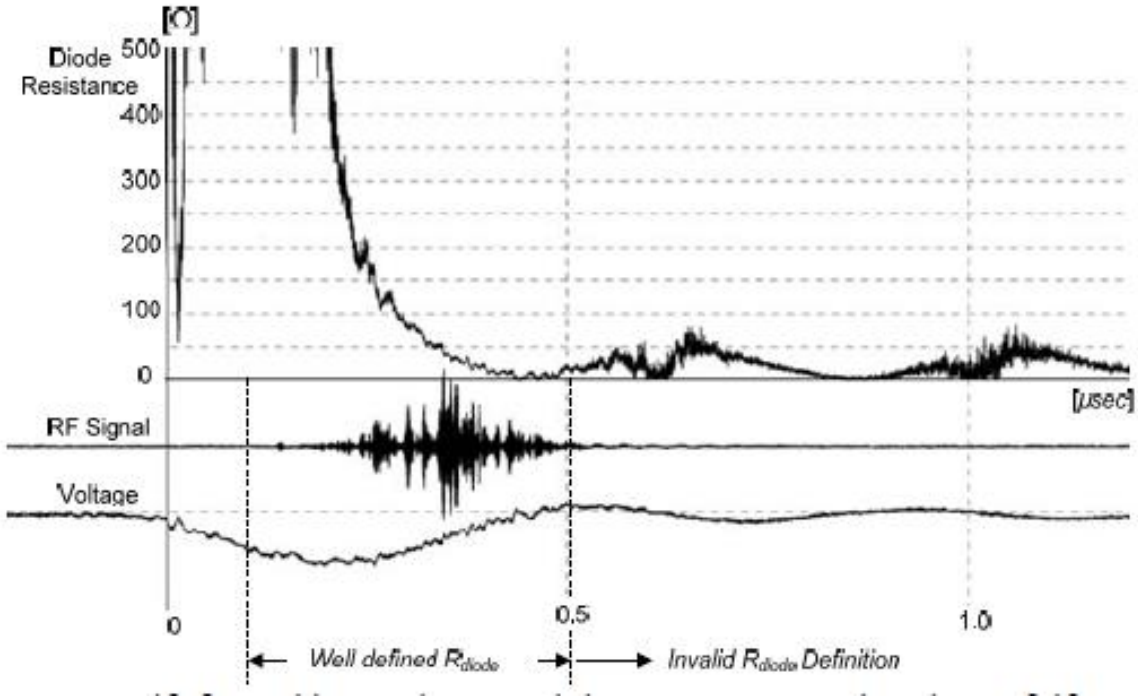

Fig. 6.81: The Descent fabric, dAK = 15mm (measurement 20080409m43): diode impedance.

Case B (64kV, 950A, 31MW, 5cm / msec)

H This test gave one of the greatest strengths, recorded from the cathode with fabric. The power of the microwave signal is approximately 10W, the observation bandwidth. The diode is bridged to 300nsec, and the waveforms are in this case very smooth. At the time of initiation of the collapse is observed an abnormal behavior and a microwave signal is not interpretation, re- Athos stream has not yet begun to receive significant value. This mark may be random interference, observing, moreover, that something happens in the channel voltage and current later. The typical microwave signal from the virtual cathode is detected when the resistance of the gap is below 100O and megistopoiei- Tai, when the resistance of the gap is approximately 30O.

H time spectrum display, Fig. 6.83, showing range extending the range of 1450MHz to 1800MHz. The predictions from the models for this shaping, as shown in the diagram of Fig. 6.76 and Fig. 6.78, showing that the sys- gkekrimeni output may be due to vibrations of the virtual cathode, with frequencies close to the plasma frequency.

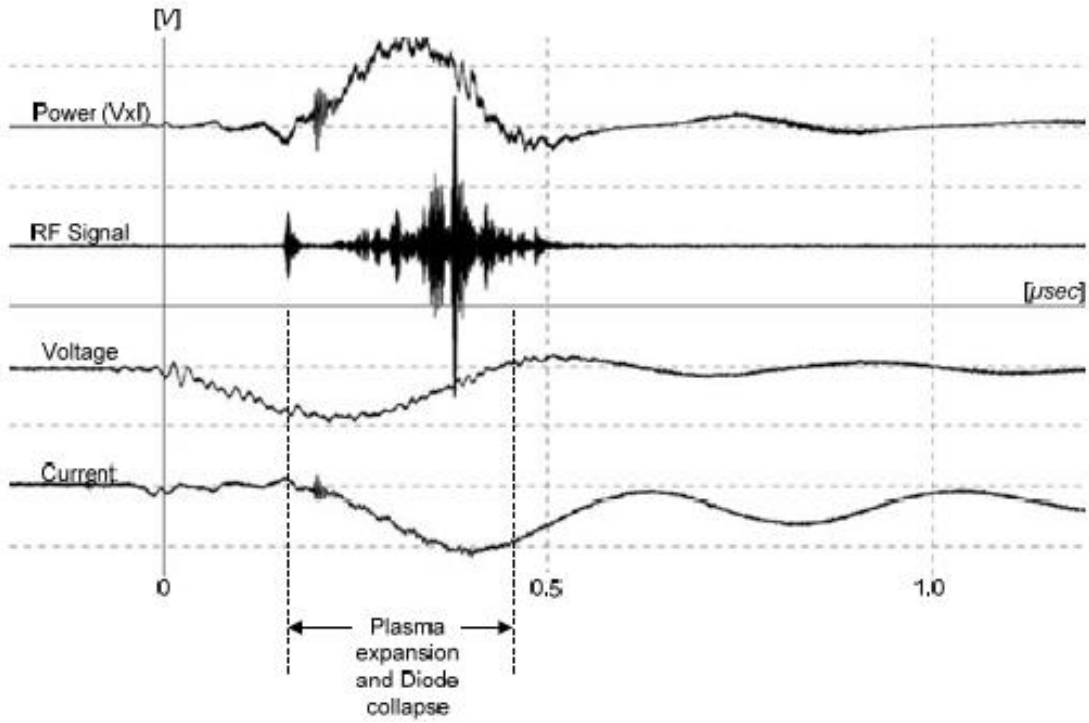

Fig. 6.82: The Descent fabric, dAK = 15mm, mesh no. '1' (measured 20080410m45): Vmax = 64kV, Imax = 950A, RFmax = 12W, Pmax = 31MW.

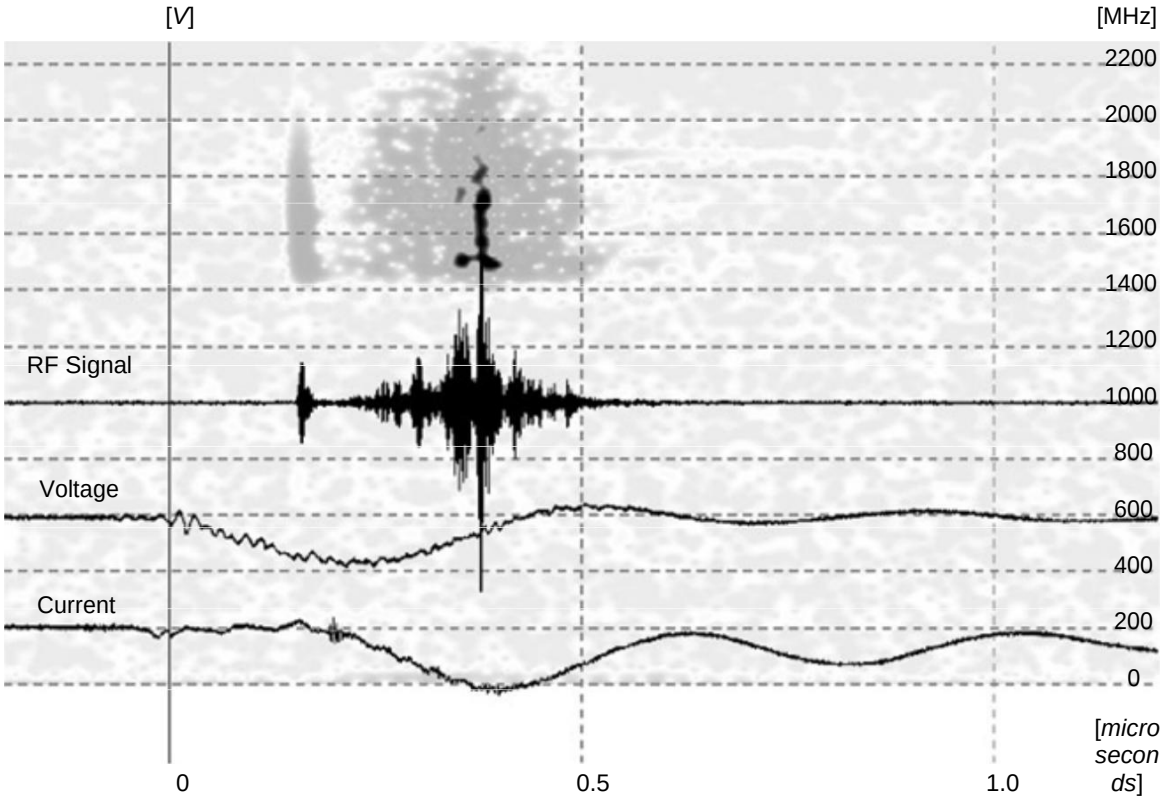

Fig. 6.83: The Descent fabric, dAK = 15mm (measurement 20080410m45): time-imaging spectrum.

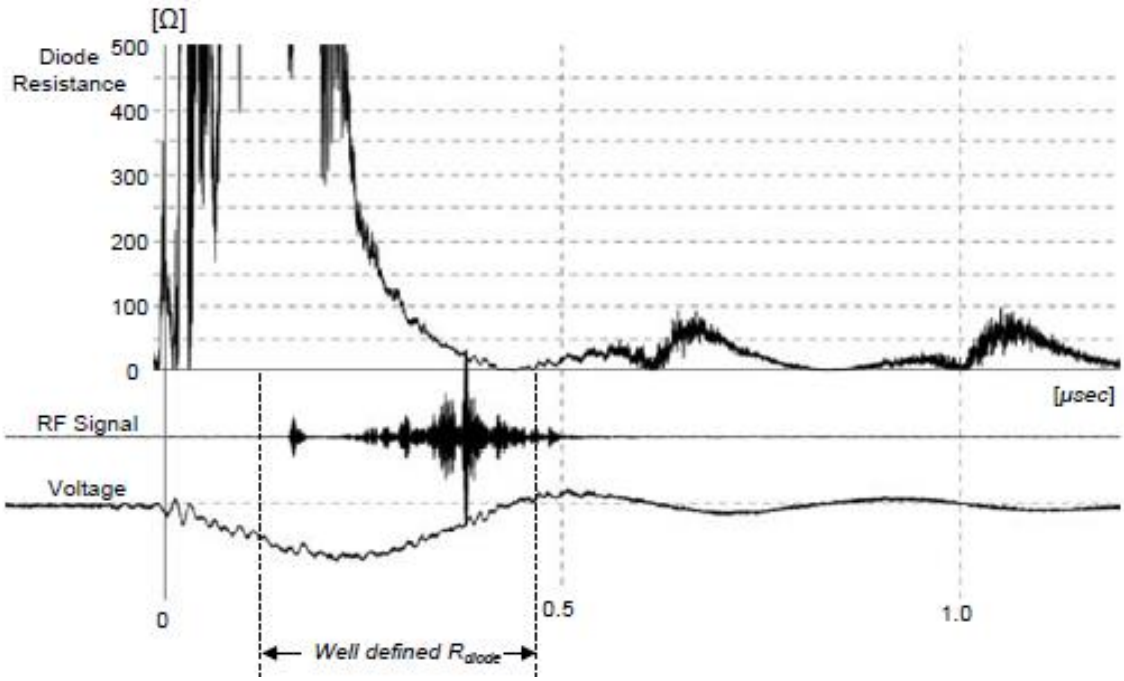

Fig. 6.84: The Descent fabric, dAK = 15mm (measurement 20080410m45): diode impedance.

In the above cases, a gap should be from the time when the voltage stops rising in the prescribed rate and a current starts flowing in the passage, until a zero voltage and normalization of power. The phenomenon lasts, with high repeatability, 300nsec. Thus, for this geometry, namely spheroidal cathode fabric spaced 15mm from the anode a- noxeidotou matrix, the propagation velocity of the plasma in the passage is estimated at ~ 5cm / microseconds, as in the case of the pin within 15mm. This observation is explained if considered a main body spread plasma, derived mainly from the cathode and partly from rising. The change in size is much smoother char- raktira, with changes of voltage, current and power exist very kroteres Asia Mi- ripples relative to pin the same gap. Those waveforms were observed with minor variations, for all the shock test. M- thanotata both the geometry and the emission of ionized gas from the fabric to Generator even conditions plasma column between the cathode and the anode. After all the gases adsorbed on the fabric are several orders of magnitude more than the metal cathodes.

The spheroidal cathode fabric, despite similar macroscopic sizes Direc- tion showing the tip, has substantially lower microwave output from the latter. This is probably due to the site of cleavage, which, as demon- chtike, not in the center of the terminal but slightly to the side. The experiments showed no significant change to the fabric surface, only a small mark is not already on the fabric, and the position noted in the following eiko- be. The asymmetry of the breakpoint can be led to the input of electrons in the waveguide with large dispersion and speeds with steep, so it was not possible to form a strong virtual cathode, as in the experiments with the pins.

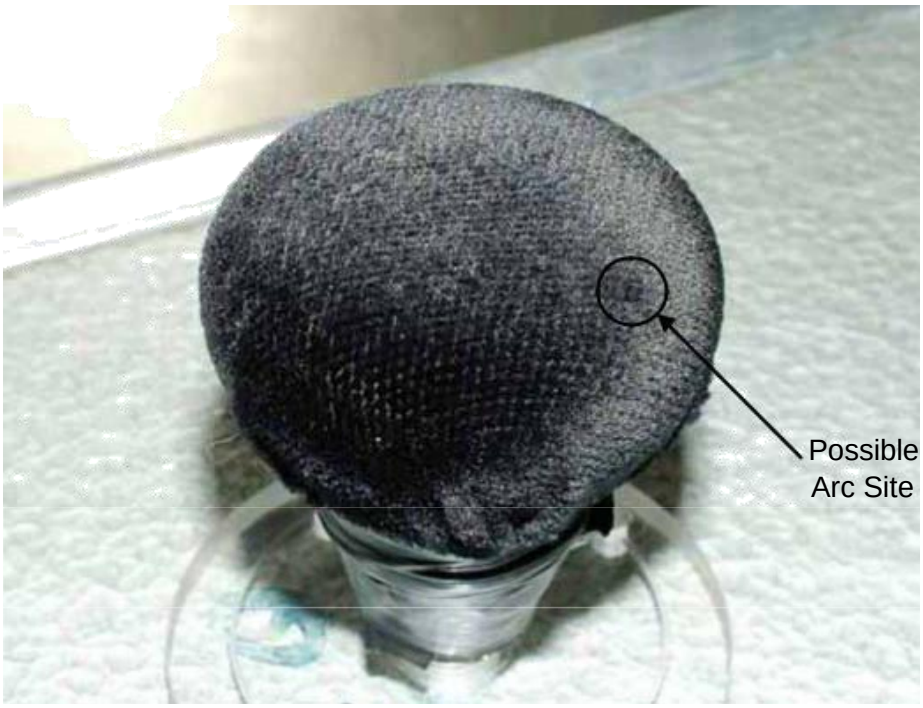

Fig. 6.85: The Descent fabric, dAK = 15mm, ~ 100 impacts. Noted the only visible sign that appeared following examination of the fabric.

One conclusion from this experiment is that it should not be used as a black cloth cathode surface because this practice is rather difficult to search for marks in the surface characteristics. However, this was the only velou- structure found quickly after searching store with fabrics. Besides, we could not use anything other than velvet, as this will paravai- NAME tradition decades, wants to field emission cathodes covered only with this type of fabric (velvet cathodes).

6.3.6. Ductile Descent with Fabric (d = 25mm)

In order to gain comprehensive insight into the behavior of the cathodes with fabric, we used stainless plug, having the same form kampyloti- Tash to the previous, but it leaves an anode-cathode distance of 25mm. The alpha krodektis he dressed with cloth (again the same black velvet) and placed in Vircator. The mesh used is the number "1". Comprised 30 holes per inch, with a hole opening 0.587mm, 0.26mm diameter wire and free surface ~ 48% and proven to provide easier passage in the electronic drain. The configuration of the passageway shown in Fig. 6.86.

Based on the nomogram of Fig. 5.20, the maximum diameter of the cathode for a distance 25mm from the anode is about 40mm. Since the diameter of that terminal is 42mm, it is not certain that electronic culverts channeled onto the grid. Indeed, signs were observed in the anode support flange and tan in the insulating cylinder Acetal, which before the start of the experiment there were not. From these observations and from the fact of very weak micro-

wave signal, we conclude that the evacuation probably driver.This the side walls of the passage and not to the grid.

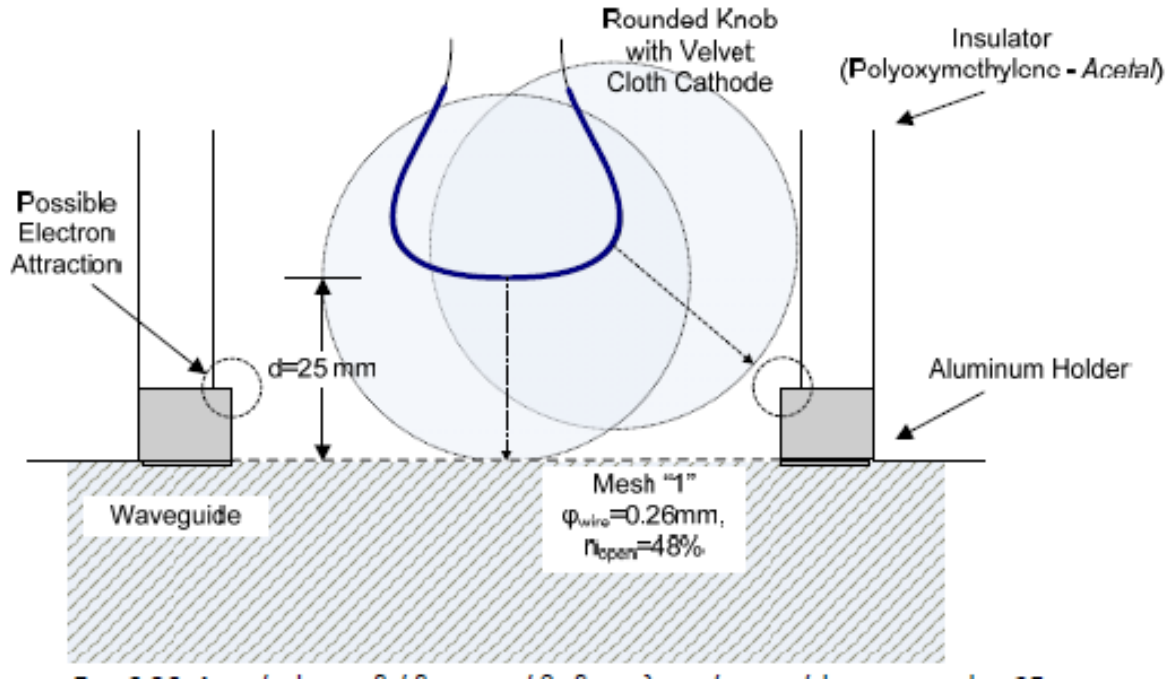

Fig. 6.86: cathode diode configuration covered with fabric and dAK = 25mm.

6.3.6.1. Macroscopic Experimental Sizes

The following tables lists the recorded peak voltages, current and power in the passage for at least ten (10) iterations, a charging pri- tefontos of 50, 75 and 100V AC. According to what has been stated in paragraphs 5.5 and 6.3.2, the loads they give impulse *0.6 / 50*With maximum widths 52, 78 and 104kV. The voltage, current and power of the diode are given as mean and the calculated dispersion *p*the recorded maximum, in any state of charge, with semiotics *<X> ± 1 · sx*. In all tests, the diode presented to withstand the impulse voltage of 54kV (primary charging voltage 50V AC).

Tab. 6.18: Descent with Fabric dAK = 25mm, Mesh "1" (Measurements 02-06-2008)

Load	50V AC	75V AC	100V AC
Max Surge	(No decay)	~ 78kV	~ 104kV
Current Ion Pump	0.2m	0.35 ~ 0.37mA	0.38 ~ 0.42mA
Lifting	×	9.5 ~ 11.5mA	13 ~ 14.5mA
Voltage typical	×	66.9 ± 2.2kV	73.0 ± 2.2kV
Typical Power	×	772 ± 12A	1000 ± 45A
Power typical	×	26.2 ± 1.7MW	38.0 ± 3.4MW
RF typical	×	**<0.1W**	**<0.1W**
Efficiency typical	×	-	-
RF max recorded	×	**0.1W**	**0.1W**

Tab. 6.19: Descent with Fabric dAK = 25mm, Mesh "1" (Measurements 04-06-2008)

Load	50V AC	75V AC	100V AC
Max Surge	(No decay)	~ 78kV	~ 104kV
Current Ion Pump	0.2m	0.25 ~ 0.35mA	0.30 ~ 0.40mA
Lifting	×	9.2 ~ 11mA	12 ~ 13mA
Voltage typical	×	56.2 ± 1.4kV	63.1 ± 2.0kV
Typical Power	×	725 ± 9.0A	989 ± 17A
Power typical	×	21.0 ± 0.7MW	32.1 ± 1.2MW
RF typical	×	**<0.1W**	**<0.1W**
Efficiency typical	×	-	-
RF max recorded	×	**0.1W**	**0.1W**

The estimated pressure in the passage area is as current of Ion Pump in mA at the moment before impact, multiplied by 10-4 Torr (see. Par. 6.1). Therefore the 0.2mA corresponding to 2 · 10-5Torr. The current of the ionization pump the moment of impact rises rapidly (within approximately 0.5sec) too, most of the cases of re- thodon pin and the cathode material with the smallest gap. This is due to the large volume of gas ejected from the fabric. Also, resetting the pressure at the low levels lasts much longer, indicating a large volume of gases released from the cathode. Longer impulse voltage pre invites greater surge current of ionization pump. The gassing seems to be lower during the second day of tests. Probably stay in abstraction from the ionization pump improves the purity of the sample.

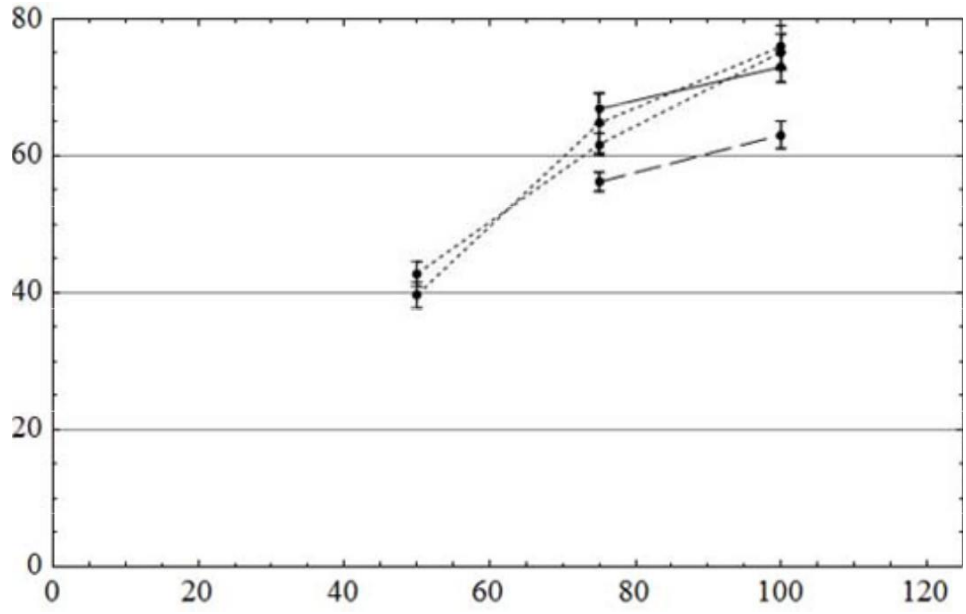

Fig. 6.87: Maximum voltage diode. Cathode fabric, first day (solid line), sec- teri day (dotted line), the cathode pin (dotted lines). Grid no. "1" dAK = 25mm.

The behavior of the gap, in terms of electrical resistance, shows a large deviation between the first and second day. The total maximum voltage of the gap

the second day is much lower, around 10kV, for exactly the same conditions Direc- tion. Probably some distortion of the fabric leading to the creation of a route with a smaller withstand voltage in this embodiment. The stream of this configuration vri- situated in the same context with the flow passage to the cathode tip, the same distance. The di- aforopoiisi current in the series of tests was small and extremely Asia Mi- Kpn dispersion.

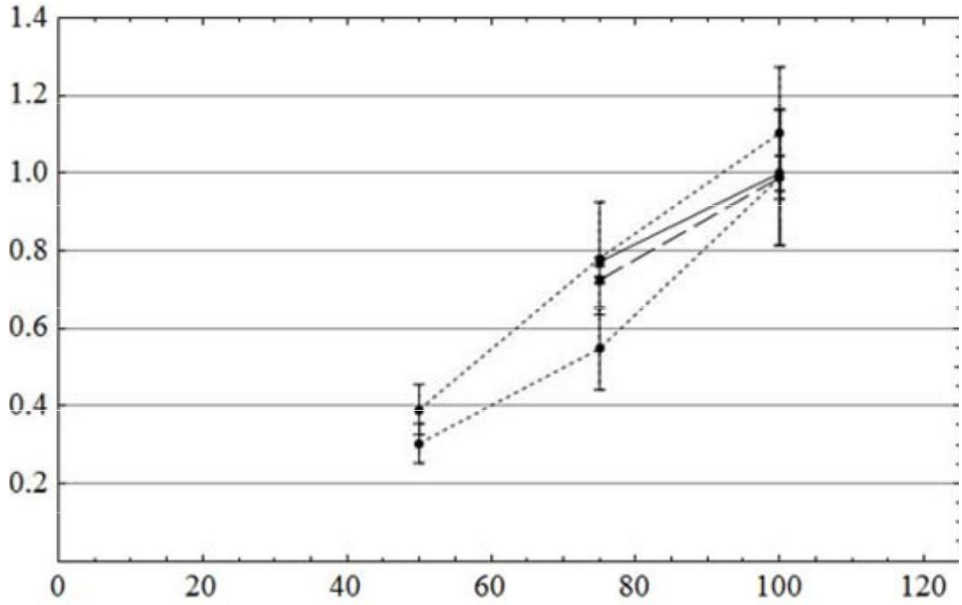

Fig. 6.88: Maximum diode current. Cathode fabric, first day (solid line), sec- teri day (dotted line), the cathode pin (dotted lines). Grid no. "1" dAK = 25mm.

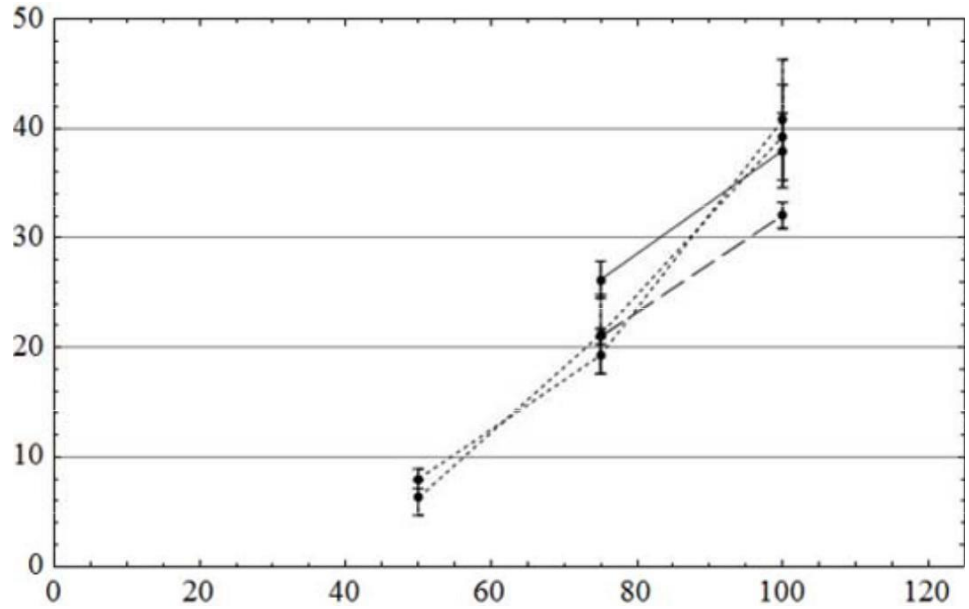

Fig. 6.89: Maximum power diode. Cathode fabric, first day (solid line), sec- teri day (dotted line), the cathode pin (dotted lines). Grid no. "1" dAK = 25mm.

6.3.6.2. Model Discharge Capacity by Diode

As seen from the experimental results from wrong design seems that this descent is not channeled electronic stream of splitting up the grid anode. During the experimental procedure signs observed in the anode support collar, tan in the insulating cylinder Acetal, and alpha sthenestata microwave signals. For these reasons, this descent is not meaningful to compare with similar cathode distance dAK = 15mm or cathodes type pin. We can, for the sake of completeness, to include a model representatives charging diode with "beam" electron emission equal to 10mm, since the diameter of the probe is 42mm and plasma spread speed equal to *u*= 5cm / microseconds, because long distance anode - cathode and thus relatively cold plasma. With these assumptions, make and model of other sizes: *k*= 2.33 · 10-6A / V3 / 2, reinforcement distance *d*= 0.025m, geometric matrix permeability the rise *n*= 48% initial voltage capacitor *V (0)=V0*= 70kV, capacitor capacity *C*= 1.2nF. The discharge capacitor visa through diode lamp developed in par. 4.3.6 and in para. 6.3.3.2.

In Fig. 6.90 show the analytical solution of the diode voltage and the sys- nypologizomeno stream passage Vircator. Once we find the dependence of the voltage in the gap, we can extract the energy of the electron beam and the area of which is set equal to the phenomenon of cathode area. Of those sizes and the permeability of the anode grid, we can calculate the diode current required to feed the kymatodigiki cavity with critical peak beam current. This stream, symbolized by the dotted line, it must be leak passage to enter in conditions of virtual cathode display in kymatodigiki cavity. The passageway leads to more current than is necessary after the first 210nsec. From that moment onwards we can predict what will import so the expected output frequencies Vircator, based on the theoretical models of the literature. Once you know the voltage and the current flowing through the diode, then we are able to illustrate approaches for frequency reflex as well as the frequency of oscillations of the cloud of virtual cathode.

The frequency of oscillation of the virtual cathode, according to what are referred brought in par. 4.1.2, is between the values *fp* and (2n) 1/2*fp*. In Fig. 6.91 Read off: the area defined by frequencies *fp* and (2n) 1/2*fp*The two estimates sys-
frequencies reflexing, non-relativistic and relativistic, as described in par. 4.1.1. Finally made and the assessment of Woo, on. (4.16) for the output frequency of a Vircator. After the first 210nsec, when the diode leads necessary currents ap- emergence virtual cathode, the output frequencies appears to lie in the range between 1 and 2GHz. Although such behavior would be desirable to Down Methods can be used in the passage of the Vircator, because of insufficient space in the chamber of the passage.

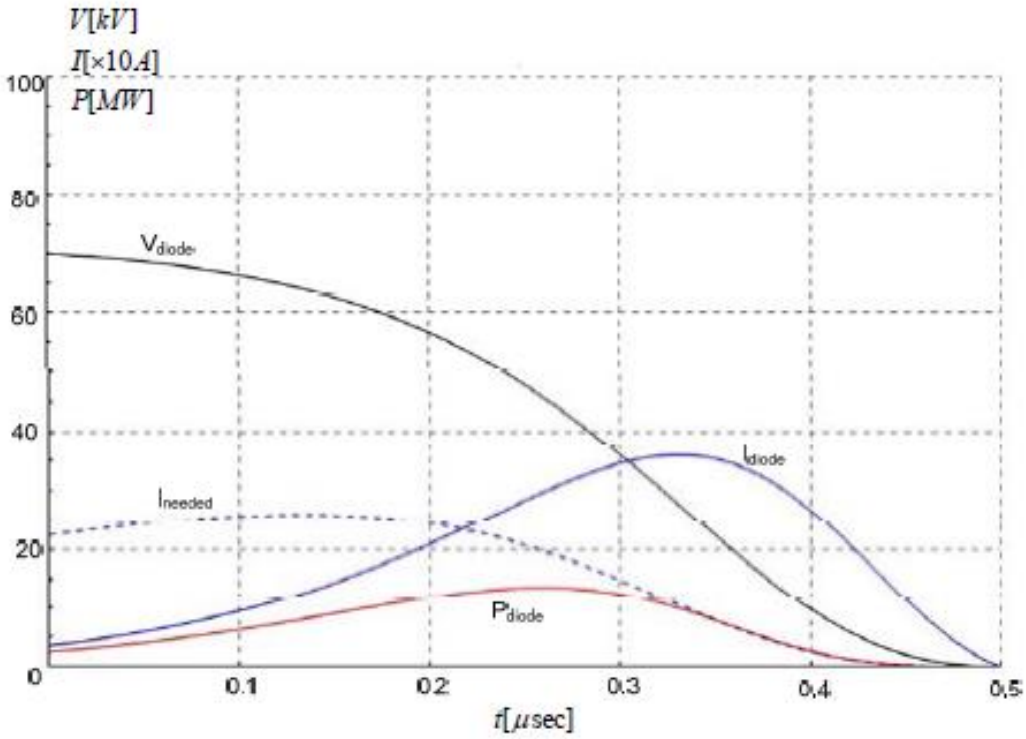

Fig. 6.90: Theoretical variation of voltage, current and power at the cathode with fabric and dAK = 25mm, for drive voltage 70kV, capacity capacitor 1.2nF, speed katarref- ing gap 5cm / microseconds (large emitting surface).

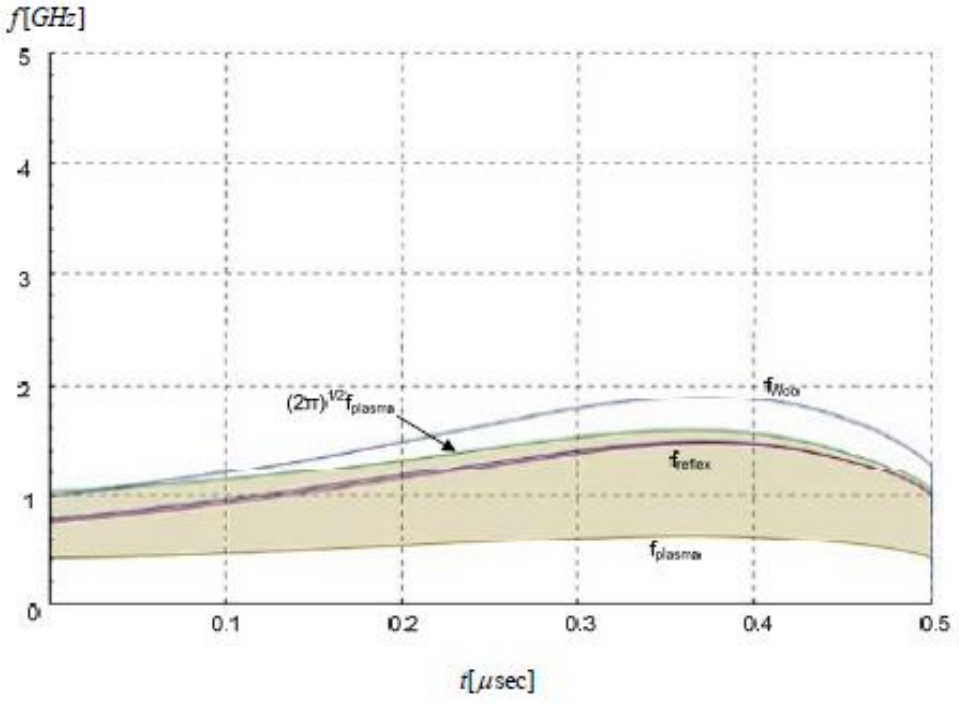

Fig. 6.91: Output frequency Assessments Vircator with descent with fabric and dAK = 25mm, for discharge voltage 70kV, capacitor 1.2nF, with spacing collapse speed 5cm / microseconds (large emitting surface).

6.3.6.3. Typical measurements

The following records are typical behavior of this diode. The microwave signal, although reflected, has negligible effect. Indicatively, the following two records translated into microwave power output 0.02W. These small signals observed when the diode consumes power when that gap EI- yes even unbridgeable. The marginal geometry but the big rise distance - lays period lead us to the conclusion that the first stream may be towed to the metallic anode diphenylmethyl kickstand secondly that may be spreading so much, D- CoE entering the waveguide with very small spatial density and being impossible the formation of a virtual cathode. Here are two typical recording waveform. The microwave signals are so weak force, so the time-range display is dominated by the noise measurement and the quantization noise of the oscilloscope.

Case A (74kV, 1000A, 39MW, 8cm / msec)

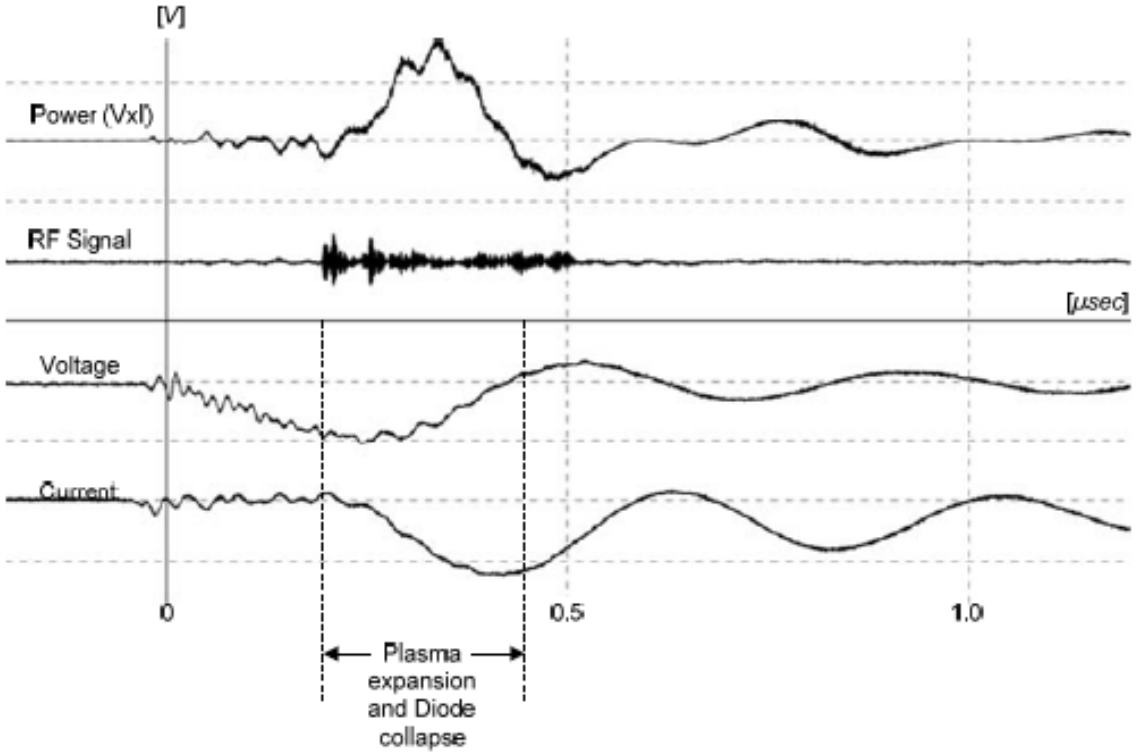

Fig. 6.92: The Descent fabric, dAK = 25mm, mesh no. '1' (measured 20080602m28): Vmax = 74kV, Imax = 1000A, RFmax = 0.02W, Pmax = 39MW.

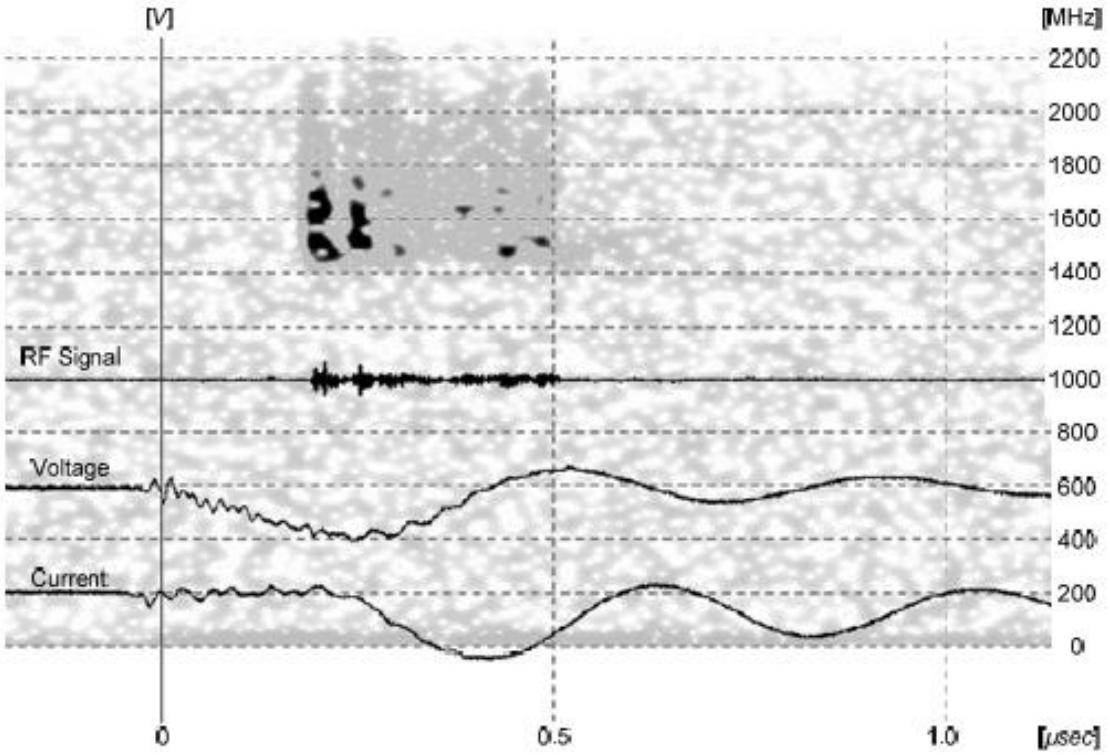

Fig. 6.93: The Descent fabric, dAK = 25mm (measurement 20080602m28): time-imaging spectrum.

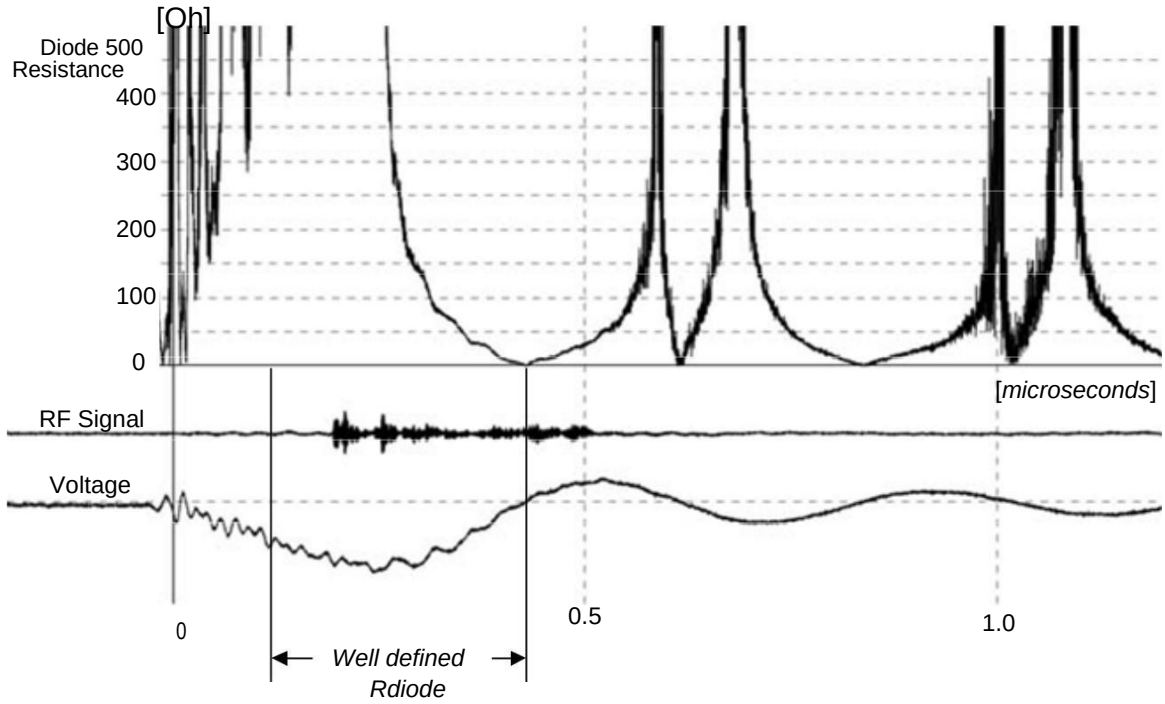

Fig. 6.94: The Descent fabric, dAK = 25mm (measurement 20080602m28): diode impedance.

Case B (62kV, 980A, 30MW, 8cm / msec)

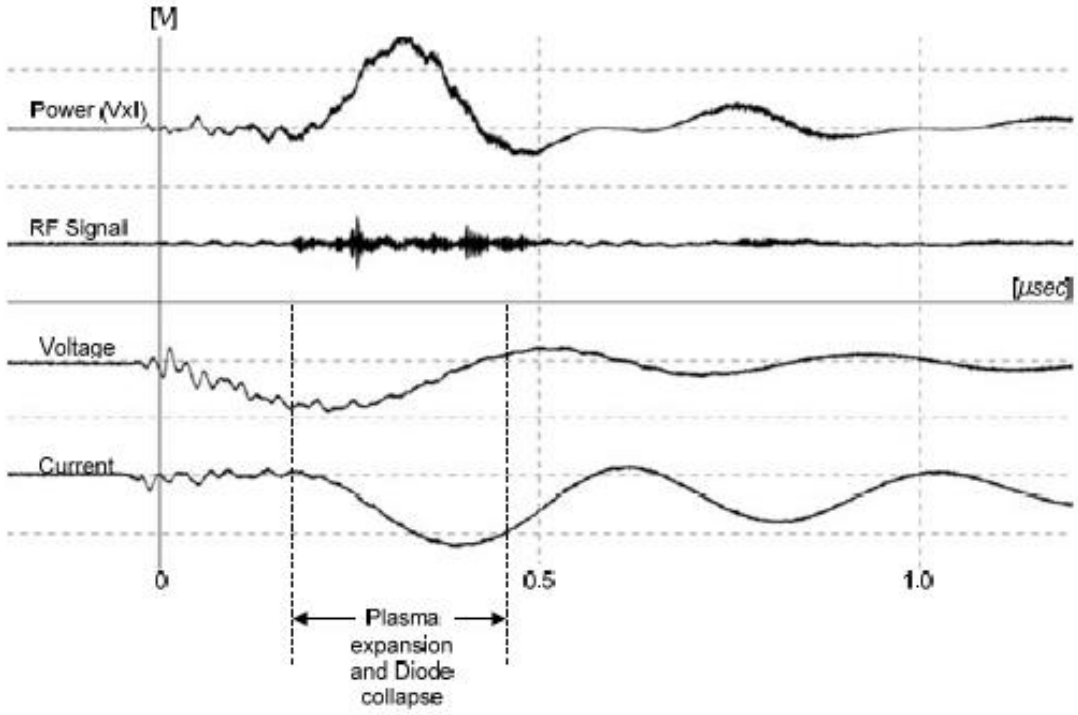

Fig. 6.95: The Descent fabric, dAK = 15mm, mesh no. '1' (measured 20080604m29): Vmax = 62kV, Imax = 980A, RFmax = 0.02W, Pmax = 30MW.

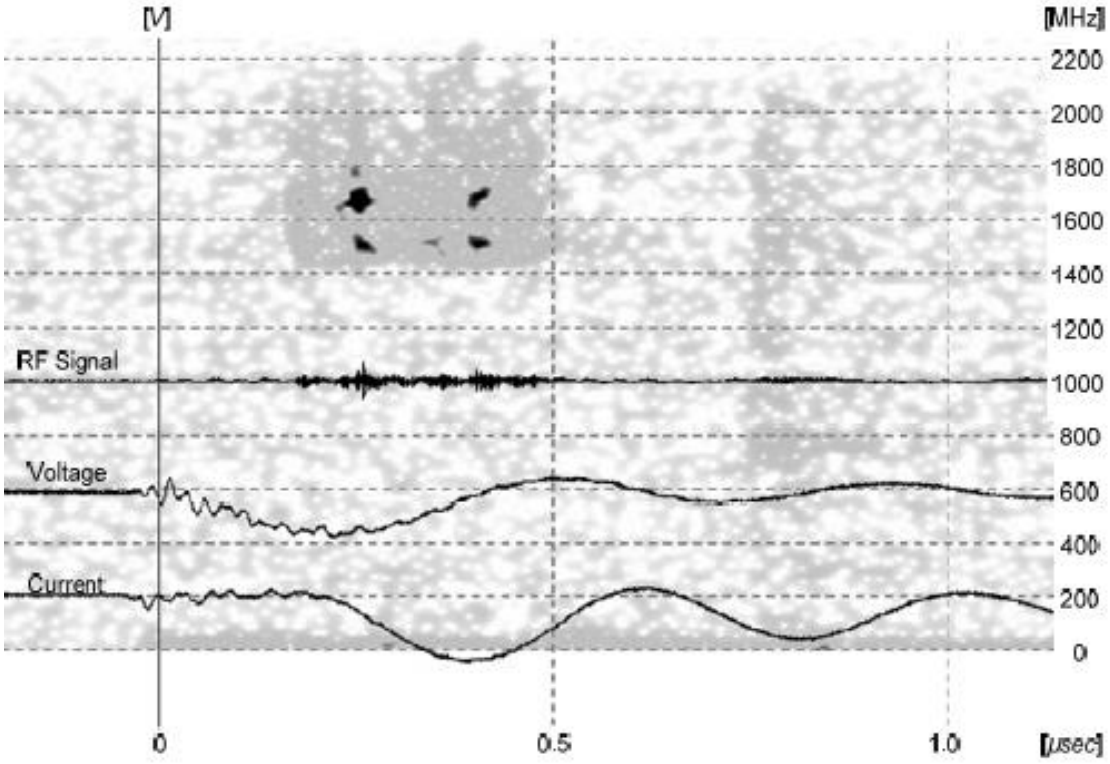

Fig. 6.96: The Descent fabric, dAK = 25mm (20080604m29 measurement) Show time-range.

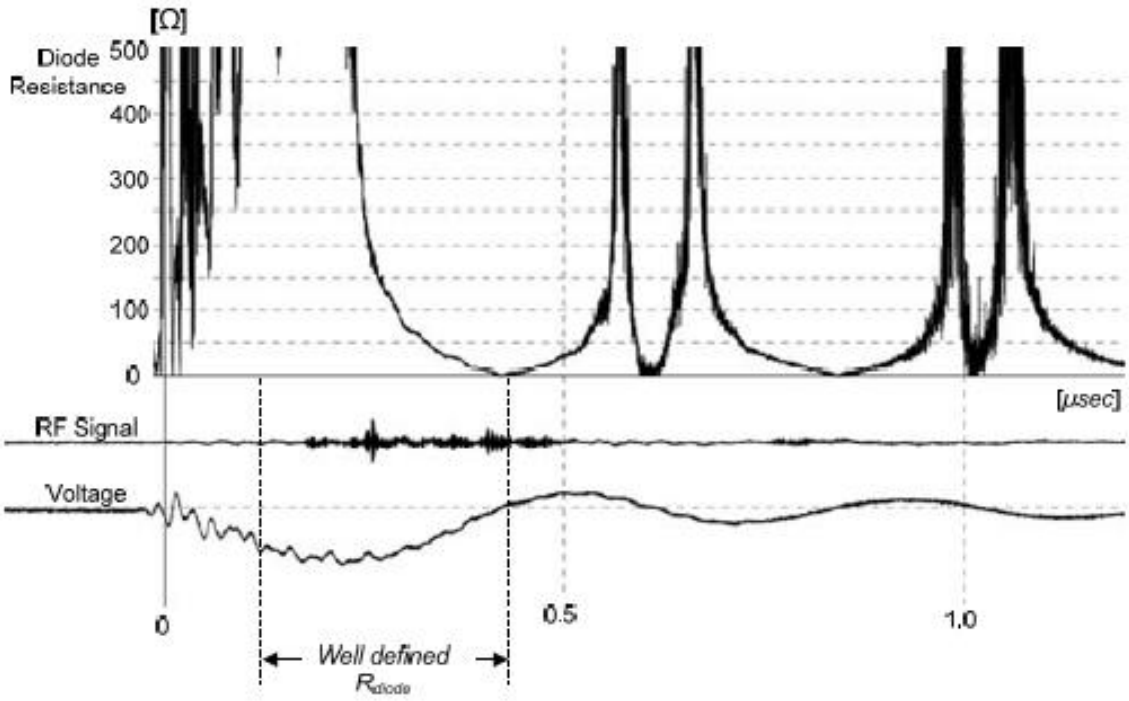

Fig. 6.97: The Descent fabric, dAK = 25mm (20080604m29 measurement): diode impedance.

In the above cases, a gap should be from the time when the voltage stops rising in the prescribed rate and a current starts flowing in the passage, until a zero voltage and normalization of power. The phenomenon lasts about 300nsec, although the gap is significantly greater, 25mm. Therefore, for this geometry, namely spheroidal descent fabric within 25mm from rising stainless mesh, the spread velocity of plasma in the diode is estimated at ~ 8cm / microseconds. Also, variations in sizes is much smoother character, to changes in the voltage, current and power to suffer much smaller ripples relative to pin the same gap. The behavior illustrated in the above waveforms were perfectly repetitive in all the tests, which is shown in small dispersions of characteristics quantities of the passageway. The absence of RF, other than a minimum power state that the current evacuation not prosepipte the grid as expected. What appeared to be the case is the power incident on the matrix support hoop, small scars, and discoloration of the cylinder of insulating material that surrounds the passage. The grid does not appear to have any distortion.

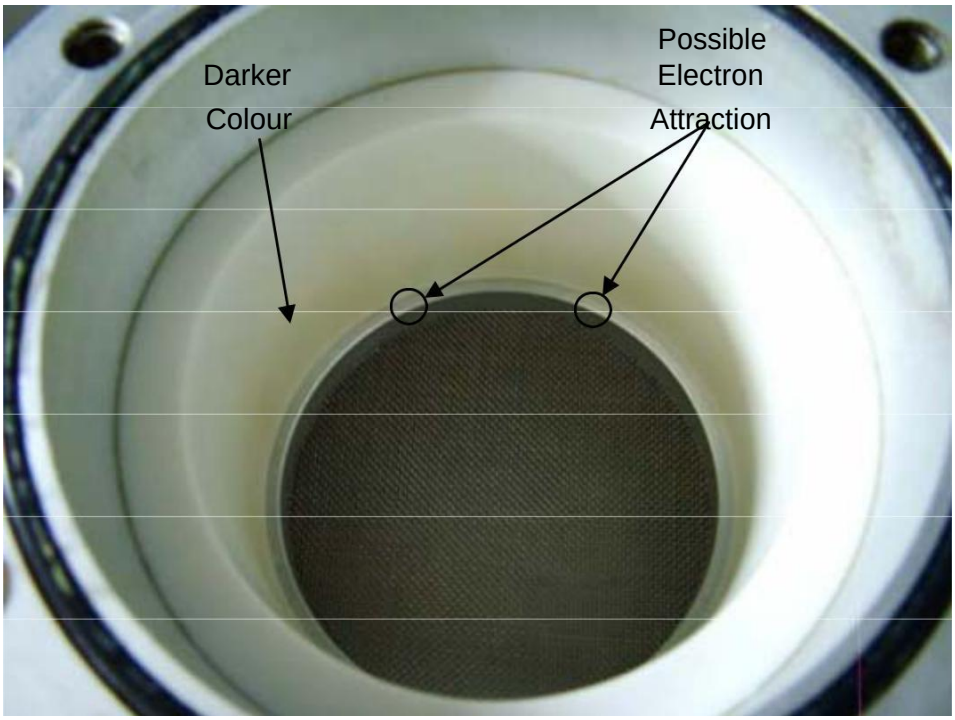

Fig. 6.98: Grid and bushing after impact with spheroidal descent fabric, dAK = 25mm, ~ 100 impacts.

The wide spacing of the collapse speed explained, if considered as the main population spread hydrogen, derived from both the cathode and the upward structure. Also, the adsorbed gas on the fabric may form a local cloud of gas around the cathode, so the split falls into divisions formula Townsend ionization of the gas present in the passage. The waveforms of voltage and currents, Tosh in the fairway, both in the case of cathode fabric spacing 15mm, and in this case, is so close, that the justification of the rapid collapse of preexisting plasma gas locally, seem justified.

6.3.7. Sandblasted Ductile Descent (d = 15mm)

Pin the geometry, shown below, is made of stainless steel. To increase the roughness of its surface in order to release current largest Mars due to field emission, the underside blasted. Already we found that this terminal when covered with fabric, produces a Cro Asia Mi- amount RF, however, the placement of the fabric during the tests has resulted in the cam release electrons from a point near the "edge" of the lower epifanei- let. Since the geometry of the component itself is very symmetrical, the electron ekly- importance when it is uncovered, should be carried out around the center. By blasting the surface and development mikrotrachytitas, we create a lot simei-, which will cause downward FEDs.

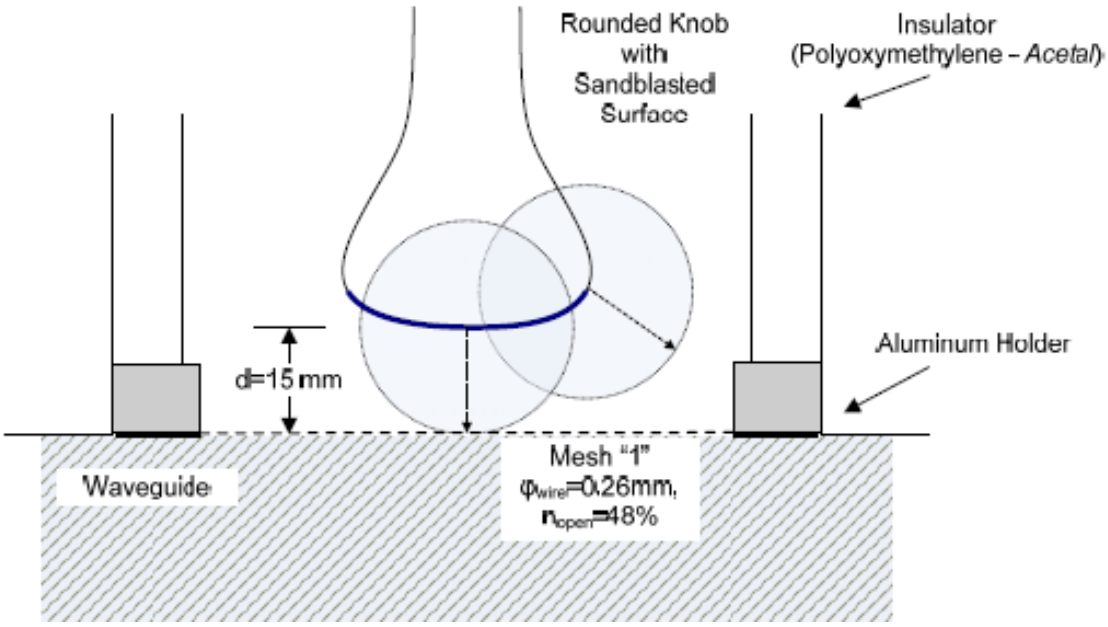

Fig. 6.99: Configuring path with sandblasted nodular cathode dAK = 15mm.

Based on the nomogram of Fig. 5.20, the maximum diameter of the cathode for a distance 15mm from the anode is about 50mm. Since the diameter of the probe so EI-42mm, with some certainty we can say that the culvert of channeled electrons tefetai the grid anode rather than the mesh support hoop.

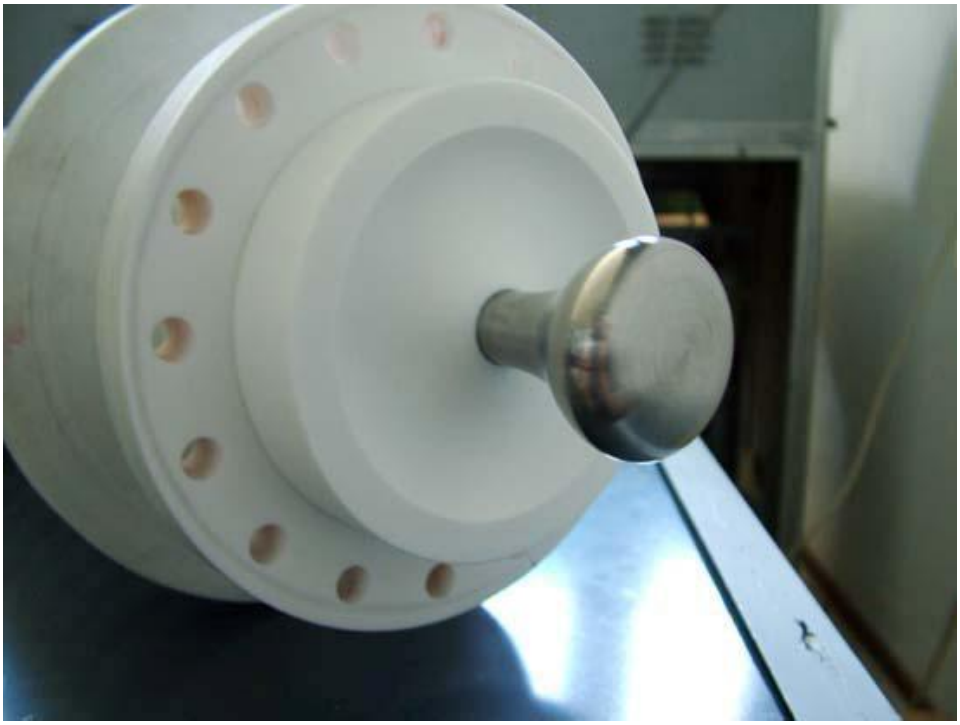

Fig. 6.100: Ductile cathode dAK = 15mm, mounted on the insulator passage.

6.3.7.1. Macroscopic Experimental Sizes

The following table lists the recorded peak voltages, currents, Tosh and power in the passage for at least ten (10) repetitions in primary charge equal to 100V AC. According to what has been stated in paragraphs 5.5 and 6.3.2, charging gives impulse *0.6 / 50*A maximum width ~ 104kV. The voltage, current and power of the diode are given as mean and the calculated dispersion *p* the recorded maximum STON in any state of charge, with the notation *<X> ± 1 · sx*. In this configuration, the gap showed resistance to all percussive lower price trends. Despite our expectations, the terminal he never showed microwave output, only the first time imposed voltage. All other times, the channel of RF frozen only writes baseband signals, declared to the interference within the system of high voltage.

Tab. 6.20: sandblasted descent dAK = 15mm, Mesh "1" (Measurements 16/07/2008)

Load	50V AC	75V AC	100V AC
Max Surge	(No decay)	(No decay)	~ 104kV
Current Ion Pump	0.2m	0.2m	0.2 ~ 0.3m
Lifting	×	×	6 ~ 9mA
Voltage typical	×	×	98.9 ± 2.9kV
Typical Power	×	×	1912 ± 37A
Power typical	×	×	81.7 ± 10.0MW
RF typical	×	×	***no RF***
Efficiency typical	×	×	-
RF max recorded	×	×	**1W** (One case)

The estimated pressure in the passage area is as current of Ion Pump in mA at the moment before impact, multiplied by 10-4 Torr (see. Par. 6.1). Therefore the 0.2mA corresponding to 2 · 10-5Torr. The current of the ionization pump the moment of impact rises rapidly (within approximately 0.5sec) over an order of magnitude. Very large amounts of power, more than twice the same distance spike, confirming there ment of many degradation centers on the cathode surface. In the absence of micro- wave signal can assume either that the output is significantly above the 2GHz, or that the great dispersion of power, is not capable of creating virtual descent into the waveguide.

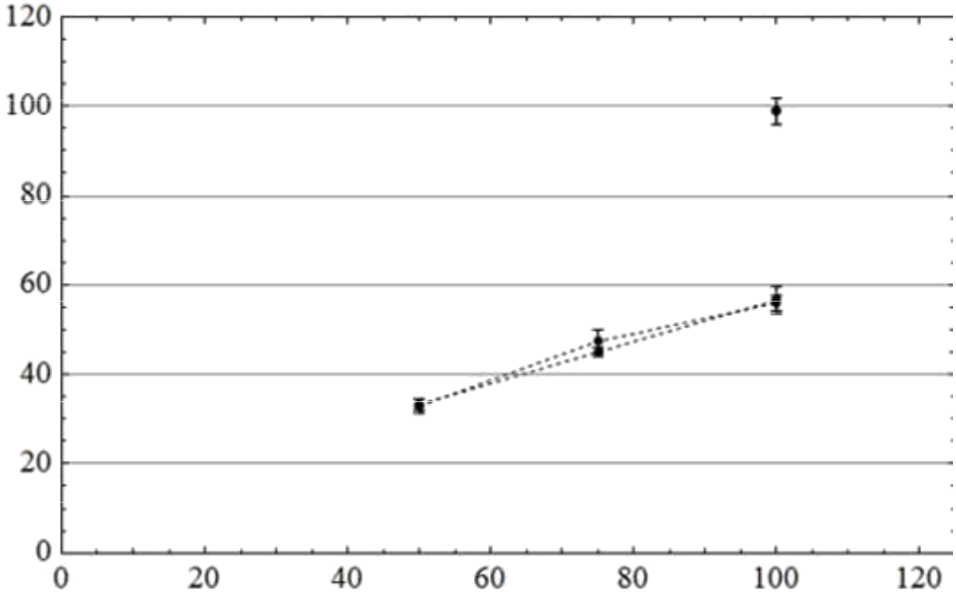

Fig. 6.101: Maximum voltage diode. Sandblasted cathode and cathode pin (dotted lines). Grid no. "1" dAK = 15mm.

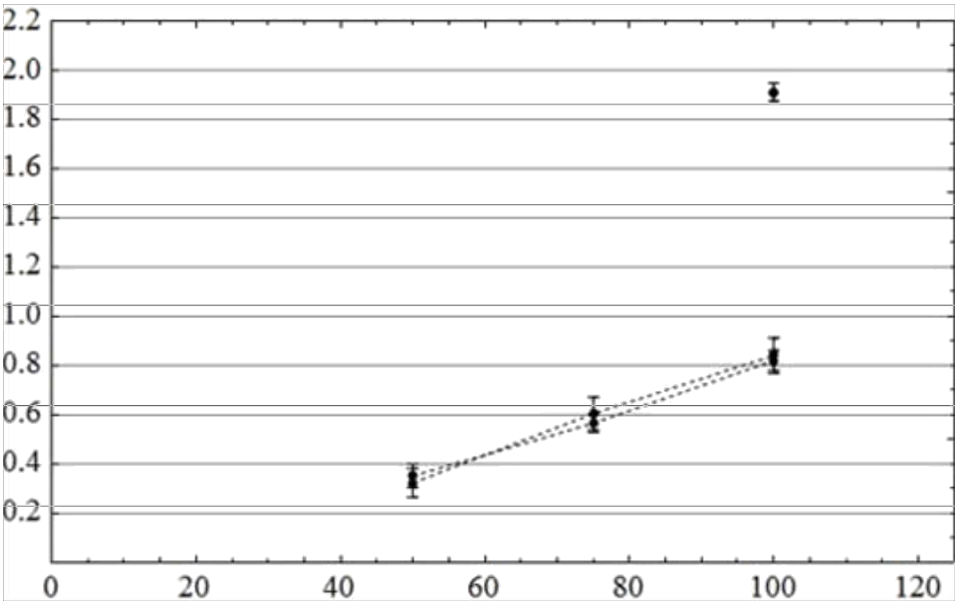

Fig. 6.102: Maximum diode current. Sandblasted cathode and cathode pin (dotted lines). Grid no. "1" dAK = 15mm.

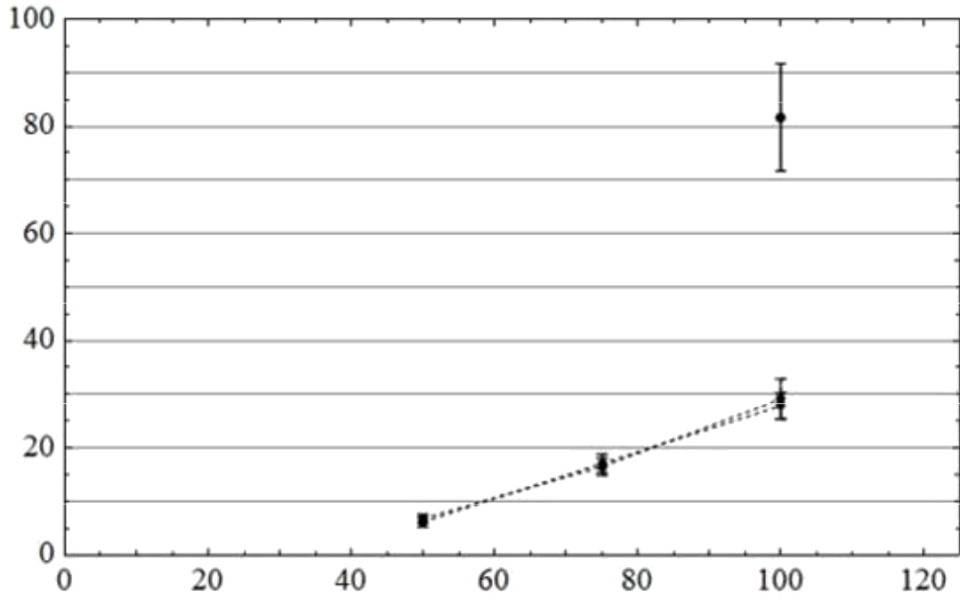

Fig. 6103: Maximum power diode. Sandblasted cathode and cathode pin (dotted lines). Grid no. "1" dAK = 15mm.

6.3.7.2. Model Discharge Capacity by Diode

The sandblasted spheroidal descent decays into voltages in the range of 100kV, and displays Diode currents too strong, approaching 2kA. The measurements showed that the clearance of 15mm collapses in 200nsec about, which leads us to de-
pologizoume the spreading velocity of plasma in 8cm / microseconds. Experimenting with the model Fri 4.3.6 and still. 6.3.3.2, we *k*= 2.33 · 10-6A / V3 / 2, distance reinforcement *d*= 0.015m, geometric anode grid permeability *n*= 48%; initial voltage capacitor *V (0)=V0*= 100kV, capacitor capacitance *C*= 1.2nF. If we define initial active radius lays period equal to 5mm, we can receive voltage changes, current and power laid sengizoun experimental results.

Simulation discharge with the above data shown in Fig. 6,104. The diode is bridged at ~ 200nsec (typical experimentally observed half) with a maximum current of 1800 (standard experimentally observed current) and maximum power ~ 80MW. In this way we have a parallel macroscopic characteristics of the cathode driving aggregates in the analytical model. Having found the dependence of the voltage in the gap, we can extract the energy of the electron beam and the area of which is set equal to the apparent area of the cathode. Of those sizes and the permeability of the anode grid, we can calculate the current appointment period required to feed the cavity with kymatodigiki critical maximum at a beam current. This stream is denoted by the dotted line. The passageway leads to more current than is necessary after the first 70nsec. From that moment onwards we can predict what will be the expected output frequencies Virca- tor, based on theoretical models.

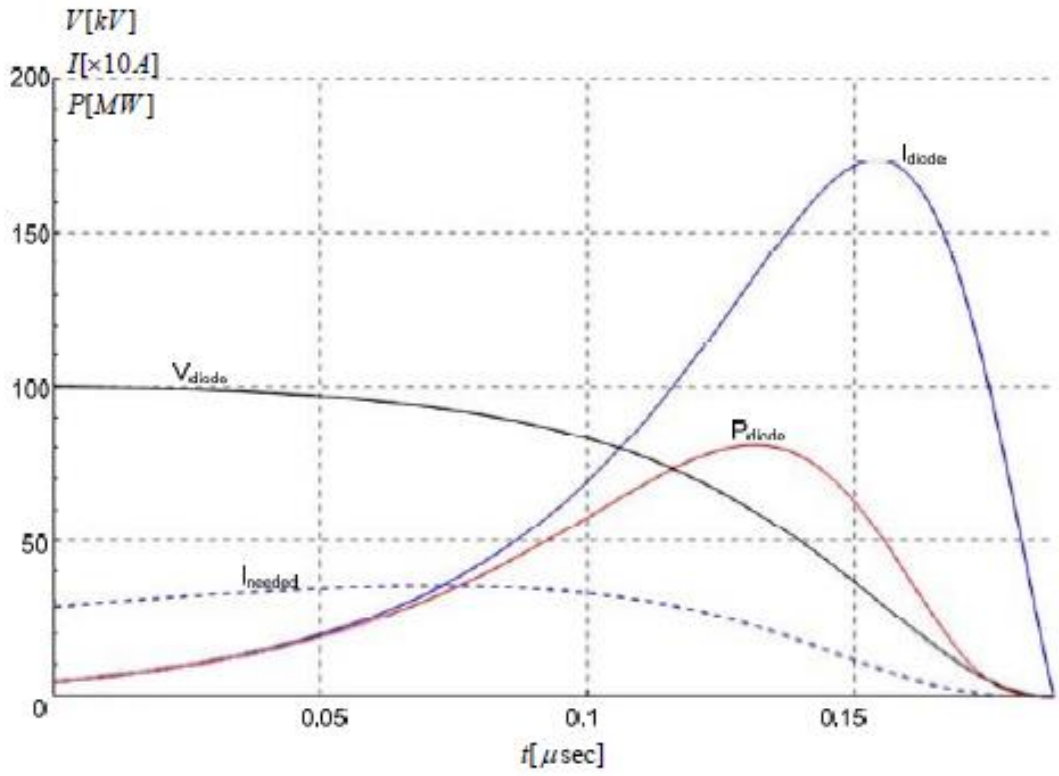

Fig. 6104: Theoretical variation of voltage, current and power sandblasted sfairo- kinds cathode dAK = 15mm, for drive voltage 100kV, capacity capacitor 1.2nF, with BRAKE gap collapse cast 8cm / microseconds.

The plasma frequency of the electron beam, which enters the inactive area can be calculated from the relativistic equation (4.42). In this expression in place of the current package *I*, Substituting the amount (4.69) multiplied by the geometrical permeability of the matrix, *n*. In the denominator of the equation (4.42) we make the appropriate anti-time dependence of the radius of the cathode, which we assume and radius of the beam. The change of plasma frequency is described by (4.71), where the coefficients b and c depend on the tension in the passage and described by equations (4.44) and (4.45). The frequency of oscillation of the virtual cathode, according to what has been reported in par. 4.1.2, is between the values *fp* and (2n) 1/2*fp*. In Fig. 6.105 marked: the area bounded by the frequencies at Timoleon Mes *fp* and (2n) 1/2*fp*The two estimates of frequency reflexing, non-relativistic and relevant tikistiki as described in par. 4.1.1. Finally made and the assessment of Woo, on. (4.16) for the output frequency of the Vircator.

When the current in the diode exceed 300A, beam energy ~ 90keV, enter the area where the current in the waveguide chamber is strong enough to be able to form the virtual cathode. This happens after the first 70nsec, D-, provided the relevant lamp output frequencies beyond 2GHz. In particular, the relativistic and non-relativistic approach to frequency of reflex BRAKE lantoseon gives frequencies higher than 2.5GHz, while the expected oscillation frequency of the virtual cathode is also well above 2GHz. The estimates of the theoretical model can justify the absence of microwave signal during testing of this terminal.

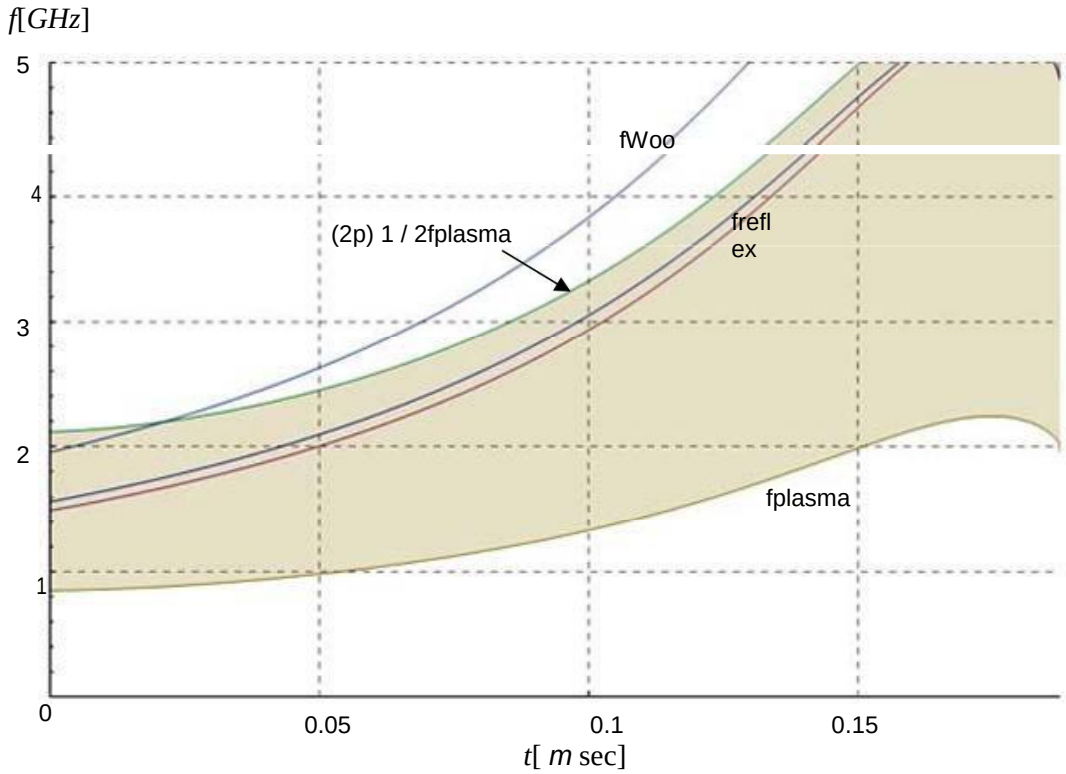

Fig. 6.105: Output frequency Assessments Vircator with sandblasted laid spheroidal structure with dAK = 15mm, for discharge voltage 100kV, capacitor 1.2nF, with spacing collapse speed 8cm / microseconds.

6.3.7.3. Typical measurements

The spheroidal terminal was sandblasted to create large signs electronic field emission due to the abnormal geometry. What we tried to achieve in this way is any reproduction of the results with the fabric. However, what is observed is very abrupt behavior of the diode, as well as zero output microwave signal other than the first test voltage enforcement in the fairway. This case is illustrated below, and the high-pitched signal, observed, is paradoxically a point where the voltage across the diode is reversed. We can safely say if this signal is due to a phenomenon import Connick descent. Moreover, it is noted that this configuration has never showed exo-structure after a plurality of shock, so the signal appeared only once to be due to local specificity, which is destroyed after the first evacuation.

Measurements with this lead, we observed a rapid collapse of the diode due to large currents that trigger intense thermal effects. The diode de- popiptei vibration very quickly after the first reversal voltage, while the liquidity but is still very high. The load levels due to the high electrical resistance tricity gap is very high. The gap begins to crumble when the voltage is 100kV, the limits that the imposed impulse voltage. The maximum liquidity automatically observed are of the order of 2kA. The gap appears to be bridged to 200nsec or less, which gives us spread velocity plasma con-

THE length of the passage about 8cm / microseconds. This figure apparently indicates D-existence cathode and anode plasma.

Case A (98kV, 1800A, 72MW, 8cm / msec)

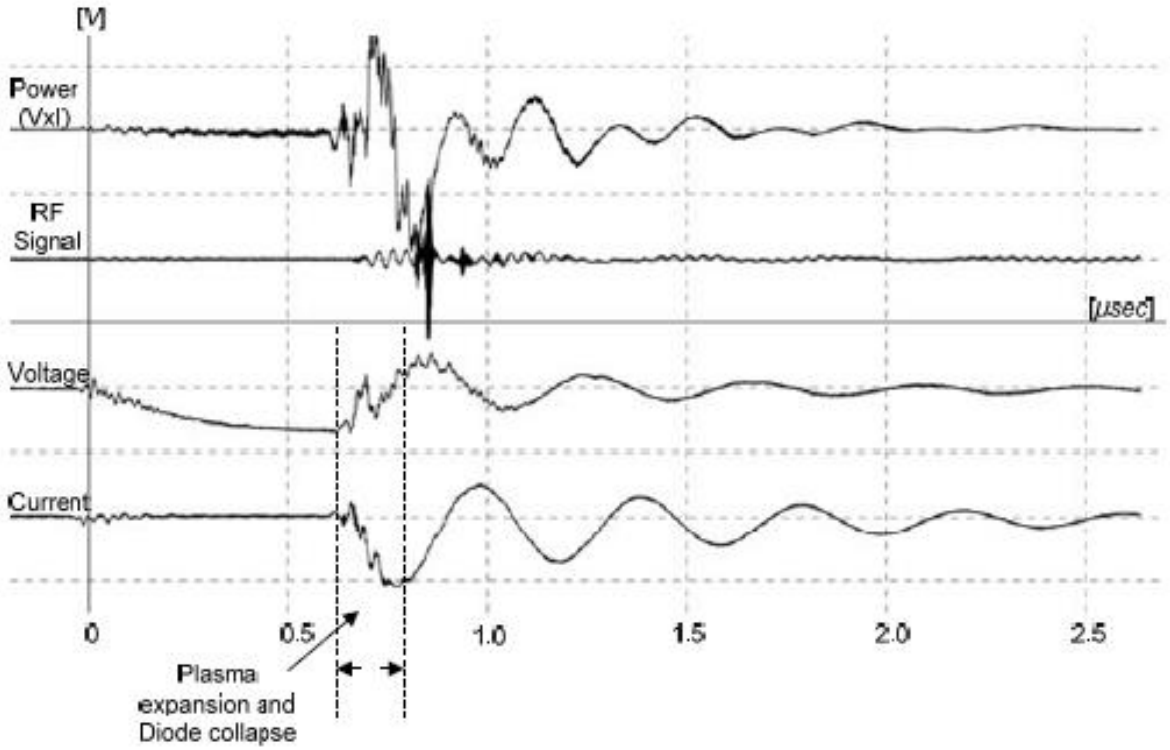

Fig. 6.106: sandblasted spheroidal descent, dAK = 15mm, mesh no. '1' (measured 20080716m00): Vmax = 98kV, Imax = 1800A, RFmax = 1W, Pmax = 72MW (unique case observation RF).

Time-range imaging in this unique case is not possible because the waveform is clipped from the recorder. The amplitude of the signal was recorded (> 40mV) surpassed placement of the scale of the instrument of 10mV / division. The clipping, suffered the waveform has been obvious as a result the appearance of spectral content in whole frequency range Nyquist 0- 10GHz sampling frequency 20GSamples / sec, something which is a direct consequence of the mathematical and shearing. Search the predominant component of the zero- crossings of the signal can place the center frequency at 1.4GHz, ie close to the cutoff threshold of the waveguide.

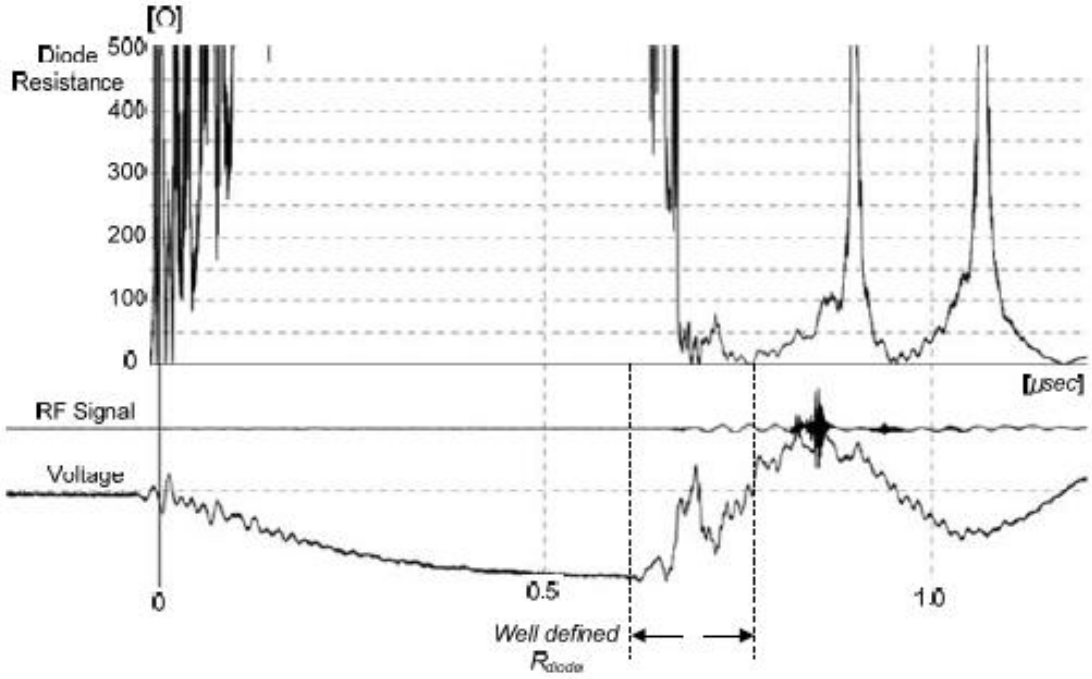

Fig. 6107: sandblasted spheroidal descent, dAK = 15mm (measurement 20080716m00): A-ntistasi passage.

Case B (101kV, 1900A, 90MW, 8cm / msec)

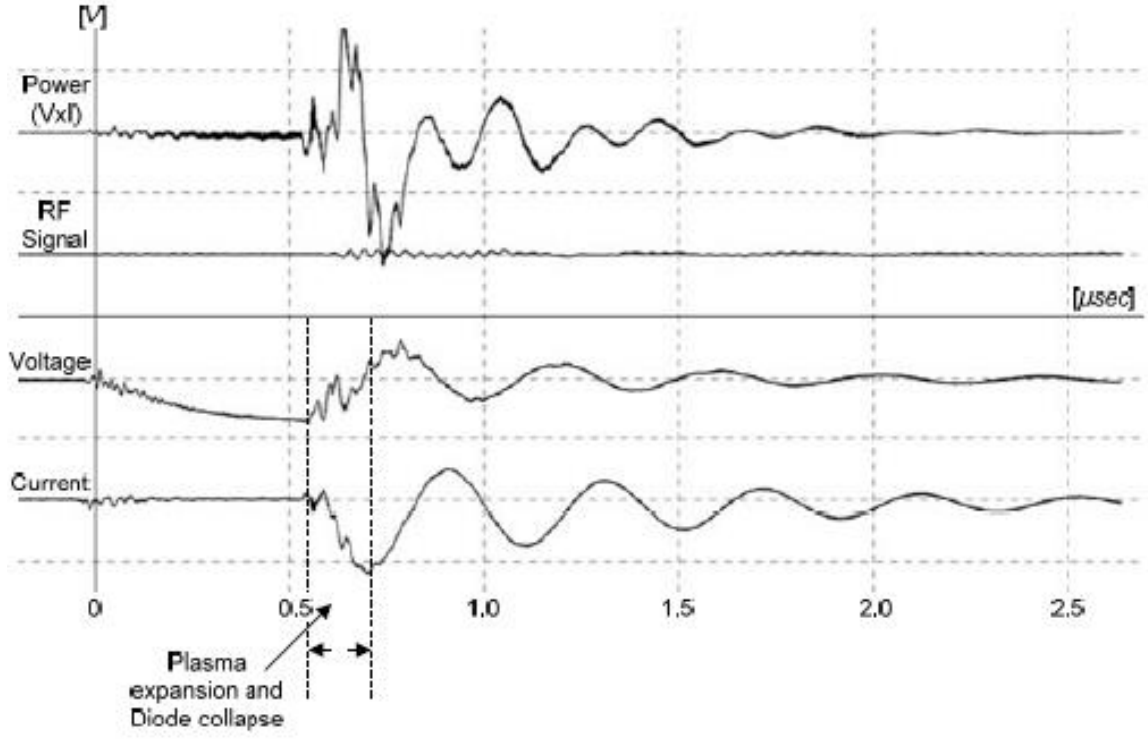

Fig. 6.108: sandblasted spheroidal descent, dAK = 15mm, mesh no. '1' (measured 20080716m08): Vmax = 101kV, Imax = 1900A, RFmax = 0W, Pmax = 90MW.

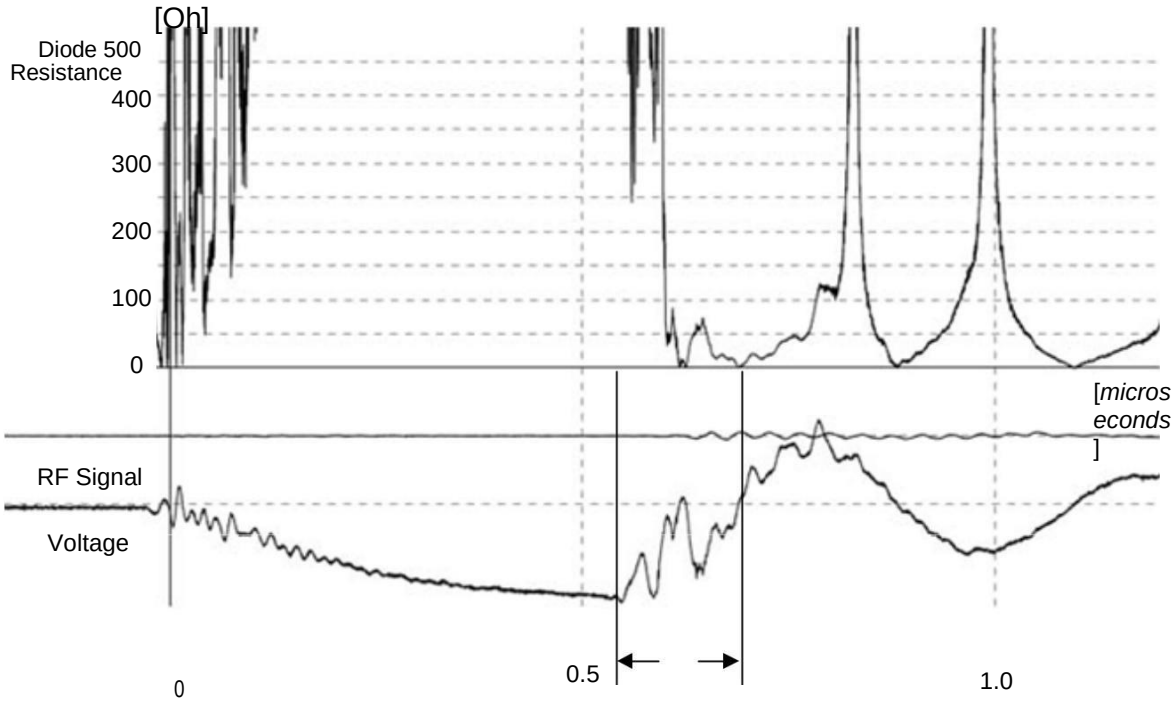

Well defined Rdiode

Fig. 6109: sandblasted spheroidal descent, dAK = 15mm (measurement 20080716m08): A- ntistasi passage.

6.3.8. Descent Multi-pin (d = 17mm)

For the sake of experimentation constructed a cathode with many pins. A o- reichalkinos 24mm diameter cylinder dug slightly, creating a socket, which placed pins. The pins mounted to the socket with tile adhesive ment and formed a cylindrical diameter area ~ 18mm. This construction was done by hand, of course, could not all the pins are at the same height. The final anode-cathode distance, the particular terminal shown final Kd 17mm, however, results in the noticed sizes compared with those of the pin to a distance 15mm from the anode. Given lychni- driving levels we are likely disruption start from the pin which is higher than all the others and to spread only in some of the neighboring countries.

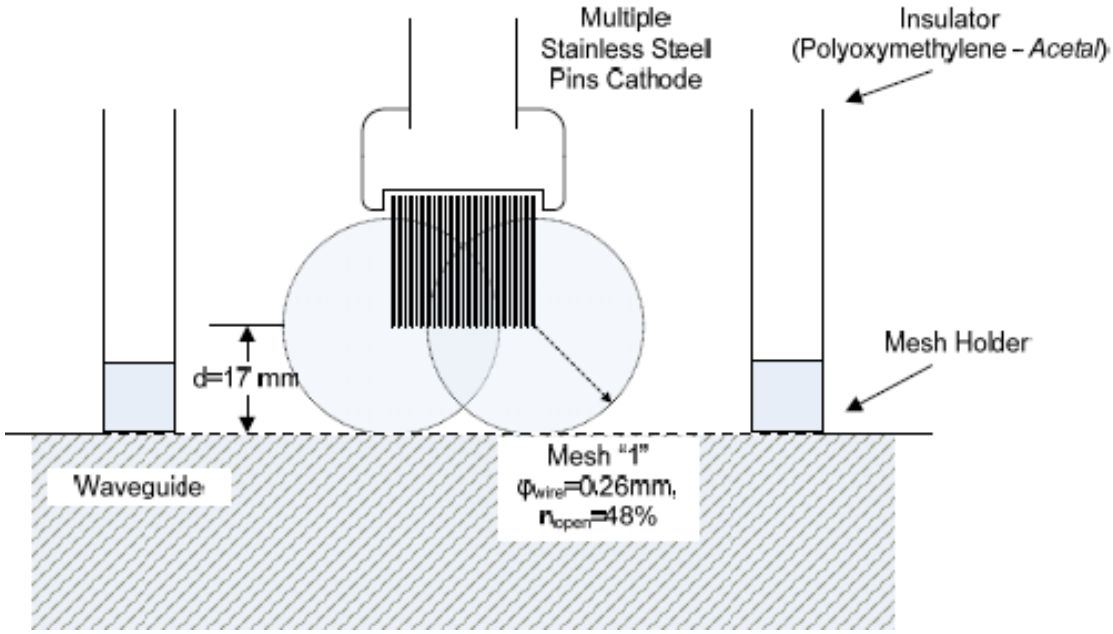

Fig. 6.110: Configuration diode with cathode pins and many dAK = 17mm.

Fig. 6111: Descent of many pins.

Based on the nomogram of Fig. 5.20, the maximum diameter of the cathode, for a distance of 17mm from the anode, is approximately 50mm. Since the diameter of the probe so EI- 18mm (stack pin), we can safely say that the culvert of electronic s channeled to the anode grid and not on the mesh support hoop.

6.3.8.1. Macroscopic Experimental Sizes

The following tables lists the recorded peak voltages, current and power in the passage for at least ten (10) iterations, a charging pri- tefontos of 50, 75 and 100V AC. According to what has been stated in paragraphs 5.5 and 6.3.2, the loads they give impulse *0.6 / 50*With maximum widths 52, 78 and 104kV.

The voltage, current and power of the diode are given as mean and the calculated dispersion *p*the recorded maximum, in any state of charge, with semiotics *<X> ± 1 · sx*.

Tab. 6.21: Descent Multi Pin dAK = 17mm, Mesh "1", (Measurements 27/03/2008)

Load	50V AC	75V AC	100V AC
Max Surge	~ 52kV	~ 78kV	~ 104kV
Current Ion Pump	0.29 ~ 0.33mA	0.37 ~ 0.45mA	0.38 ~ 0.53mA
Lifting	4 ~ 4.5m	5.8 ~ 6.6mA	7 ~ 8.2mA
Voltage typical	49.3 ± 3.0kV	78.3 ± 6.3kV	89.1 ± 5.7kV
Typical Power	720 ± 95A	1335 ± 99A	1645 ± 55A
Power typical	13.1 ± 1.7MW	41.1 ± 5.7MW	65.2 ± 5.5MW
RF typical	**0.1 ~ 0.5W**	**0.2 ~ 2W**	**0.5 ~ 5W**
Efficiency typical	10-8 ~ 6 · 10-8	10-8 ~ 2 · 10-7	2 · 10-8 ~**4 · 10-7**
RF max recorded	**1W**	**7W**	**12W**

Tab. 6.22: Descent Multi Pin dAK = 17mm, Mesh "1", (Measurements 03/28/2008)

Load	50V AC	75V AC	100V AC
Max Surge	(Not out)	~ 78kV	~ 104kV
Current Ion Pump	-	0.28 ~ 0.36mA	0.40 ~ 0.53mA
Lifting	-	5.8 ~ 7.2mA	6 ~ 8.1m
Voltage typical	-	72.5 ± 4.1kV	85.8 ± 10.7kV
Typical Power	-	1187 ± 125A	1611 ± 131A
Power typical	-	37.9 ± 6.7MW	72.6 ± 12.0MW
RF typical	-	**0.5 ~ 10W**	**0.5 ~ 5W**
Efficiency typical	-	10-8 ~ 4 · 10-7	10-8 ~ 7 · 10-8
RF max recorded	-	**12W**	**6W**

Tab. 6.23: Descent Multi Pin dAK = 17mm, Mesh "1", (Measurements 03/31/2008)

Load	50V AC	75V AC	100V AC
Max Surge	~ 52kV	~ 78kV	~ 104kV
Current Ion Pump	0.23 ~ 0.29mA	0.29 ~ 0.35mA	0.36 ~ 0.40mA
Lifting	2.5 ~ 3.5m	5 ~ 6.2mA	5.8 ~ 6.8mA
Voltage typical	50.3 ± 2.9kV	71.5 ± 4.9kV	80.4 ± 3.9kV
Typical Power	790 ± 46A	1257 ± 125A	1593 ± 63A
Power typical	11.0 ± 3.4MW	35.8 ± 8.5MW	49.6 ± 8.3MW
RF typical	**0.1 ~ 0.5W**	**0.2 ~ 5W**	**0.5 ~ 5W**
Efficiency typical	10-8 ~ 10-7	10-8 ~ 5 · 10-7	10.8 ~ 3**· 10-7**
RF max recorded	**2W**	**12W**	**12W**

The estimated pressure in the passage area is as current of Ion Pump in mA at the moment before impact, multiplied by 10-4 Torr (see. Par. 6.1). Therefore the 0.2mA corresponding to 2 · 10-5Torr. The current of the ionization pump the moment of impact rises rapidly (within approximately 0.5sec) over an order of magnitude. Longer impulse voltage causes, naturally, greater surge current pump ioni- tion. The gassing seems to be lower in the next few days testing.

The descent with many spikes gave small amounts of microwave signal and sizable diaspora in macroscopic drive sizes. The offered power in the passage, as seen from the recorded values, takes prices from 40MW to 80MW, mainly due to unstable collapse the gap. The largest recorded that Timoleon RF Mes reach 12W, significantly smaller amounts of power from re- Methods tip.

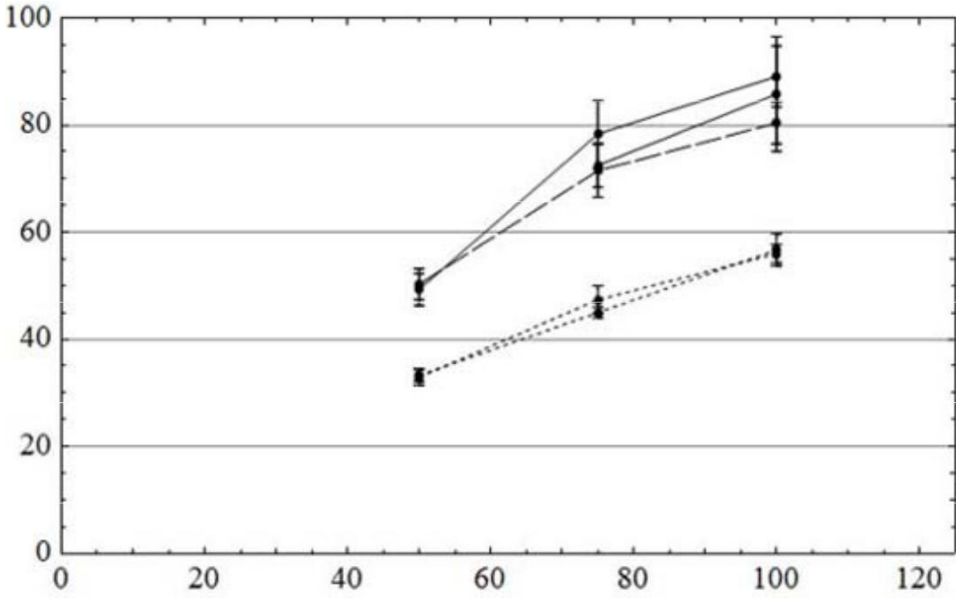

Fig. 6.112: Maximum voltage diode. Descent multi-pin first day and second day (solid lines), the third day (dotted line), the cathode pin (dotted Secretary mesh). Grid no. "1" dAK = 15mm.

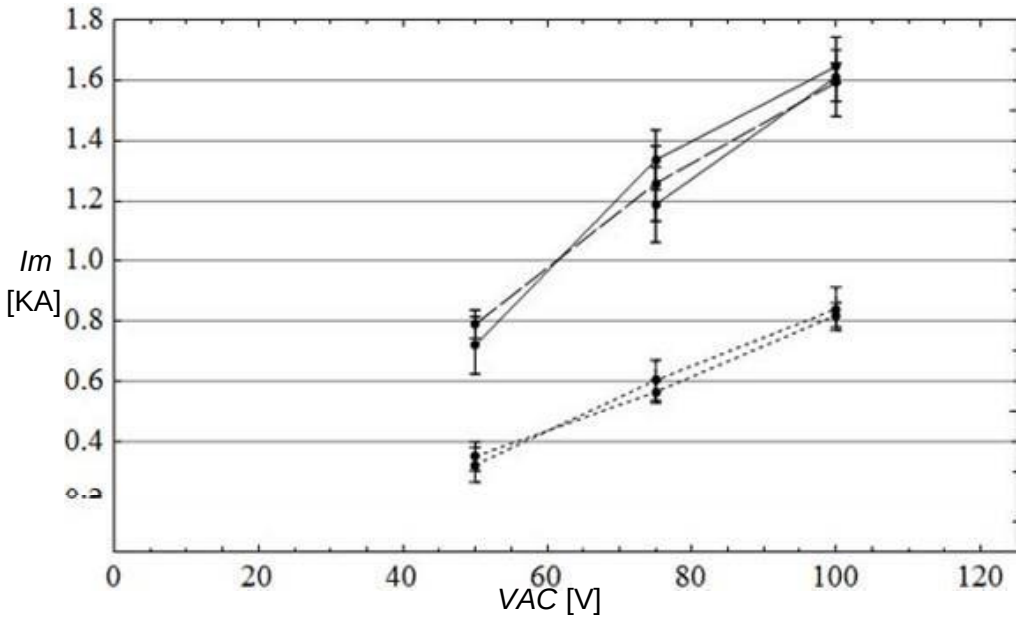

Fig. 6.113: Maximum diode current. Descent multi-pin first day and second day (solid lines), the third day (dotted line), the cathode pin (dotted Secretary mesh). Grid no. "1" dAK = 15mm.

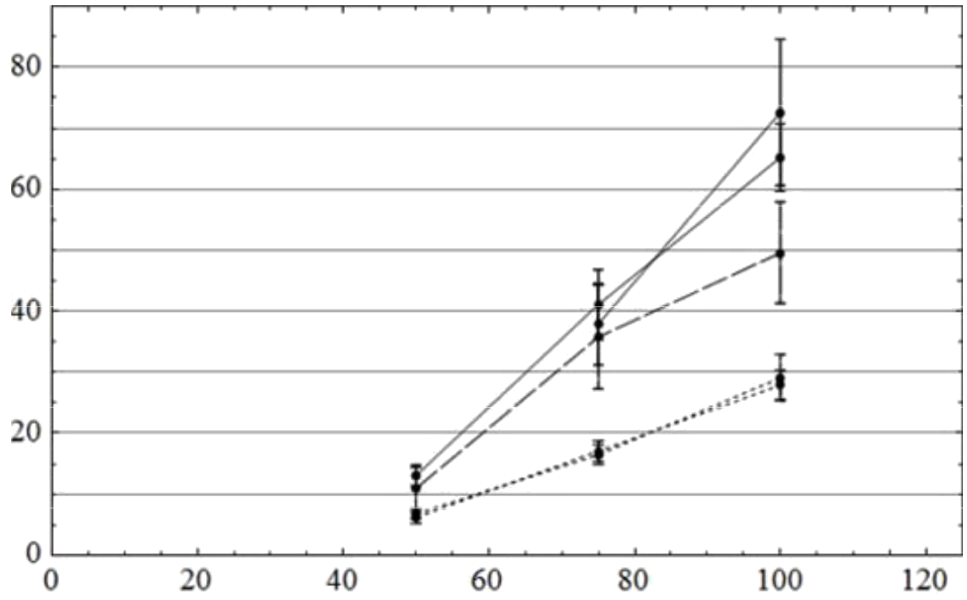

Fig. 6114: Maximum power diode. Descent multi-pin first day and second day (solid lines), the third day (dotted line), the cathode pin (dotted Secretary mesh). Grid no. "1" dAK = 15mm.

6.3.8.2. Model Discharge Capacity by Diode

The descent with many pins shows high dispersion in drive sizes. The not very symmetrical placement of pins onto the brass strain results do not know what is the total number of pins that con- tribute plasma explosive electronic emission. Trying to anaparagou- to rear sizes, consider the following theoretical model: Given a driving voltage, say the 75kV, a typical maximum current is 1000A. The power diake- mind in this case is around 35MW. The experimental results showed that bridging the gap typically takes 200-400nsec for all voltages Direc- tion. Therefore, the calculated collapse speed for the gap of 17mm is between 4 and 7cm / microseconds. Transporting these parameters in the model of Fri 4.3.6 and still. 6.3.3.2, we *k*= 2.33 · 10-6A / V3 / 2, distance reinforcement *d*= 0.017m, geometri- RH anode grid permeability *n*= 48% initial voltage capacitor *V (0)=V0*= 75kV, coun- ritikotita capacitor *C*= 1.2nF. If we define initial active cathode radius equal to 2mm, we can take voltage changes, current and power approaching investigational results. The effective radius is substantially represents the start in- kriktikis electron emission from only some of the cathode pins. The simulation importance discharge with the above data is shown in Fig. 6.115. Bo- then sible to calculate the diode current required to feed the kyma- todigiki cavity with critical peak beam current. This stream is denoted by the dotted line. The passageway leads to more current than is necessary after the first 120nsec. From that moment onwards we can see what the anamenome- images output frequencies Vircator, based on theoretical models.

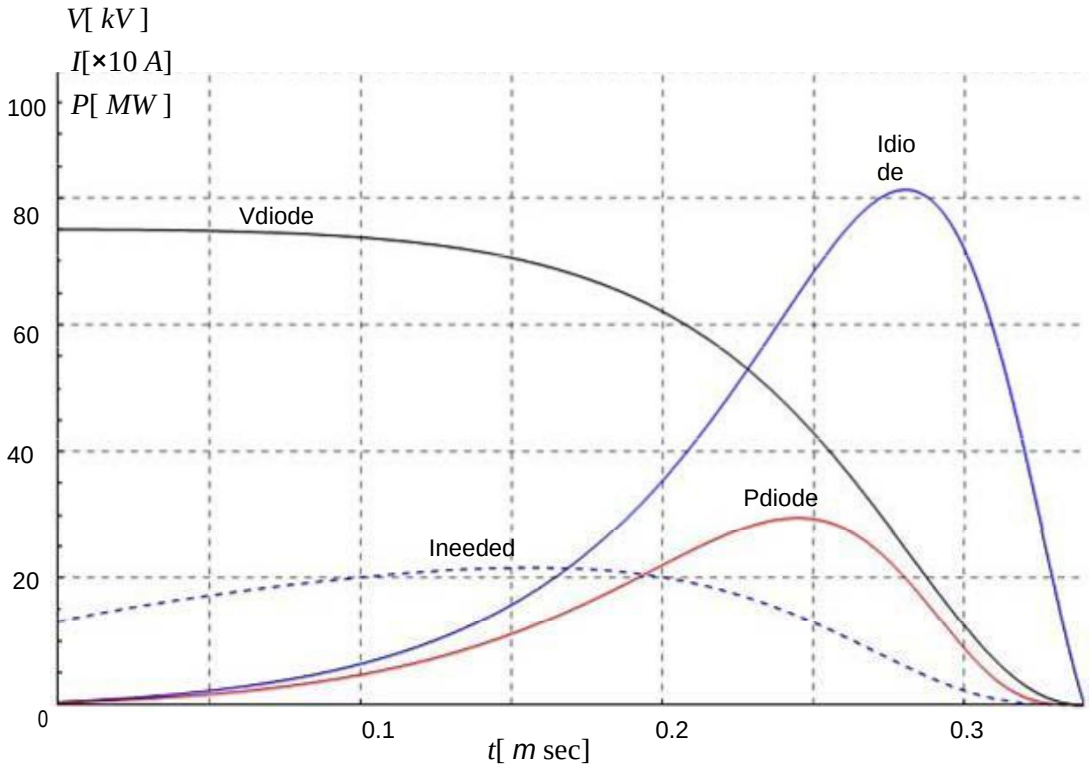

Fig. 6.115: Theoretical variation of voltage, current and power at the cathode multi-pin dAK = 17mm, for drive voltage 75kV, capacity capacitor 1.2nF, rapidly collapse spacing 5cm / microseconds.

H plasma frequency of the electron beam, which enters the inactive area can be calculated from the relativistic equation (4.42). In this expression in place of the current package *I*, Substituting the amount (4.69) multiplied by the geometrical permeability of the matrix, *n*. In the denominator of the equation (4.42) we make the appropriate anti-time dependence of the radius of the cathode, which we assume and radius of the beam. The change of plasma frequency is described by (4.71), where the coefficients b and c depend on the tension in the passage and described by equations (4.44) and (4.45). The frequency of oscillation of the virtual cathode, according to what has been reported in par. 4.1.2, is between the values *fp* and (2n) 1/2*fp*. In Fig. 6116 marked: the area bounded by the frequencies at Timoleon Mes *fp* and (2n) 1/2*fp*The two estimates of frequency reflexing, non-relativistic and relevant tikistiki as described in par. 4.1.1. Finally made and the assessment of Woo,
Eq. (4.16).

H path leads higher current than necessary after the first 170nsec. From that moment onwards we can see what will be the expected output frequencies Vircator, based on theoretical prediction models. The output frequencies are shown removed from the 2GHz. It is important to note that there is a region in which the flow passageway is sufficiently strong to have formations tion virtual cathode. However, forecasts for output frequencies quickly removed from the area of 1.8 to 2GHz.

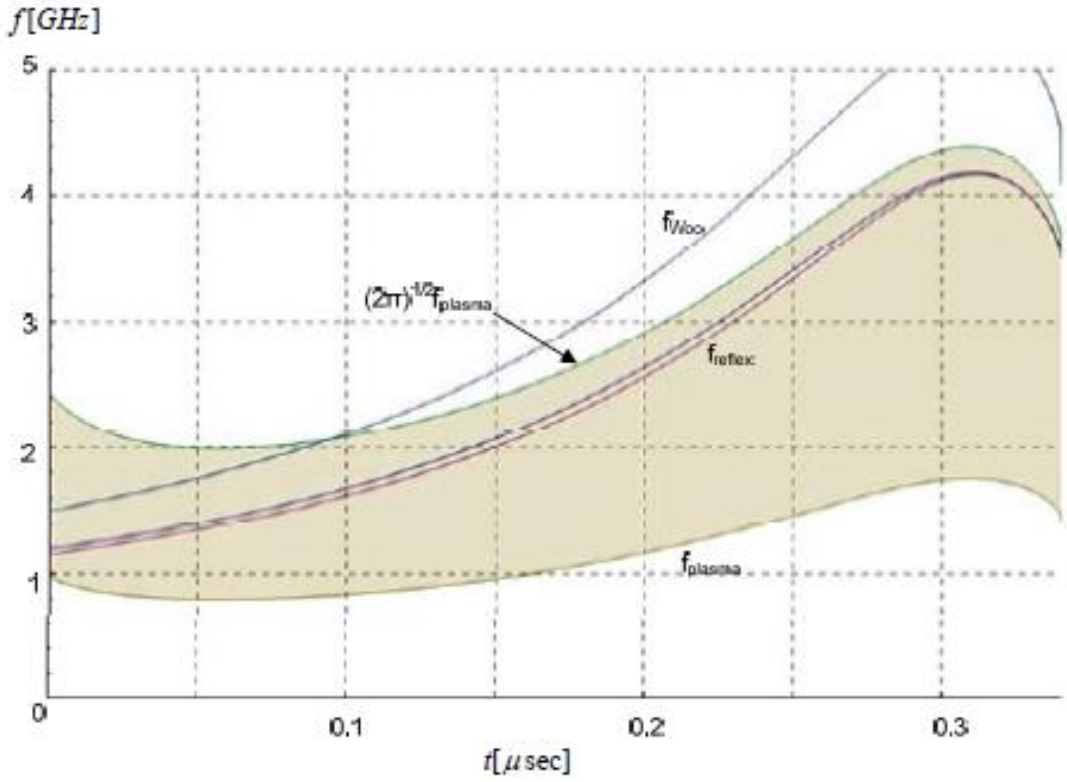

Fig. 6116: Output frequency Assessments Vircator descent with many pins with dAK = 17mm, for discharge voltage 75kV, capacitor 1.2nF, with clearance speed crash 5cm / microseconds.

6.3.8.3. Typical measurements

The diode configuration with multiple cathode pin exhibits quite anomalous behavior at the time of collapse. Bridging the gap typically lasts 200- 400nsec for all driving voltages. The calculated collapse speed EI- yes between 4 and 7cm / microseconds and reasonably attributable to the plasma spread both the anode and the cathode. During the phenomenon, the voltage and current of the diode fluctuate always the diode switches to talantou- next behavior. The interest in this configuration is the presence of small ypsi- often signals that occur before the collapse of the gap. Where appropriate due to small currents emitted by one of the pins and alpha coma while the trend is quite lower. Without being able to cause intense thermal marking the electrodes and start the collapse process, these streams where appropriate passing vertically waveguide and excite microwave signals, without forming part of a virtual cathode phenomenon.

Case A (74kV, 1000A, 33MW, 5cm / msec)

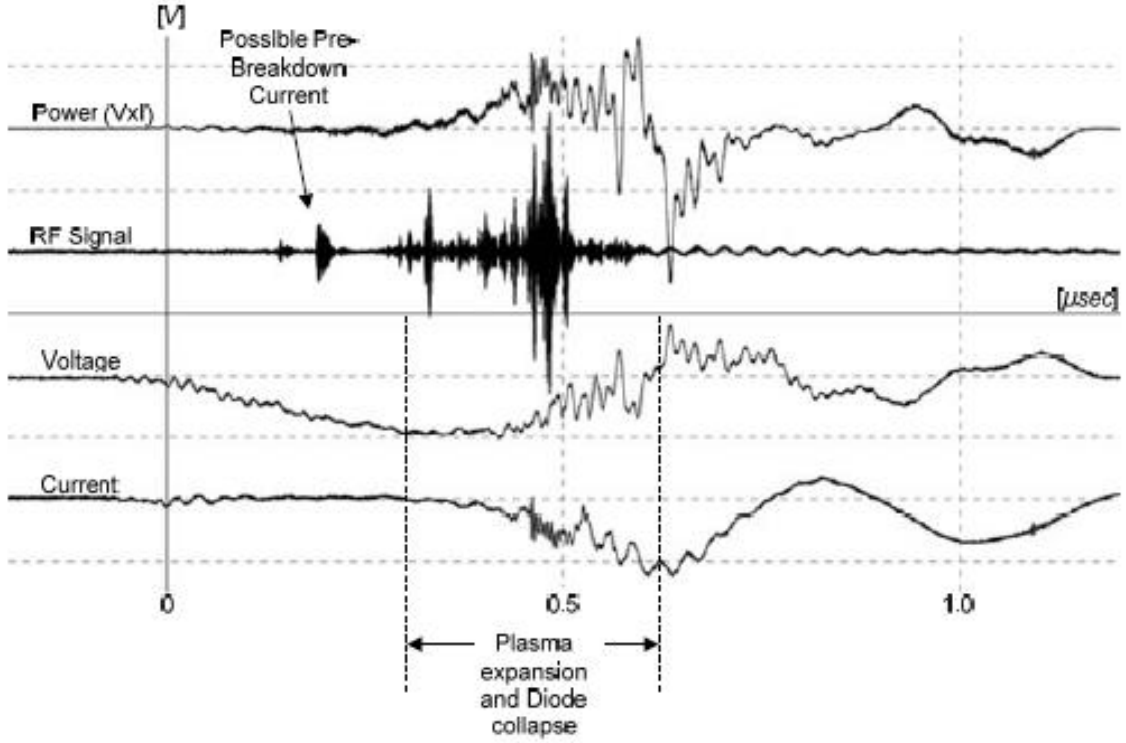

Fig. 6117: Descent many pin dAK = 17mm, mesh no. '1' (measured 20080328m05): Vmax = 74kV, Imax = 1000A, RFmax = 4W, Pmax = 33MW.

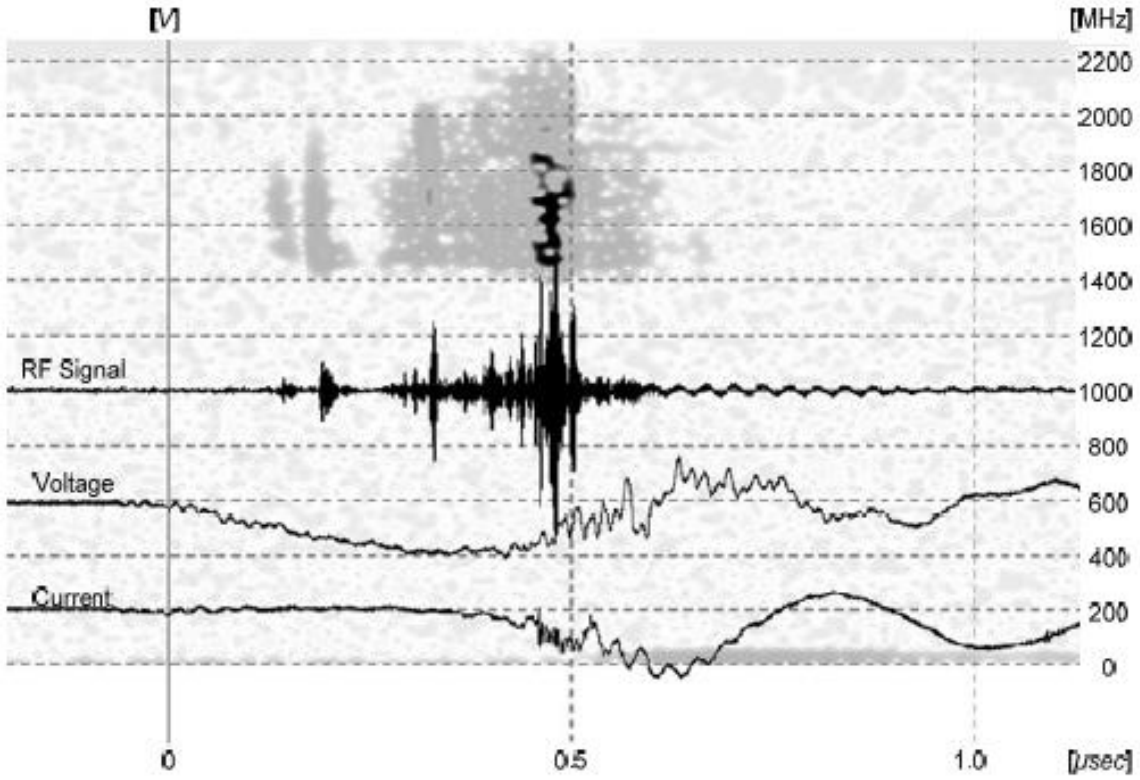

Fig. 6118: Descent many pin dAK = 17mm (measurement 20080328m05): Show chro-mind-spectrum.

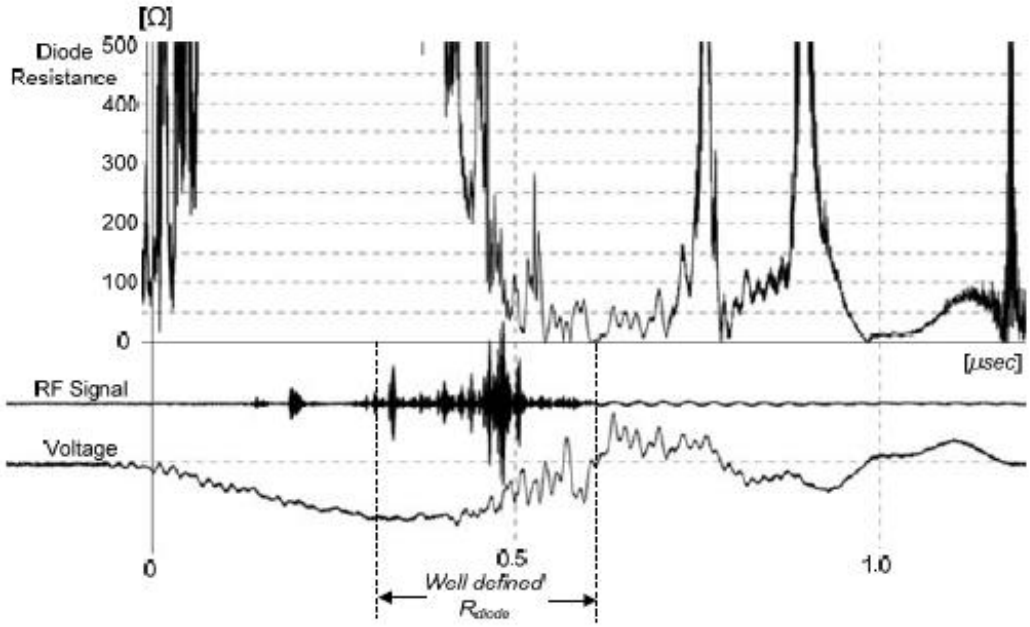

Fig. 6119: Descent many pin dAK = 17mm (measurement 20080328m05): Resistance appointment period.

Case B (76kV, 1300A, 35MW, 5cm / msec)

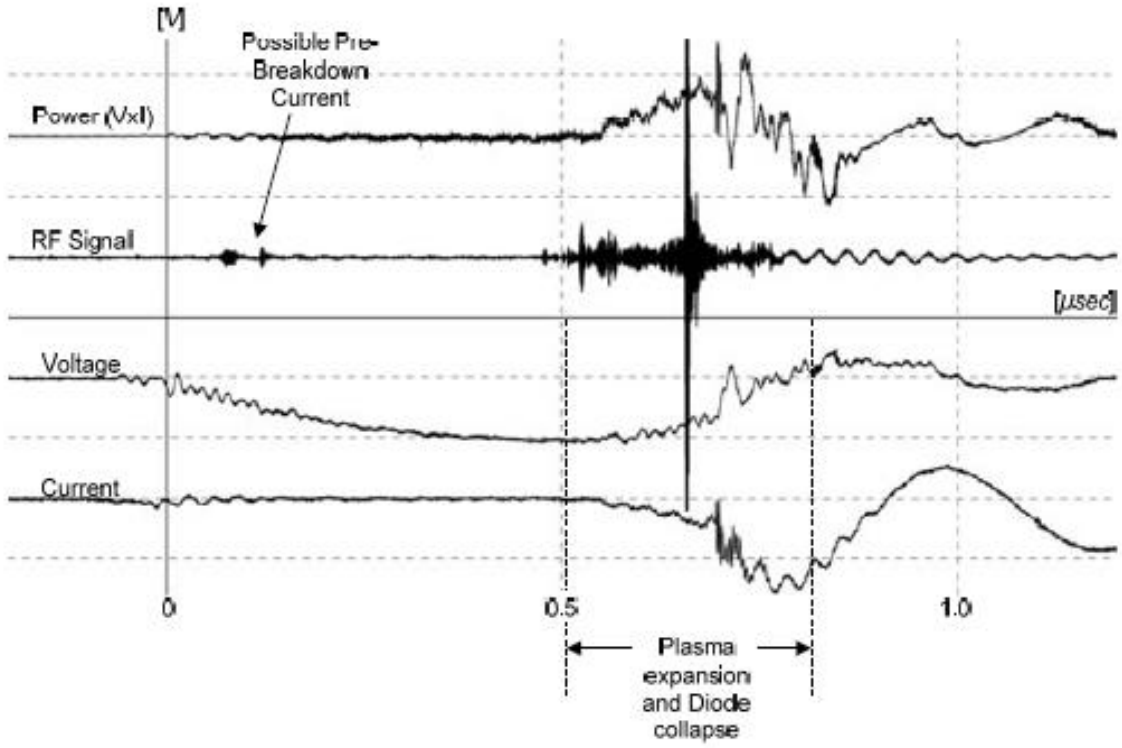

Fig. 6120: Descent many pin dAK = 17mm, mesh no. '1' (measured 20080331m28): Vmax = 76kV, Imax = 1300A, RFmax = 12W, Pmax = 35MW.

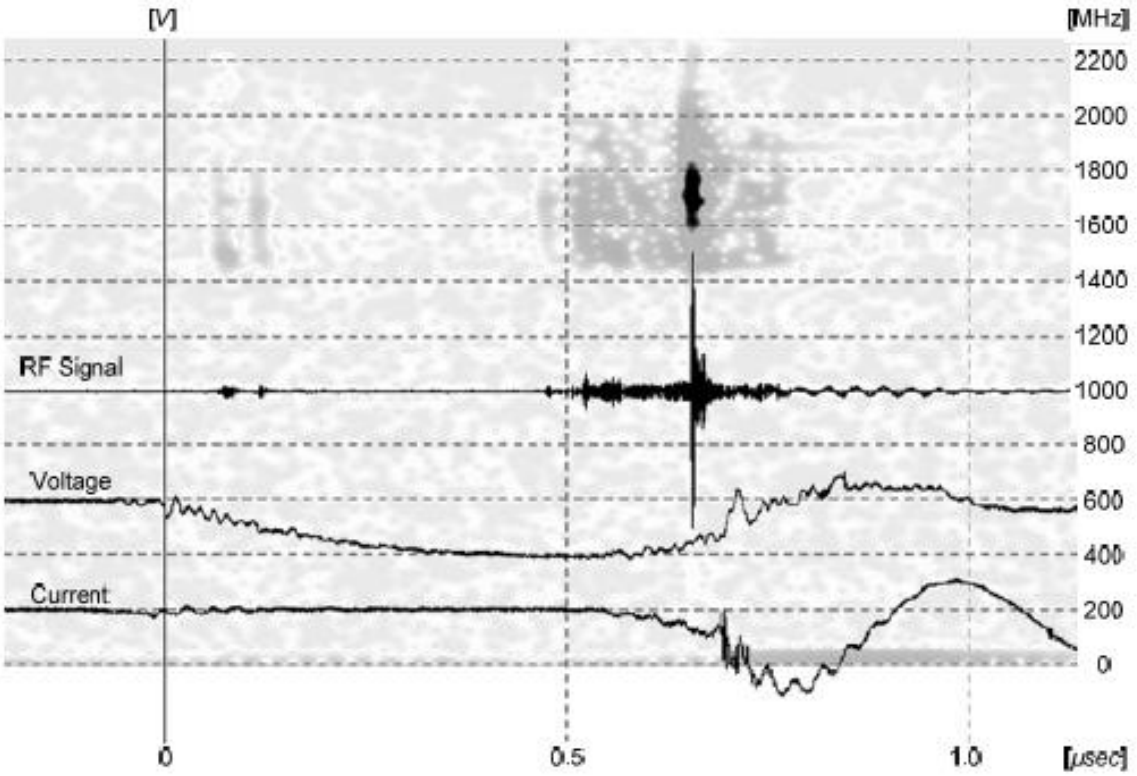

Fig. 6121: Descent many pin dAK = 17mm (measurement 20080331m28): Show chro-mind-spectrum.

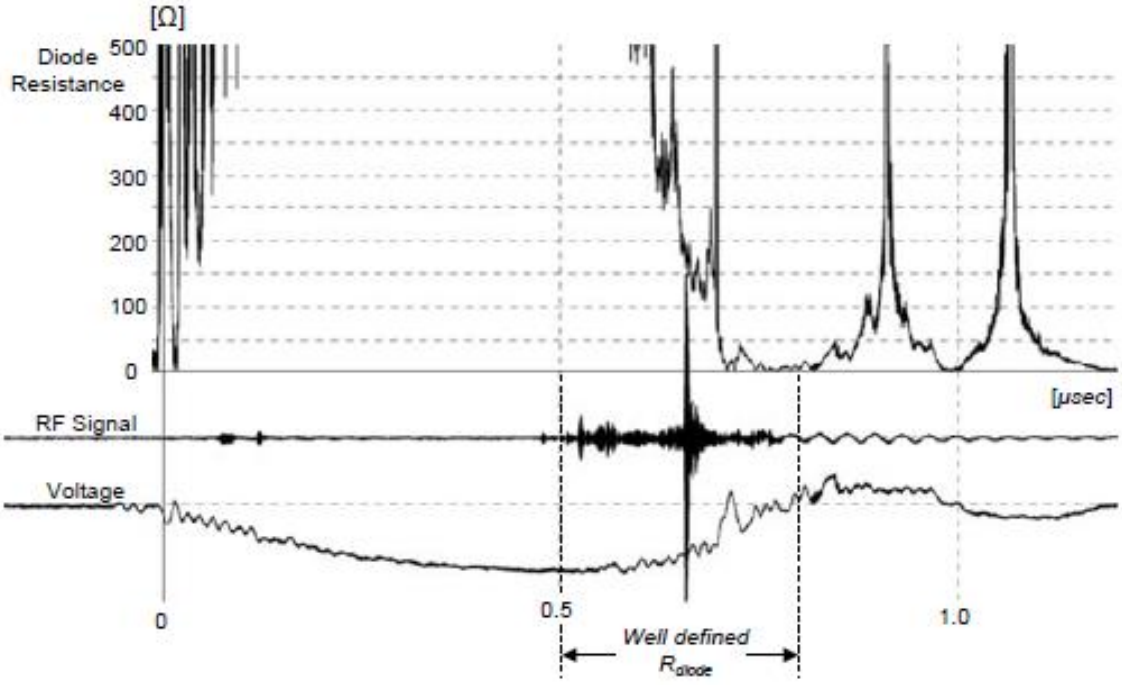

Fig. 6122: Descent many pin dAK = 15mm (measurement 20080331m28): Resistance appointment period.

6.3.9. Cylindrical Descent with Grooves (d = 14mm)

For further experimentation, a cathode formed of aluminum, which has a cylindrical shape with a 30mm cross-section and has grooves on the bottom. It was constructed by hand, unlike the stainless steel cathodes, as it leaves a distance of 14mm from the anode.

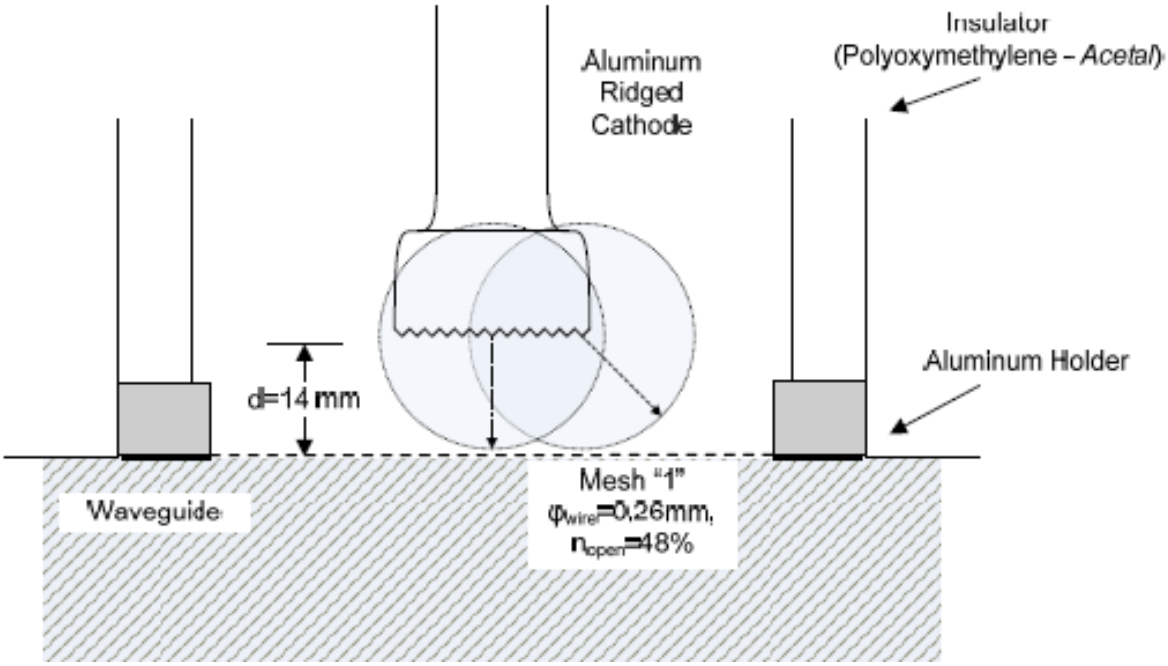

Fig. 6.123: Configuration diode with cathode concentric grooves and dAK = 15mm.

Based on the nomogram of Fig. 5.20, the maximum diameter of the cathode for a distance 14mm from the anode is about 50mm. Since the diameter of the probe so EI-30mm, we can safely say that the drain of electrons injected into the grid anode rather than the mesh support hoop.

Fig. 6124: Descent grooved, dAK = 14mm.

6.3.9.1. Macroscopic Experimental Sizes

The following tables lists the recorded maximum voltage values, liquidity Matos and power in the diode, for at least ten (10) repetitions in charge protefo- dos equal to 100V AC. According to what has been stated in paragraphs 5.5 and 6.3.2, charging gives impulse *0.6 / 50*A maximum width ~ 104kV. The voltage, current and power of the diode are given as mean and the calculated dispersion *p* the maximum katagegramme- images in any state of charge, with the notation *<X> ± 1 · sx*. In this configuration, the gap had a resistance value smaller impulse voltages.

Tab. 6.24: Descent with Grooves dAK = 14mm, Mesh "1", (Measurements 18-04-2008)

Load	50V AC	75V AC	100V AC
Max Surge	(No decay)	(No decay)	~ 104kV
Current Ion Pump	0.2m	0.2m	0.2 ~ 0.25m
Lifting	×	×	6.8 ~ 7.8mA
Voltage typical	×	×	112 ± 3.0kV
Typical Power	×	×	2041 ± 36A
Power typical	×	×	64.6 ± 15MW
RF typical	×	×	***no RF***
Efficiency typical	×	×	-
RF max recorded	×	×	no RF

Tab. 6.25: Descent with Grooves dAK = 14mm, Mesh "1", (Measurements 21-04-2008)

Load	50V AC	75V AC	100V AC
Max Surge	(No decay)	(No decay)	~ 104kV
Current Ion Pump	0.18mA	0.18mA	0.18 ~ 0.25m
Lifting	×	×	6.2 ~ 8.1m
Voltage typical	×	×	99.1 ± 7.1kV
Typical Power	×	×	1934 ± 53A
Power typical	×	×	32.0 ± 12.0MW
RF typical	×	×	***no RF***
Efficiency typical	×	×	-
RF max recorded	×	×	no RF

The estimated pressure in the passage area is as current of Ion Pump in mA at the moment before impact, multiplied by 10-4 Torr (see. Par. 6.1). Therefore the 0.2mA corresponding to 2 · 10-5Torr. The current of the ionization pump the moment of impact rises rapidly (within approximately 0.5sec) over an order of magnitude. It was observed that the E- enemas gas is smaller at the second day of testing. This stood importance never showed microwave output. This might be due to the occurrence of microwave radiation at frequencies well above 2GHz, and the large surface of the stream, which, in combination with the available capacity Direc- tion, attaches rheumatic patients densities, not capable of generating phenylbutyl acted, virtual cathode.

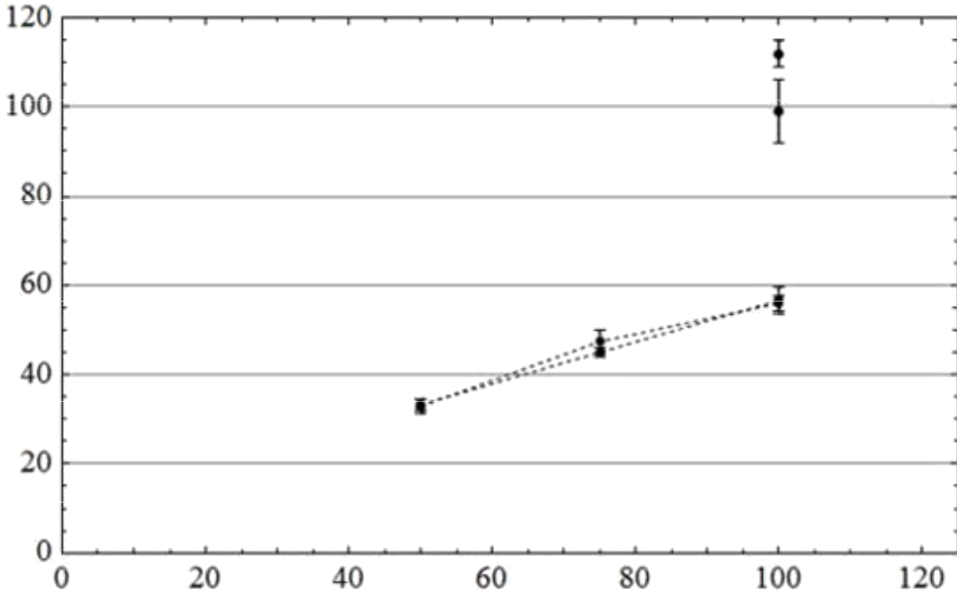

Fig. 6.125: Maximum voltage diode. Descent grooves, first and second day, pin cathode (dotted lines). Grid no. "1" dAK = 15mm.

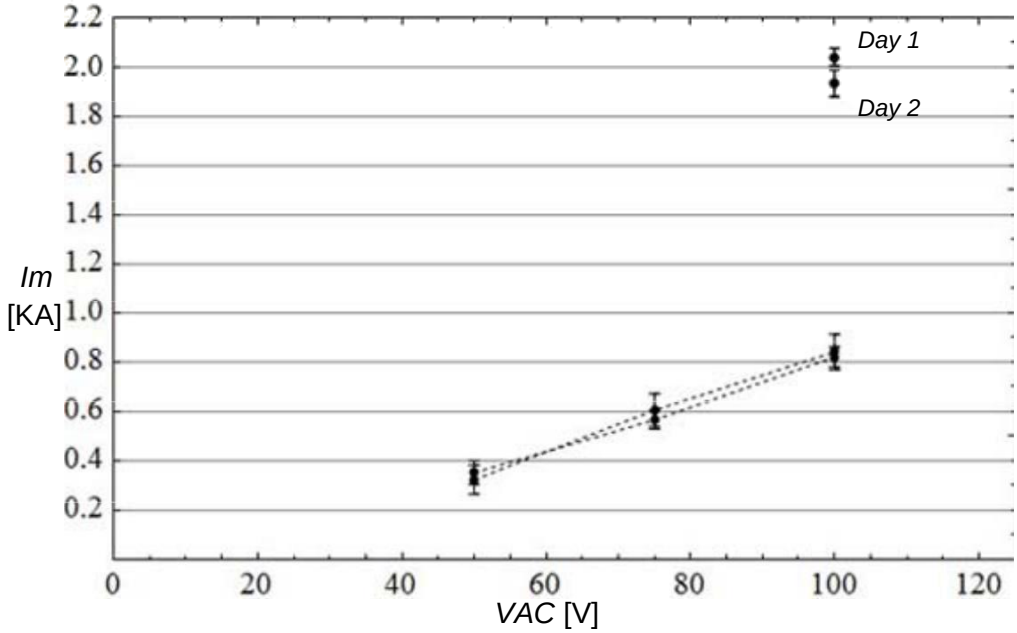

Fig. 6.126: Maximum diode current. Descent grooves, first and second day, laid spike Give (dotted lines). Grid no. "1" dAK = 15mm.

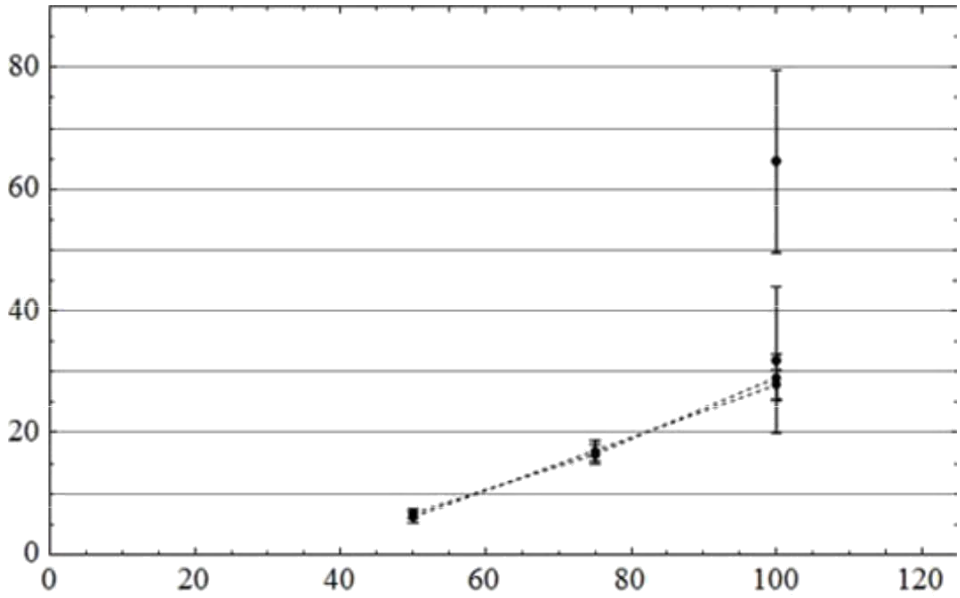

Fig. 6.127: Maximum power diode. Descent grooves, first and second day, laid spike Give (dotted lines). Grid no. "1" dAK = 15mm.

6.3.9.2. Model Discharge Capacity by Diode

H cathode grooves cleaved to impulse voltages on the order of 100kV. The currents are strong enough in the area of 2kA. The collapse of the gap is po- sewage quickly and lasts for about 200nsec, and in some cases even less. The collapse speed arises, therefore, from 7 to 10cm / microseconds. To reproduce drivers sizes, we examine the following theoretical model. The- oroume charging voltage of 100kV capacitor gap and the collapse speed 8cm / microseconds. Adjusting the theoretical simulation with experimental results, we find that the original effective radius of the cathode is about 5mm. Therefore we identified as being at the cathode does not emit electronic current across the surface, but a portion thereof. Transporting these parameters in the model of Fri 4.3.6 and still. 6.3.3.2, we *k*= 2.33 · 10-6A / V3 / 2, distance reinforcement *d*= 0.014m, geometric di- impermeability mesh anode *n*= 48% initial voltage capacitor *V (0)=V0*= 100kV, a capacity capacitor ness *C*= 1.2nF. If we define initial active cathode radius equal to 5mm, can we take voltage changes, current and power that approaches the experimental results Kd. The effective radius is essentially represents the start explosives tion electron emission from only a portion of the cathode surface. Simulation discharge with the above data shown in Fig. 6.128. Then we can calculate the diode current required to feed the kymatodigiki cavity with critical peak beam current. This stream is denoted by cov diasti- line. The passageway leads to more current than is necessary after the first 80nsec. From that moment onwards we can see what will be the expected frequency output quantities of Vircator, based on theoretical models.

H plasma frequency of the electron beam, which enters the inactive area can be calculated from the relativistic equation (4.42). In this expression in place of the current package *I*, Substituting the amount (4.69), multiplied by

geometrical permeability of the matrix, *n*. In the denominator of the equation (4.42) we make the appropriate anti-time dependence of the radius of the cathode, which we assume and radius of the beam. The change of plasma frequency is described by (4.71), where the coefficients b and c depend on the tension in the passage and described by equations (4.44) and (4.45).

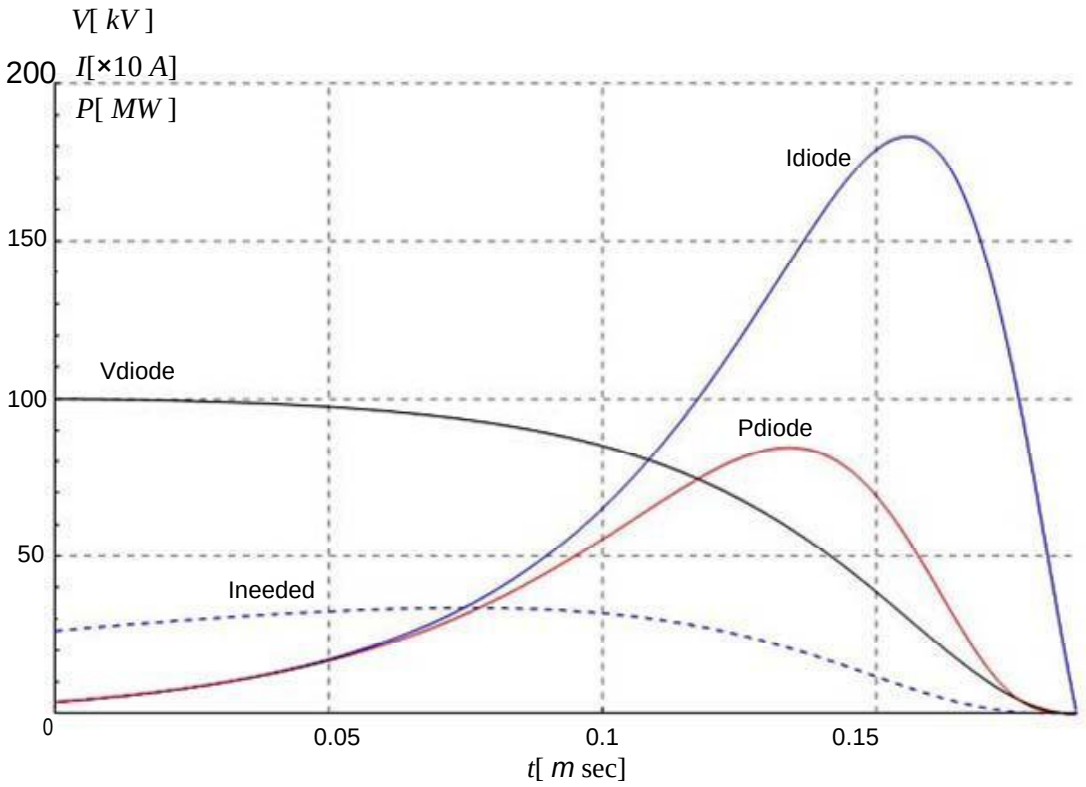

Fig. 6.128: Theoretical variation of voltage, current and power slot cathode dAK = 14mm, for drive voltage 100kV, capacity capacitor 1.2nF, rapidly collapse gap 8cm / microseconds.

The frequency of oscillation of the virtual cathode, according to what are referred brought in par. 4.1.2, is between the values *fp* and (2n) 1/2*fp*. In Fig. 6.129 im- reduced: the area bounded by the frequencies prices *fp* and (2n) 1/2*fp*, Both in-
SSESSMENT frequency reflexing, non-relativistic and relativistic as DESCRIBED out in par. 4.1.1. Finally made and the assessment of Woo, on. (4.16) for the frequency output of Vircator. When the current in the diode exceed 300A, beam energy ~ 90keV, enter the area where the current in the waveguide chamber is AP- CTDC powerful to be able to form the virtual cathode. But what happens after the first 80nsec, where the planned output frequencies of light are quite sta- tion from 2GHz. In particular, the relativistic and non-relativistic approach to the frequency of oscillation reflex gives frequencies higher than 2.5GHz, while the expected oscillation frequency of the virtual cathode is also quite sta- tion from 2GHz. The estimates of the theoretical model can justify a- Pusan microwave signal during testing of this terminal.

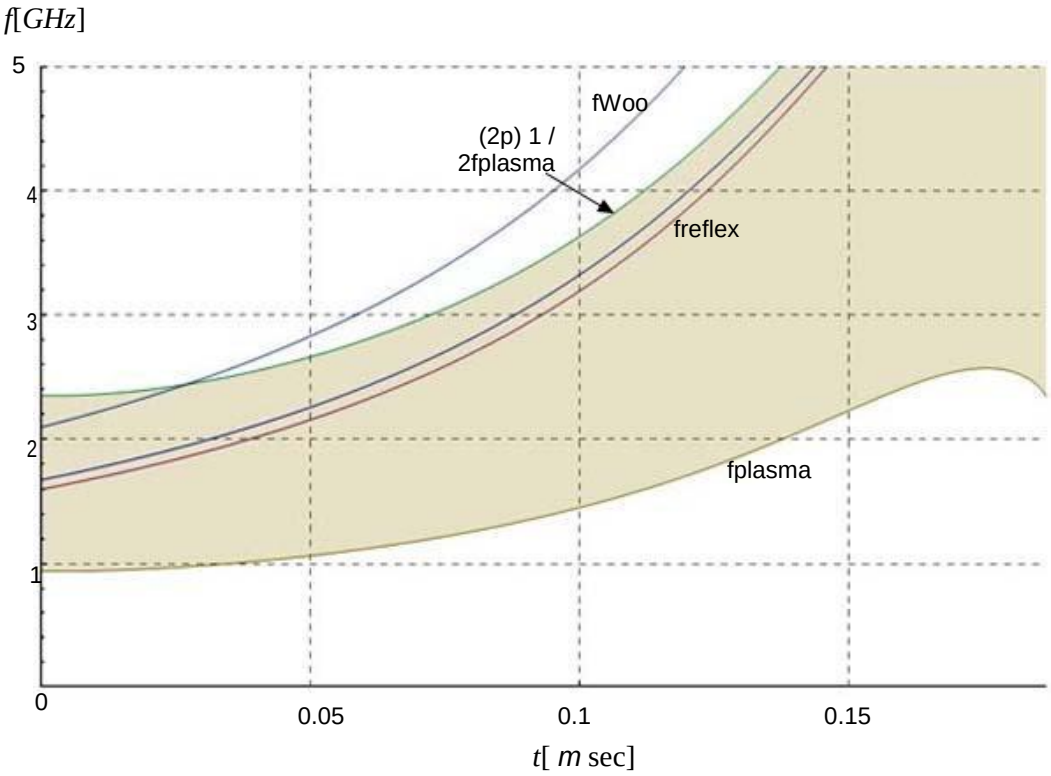

Fig. 6.129: Output frequency Assessments Vircator grooved cathode, with dAK = 14mm, for discharge voltage 100kV, capacitor 1.2nF, with collapse speed diake- mind 8cm / microseconds.

6.3.9.3. Typical measurements

The cathode is of resistance to all smaller voltage levels and cleaved only the impulse amplitude 100kV. The collapse of the gap is very rapid and di- long about 200nsec, and in some cases even less. The speed of collapse arises therefore from 7 to 10cm / microseconds. The variation in sizes during the degradation phenomenon is very high.

Case A (106kV, 2000A, 55MW, 8cm / msec)

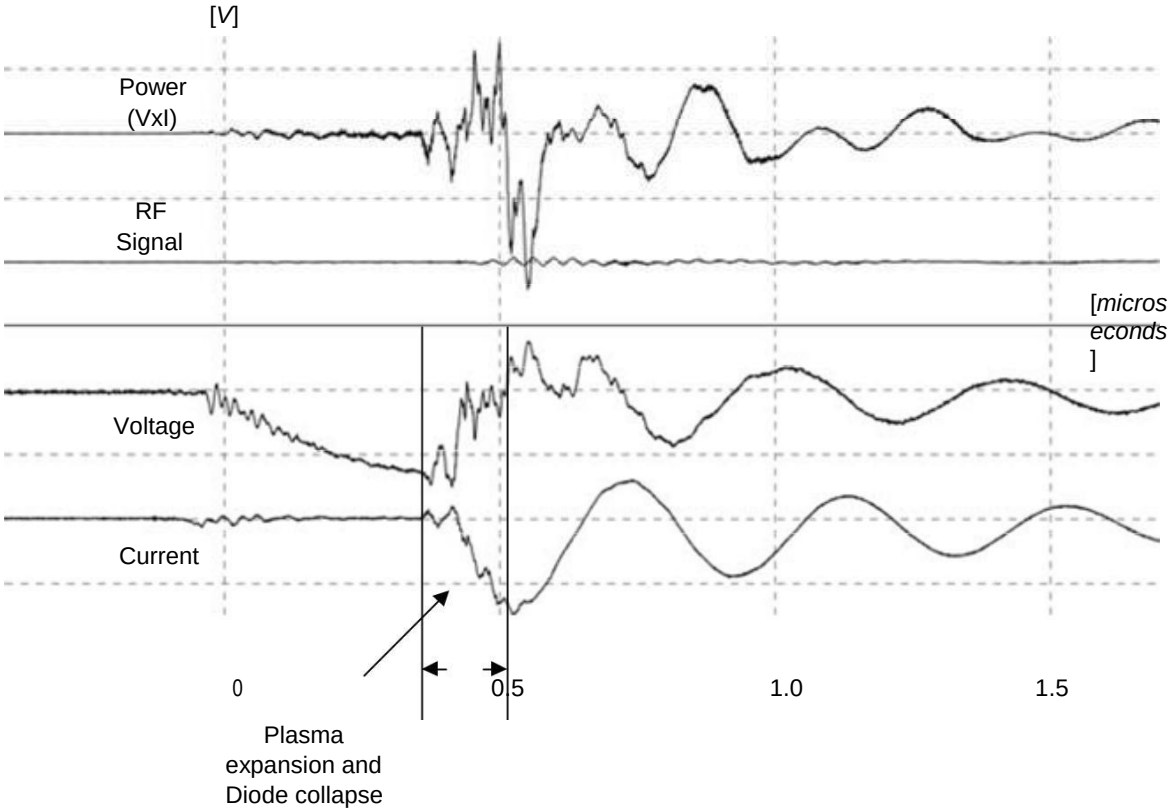

Fig. 6.130: Descent grooved, dAK = 14mm, mesh no. '1' (measured 20080418m03): Vmax = 106kV, Imax = 2000A, RFmax = 0W, Pmax = 55MW.

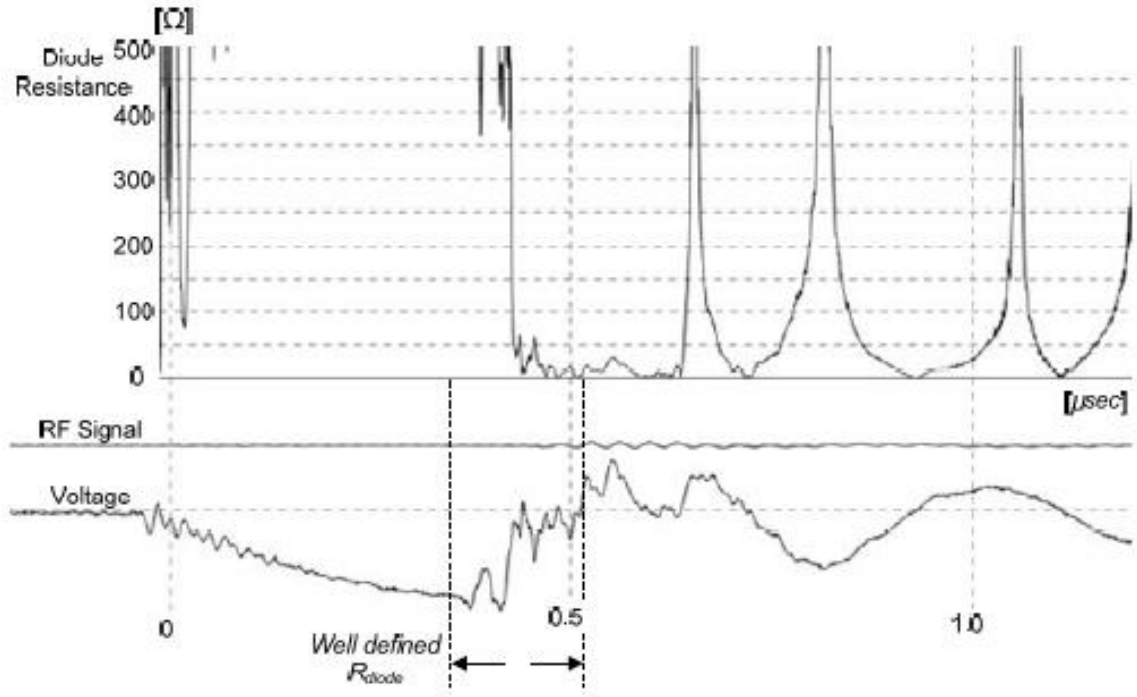

Fig. 6131: Descent grooved, dAK = 14mm (20080418m03 measurement): Resistance appointment period.

6.4. Observation of X Rays

Naturally, the actions which the electrons are accelerated to the lamp, be producing rays X, both the anode and the metal walls of the waveguide, at the points reached by the electron beam. In order to have some insight into the production of X-rays from the lamp, placed two aktinogra- fika Kodak film X-Omat (Ready Pack), measuring approximately 24cmx30cm, just below the lamp and on the side thereof. These films are packed in photo- tostegi folder and can be used independently, for exposure to rays X, coun- Piq need other equipment. The film, which was placed under the lamp was level and in full contact with the lower surface of the waveguide. The film, which was replaced on the side, made good contact only with the waveguide, but with the metallic curved neck, which resulted in a slightly distorted image. For the exhibition of the films were completely at random, 100 shocks in lamp voltage appointed period that reached approximately 90kV. The cathode used in this se- ries shock was spike with anode-cathode distance of 2.5cm. The film thereafter appeared in radiology and laboratory results were omologoume- fore very interesting. In Fig. 6132 shows the X-ray from the underside of the waveguide positioned above the draft Vircator, to the situation during experiment for viewing of the result. We observe that there is very E- Don irradiation from the area just below the passage, due to the electrons that strike the bottom surface of the waveguide. There is also a "shadow", which coincides with the position of the irises in the waveguide, and is evident by the rapid depreciation of the power of radiation at a distance.

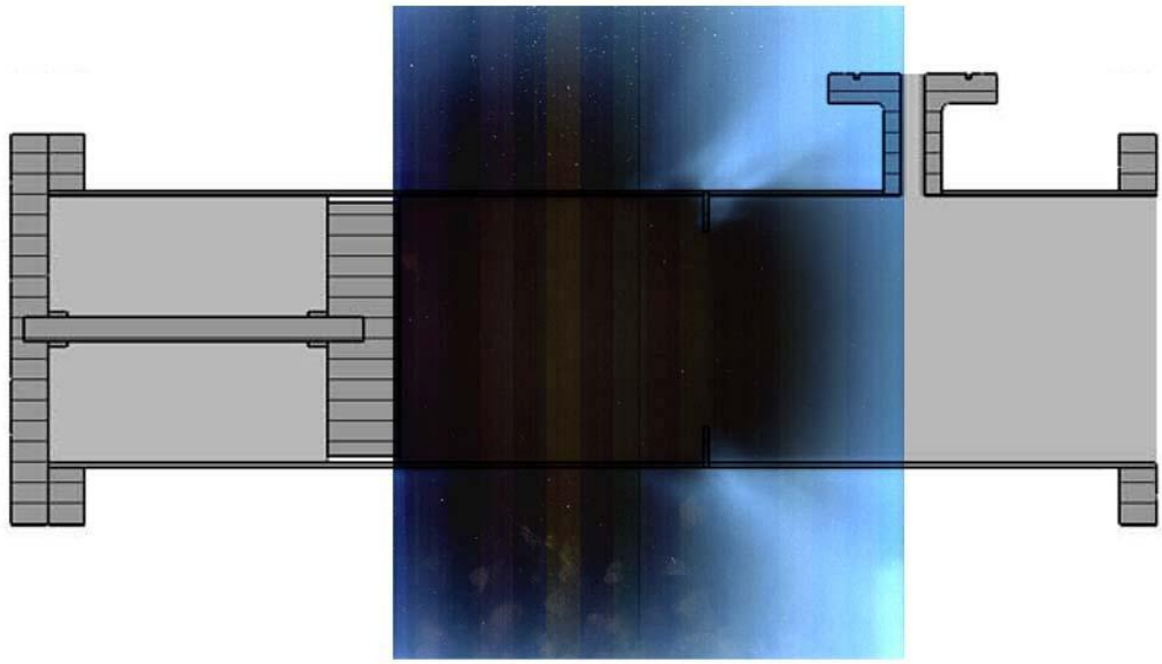

Fig. 6132: X-appeared after 100 strokes with diode voltage ~ 90kV and cathode pin (dA-K = 2.5cm).

In Fig. 6133 shows the X-ray from the side of the waveguide positioned above the draft Vircator, to the situation during experiment for viewing of the result. To emphasize that around the metal neck, the film was kampy- Spent and therefore the radiograph shows a not very clear illustration of the? Monosaccharide from the device. Low beside the waveguide, the image is representative, after the film was in good contact with the outer surface. Discrimination nontai clean the shadows left by irises and epoxy resins, which been used even at the base of the metal neck and points stuck the irises. Intense a- ktinovolisi X rays is so the lower surface of the waveguide, and the area of the passage. The shadow of the anode region is the component that secures the metal mesh, and in general a large amount of me- metals and resins in that region. Also, the formulations are distinguished, due under the screws seal the insulator onto the waveguide.

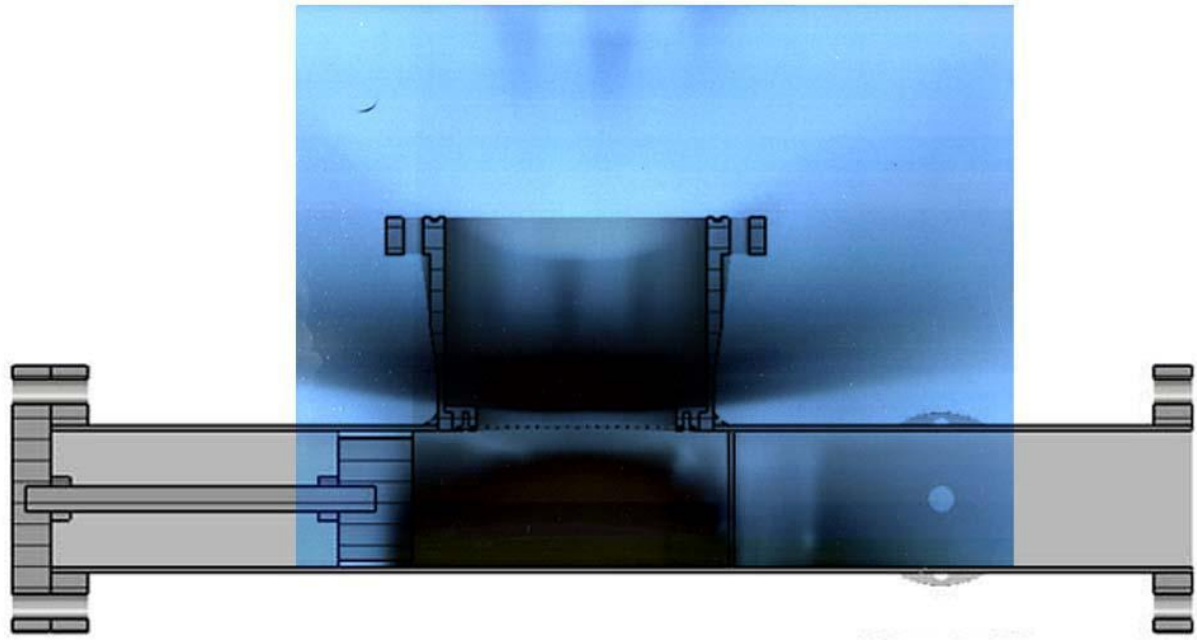

Fig. 6133: X-appeared after 100 strokes with diode voltage ~ 90kV and cathode pin (dA-K = 2.5cm).

To estimate the output radiation from the device used only di- athesimo gauge the InoVision 451B of Victoreen (Fluke), which detects X akti- images from operations 7keV over [136]. This body is essentially unfit for one such measurement, because the phenomenon is very short, osis and pulse the lamp. Production of x-ray done for a period of less than 500nsec in any impact, while the instrument is not prescribed for as short pulse. Specifically, the response of the instrument according to the manufacturer is 2sec. Measurements were taken at three distances from the lamp, showed tech- tragoniki reducing power ray X, in accordance with the theoretical prediction. We do not know whether they can be an indication of the average radiation dose produced by Vircator, but prove the exponential decrease with distance.

Specifically, at 40cm from the lamp and to the plane of the waveguide, the *maximum* SO-night per impact recorded was 0.1mSv, at 60cm from the lamp was 0.04mSv while at 140cm from the lamp was 0.01mSv. These data are adjusted for the model

$$D = a \cdot \frac{1}{xb} \quad , \tag{6.25}$$

with $a \cong 276$ and $b \cong 2.15$, ie very close to 2. The results are summarized in the following chart.

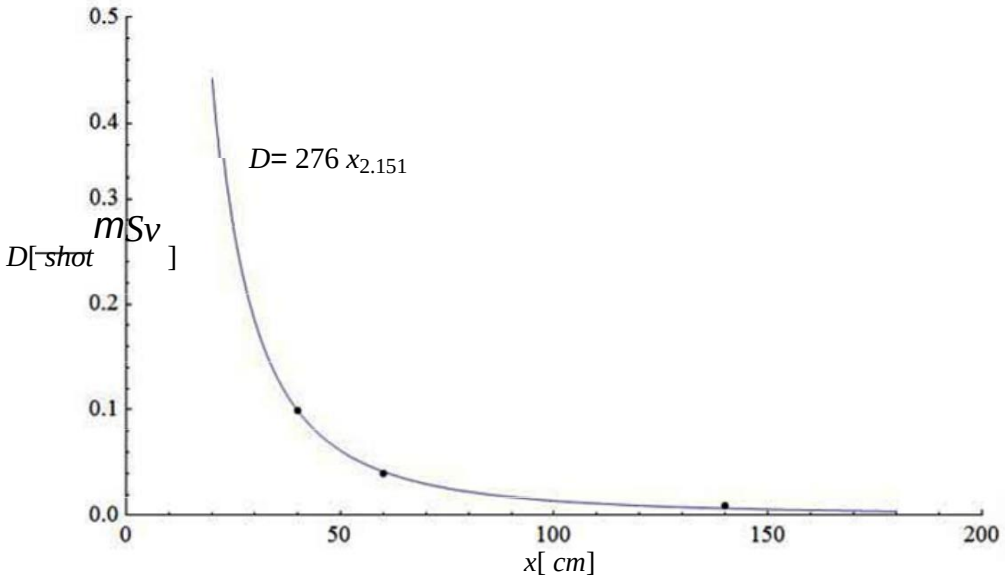

Fig. 6.134: Measured X-ray dose in relation to the distance from the lamp, for Direc- tion at 100kV.

These amounts, which relate to three distances from the lamp are a predominant amount cumulative dose was observed in a pulse of light. The instrument used, the Victoreen 451B has a small ionization chamber, about 350cm2. The logic of the divider in this case consists of the total load produced by ionizing process and collected in the anode electrode or-Ganos. Because the phenomenon takes a long while, the ionized particles experience reunification therefore load neutralized prior record the total MR "population" of the measuring instrument. The reconnection process of operators and ultimately recorded dose for X-ray pulses of short duration is complex and requires parameters of the instrument, which we are not able to know, O how pressure ionizable gas (ionization chamber organ), type the appliance to the gas used, mobility operators tend ion collector and the format, such as the diode collecting the ionization derived from the rays X.

The only way to determine the cumulative production of X-rays from such a device is using radiological film, which is subject to cumulative alteration of chemical composition thus constitutes an integrator of radiation. Have knowledge ozone characteristics color response of the film, relative to the radiation is incident, and by a calibration of the film by a known source, borou-

with, from coloring, to find the dose of radiation they hit. For this experiment, the images appeared, Fig. 6132 and Fig. 6133, They can be compared to color with a typical chest X-ray. This type of radiography using doses of one mSv, up 10mSv. Assuming that the film has been illustrated an equivalent dose of a radiography tho- Pakala, the black area corresponds to a dose 1mSv, which as we have said, have come from 100 replications. Therefore, a distance of the order of 5cm from the lamp, wherein *We believe* it's in the film, each impact delivers dose 10mSv. From exponential party law calculated previously, the dose per impact at 5cm would be eight (!) MSv, a figure that is, if anything, in the same order of magnitude as our assumptions. Based on these assumptions, it is not unreasonable to assume that the measured doses of the instrument within a range of magnitude in terms of output SO- importance in mSv from Vircator, for diode driving to 100kV. Assuming that the instrument response gives amounts so unrealistic that we are 100 times below the actual levels of radiation, the dose per impact falls in a relatively small amount of 0.1mSv at 5 meters from the lamp.

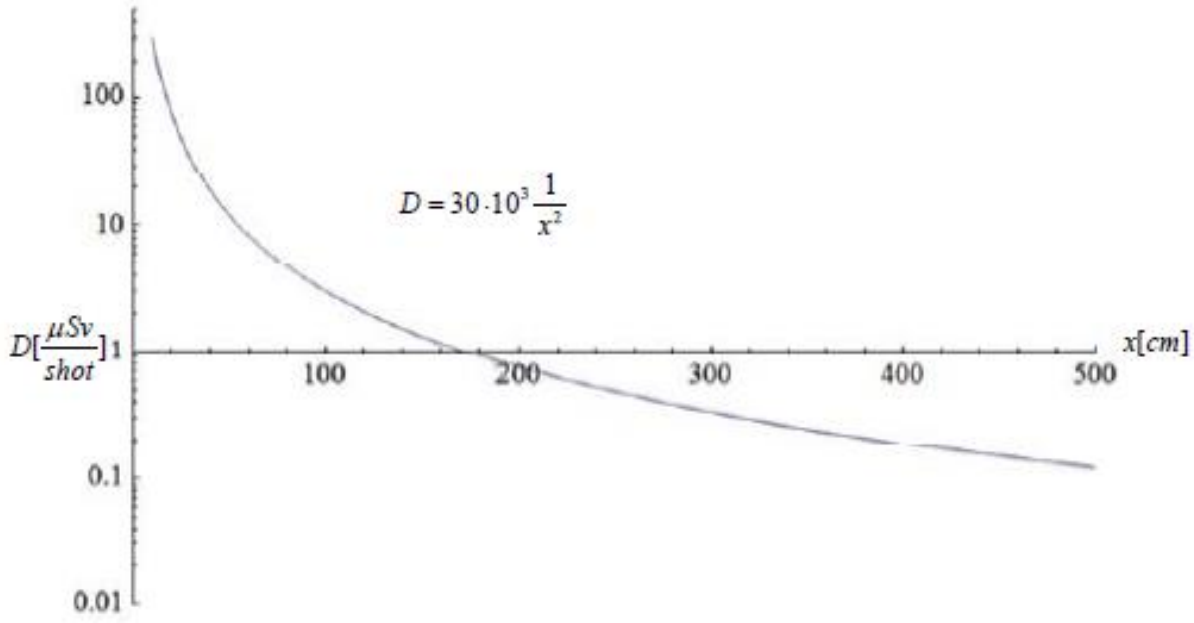

Fig. 6.135: Adverse scenario producing X-rays per impact (100 times more potent than the measured values), in relation to the distance from the lamp, driving the 100kV.

For the safety of experiments, if they are to become an even larger voltage levels, it is necessary not in sight of the lamp, with me- solavisi of an appropriate partition. Concrete is very good shielding rays X, when it comes to a typical thick structural body. Alternatively or additionally, the waveguide may be coated with a thick lead sheet only 2mm, thus reducing the radiation several hundred times. For the effectiveness of the shield of lead, in relation to the effects of radiation X, should be study with the factors weakening of the data to ionizing radiation (X-ray Mass Attenuation Coefficients) [137]. Relevant study is developed in

following paragraph, 7.2.6, since the lamp with leaves of lead mo- coverage was necessary in the new round of experiments with higher voltages.

6.5. Pressure Effect

Tests lamp made, as already mentioned, the ionization pump co dedemeni the body of the lamp and continuous pumping. Each impact is pressure poly- XVIA calculated approximately 10-5 Torr. In order to determine whether the increased Meni pressure affects the microwave output, a series of tests were conducted, in which the ionization pump remained sealed, leaving Vircator without antli- importance. Tests with an increased pressure were to tip cathode dAK = 25mm (see. Par. 6.3.4), the grid number "6", which carries 150 orifices per inch, with a mesh width of 0.109mm, diameter of wire 0.06mm and free surface of ~ 41%.

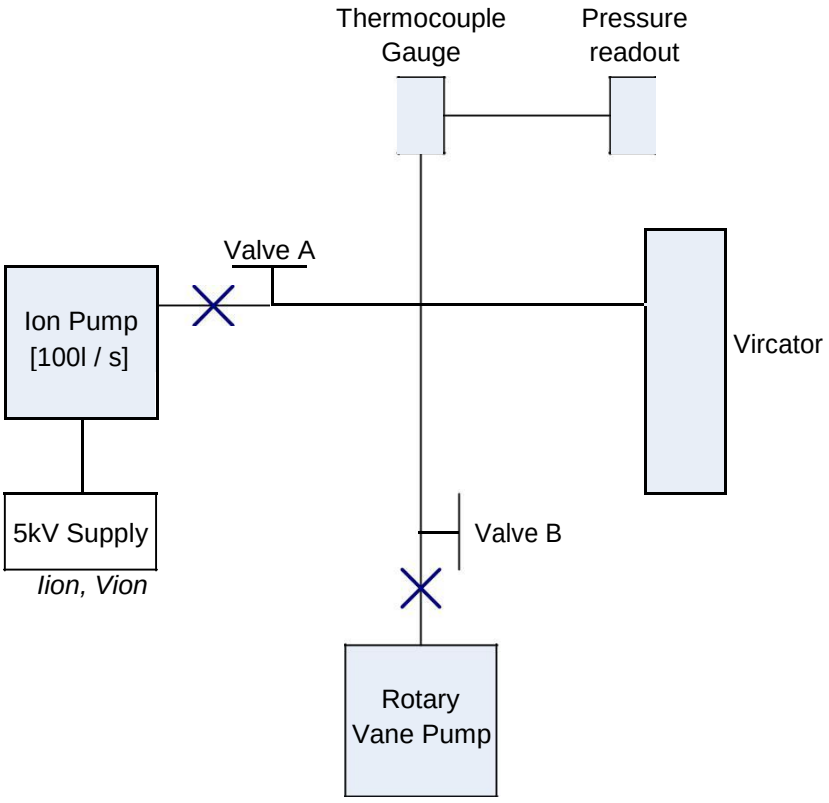

Fig. 6.136: Tests Vircator without associated drainage system.

For these tests, after each shock, take measurements of pressure with thermal mozefgos. As mentioned above (see. Par. 6.1), the indicator thermozef- reasons (Thermocouple gauge) has an operating range of up 1mTorr 760Torr. Since me- measurements it became apparent that each impact raises the total pressure of space 0.2 with 2mTorr. Leakages in the atmosphere are considered negligible and the rate deregulation of frozen gases from the interior surfaces also considered low because the piece has remained in abstraction from the ionization pump for some time. There- fore, the release of gases only from the areas affected by the shock current. The gases, which are responsible for increasing the pressure in each outbreak

night, probably H2, H2O and blocked air gases deep sti- vades metals.

Since the tests were conducted, there was negligible diversification of micro- wave output during the first shock without pumping, ie in the first 10mTorr pressure. Note that already the first impact brings the specimen in the region of 1mTorr pressure, resulting to have no ability to control the phenomenon in the range of 10-4 Torr. Macroscopic specimen sizes for pressures up 10mTorr shall remain relatively undifferentiated, with the only effect slightly faster collapse of the gap and the relatively larger diode currents. However, a striking resemblance to those described in [65], and developed in par. 4.2.4, there seems to be a threshold around 10mTorr, above which the conduct of Vircator changes drastically. The passageway collapses much more quickly, visibly stronger currents, with non Mechanism decomposition gases (Townsend and culverts). Filling plasma is ragdai- a while microwave output continuously limited until it is reset completely to the re- Rioja ~ 50mTorr more.

Two representative recordings are shown in the following graphs. At first, Fig. 6137, recorded an impact with light pressure 4mTorr. It is a charac- raktiristiki test, the pressure range up to 10mTorr. The macroscopic aggregates are driving the same in the case of a high vacuum. The microwave output is always present with the same randomness distinguishing between measurements in a high vacuum. The voltage and current are broadly the same behavior that characterizes the measurements with the pin cathode dAK = 25mm.

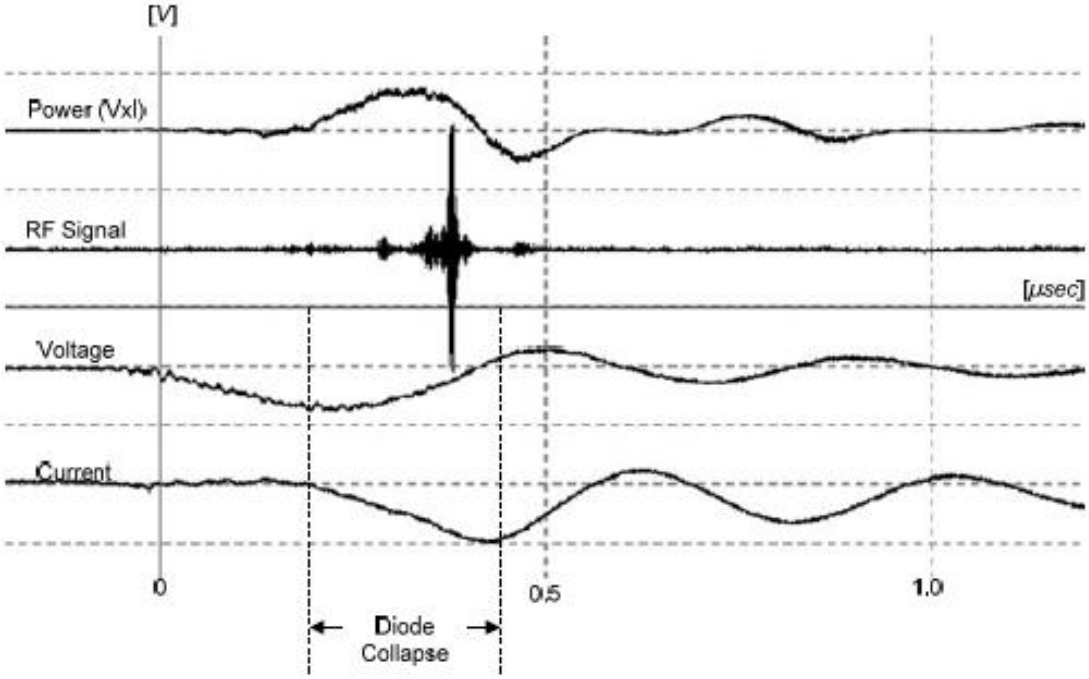

Fig. 6137: Descent pin, dAK = 25mm, mesh no. '6' (measured 20080617m11): Vmax = 52kV, Imax = 800A, Pmax = 17MW, pressure 4mTorr.

Continuing experiments without pumping the waveguide, the pressure in struc- light ciently increases after each high-voltage shock. With the progress of testing production

kept constant increase in the power diode and faster katarref- ing times the gap. The microwave output is limited in time and in place, as we pass the threshold of 10mTorr. Referring to Fig. 6.55 and Fig. 6.58, we find that such a range and diversity of microwave pulse is absent now, with the output limited to weak signals around a short duration 30-40nsec. The voltage collapses very quickly and the current increases rapidly, as shown in Fig. 6.138, measured on approximately 40mTorr. From 50mTorr then, except for a few insignificant exceptions, the microwave output is practically in- xafanistei.

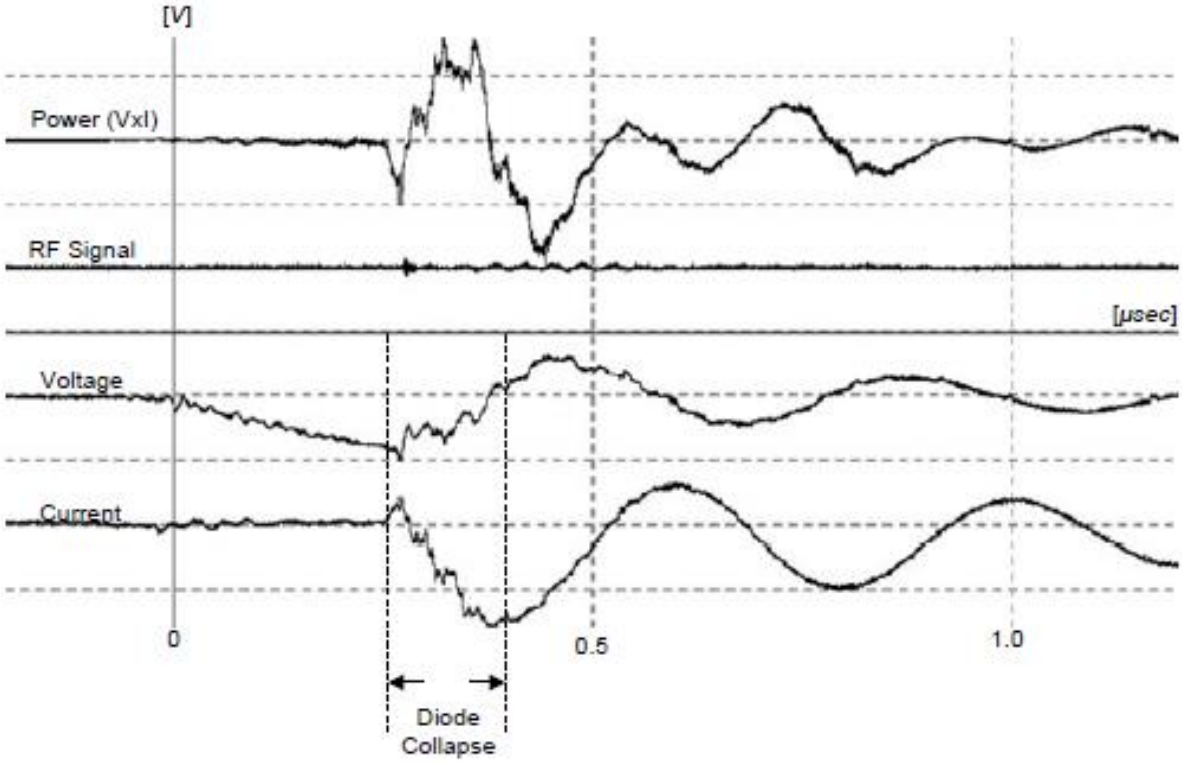

Fig. 6138: Descent pin, dAK = 25mm, mesh no. '6' (measured 20080617m52): Vmax = 71kV, Imax = 1320A, Pmax = 35MW, pressure 40mTorr.

Fig. 6139: High Voltage Laboratory, NTUA, 10.2007 - 07.2008 ...

7. Extension System Vircator

Tests of lamp Vircator, the single-stage impulse device VDE-b, showed that it is possible to drive with a large force, since the striking voltage is relatively narrow and slowly varying (~ 100kV form 0.6 / 50). Furthermore, the tests so far, the capacitive divider, which is directly connected to the core and provides the majority of the current in the diode lamp, E- has small capacity, 1200pF. Therefore, it was decided to construct a multi tertiary generator Marx, larger capacity, which will provide the possibility of driving with considerably more pulses potencies.

As will be shown subsequently designed a multi-stage impulse generator Marx, based on 50kV voltage capacitors and capacity 100nF each. The provision of this provision is to eight steps, giving theoretically able to drive lamp with 400kV voltage. Inserting or not resistance between arrays cess capacitor and the lamp, we can drive current as large as in- pitrepei vacuum diode lamp and any external resistance. Since coun- ritikotita Knock device is significantly larger than those hitherto used, the lamp driving currents can amount to tens of kA, resulting in a pulsed DC power supply to light several hundred MW or even GW. The following sections present the me- say made for the high-voltage system and experimental results of the tests conducted.

7.1. Multistage Impulse Generator

The multistage impulse Marx generators are based on a very simple philosophy. A capacitor bank is charged with DC voltage in parallel and discharged in series, using a scintillator. In a generator Marx, the capacity capacitors *C* loaded in parallel from the source *V0*Through resistor *R1* and resistors *R*. If the spark collapse almost simultaneously, the capacitors are automatically affiliated in series. The scintillators are designed so that this tier has slightly less electrical resistance than others. Alternatively the first spark ignited a small spark or, even, and high-intensity laser (laser triggered spark gap). With N capacitors (N. *steps*) Across the load *Rload* Voltage will appear theoretically equal to *NV0*. If there are no reactors in gov-

circuit and the resistance of the load is purely resistive, the voltage will rise to a maximum of non Timoleon, *NV0*Almost instantaneously. The total capacity of the generator is Marx *C*/ N due to the series connection of the capacitors and hence the voltage at the load deteriorates EXPO- ing time constant *t*=*RloadC*/*N*. Important condition for the Marx generator constitutes the resistance of the load to be sufficiently lower than the resistance of the device *R*, That the voltage apportioned almost entirely on *Rload*. In our case, the cross cutters *S* are simple passive spark gap (spark gaps), the geometry of o what determines their electrical resistance.

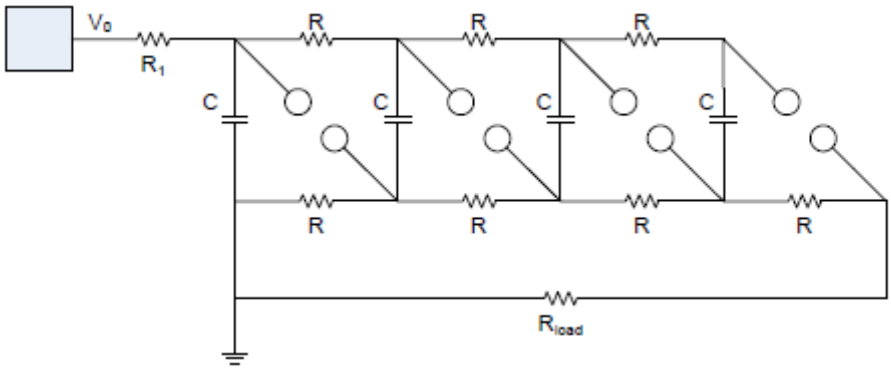

Fig. 7.1: Multistage (tetravathmia) Marx generator.

For this experimental setup sought air capacitors, impulse discharge, voltage 50kV. The 50kV is a charge voltage easily generated, fairly large value in order to multiply at very high voltages with a few steps, while the phenomenon Corona to 50kV is not important whether the conductors of the device are me- godet but not cumbersome sections.

For the implementation of the Marx generator used capacitors voltage DC 50kV and capacity 100nF each. The capacitors they have a parallelepiped shape with dimensions 35.5cm x 10.5cm x 14.5cm, while small sides have threads sup- port M10. The resistors of multistage impulse device chosen is pre- crossed out for DC voltage of 70kV and power 55W [138]. It is cylindrical in shape, 16cm long and cross 30.5mm. The resistors have threaded mounting M8 on both sides. Used 1MO resistors levels of provision and 10MO for charging resistance.

Due to the high resistance value, the Marx generator is very slow chro- nous charging and discharging vacuum load. Selected high value resistors to significantly limit the required charging current from the DC supply. Com- ing, large value resistors eliminate transients between steps during the discharge, thus the sum of the voltage at the output is completely in accordance with the number of stages of the generator.

The following paragraphs present the studies for the electrical behavior of the impulse device, the design estimates for electric strength, the Study for spark plugs and experimental results from the Marx generator.

Fig. 7.2: Capacitor discharge impulse 50kV (left) and resistance 70kV, 55W (de- Xia). The resistors 1MO and 10MO have identical dimensions.

7.1.1. Study Characteristics Charge

For charging the battery of capacitors available high voltage DC power supply (WK125N5 Glassman High Voltage, [139]), 600W power and maximum output voltage 120kV. The
load resistance of 10MO is a limiting factor of the current cargo tisis. In 50kV voltage, maximum charging current, even in the absence of the restriction of the feeder would 5mA. The power supply starts from zero voltage and the output can be adjusted either by potentiometer or analog control signal.

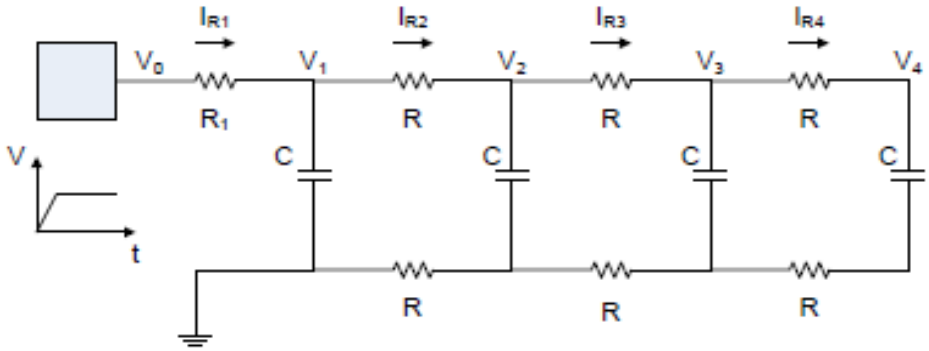

Fig. 7.3: Charging circuit four-stage Marx generator.

The charging circuit is simulated using suitable software package (Agilent ADS). Without loss of generality, we can consider the case BRAKE importance output to rise linearly from 0kV to 50kV within 2sec, by manipulating the power supply. Once the 2sec and then the charging voltage remains constant and equal to 50kV. What we observe is that the levels are loaded with great steadily years, but trends in higher grades attend well enough

tend tier. Therefore, when caused disruption of the spark plug of the first step, the output will approach pretty well tended N*V1*Wherein *V1* the voltage at which the first capacitor is charged. The array of capacitors with charging resistance 10MO and resistance levels 1MO approaches the maximum voltage of 50kV in time 15sec. Specifically, in 15sec tier is charged at 47.8kV, while in 20sec to 49.3kV, where we refer to the charging scenario with ramping voltage within 2sec.

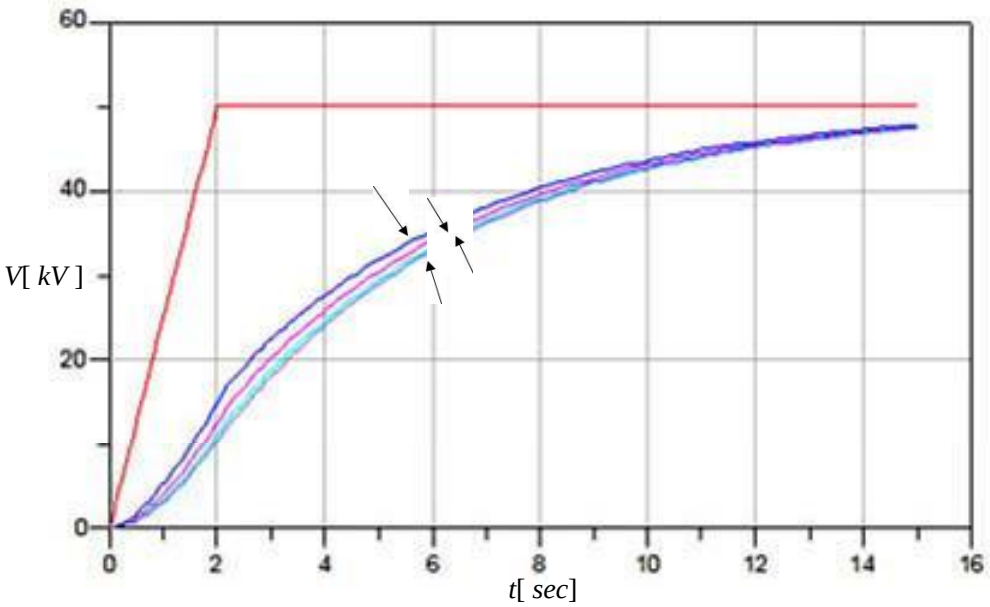

Fig. 7.4: Trends levels.

The charging current is relatively small, decay time. The Mo-screen where the power of resistance of the resistor *R1* is exceeded in the first ~ 4sec. At this stage, the product $IR12 \cdot R$ exceeding 55W for a short time and reaches 120W. The total period during which the power consumption in a- ntistasi is greater than allowable, the order of 2.5sec, this in- Narita charging. It is understood that if the increase in power supply voltage from 50kV to 0kV done in longer (greater than 6sec), the limit of thermal power charging resistance is not exceeded at any time.

The simulation can be repeated for a larger number of stages. For example, an array Marx with 8 levels same data (*C*= 100nF, *R1*= 10MO and *R*= 1MO) It requires about 40sec To charge the 48.6kV. In 50sec the array It is charged to 49.4kV. The results of these simulations on our character- ktiristikes charge give a feeling of repetition rate shock, which varies in the limits of 0.1Hz. Since it is desirable to accelerate this rate, smaller charging resistors should be sought in effect greater power supply capacity. For example, this oktavath- a generator is charged to 50kV within 7 sec, if the load resistance is 1MO and resistance generator 100k. The maximum instantaneous load current is 16mA, or- TOI momentary feed-in power 800W.

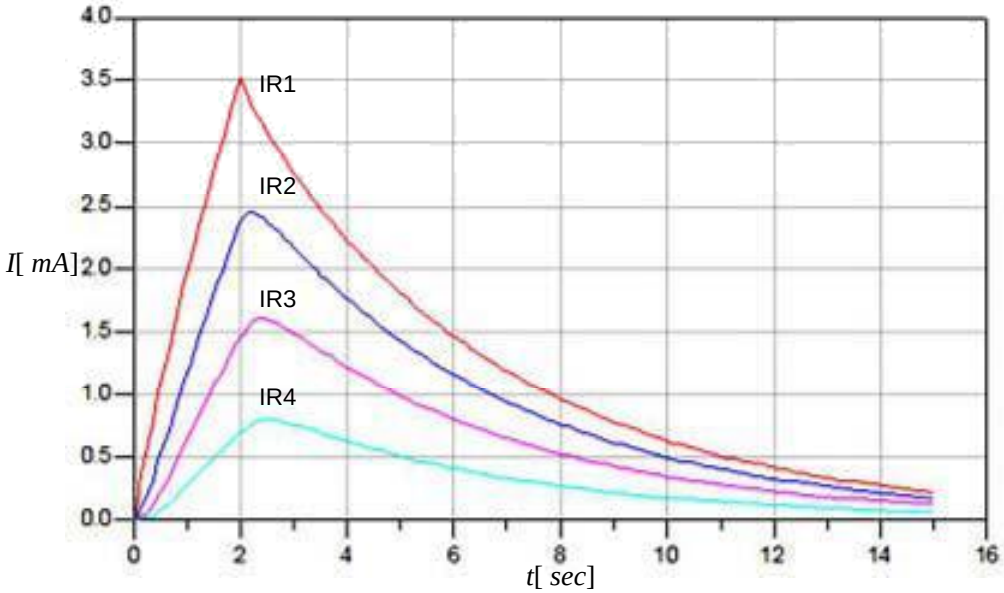

Fig. 7.5: Streams steps.

The oktavathmia percussive device may be charged at a rate of 50kV 1Hz, if the load resistance is 200k and resistors levels 20kO. The maximum charge current that would be required in this case is 140mA, i.e. instantaneous power Food fodosias 7kW. The load resistance R must always be sufficiently greater than the resistance of the array. A good rule of thumb is 10 times greater. In this way there is equipartition of voltages in steps of the Marx generator in the charging phase. Resistance levels can not be different, because, especially during the phase of discharge, created unequal distributions trends, potentially ded appearance arcing resistors, which currently katapo- moving from larger tendencies of their electricity resistance.

7.1.2. Study Characteristics Discharge

The discharge of a Marx generator is the collapse of the first gap, fact that has lead to the cataclysmic collapse all other spark Ston. At this time, the capacitors are automatically connected in series and thus have the effect of so-called "egermeni 'capacity (erected capacitance), equal to *C*/*N*. The circuit due to large displays great inductance, which is relatively difficult to measure. Since we are talking about air circuit, from which alpha pousiazoun magnetic materials, we can use the empirical relationship that 1m loop displays from 0.5 to 1mI inductance, depending on the angle sections of pipeline. Safe method for determining the inductance of the arrangement is by imposing oscillations of voltage and current when the impulse device discharged, no damping resistors at pin essay - plate or equivalent. These oscillations have been observed in experimental measurements and place the aftepago- earth circuit in the region of 5mI. For example, the three stage discharge sys-correlation in barb-plate specimen revealed current oscillations with a period 2.6msec.

Therefore, a total capacity of three steps equal to 33nF (*N.*= 3), the inductance of the circuit is calculated in 5.13mI accordance with the relationship:

$$fLC = \frac{1}{I_{LC}} = \frac{1}{2Fr.\sqrt{Ltot\ Ctot}} = \frac{1}{2Fr.\sqrt{\left(NLstage + Lext\right)\frac{C_{stage}}{N}}} \quad (7.1)$$

Placing additional steps in the array increases the length of my conducting dro- in the discharging phase and, in result, the inductance of the circuit. The dimensions of the experiment are determined by the height of the device (~ 1.5m), by Mr. Non- conductive way between successive steps (~ 1m) and the distance the light-specimen (about 1.5m away from the device). Furthermore, each capacitor having its own considerable inductance because of the large stretching. The use of very thick pipes allows to estimate the inductance in 0.5M per me- nitro conductive street, resulting in an initial estimate of the total inductance of the circuit generator Marx-lamp Vircator in 5mI. The simulation of bo- provision psi be done, if we consider the spark that anoiktokyklomata transitioning to short circuit resistance <1h, within a very short time. Using ADS, we can simulate the following circuit discharge tetravathmias gennitri- let:

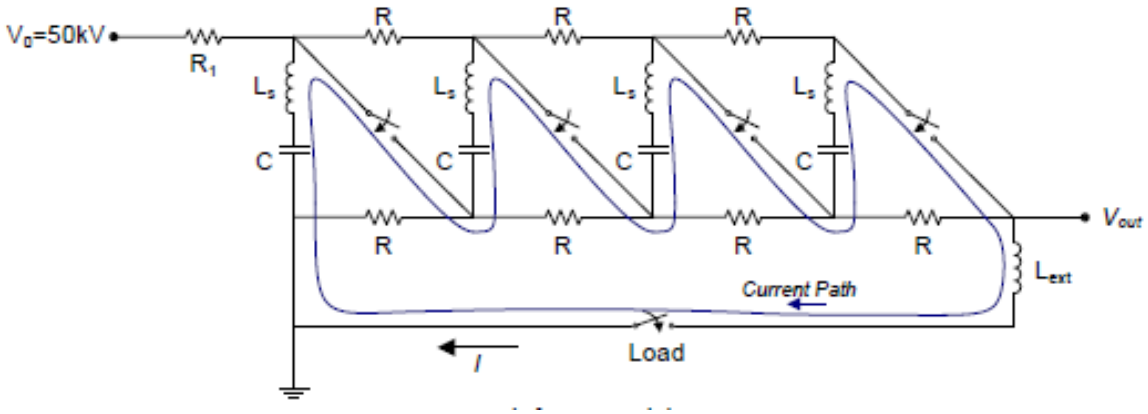

In this circuit we capacitors *C* equal to 100nF, resistors *R* equal 1MO, inductions levels *Ls* equal to 0.5 M and the external inductance equal 3mI. Switches - spark "closed" with time delay 100nsec the first with a characteristic impedance changes from infinite to 0.1O with tetragoni- parties law within 500nsec. The load - path is simulated with a switch, which closes with a characteristic impedance, which changes from infinite to 1h within 1msec. The character- ktiristikes voltage and current, obtained are the following:

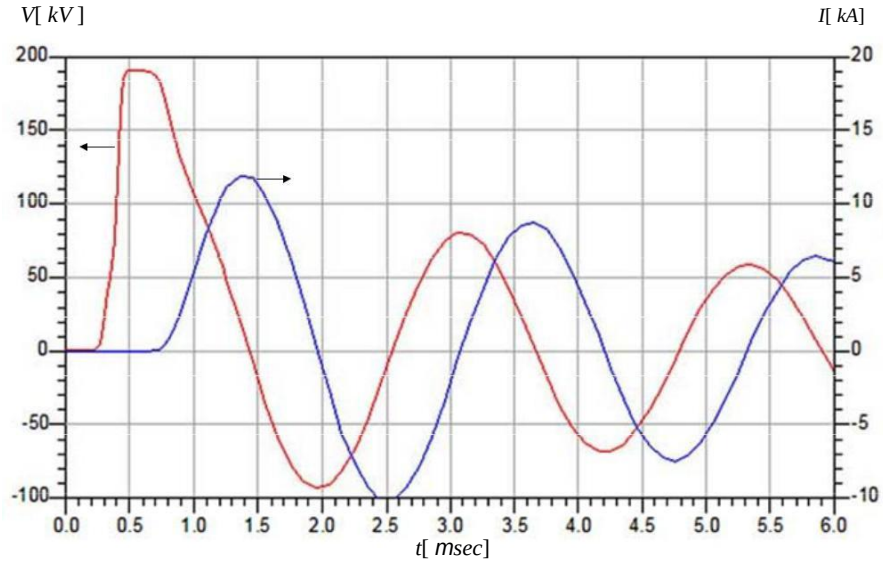

Fig. 7.7: Simulated typical voltage and current.

The resistors placed in the circuit is estimated, however intense oscillating behavior is apparent that occurs because of the large capacity and inductance of the closed loop and the low-impedance that displays the circuit altogether. For discharge voltage 200kV (4 steps), an impulse discharge into the arc can display currents in the range of 10kA. The current is direct importance dependence of the transition resistance of the gap, when the load of the generator is Marx diode lamp. Adding external resistor can damp the oscillations, since these are undesirable. The resistance, which may be used should be a small value so as not to significantly limit the current representatives charging and has electrical resistance of at least *NV0*Wherein *V0* the charging voltage levels and *N* the number of stages used. The use of a corresponding situation 10 ohms, the discharge circuit of Fig. 7.6, imparts characteristics critical alpha posvesis, as illustrated by the following simulation:

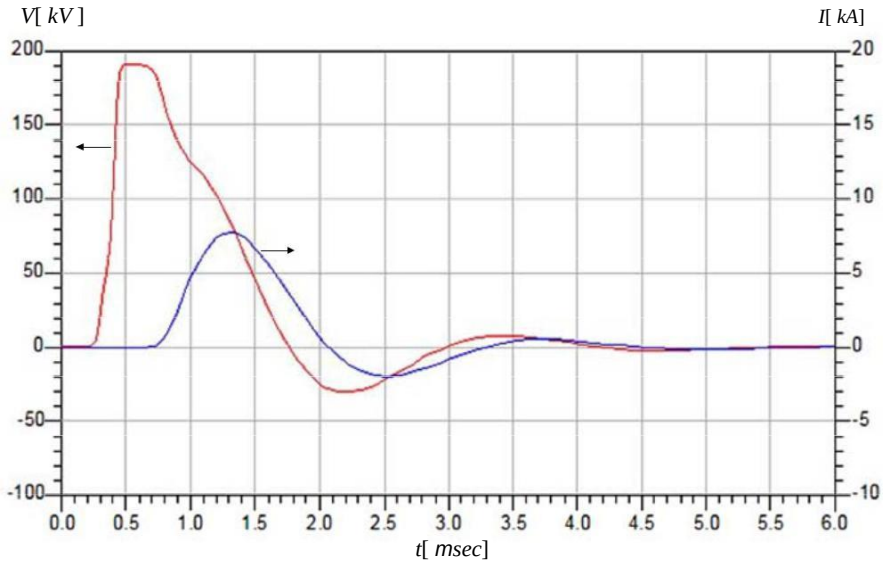

Fig. 7.8: Simulated undamped characteristic, using impedance 10 ohms.

In the case of damped oscillations, the relation (7.1) is amended as

$$f_d = f_0\sqrt{1-g^2}\ , \tag{7.2}$$

where c is a parameter *RLC* circuit *serial* equal to

$$g=\frac{R}{2}\sqrt{\frac{C}{L_{tot}}}=\frac{R}{2}\sqrt{\frac{\frac{C_{stage}}{N}}{(NL_{stage}+L_{ext})}}\approx\frac{R}{2N}\sqrt{\frac{C_{stage}}{L_{stage}}}\ , \tag{7.3}$$

when the "external" inductance is much smaller than the cumulative inductance of all levels. With *fd* denotes the frequency of damped talantose- s, while *f0* the natural frequency of the LC circuit without damping.

7.1.3. Design and Testing sparkle

To achieve multiplication of the voltage, the capacitors are placed in series by use of spark gap (spark gaps). Since it is not easy to use triggered gaps (triggered spark gaps), it was decided to construct sfairoei- don scintillator, made of machined aluminum. Alpha-krodektes shaped smooth, allowing more specific characteristic of electrical resistance in small-medium gaps. The scintillators manufactured, E to contain a back side of M10 threaded socket for mounting stem diameter 16mm, while the front side (flash side) has an approximate form of sphere diameters 40mm. Drawn terminal shown below in Fig. 7.9, while re- taskefasmenoi scintillators, with their support member, in Fig. 7.10.

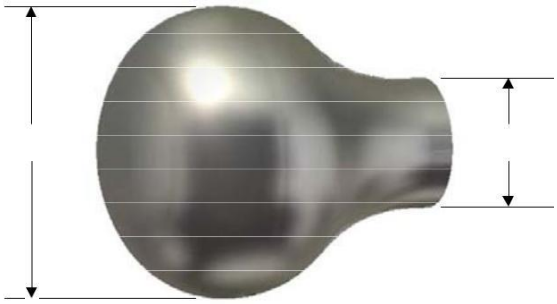

Fig. 7.9: The terminal is designed scintillator.

The spark plugs were tested using a DC power supply in order to determine the character-ktiristiki their electrical resistance as a function of distance. The experiment to document the electric resistance is shown below (Fig. 7.10). Two resistors of 10MO limit the current in the phase which is split gap, and formed arc. The electric arc can and maintained even for those patients predicted current values. For example, cleavage at 50kV through the overall resistance of 20MO mean arc current of 2.5mA. Falling BRAKE

ing divided equally in two identical resistors, since the arc emergence ordinates negligible resistance. For measurements, the ignition plugs and resistances were adapted to the frame acrylic glass of multistage generator.

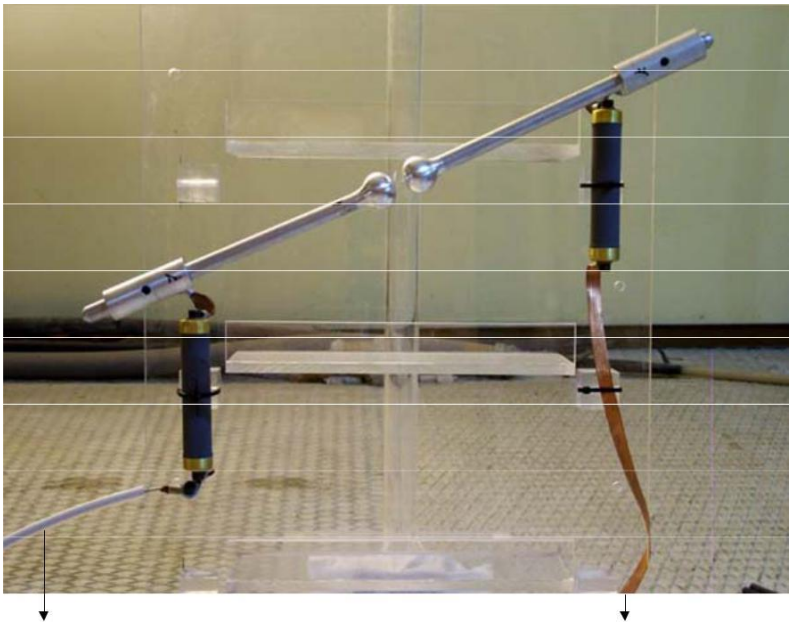

Fig. 7.10: Testing electrical gap resistance.

The decay rates of the gap, recorded, listed in the diagram, Fig. 7.11. Reducing the degradation values at electric field intensity by dividing the voltage with distance, observed that the strength approaching 30kV / cm for small distances. As the gap increases, the partial proekkenoseis the Corona effect and long kroskopiki altering the range of the enhancing agent pediakis intensive causing the cleavage of the gap smaller analog electric field values.

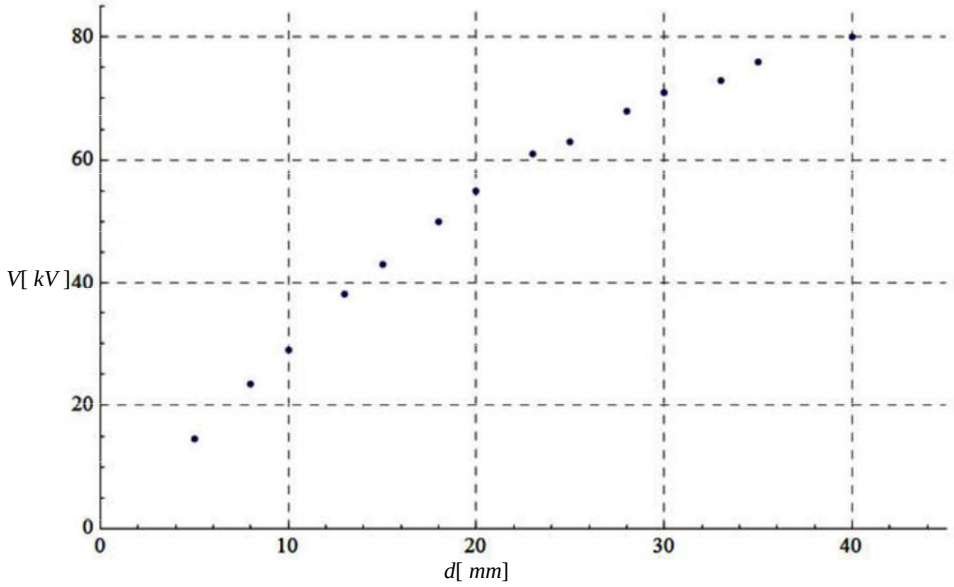

Fig. 7.11: Decomposition of spark voltage as a function of the gap.

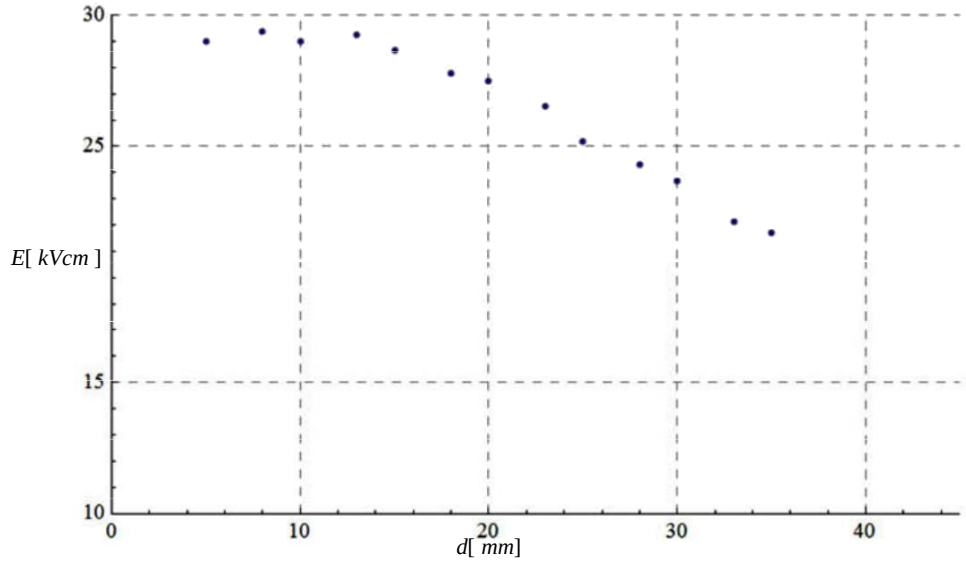

Fig. 7.12: Equivalent electrical gap resistance.

The apparent electrical resistance of the spark gap is 20kV / cm, when the scintillators are 4cm. Due to the size of the generator load, we should not exceed 50kV, so the spark must be placed at a distance of at most 18mm (see. Fig. 7.11).

The electric arc occurs, the characteristics traveling electric arc or "scale of Jacob» (Jacob's Ladder), characteristically called. Xe- China from the center of scintillators and gradually promoted to the external periodic Xe of scintillators. The breakdown voltage is reproducible with high accuracy. Let im- reduced that the tests were a typical dry day since the atmospheric moisture results in great randomness in the characteristic cleavage of scintillators. In the following picture with slow shutter speed and in a dark place, it seems the low current arcing between the scintillators.

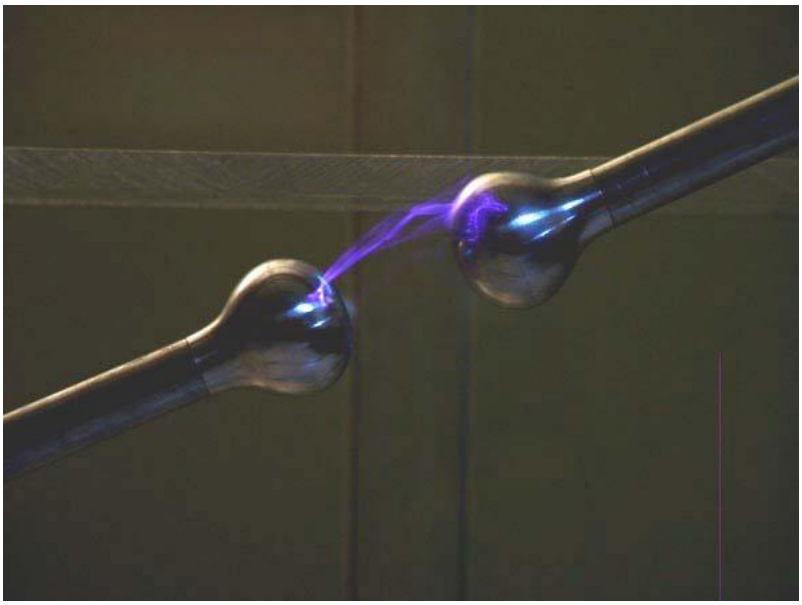
Fig. 7.13: Electric arc between scintillators, when the gap stress tests.

In the above tests, the sound of the electric arc is weak, since their total current of the test circuit is limited to a few mA. However, when the device is connected to a low impedance load, the very strong discharge currents of the capacitors, resulting in the production of strong click from the device.

7.1.4. Construction multistage Generator

The multistage generator mounted on a frame made of acrylic glass (Plexiglas). Eight steps were provided, spaced steps 22cm. The total height of the device is 2m. Each capacitor is placed horizontally in a suitable rack, and the resistances between the tiers supported laterally generator Marx, onto guides acrylic glass (see. Fig. 7.14). Their support in the vertical position is done using plastic clamps through hole. The back of the device formed by two pieces of acrylic glass, width 55cm, height 1m and thickness 10mm. The two pieces were welded together and their association amplified by two additional longitudinal the tracks 1m height and width of 8cm, also acrylic thickness 10mm.

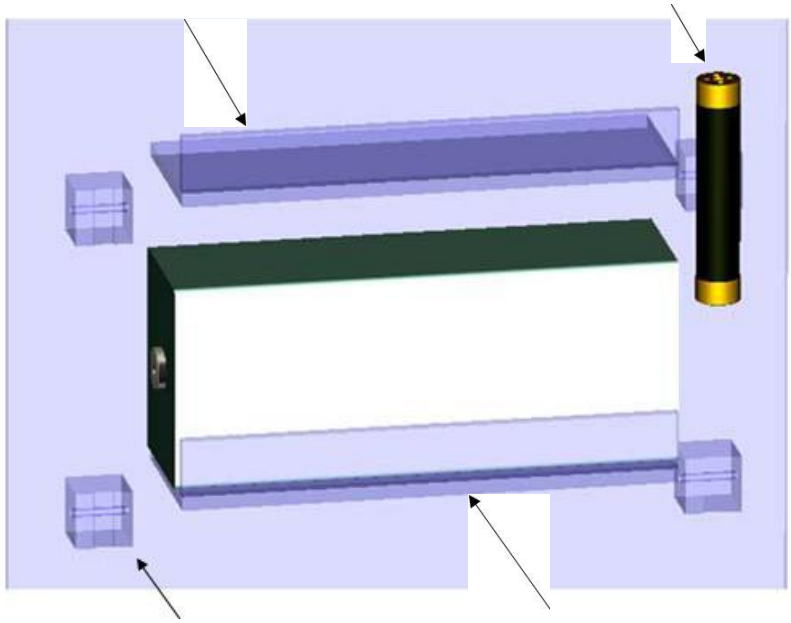

Fig. 7.14: Installing capacitors and resistors in multistage generator.

The mounting of the device are two trapezoidal pieces 50cm height and base width 40cm. The shoe of the device is a rectangular piece of 40cm on 55cm, thickness 10mm. This part also functions as insulation against the ground alpha- Fu bringing the charging voltage of 50kV is from below, using insulated high voltage cable. The model of the first four steps of the re- assembly sented in Fig. 7.15 left.

The scintillators consist of a horizontal rod, which rely on the device back. This strain retains the beads in height 18cm, or about 7cm outside capacitors. A cylinder length 8cm, 30mm outer diameter and inner diameter of 16mm, is the guide to the horizontal members of a spark

Ston. Cylinders - drivers carry a small threaded hole on the outer side. In this manner, using screw type without Allen head adjusted to an executive horizontal with spheroidal terminal of the spark plug at the desired distance. RH The electrical connection of resistors, capacitor and scintillator to each node of outbreak ment layout is done using large diameter pipeline, for oppression of mind phenomena Corona during the charging phase (see. Fig. 7.15 right). The impulse device was designed to be easily detachable to prosthafairountai quickly tiers for achieving shock test voltages up to 400kV. As shown in the model of Fig. 7.15 left, first lower resistance is the load resistance of 10MO. The adduct is made by the voltage insulated cable, which is connected to the lower terminal. The piece of Plexiglas base serves as insulation of this terminal, which is under voltage, the territory in which the multistage generator based.

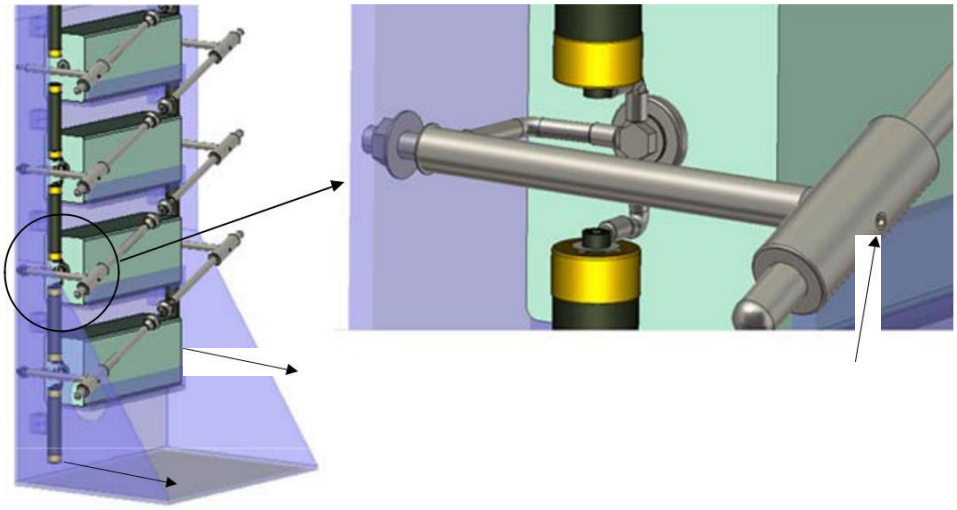

Fig. 7.15: View of multistage generator (left) and detail of connections and mounting strain of the spark (right).

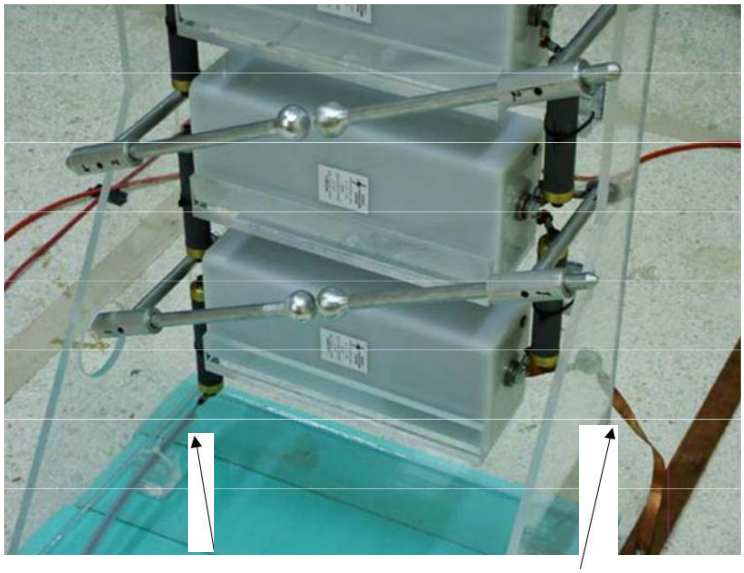

Fig. 7.16: View of the first two stages, with the voltage supply cable.

7.1.5. Study of Electric Resistance

During the discharge of the capacitor array of scintillators short stems cyclone and said it was the same potential. As a result, the arm of the scintillator directly above step displays instantaneous potential greater than a voltage during charging.

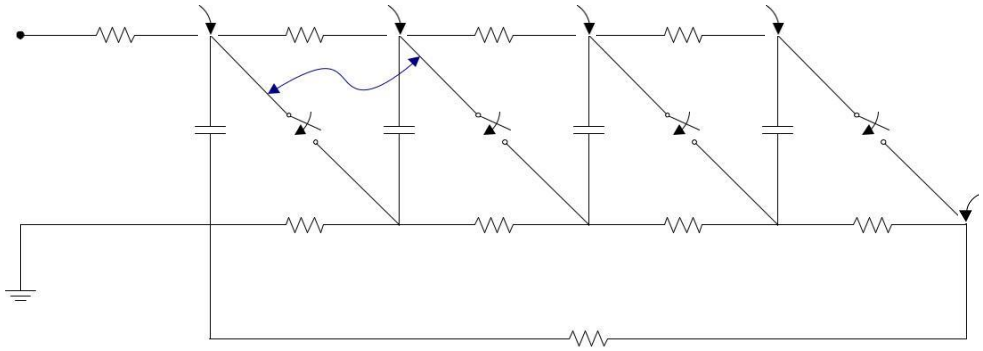

Fig. 7.17: Difference between capacity levels during discharge.

The following exact model generator Marx, Fig. 7.18, a straight line im- reduced the shortest distance that occurs between successive metal members KON steps. This distance of areas with a strong geometry, therefore an believers Thanos arcing between levels during the discharge phase, there will be between them. Given the scale of construction, the shortest distance between successive steps is about 16cm.

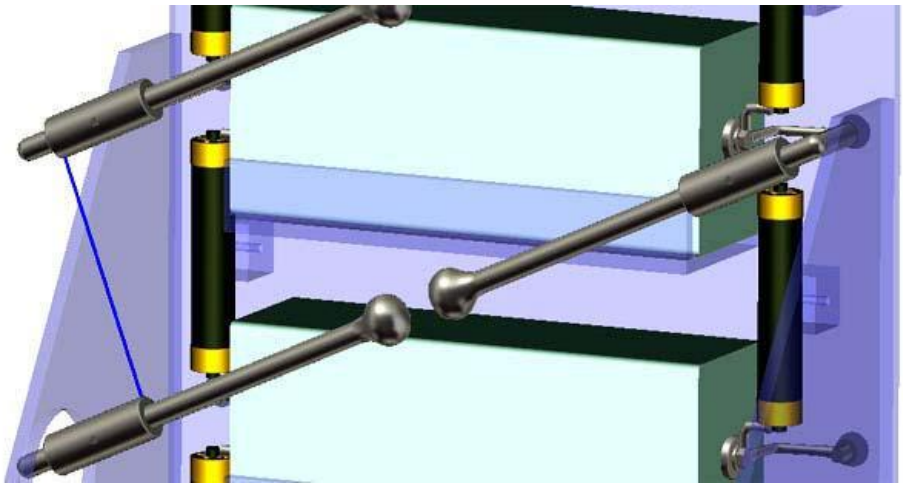

Fig. 7.18: Potential arcing points during discharge.

In order to determine the electric strength between the steps, the model generator we outbreak ment between the upper and lower arm potential difference equal to 50kV, as that is the maximum voltage of each step. Along the line marked on the model of Fig. 7.18, with the lower point is the beginning me- measurement of the segment (lower potential) depict the change in the electric field, in the following diagram:

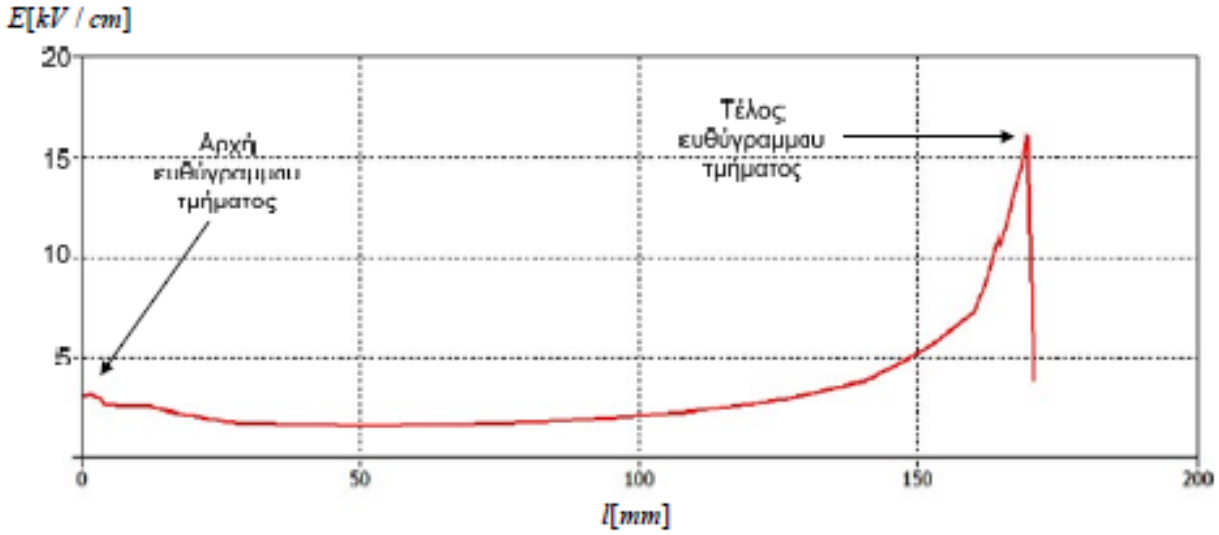

Fig. 7.19: electric field simulation for V = 50kV.

From the simulation using the Microwave Studio of CST, it is apparent that pediaki aid appears under the stronger geometry upper stele- objectives. The pediaki aid leads to appearance of an electric field sufficiently less than 30kV / cm, the arm with the highest potential. It is therefore unlikely to re- ratirithei arcing between tiers in the phase of discharge of the device.

7.1.6. Inductance Study

The Marx generator presents inductance per step, which depends on their total length of the duct connecting the modules together and the afte- pagogi, showing the high voltage capacitor. In this embodiment, the conductive trace their total current from one stage to the next is approximately 1.2m. Therefore, the inductance per step resulting sizeable price. In order to assess the magnitude of inductance per grade *Lstage*. (See expressed night (7.1)), we use the model of the Marx generator and replace the capacitor with a conductive cylindrical body large diameter. Then, using a stimulus in the form of port S-parameters, and calculate the inductance from fa- Dusty part reflectance. In Fig. 7.20 below shows how we are looking at the inductance, at the stage of discharging. The electric arc is mo- ntelopoiithei like a small conductive cylinder between the beads. The capacitor consideration during the discharge phase of conducting fully, so a large conductive cross sectional roller is inserted as a carrier of electricity. The metal members designated by aluminum. Finally, between the first and second tier terminal, the resistance is removed, since it contributes to the transient, and is positioned tithei one port S-parameters, characteristic impedance 50 ohm, in which recorded lampblack voltage and current versus frequency.

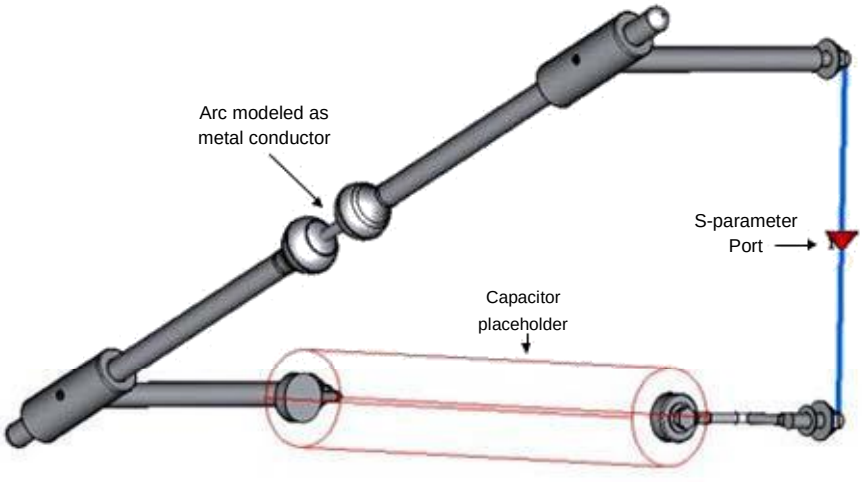

Fig. 7.20: Study inductance per grade.

The sizes of the discharge current move in the range of MHz, therefore simulate the above model for frequencies 0 to 15MHz. The results for the inductance of the model shown in Fig. 7.21.

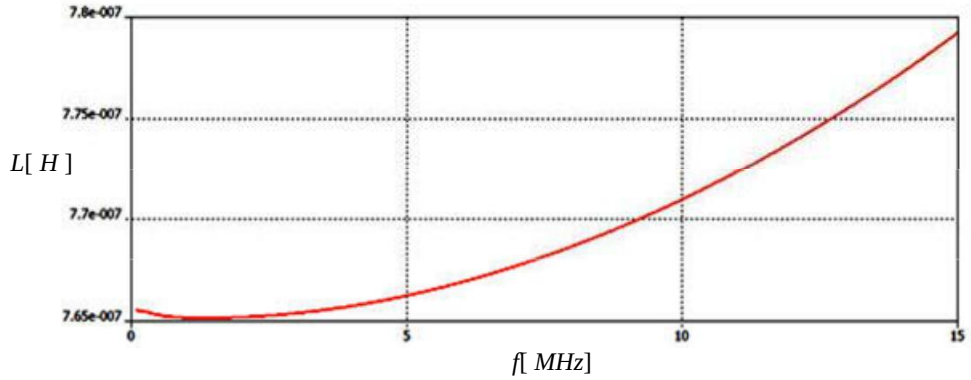

Fig. 7.21: inductance per grade until 15MHz.

We observe that the inductance in the region of 0.76 to 0.78ml per vathmi- da. This figure is expected and is consistent with the dimensions of the conductive loop. The premise for the capacitor is logical if we accept that the electric current through it occupies the entire volume and flow in a manner parallel to its axis. Furthermore, the study for high voltage resistance, presented in section 7.2.1 showed that the simulations lead to estimation of in-tepagogis confirmed both theoretically by the approximate formulas pipeline leak angle of current, and by experimental measurements.

7.2. New Experimental Device

The former test lamp, with single-stage impulse device VDE-b, did not allow driving with great force, since the striking voltage is relatively narrow and slowly varying (~ 100kV form 0.6 / 50). The new experimental setup a-

potelei a transfer of Vircator system, replace the system odigi- ing high voltage from the new multistage impulse device. The generator Marx, the capacitors were first liberalized capacities, offers the possibility to drive with significantly higher pulse powers, both in voltage and in terms of power. The new experimental setup described below, the light moved with re- relkomeno vacuum system to a new area where the new synegkatastathike polyvath- a Marx generator.

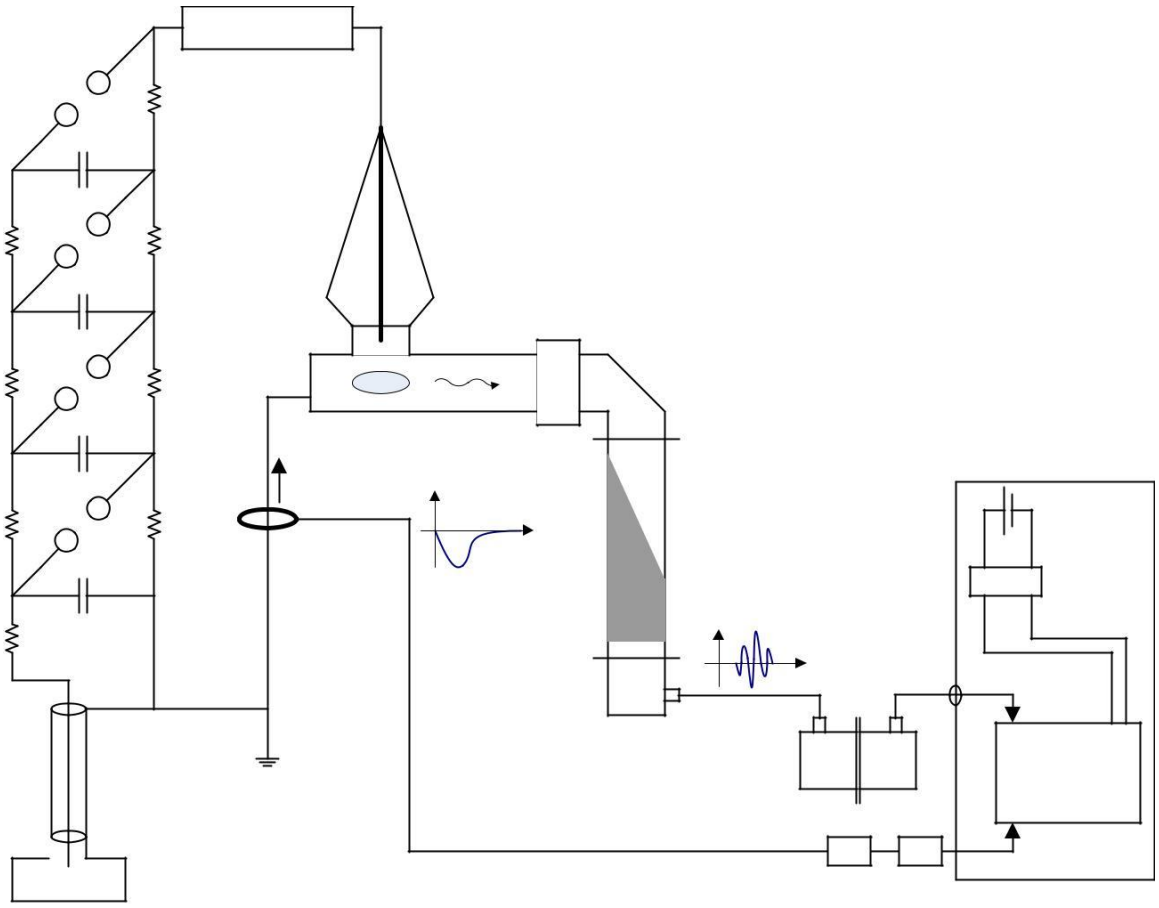

Fig. 7.22: Diagram of the new installed system.

The new high-voltage device may cause the lamp Vircator with voltages up to 400kV and currents depending on the configuration of the diode, the inductance of the system and the interference resistance of the front, if necessary. Currents, exceeding 10kA can be observed with appropriate configuration. The addition levels and adjustment of the spark gaps can be amended CAM total voltage and total capacity will lead the lamp.

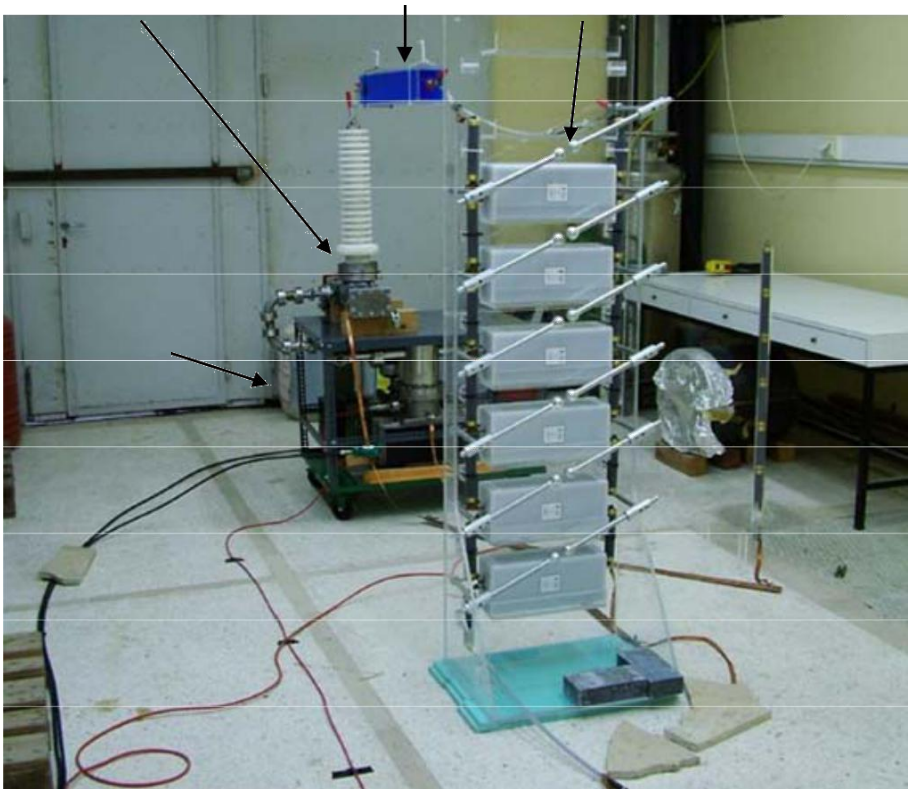

Fig. 7.23: Photograph of experimental setup with multi-stage Marx generator.

7.2.1. High Voltage Resistance Front

The multistage impulse device, due to the large dimensions of the circuit, pre- sented significant inductance. To avoid LC oscillations, but also relevant limitation of output current, appropriate to place a small a- ntistasi price and high electrical resistance between the core and the genni- three Marx (see. Fig. 7.24). The preferred use of metal salt solution resistance due to the ease of manufacture.

Resistance to salt solutions are often used in high voltage applications. The aqueous salt solutions have very high electrical resistance, high thermal mochoritikotita and can be prepared easily in the desired resistance value by varying the concentration of the dissolved salt. Where required very small resistance values in the range of tens or Oh Oh, the preparation of highly concentrated solutions are needed. It must be compatible type electrode with salt used in order not to place the electrochemical reactions, which alter the texture of the electrode and solution; Tos. In Tab. 7.1 indicated certain salts, typically used in such applications.

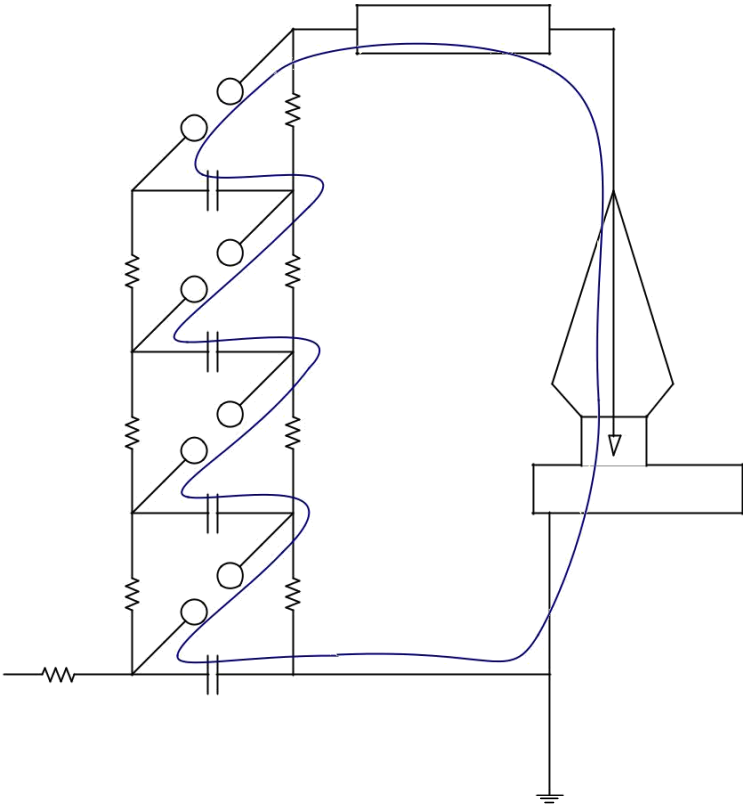

Fig. 7.24: High Voltage Resistance Front.

Tab. 7.1: Properties of Electrolyte and Electrode

Union	Molecular weight [G / mol]	Solubility 0oC [G / lt]	Compatibility with n-lektrodia
Aluminum nitrate Al (NO3) 3 · 9H2O	212.99 (a) 375.13 (h) [1]	637 (h)	Stainless steel rehearsing
Cupric Sulfate CuSO4 · 5H2O	159.60 (a) 249.68 (h)	316 (h)	Copper
Aluminum Sulfate-Potassium KAl (SO4) 2 · 12H2O	474.39 (h)	114 (h)	Aluminum
Potassium Chloride KCl	74.56	344	Stainless steel rehearsing
Potassium dichromate K2Cr2O7	294.19	49	Copper, Stainless Steel, Oreichal-Mr.
Silvernitrate AgNO3	169.88	1220	Stainless steel rehearsing
Sodium Chloride NaCl	58.44	357	Stainless steel rehearsing
Sodium dichromate Na2Cr2O7 · 2H2O	261.97 (a) 298.00 (h)	2380 (a) 1800 (h)	Copper, Stainless Steel, Oreichal-Mr.
Sodium thiosulfate Na2S2O3 · 5H2O	158.11 (a) 248.18 (h)	794 (a) 500 (h)	Aluminum

[1] (A) - the anhydrous form, (h) - hydrate

For the construction of high voltage resistance forehead prepared solution 1300gr hydrated copper sulfate (copper sulphate) in 4lt H2O. The hydrated CuSO4 having a molecular weight of ~ 250gr / mol, and the anhydrous ~ 160gr / mol. Dissolving 1300gr hydrated CuSO4 in sys-gkekrimeni water, prepare a solution of about 5.2mol CuSO4 in their total amount of 4.5kg solvent (H2O). Accordingly, the molar *m*[Mol substance / kg solvent] is estimated at around 1.15mol / kg. The nearly saturated solution manufacturer; y has conductivity in the range of 4.0-4.5Sm-1, at a temperature of 20 ° C [140].

The container of resistance constructed by acrylic glass (Plexiglas) with internal (useful) Dimensions 8cm x 10cm x 48cm. Used acrylic glass thickness 10mm. On the short sides of the parallelepiped mounted electrical terminals of the resistor. They are made of brass, with 4cm diameter and thickness 3mm. Among cyclic terminals and acrylic glass placed rubber, to seal the holes in the container.

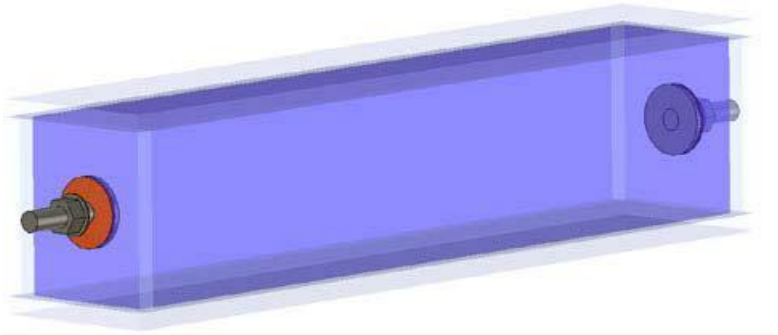

Fig. 7.25: High voltage resistance front with a solution of CuSO4.

The container was filled with the prepared solution and measured using our gennitri-signals and oscilloscope. Note that the resistors salt solutions should be measured in the value of the ohmic resistance with DC method (such as a tester or AC DC), since the surface layers are formed and other defects on the surfaces of the electrodes. The generator sinusoidal signals used has internal resistance 50R and can result signal stou maximum amplitude 10V to high load resistance. The amplitude of the signal monitored by online signal generator to oscilloscope 10MO. Connecting paralli- la resistance was found voltage drop in the measured signal, with the following change in frequency:

Tab. 7.2: Voltage resistance CuSO4

Frequency f	Signal Width	Width under load
1kHz	10V	2.2V
10kHz	10V	2.2V
100kHz	10V	2.2V
500kHz	10V	2.4V
1MHz	10V	2.5V
1.5MHz	10V	2.8V
2MHz	10V	3.2V
5MHz	10V	5.9V
10MHz	10V	8.2V

With appropriate calculations, the above R-L behavior can be matched precisely to a load with real resistance R = 14.5 and inductance 1.4mH. Taking into account that was used to measure thin stranded wire total length ~ 60cm, the inductance of the copper sulphate resistance is less than this value. A thin 0.5mm wire diameter and 60cm length have inductance of about 0.8mH ([133], [134]). Therefore the load of CuSO4 should exhibit an overall inductance of about 0.6M.

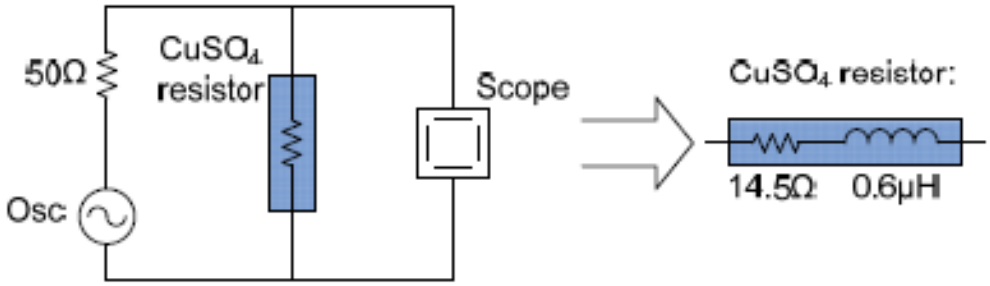

Fig. 7.26: Resistance measurement CuSO4.

The value of the real part of the resistance, which is determined experimentally, sys- coincides with conductivity conductor resistance value 4.1Sm-1 (~ 1.1mol / kg CuSO4 at a temperature of 20oC, [140]), 48cm in length and area of 80cm2. Simulations of Accountants resistance due to low frequencies from 0Hz to 15MHz, show little dependence both resistance and inductance of the frequency. Simulating the migration model of high voltage resistor with conductive material 4.1S / m, relative dielectric constant *E0* equal to 81 and a magnetic permeability *M0* equal to 1 (water with dissolved salt known conductivity), together with the terminals and Plexiglas, shows how the real-part of the resistance gradually changes from 14.5 up to 15.5, and the inductance of the structure is between 0.528 and 0.530ml (see. Fig. 7.27).

Both the experimental measurements and simulations agree that the high voltage resistor is the real part value between 14.5 and 15.5, and the inductance value between 0.5 and 0.6. The load, built, hung from the ceiling of do- eyes by line. It enables comparison figures when it paremvalle- Tai in the layout when bypassed by shorting out the appropriate terminals.

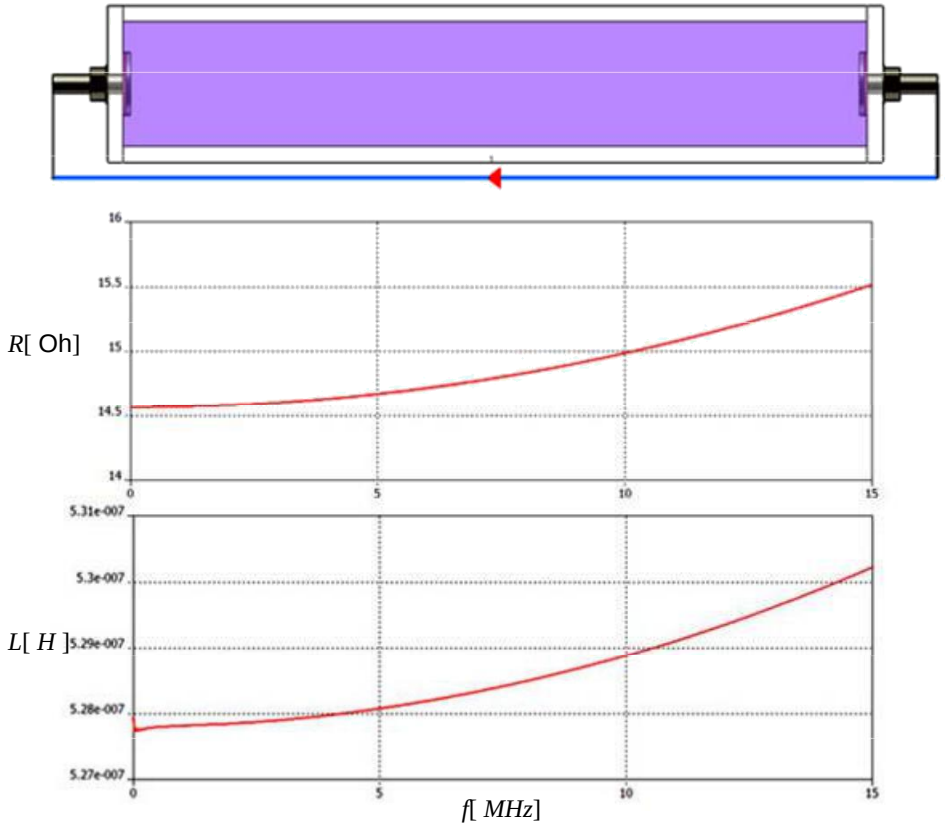

Fig. 7.27: Simulated resistance CuSO4.

7.2.2. Vacuum System

The vacuum system remains the same and the new installation site. Refer to paragraphs 5.3 and 6.1, for the exact description of the vacuum system lychni- let. The only peculiarity of the migrated system is that the stream of antli- let ionization does not approach the previous minimum levels of 0.16mA. Instead, gov- raging about 0.20mA, which may be due to aging of the lamp body, said transfer, vibration and aging. In result, the pre-existing small leaks may have been boring, worsening the minimum achievable vacuum. These new levels of ionisation current, however, does not represent a significant change in the pressure prevailing in the device. It is estimated that the gap is around 2 · 10-5Torr. The assessment is based, as mentioned in para. 6.1, to correspond cess stream of ionization pump and the vacuum prevailing therein, and the relationship of the pressures of interconnected volumes by conduction tubular sations. Note that the transfer, the ionization pump remained out of service for some time and came necessarily into contact with large pressures. As a result, De- chtike large amount of adsorption, which required disassembly and the careful cleaning of the ionization cell in a special ultrasonic bath (ul- trasound bath) for days.

7.2.3. Measuring Device

To draw conclusions about the behavior of the lamp, we measure the current and the microwave signal directly to the oscilloscope bandwidth and sampling 2GHz 20GSamples / s (see. Par. 6.2). Voltage impulse device in pres- ence tests could not be measured. Note that to record the trend was the attempt to construct a resistive divider with high voltage resistance 6MO and low voltage resistance 50R. The high voltage resistor formed by six of the resistors 1MO who purchased for the generator Marx, a total tensile strength 420kV, according to their specifications. The resistance of 50 ohm placements was in a small metal box with BNC output terminal. However, it turned out that the function of the resistive divider unsatisfactory. The direct connection of re- tameristi the oscilloscope showed record radio signals by back BRAKE ment of 20mV. This meant that the construction of the divider had good immunity to electromagnetic interference. The high divider and self-construction of the connection to the low voltage resistance resulted recording marks by the air, let alone in the discharging phase generator Marx, something not diakindynefthike ever, even with incoherent the resistive divider. The ohmic katame- Excellent routed but unattached, distinguished in Fig. 7.23 right.

The current measured is the ground current of the lamp and recorded through the current transformer 1025 of Pearson Electronics, with Bandwidth 4MHz, peak current 20kA and transformation rate 25Volt / 1kA an open load. At 50W this relationship, according to the manufacturer, is half, ie 12.5V / 1kA. Therefore, two 46dB attenuators or 200: 1 (6dB + 40dB = 1: 2 + 1: 100), so that the degraded signal in the order of 1V per 16kA passing current. In other be- on the transformation ratio is **1V / 16000A** current. This signal is driven to re- nali digital oscilloscope DSO80204V of Agilent.

Two attenuators, so the signal amplitude to ypoviva- Zeta in *two successive stages*So as not to exceed the tensile strength of victories coaxial attenuators. For example, a current amplitude 10kA would result in the appearance in the output voltage current transformer equal to 125V (50 ohm load). This mark will be relegated at 62.5V from the first attenuator and 62.5V about the second attenuator. The coaxial attenuators have, in accordance with their specifications, pressure limit for pulse corresponding to instantaneous power 200W. At 50W, the power is equivalent to a threshold voltage 100V. Therefore, by placing two attenuators in this order of succession, the power surge loses half width of the first export stheniti (6dB) and the remaining half of the width of the other attenuator (40dB). The difference that provision allows us to measure up to 16kA power safely, without deposits shifted from hypertension coaxial attenuators.

The microwave signal, after undergoing attenuation of the microwave load at the output of the lamp, is driven via coaxial cable to another channel palmo- graph, where he recorded for the range of 1.4GHz (Cut WR430 kymatodi- Woo) up to ~ 2GHz, which It is the analog bandwidth of the oscilloscope. The attenuation is variable with the frequency varies, as illustrated in the diagram of Fig. 5.28, with an average value of about **43dB**, If we calculate the total losses of the coaxial cable used by the lamp until the system of recording. In the RF channel is also a device two WR430-to-N-Type adapted

Gihon connected together (back-to-back), so that the microwave signal is still a high-pass filter to lower the cutoff frequency 1.4GHz.

The new experimental arrangement tested a new method for the measurement of microwave sional signal oscilloscope. Build a small antenna with a parallel polarization in the electric field of the TE10 rate and placed in the center of the small plef- ket of WR430 waveguide mounted onto a suitable gasket. The construction and the measurement of the electric field probe described in par. 7.2.4. The average coupling with the microwave signal is approximately **46dB**, In the frequency range of the first rate.

The two channels, RF and power respectively driven to channels CH1, and CH4 oscilloscope DSO80204V of Agilent, who no longer is in a shielded cage because there is no available Faraday cage at the new test site. An effort to create a "cage" of tin sheet metal screw cap RES obtain, because this construction did not provide substantial isolation from external Electromagnetic interference. The oscilloscope remains inside the metal box and consideration during the conduct of experiments powered by car battery 12V, 44Ah, me-physical inverter voltage DC / AC. The battery is used to maintain the oscilloscope to completely free capacities. The overall configuration along with the metering system, shown schematically in Fig. 7.22.

7.2.4. Probe Electric Field

The suspicion that the microwave attenuator (see. Par. 5.4) can exhibit nonlinear behavior at higher powers, led to the construction of a probe for detecting the microwave signal into kymatodigiki cavity. Of utilization was a flange FDP22, i.e. the flange waveguide WR430, a thickness of 23mm. On the short side of the opened thread M16 and adapted appropriately aluminum tube with inner diameter opening Ø12 and outer diameter Ø20. At the free end of this tube adapted N-type connector and the pin was glued a coaxial stem to create in this way one TEM line transport of the electrical signal. The tip of the pin, therefore, was extended until it protrudes 3mm inside and has a short stem length 6mm pediakes parallel to lines of the electric field of the TE rates. This provision may take samples of the electric field at any frequency, since essentially comprises a small monopole, mounted inside the waveguide.

To verify the transfer of power to probe the electric field mo- ntelopoiithike provision and simulated in the frequency domain. For the frequency range under examination, the rates, which is likely to be excited, are TE10, and TE20, with cutoff frequencies of 1.37GHz and 2.74GHz respectively. These rates have electric field parallel to the short dimension of the waveguide, it is therefore in parallel with the electric probe. The rate TE01, also by cutting the 2.74GHz, has an electric field vector parallel to the long side of the waveguide and we assume that it is rather difficult to excite by electronic oscillations in the lamp.

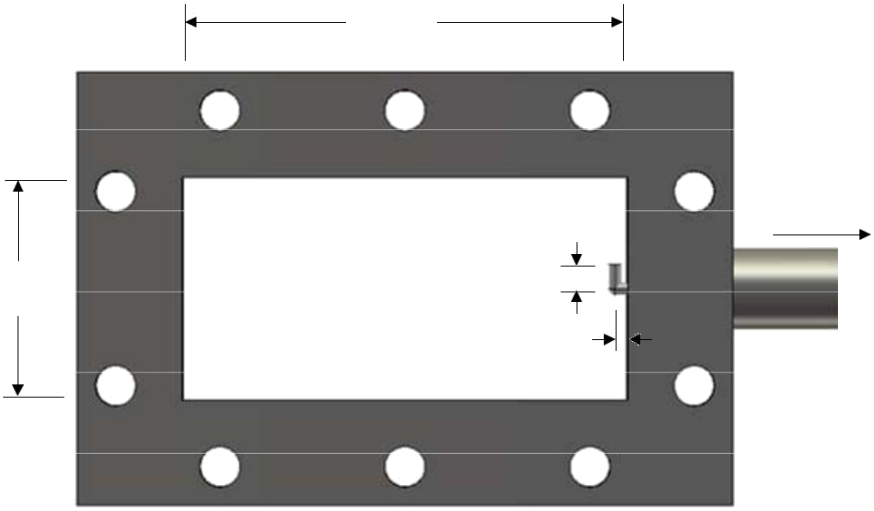

Fig. 7.28: Probe electric field positioned in flange waveguide WR430.

The simulation of the probe gives the following coupling results for TE10 and TE20 rates:

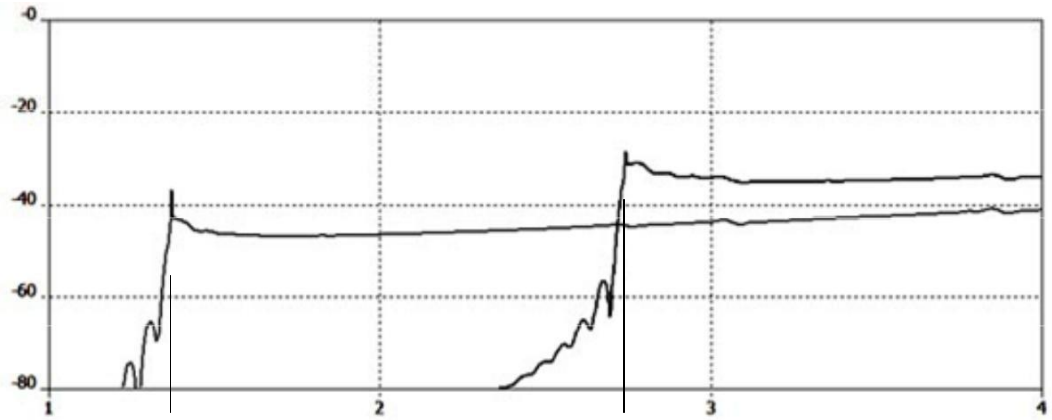

Fig. 7.29: Simulation of electric field probe.

Note that the coupling with the first rate is less than -40dB in sys- frequencies to 4GHz. Raising of second rate will lead to coupling coefficient below -30dB the TE20 rate, for frequencies up to 2.74GHz 4GHz. Antilamvano- here we are that the coupling ratio will rise with increasing frequency. Based on the results parapa- Upper constructed and the probe measured the microwave signal. The measurement was made with network analyzer, frequency range 1 up to 4GHz, using two komma- price waveguide, and using two WR430 to N-type adaptors. The results of measurements of the reflection coefficient S11 and S21 transit rate for netting WR430 adaptor and probe output is:

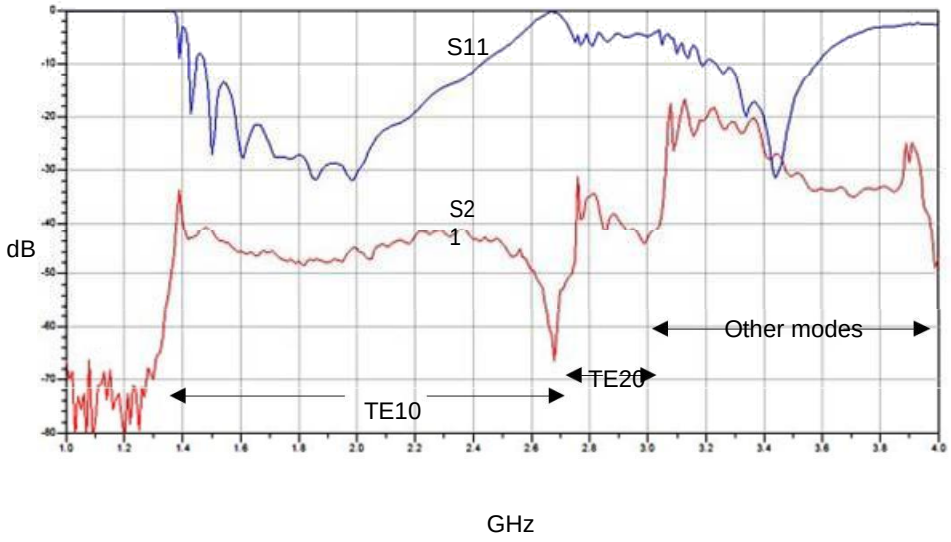

Fig. 7.30: Simulation of electric field probe.

Since the N-type adapters in this waveguide used, yes EI- unpredictable their behavior in upper class rates. However, the coincidence of the first rate in the transit area is very good and seems concludes with and the signal from the TE20 rate. The specification adapters clearly does not provide frequencies above 2.6GHz, as is reflected in S11. The coupling at 1.6GHz is -46dB, -48dB at 1.8GHz is 2GHz and is - 46dB. The electric field probe inserted at the output of the lamp, immediately after the piece waveguide bend of 90o.

7.2.5. Voltage divider

In order to measure the voltage in the essay, attempted to construct a petri divided voltage with the materials at our disposal, that some of the resistors 1MO generator Marx. The resistors have electrical strength 70kV, power 55W ([138]). It is cylindrical, 16cm in length and sectional 30.5mm (see. Fig. 7.2). The resistors have threaded mounting M8 on both sides. Six such resistances, which were placed in a tube of Plexiglas, single di- immeasurable 32mm and 38mm outer diameter. The cylinder of Plexiglas, height 1m, was placed onto a square base, also from acrylic, with four legs for support. The six resistors provide a comprehensive theoretical electrical resistance of the order of 420kV.

At the end of the last high voltage resistance placed terminal BNC, sub- tos that the pin to bring the degraded voltage signal. The low voltage resistance the- pothetithike inside a small metal box, which was adapted BNC akrode- officer for signal transfer to the measuring instrument. As a resistor used two resistors of 100O, connected in parallel, type SMT (surface mount type), which are used in high frequency applications and are free in- tepagogis. The reason allocation of this provision is 1V / 120kV, however if connected oscilloscope 50 ohm characteristic impedance, such as Agilent DSO80204B used so far, why sharing is 1V / 240kV.

Fig. 7.31: First voltage divider.

The divider was tested as cargo remaining unattached. This test is done to determine that it has planned high-impedance load operation and relevant electric strength. However, after three repetitions with impulse generator equip- structure on the 250kV (see. Par. 7.3), the divider collapsed creeping ekke- Union. The discharge was reduced internal surface of the acrylic tube and leave visible marks on the tanning acrylate and onto the resistors. The representative high voltage stops do not appear to have undergone any change in their electrical characteristics. Surprisingly, only one of the two low-voltage resistors combusted ex- Tías phenomenon.

The most probable explanation for the fall is the growth of abnormal electrical re- oxide at the interface between the resistor and the dielectric. Additionally, charging with static electricity acrylic is another possible cause worsening diile- tricity strength of the column divider. The three repetitions were made with the typical charging rate of the battery six steps to 43kV, which is around 20sec, Pact along the lines described in paragraph 7.1.1. Following this re- ristatiko an urgent change of approach for building a divider BRAKE ing.

Fig. 7.32: High voltage divider resistors. Distinguished mark of your erpou- discharge surface resistances and signs in acrylic tube.

7.2.6. Shielding Lamp by X-rays

According to the theory of absorption of photons by the material, one monoenergi- tion ray beam *c*Which is incident on material specific gravity *p*Thickness *t,* leaving export sthenimeni having energy fraction equal to

$$n = \exp\left(-\frac{m}{p^{E}} I_{,E}\, pt\right). \qquad (7.4)$$

The weakening of the materials is not constant but depends on the energy anafo- ket of the incident photons. This is because the attenuation factor *m / r* It is a function of incident energy. To calculate the weakened importance of materials, lead and aluminum, X-ray, look up the list of sys- nteleston attenuation (X-ray Mass Attenuation Coefficients) [137]. We quote the following table with some values for the attenuation coefficients:

Tab. 7.3: attenuation coefficient Pb and Al

Energy (keV)	(M / r) Pb [cm2 / gr]	(M / r) Al [cm2 / gr]
10	130	26.3
20	86.4	3.44
50	8.04	0.36
100	5.55	0.17
200	0.99	0.12
300	0.40	0.10
400	0.23	0.09
500	0.16	0.08

O Lead has a specific gravity 11.35gr / cm3, while aluminum only 2.7 gr / cm3. Additional o core lead is comparatively much larger mass number from aloumi-

hexafluorophosphate, therefore the shielding offered lead against X-ray is more effective than any other industrial material (concrete, steel, etc.). For some thicknesses of materials, we export the following impairments table for X-rays and energies up 400keV.

Tab. 7.4: impairments Pb and Al, various thicknesses shields

Action (KeV)	2mm Pb	6mm Pb	2mm Al	50mm Al	6mm Pb + 2mm Al
10	-	-	10-7	-	-
20	-	-	0.15	10^{-21}	-
50	10-8	10^{-24}	0.82	0.01	10^{-24}
100	10-6	10^{-17}	0.91	0.10	10^{-17}
200	0.10	10-3	0.93	0.19	10-3
300	0.4	0.06	0.94	0.26	0.06
400	0.6	0.21	0.95	0.29	0.20

We observe that a thick sheet of lead 2mm practically absorbs all radiant energy up to 50keV. The 6mm lead an effective shield for in--effects until 200-300keV, but from 300keV and above require more thora- kisi. In order to shield the light rays from the output X, the set of waveguide dressed with a sheet of lead thickness 2mm. A second portion was proste- above the first, the middle portion of the waveguide, while the body of the lamp around the area of the passage dressed whole three lead sheets, thickness 2mm. The neck, due to the construction of the insulator, may be shielded to a certain height as shown in the following picture. The cumulative shield the lamp is now sufficient for operations up 300keV.

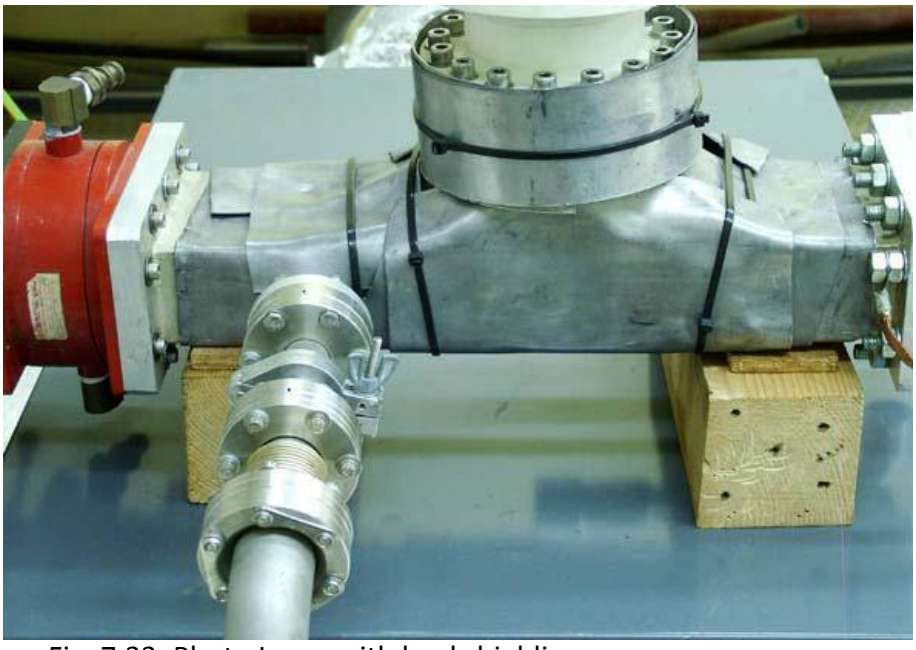

Fig. 7.33: Photo Lamp with lead shielding.

Recall that X radiation observations during experiments with 100kV impulse voltage (see. Par. 6.4) with the naked waveguide showed that the resulting struc-

tions per impact were: at 40cm from the lamp and to the plane of the waveguide, *maximum* dose 0.1mSv in 60cm from the lamp, *maximum* dose 0.04mSv while at 140cm from lychni- a, *maximum* 0.01mSv dose. Dosimetry new experimental setup for voltages above 100kV not currently conducted. However, experiments conducted by the lamp at a distance of 5m, using extra special unitary lead apron, as a measure pre- storage.

7.3. Testing Marx Generator

The multistage generator was installed in the center of a spacious room (IASA, Department of Physics), with distances from other objects at least 1.5m. The neigh- thrust system was using rectangular copper rod, width 40mm, and associations with level braided copper (shield), width 15mm. The only departure of the impulse grounding ligated into the building's grounding conductor, which is at a very great distance, until the local substation. The scenario ground is unsuitable for tech- TolC type applications, the high voltage laboratories must have funda- ventricular ground with rectangular mesh just below the floor of testing, covering the entire premises ([141]) . One thought was to create a small grounding grid in open space, located just outside the area as- Kimonos, a total distance of approximately 5m from the field tests. However soil resistivity measured by the method of the four electrodes and the value was close to 400Om. H value would require a very large network of radio vdous copper sunken into the ground, in order to achieve grounding resistance mo- nopsifias price. The idea was abandoned because the creation of such "local" impulse land would require to fill the space with copper. Specifically, it was estimated that it would require 25 copper rods, length 1.5m diameter Ø16, immersed in the territory, positioned vertically netting 5x5, with 2.5m distance between them.

In discharges of Marx generators, a crucial role plays the return path of the current passing through the core, array of capacitors. For this reason, large diameter pipes are used for the lamp connections with polyvath- a device. A single node is used for attachment of the ground point to the building grounding system. For routing was used typical conductor cross section 50mm2, length of 7 meters. From this point onwards used the regional grounding bar of laboratory, which is heading up the substation, at a distance of but over 20m.

The two pieces of acrylic, designed to form the Ba- importance of oktavathmias generator glued successfully together. The placement of the capacitors and resistors made according to the design and loading of genni- triplet successfully tested. The use of resistors 1MO, the side of the zero potential of the capacitors, offers a high resistance conductive path to the ground node. Therefore, the multistage Marx generator can be tested without re- Nena external load. The timing of the gaps of the generator is successful when, upon discharge, all experience gaps arc. The discharge currents in this case is small, and therefore, the noise of discharge is too small. However, this method allows to confirm that the Load Generator Zeta as provided even collapse that happens all the gaps, in-

pomenos summation of voltage at the output. Test Example of the multistage arrangement without external load shown in the following picture, Fig. 7.34, which is a frame of video, which is obtained in low light. Electric arcs of scintillators are weak, so full lighting is not bright, as we refer to currents of a few tens of mA. If the manual adjustment is a gap failed, some steps not exhibit electrical arcing.

In order to achieve a desired output voltage, calculate how much is required to be the charging voltage levels. In this charging voltage should be re- tarrefsei the scintillator tier. From this moment, the output voltage is approximately equal to the product of the charge voltage, on the steps used by a factor of ~ 95%, which depends on the capacity of the as-Kimi and parameters of the external circuit . The gaps are adjusted, to agree- with the experimental recordings, which are reflected in Fig. 7.11. The first clearance is set to the required breakdown voltage, while the other set about 30% higher standards in order to ensure the initial collapse of the first gap. No there is no reason, in the next gaps be regulated at progressively greater distances. The adjustment of the distances of the scintillator is made with calipers and the test genni- triplet made to the aforementioned method, the Marx generator is unladen.

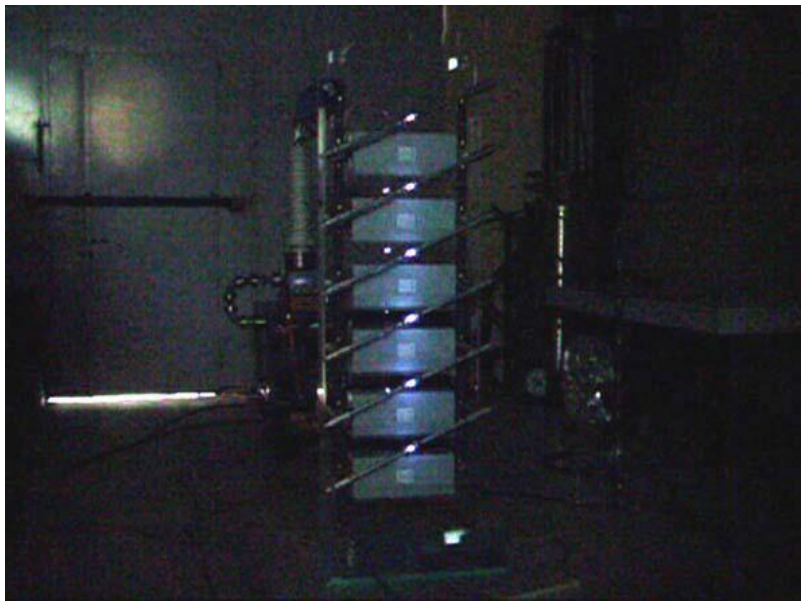

Fig. 7.34: Synchronization Testing interstices of multistage generator without load.

Before drive output voltage to the lamp, built a akidas- plate essay, to confirm the operation of the multistage generator load, simulating the Vircator. Two parallel blocks parts made of aluminum stereothi- even while roller from Acetal, at a distance of 20cm. At the top placements sheet was a support guide, through which passes a compact cross roller 16mm, the tip of which amounted to spike. Placing the tip a few cm RES à-vis the plate, led the output of the multistage generator in this essay.

Fig. 7.35: Essay pin-plate controls the generator Marx.

As shown in the following figure, the channel voltage in the essay is successful. This picture is a frame from a video which was taken in discharge established within three stage generator, a charging voltage 40kV / grade. The voltage discharge EI- yes above 100kV, while the discharge current without being measured, causes very iota schyro click.

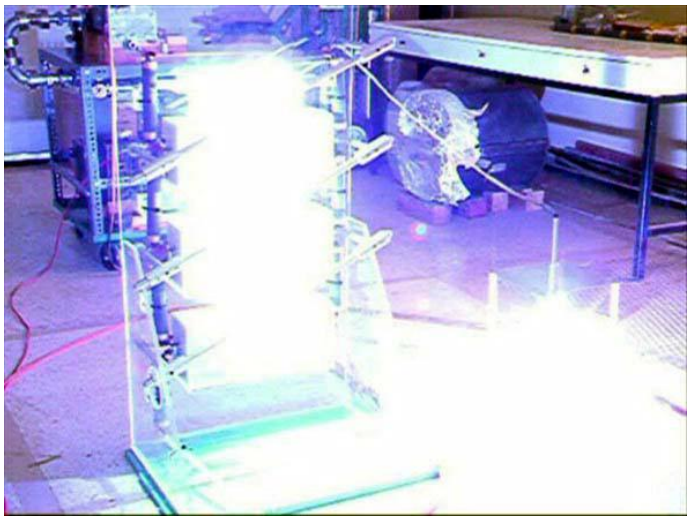

Fig. 7.36: Discharge generator directly to the plate pin essay.

After experimentally documented that the multistage generator can be synchronized and result output voltage, the high voltage resistance of front and then the lamp was connected to the outlet. The resistance kept horizontal, mounted on the ceiling of the room by line. High voltage connections are braided copper conductor (shield) which is suspended in space. The multistage device was confirmed to successfully leading the trend to light in principle by the large increase observed for the first time in the current of ionization pump. Note that, in these experiments automatically, the lamp remains under constant pumping to maintain the vacuum conditions. In the following photo from Video frames can distinguish the activation of the last spark, suggesting successful driving voltage to
Vircator.

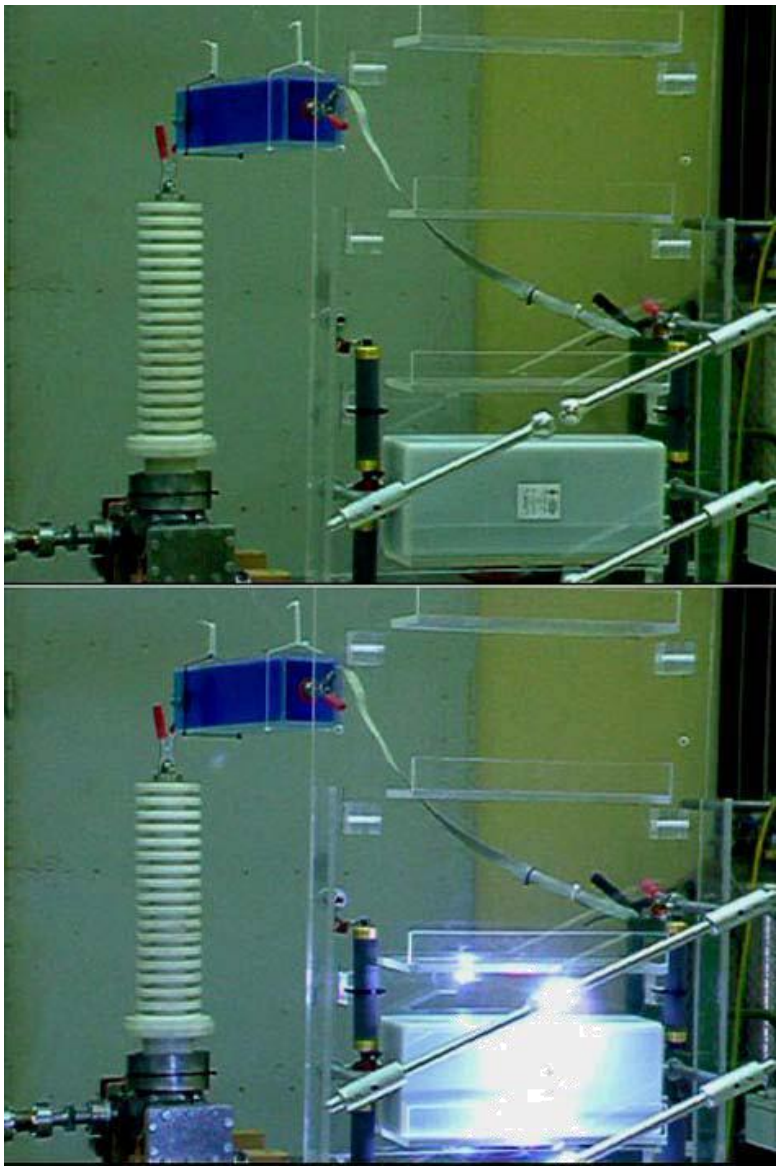

Fig. 7.37: Discharge Marx generator to light through the high-voltage resistance.

7.4. New Experimental Results System Vircator

The first tests were carried out with Vircator layout VDE-b, we have in previous outline (see. Par. 5.5 and par. 6.3), with front resistance RF = 208O, capacitor Load ing CC = 6000pF capacitor and CL shock = 1200pF, formed simultaneously as chori- nity divider. This arrangement could lead to the light with a maximum impulse voltage of 115kV, with a rise time of 10% -90% approximately equals 600nsec and impulse current, which largely provided by the capacitive divider and generally depends Tai the transition resistance shows the anode-cathode gap lychni- let. New tests were made with the multistage generator Marx, to formulations 4, 5 and 6 steps, using or not the high voltage resistance exceeding 40kV charging vathmi- don. The use of multistage generator allowed the driving equivalent capa- from 25nF to 16.67nF and trends up to 240kV. Initially the diode used

with pin type cathode, with the anode-cathode distance of 25mm, as the device which yielded the greatest powers in the testing phase with single-stage impulse ment provisions.

7.4.1. Descent Pin (d = 25mm)

For experiments with waveguide Vircator and testing the multistage outbreak STICK generator, originally used the pin-type cathode, because, since the series of experiments with single-stage configuration VDE-b, provided the larger sizes mikrokyma- tion radiation.

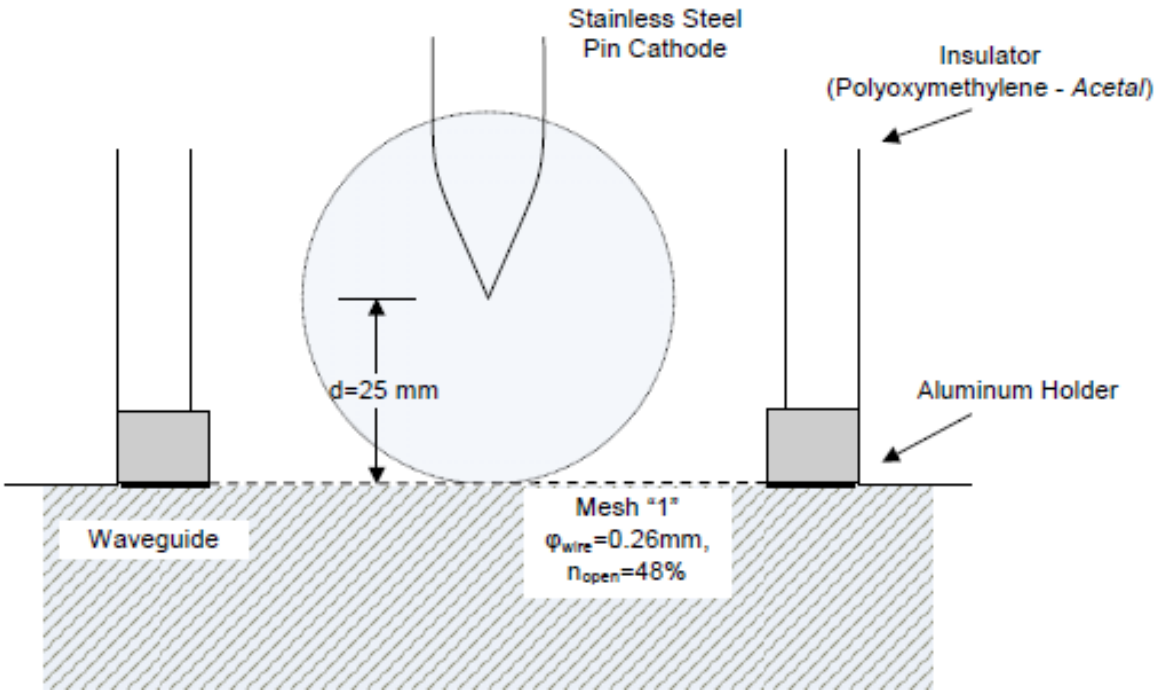

Fig. 7.38: Configuring a pin diode cathode and dAK = 15mm.

For measurements originally used the mesh number "1", which comprised 30 holes per inch, with a mesh 0.587mm, 0.26mm diameter wire surface should be free E- ~ 48%. Then a new grid was used, the grid number "7", with 10 holes per inch, with an opening hole 2.2mm, 0.34mm diameter wire and surface should be free in- ~ 75%.

7.4.1.1. Macroscopic Experimental Sizes

The pin cathode was tested at various voltages to the multistage generator. Specific experiments it was not possible to measure the voltage because of problems due to the resistive divider. Here are some driving sizes experiments pin cathode dAK = 25mm and matrices "1" and "7".

Tab. 7.5: Descent Pin dAK = 25mm, Mesh "1"

Formation	Theoretical Vmax	Ityp	RF max (mV)
4st. / 21kV / CuSO4	~ 80kV	1200A	400
4st. / 21kV	~ 80kV	2200A	240
5st. / 21kV / CuSO4	~ 100kV	1400A	400
5st. / 21kV	~ 100kV	1900A	700
5st. / 31kV / CuSO4	~ 150kV	2000A	760
5st. / 31kV	~ 150kV	3200A	400
5st. / 31kV / CuSO4	~ 150kV	1900A	800
6st. / 31kV / CuSO4	~ 180kV	2100A	750
6st. / 31kV / CuSO4	~ 180kV	2100A	1200

Tab. 7.6: Descent Pin dAK = 25mm, Mesh "7"

Formation	Theoretical Vmax	Ityp	RF max (mV)
6st. / 31kV / CuSO4	~ 180kV	2300A	450
6st. / 31kV	~ 180kV	3500	250
6st. / 38kV / CuSO4	~ 220kV	2500A	450

The microwave output was tested with the probe electric field (see. Par. 7.2.4) and found the same power levels with microwave attenuator. This test was made in order to solve some doubts that had been raised concerning possible non Secre- pacity of microwave attenuator at high powers. The following measurements have been conducted with microwave attenuator.

7.4.1.2. Typical measurements

Case A (5 stages, 31kV / stage, no resistor, 3200A)

In this recording, driving the lamp about 5 steps, without using anti limitation situation and charging levels equal to ~ 31kV. The theoretical maximum voltage to the lamp is ~ 150kV, when the diode is still in the early stages of katarref- ing at the beginning of the phenomenon, when it displays great resistance. The maximum current recorded is 3.2kA. Microwave signal occurs when the path has not short-circuited. However this can not be directly detected due to failure to record the voltage. We understand that the light is not bridged, as the change of current exhibits characteristic small fluctuations, before going to smooth behavior. Since the durations of phenomena speculate that the diode is bridged within 400 500nsec, namely a time slightly smaller than observed in the previous measurement series (see. Παρ. 6.3.4.3). The output frequency shown by the time-spectrum diagram that follows a path to higher values as the phenomenon develops. This development can be predicted using the migration model discharge capacity through the passage of Vircator (see. Par. 4.3.6).

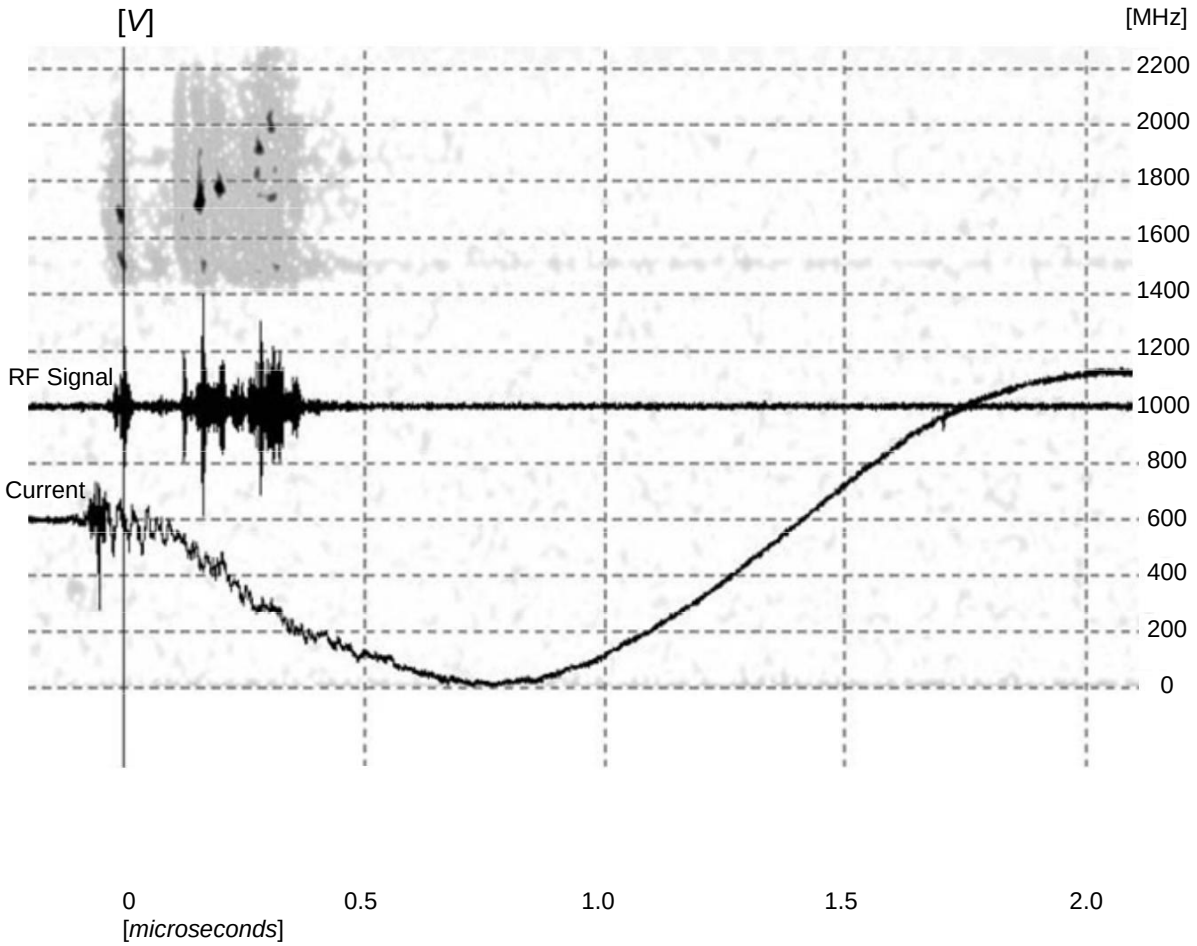

Fig. 7.39: The Descent pin, dAK = 25mm (measurement 20090409m34): *N*= 5, Vcharge = 31kV, Imax = 3200A, RFmax = 60W.

Case B (6 stages, 31kV / stage, CuSO4 resistor, 2200A)

In this recording, driving lamp about six steps and inserted high voltage resistance of solution CuSO4. Charging levels are ~ 31kV, in- pomenos theoretical maximum voltage to the lamp is ~ 180kV, when the diode is following but in the early stages of the collapse, at the beginning of the phenomenon, when it displays great resistance. The maximum current recorded is 2.2kA. Microwave signal occurs when the path has not short-circuited. We understand that the light is not bridged, as the change of current exhibits characteristic small fluctuations, before going to smooth behavior. This stage is calculated on the 500nsec, observing the variation waveform of the current.

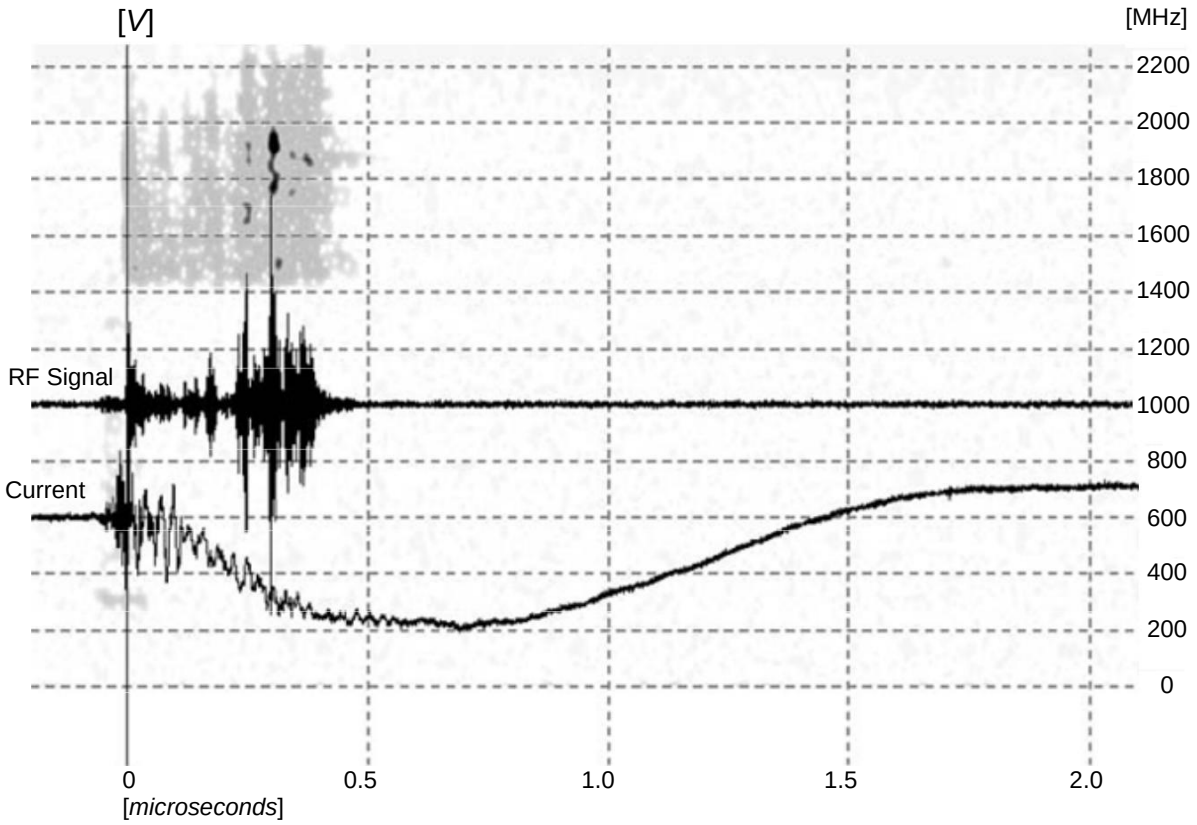

Fig. 7.40: The Descent pin, dAK = 25mm (measurement 20090411m11): *N*= 6, Vcharge = 31kV, CuSO4 resistor, Imax = 2200A, RFmax = 250W.

7.4.2. Descent with cylindrical accretion Cu (d = 3mm)

A novel method for achieving high roughness on the surface of the cathode doki- mastike the new experiments. A cylindrical cathode is aluminum, diameter 35mm, suitably adjusted to stem diameter 16mm, to leave very little alpha postasi the grid. The underside of the electrode was immersed in solution CuSO4, while as the anode was used a piece of copper. Connecting negative terminal of a DC power supply to the cathode and the positive pole of the power supply to the track copper, we can achieve by electrolysis to create a very thin porous layer of copper. The result of fitting uneven pure metallic copper with low affinity to aluminum, which is easily removed by scraping. The result of the electrolysis appears images of Fig. 7.42.

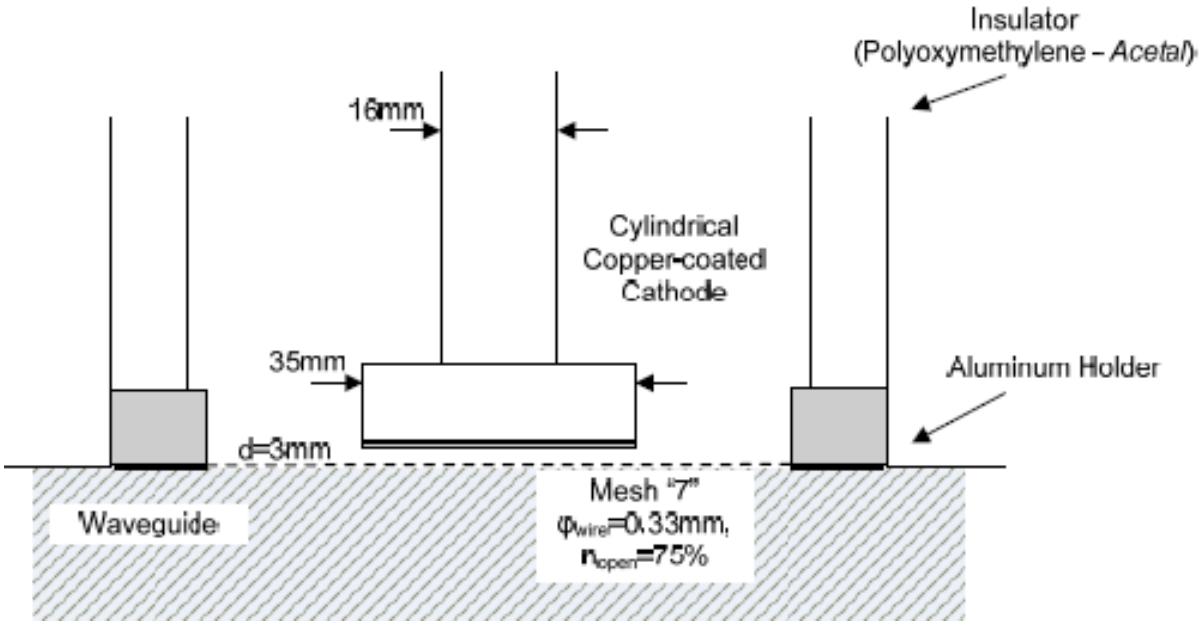

Fig. 7.41: Configuring diode with cylindrical cathode copper accretion and dAK = 3mm.

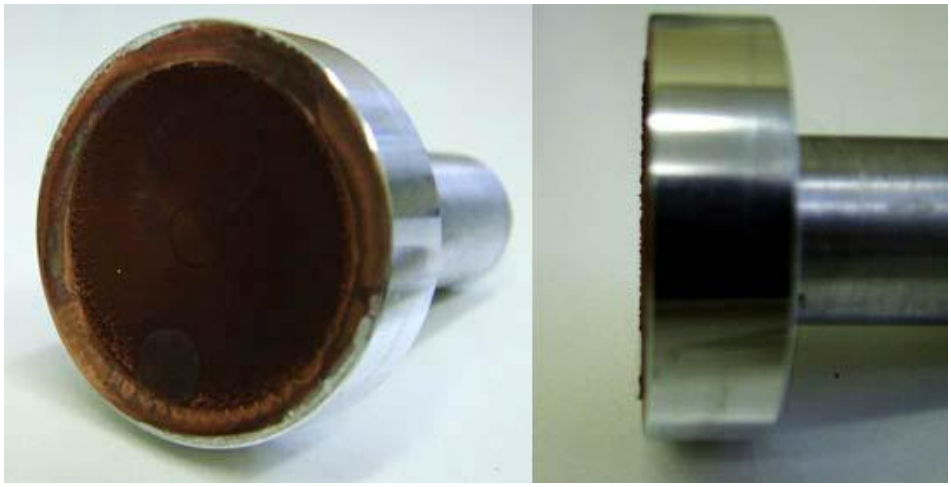

Fig. 7.42: Cylindrical cathode copper accretion.

The length of that cathode, 56mm, was such that the distance from the grid is a 3 to 4mm. As shown by the measurements, the passage collapses into a very short time, in the order of 100nsec, without any appearance of micro- wave signal. This descent, however, helps to document the me- tavatikis temporal behavior of the RLC circuit consisting of the generator Marx, high voltage resistance and the distributed inductance loop.

7.4.2.1. Macroscopic Experimental Sizes

The rapid closing of the gap leads the circuit in simple oscillating RLC of Conduct. We can practically ignore the transitional nonlinear behavioral Pa diode, since the contribution lasts little. With six levels and ~ 31kV charging voltage per step, with theoretical initial drive voltage of 180kV, the current pro-

bidders multigrade device is 3kA, interpolated resistance and 4.5kA, without resistance CuSO4.

Tab. 7.7: Cylindrical Descent with accretion Cu, dAK = 3mm, Mesh "7"

Formation	Theoretical Vmax	Ityp	RF max (mV)
6st. / 31kV / CuSO4	~ 180kV	3100A	-
6st. / 31kV	~ 180kV	4500	-

7.4.2.2. Typical measurements

Case A (6 stages, 31kV / stage, CuSO4 resistor, 3100A)

From this graph we realize that the diode is bridged, as the change of current exhibits characteristic small fluctuations, before going to smooth behavior. This stage is calculated on the 150nsec, paratiro- ing the variation waveform of the current. Simulations can be confirmed that the waveform responds to the discharge of an RLC circuit with R≈15O, C≈16nF and L≈8.6mI. Placing at 0.8 to 0.9mH inductance every tier one show for the rest of circuit (conductors high voltage connections, grounding conductors and high voltage resistance) *Lext* from 3.2 to 3.8mI. Interestingly, that absent the microwave output of the tests conducted.

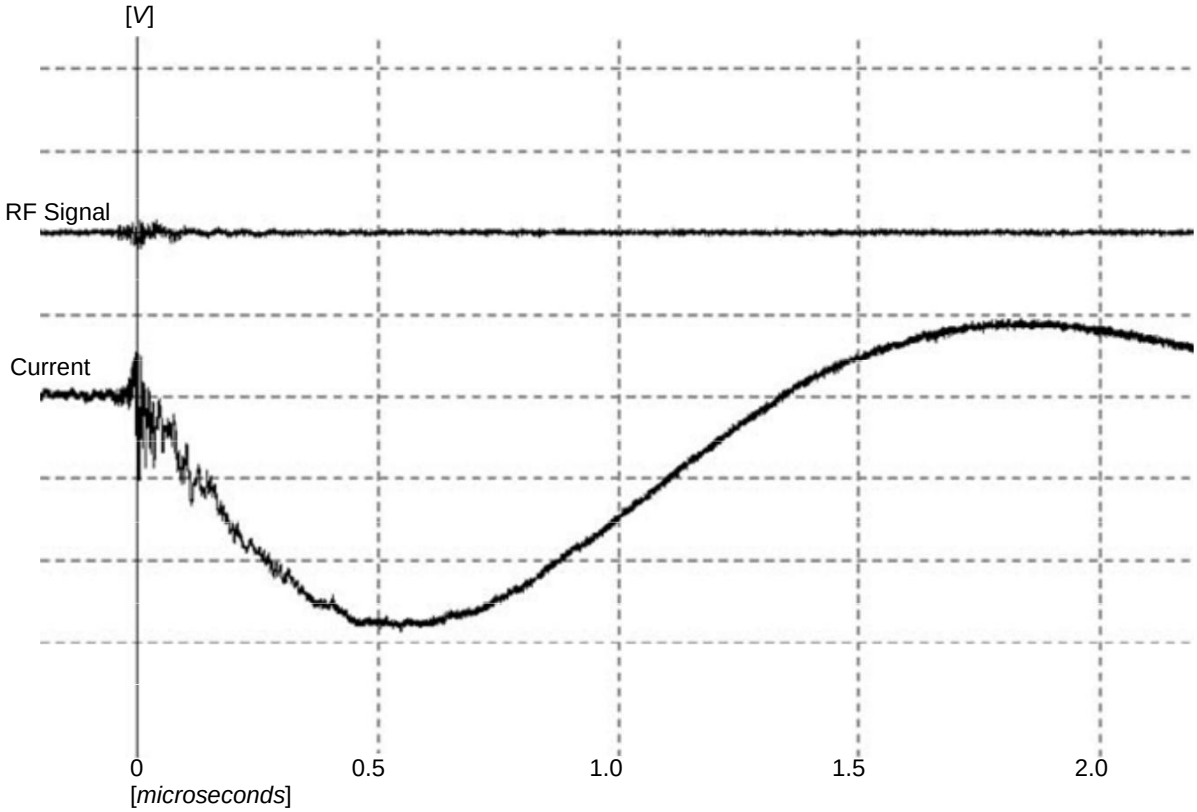

Fig. 7.43: Cylindrical cathode Cu, dAK = 3mm (measurement 20090411m11): *N*= 6, Vcharge = 31kV, CuSO4 resistor, Imax = 3100A.

The absence of observed microwave signals probably due to the fact the spectral content at very high frequencies, which is justified by the theoretical models and anode-cathode just 3mm.

7.4.3. Descent with cylindrical accretion Cu (d = 9mm)

Measurements with the cylindrical cathode with a distance 3mm from the grid not parousi- Asan microwave output, observed the oscilloscope bandwidth 2GHz. Down taskefastike another cathode by the same method unseated Cu. This Down Methods diameter 40mm and leaves away from the grid anode approximately 9mm. The passageway formed by a stainless steel grid number "7", with transit Food 0.33mm wire and geometrical permeability of 75%.

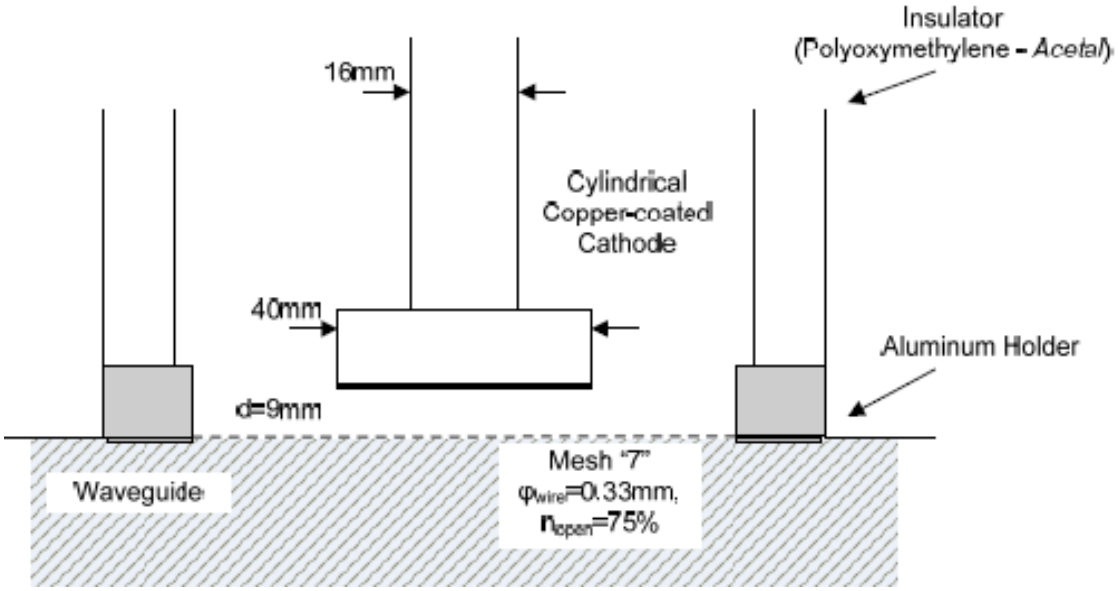

Fig. 7.44: Configuring diode with cylindrical cathode copper accretion and dAK = 9mm.

7.4.3.1. Macroscopic Experimental Sizes

Observations of the behavior of power suggest that the gap collapses in about 400 500nsec. The gap is considered to have collapsed by now, that the measured current does not show sharp fluctuations but has switched to a smoother behavior. These numbers translate into significantly low speeds katarref- ing gap of around 2cm / microseconds. This is probably due to epika- thisi Cu on the lower surface of the cathode. The presence of copper in combination with the large surface of the electrode leads to a wider distribution of current, thus in Asia Mi- kroteri heat strain of the cathode. In addition, copper is a heavy item, so the copper plasma derived from the cathode, has smaller thermal diffusion velocities. With six levels and ~ 31kV charging voltage per grade, with a theoretical

initial driving voltage of 180kV, the current provided by the multistage arrangement is 2.5kA, interpolated resistance and 3.5kA, without resistance CuSO4.

Tab. 7.8: Cylindrical Descent with accretion Cu, dAK = 3mm, Mesh "7"

Formation	Theoretical Vmax	Ityp
6st. / 31kV / CuSO4	~ 180kV	2500A
6st. / 31kV	~ 180kV	3500

Notably, for one set of measurements, allocated digital palmo- graph DSO90604, an analog bandwidth equal to 6GHz and sampling frequency 20GSamples / sec. While the measurement with a digital oscilloscope of 2GHz had re- we record patients microwave signals during this phenomenon, the measurements with the new oscilloscope showed impressive results. Established for the first time we conjecture that, in many cases, the output of spectral Vircator is included we have a significantly higher frequencies.

7.4.3.2. Typical measurements

Case A (6 stages, 31kV / stage, CuSO4 resistor, 3100A)

In this recording, driving the lamp is made with six levels, using limiting resistor ing and loading levels equal to ~ 31kV. The theoretical maximum voltage to the lamp is ~ 180kV, when the diode is still in the early stages of the collapse, at the beginning of the phenomenon, when it displays great resistance. The maximum current recorded is 3.1kA. Microwave signal occurs when the path has not short-circuited. However this can not be directly detected due to failure of recording the trend. We understand that the light is not bridged, as the change of current exhibits characteristic small fluctuations, before going to smooth behavior. Some small parasites in the waveform displayed, O when the connection multistage impulse function with high voltage resistance front and the essay makes good electrical contact. Note that Electrical connection of the last stage of the Marx generator with one end of the resistance, as the other end of the resistance with the top of the insulator tube becomes a me- tallikes pincers and used as connecting duct Interleaved Copper (blue-ntaz).

Since the durations of phenomena speculate that the diode is bridged within 400nsec, plasma spread speed of 2cm / microseconds. High frequencies can be predicted using the model discharge capacity through the passage of Vircator (see. Par. 4.3.6), but the model is no longer suitable, since intervention is denied high voltage resistance front

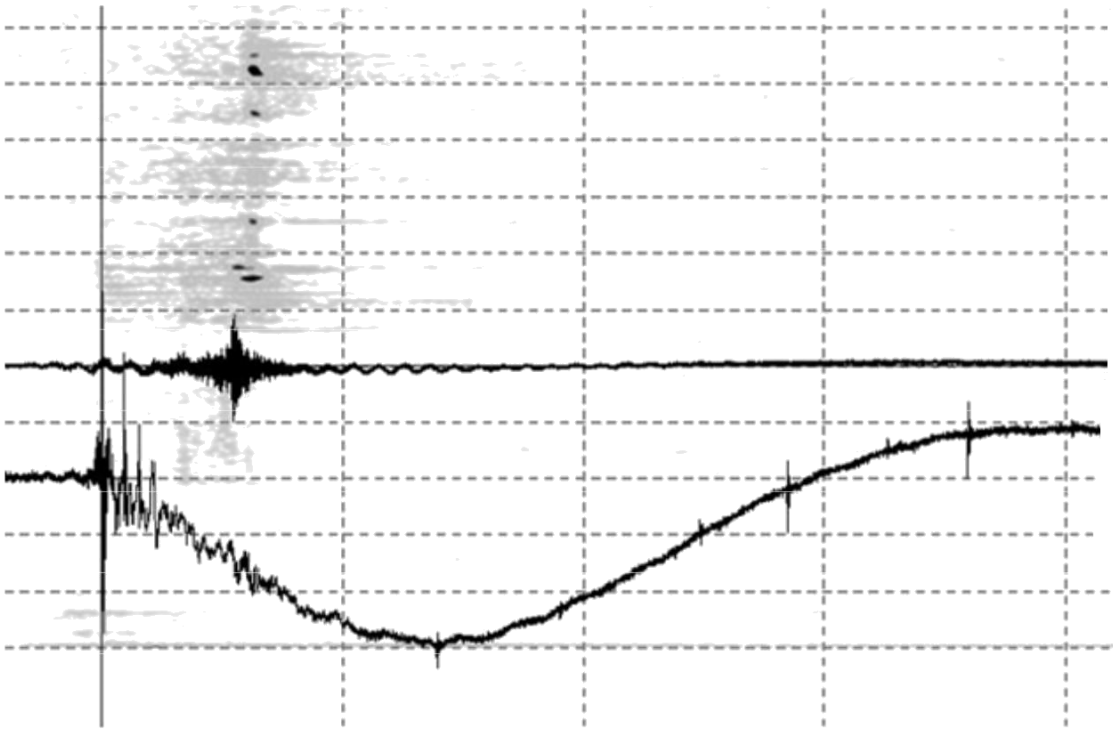

Fig. 7.45: Cylindrical cathode Cu, dAK = 9mm (measurement 20090515m03): *N*= 6, Vcharge = 31kV, CuSO4 resistor, Imax = 2500A, RFmax = 800W.

8. Suggestions for Future Research

In the present research, results were presented for the original waveguide Vircator, designed, constructed and tested experimentally. The initial experimental work was conducted at the Laboratory of High Tase- s premises of NTUA. To this end, it settled a mono- Primary impulse type device VDE-b, according to what has been described in Chapters 5 and 6. The device enabled with results with percussive waveforms doki- bution type 0.6 / 50, with a maximum width of driving 110kV. The lychni- driving currents let was approximately 1-2kA, amounts directly dependent on the drive voltage level and capacity of the high voltage system. The light seemed to bear micro- wave radiation from virtual cathode oscillations, but in small amounts of power and yields touched the limits 10-5. Small amounts of RF produced, apodido- are in low lamp drive sizes, especially in the very small currents. The persuasive sutures performed with the single-stage impulse device allowed the original documentation of the behavior of the lamp. Having the ability to record voltage and current tests revealed the behavior of the specimen with various combinations of voltage levels and anode and cathode electrodes. These experiments were completed, when a great variety of configurations measured, and Vircator doki- mastike the highest possible voltage levels.

To achieve higher levels of microwave power was decided the construction of a multistage impulse high voltage device. The impulse generator type Marx, it was possible to drive the Vircator with higher potencies. The multistage generator based on charging voltage capacitors 50kV and capacity 100nF. The infrastructure of the Marx generator offers composable up to eight degree midon for test voltages up to 400kV. The generator was installed in a new space, the Physics Department of the University of Athens, and successfully tested, leading the lamp. The current capacity of the multistage impulse generator is much higher than the one-stage arrangement. Limited mainly by the large inductance that displays the multistage generator size is increased by long in- naerion electrical connections required for the achievement of the necessary safe distances.

During the phase of experiments with single-stage impulse VDE-order b, the tip cathodes gave larger amounts of microwave radiation effect benefi- invoiced by the concentrated power transmission and therefore show stronger virtual cathode in kymatodigiki cavity. Such cathodes are, however,

They exhibit high resistance and not allow the pumping of large amounts of power, to the extent, of course, the capacity and the induction of impulse source of the permit. The light was tested under the new driving conditions, showing growth in Asia Mi- krokymatiki power.

For the observation of high frequency signals used two systems me- measurements. One involved the use of a microwave attenuator, implemented with absorbent material within the waveguide of the same dimension. At the output of the signal attenuator taken with adapter to coaxial cable. The second system includes receiving using a small probe electric field within the kymatodigikis route in order to take a sample of the microwave signal, back to coaxial CABLES. The observation of the signals became a digital storage oscilloscope with a bandwidth of 1.4 (the first rate cut-off frequency) up to approximately 2.1GHz. Sometimes used heterodyned technique allowing control signals to the 3.4GHz. These measurements, made in configurations pin cathode, showed no spectral content greater power in the region 2.1 to 3.4GHz, than in the region 1.4 to 2.1GHz. In all measurements, the energy of the microwave signal falls under the direct observation zone oscilloscope.

The realized Vircator lamp system passed the first stage of development, which is to address the problems of the operation itself. Overcome critical problems, such as leaks of light in a vacuum, the construction of high voltage components, obtaining experimental measurements free of interference. The overall behavior of the device has now been established, so that we can pre voume improvements in partial or total redesign of Vircator system.

A first possibility of future work is to design improved poly- XVIA. The microwave signals, which are recorded, studied and found that the spectral content takes several frequencies in the observation bandwidth to a patient preferably in the range between 1.7 and 1.9GHz, due sys- ntonizomenis cavity installed in the waveguide. Incorporating the poly- XVIA suitable machining modifications, such as the ability to change the coordination ers cavity and the distance cathode from the anode without requiring disassembly of the essay, we will have the opportunity to drastically accelerate the experimental procedure. To modify this requires use of suitable acces- sories vacuum (motion feedthroughs) and redesign of the body of Vircator, for which already given guidelines. In this way, can in- xetastei depth effect of the geometrical characteristics of kymatodigikis Com- versity and the passage in the microwave output of the Vircator.

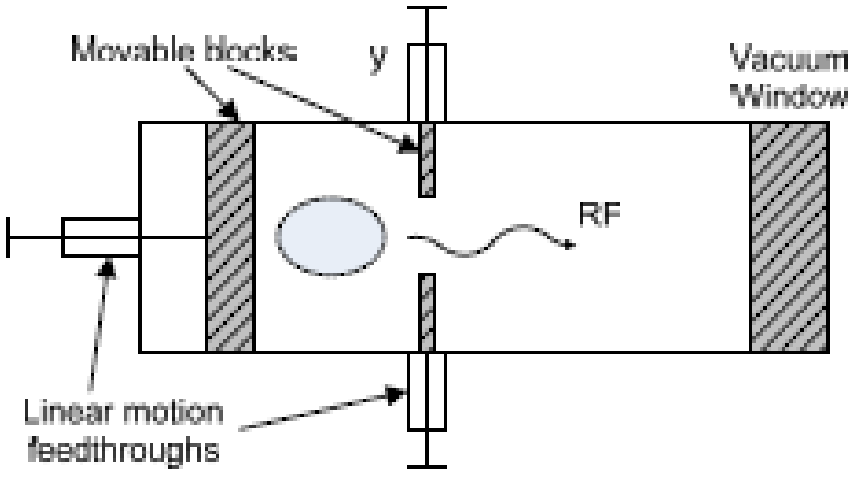

Fig. 8.1: Vircator with externally adjustable geometric parameters.

Secondly, it can be designed a new Marx generator, based appro- Luce capacitors placed inside the container with an insulating oil or gas is high elec- tricity resistance as sulfur hexafluoride, SF6. This will reduce to the maximum extent possible the total length of the impulse device. Thus, it will significantly reduce the inductance and is achievable larger drive currents and speed waveforms. In such a generator system Marx, the high voltage insulator tube passage can be insulator and supply voltage to the diode, making the lamp "integral" part of the multistage generator.

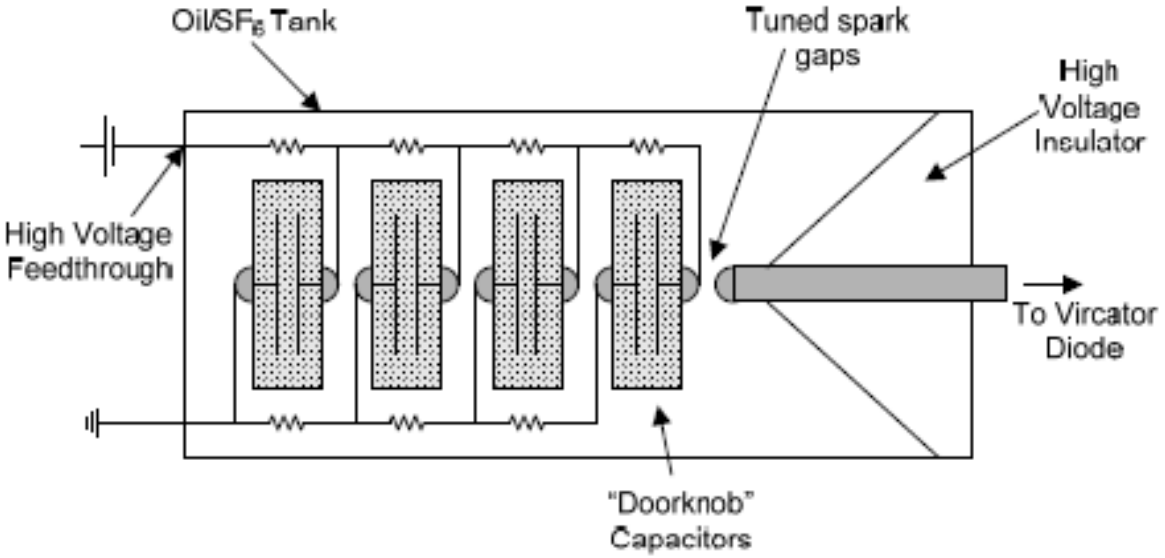

Fig. 8.2: Generator Marx low inductance.

To achieve faster shock repetition rates in the light, bo- psi appropriately modified the drainage system. The vacuum pump works best when it is connected to the volume to be pumped through a network of high conductivity pipe. Therefore, the lamp can be made larger window antli- ing gap, which however should skepasthei with stainless mesh to prevent the passage of radiation to the network and pumping disorder micro- wave field.

An important element in Vircator function are the materials and the geometry of the anode and cathode. As for the cathode, the study can be extended to re- search for new materials and techniques, such as full metal cathodes engraved with micro-mechanical, with carbon cathodes or cathodes coated from compounds Lu large molecular weight, such as cesium iodide. In this way they will reduce significantly the plasma spread speed and attained Microwave longer pulses.

The microwave output Vircator at higher frequencies, not observed so far, it may be possible to design the new measuring system. The output of the lamp can be divided into several zones, using an appropriately calibrated probes and then driven through zonoperaton filters in heterodyne De- cators. This will determine if there is a spectral content at much higher frequencies. The bandpass signals can also be observed with crystalline fast response detectors, to determine the total energy content of microwave output. Using finally digital oscilloscope with were first liberalized bandwidth can illuminate directly on the behavior of lychni-

let at much higher frequencies. In any event, the sampling system of the microwave power exhibits a transfer function which depends on the induced rhythms to the lamp, to which should be given special qualifi- Xe.

The elaborated system, which has been studied extensively and presented in this thesis, if you receive the proposed extensions, has multiple useful and interested Ruse applications.

It will be possible to create a technically simple microwave system ypsi- glycol power with high pulse repetition rate, easily customizable, coordinating ers in frequency and low in volume. As such, the system can Vircator operating tourgisei as a simple and effective tool documentation EMC devices and detection sensitivity to electromagnetic interference. Sys- gkekrimena, the implementation of a Vircator system with choice of frequency output Tash, by appropriate adjustment of the geometrical characteristics and me- gethon driving allows the study of immunity to electromagnetic devices re- interferences in a wide frequency range and power.

A lamp system Vircator with adjustable output characteristics can be effec- lesei microwave source of high power, for use in pulsed radar very long distance. The maximum range of a radar is proportional to the fourth root class of iota schyos broadcast. Therefore, emitting a Vircator force 103 times greater than the traveling wave tube of a radar, may be covered approximately six times greater radius. Also, a small volume of high power microwave system with light Vircator, transmitting at UHF frequencies, can be placed in a flying device and used in subsurface mapping radar, to detect mines, geological formations, archaeological sites.

The lamp Vircator, a microwave source of very high power, can be used been in other applications, such as gas ionization time of pulse of electromagnetic signals, the study of the atmosphere, even in the production of hot plasma- Tos fusion devices. There is even the possibility of a Vircator be used as output stage in aid provision microwave signals by kleidoma- Tosh output frequency techniques by external driving signal. In this case, the relaxed preferably output frequency of "free» Vircator will fall at a frequency, which can be exploited in particle accelerators high ENERGY crops.

REFERENCES

[1] I. Langmuir and L. Tonks, "Oscillations in Ionized Gases," *Phys. Rev.,* vol. 33, pp. 195-210, 1929.

[2] MN Saha, "On a Physical Theory of Stellar Spectra," *Proc. R. Soc. A,* vol. 99. no. 697, pp. 135-153, 1921.

[3] J. A. Bittencourt, *Fundamentals of Plasma Physics*, 3rd ed .: Springer, 2004.

[4] C. D. Child, "Discharge from Hot CaO," *Phys. Rev.,* vol. 32, no. 5, pp. 492-511, 1911.

[5] I. Langmuir, "The Effect of Space Charge and Residual Gases on Thermionic Currents in High Vacuum," *Phys. Rev.,* vol. 2, no. 6, pp. 450-486, 1913.

[6] J. Benford, E. Schamiloglu, and J. A. Swegle, *High Power Microwaves*, 2nd ed .: Taylor & Francis, 2006.

[7] HR Jory and AW Trivelpiece, "Exact Relativistic Solution for the One-Dimensional Diode," *J. Appl. Phys.,* vol. 40, no. 10, pp. 3924-3926, 1969.

[8] JW Luginsland, YY Lau, and RM Gilgenbach, "Two-Dimensional Child-Langmuir Law," *Phys. Rev. Lett.,* vol. 77, no. 22, pp. 4668-4670, 1996.

[9] YY Lau, "Simple Theory for the Two-Dimensional Child-Langmuir Law," *Phys. Rev. Lett.,* vol. 87, no. 23, pp. 1-3, 2001.

[10] Y. Li, F. He, C. Liu, and J. Sun, "Two-Dimensional Child-Langmuir Law for Planar Diode with Finite-Radius Emitter," *5th Int. Conf. on Vacuum Electron Sources (IVESC 2004). Proceedings,* pp. 263-264, 2004.

[11] I. Langmuir and KB Blodgett, "Currents Limited by Space Charge between Coaxial Cylinders," *Phys. Rev.,* vol. 22, no. 4, pp. 347-356, 1923.

[12] X. Chen, J. Dickens, EH Choi, and M. Kristiansen, "Space-charge limited current for 1-D cylindrical diodes," *14th IEEE Int. Conf. on Pulsed Power (PPC-2003). Digest of Technical Papers,* vol. 1, pp. 467-470, 2003.

[13] L. Tonks, "Space Charge as a Cause of Negative Resistance in a Triode and Its Bearing on Short Wave Generation," *Phys. Rev.,* vol. 30, no. 4, pp. 501-511, 1927.

[14] C. K. Birdsall and W. B. Bridges, *Electron Dynamics of Diode Regions*: Academic Press Inc., 1966.

[15] CE Fay, AL Samuel, and W. Shockley, "On the Theory of Space Charge between Parallel Plane Electrodes," *Bell Sys. Tech. J.,* vol. 17, no. 1, pp. 49-79, 1938.

[16] M. Reiser, *Theory and Design of Charged Particle Beams*: Wiley, 1994.

[17] V. L. Granatstein and I. Alexeff, *High-Power Microwave Sources*: Artech House, 1987.

[18] JD Lawson, "On the classification of electron streams," *J. Nucl. Energy, Part C Plasma Phys.,* vol. 1, no. 1, pp. 31-35, 1959.

[19] M. Abramowitz and I. A. Stegun, *Handbook of Mathematical Functions with Formulas, Graphs, and Mathematical Tables*. New York: Dover, 1972.

[20] E. W. Weisstein, "Dawson's Integral," in *MathWorld - A Wolfram Web Resource.*:http://mathworld.wolfram.com/DawsonsIntegral.html.

[21] H. Alfvén, "On the Motion of Cosmic Rays in Interstellar Space," *Phys. Rev.,* vol. 55, no. 5, pp. 425-429, 1939.

[22] CL Olson and JW Poukey, "Force-neutral beams and limiting currents," *Phys. Rev. A,* vol. 9, no. 6, pp. 2631-2634, 1974.

[23] LS Bogdankevich and AA Rukhadze, "Stability of Relativistic Electron Beams in a Plasma and the Problem of Critical Currents," *Sov. Phys. Usp.,* vol. 14, no. 2, 1971.

[24] JA Nation and M. Read, "Limiting currents in unneutralized relativistic electron beams," *Appl. Phys. Lett.,* vol. 23, no. 8, pp. 426-428, 1973

[25] OW Richardson, "Thermionic Phenomena and the Laws Which Govern Them," Nobel Lecture, December 12, 1929.

[26] S. Dushman, "Electron Emission from Metals as a Function of Temperature," *Phys. Rev.,* vol. 21, no. 6, pp. 623-636, 1923.

[27] MD Campbell-Miller and B. Simard, "First ionization potentials of tungsten and rhenium by mass-selected double-resonance ionization spectroscopy," *J. Opt. Soc. Am. B,* vol. 13, no. 10, pp. 2115-2120, 1996.

[28] R. L. Boxman, D. M. Sanders, and P. J. Martin, *Handbook of Vacuum Arc Science and Technology: Fundamentals and Applications*: Noyes Publications, 1995.

[29] M. Lenzlinger and EH Snow, "Fowler-Nordheim Tunnelling into Thermally Grown SiO2," *J. Appl. Phys.,* vol. 40, no. 1, pp. 278-283, 1969.

[30] RH Fowler and L. Nordheim, "Electron Emission in Intense Electric Fields," *L. Proc. R. Soc.,* vol. 119, no. 781, pp. 173-181, 1928.

[31] R. Gomer, *Field Emission and Field Ionization (AVS Classics of Vacuum Science and Technology)*: Springer, 1993.

[32] E. Hantzsche, "The Thermo-Field Emission of Electrons in Arc Discharges," *Beitr. Plasmaphys.,* vol. 22, no. 4, pp. 325-346, 1981.

[33] CA Spindt, KR Shoulders, and LN Heynick, "Field emission cathode structures and devices utilizing such structures." vol. 3755704 U. S. Pat. Office, 1973.

[34] PR Schwoebel, CA Spindt, and CE Holland, "Spindt cathode tip processing to enhance emission stability and high-current performance," *J. Vac. Sci. Technol. B,* vol. 21, no. 1, pp. 433-435 2003.

[35] CA Spindt, I. Brodie, L. Humphrey, and ER Westerberg, "Physical properties of thin-film field emission cathodes with molybdenum cones," *J. Appl. Phys.,* vol. 47, no. 12, pp. 5248-5263, 1976.

[36] ID Chalmers and BD Phukan, "Photographic Observations of Impulse Breakdown in Short Vacuum Gaps," *J. Phys. D: Appl. Phys.,* vol. 12, pp. 1285-1292, 1979.

[37] GA Mesyats, "Primary and secondary processes of explosive electron emission," *J. Appl. Mech. Tech. Phys.,* vol. 21, no. 5, pp. 690-695, 1980.

[38] R. J. Barker and E. Schamiloglu, *High-power Microwave Sources and Technologies*: IEEE Press, 2001.

[39] RB Miller and KW Habiger, "A review of recent progress in Reltron tube design," *12th Int. Conf. on High-Power Particle Beams (BEAMS '98),* vol. 2, pp. 740-743, 1998.

[40] L. Li, L. Liu, J. Wen, and Y. Liu, "Effects of CsI Coating of Carbon Fiber Cathodes on the Microwave Emission From a Triode Virtual Cathode Oscillator," *IEEE Trans. Plasma Sci.,* vol. 37, no. 1, pp. 15-22, 2009.

[41] DV Giri and FM Tesche, "Classification of Intentional Electromagnetic Environ- ments (IEME)," *IEEE Trans. Electromagn. Compat.,* vol. 46, no. 3, pp. 322-328, 2004.

[42] I. A. Stathopoulos, *High Voltages I*: Ed. Simeon.

[43] A. V. Gaponov-Grekhov and V. L. Granatstein, *Applications of High-Power Microwaves*: Artech House, 1994.

[44] SH Gold and GS Nusinovich, "Review of high-power microwave source research," *Rev. Sci. Instrum.,* vol. 68, no. 11, pp. 3945-3974, 1997.

[45] M. Haworth, R. Adler, B. Anderson, M. Connaughton, W. Dungan, J. Enns, J. Metz, P. Pelletier, R. Platt, J. Polaco, R. Rupp, L. Thode, and D . Voss, "Experimental observation of two microwave radiation mechanisms with widely separated frequencies during the output pulse of a high-voltage virtual cathode oscillator," *Appl. Phys. Lett.,* vol. 59, no. 4, pp. 408-410, 1991.

[46] SC Burkhart, RD Scarpetti, and RL Lundberg, "A virtual-cathode reflex triode for high-power microwave generation," *J. Appl. Phys.,* vol. 58, no. 1, pp. 28-36, 1985.

[47] HA Davis, RR Bartsch, LE Thode, EG Sherwood, and RM Stringfield, "High- Power Microwave Generation from a Virtual Cathode Device," *Phys. Rev. Lett.,* vol. 55, no. 21, pp. 2293-2296 1985.

[48] CA Kapetanakos, PA Sprangle, RA Mahaffey, and J. Golden, "High-Power Microwaves from a Non-Isochronous Reflecting Electron System (NIRES)." vol. 4150340 U. S. Pat. Office, 1979.

[49] D. Price, D. Fittinghoff, J. Benford, H. Sze, and W. Woo, "Operational Features and Microwave Characteristics of the Vircator II Experiment," *IEEE Trans. Plasma Sci.,* vol. 16, no. 2, pp. 177-184, 1988.

[50] W.-Y. Woo, "Two-dimensional Features of Virtual Cathode and Microwave Emission," *Phys. Fluids,* vol. 30, no. 1, pp. 239-244, 1986.

[51] DJ Sullivan, "High Power Microwave Generation from a Virtual Cathode Oscillator (Vircator)," *IEEE Trans. Nucl. Sci.,* vol. 30, no. 7, pp. 3426-3428, 1983.

[52] W. Jiang, K. Masugata, and K. Yatsui, "Mechanism of Microwave Generation by Virtual Cathode Oscillation," *Phys. Plasmas,* vol. 2, no. 3, pp. 982-986, 1995.

[53] BV Alyokhin, AE Dubinov, VD Selemir, OA Shamro, KV Shibalko, NV Ste- panov, and VE Vatrunin, "Theoretical and Experimental Studies of Virtual Cathode Microwave Devices," *IEEE Trans. Plasma Sci.,* vol. 22, no.5, pp. 945-959, 1994.

[54] M. Yatsuzuka, M. Nakayama, M. Tanigawa, S. Nobuhara, D. Young, and O. Ishihara, "Plasma Effects on Electron Beam Focusing and Microwave Emission in a Virtual Cathode Oscillator," *IEEE Trans. Plasma Sci.,* vol. 26, no. 4, pp. 1314-1321, 1998.

[55] HA Davis, RD Fulton, EG Sherwood, and TJT Kwan, "Enhanced-Efficiency, Narrow-Band Gigawatt Microwave Output of the Reditron Oscillator," *IEEE Trans. Plasma Sci.,* vol. 18, no. 3, pp. 611-617, 1990.

[56] HA Davis, RR Bartsch, TJT Kwan, EG Sherwood, and RM Stringfield, "Giga- watt-level microwave bursts from a new type of virtual cathode oscillator," *Phys. Rev. Lett.,* vol. 59, no. 3, pp. 288-291, 1987.

[57] RA Mahaffey, P. Sprangle, J. Golden, and CA Kapetanakos, "High-Power Micro- waves from a Nonisochronic Reflecting Electron System," *Phys. Rev. Lett.,* vol. 39, no. 13, pp. 843-846 1977.

[58] PA Lindsay, WK Toh, and X. Chen, "The Influence of an Axial Magnetic Field on the Performance of a Coaxial Vircator," *IEEE Trans. Plasma Sci.,* vol. 30, no. 2, pp. 1186-1195, 2002.

[59] EN Egorov and AE Hramov, "Investigation of the Chaotic Dynamics of an Electron Beam with a Virtual Cathode in an External Magnetic Field," *Plasma Physics Reports,* vol. 32, no. 8, pp. 683-694, 2006.

[60] KG Kostov, NA Nikolov, and VA Spassov, "Excitation of Transverse Electric Modes in Axially Extracted Virtual Cathode Oscillator," *Elect. Lett.,* vol. 29, no. 12, pp. 1069-1070, 1993.

[61] KG Kostov, NA Nikolov, IP Spassovsky, and VA Spassov, "Experimental study of virtual cathode oscillator in uniform magnetic field," *Appl. Phys. Lett.,* vol. 60, no. 21, pp. 2598-2600, 1992.

[62] KG Kostov and NA Nikolov, "Microwave generation from an axially extracted vir- tual cathode oscillator with a guide magnetic field," *Phys. Plasmas,* vol. 1, no. 4, pp. 1034-1039, 1994.

[63] AE Dubinov and VD Selemir, "Microwave generation features in a vircator with an inhomogeneous magnetic field in the interaction region," *Tech. Phys. Lett.,* vol. 27, no. 7, pp. 557-559, 2001.

[64] TJT Kwan, "High-Efficiency, Magnetized, Virtual-Cathode Microwave Generator," *Phys. Rev. Lett.,* vol. 57, no. 15, pp. 1895-1898, 1986.

[65] VD Selemir, AE Dubinov, BG Ptitsyn, AA Evseenko, VA Letyagin, RK Nur- galiev, VG Suvorov, and AV Sudovtsov, "The Influence of Vacuum Conditions on the Microwave Generation in a Vircator," *Tech. Phys. Lett.,* vol. 27, no. 11, pp. 967- 969, 2001.

[66] L. Li, T. Men, L. Liu, and J. Wen, "Dynamics of virtual cathode oscillation analyzed by impedance changes in high-power diodes," *J. Appl. Phys.,* vol. 102, no. 12, 2007.

[67] E.-H. Choi, M.-C. Choi, Y. Jung, M.-W. Chong, J.-J. Ko, Y. Seo, G. Cho, HS Uhm, and H. Suk, "High-Power Microwave Generation from an Axially Extracted Virtual Cathode Oscillator," *IEEE Trans. Plasma Sci.,* vol. 28, no. 6, pp. 2128-2134, 2000.

[68] CS Hwang and MW Wu, "A High Power Microwave Vircator with an Enhanced Efficiency," *IEEE Trans. Plasma Sci.,* vol. 21, no.2, pp. 239-242, 1993.

[69] FJ Agee, "Evolution of Pulse Shortening Research in Narrow Band, High Power Microwave Sources," *IEEE Trans. Plasma Sci.,* vol. 26, no. 3, pp. 235-245, 1998.

[70] FR Schwirzke, "Vacuum breakdown on metal surfaces," *IEEE Trans. Plasma Sci.,* vol. 19, no. 5, pp. 690-696, 1991.

[71] DJ Sullivan, "High Power Microwave Generator using Relativistic Electron Beam in Waveguide Drift Tube." vol. 4345220 U. S. Pat. Office, 1982.

[72] L. Liu, L.-M. Li, X.-P. Zhang, J.-C. Wen, H. Wan, and Y.-Z. Zhang, "Efficiency Enhancement of Reflex Triode Virtual Cathode Oscillator Using the Carbon Fiber Cathode," *IEEE Trans. Plasma Sci.,* vol. 35, no. 2, pp. 361-368, 2007.

[73] W. Jiang, J. Dickens, and M. Kristiansen, "Efficiency Enhancement of a Coaxial Virtual Cathode Oscillator," *IEEE Trans. Plasma Sci.,* vol. 27, no. 5, pp. 1543-1544, 1999.

[74] J. Mankowski, X. Cheng, J. Dickens, M. Kristiansen, and EH Choi, "Efficiency Results from a Coaxial Vircator using a Simple Feedback Technique," *14th IEEE Int. Conf. on Pulsed Power (PPC-2003). Digest of Technical Papers,* vol. 1, pp. 455-458, 2003.

[75] AN Didenko, AG Zherlitsyn, and GV Melnikov, "Research of Microwave Genera- tion Efficiency for Triode with Virtual Cathode (Vircator Triode)," *12th Int. Conf. on High-Power Particle Beams (BEAMS '98),* pp. 65-68, 1998.

[76] HE Brandt, "High Power Millimeter-Wave Source." vol. 4553068 U. S. Pat. Office, 1985.

[77] TJT Kwan and CM Snell, "Virtual Cathode Microwave Generator having Annular Anode Slit." vol. 4730170 U. S. Pat. Office, 1988.

[78] T. Ohkawa, "Microwave Generation by Virtual Cathode with Phase Velocity Match-ing." vol. 4745336 U. S. Pat. Office, 1988.

[79] RW Schumacher, J. Hyman, R. Harvey, and J. Santoru, "Plasma-Assisted High-Power Microwave Generator." vol. 4912367 U. S. Pat. Office, 1990.

[80] G. Convert and JP Brasile, "Electron Beam Device Generating Microwave Energy via a Modulated Virtual Cathode." vol. 5164634 U. S. Pat. Office, 1992.

[81] AJ Durand, "Microwave Generator with Virtual Cathode." vol. 2004/0245932 U. S. Pat. Office, 2004.

[82] S. Burkhart, "Multigigawatt microwave generation by use of a virtual cathode oscilla-tor driven by a 1-2 MV electron beam," *J. Appl. Phys.,* vol. 62, no. 1, pp. 75-78, 1987.

[83] R. Platt, B. Anderson, J. Christofferson, J. Enns, M. Haworth, J. Metz, P. Pelletier, R. Rupp, and D. Voss, "Low-frequency, multigigawatt microwave pulses generated by a virtual cathode oscillator, " *Appl. Phys. Lett.,* vol. 54, no. 13, 1989.

[84] RF Hoeberling and MV Fazio, "Advances in Virtual Cathode Microwave Sources," *IEEE Trans. Electromagn. Compat.,* vol. 34, no. 3, pp. 252-258, 1992.

[85] GA Huttlin, MS Bushell, DB Conrad, DP Davis, KL Ebersole, DC Judy, PA Lezcano, MS Litz, NR Pereira, BG Ruth, DM Weidenheimer, and FJ Agee, "The reflex-diode HPM source on Aurora," *IEEE Trans. Plasma Sci.,* vol. 18, no. 3, pp. 618-625, 1990.

[86] W. Jeon, KY Sung, JE Lim, KB Song, Y. Seo, and EH Choi, "A Diode Design Study of the Virtual Cathode Oscillator With a Ring-Type Reflector," *IEEE Trans. Plasma Sci.,* vol. 33, no. 6, pp. 2011-2016, 2005.

[87] KY Sung, W. Jeon, Y. Jung, JE Lim, HS Uhm, and EH Choi, "Influence of Anode-Cathode Gap Distance on Output Characteristics of High-Power Microwave From Co-axial Virtual Cathode Oscillator," *IEEE Trans. Plasma Sci.,* vol. 33, no. 4, pp. 1353-1357, 2005.

[88] X. Chen, WK Toh, and PA Lindsay, "Physics of the Interaction Process in a Typical Coaxial Virtual Cathode Oscillator Based on Computer Modeling Using MAGIC," *IEEE Trans. Plasma Sci.,* vol. 32, no. 3, pp. 1191-1199, 2004.

[89] MU Karlsson, F. Olsson, G. Filipsson, E. Edbom, BO Bergman, T. Hurtig, P. Appel- gren, M. Elfsberg, A. Larsson, C. Nylander, and SE Nyholm, "Comparison Between Experimental and Numerical Studies of a Reflex Triode, " *15th IEEE Int. Conf. on Pulsed Power (PPC-2005). Digest of Technical Papers,* pp. 210-213, 2005.

[90] SA Kitsanov, AI Klimov, SD Korovin, IK Kurkan, IV Pegel, and SD Polevin, "A Vircator With Electron Beam Premodulation Based on High-Current Repetitively Pulsed Accelerator," *IEEE Trans. Plasma Sci.,* vol. 30, no. 1, pp. 274-285, 2002.

[91] AE Dubinov, IA Efimova, KE Mikheev, VD Selemir, and VP Tarakanov, "Hybrid Microwave Oscillators with a Virtual Cathode," *Plasma Physics Reports,* vol. 30, no. 6, pp. 496-518, 2004.

[92] SA Kitsanov, AI Klimov, SD Korovin, BM Kovalchuk, IK Kurkan, SV Loginov, I. V. Pegel, SD Polevin, SN Volkov, and AA Zherlitsyn, "S-Band Vircator With Elec- tron Beam Premodulation Based on Compact Pulse Driver With Inductive Energy Storage," *IEEE Trans. Plasma Sci.,* vol. 30, no. 3, pp. 1179-1185, 2002.

[93] D. Biswas and R. Kumar, "Efficiency Enhancement of the Axial VIRCATOR," *IEEE Trans. Plasma Sci.,* vol. 35, no. 2, pp. 369-378, 2007.

[94] G. Singh and S. Chaturvedi, "PIC Simulation of Effect of Energy-Dependent Foil Transparency in an Axially-Extracted Vircator," *IEEE Trans. Plasma Sci.,* vol. 32, no. 6, pp. 2210-2216, 2004.

[95] G. Singh, A. Majalee, and S. Chaturvedi, "Two-Dimensional PIC Simulation of some Narrowband and Ultra-Wideband HPM Sources," *14th IEEE Int. Conf. on Pulsed Power (PPC-2003). Digest of Technical Papers,* vol. 2, pp. 1139-1142, 2003.

[96] D. Biswas and R. Kumar, "Modelling and Simulation of the Virtual Cathode Oscillator," Trombay, Mumbai: Theoretical Physics Division, Bhabha Atomic Research Centre, 2005.

[97] DJ Sullivan, "Autoacceleration via Virtual Cathode Oscillation," *IEEE Trans. Nucl. Sci.,* vol. 26, no. 9, pp. 4274-4276, 1979.

[98] TJT Kwan and HA Davis, "Numerical simulations of the reditron," *IEEE Trans. Plasma Sci.,* vol. 16, no. 2, pp. 185-191, 1988.

[99] SD Korovin, SA Kitsanov, AI Klimov, IK Kurkan, IV Pegel, SD Polevin, VV Rostov, and VP Tarakanov, "Tunable Vircators with E-beam Premodulation," *Pulsed Power Plasma Science (PPPS-2001). Abstracts,* pp. 495-499, 2001.

[100] SD Polevin, AM Efremov, AA Zherlitsyn, SA Kitsanov, AI Klimov, SD Korovin, B. M. Kovalchuk, IK Kurkan, OP Kutenkov, SV Loginov, and IV Pegel, "S-band Vircator with Electron Beam Premodulation Based on Compact Inductive Energy Storage Generator," *Pulsed Power Plasma Science (PPPS-2001). Digest of Technical Papers,* vol. 2, pp. 1642-1645, 2001.

[101] W. Jiang, K. Woolverton, J. Dickens, and M. Kristiansen, "High Power Microwave Generation by a Coaxial Vircator," *12th IEEE Int. Conf. on Pulsed Power (PPC-1999). Digest of Technical Papers,* pp. 194-197, 1999.

[102] X. Chen, J. Dickens, EH Choi, J. Mankowski, LL Hatfield, and M. Kristiansen, "Cavity Resonance Effect on a Coaxial Vircator," *14th IEEE Int. Conf. on Pulsed Power (PPC-2003). Digest of Technical Papers,* pp. 1165-1168, 2003.

[103] X. Chen, J. Dickens, J. Mankowski, LL Hatfield, EH Choi, and M. Kristiansen, "Microwave Frequency Determination Mechanisms in a Coaxial Vircator," *IEEE Trans. Plasma Sci.,* vol. 32, no. 5, pp. 1799-1804, 2004.

[104] Y. Yin, D. Zhu, and S. Liu, "Study of a Coaxial Vircator With a Three-Mirror Quasi-Optical Resonant Cavity," *IEEE Trans. Plasma Sci.,* vol. 34, no. 1, pp. 18-22, 2006.

[105] J. Mankowski, Y. Chen, J. Dickens, A. Neuber, and R. Gale, "A Low-Cost Metallic Cathode for a Vircator HPM Source," *15th IEEE Int. Conf. on Pulsed Power (PPC-2005). Digest of Technical Papers,* pp. 66-69, 2005.

[106] Y. Chen, J. Mankowski, J. Walter, and M. Kristiansen, "Cathode and Anode Optimization in a Virtual Cathode Oscillator," *IEEE Trans. Dielect. Elect. Insulation,* vol. 14, no. 4, pp. 1037-1044, 2007.

[107] YJ Chen, J. Mankowski, J. Walter, and M. Kristiansen, "Virtual Cathode Oscillator Component Optimization," *Power Modulator Symposium, 2006. Conference Record of the 2006 Twenty-Seventh International,* pp. 157-160, 2006.

[108] D. Price and HM Sze, "Phase-Stability Analysis of the Magnetron-Driven Vircator Experiment," *IEEE Trans. Plasma Sci.,* vol. 18, no. 3, pp. 580-585, 1990.

[109] D. Price, H. Sze, and D. Fittinghoff, "Phase and frequency locking of a cavity vircator driven by a relativistic magnetron," *J. Appl. Phys.,* vol. 65, no. 12, pp. 5185-5189, 1989.

[110] M. Onoi, K. Minami, and M. Yatsuzuka, "Repetitive Operation of Virtual Cathode Oscillator in an Axial Magnetic Field," *14th IEEE Int. Conf. on Pulsed Power (PPC-2003). Digest of Technical Papers,* vol. 2, pp. 1154-1157, 2003.

[111] HA Davis, RR Bartsch, TJT Kwan, EG Sherwood, and RM Stringfield, "Ex- perimental confirmation of the reditron concept," *IEEE Trans. Plasma Sci.,* vol. 16, no. 2, pp. 192-198, 1988.

[112] VD Selemir, AE Dubinov, EE Dubinov, IV Konovalov, and AV Tikhonov, "A hy- brid microwave generator based on a vircator-TWT (Virtode) system," *Tech. Phys. Lett.,* vol. 27, no. 7, pp. 583-585, 2001.

[113] AE Dubinov, VD Selemir, and AV Tsarev, "Phased Antenna Arrays Based on Vircators: Numerical Experiments," *Radiophysics and Quantum Electronics,* vol. 43, no. 8, pp. 637-642, 2000.

[114] H. Sze, D. Price, and B. Harteneck, "Phase locking of two strongly coupled vircators," *J. Appl. Phys.,* vol. 67, no. 5, pp. 2278-2282, 1990.

[115] H. Sze, D. Price, B. Harteneck, and N. Cooksey, "A master-oscillator-driven phase-locked vircator array," *J. Appl. Phys.,* vol. 68, no. 7, pp. 3073-3079, 1990.

[116] BM Novac, M. Istenic, J. Luo, IR Smith, J. Brown, M. Hubbard, P. Appelgren, M. Elfsberg, T. Hurtig, C. Moller, A. Larsson, and SE Nyholm, "A 10- GW Pulsed Power Supply for HPM Sources, " *IEEE Trans. Plasma Sci.,* vol. 34, no. 5, pp. 1814-1821, 2006.

[117] TA Holt, AJ Young, MA Elsayed, JW Walter, AA Neuber, and M. Kristiansen, "Images From the Development of a High-Power Microwave System," *IEEE Trans. Plasma Sci.,* vol. 36, no. 4, pp. 1414-1415, 2008.

[118] A. A. Neuber, *Explosively Driven Pulsed Power: Helical Magnetic Flux Compression Generators*: Springer, 2005.

[119] EH Choi, MC Choi, SH Choi, KB Song, Y. Jung, YH Seo, HM Shin, HS Uhm, D. W. Lim, CH Kim, JM Lee, and JW Ahn, "Characteristics of Diode Perveance and Vircator Output Under Various Anode-Cathode Gap Distances," *IEEE Trans. Plasma Sci.,* vol. 30, no. 5, pp. 1728-1732, 2002.

[120] W. Jiang, K. Woolverton, J. Dickens, and M. Kristiansen, "High Power Microwave Generation by a Coaxial Virtual Cathode Oscillator," *IEEE Trans. Plasma Sci.,* vol. 27, no. 5, pp. 1538-1542, 1999.

[121] W. Jeon, JE Lim, M. Moon, KB Jung, WB Park, HM Shin, Y. Seo, and EH Choi, "Output Characteristics of the High-Power Microwave Generated From a Coaxial Vir- cator With a Bar Reflector in a Drift Region, " *IEEE Trans. Plasma Sci.,* vol. 34, no. 3, pp. 937-944, 2006.

[122] J. Benford, H. Sze, W. Woo, and B. Harteneck, "Virtual-cathode oscillator emission by a pinched diode," *Phys. Rev. Lett.,* vol. 56, no. 4, pp. 344-346, 1986.

[123] H. Sze, J. Benford, W. Woo, and B. Harteneck, "Dynamics of a virtual cathode oscillator driven by a pinched diode," *Phys. Fluids,* vol. 29, no. 11, pp. 3873-3880, 1986.

[124] CS Hwang, MW Wu, PS Song, and WS Hou, "High power microwave genera- tion from a tunable radially extracted vircator," *J. Appl. Phys.,* vol. 69, no. 3, pp. 1247- 1252, 1991.

[125] J. Benford, D. Price, H. Sze, and D. Bromley, "Interaction of a vircator microwave generator with an enclosing resonant cavity," *J. Appl. Phys.,* vol. 61, no. 5, pp. 2098-2100, 1987.
[126] BM Marder, MC Clark, LD Bacon, JM Hoffman, RW Lemke, and PD Cole- man, "The split-cavity oscillator: a high-power E-beam modulator and microwave source," *IEEE Trans. Plasma Sci.,* vol. 20, no. 3, pp. 312-331, 1992.
[127] R. E. Collin, *Field Theory of Guided Waves*, 2nd ed .: Oxford University Press, 1991.
[128] www.matweb.com, "Overview of materials for Acetal Copolymer, Unreinforced," 2008.
[129] J. F. O'Hanlon, *A User's Guide to Vacuum Technology*: Wiley, 2003.
[130] Agilent, *Infiniium DSO80000B Series Oscilloscopes and InfiniiMax Series Probes, Data Sheet*.
[131] Schaffner, *MD-200 High Voltage Differential Probe, Data Sheet*.
[132] Pearson, *Model 1025 Wideband Current Transformer, Data Sheet*.
[133] F. E. Terman, *Radio Engineers' Handbook*: McGraw-Hill, 1943.
[134] F. W. Grover, *Inductance Calculations*: Dover, 1962.
[135] GA Mesyats and EA Litvinov, "The volt-ampere characteristic of a diode with point cathode in the explosive electron emission mode," *Rus. Phys. J.,* vol. 15, no. 8, pp. 1235-1237, 1972.
[136] Victoreen, *InoVision Model 451B, Data Sheet*.
[137] physics.nist.gov, "X-Ray Mass Attenuation Coefficients."
[138] Nicrom, *High Voltage Power Resistors Series 500, Data Sheet*.
[139] Glassman, *WK Series Extended Current 500 Watt Regulated High Voltage DC Power Supplies, Data Sheet*.
[140] M. Bester-Gogac, "Electrical Conductivity of Concentrated Aqueous Solutions of Divalent Metal Sulfates," *J. Chem. Eng. Data,* vol. 53, no. 6, pp. 1355-1359, 2008.
[141] M. S. Naidu and V. Kamaraju, *High Voltage Engineering*, 2 ed .: McGraw Hill, 1995.